GARNET-ORTHOPYROXENE ASSEMBLAGES AS PRESSURE-TEMPERATURE INDICATORS.

An experimental study with applications to granulites from Enderby Land, Antarctica.

by

Simon Leigh Harley, B.App.Sc.(Hons.)

Submitted in fulfillment of the requirements
for the degree of Doctor of Philosophy.

University of Tasmania

Hobart

1981

This thesis contains no material which has been accepted for the award of any other degree or diploma in any university, and to the best of my knowledge and belief, contains no copy or paraphrase of material previously published or written by another person, except where due reference is made in the text of this thesis.

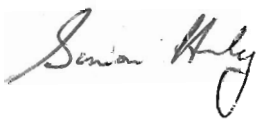

S.L. Harley.
University of Tasmania.
September, 1981.

CONTENTS

* * * * * *

LIST OF FIGURES

Page

LIST OF PLATES

LIST OF TABLES

* * * * * * * * *

ABSTRACT

Granulites from the Napier province, Enderby Land, Antarctica were metamorphosed at 900-950 °C and 7-10 kilobars during and subsequent to a major tectonothermal episode at 3000 million years before the present. Rocks presently exposed at the surface in southwestern Enderby Land indicate a regional increase in pressures of metamorphism towards the Scott Mountains - Casey Bay region, where crustal thicknesses of at least 30 kilometres were attained at that time.

Subsequent to the peak granulite facies metamorphic event, the Napier province granulites underwent a prolonged phase of near-isobaric cooling at depth to P-T conditions of 650-700 °C and 5-8 kilobars by 2500 million years before the present.

A study of the pyroxene granulites from the Napier province demonstrates the near-isobaric cooling path in the development of a variety of retrograde corona textures involving the formation of garnet by reactions between pyroxenes, plagioclase, and opaque phases. Garnet-orthopyroxene bearing felsic and pelitic granulites display a variety of recrystallisation and corona textures which usually involve the formation of secondary garnet and , occasionally, orthopyroxene. Chemical zoning in these minerals, and the compositions of distinct generations of the garnets and pyroxenes , are used to constrain the P-T metamorphic evolution of these granulites, and hence the evolution of the Napier province.

The P-T conditions of metamorphism and cooling history of the granulites of the Napier province have in part been determined by the application of several previously calibrated geothermometers and geobarometers to mineral assemblages common throughout the province. Most information on the physical conditions of metamorphism and later cooling suggested by zoning relationships in coexisting phases has been obtained, however, using a new experimental calibration of the P-T-compositional dependence of the solubility of Al_2O_3 in orthopyroxene coexisting with garnet, and an experimental study of the distribution of Fe and Mg between garnet and orthopyroxene.

The P-T-compositional dependence of the solubility of Al_2O_3 in orthopyroxene coexisting with garnet has been experimentally

determined in the P-T range 5-30 kilobars and 800-1200 °C in the system $FeO-MgO-Al_2O_3-SiO_2$ (FMAS) and extended into the system $CaO-FeO-MgO-Al_2O_3-SiO_2$ (CFMAS) in a further set of experiments designed to quantify the effects of the calcium content of garnet on the Al_2O_3 content of coexisting orthopyroxene. The geobarometer developed from these experimental studies, and applied to granulites from the Napier province, compares favourably with recent experimental data obtained by other workers, and yields reasonable and consistent results for a variety of well-documented natural occurrences previously reported in the literature.

The P-T-compositional dependence of the distribution of Fe and Mg between garnet and orthopyroxene has been experimentally calibrated in FMAS and CFMAS , enabling the construction of an approximate geothermometer for use in granulite facies assemblages and in garnet peridotite xenoliths. Non-ideal, model-dependent interaction parameters for garnet, derived from Fe-Mg distribution experimental data obtained in CFMAS, are in good agreement with previous estimates by other experimental investigators.

ACKNOWLEDGEMENTS

It is with the greatest pleasure that I acknowledge my supervisor, Professor D.H. Green, for his suggestion of the experimental project which constitutes a major part of this thesis, for his endeavour which allowed me a field season in Enderby Land, and for his guidance and good sense of humour throughout the course of this study.

I have also benefitted from discussions with many people on aspects of this project : Dr. R.F. Berry, Dr. L.P. Black, Dr. D.J. Ellis, Mr. R. N. England, Dr. E. Grew, Mr. K.L. Harris, Dr. C. Hatton, Dr. B.J. Hensen, Dr. P.R. James, Mr. K. Nickel, Mr. N. Ortez, Dr. R. Powell, Mr. M. Sandiford, Dr. J.W. Sheraton, Dr. V. Wall, Dr. J. Walshe, Dr. C. Wilson.

I am particularly grateful to the following people with whom I was fortunate enough to spend many enjoyable hours in the field : Dr. L.P. Black, Mr. R.N. England, Dr. M. Etheridge, Dr. P.R. James, Mr. M. Sandiford, Dr. V. Wall, and Dr. C. Wilson.

I am indebted to the following workers who provided me with some of the samples which form the basis of the work on Enderby Land. Dr. D.J. Ellis, Dr. P.R. James, Dr. R. Oliver, Dr. J.W. Sheraton, and Mr. R.J. Tingey.

From November 1979 till April 1980 I undertook field work in Enderby Land, Antarctica, as a research scientist attached to the 1979-1980 Australian National Antarctic Research Expedition summer program. I thank the Director of the Antarctic Division, Department of Science, for providing me with this opportunity and also thank the officers of the Antarctic Division and the expeditioners at Mawson and Mount King who gave invaluable assistance with logistic support and in the field. In particular, I am indebted to Sid Kirkby, Vic Barkell, Dave Hardy, and Shane Rollins for enabling me to camp at isolated sites for prolonged periods of time.

I am grateful to Mr. K.L. Harris for his instruction and assistance in the high-pressure laboratory as well as his sometimes tuneful and lyrical renditions of many songs. Assistance with the electron microprobe was given by W. Jablonski, R. Lincolne, and B.J. Griffin. I thankall these for their help and in particular am indebted to B.J. Griffin for his instruction in the use of the microprobe.

This project was financed by a Commonwealth Postgraduate Research Award. I thank Mrs. N. Gill, Mrs. J. Pongratz, and Mrs. A. Brooks for typing this thesis.

I would also like to thank the many students and the staff of the Geology Department, University of Tasmania, for making the department an enjoyable place in which to work, and for their ability to laugh both in the face of adversity and at the occasional satirical ballad I have been known to produce.

Finally, I thank Ron Berry and George Jenner for their continued friendship and sometimes stimulating rhetoric; Bryan Stait for his guidance to the hallowed doors of various establishments and his ability to exchange ideas on metamorphic petrology and Ordovician cephalopoda (which forms a negligable part of this thesis); Dr. Clive Burrett and Dr. Asahel Bush for their sometimes cynical support; and lastly Miss Veronika Lanzlinger for her understanding friendship, sense of humour, and fine taste in music and rocks. Sanity is a precarious path, and without the help of these people I may have stayed on it.

GLOSSARY OF ABBREVIATIONS AND SYMBOLS USED IN THE TEXT

a_j^i	activity of component i in phase j
Ab	albite
An	anorthite
Apat	apatite
alm	almandine
biot	biotite
CaTs	Calcium Tschermaks molecule
cd	cordierite
cpx	clinopyroxene
Di	diopside
En	enstatite
Fs	ferrosilite
ga, gar	garnet
Hd	hedenbergite
hy	hypersthene
ilm	ilmenite
Jd	jadeite
$K_{D\,Fe-Mg}^{i-j}$	distribution coefficient for Fe-Mg partitioning between phase i and phase j.
Kspar	K-feldspar
MgTs	Magnesium Tschermaks' molecule
mt	magnetite
Ol	olivine
opx, op	orthopyroxene
osu	osumilite
P	pressure in kilobars
pig	pigeonite
plag	plagioclase
py	pyrope
pyx	pyroxene
qz	quartz
R	universal gas constant, 1.9872
Sa	sapphirine
sill	sillimanite
Sp	spinel
T	temperature in °C or °K
V_{298}^o	standard molar volume of a phase, at 298°K.
ΔV_r°	standard molar volume change of reaction.
W_{FeAl}^{opx}	regular solution parameter for non-ideal Fe-Al interactions in the opx M1 site.
W_{FeMg}^{M2}	regular solution parameter for non-ideal Fe-Mg interactions on the opx M2 site
W_{FeMg}^{M1}	regular solution parameter for non-ideal FeMg interactions on the opx M1 site
W_{CaMg}^{ga}	regular solution parameter for non-ideal Ca-Mg interactions in garnet.
X_{Al}^{opx}	Al/2 in orthopyroxene
X_{Al}^{sa}	AFM ratio (Al_2O_3/Al_2O_3-FeO-MgO) of sapphirine
X_{Ca}^{ga}	Ca/Ca-Mg-Fe of garnet
X_{Mg}^i	Mg number (Mg/Mg+Fe) of phase i as a mole fraction
$\Delta H_{1,T}^o$	standard state enthalpy of reaction at 1 bar and T of interest, in cal/mole.
ΔS_T^o	entropy of reaction at T of interest, in cal/mole/°K
$\Delta G_{1,T}^o$	standard state free energy change of reaction at 1 bar and T of interest, in cal/mole

Chapter 1

INTRODUCTION

INTRODUCTION

This thesis presents the results of an experimental study of the P-T dependence of the solubility of Al_2O_3 in orthopyroxene coexisting with garnet and the application of this barometer-thermometer, in combination with other Fe-Mg exchange geothermometers, to granulite facies metamorphic rocks from Enderby Land, Antarctica.

In the past decade there have been considerable advances in the quantitative estimation of pressures and temperatures of metamorphism, based on data obtained from the analysis of compositions of phases coexisting in divariant and trivariant equilibria. Experimental work has led to the calibration of a number of Fe-Mg exchange thermometers, the pyroxene "solvus" thermometer, and other barometers and thermometers which are applicable, with varying degrees of uncertainty and reliability, to granulite facies metamorphic rocks, eclogites, and peridotites.

An important barometer which has been developed from experimental studies, chiefly in chemical systems approaching peridotite compositions, is the pressure dependence of the solubility of Al_2O_3 in orthopyroxene coexisting with garnet (Boyd, 1973; Wood and Banno, 1973; Wood, 1974). Application of this barometer to crustal granulites and garnet peridotites has, in some cases, yielded unrealistic pressures of formation for such rock types and has cast doubt on the reliability of this barometer.

In the first part of this thesis, the solubility of Al_2O_3 in orthopyroxenes coexisting with garnet is experimentally re-calibrated in a P-T-X range applicable to granulite parageneses. Thermodynamic analysis of the experimental data results in the formulation of equations from which the pressures of formation of granulites and

peridotites can be estimated. In Chapter 2, experimental results in the simple system FeO-MgO-Al_2O_3-SiO_2 are presented. The experimental approach is further extended to CaO-bearing systems in Chapter 3. Along with a practical barometer based on Al_2O_3 solubility in orthopyroxenes coexisting with garnet, a thermometer based on Fe-Mg exchange between garnet and orthopyroxene in the FMAS and CFMAS systems is obtained from the experimental data of Chapter 2 and Chapter 3. Application of both experimentally-derived techniques enables the simultaneous estimation of the P-T conditions of formation of garnet-orthopyroxene-bearing parageneses.

The geobarometer equations derived in Chapter 2 and Chapter 3 are compared in Chapter 4 with previous experimental data obtained by other workers in the systems MAS, CMAS, and CFMAS. These experimental data constitute independent data sets by which the accuracy of equations derived in Chapter 2 and Chapter 3 may be judged. The consistency of these equations with the most recent MAS and CMAS data is demonstrated in Chapter 4.

The Al_2O_3-geobarometer is applied to some well documented natural garnet-orthopyroxene-bearing parageneses in Chapter 4. These parageneses include garnet-peridotite inclusions in kimberlites; garnet-peridotite and orthopyroxene-eclogite bodies and masses in crustal gneisses; and granulites from regional metamorphic belts worldwide. The overall consistency and reliability of the Al_2O_3 barometer derived herein, given reasonable temperature estimates, are illustrated by these examples.

In the second part of the thesis (Chapters 5, 6 and 7) the garnet-orthopyroxene barometry/thermometry techniques are combined with other geothermometers and geobarometers including garnet-clinopyroxene Fe-Mg distribution thermometry; two-pyroxene thermometry;

calcium Tschermak's-anorthite-quartz barometry; and phase stability and topological constraints in a detailed study of the metamorphic conditions and evolution of an Archaean granulite facies terrain, the Napier Complex of Enderby Land, Antarctica.

A wide range of two-pyroxene and garnet-clinopyroxene granulites are considered in Chapter 5. The P-T evolution of these rock types is evaluated, based on textural criteria and the application of various geothermometers/barometers to the mineral assemblages.

The metamorphic history of Enderby Land is further elucidated in an extensive study of the common garnet-orthopyroxene-bearing assemblages found in the granulites. The barometry/thermometry techniques developed in Chapter 2 and Chapter 3 are applied to such granulites and P-T evolutionary paths on both local (single sites) and regional scales are constructed from a combination of the P-T techniques with textural observations and mineral zoning patterns

The data outlined in Chapter 5 and Chapter 6 are combined in Chapter 7 to produce a regional synthesis of the P-T metamorphic evolution of the Napier Province, for the time span 3000-2500 ma. The tectonic implications of the P-T evolutionary path of this Archaean craton are also considered in this chapter and possible models of Archaean crustal processes are briefly assessed.

Chapter 2

AN EXPERIMENTAL STUDY OF THE SOLUBILITY OF Al_2O_3 IN ORTHOPYROXENE COEXISTING WITH GARNET IN THE SYSTEM $FeO-MgO-Al_2O_3-SiO_2$ and the DISTRIBUTION OF Fe-Mg BETWEEN GARNET AND ORTHOPYROXENE AT 800-1200°C and 5-30 KBAR

2.1 INTRODUCTION

The pressure and temperature dependence of the solubility of Al_2O_3 in orthopyroxene coexisting with garnet has long been recognised amongst experimental workers and petrologists concerned with garnet peridotites (Boyd and England, 1964; Green and Ringwood, 1967, 1970), and more recently petrologists concerned with crustal granulites. Earlier experimental calibrations of the Al_2O_3 content of enstatite as a function of P and T (Boyd and England, 1964; MacGregor, 1974) in the $MgO-Al_2O_3-SiO_2$ system have been used widely, in conjunction with other geothermometers, to construct "paleogeotherms" for mantle-derived garnet peridotites (Boyd, 1973; Boyd and Nixon, 1975, Nixon and Boyd, 1973; Carswell and Gibb, 1980; Mitchell, 1978). The most widely used geobarometer-geothermometer equation has been that developed by Wood (1974). This calibration was based upon the experimental data of MacGregor (1974) in the $MgO-Al_2O_3-SiO_2$(MAS) system, and on experimental data obtained by Wood (1974) in the FeO-MgO-$Al_2O_3-SiO_2$ (FMAS) system and CaO-FeO-MgO-$Al_2O_3-SiO_2$ (CFMAS) system. This calibration was compared with the multicomponent pyrolite composition data of Green and Ringwood (1970) and found to give reasonable duplication of their run conditions.

More recently, much more experimental data has accumulated on the solubility of Al_2O_3 in orthopyroxene coexisting with garnet in the MAS system (Arima and Onuma, 1977; Howells and O'Hara, 1975, 1978; Danckwerth and Newton, 1979; Lane and Ganguly, 1981; Hensen and Essene, 1971), in the CMAS system (Akella, 1976; Howells and O'Hara, 1978); and in CFMAS or natural mineral systems (Akella, 1973, 1974; Hensen, 1973; Mori, 1978; Ellis,1979). Despite the proliferation of

data in compositions relevant to garnet lherzolites, several inconsistencies remain and the experimental data is subject to large uncertainty, particularly in the CMAS and CFMAS systems (Howells and O'Hara, 1978).

In the MAS system, recent data (Lane and Ganguly, 1980) have tended to give support to lower Al_2O_3 contents in enstatite, for a given P and T, than found by Boyd and England (1964). These new data are in broad agreement with most of the data of MacGregor (1974). The details of the previous experimental data in the MAS, CMAS and CFMAS systems will be discussed along with some new MAS data in Chapter 4

In the FMAS system, the only experimental data remains that of Wood (1974), and Holdaway (1971). The experiments of Wood (1974) were undertaken using seeded glass starting mixes (X_{Mg} =.50 glass with seeds of natural almandine-pyrope garnet (X_{Mg} = .25 , X_{Ca} = .05) and synthetic aluminous orthopyroxene (X_{Mg} =.70 , Al_2O_3 = 12.3 wt %)) only, and no reversals using mineral-mix or low-Al_2O_3 seed types were attempted. In addition, these experiments were of relatively short durations for higher temperature runs (20 hours), and the lower temperature runs resulted in quite strongly zoned garnets and probably in strongly zoned orthopyroxenes too. As centres of pyroxene grains were analysed and SiO_2 was estimated from difference, the quality and representability of the data is open to some question. The experiments were performed on a very narrow range of bulk compositions with respect to X_{Mg}, thus the experimental data set represented only an initial and incomplete exploration into the FMAS system. This data was combined with the earlier MAS data, and CFMAS data of Wood (1974), to produce a general equation governing Al_2O_3 in orthopyroxene coexisting with garnet as a function of P, T, X_{Mg}^{opx} and X_{Ca}^{garnet}

Workers in granulite terrains, where garnet-orthopyroxene bearing assemblages occur over a wide range of compositions in pelitic and metabasic rocktypes (X_{Ca}^{ga} = zero to .2, X_{Mg}^{opx} = .2 - .75), have in recent times applied the Wood (1974) barometer to these metamorphic rocks. The results in these natural occurrences have, at times, been inconsistent with observed phase assemblages (Ellis, 1980), and in some cases the Wood (1974) equation has given very low or negative pressures (O'Hara and Yarwood, 1978). Such inconsistencies point to the inadequacies of the thermodynamic extrapolations from data in MAS, necessitated in the Wood (1974) treatment.

In order to obtain more reliable and extensive data on which to base pressure estimates for granulite facies rocks in particular, I have undertaken an experimental programme aimed at determining the Al_2O_3 contents of orthopyroxenes in equilibrium with garnet plus quartz in the FMAS system and the CFMAS system. The experimental results of work in CFMAS will be presented in Chapter 3.

In the FMAS system, experiments have been undertaken over the pressure-temperature range 5 to 30 kb and 800-1200°C, at a nominal pressure spacing of 2.5 kbars. A number of bulk X_{Mg} compositions have been used at all run conditions to determine the dependence of X_{Al}^{opx} upon X_{Mg}. In addition, several runs have been performed using "reversal" mixes as a check on the validity of results using seeded glass mixes.

For the purposes of an experimental study aiming to determine the equilibrium content of Al_2O_3 in a phase, a "reversal" constitutes growing that Aluminous phase from both an Al-richer starting composition and an Al-poorer precursor.

An Al-richer precursor is exemplified by an aluminous glass mix

(A/AFM = 15 to 20), seeded with garnet to promote garnet nucleation and hence a more rapid approach to equilibrium. In this type of mix, the original glass devitrifies to Al-rich pyroxene and this must further exsolve to a lower-alumina orthopyroxene while the higher alumina phase (garnet) is growing. Thus, orthopyroxenes formed from such a mix would be expected to approach the equilibrium X_{Al} value from the high-Al side as growth of garnet proceeds. Experimental orthopyroxenes formed in this way may be zoned, with a decrease in X_{Al}^{opx} from cores to rims.

An Al-poorer predecessor for the growth of a phase of variable Al_2O_3 content is provided by a mineral mixture of finely ground garnet + orthopyroxene (low or no Al_2O_3) + quartz. In such a starting mix, Al_2O_3 can only be incorporated into the pre-existing orthopyroxene through consumption or "dissolution" of the aluminous phase, garnet. As ionic exchange (Fe = Mg, Al) proceeds, garnet will be consumed in total but will change composition (in terms of X_{Mg}) in the process. Pyroxene seeds would also change composition by incorporating progressively more Al_2O_3 to approach the equilibrium X_{Al} value from the low-Al side. Pyroxene would also change composition in terms of X_{Mg}, in an opposite sense to the garnets. In mineral mix runs, therefore, pyroxenes would be expected to zone outwards to a *maximum* Al_2O_3. The direction of X_{Mg} change depends on the relative X_{Mg}^{seed} with respect to X_{Mg}^{bulk}. Using almandine and enstatite seeds only, the orthopyroxene will become more Fe, Al rich, while the garnet will become more magnesian rimwards

The reasoning above is the basis for the interpretation of the analytical data on the experimental run products in this study.

The experimental data obtained also provide information on the

distribution of Fe-Mg between garnet and orthopyroxene ($K_{D_{FeMg}}^{ga-opx}$) as a function of P, T, X_{Al}^{opx}, and X_{Mg}. It is necessary here to point out that K_D data is heavily dependent on the X_{Mg}^{ga} attained in any experiment. Garnet produced in these, and in most subsolidus experiments, is quite often strongly zoned and thus X_{Mg}^{ga} is a difficult variable to constrain. In some experiments garnets analysed may not have attained their equilibrium Xmg value, and there also exists a possibility that they may overshoot this value (Danckwerth and Newton, 1979; and discussion section 4.5).

For the purposes of Fe-Mg exchange equilibria, a "reversal" consists of attaining similar Xmg values (and hence a similar K_D) in the participating phases whether approaching from a more magnesian seed or a more iron rich seed composition. Thus, a pyrope (or pyropic ga)-ferrosilite seeded mix ($K_D = 0$) would consitute a reversal type mix to the almandine + enstatite + quartz mineral mix or the almandine + enstatite seeded glass mixes (K_D's = ∞) mostly used in the experiments. A reversal mix of this type has been used only in a few experiments at 1050°C and one experiment at 900°C.

Experiments considered in this chapter have been performed mostly in Fe capsules. It is found (section 2.5) that iron enters the mix from the capsule walls, both as Fe-metal and as FeO addition into the equilibrating phases. Such FeO addition results in a change in bulk composition through the duration of a run. In response to such changes, the phases take up FeO. As orthopyroxene reacts at a faster rate than garnet (section 2.5), FeO may be preferentially incorporated into orthopyroxene over garnet as the experiment proceeds. This will result in illusory low $K_{D_{FeMg}}^{ga-opx}$ at any particular (P,T) condition as the measured garnet composition is actually in Fe-Mg

equilibrium with an orthopyroxene of more magnesian composition than that measured.

In view of the uncertainty associated with obtaining K_D data from runs performed in Fe-capsules, few reversals of $K_{D_{FeMg}}^{ga\text{-}opx}$ using alternate seed types have been attempted. K_D data obtained in Fe capsules have been compared with unreversed and reversed K_D data obtain in graphite capsules run under the same (P,T) conditions, and a general empirical adjustment has been made accordingly to account for FeO addition. This problem is further discussed in section 2.5.

2.2. THERMODYNAMIC CONSIDERATIONS

I. Al_2O_3 SOLUBILITY IN ORTHOPYROXENE COEXISTING WITH GARNET

The reaction governing the Al_2O_3 content of orthopyroxene in equilibrium with garnet may be written as :

$$Mg_2Si_2O_6 + MgAl_2SiO_6 = Mg_3Al_2Si_3O_{12} \qquad (1)$$

orthopyroxene solid solution — garnet

(Boyd and England, 1964; MacGregor, 1974; Wood and Banno, 1973; Wood, 1974).

On the basis of Xray evidence and crystal-chemical constraints (Ganguly and Ghose, 1975, 1980), Lane and Ganguly (1981) considered that the maximum Al-content of an orthopyroxene was equivalent to the pyrope composition. These authors have accordingly analysed their MAS data using the relation:

$$Mg_3Al_2Si_3O_{12} = Mg_3Al_2Si_3O_{12}$$

orthopyroxene — garnet

defining a "quadrienstatite" (QEn = $Mg_4Si_4O_{12}$) - "orthopyrope" (Opy = $Mg_3Al_2Si_3O_{12}$) solid solution series and writing activity-composition relations for orthopyroxenes appropriately. The choice of end-member is purely arbitrary however, and my analysis proceeds using relationships derived from equation (1). The data can be analysed using formulations derived from (2), and an analysis of this type has been carried out, yielding a barometry-thermometry equation which appears to offer no advantage over that derived from an analysis of the experimental data based on equation (1).

A full and detailed thermodynamic analysis of both garnet-

orthopyroxene, Fe-Mg exchange equilibria and the Al_2O_3 contents of orthopyroxene coexisting with garnet is presented in Appendix One. Only a brief outline of the approach used will be presented here.

The equilibrium condition for reaction (1) can be rearranged to give (Wood and Banno, 1973)

$$\Delta G^{o}_{P,T} = - RT \, Ln \, K$$

$$= - RT \, Ln \left\{ \frac{a^{garnet}_{Mg_3Al_2Si_3O_{12}}}{a^{opx}_{Mg_2Si_2O_6} \cdot a^{opx}_{MgAl_2SiO_6}} \right\} \quad (3)$$

and $$\Delta G^{o}_{P,T} = \Delta H^{o}_{1,T} - T\Delta S^{o}_{1,T} + \int_{.001}^{P} \Delta V^{o} \, dP$$

$$\simeq \Delta H^{o}_{1,T} - T\Delta S^{o}_{1,T} + P\Delta V^{o}$$

where P is in kilobars, T is in ° Kelvin, and ΔV^{o} is the standard volume change of reaction (1):

$$\Delta V^{o} = V^{o}_{Mg_3Al_2Si_3O_{12}} - V^{o}_{Mg_2Si_2O_6} - V^{o}_{MgAl_2SiO_6}$$

The aim is to extract values of $\Delta H^{o}_{1,T}$ and $\Delta S^{o}_{1,T}$ from experimental data obtained over a P-T range. To evaluate these parameters we require an expression for ΔV^{o} and activity-composition relations describing the solid-solution properties of the phases involved in reaction (1).

Garnet has initially been treated as an ideal binary solid solution in FMAS, thus

$$a^{ga}_{Mg_3Al_2Si_3O_{12}} = (X^{ga}_{Mg})^3$$

(Wood and Nicholls, 1979).

Subsequent thermodynamic analysis of reaction (1) has indicated that

garnet can best be treated, in FMAS, as a single component phase for the purposes of Al-exchange with orthopyroxene. Hence garnet can be expressed as $M^{2+}_3Al_2Si_3O_{12}$, where

$$M^{2+} = Mg, Fe,$$

and then $a^{garnet}_{M^{2+}_3Al_2Si_3O_{12}} = 1.$

This approach is analogous to that of Wood (1974).

Orthopyroxene has been treated as a two-site symmetric regular solution (Thompson, 1969) with reciprocal terms (Sack, 1979) included. The M1 site has been treated as a ternary (Fe,Mg,Al) symmetric regular solution, while in FMAS the M2 site has been described in terms of a binary symmetric regular solution (Fe,Mg). Cross-site interaction terms have also been included. Full activity-composition expressions for $Mg_2Si_2O_6$ and $MgAl_2SiO_6$ are presented in Appendix One.

Adopting the method of Wood and Banno (1973), Mg-Al orthopyroxenes have been assumed to mix ideally at one bar, and non-ideal (regular solution term W^{opx}_{MgAl}) Mg-Al interactions at higher pressures have been ascribed to an excess volume of mixing term. Incorporation of this term, derived from the molar volume data of Skinner (1964) and Danckwerth and Newton (1978), into the standard molar volume change of reaction (ΔV^o) results in a (P,T) dependent volume of reaction, ΔVr, where

$$-\Delta Vr = 183.3 + 178.98 \{X^{opx}_{AL}(1 - X^{opx}_{AL})\} \text{ cals/kbar} \qquad (4)$$

This volume term ($= \Delta V^o + \Delta V^{excess}$) accounts for the Mg-Al non-identity on the M1 site of orthopyroxene and for the pressure-dependent of Fe-Al interactions on the M1 site. In this approach it is implicitly assumed that the volume behaviour of $Mg_2Si_2O_6$ - $MgAl_2SiO_5$

orthopyroxenes and $Fe_2Si_2O_6$ - $FeAl_2SiO_6$ orthopyroxenes are similar.

In a similar approach to that used by Wood (1974), the remaining non-ideal interactions in orthopyroxene are attributed to an excess enthalpy term related to Fe-Al interactions on the M1 site. This term is of the form

$$W^{M1}_{FeAl} \ (1 - X^{opx}_{AL}) \ (1 - 2X^{opx}_{AL}) \ (1 - X^{opx}_{Mg}),$$

and represents a net apparent excess energy terms. The value of W^{M1}_{FeAl} derived from the experimental data is thus a partly empirical estimate.

Several assumptions, referred to in Appendix One, are critical in the derivation of this model and are responsible for the possible limitations of the use of reaction (1) as a barometer-thermometer:

(a) site occupancies of Fe and Mg on M1 and M2 can be ignored and X^{opx}_{Mg} or X^{opx}_{Fe} may be used instead. Major errors in pressure estimates may occur where M1-M2 ordering of Mg and Fe is extreme;

(b) the magnesium numbers of the coexisting garnet and orthopyroxene can be ignored except for the interactions with aluminium on the M1 site;

(c) non-ideal Fe-Mg interactions on the M1 and M2 sites of orthopyroxene are generally small enough to be neglected in aluminous orthopyroxenes. These on-site interactions can be balanced or negated by several cross-site (reciprocal) terms which then can also be ignored.

With this approach and these assumptions, we arrive at a simplified expression relating the Al_2O_3 contents of orthopyroxene coexisting with garnet in FMAS to P,T and X^{opx}_{Fe} : (equation (25) in

Appendix one).

$$\Delta H^{o}_{1,T} - T\Delta S^{o}_{1,T} + P\Delta Vr = RT \ln \{X_{Al}(1 - X_{Al})\} + W^{M1}_{FeAl}[(1-2X^{opx}_{Al})(1-X^{opx}_{Al})(1-X^{opx}_{Mg})] \quad (5)$$

The experimental data to be presented below are analysed according to this expression, defining

$$X^{opx}_{Mg} = (Mg/Mg+Fe)^{opx}$$

$$X^{opx}_{Al} = Al/2$$

and ΔVr as given in equation (4).

Equation (5) essentially treats the reaction (1) as an alternate reaction of the form

$$M^{2+}_2Si_2O_6 + M^{2+}Al_2SiO_6 = M^{2+}_3Al_2Si_3O_{12}$$

where M^{2+} = Mg, Fe.

In this form, no entropy of mixing arises from the presence of Fe and Mg in garnet or orthopyroxene except for distinguishable mixing with Al on the M1 site of orthopyroxene. i.e. Fe and Mg are indistinguishable in reaction (1) except for interactions with alumina. The variation of X^{opx}_{Al} with X_{Mg} is attributed only to differences in the mixing of Mg and Fe with Al in the orthopyroxene. The effects of addition of Fe^{2+} to the MAS system are not regarded as dilution effects but as results of the different mixing properties between the $(MgAl)_{M1}$ and $(FeAl)_{M1}$ components in a simplified orthopyroxene. This is a rather simple view of the macroscopic

activities of the garnet and orthopyroxene solid solutions participating in reaction (1). This macroscopic model arises from the interaction of a number of complicated effects in the orthopyroxene solid solution. In this regard, the W^{M1}_{FeAl} value derived from the experimental data should be viewed solely as a regression parameter. It is *not* a value to be used unquestioningly as an input to other quite different reactions involving orthopyroxene and other aluminous phases.

II. GARNET-ORTHOPYROXENE Fe-Mg EXCHANGE

The distribution of Fe^{2+} and Mg between coexisting garnet and orthopyroxene is governed by the following reaction:

$$\underset{\text{pyrope}}{\tfrac{1}{3}\,Mg_3Al_2Si_3O_{12}} + \underset{\text{ferrosilite}}{\tfrac{1}{2}\,Fe_2Si_2O_6} = \underset{\text{enstatite}}{\tfrac{1}{2}\,Mg_2Si_2O_6} + \underset{\text{almandine}}{\tfrac{1}{3}\,Fe_3Al_2Si_3O_{12}} \qquad (6)$$

for which the condition of equilibrium is

$$\Delta G^{o}_{1,T} + \int_{.001}^{P} \Delta V^{o}_{6}\, dP = -RT \ln \left\{ \frac{(a^{ga}_{Fe_3Al_2Si_3O_{12}})^{\frac{1}{3}}}{(a^{ga}_{Mg_3Al_2Si_3O_{12}})^{\frac{1}{3}}} \cdot \frac{(a^{opx}_{Mg_2Si_2O_6})^{\frac{1}{2}}}{(a^{opx}_{Fe_2Si_2O_6})^{\frac{1}{2}}} \right\} \qquad (7)$$

$(\Delta V^{o}_{6})_{298°K}$ is -22.86 cal $kbar^{-1}$, calculated from molar volume data given in table A1.1. In the subsequent thermodynamic analysis, ΔV^{o}_{6} is assumed to be independent of P and T, i.e. the effects of isothermal

compression and thermal expansion are ignored.

A full thermodynamic discussion of reaction (6) is presented in Appendix One, and only a summary of the approach is presented here.

In FMAS, garnet is treated as an ideal binary solid solution between pyrope and almandine. This solution model is considered reasonable in view of the similar molar volumes of the end members and the near linear volume-composition curve between almandine and pyrope.

Orthopyroxene is again treated as a two-site symmetrical regular solution, with Fe-Mg mixing on the M2 site and Fe-Mg-Al mixing on the M1 site. Reciprocal interactions across sites are also considered in the approach of Appendix One.

In order to derive a practical geothermometer based on $K_{D_{FeMg}}^{ga\text{-}opx}$*, site occupancies of Fe and Mg on the M1 and M2 sites of orthopyroxenes are ignored and approximated by the following terms:

$$X_{Fe}^{M1} = (1 - X_{AL})\ X_{Fe}^{opx}$$

and

$$X_{Fe}^{M2} = X_{Fe}^{opx},$$

where X_{Fe}^{opx} is the (Fe/Fe + Mg) ratio of the orthopyroxene.

Consideration of the relative contributions of non-ideal Fe-Mg, Mg-Al and Fe-Al interactions both on individual sites and across sites of the orthopyroxene solid solution (Appendix One) indicates that the orthopyroxene can be adequately modelled assuming near random Fe-Mg

---

* defined as $$K_D = \left(\frac{X_{Fe}^{ga}}{X_{Mg}^{ga}}\right) \cdot \left(\frac{X_{Mg}^{opx}}{X_{Fe}^{opx}}\right)$$

distribution on sites, an excess energy term resulting from Fe-Mg mixing (W^{opx}_{FeMg}), and excess energy terms resulting from Mg-Al and Fe-Al interactions on the M1 site ($W^{M1}_{MgAl} - W^{M1}_{FeAl}$). These terms can be combined with the ideal solid solution model for garnet to yield equation (34) of Appendix One.

$$-RT \ln K = -RT \ln K_D - (1 - 2X^{opx}_{Mg}) W^{opx}_{FeMg} - \tfrac{1}{2}X_{Al}(W^{opx}_{MgAl} - W^{opx}_{FeAl})$$

$$= \Delta H^{o}_{1,T} - T\Delta S^{o}_{1,T} + P\Delta V^{o}_{1,298} \qquad (8)$$

This equation has been used to analyse the experimental data obtained in FMAS. If, instead of assuming ideality, we assume a symmetric regular solution model for Fe-Mg garnets, the term

$$(2X^{ga}_{Mg} - 1)\ W^{ga}_{FeMg}$$

will be added to the expression in equation (8). The magnitude of W^{ga}_{FeMg} can be estimated by incorporation of this term into the analysis of the experimental data, however the derived value will be subject to large uncertainty resulting from FeO addition into mixes and the use of unreversed K_D data.

2.3 EXPERIMENTAL STARTING COMPOSITIONS

A series of simple system FeO-MgO-Al_2O_3-SiO_2 (FMAS) starting mixes were prepared using analytical grade reagents. Three basic types of mix were used in the experiments:

(1) seeded glass mixes

(2) mineral mixes

(3) seeded sintered oxide mixes.

(1) Seeded glass mixes.

Analyses of glasses used in the experimental programme are presented in table 2.1. A number of FMAS glasses of similar A/AFM ratio (.15 or .20), covering a broad X_{Mg} range (X_{Mg} = .30, .45, .50, .60) were synthesised from analytical grade Fe_2O_3, MgO, SiO_2 and Al_2O_3 reagents stored in a desiccator.

The pure oxide reagents were ground together under acetone in an agate mortar up to four times to achieve homogeneity. Ground mixes were then sintered in a one atmosphere furnace at 900°C for 12 hours. The pelletised, sintered oxide mixes were than reground and loaded into large capacity (50mg) graphite capsules with tight fitting lids. These mixes were then run in a piston cylinder apparatus at 10kbar and 1400-1450°C to produce homogeneous green glasses generally devoid of any quench crystals. Raman spectra of such glasses indicated the presence of minor quantities of CO_2.

Glasses manufactured by this technique were used for most of the experiments, however an alternative set of glasses was manufactured for the final experiments to try to overcome iron-addition problems encountered when running glasses manufactured using the graphite

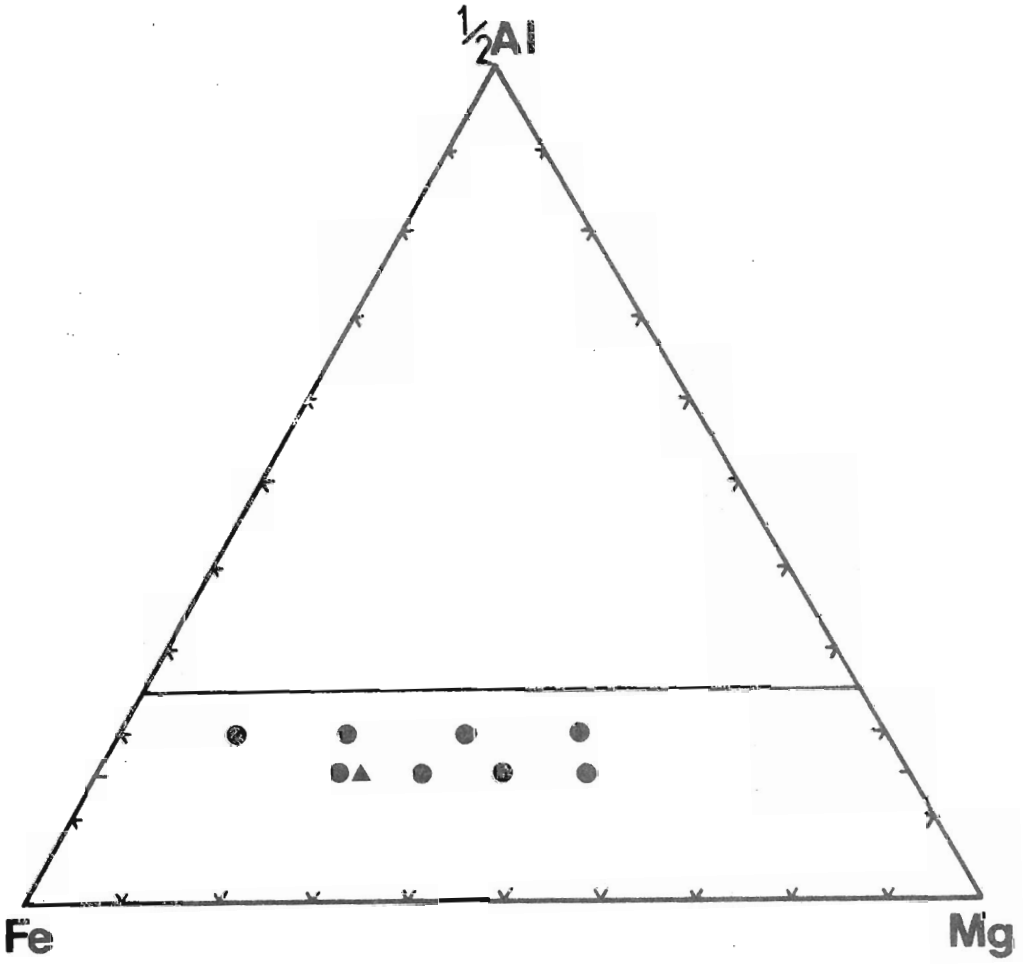

Fig. 2.1 $\frac{1}{2}$Al-Fe-Mg diagram showing compositions of starting mixes used in FMAS experiments. Filled circles - glass starting mixes (A15 and A20). Filled triangle - M33A15 mineral mix. All mixes lie between garnet composition (Fe-Mg tieline at A25) and orthopyroxene . Quartz present in excess.

Table 2.1 COMPOSITIONS OF GLASS STARTING MIXES USED IN FMAS EXPERIMENTAL PROGRAMME

	M15A20 1 atm.	M30A20 hi. P	M45A20 hi. P	M60A20 hi. P	M30A15 hi. P	M40A15 hi. P	M50A15 hi. P	M60A15 hi. P
SiO_2	55.00	54.18	53.33	53.95	54.87	55.02	55.85	56.72
Al_2O_3	12.38	12.89	13.70	14.45	10.79	10.49	10.73	10.99
FeO	29.71	25.74	22.05	16.98	27.21	24.87	21.44	17.57
MgO	2.94	6.29	10.31	14.09	7.11	10.49	12.01	14.76
X_{Mg}	15.10	30.32	45.45	59.66	31.80	40.20	50.10	60.15
$\frac{1}{2}Al/\frac{1}{2}Al+Fe+Mg$	19.90	19.67	19.27	19.48	16.00	14.95	15.00	15.02

capsule technique.

The second set of glasses were prepared using oxide reagents plus Fe metal, present in appropriate proportions such that the reaction

$$Fe + Fe_2O_3 = 3\ FeO$$

would proceed in the mixes during glass manufacture to produce the correct amount of FeO. Ground mechanical mixes of the reagents were sintered as before, and the sintered oxide + Fe metal pellets were then run in an atmospheric furnace at 1350°C, held in a Pt bucket with a continuous atmosphere of Argon to limit oxidation. Glasses produced by this technique were generally green, devoid of CO_2, and contained fine quench crystals of quartz. Analyses and the theoretical compositions of these glasses are presented in table 2.1.

Both methods of synthesis produced glasses close to the theoretical compositions required in the field garnet-orthopyroxene-quartz.

Glasses to be used in the experimental runs were seeded with finely ground mineral grains synthesised following methods outlined below. The following seed combinations were used:

(a) pyrope + ferrosilite

(b) almandine + enstatite

Combination (b) was most extensively used as these seeds reacted with the glass mixes much more completely. The seeds were added to the glasses to make up a total of 7 to 8 weight percent of the final seeded glass mix. The glass + seeds mixes were then re-ground to ensure homogeneous grainsize and distribution of seeds.

(a) Preparation of seeds.

Pyrope was synthesised from analytical grade MgO, Al_2O_3, and SiO_2

mechanically ground together, sintered at 900°C for 12 hours and then run in a piston cylinder appartus at 1100°C, 30 kilobar for two hours. Such syntheses were performed in large diameter (3mm) sealed platimum capsules. A small quantity of water was added to the mix to promote reaction. Clear, dodecahedral granular pyrope, apparently free of inclusions, was the product, as confirmed by XRD patterns and probe analyses.

Almandine was synthesised from Fe_2O_3-Al_2O_3-SiO_2 mechanical ground, sintered oxide mixes in a piston cylinder apparatus at 1050°C and 20 kbar for five hours. Syntheses were performed in large diameter (3mm) gold capsules, unsealed to allow reduction of Fe_2O_3. One synthesis run yielded homogeneous, dodecahedral brown-green almandine with few inclusions of spinel and unreacted quartz. Another synthesis run reacted only partially and yielded almandine, almandine with spinel inclusions, and some possible olivine. The almandine from the first synthesis was used in most of the experimental runs. EPM analyses of this almandine indicate its stoichiometry but also confirm the presence of some fine spinel inclusions.

Ferrosilite was synthesised from analytical grade Fe_2O_3-SiO_2 reagents ground under acetone, sintered at 900°C and 1 atm for 12 hours and loaded into $Ag_{50}Pd_{50}$ large diameter (3mm) capsules. These mixes were then run in a piston-cylinder apparatus at 1100°C, 25 kilobar for two hours to produce homogeneous green ferrosilite, confirmed by XRD patterns and EPM analyses.

Enstatite was synthesised by Mr. G.A. Jenner from analytical grade MgO and SiO_2. The mechanically ground, sintered mix was run in an atmospheric furnace at 1300°C, for 96 hours.

(2) Mineral Mixes

Initially, a set of mixes containing enstatite-ferrosilite-pyrope-almandine-quartz, ground together under acetone in an agate mortar to 2.5 μm grainsize, were prepared to provide "exsolution" type mixes i.e. aluminous orthopyroxene being formed at the expense of the aluminous phase garnet. The seeds were mixed together in such proportions to produce mixes with A/AFM ratios of .15, and X_{Mg}^{mix} = .40, .50 or .60. It was found in an early set of experiments (T412, see experimental section) that such a mineral mix was unsuitable for experimental determination of Al_2O_3 in orthopyroxene for the following reasons (see Appendix Two):

(a) the pyroxene grains were very strongly zoned, and small grainsizes prohibited interpretation of the zoning;

(b) abundant garnet nucleii prohibited grain growth, hence small grainsizes (5 μm) resulted;

(c) pyrope nucleii often failed to react strongly, thus the effective A/AFM ratios of the mixes were less than .15, inhibiting the growth of Al-orthopyroxene by migration of Al from garnet.

An alternative mineral mix of almandine + enstatite + quartz was prepared from seeds described above mechanically ground under acetone in an agate mortar. The minerals were combined in such proportions to produce a mix of A/AFM = .15 and X_{Mg}^{mix} = .33. This mineral mix was used exclusively in later experimental runs as an "exsolution" type mix. For lower temperature runs approximately 10 weight percent of an X_{Mg} = .30, A/AFM = .15 glass mix was added to the mineral mix to promote reaction and consumption of garnet seeds.

(3) Sintered Oxide Mixes (seeded)

Sintered oxide mixes were prepared using the initial steps of the procedures outlined for preparation of the glass mixes. Sintered oxide mixes were seeded with 7 to 8 weight percent almandine plus enstatite and re-ground to ensure homogeneity in composition and grain-size. A mix of this type was used in one experiment only, to compare reaction rates and achievement of equilibrium with seeded glass mixes.

2.4 EXPERIMENTAL TECHNIQUES

Experiments were carried out using ½ inch piston cylinder apparatus at the Geology Department, University of Tasmania. Experimental techniques are similar to those employed by Green and Ringwood (1967). Temperature was measured using a Pt/Pt 90 Rh10 thermocouple and recorded temperatures were controlled to within ±5°C of the set point. Owing to the long duration of the experiments (see below), the current required to maintain the temperature at the set point increased during the runs. The increase in required EMF and input current is ascribed to degradation of the graphite heater by water released from dehydrating talc in the initial stages of the runs. Thermocouple poisoning by Ag, Au or Fe was checked for by EPM qualitative analysis of thermocouple beads. In beads analysed, spectra show only Pt and Pd, with no Fe or Ag detected. The runs for which thermocouple beads were analysed were typical long duration runs with normal input current drift, and hence thermocouple poisoning is considered to be unimportant in the whole series of runs (Brey and Green, 1975). The set temperatures are thus regarded as the true initial and final temperatures despite the current drift.

All runs were of the "piston-in" type. For runs at pressures of greater than 10 kbar, the assembly was brought up to near the required pressure and temperature, and, when at the nominated temperature, the pressure was increased to the required value. Lower pressure runs were overpressed by 2 to 4 kilobars then bled off to just below the required pressure when the nominated temperature was reached. The pressure was then boosted to the required value. This latter procedure was employed to limit the possibility of thermocouple extrusion.

Nominal pressures are accurate to ±1 kbar (Green and Ringwood, 1967), although it is considered that the precision in pressure measurement for this series of experiments may be ± 5 kbar because of the piston-in techniques employed for all runs. Pressures were calculated from load pressures using a -10% friction correction.

All runs were undertaken in a "buffer assembly" consisting of an outer talc sleeve, a pyrex sleeve and an inner graphite heater sleeve. Boron Nitride inserts were fitted into the graphite sleeve and housed the sample capsule. Any gaps in BN sleeves or buckets were filled with BN powder.

All samples were run in sealed, large diameter (3mm, "buffer" size) noble metal outer capsules. Pt outer capsules were used for 1150°C and 1200°C runs, while $Ag_{75}Pd_{25}$ or $Ag_{50}Pd_{50}$ outer capsules were used for the lower temperature experiments. These outer capsules were all sealed under an Argon stream with a graphite arc welder.

The sample capsules (inner capsules) were specpure Fe or carbon rods, sealed with lids inside the noble metal outer capsules. Fe capsules were found to alloy with the noble metal containers along their boundary. In order to run different compositions (in terms of X_{Mg}^{mix}) or starting materials simultaneously, the Fe- or carbon capsules were prepared with up to four separate sample holes in each (Ellis, 1979). Approximately 3 to 6 mg of sample could be packed into each of these holes (1mm diameter).

Graphite multibore capsules were used only for some higher pressure experiments in FMAS, as at low pressures (<10 kb approx.) graphite is more reducing than metallic iron (Ellis, 1979) To promote reaction, small quantities of water were added to the lower temperature runs (see Run Details, Table 2.2).

Typical run durations were:

28 days at 800°C

20 days at 900°C

16 days at 975°C

8 days at 1050°C

and 4 days at 1150°C.

These run durations were apparently sufficient to enable a close approach to equilibrium in both glass starting mixes and mineral mixes at higher temperatures, while at 900°C and 800°C the almandine-enstatite-quartz mineral mixes generally showed very strong zoning.

2.5 EXPERIMENTAL RESULTS

(1) THE PROBLEM OF IRON ADDITION

In specpure Fe capsules a general problem encountered in the experimental results was the addition of Fe from the capsule into the sample. Most run products were granuloblastic fairly equigranular polygonal mosaics of garnet, orthopyroxene and quartz with additional polygonal Fe metal as a product in the mosaic. In runs where some melting occurred (see below), Fe metal areas and quartz become globular and the garnets and orthopyroxenes subhedral.

The Fe metal globules or grains were not produced by reduction of the charges. Area scans of run products show that silicate areas exclusive of metallic Fe grains are more Fe rich than the starting X_{Mg}^{mix}, indicating the addition of FeO. Visual evidence of Fe-metal migration into the capsule centre was accompanied by analytical evidence for extensive FeO addition. This Fe-migration and FeO addition was temperature- and mix-dependent. Addition was found to be more extensive and complete at higher temperatures in all mix types, with Fe-metal forming large globular areas (T450). At lower temperatures (900-800°C), Fe-addition was less extensive and some mixes indicated a zoning in the amount of addition, with core areas of sample bores closer to the original X_{Mg}^{mix} than areas near the rims of the sample chamber. This feature was particularly true of mineral mix samples (e.g. in T680) where FeO-addition at lower temperatures was confined to a narrow zone near the bore wall and Fe-blebs were only found near the walls. In other runs (T694, T478) mineral mixes and glass + seeds show a zonal arrangement of Fe-blebs in the sample chamber, with coarser Fe-blebs near the walls and a greater density of Fe-blebs near the walls also (plate 2.2).

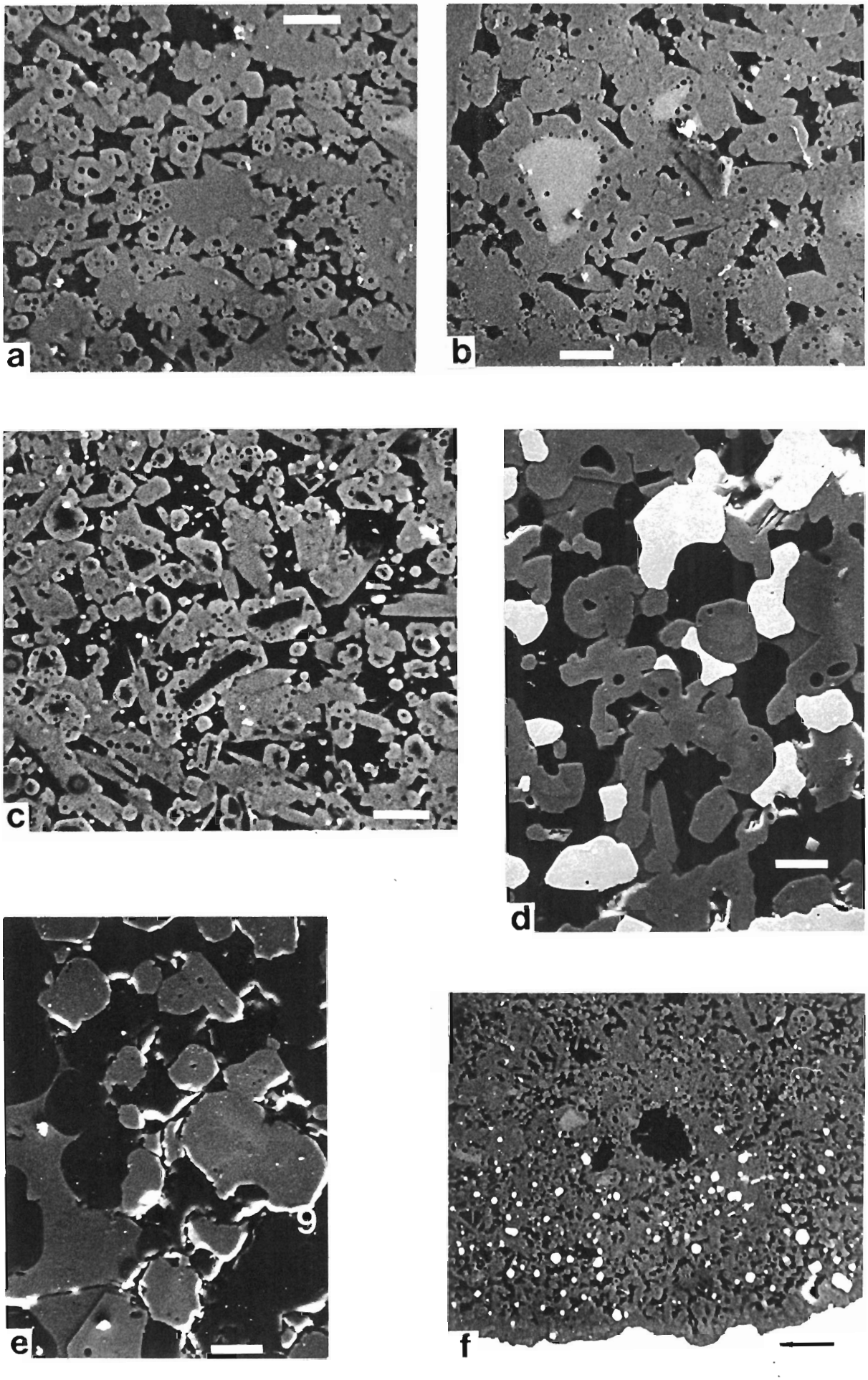

Plate 2.1

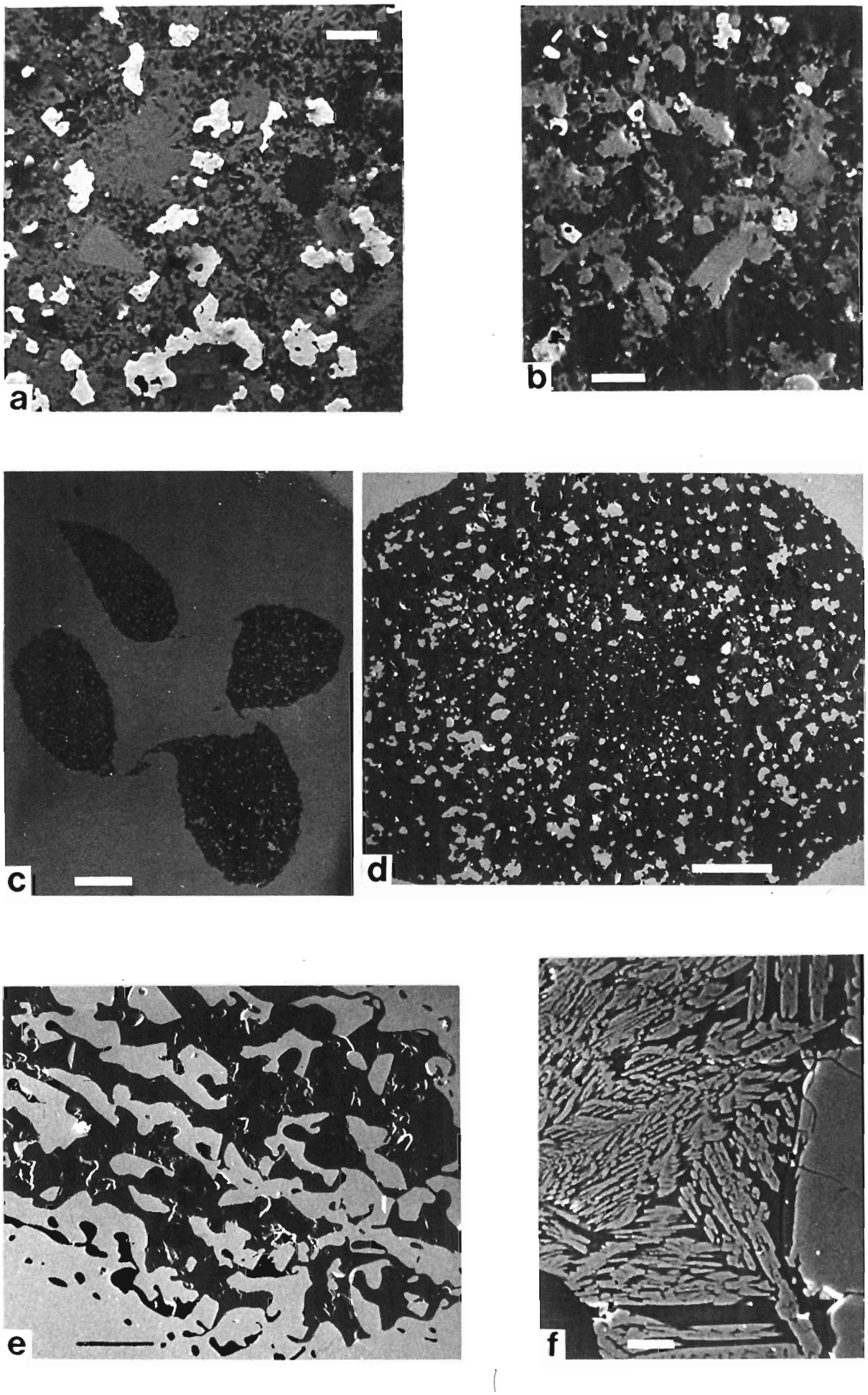

Plate 2.2

The Fe-addition was mix dependent, with glass mixes suffering more addition than mineral mixes or oxide mixes held under the same run conditions.

In one run (T720, 800°C, 7.5 kbar), Fe addition was so extensive that on the edges of the sample chamber all quartz in the mix was consumed and olivine formed along with Fe-rich garnet and orthopyroxene. This indicated the progressive consumption of quartz to form ferrosilite in orthpyroxene:

$$\underset{\text{added}}{2FeO} + \underset{\text{quartz}}{2SiO_2} = \underset{\text{in opx}}{Fe_2Si_2O_6}$$

followed by the consumption of orthopyroxene ($X_{Mg}^{opx} = .2$) to form olivine (Fo 10) when the SiO_2 was exhausted:

$$Fe_2Si_2O_6 + \underset{\text{added}}{2FeO} = 2Fe_2SiO_4$$

$$Mg_{.2}Fe_{.8}SiO_3 + FeO = (Mg_{.1}Fe_{.9})_2SiO_4 \quad \text{in T720.}$$

Initially, it was considered that the FeO may have been added as a result of Fe^{3+} being present in the synthetic glasses. However, the presence of Fe addition in the mineral mixes synthesised under conditions where no Fe^{3+} would exist in the almandine or ferrosilite contradicted this. Raman spectra of glasses showed no Fe^{3+} in them, but did indicate some $CO_3^{=}$ which could flux Fe metal into the mix and provide appropriate redox equilibria.

Initial devitrification of glass containing $(CO_3)^{=}$ can be assumed to release CO_2 which then reacts with Fe metal of the capsule

$$Fe\ (metal) + CO_2 = CO + Fe^{2+} + O^{2-}$$

then:

$$Fe^{2+} + O^{2-} = FeO,$$

and in the presence of quartz

$$FeO + SiO_2 = FeSiO_3 \text{ (in orthopyroxene)}$$

Thus, the extent of FeO addition into the phases is controlled by the CO_2 present, the diffusion of Fe^{2+} through the mix, and by the prevailing fO_2.

The presence of Fe-addition, particularly marked at high temperatures, has a significant effect on $K_{D_{Fe-Mg}}^{ga-opx}$, while apparently having little direct effect on X_{Al}^{opx} in these experiments. In runs where iron addition has only occurred on the margins of capsules, it is found that orthopyroxene preferentially becomes more Fe-rich than garnet. Garnets sometimes show zonation from almandine seed cores to more Mg-rich compositions, as is usual in these runs, and then a reverse zoning to slightly more almandine rich compositions in areas where marked FeO addition has occurred (e.g. T720, T764). However, orthopyroxene is strongly Fe-enriched while not displaying such zoning (Appendix Two). In higher temperature runs where Fe-addition occurs throughout a sample it is thus to be expected that orthopyroxenes will be enriched in Fe more than the garnets, resulting in erroneously low $K_{D_{Fe-Mg}}^{ga-opx}$. High pressure runs duplicated in graphite capsules (T454), K_D's derived from some mineral mix type samples, and later runs in the CFMAS system indicated that $K_{D_{Fe-Mg}}^{ga-opx}$ determined from experiments using glasses, where Fe-contamination is greatest, should be increased by 0.2. This is further discussed and evaluated in the analysis of K_D data (section 2.5).

(2) PRESENCE OF A MELT FRACTION

In high temperature runs at 1050°C and 1150 °C particularly, a

very minor aluminous Fe-rich melt fraction was detected interstitial to the other phases. In T544, at 1150°C and 7.5 kbar, appreciable melting occurred and resulted in the consumption of virtually all garnet and the formation of very coarse subhedral orthopyroxene with aluminous quench rims. In T535, at 1050°C and 5 kbar melting was accompanied by the consumption of garnet and the production of other phases (Spinel) as the bulk compositions of the mixes were outside the garnet-opx-quartz stability field for those conditions.

In T545 (1150°C, 12.5 kbar) melting and melt segregation occurred in at least one mix, producing a coarse granular to subhedral garnet-orthopyroxene area and a separate area of melt plus quench highly aluminous quench orthopyroxene (Plate 2.2). A similar effect occurred in a run prepared in a graphite multibore capsule, T749 (1050°C, 17.5 kbar), and particularly was prominent in a number of CMAS runs (see Chapter 4). In such runs, while pyroxenes adjacent to melt areas were probed, only coexisting garnet and orthopyroxenes well away from segregated melt areas were used in the reduction of experimental data.

Compositions of melts in FMAS runs are reported in Table 2.3. It is noteworthy that these melts are more Fe-rich than garnets also present in these runs, and range in Mg-number from .20 to .35. Previous workers (T.H. Green, 1977) have suggested that melts in a garnet-bearing pelitic system will be less magnesian than coexisting garnets at temperatures above 950°C. All melts formed in these FMAS model pelitic symple system mixes and in CFMAS mixes support this contention. Thus

$$K_{D_{Fe-Mg}}^{ga-liq} = \frac{(Fe/Mg)^{ga}}{(Fe/Mg)^{liq}}$$

is <1 for all runs in this series where melt was generated.

(3) RUN PRODUCTS - FMAS

Experiments generally yielded granuloblastic lobate to polygonal mosaics of garnet-orthopyroxene-quartz and Fe metal. In most runs original almandine garnet cores remained, rimmed by poikiloblastic zones of more magnesian garnet (plate 2.1). Garnets contained inclusions of quartz and sometimes orthopyroxene. Orthopyroxenes were usually polygonal to subhedral, free of quartz inclusions, but containing some garnet inclusions (plate 2.1). Quartz grains were usually lobate to ovoid. Grainsizes varied depending on the starting material, the presence of melt, and the temperature. Runs at 800°C produced grains up to 10 μm diameter. At higher temperatures grainsizes varied from 10 μm to 40 μm, with garnets up to 100 μm growing in runs where melt was present (e.g. T534). Garnets were generally coarser than coexisting orthopyroxenes, and of similar diameter to Fe-globules.

In mineral mix type experiments, almandine cores persisted and strongly zoned garnets resulted particularly at lower temperatures (900°C, 800°C). Orthopyroxenes were strongly zoned in some low temperature runs (T680, T501), from Mg-rich cores to Fe, Al richer rims. In the higher temperature runs (1050, 1150, 975°C) the orthopyroxenes were usually fairly homogeneous (Appendix Two), although sometimes zoned to Al-richer rims. Garnets in these runs usually consisted of relict Almandine cores (5 μm) surrounded by broad rims (5-15 μm) of Mg richer garnet.

In glass starting compositions, relatively homogeneous orthopyroxenes grew (Appendix Two). These show some variation in X_{Mg} but little scatter in Al_2O_3 contents. Garnets were often only weakly zoned when small (5-10 μm), but coarser garnets commonly contained small almandine rich cores surrounded by broad zones of Mg-richer

garnet (5-20μm). Within runs some variation in Xmg of garnet and orthopyroxene could be related to the positions of the particular grains in the sample, with lower X_{Mg}^{rim} garnets and pyroxene found near the capsule walls.

Some multibore experiments resulted in ovoid, sigmoidal or elongate capsule shapes (plate 2.2), and in two runs (T720, T709) the Fe-lids may have been separated from the bores. At high temperatures, deformation of the capsules was aided by the presence of some melt. In the runs T720 and T546 the individual sample bores are particularly deformed and some mixing of the samples may have been possible. These runs have very high amounts of Fe-addition into the silicate phases possibly promoted by H_2O-CO_2 fluxing of the samples enhanced by the deformation. Run T720 (900°C, 7.5 kb), where olivine has formed in two mixes, has been excluded from the data analysis of $K_{D_{Fe-Mg}}^{ga-opx}$. The olivine-bearing mixes have been excluded from the analysis related to X_{Al}^{opx}.

Other runs (T694, T720, T709), where garnets show reverse zoning from pyropic compositions near rims to more almandine-rich compositions closest to the rims, have also been excluded from the data set used to analyse Fe-Mg distribution.

Details of all runs in the FMAS system are presented in Table 2.2. Individual run products are depicted in partial ½Al-Fe-Mg diagrams presented in Appendix Two. Compositional data derived from the experiments and compiled in Table 2.2 have been extracted from the analytical data of Appendix Two based on criteria previously referred to. For glass type starting mixes, clusters of orthopyroxene analyses have been averaged to give $\bar{X}_{Al}^{opx}$, $\bar{X}_{Mg}^{opx}$ and σ values. In these mixes,

TABLE 2.2 FMAS EXPERIMENTAL RUN DETAILS.

P Equation	Run	P kbar	T °K	Capsule	Outer Capsule	Mix	X^{opx}_{Al}	X^{opx}_{Mg}	X^{ga}_{Mg}	Melt	Time (Hours)	Texture Comments	Other General Comments	K_D
23.0	T821	30	1473	C	Pt	mineral mix	.080 (.003)	.593 (.004)	.459 (.011)		53.5	Opz and ga coarse, some Ca present. Very coarse & segregated ga coarse, zoned. polygonal to subhedral. Opx zoned fine grained granular	Cupsate, signoidal deformed bores. Fe added across to MAS mix, not closed. Melt segregation and quench textures. Ca added across to non-Ca mixes. Only minor zoning.	1.72
25.6						glass mix	.070 (.003)	.601 (.004)	.480	present				1.63
30.1						MAS mix	.080 (.003)	.913 (.005)	.857					1.60
21.0	T820	25	1473	C	Pt	M45 A20 glass	.100 (.003)	.589 (.003)	.470		54.3	Polygonal granuloblastic, with area of melt + quench fine granular pyrope and interstitial opx	Elongate bores, melt segregation in M45 mix. Fe added across to MAS mix. Only minor zoning.	1.61
23.8						MAS oxides	.132 (.005)	.955 (.006)	.950					1.01
18.5	T454	20	1423	C	Pt	M30 A15 glass	.095 (.004)	.523 (.007)	.390		125.5	Very coarse garnets and opx, interstitial quartz	Slightly elongate bores. Fe-loss to graphite apparent. Good clustering of analyses.	1.72
20.3						M50 A15 glass	.109 (.010)	.703 (.006)	.585					1.68
19.6						M60 A15 glass	.120 (.006)	.727 (.006)	.626			Polygonal granuloblastic.		1.59
16.1	T478	17.5	1423	Fe	Pt	Seeded oxide	.108	.466	.378		96	Fine granular. Opx near run walls lower X_{Mg}	Fe blebs more abundant on rim of run, and coarser in size. Zonal arrangement. Abundant Fe blebs (fine). Zoning pronounced in oxide mix. Common Fe lobate blebs, possibly more Fe blebs in centres of runs than on rims where coarser opz occurs. Good clustering analyses.	1.44*
16.5							.080	.324	.220					1.70
15.8						M40 A15 glass	.103 (.009)	.420 (.006)	.341			Poikiloblastic ga and polygonal hyp. Coarse		1.40*
13.9	T461	15	1423	Fe	Pt	M30 A15 glass	.113 (.013)	.362 (.004)	.284		96.5	Polygonal granuloblastic ga-opx-qz, coarse		1.43*
14.8						M40 A15 glass	.117 (.011)	.433 (.006)	.350			"		1.42*
14.8						M50 A15 glass	.141 (.007)	.533 (.007)	.468			"		1.30*
13.7	T545	12.5	1423	Fe	Pt	M30 A15 glass	.124 (.008)	.400 (.008)	.305	present	95.5	Coarse polygonal; separation to ga rich and poor parts.	Elongate bores, Fe blebs and areas blanket across bores as elongate lobate forms (Bores become xenomorphic). Melt present and some segregation occurs X_{Al} scatter in M30 mix opx.	1.52*
						M45 glass	.153 (.006)	.504 (.007)	-	present		Opx only, polygonal and v. coarse.		
						M60 glass	.178 (.004)	.569 (.006)	-	present		Opx, plus aluminous melt phase		
	T450	10	1423	Fe	Pt	M30 glass	.198 (.016)	.400 (.004)	-	present	97	Coarse subhedral opx, ovoid qz and Fe. Some melt.	Coarse Fe globules throughout the mixes, very coarse (>300μm) grainsize. Bores not deformed.	
						M40 glass	.203 (.017)	.463 (.006)	-			Subhedral opx, ovoid qz, Fe, melt.		
						M50 glass	.200 (.020)	.546 (.010)	-			Opx and melt, qz.		
	T534	7.5	1423	Fe	Ag/Pd $Ag_{50}Pd_{50}$	glass mixes					18 outer capsule melted	Very coarse (100μm) erhedral opx and interstitial Al rich melt.	Very coarse and irregular Fe blebs. Undeformed bores Grainsizes up to 200 μm.	

NUMBERS IN PARENTHESES - STANDARD DEVIATIONS FROM THE LISTED VALUES.

* K_D VALUES WHICH HAVE BEEN ADJUSTED UPWARDS BY .2 IN THE ANALYSIS OF THE DATA.

	T544	7.5	1423	Fe	Pt	glass mixes	-	-	-	present	96	Resultant very homogeneous melt phases. Garnet totally consumed.	Bores lobate or cuspate with vast Fe metal invasion as blebs and areas up to 300μm.	
	T469	5	1423	Fe	Pt	M30 glass				present	96	Very coarse grainsizes, no go. Opx very coarse subhedral grains with wide variations in X_{Al}	Massive Fe metal invasion, blebs and areas of Fe still attached to capsule walls. Bores elongate and deformed	
						M40 glass				present				
						M50 glass				present				
16.0 - 17.6	T439	20	1323	Fe	Au	M40 glass	.067 (.004)	.418 (.005)	.285		288	Grainsize >10μm, granuloblastic.	Fe blebs more common near capsule walls. Outer capsule deformed and one mix (M60) is adjacent to Au outer capsule. No Fe blebs occur when near Au. Bores only slightly elongate.	1.802
						M50 glass	.070 (.005)	.514 (.007)	.384			Coarse granuloblastic homogeneous.		1.69 *
18.3						M60 glass	.076 (.009)	.590 (.010)	.474			Coarse granuloblastic homogeneous		1.60 *
16.6	T749	17.5	1323	C	$Ag_{75}Pd_{25}$	M45 A20	.092 (.002)	.610 (.003)	.460 (.005)		188	Coarse grains, to 20μm	Slightly deformed bore, good clustering of analyses.	1.84
16.6						M60 A20	.109 (.004)	.708 (.003)	.577 (.008)	present		Coarse ga+opx+qz and interstitial melt (20-40μm).	Abundant melting, melt segregation. Elongate deformed bore.	1.77
16.1	T754	17.5	1323	C	$Ag_{75}Pd_{25}$	M33 min mix	.077 (.004)	.490 (.002)	.348 (.006)		236	Fine excellent granuloblastic homogeneous. Zoned Ga.	Coarse grainsize;cracks in graphite between bores.	1.80
15.9	T493	15	1323	Fe	Pt	M30 A15	.060 (.020)	.357 (.007)	.270		216	Poikiloblastic ga and granular opx. Zoned ga.	Bores undeformed. Fe coarse blebs throughout each bore (10μm sizes or greater) concentrated more near run rims. Opx zoned in X_{Mg} in the M60 and M30 bores? Fe blebs occur around margins of each bore only, and none in centres. X_{Mg} zoning strong in garnets X_{Al} zoning v.strong in opx, Al_2O_3 increasing to rims.	1.50 *
15.9						M40 A15	.070 (.018)	.434 (.012)	.338			Poikilo ga, granuloblastic coarse texture.		1.50 *
14.8						M60 A15	.095 (.011)	.535 (.008)	.464			Coarse granuloblastic, poikilo ga.Zoned ga.		1.33 *
12.7	T412	12	1323	Fe	Au	M40 multi min mix	.110	.496	.350		216	Fine grained, many seeds survive, pyrope and alm seeds common, Zoning Strong. In equigranular but polygonal.		1.83
12.9						M50 multi min mix	.130	.590	.420					1.99
13.5						M60 multi min mix	.140	.670	.540					1.73
10.1	T696	10	1323	Fe	Ag Pd 50 50	M30 glass	.092 (.009)	.274 (.002)	.210	interstitial	260	Poikoloblastic polygonal ga, ovoid quartz	Very coarse Fe blebs 10μm to 50μm, irregular shapes, Deformed outer capsule.	1.42 *
10.3						M40 glass	.126 (.007)	.418 (.006)	.330	interstitial		Minor poikilo. ga; polygonal opx and ovoid quartz		1.45 *
9.6	T415	10	1323	Fe	Au	M50 glass (Alm+Alen)	.174 (.025)	.518 (.007)	.409		216	pologonal granuloblastic, coarse. Opx zoned X_{Al} polygonal granuloblastic, coarse, homogeneous	Fe blebs throughout each bore,some have more Fe near walls, and zoning to coarser blebs near walls. Ga shows X_{Mg} zoning.	1.55 *
9.4						M50 glass (Alm+en)	.180 (.026)	.515 (.014)	.407					
9.2	T415	10	1323	Fe	Au	M50 glass (Py+Fs)	.182 (.022)	.506 (.012)	.364		216	Coarse polygonal granuloblastic. Py relict.	Strong zoning in X_{Al} in opx for each run type.	1.79
10.0	T387	10	1323	Fe	Au	M50 multi-mineral mix	.180	.565	.430		239	Very fine grainsizes in all bores.Relict seed cores common (ga).Fine granuloblastic textures but inhomogeneous grainsizes.	Very strong zoning in Py and Alm cores to rims.	1.72
10.5						M60 multi-mineral mix	.200	.660	.560				Strong zoning in Al_2O_3 in opx, increasing to rims. Qz inclusions common in opx. Little Fe addition. Inhomogeneous runs.	1.53
9.1						M40 multi-mineral mix	.160	.490	.310					2.14
6.8	T527	7.5	1323	Fe	$Ag_{50}Pd_{50}$	M30 A20	.177 (.013)	.306 (.010)	.243		152	Good grainsizes >10μm, granuloblastic; X_{Mg} & X_{Al} zoning in opxs for M30 and M45 mixes.	Fe blebs common throughout bores, concentrated in central areas and out to just inside walls where coarser opx occurs. Qz inclusions in garnet.	1.37 *
7.5						M45 A20 glass	.209 (.012)	.415 (.017)	.345					1.35 *
						M60 A20	.251 (.018)	.311 (.016)	-			Fine granuloblastic opx, interstitial melt, no ga.		

P Equation	Run	P kbar	T °K	Capsule	Outer Capsule	Mix	X^{opx}_{Al}	X^{opx}_{Mg}	X^{ga}_{Mg}	Melt	Time (Hours)	Texture Comments	Other General Comments	K_D
	T535	5	1323	Fe	$Ag_{50}Pd_{50}$	M60 glass	.247 (.008)	.543 (.012)	-	present	189	Coarse euhedral opx occurs in melt; ovoid qz blebs. Some metastable aluminous phases.	Fe blebs very common, especially near centres of bores. Wall areas free of Fe blebs, opx common here.	
						M45 glass	.244 (.008)	.464 (.007)	-	present				
						M30 glass	.237 (.010)	.326 (.005)	-	present				
	T443	5	1323	Fe	Pt	M30 glass	.224 (.017)	.363 (.012)	-	present	298.7	ga being resorbed, coarse opx formed and aluminous melt (?).	Fe blebs homgeneously throughout bores, coarse grainsize (> 10µm). Aluminous opx in each bore has strong scatter in X_{Mg}.	
						M40 glass	.183 (.020)	.418 (.008)	-	present				
						M50 glass	.230 (.015)	.475 (.012)	-	present				
13.8	T760	15.0	1248	C	$Ag_{75}Pd_{25}$	M33 min. mix	.080 (.011)	.551 (.005)	.370 (.008)		385	ga strongly zoned, medium granuloblastic	Bore slightly elongate	2.00
14.1						M45 A20 glass	.081 (.003)	.574 (.004)	.413 (.004)			Strongly poikiloblastic ga Coarse granuloblastic	Bore deformed, elongate to sigmoidal.	1.78
13.0	T703	12.5	1248	Fe	$Ag_{50}Pd_{50}$	M33 A15 min.mix	.064 (.012)	.411 .421	.294 .312		359	Poik.ga, good grainsize. Relict alm cores common.	More hypersthene on run margin, ga+qz in centre, Strong X_{Mg} zoning in both mixes. More Fe blebs rimwards.	1.67 *
13.6														1.60 *
13.4						M40 glass	.063	.420	.310			Poikiloblastic subhedral ga		1.61 *
12.8							.070	.440	.318			Prismatic-granular hyp.		1.68 *
8.8	T694	10	1248	Fe	$Ag_{50}Pd_{50}$	M30 A20	.082 (.007)	.312 (.003)	.210 .200		387	Poik. ga, coarse; opx mostly on run margin.	Zoned and reverse zoned ga, late Fe addition. Run was off for 16 hours after the first day.	1.70 1.81
8.8						M40 A20	.104 (.005)	.410 (.008)	.295			Granuloblastic good mosaic		1.65 *
8.7						M60 A20	.128 (.010)	.490 (.008)	.370			Granuloblastic coarse, also interstitial garnets. Opx dominates near run margin.	Reverse zoning in garnets common, adjusting to Fe addition. Fe blebs coarse and common, homogeneous through bores.	1.64 *
7.4	T709	7.5	1248	Fe	$Ag_{50}Pd_{50}$	M15 A20 glass	.071 (.005)	.192 (.007)	.130		380	Moderate grainsize granuloblastic.	Fe addition into phases and as numerous blebs in all mixes. Lid of capsule pinched upwards. Massive Fe addition resulting in 75µm blebs. Min.Mix has less Fe metal in centre of bore.	1.59 *
7.6						M30 A20 glass	.082 (.008)	.253 (.008)	.193			Moderate grainsize granuloblastic		1.42 *
7.1						M33 min. mix	.091 (.004)	.267 (.004)	.200			In centre coarse poik.ga and finer opx, good X_{Mg} clustering.		1.46 *
7.7						M45 A20 glass	.100 (.011)	.336 (.009)	.258			Variable, granuloblastic but strong zoning.	Reverse zoning in garnets, X_{Mg} zoning in opx strong too (M45)	1.45 *
5.3	T546	5	1248	Fe	$Ag_{50}Pd_{50}$	M33 min. mix	.141 .148	.315 .336	.225 .230		480	Small grainsize, qz inclusions in ga. X^{opx}_{Mg} zoning.	Good reversal in X_{Al}. Capsule deformed, some bores sigmoidal (M30) or elongate (M60), may be some mixing at edges of close bores. Fe blebs (10-30µm) spread throughout.	1.58
5.4														1.70
5.2						M30 A20 glass	.154 (.008)	.333 (.008)	.230			Scatter in X_{Mg} and X_{Al}, granuloblastic.		1.67
5.3						M45 A20 glass	.190 (.011)	.396 (.013)	.264			Medium grained granuloblastic.		1.80
						M60 A20 glass	.205 (.011)	.452 (.011)	-			Coarse prismatic to granular opx. No garnet.	Scatter in opx X_{Al} and X_{Mg} due to non-formation of ga (M60)	

P Equation	Run	P kbar	T °K	Capsule	Outer Capsule	Mix	X^{opx}_{Al}	X^{opx}_{Mg}	X^{ga}_{Mg}	Melt	Time (Hours)	Texture Comments	Other General Comments	K_D
9.7	T501	10	1173	Fe	Au	M30 A15 glass	.065 (.011)	.415 (.004)	.250		510	Granuloblastic, fine, zoned opx+ga in X_{Mg}	Fe Addition from walls only on edges of bores, zonal Fe bleb pattern outwards. 2 bores deformed. Marked scatter in X_{Al} and X^{opx}_{Mg}	2.12
9.8						M40 A15 glass	.079 (.007)	.499 (.012)	.332			Granuloblastic, fine zoned opx in X_{Mg}.		2.00
10.1						M60 A15 glass	.103 (.008)	.633 (.012)	.455			Granuloblastic, fine and ga not common.		2.07
6.2	T720	7.5	1173	Fe	$Ag_{50}Pd_{50}$	M33 min. mix	.056 (.007)	.200 (.010)	.100 .140	.112 = olivine X_{Mg}	479	Qz abundant in centre of bore with prismatic opx, poikilo. ga. More Fe rich opx, ga & olivine on walls.	Strongly deformed capsule, with mix in zone between outer and Fe capsule, sigmoidal bores. Abundant Fe addition as blebs and into phases. Lid lifted off inner capsule, allowing H_2O, CO_2 access and exchange. Run off after 2 days, then recommended. This possibly stabilised Mg richer garnet which zoned back to more Fe-rich as more Fe addition occurred. Hence normal and reverse zoning (Alm→Pyropic →more Fe rich) in ga in M30, M33 min.mix, and M45 mix. These are unreliable for K_D.	2.25 1.81
6.8						M30 A20 glass	.055 (.006)	.217 (.008)	.125 .143			Granuloblastic, poikilo.ga and polygonal opx. Higher X_{Mg}, ga qz in centre. Coarser and low X_{Mg} rim.		1.93 1.66
7.3						M45 A20 glass	.064 (.007)	.296 (.009)	.170 .183			In centre, equant opx, qz Fe blebs and poikilo ga Rim region little or no qz, granuloblastic ga + opx		2.05 1.88
6.7						M60 A20 glass	.080 (.007)	.352 (.004)	.202	.233 = olivine X_{Mg}		ga coarse, common on bore margin. Olivine produced on run margin with opx+ga+Fe, qz consumed. Opx zoned hi Al to low Al.		2.14
6.6	T857	7.5	1173	C	Pt	M50 A15 py+fs seeds	.139 (.004)	.548 (.006)	.368		465	Elongate subhedral opx 10-20μm; polygonal ga	Excellent zoning in ga on earlier seeds. Fine ga rim coarse opx and show less zoning. Zoning Fe rich ga to Mg richer ga well developed towards rims of grains.	1.98
6.6						M33 mineral mix	.142 (.008)	.573 (.007)	.387			10-15μm anhedral opx + ga; qz abundant.		2.13
5.7	T532	5	1173	Fe	$Ag_{50}Pd_{50}$	M30 A20 glass	.095 (.016)	.367 (.013)	.263		422	Fine granuloblastic ga+opx +qz. Scatter in opx.	Fe globules mainly in rims of bores, X^{opx}_{Mg} in these areas is less than in core of bores. Zoning in bulk compositions from cores to rims of bores.	1.62
5.7						M45 A20 glass	.122 (.012)	.455 (.007)	.315			Fine granuloblastic ga+opx+ qz. Zoning in ga.		1.81
						M60 A20 glass	.120 (.014)	.496 (.008)	-			Granuloblastic to prismatic opx, no ga but some Sp type phase.		
	T807	10	1073	Fe	$Ag_{75}Pd_{25}$	M33 A15 min.mix	.045	.680	-		745	Relict ga cores, unreacted areas and some fine new opx.	Poor reaction and strong zoning in min.mix, glass (1atm type) showed melting. Hardly any Fe addition, bulk mixes constant, glasses unreactive(!) (1 atm furnace glasses). Failed.	
						M50 A20 glass	-	-	-			Some recryst ga and hi Al inclusions		
						M50 A20 glass	-	-	-	present		Relict resorbed, Almandine in melt.		
2.4	T680	5	1073	Fe	$Ag_{75}Pd_{25}$	M33 min mix	.108 (.008)	.451 (.005)	.254		673	Inhomogeneous grainsizes, common relict ga+opx cores. X_{Al} increases in opx rim wards. Strong X_{Mg} zoning.	Few Fe blebs, mix strongly zoned opx and ga; some Fe blebs near walls.	2.40
2.5						$M_{45}A_{20}$ glass	.101 (.009)	.431 (.009)	.250			homogeneous fine granular ga poikilo.	Reverse min mix as had Fe addition homogeneously.	2.27
2.5						$M_{15}A_{20}$ glass	.059 (.013)	.259 (.005)	.145			coarser ga than opx, coarser opx near rim walls.	Fe blebs very common, good clustering ga, some X_{Mg} spread for opx.	2.15
1.8						$M_{30}A_{20}$ glass	.094 (.009)	.374 (.007)	.210			very fine grained 5μm poikilo ga, some relict Almandine cores. Opx fine.	Fe blebs mostly on margin of rim X_{Al} in opx zoned to lower at rims, minima taken.	2.25

clusters of analyses usually occur with some additional higher $\bar{X}_{Al}^{opx}$ analyses often falling on mixing lines towards garnet. Maximum X_{Mg}^{ga} garnets have been selected where almandine was the original seed type. Where orthopyroxenes have been found to be zoned to lower Al_2O_3 rims, these low X_{Al}^{opx} analyses have been used as the equilibrium values.

In mineral-mix starting mixes, the high X_{Al}^{opx} orthopyroxene analyses or clusters have been selected as equilibrium products. Where mineral-mix and glass type mixes have been run under the same P-T conditions, these high X_{Al}^{opx} analyses overlap with the lower X_{Al}^{opx} orthopyroxenes in the glass mixes (e.g. T821, T753, T760, T703, T709, T746, T720, T680). At lower temperatures (800-900°C) strong zoning in the orthopyroxenes formed in mineral-mix type starting materials (see T680), renders the interpretation of equilibrium X_{Mg}^{opx} and X_{Al}^{opx} difficult without the presence of the alternative glass starting mixes.

Py-Fe-Alm-En multi-mineral mixes (T412 - 12.5 kb 1050°C, T387 - 10 kb, 1050°C) yielded very strongly zoned garnets and orthopyroxenes strongly zoned in X_{Al}^{opx} (Figure , Appendix Two). Equilibrium Al_2O_3 contents in orthopyroxene in these runs are virtually impossible to isolate, although the higher X_{Al}^{opx} analysis overlap with analyses of orthopyroxenes grown from glass starting materials and thus these have been reported in Table 2.2. These mixes have not suffered Fe-addition, and garnet rim compositions both on pyrope and almandine seeds approach values consistent with X_{Mg}^{opx} and X_{Mg}^{bulk}. Thus K_D values from these runs would appear to be reliable and reversed values.

(4) ALUMINA SOLUBILITY IN ORTHOPYROXENE IN FMAS

Alumina contents of orthopyroxenes in equilibrium with garnet at variable X_{Mg}^{opx} are presented in figures 2.2, 2.3 and 2.4. X_{Al}^{opx} is

Table 2.3 COMPOSITIONS OF MELTS GENERATED IN FMAS EXPERIMENTS.

	T443 (1050°C, 5 kb)		T450 (1150°C, 10 kb)			T469 (1150°C, 5 kb)			T545 (1150°C, 12.5 kb)
SiO_2	47.70	48.77	46.01	45.03	47.34	50.25	49.93	49.86	45.37
Al_2O_3	16.59	15.23	18.90	14.68	17.97	17.33	16.57	16.16	20.71
FeO	28.73	29.63	31.85	35.40	31.87	26.32	24.98	27.12	29.77
MgO	4.64	3.03	1.86	4.24	1.29	5.47	8.51	6.86	3.23
TOTAL	90.29	89.92	90.58	94.80	88.70	95.67	93.46	93.56	89.86
X_{mg}	22.36	15.42	9.51	17.6	6.74	27.05	37.76	31.10	16.22

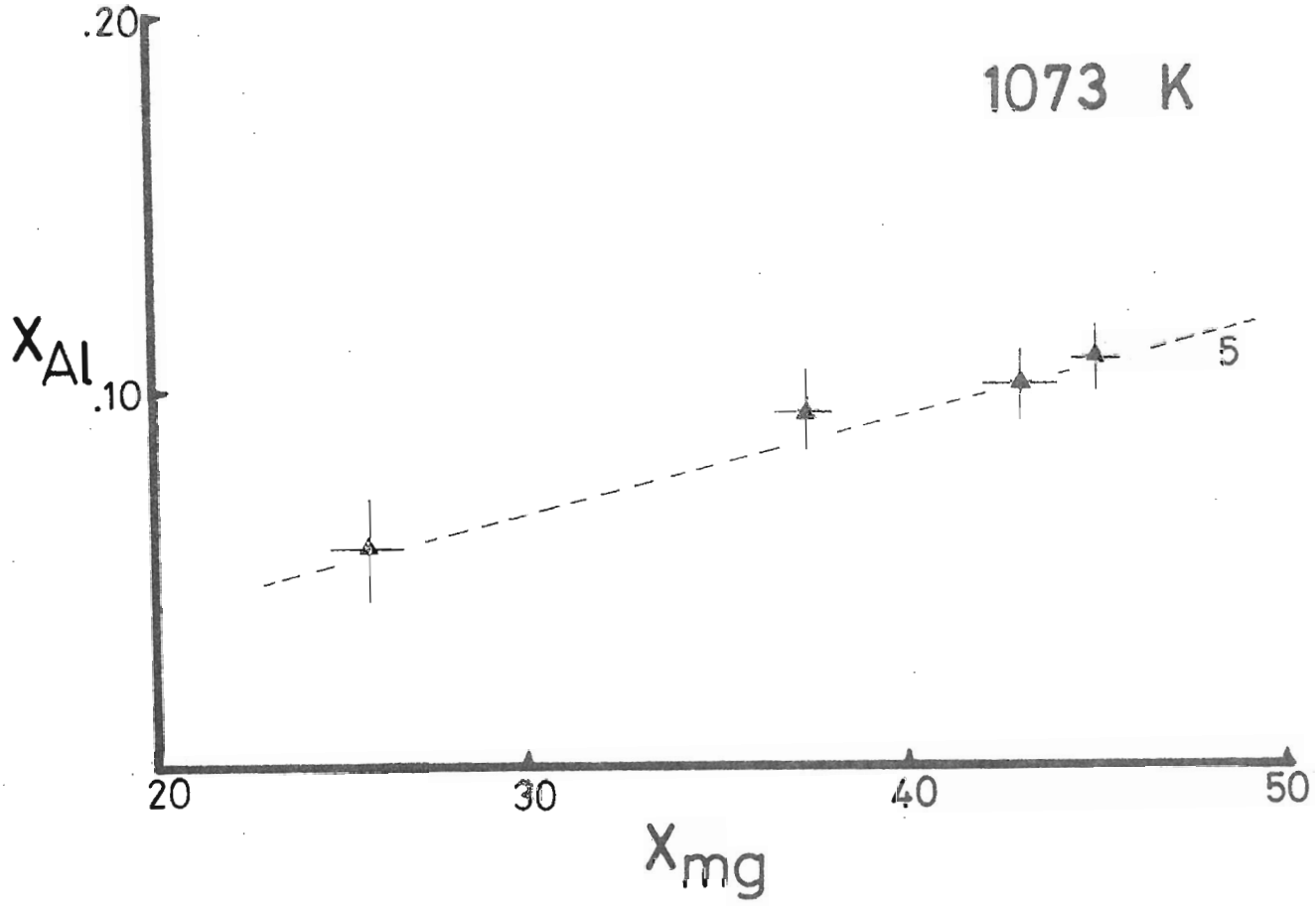

Fig. 2.2 Alumina contents of experimental orthopyroxenes in equilibrium with garnet at variable X_{Mg}^{opx} and at 1073 K (800 °C) and 5 kbar.

X_{Al} : (Al/2) for orthopyroxene

X_{Mg} : (Mg/Mg Fe)*100 for orthopyroxene

Error bars represent one standard deviation.

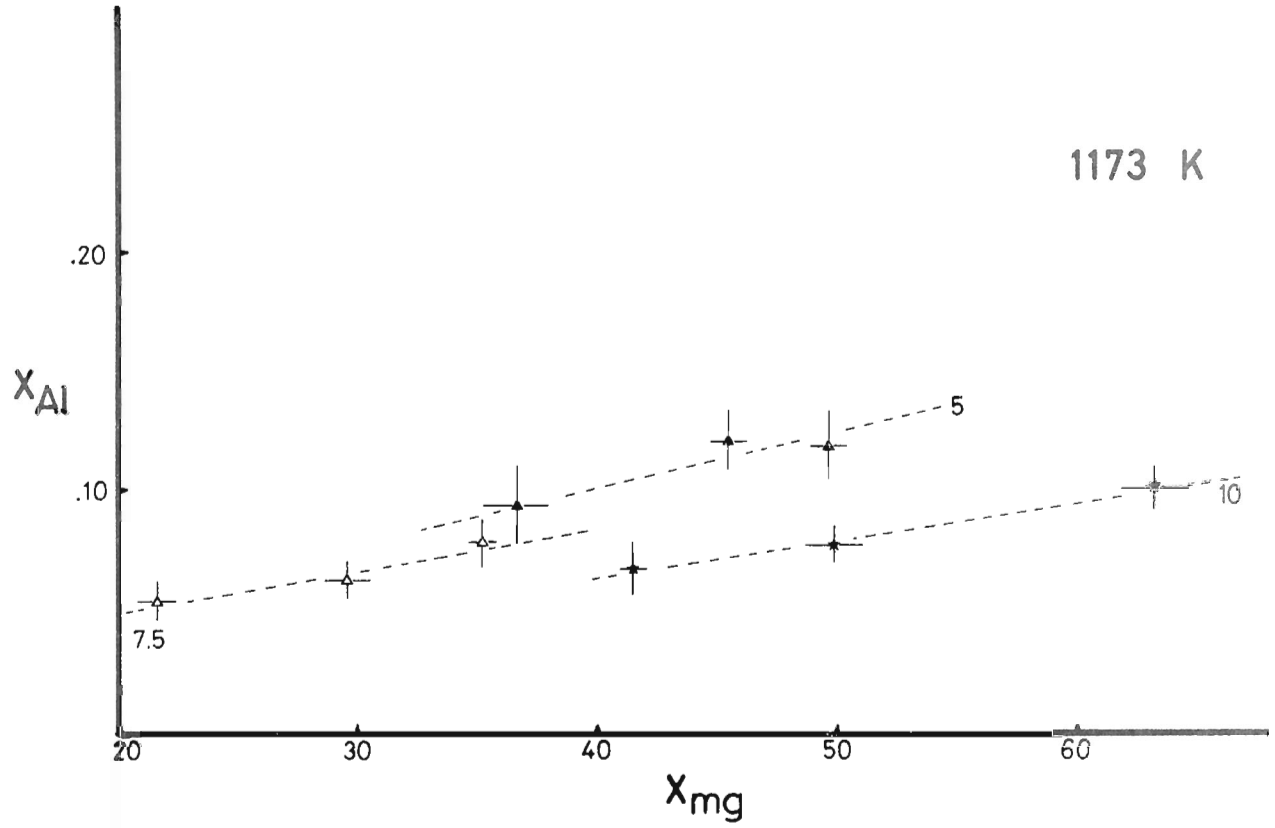

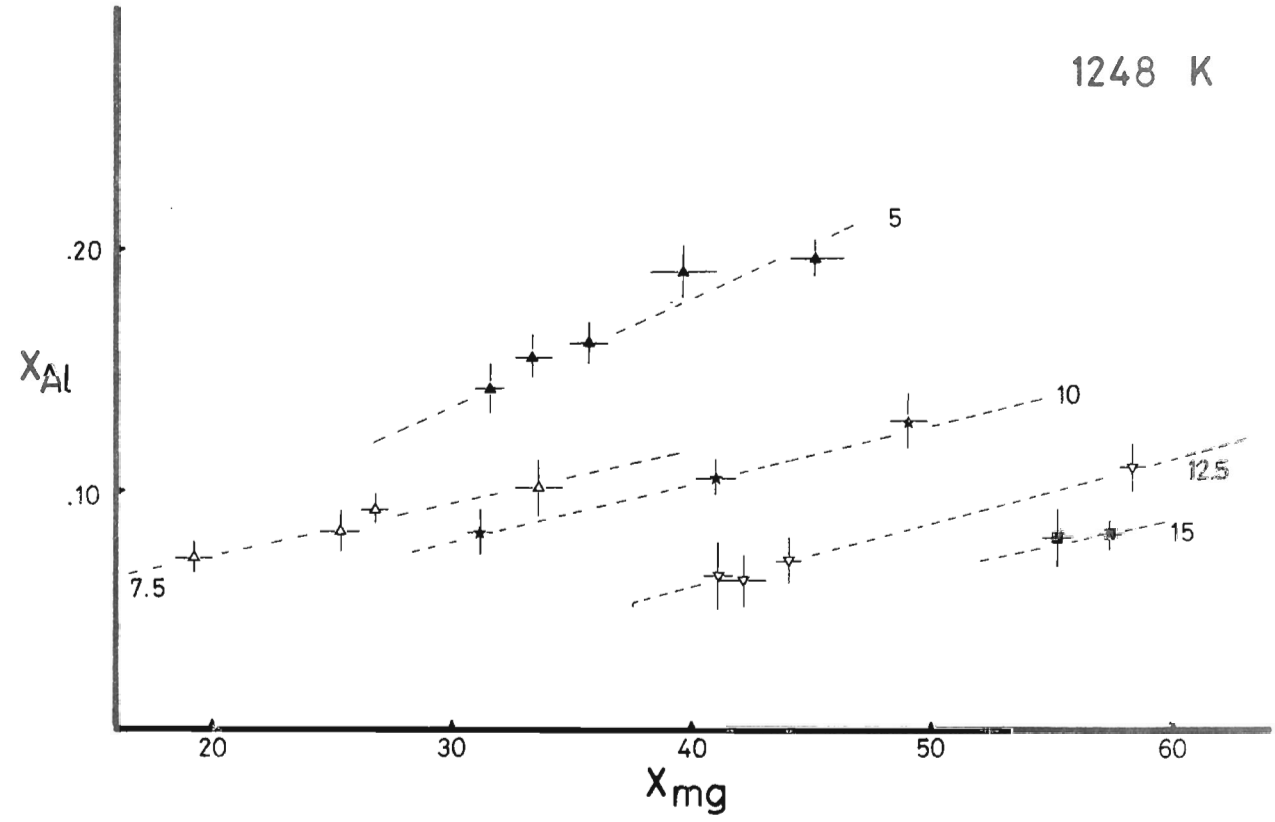

FIG. 2.3 X_{Al} (opx) variation with X_{Mg} (opx) at 1173°K (900°C) and 1248°K (975°C). Dashed lines join isobaric data, pressures as indicated.

$X_{Al} = Al/2$ (opx)

$X_{Mg} = (Mg/Mg+Fe) \times 100$ (opx)

error bars = 1 standard deviation (1 σ)

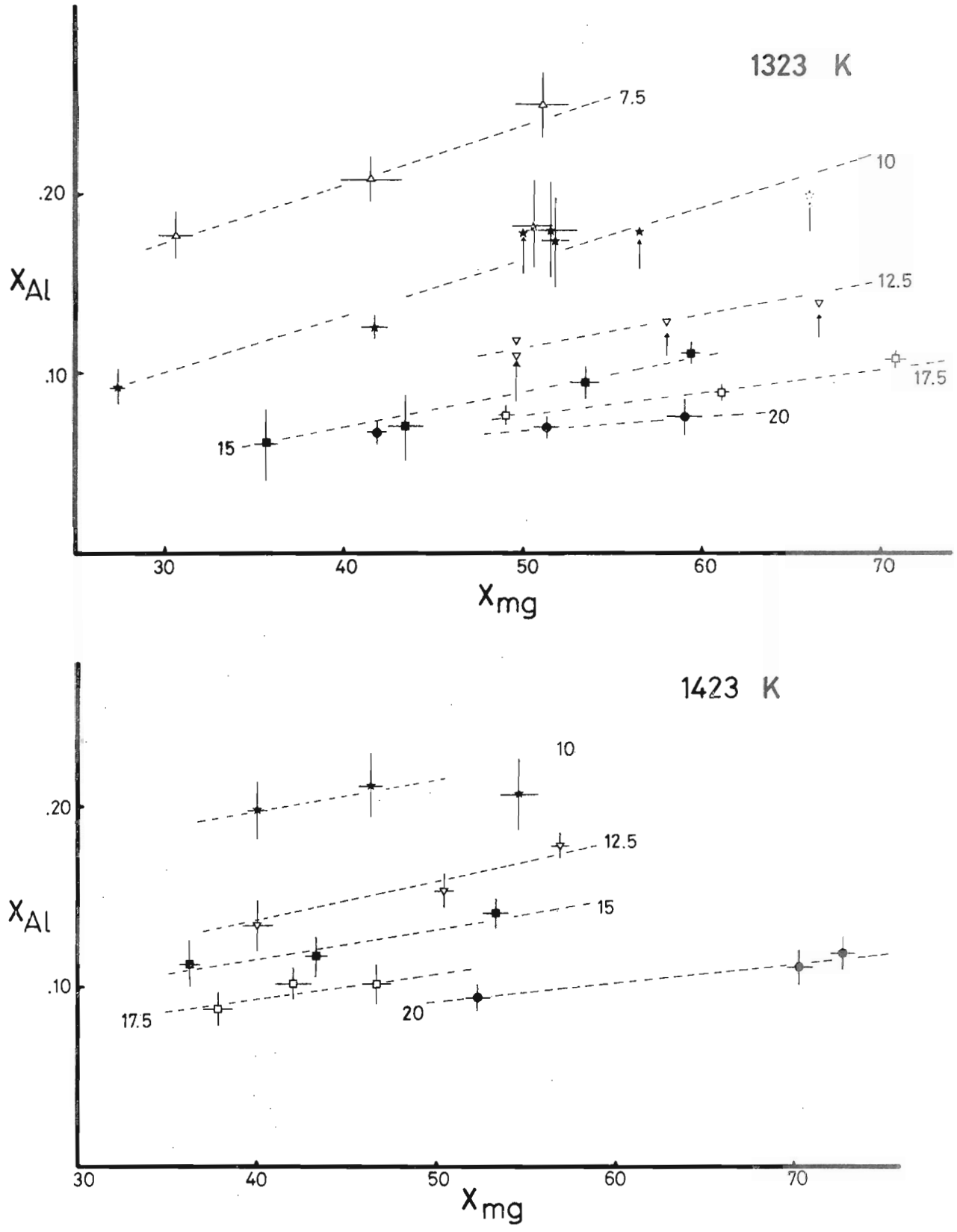

FIG. 2.4 X_{Al} (opx) variation with X_{Mg} (opx) at 1323°K (1050°C) and 1423°K (1150°C). Dashed lines connect isobaric data. arrows = direction of approach to equilibrium for mineral mix starting materials.
error bars = 1 σ

defined as Al/2, and the values depicted are average values derived from the analytical data as described above, with error bars corresponding to 1σ in X_{Mg} and X_{Al}.

In agreement with previous work in MAS, CMAS and FMAS, alumina contents of orthopyroxene *increase* with increasing temperature at constant P and X_{Mg}^{opx}. Alumina contents *decrease* with increasing P at constant T and X_{Mg}^{opx}.

It can readily be seen that, at any particular P and T, X_{Al}^{opx} varies with X_{Mg}^{opx}, with more Fe-rich pyroxenes containing less alumina (when in equilibrium with garnet). At any one temperature, $\frac{\partial X_{Al}^{opx}}{\partial X_{Mg}^{opx}}$, the slopes of the curves in the figures 2.1-2.3, usually increases with decreasing P. This effect can be alternately viewed as an increase in this slope with increasing overall X_{Al}^{opx}. By comparison of the different isothermal data sets, it is also apparent that the slopes vary with increasing T.

Adopting the thermodynamic approach developed in section 2.2, equation (22) has been applied to the experimental data to extract the parameters $\Delta H_{1,T}^{o}$, ΔS_{T}^{o}, and W_{FeAl}^{opx}. Multiple linear regression and stepwise regression techniques have been used to fit the experimental data to equation (5)(Table 2.4). Data sets at constant temperature have been normalised to 1 bar using the partial molar volume change of the reaction (1), and linear regressions performed to derive $(W_{FeAl}^{opx})_T$ and $\Delta H_{1,T}$, where $-\Delta G_{1,T}^{o}$ is $-(RT \ln\{(1-X_{Al})X_{Al}\} - P\Delta V_r)$, are presented for various temperatures in figure 2.5. Over the temperature range 900°C-1150°C, a constant slope of W_{FeAl}^{opx} = 5157 cal ± 200 is an adequate representation of the data (see table 2.4).

In the 1173°K plot, there is a small P dependence to the $-\Delta G_{1,T}^{o}$

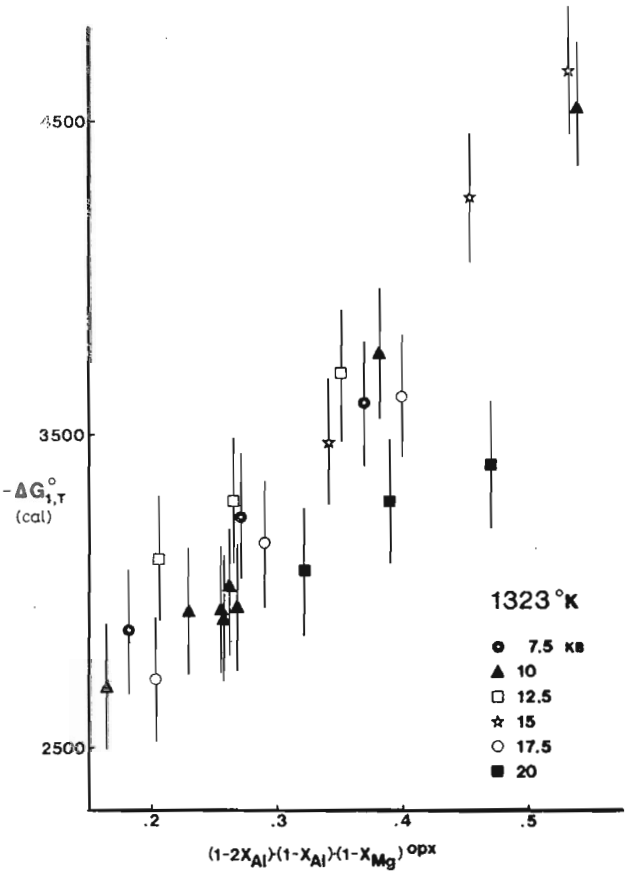
4500
3500
2500
$-\Delta G^{\circ}_{1,T}$ (cal)
1323 °K
7.5 KB
10
12.5
15
17.5
20
.2
.3
.4
.5
$(1-2X_{Al})\cdot(1-X_{Al})\cdot(1-X_{Mg})^{opx}$

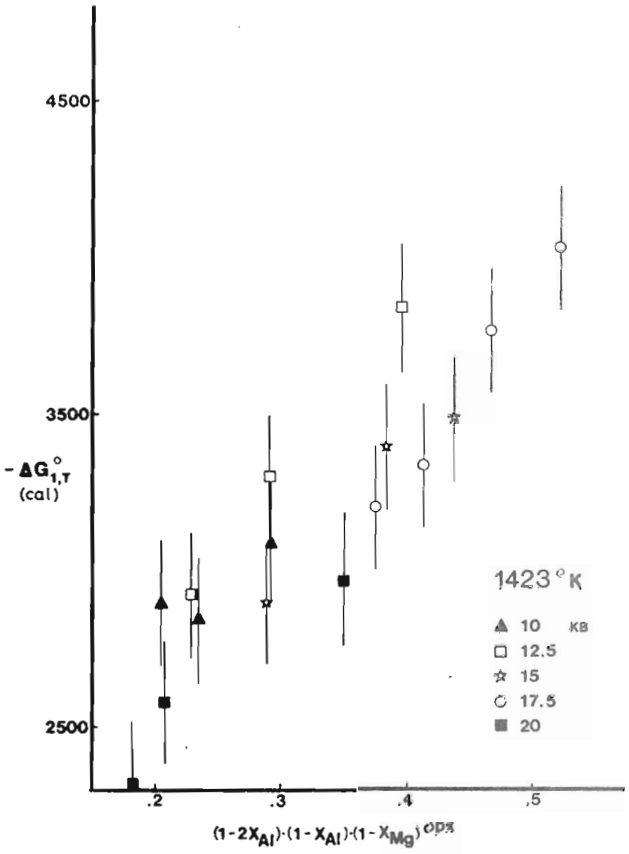
4500
3500
2500
$-\Delta G^{\circ}_{1,T}$ (cal)
1423 °K
10 KB
12.5
15
17.5
20
.2
.3
.4
.5
$(1-2X_{Al})\cdot(1-X_{Al})\cdot(1-X_{Mg})^{opx}$

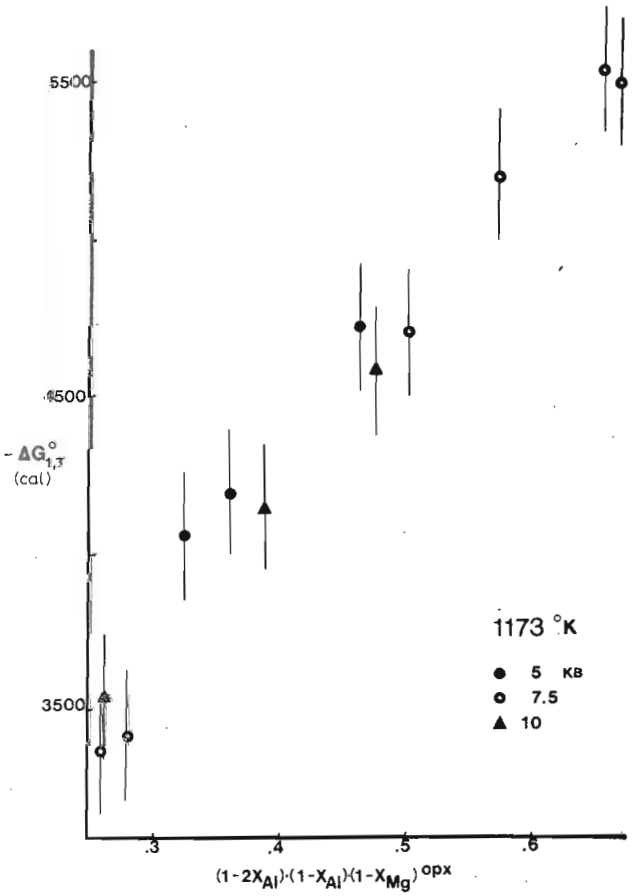
5500
4500
3500
$-\Delta G^{\circ}_{1,T}$ (cal)
1173 °K
5 KB
7.5
10
.3
.4
.5
.6
$(1-2X_{Al})\cdot(1-X_{Al})\cdot(1-X_{Mg})^{opx}$

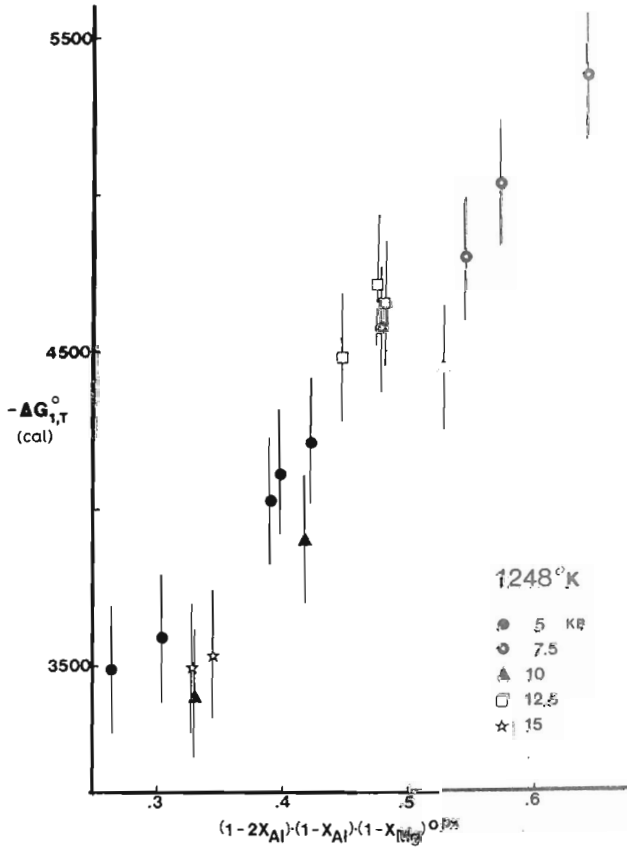
5500
4500
3500
$-\Delta G^{\circ}_{1,T}$ (cal)
1248 °K
5 KB
7.5
10
12.5
15
.3
.4
.5
.6
$(1-2X_{Al})\cdot(1-X_{Al})\cdot(1-X_{Mg})^{opx}$

data, with the 5 kb data plotting at higher values than the 7.5 and 10 kb data. In the 1248°K data, while the 10 kb and 15 kb data plot at lower $-\Delta G^{o}_{1,T}$ values than the 5 and 7.5 kb data, the 12.5 kb points plot above the latter data and thus the pressure dependence at this temperature is not systematic.

Data collected at 1323°K (figure 2.5) show no systematic pressure dependence except for the 20 kb data, which deviates strongly from the $W^{opx}_{FeAl} = 5157$ line. This deviation may result from the possibility of erroneously high Al_2O_3 estimated from microprobe analyses where background and overlap corrections are of critical importance at these low concentrations. 10 kb and 12.5 kb data plot at higher $-\Delta G^{o}_{1,T}$ values than data obtained from higher pressure runs at 1423°K.

A minor pressure correction derived from these data, W_V, could be applied in obtaining a better overall fit to the experimental data. However, the error brackets on the $-\Delta G^{o}_{1,T}$ values, derived only from analytical uncertainties, do not permit such a correction to be made. Thus,this apparent pressure or excess volume effect has been ignored.

Best fit regression lines with the constraint of a slope of 5157 ± 200 cals can be fitted to the data at each temperature and values of $(\Delta H^{o}_{1,T})_{X_{Mg}=1.00}$ obtained from the intercepts of these lines with the ordinate axis. The differences between $(\Delta H^{o}_{1,T})_{X_{Mg}=1}$ values at different temperatures gives the entropy ΔS^{o}_{T}.

Multiple linear regression of all data including 800°C data have yielded values of $\Delta H^{o} = -5020$ cals mol^{-1}, and $\Delta S^{o}_{T} = -2.507$ cals $mol^{-1}K^{-1}$. Examination of the 800°C data reveals that this data falls approximately on the best fit regression line of slope 5157 cals obtained for the 1173°K data. This would suggest that either ΔS is near zero between 800°C and 900°C, or ΔH is larger at these temperatures, or

Table 2.4 MULTIPLE LINEAR REGRESSIONS OF FMAS EXPERIMENTAL DATA

(1) X_{Al}^{opx} DATA

DATA SET	NO. OF CASES	ΔS cal mol^{-1} K^{-1}	ΔH_T cals	W_{FeAl} cals	R
all T	63	-2.507	-5020	5157	.92
		(.328)	(224)	(257)	
1073°K	4	-	-1933	5261	.99
			(80)	(443)	
1173°K	9	-	-2349	4825	.98
			(92)	(239)	
1248°K	18	-	-1708	5748	.89
			(189)	(495)	
1323°K	21	-	-1865	4641	.81
			(246)	(516)	
1423°K	11	-	-1461	4856	.89
			(184)	(557)	
1073°K	60	-3.357	-6143	5157	.81
data deleted		(.324)	(197)	given	
1073°K and	57	-2.93	-5650	5157	.91
1323°K, 20		(.30)	(200)	given	
kb data out					

(2) $K_{D\,Fe\text{-}Mg}^{ga\text{-}opx}$ DATA ($RT\ln K_D$ vs. T and parameters)

DATA SET	NO. OF CASES	ΔS cal m^{-1}K^{-1}	ΔH cals	W_{FeMg}^{opx}	$(1/2)W_{FeAl}^{opx}$	W_{FeMg}^{ga}	R
K_D .2	40	-2.58	-4514	169	589	0	.86
Fe capsules		(.26)	(153)	(129)	(602)	given	
" "	40	-2.75	-4504	102	2579	0	.84
		(.29)	(172)	(143)	given	given	
" "	40	-2.46	-4019	517	2579	500	.85
		(.26)	(155)	(129)	given	given	
" "	62	-2.12	-3688	575	"	"	.70
		(.31)	(215)	(121)			
" "	40	-2.29	-3728	766	"	800	.87
		(.24)	(145)	(121)		given	
adjusted K_D	55	-1.41	-2619	600	1500	874	.91
, C-capsules		(.22)	(133)	given	given	(91)	
K_D's also	55	-1.57	-2748	400	2579	694	.86
		(.27)	(166)	given	given	(114)	
" "	55	-2.42	-4000	600	2579	0	.85
		(.27)	(200)	(200)	(200)	given	

NUMBERS IN PARENTHESES - STANDARD DEVIATIONS

that the Alumina contents measured in orthopyroxenes formed at 800°C and 5 kb are too high in comparison to all other data. Two mixes used at 800°C were reversal mixes, and an overlap of Al_2O_3 contents was obtained at similar X_{Mg}^{opx} for orthopyroxenes grown from both glass and mineral mixes. This "reversal" is difficult to ignore, however the mineral mix orthopyroxenes are very strongly zoned even on rims, and all mixes show textures which indicate widespread disequilibrium (Plate 2.2). Possibly equilibrium Al_2O_3 contents may be lower than those reported for this run (T680).

Ignoring the 1073°K (800°C) data results in a better multiple linear regression fit (Table 2.4) to all the higher temperature data. The ΔS value obtained (2.93 ± .300) is subject to the largest uncertainty of any of the regression parameters.

Temperature and the compositional variable $(1-2X_{Al})(1-X_{Al})(1-X_{Mg})^{opx}$ account for 95 percent of the variation in $\Delta G^o_{1,T}$. Other possible minor effects, including the terms W^{ga}_{FeMg}, W_v, and $\Delta\bar{G}^o_{Fe\ Al}$ may be responsible for the remainder of the variation. However, much of this variation may also be a result of experimental or analytical inaccuracies. It is doubtful that consideration of the minor effects will significantly improve the fit to experimental data which have inherent errors of ± .5 kbar and ± 10°C at least. The resultant geobarameter is considered to have an inherent error of ± 1 kbar due to experimental and analytical errors alone. In application to natural rocks, this error will be magnified by errors necessarily associated with temperature estimation.

Returning to the experimental data, the pressure calculated using derived regression values can be compared with the nominal experimental pressures for all seventy-five cases.

Pressures have been calculated using the equations

$$P_1(\text{kbar}) = \frac{-1}{\Delta V_r}[(R \ln K - 2.507)T + 5020 + 5157(1-X_{Al})(1-2X_{Al})(1-X_{Mg})^{opx}],$$

the best-fit equation derived from a data set including the 800°C run, and

$$P_2(\text{kbar}) = \frac{-1}{\Delta V_r}[(R \ln K - 2.930)T + 5650 + 5157(1-X_{Al})(1-2X_{Al})(1-X_{Mg})^{opx}], \quad (9)$$

the best fit equation derived when 800°C data is excluded.

In these equations

$$-\Delta V_r = 183.3 + 178.98\,(1-X_{Al})(X_{Al}) \text{ cals kbar}^{-1}$$

$$K = (1-X_{Al})(X_{Al})$$

and T is in degrees Kelvin.

Minimising the error on W_{FeAl}, other intermediate values of ΔS and ΔH can be obtained which also give excellent fits of $P_{calculated}$ with $P_{nominal}$.

In figure 2.6, P_{calc} is plotted against $P_{nominal}$ for regressed values of ΔH and ΔS. In general, the agreement between calculated and nominal pressures is very good ($r = 0.977$, slope $= 0.904$, intercept $= 0.957$) for data other than the 800°C data, which gives calculated pressures of less than 5 kbar. Taking into account the errors on the calculated and nominal pressures, the equation (9) is an excellent fit to all the experimental data.

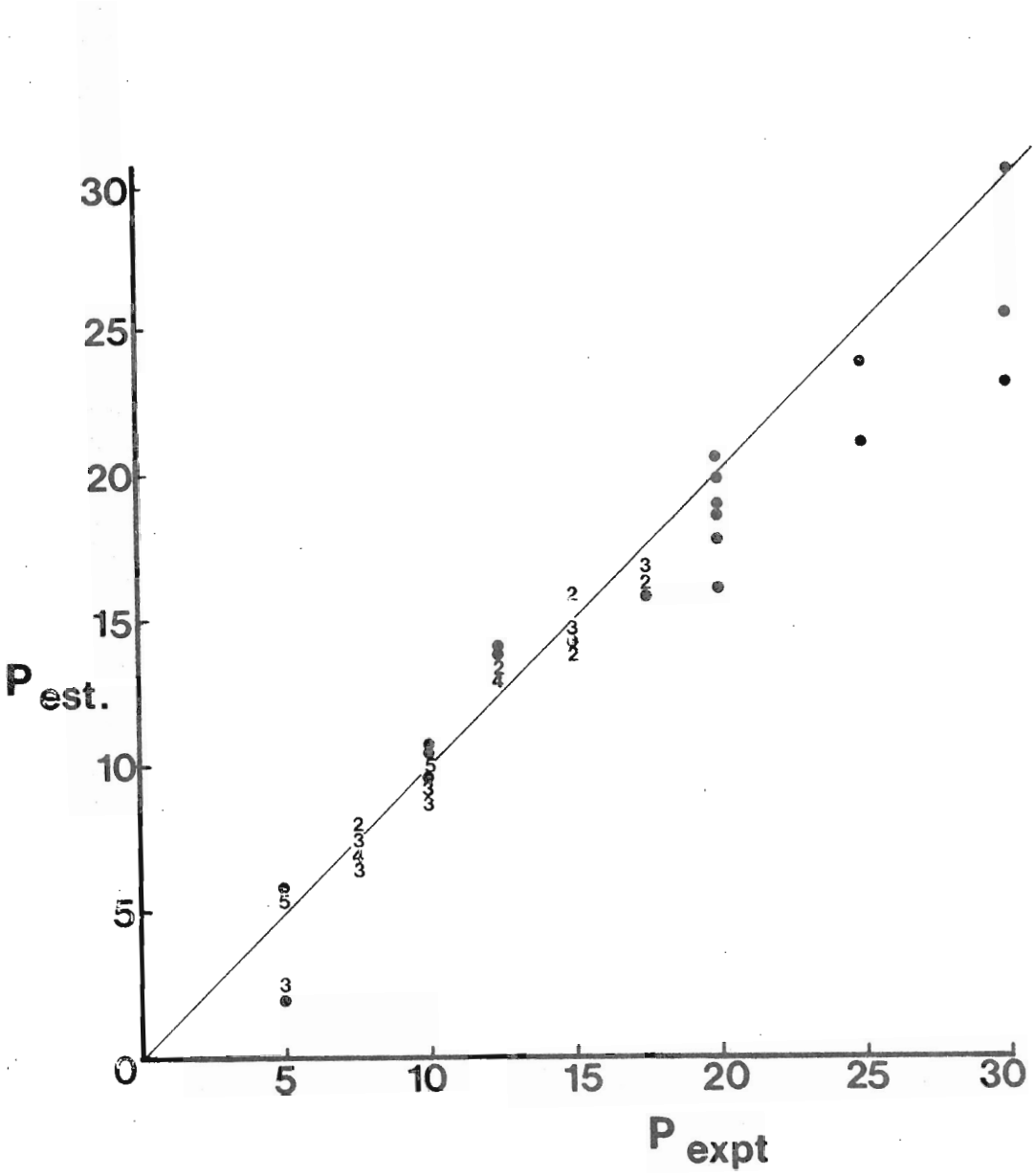

Fig. 2.6 P estimated by equation 2(9) plotted against experimental P for all experimental data, including those higher P data not used in the formulation of the equation. Small numbers indicate the number of data points giving one P estimate. All pressures in kbar.

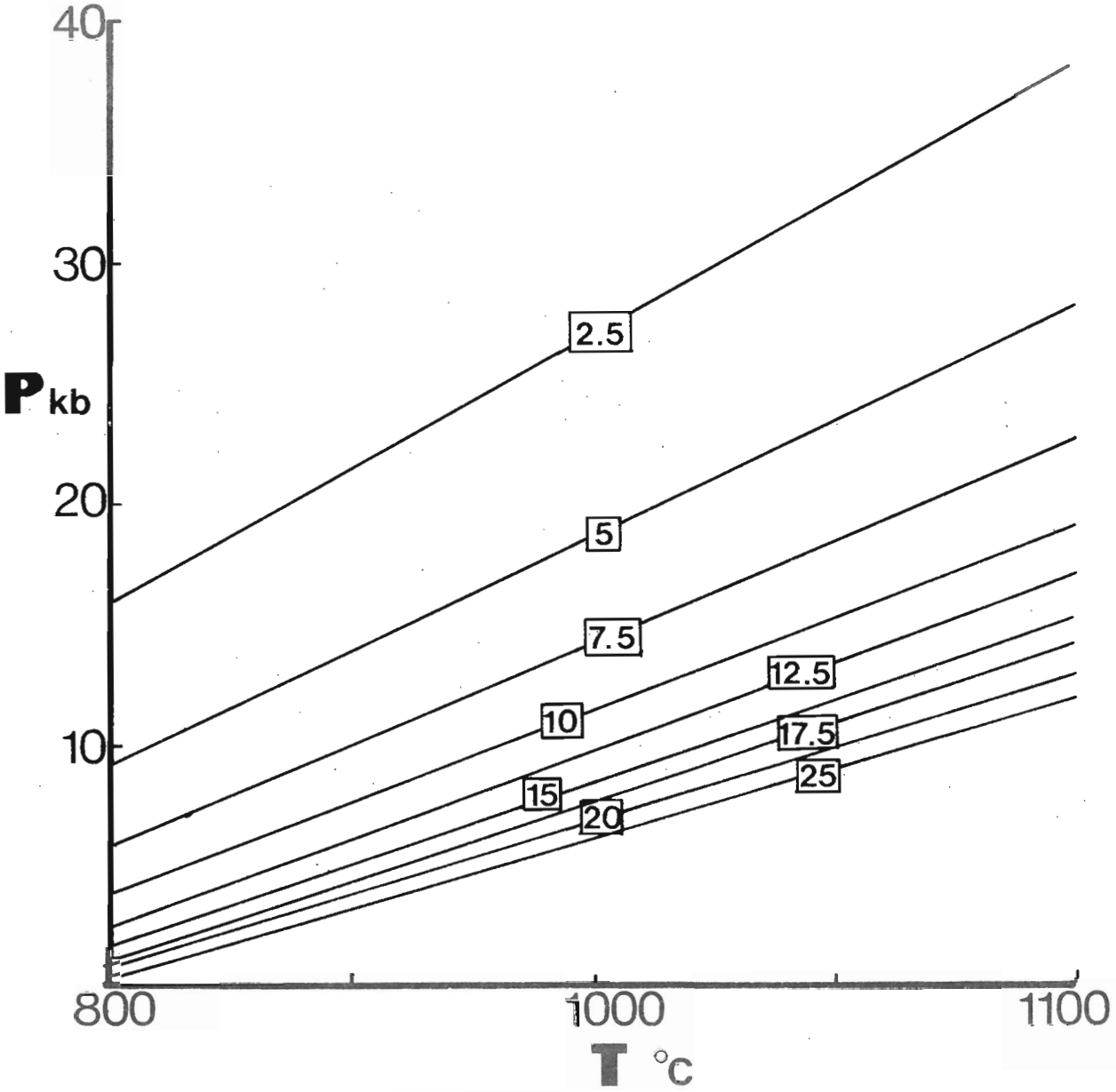

Fig. 2.7 X_{Al}^{opx} (Al/2) isopleths for hypothetical X_{Mg}^{opx} - 50 orthopyroxene in equilibrium with Fe-Mg garnet.

(5) OLIVINE-ORTHOPYROXENE AND GARNET-OLIVINE RELATIONSHIPS AT 900°C, 7.5 kbar

Massive iron addition into charges run in an iron capsule under these conditions resulted in the formation of Fe-rich olivines coexisting with orthopyroxene and garnet in the absence of quartz (page 334 , Appendix Two).

Garnet-olivine Fe-Mg partitioning in the two compositions can be compared with K_D's predicted from the experimental work of O'Neill and Wood (1979). $K_{D_{Fe-Mg}}^{ga-ol}$ values derived from the data of T720 are subject to considerable uncertainty resulting from widespread X_{Mg} zoning in the garnets. Rims of garnets near the walls of the sample capsules involved are more Fe-rich than those from the central parts of these changes where olivine is absent and quartz is present. Using the former X_{Mg}^{ga} values, $K_{D_{Fe-Mg}}^{ga-ol}$ ranges from 1.137 ± .015 (at X_{Mg}^{ol} = .112) to 1.194 ± .030 (at X_{Mg}^{ol} = .233). These values are in good agreement with the 1000°C, 30 kb data of O'Neill and Wood (1979). Allowing for the pressure effect on K_D for the reaction

$$3Fe_2SiO_4 + 2Mg_3Al_2Si_3O_{12} = 2Fe_3Al_2Si_3O_{12} + 3Mg_2SiO_4,$$

at 7.5 kbar this data (O'Neill and Wood, 1979, fig. 1) would correspond to a lower temperature of around 900°C, in good agreement with the P-T conditions of T720.

Calculation of T_{ga-ol} using the modified equation of O'Neill and Wood (1980), yields temperatures of 790°C and 860 °C for the garnet-olivine pairs generated at 7.5 kbar and 900°C in T720.

Compositions of coexisting olivine and orthopyroxene yield $K_{D_{Fe-Mg}}^{ol-opx}$ values which are consistent with the calculated values of Sack (1980), K_D values of 2 ± .13 (at X_{Mg}^{ol} = .112) and 1.79 ± .16 (at

X_{Mg}^{ol} = .233) fall within the 800°C-1000°C envelope of Sack (1980) Figure 6. If these K_D values are accepted as equilibrium data, they lend support to the orthopyroxene solution formulation of Sack (1980). It should be noted, however, that the orthopyroxenes generated in T720 are aluminous. The possible effects of Al_2O_3, which are not considered in the treatment of Sack (1980), may render a direct comparison of the data unreliable.

(6) $K_{D_{Fe-Mg}}^{ga-opx}$ RELATIONSHIPS

Variation of K_D with P,T and composition.

$K_{D_{Fe-Mg}}^{ga-opx}$ values extracted from graphite capsule runs, and adjusted values derived from iron capsule runs have been analysed using equation (8) to extract values of ΔH^o, ΔS_T^o, and W_{FeMg}^{ga}. In this analysis W_{Fe-Mg}^{opx} and W_{FeAl}^{opx} have been introduced as fixed values derived from other experimental data.

Multiple regression techniques have been applied to 40 selected data points from the experimental results. The data excluded from this analysis have unreasonably high zoning in X_{Mg}^{ga} or X_{Mg}^{opx}, or the equilibrium garnet compositions are not reliable because of reverse zoning or the presence of olivine.

The raw K_D values from all experimental data are plotted for various temperatures in figures 2.8 to 2.10. Large uncertainties in the K_D values obscure variations in K_D with Pressure and X_{Mg}^{opx}, however $K_{D_{FeMg}}^{ga-opx}$ usually increases with increasing Pressure (at constant T and X_{Mg}^{opx}). In general, $K_{D_{Fe-Mg}}^{ga-opx}$ decrease consistently with increasing Temperature (at constant P and X_{Mg}^{opx}).

Comparison of graphite capsule runs and multi-mineral mix runs

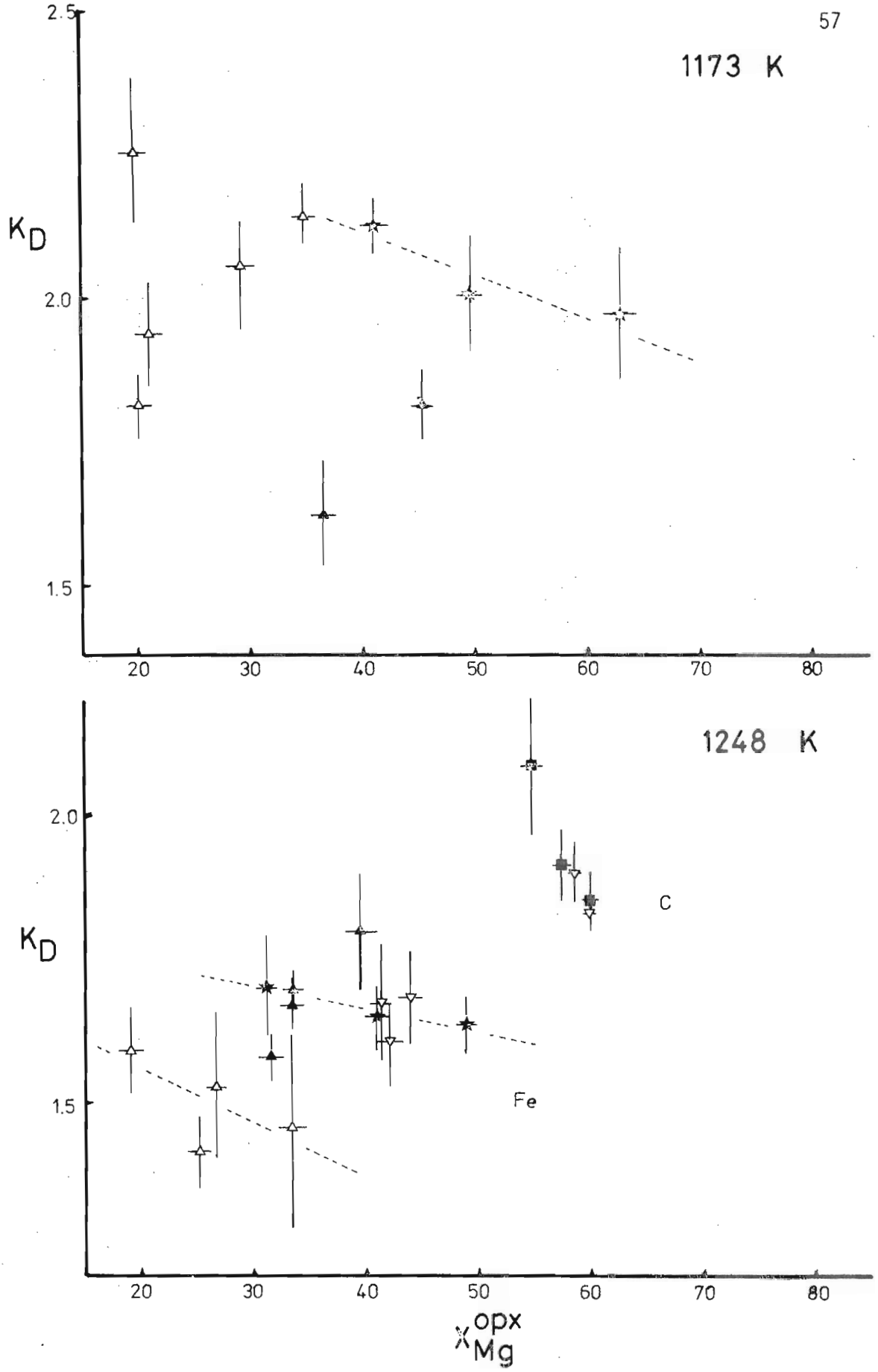
1173 K
K_D
2.5
2.0
1.5
20
30
40
50
60
70
80
1248 K
K_D
2.0
1.5
C
Fe
20
30
40
50
60
70
80
X^{opx}_{Mg}

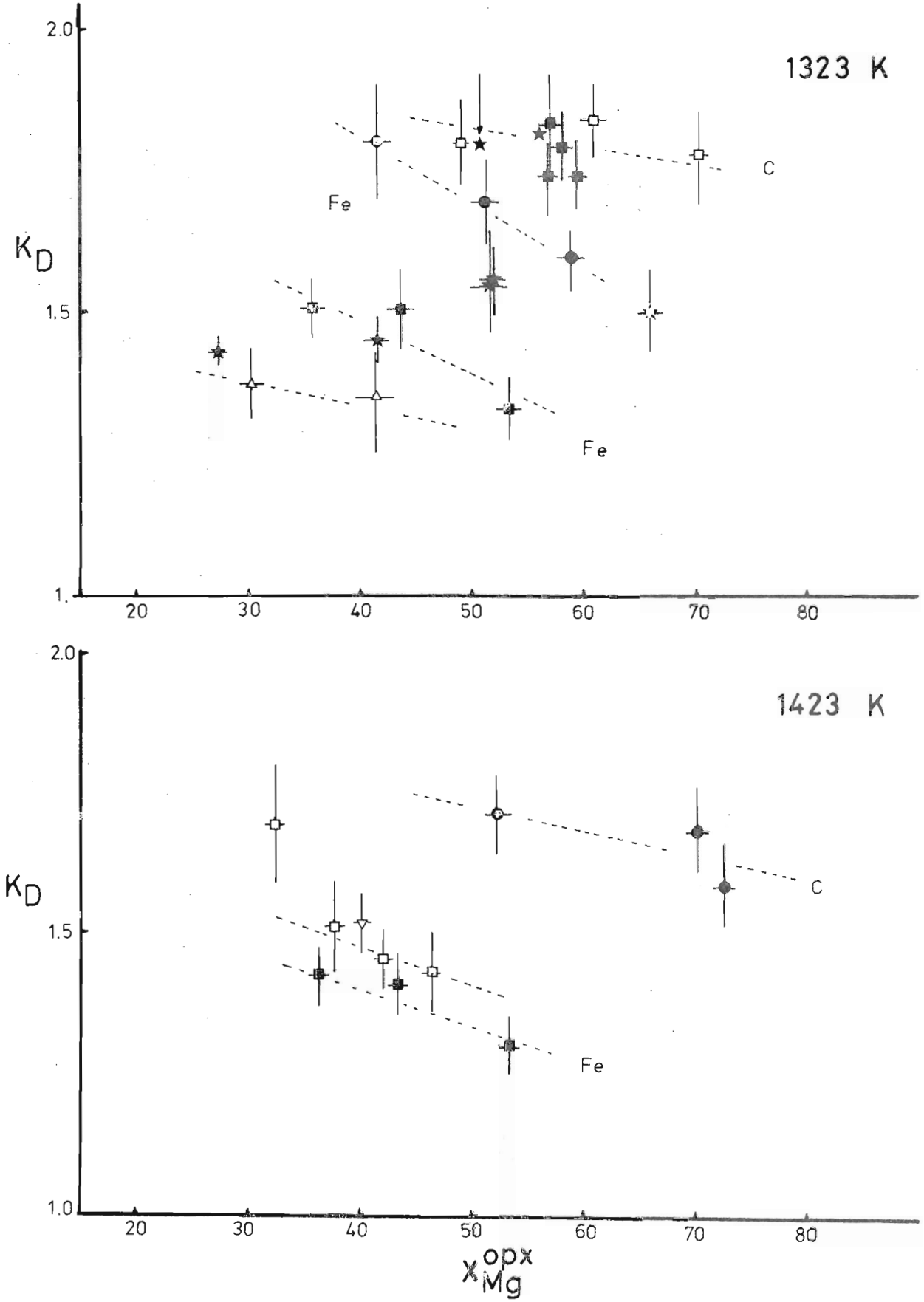
1323 K
2.0
1.5
1.
K_D
Fe
Fe
C
20
30
40
50
60
70
80
1423 K
2.0
1.5
1.0
K_D
Fe
C
20
30
40
50
60
70
80
x^{opx}_{Mg}

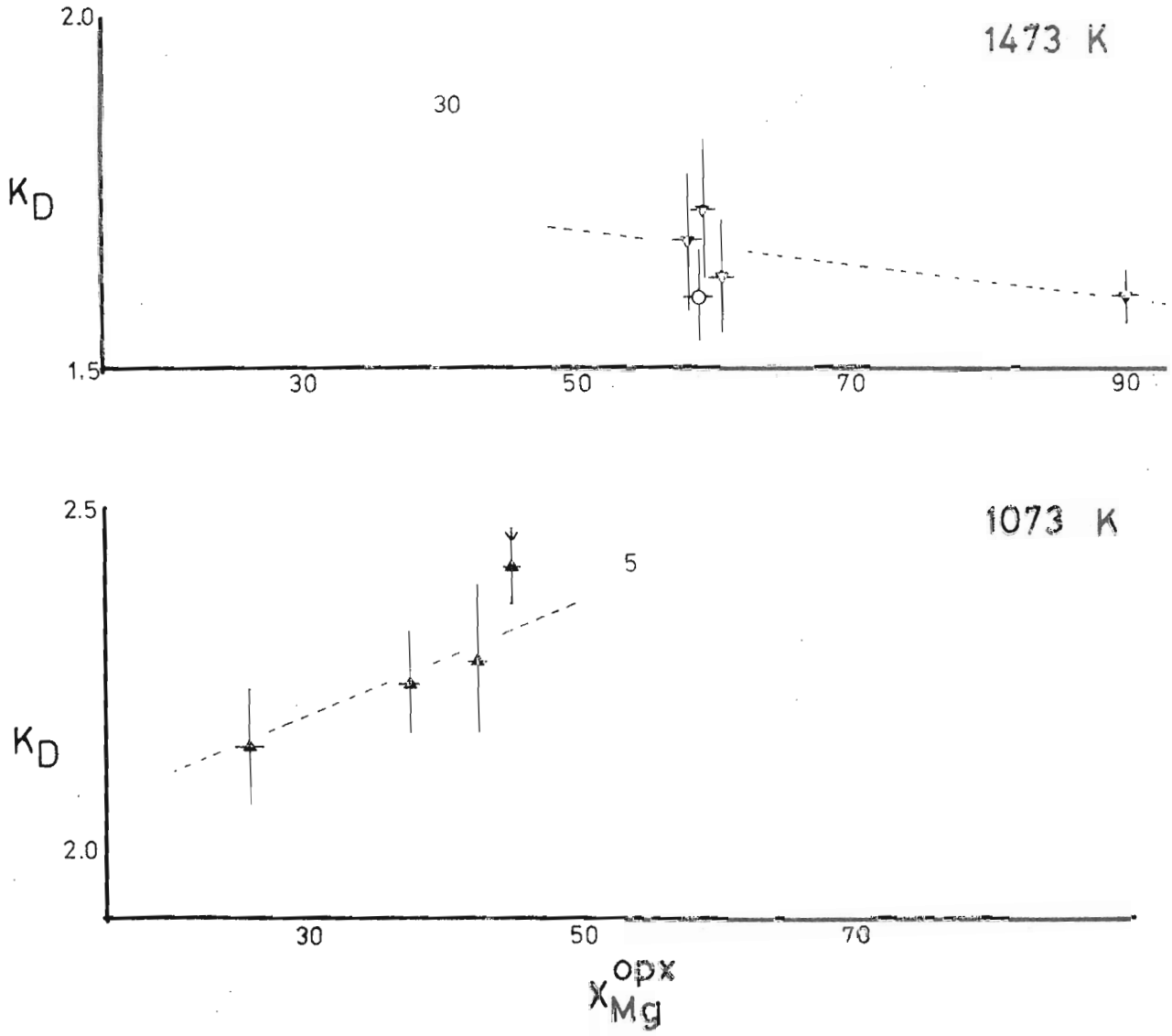

Fig. 2.10 Values of $K_{D_{Fe-Mg}}^{ga-opx}$ obtained at 1473 °K and 1073 °K, plotted against X_{Mg}^{opx}. Dashed lines connect isobaric K_D data. Pressure symbols :

▲ 5 ○ 25 ▽ 30 kbar

with glass mix runs indicates that Fe-addition into the latter mixes results in an apparent decrease in K_D (of up to .2). In particular, multi-mineral mix runs at 10 kb and 1050°C give the values of 1.5-1.6, whereas seeded glass mixes under the same conditions give K_D's of 1.3 to 1.4. These values, and K_D values obtained from seeded glass mixes where Fe-addition has been important, have been adjusted upwards by .2. Adjusted K_D values for the experiments used in this analysis are asterisked in Table 2.2.

Multiple regressions of this adjusted data according to equation (8) yields ΔS_T = -2.42 $calK^{-}mol^{-1}$ and $\Delta H_{1,T}$ = -4000 $calmol^{-1}$ (Table 2.4). The large errors in K_D measurement, the problems of accounting for iron addition, and the small temperature dependence of $K_{D_{Fe-Mg}}^{ga-opx}$, result in wide scatter of the data and hence a poor regression fit.

All K_D data have been normalised to 1 bar using a constant volume change of reaction, $\Delta V^{o}_{(6)}$. The presence of alumina in the orthopyroxene introduces some error here, in that there will be an excess molar volume change related to the partial molar volumes of $Fe_2Si_2O_6$ and $Mg_2Si_2O_6$ in Al-orthopyroxenes. The pressure dependence of $K_{D_{Fe-Mg}}^{ga-opx}$ may thus be greater in FMAS than in the simple case where no Al_2O_3 is dissolved in the orthopyroxene.

Using the derived values of ΔS and ΔH, equation (8) can be rearranged to construct a geothermometer based on $K_{D_{Fe-Mg}}^{ga-opx}$ in FMAS:

$$T_{(°K)} = \frac{4000 + 22.86\ P\ (kbar) + 2576\ X_{Al}^{opx} - 600\ (X_{Mg}^{ga} - X_{Mg}^{opx})}{R \ln K_D + 2.42} \qquad (10)$$

Temperatures calculated using equation (10) above are compared with nominal run temperatures for the FMAS experiments in figure 2.11. There is wide scatter of estimated temperatures because of the poor

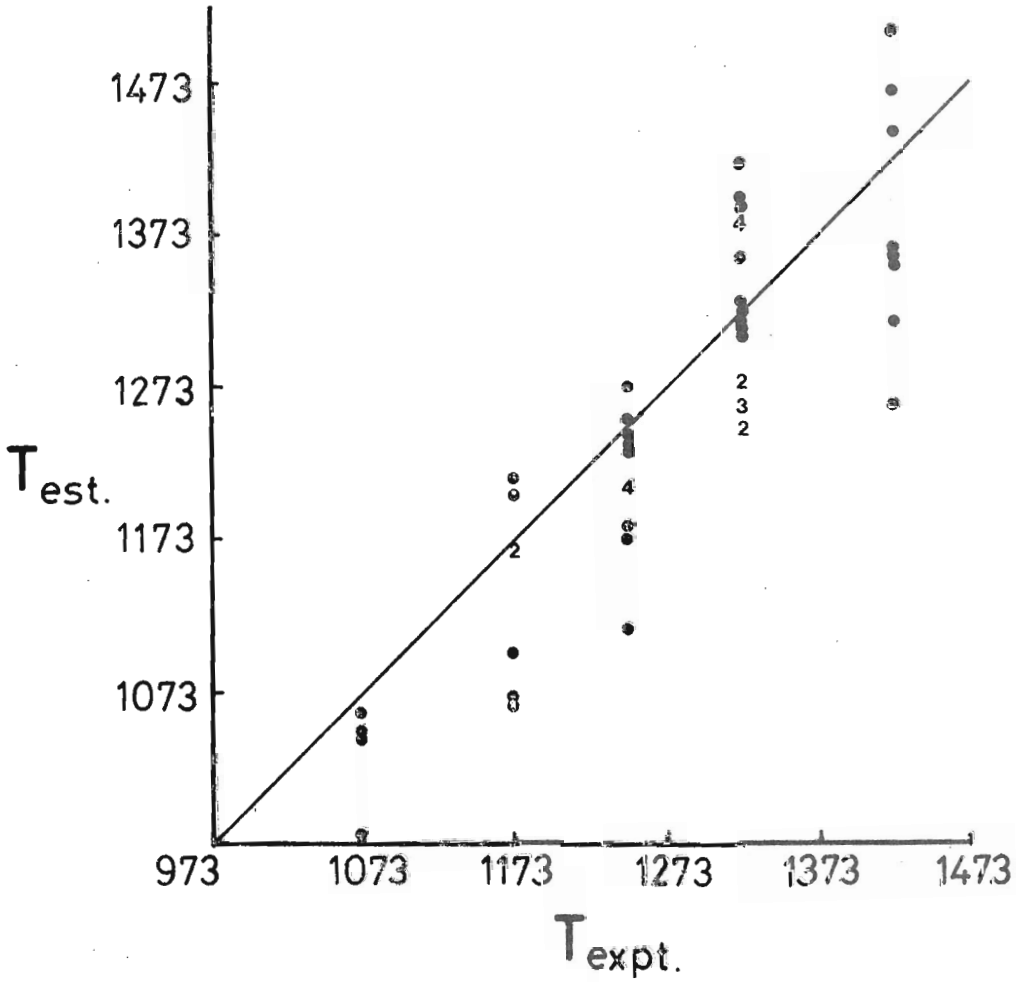

Fig. 2.11 Testimated via equation 2(10), plotted against nominal experimental T for 55 data points in C and Fe capsules. Fe capsule K_D data used in this fit have been adjusted upwards by 0.2, by comparison with C-capsule data (Fig. 2.8, Fig. 2.9)

quality of the data and the large uncertainties in ΔS^{o}. Equation (10), based on *adjusted* data, reproduces the experimental run temperatures to within ± 60°C.

Equation (10) must be applied with some caution to natural rocks because of the large errors inherent in the thermometer and the assumptions involved in the experimental data base. Compositional effects of Ca and Mn in garnet increase K_D markedly at constant P and T, and must be included in developments of equation (10)(Chapter 3). Even with these other effects included, it is unlikely that the $K_{D_{Fe\text{-}Mg}}^{ga\text{-}opx}$ thermometer derived herein can be used as a reliable estimate of absolute temperatures. Relative temperature differences between samples may be more reliably inferred, however.

Chapter 3

AN EXPERIMENTAL STUDY OF THE EFFECT OF Ca ON THE Fe-Mg DISTRIBUTION BETWEEN GARNET AND ORTHOPYROXENE AND THE SOLUBILITY OF Al_2O_3 IN ORTHOPYROXENE COEXISTING WITH GARNET IN CaO-FeO-MgO-Al_2O_3-SiO_2

3.1 INTRODUCTION

Natural garnet-orthopyroxene assemblages, both in garnet peridotites and in granulites, rarely approach the FMAS end member system for which the barometry and thermometry developed in Chapter 2 is directly applicable. A major additional component, calcium, must be considered before the experimentally calibrated garnet-orthopyroxene barometry and thermometry can be applied to natural rocks. In particular, the calcium content of garnet coexisting with orthopyroxene will have marked effects on $K_D^{ga\text{-}opx}{}_{Fe\text{-}Mg}$, by analogy with garnet-clinopyroxene (Ellis and Green, 1979) and garnet-olivine (O'Neill and Wood, 1979) Fe-Mg distributions, where K_D values increase with increasing Ca-content of the garnet at constant P and T.

Previous experimental investigations in CMAS (Howells and O'Hara, 1978 ; Akella, 1976 ; Perkins and Newton, 1980) and in CFMAS (Wood, 1974 ; Hensen, 1973 ; Akella and Boyd, 1973 ; Mori and Green, 1978) have shown that the Ca-content of garnet coexisting also has a dramatic effect on the solubility of Al_2O_3 in orthopyroxene at constant P and T, with less Al_2O_3 entering the orthopyroxene in comparison with Al_2O_3 contents determined in simpler systems (FMAS, MAS) at the same conditions.

In this chapter, the FMAS experimental program is extended to the CFMAS system, with the object of determining the effects of variable Ca-contents of garnet upon both the solubility of Al_2O_3 in orthopyroxene and the distribution of Fe and Mg between garnet and orthopyroxene at near-constant X_{Mg}^{opx} and for a range of pressures and temperatures. The evaluation of such Ca-effects will allow the development of garnet-orthopyroxene barometry and thermometry which is directly applicable to a wide range of rock types.

3.2 GARNET SOLID SOLUTIONS in the system $CaO-MgO-FeO-Al_2O_3-SiO_2$

Activity-composition relationships in multicomponent garnets have been studied by several workers on the joins Pyrope-Almandine and Pyrope-Grossular (Kolesnik *et al.*, 1979; Hensen *et al.* 1975; Newton *et al.*, 1977; Jenkins and Newton, 1979; Haselton and Newton, 1980; Perkins and Essene, 1977), and Almandine-Grossular (Cressey *et al.*, 1978; O'Neill and Wood, 1979). Three distinct approaches have been used in the estimation of the activity coefficients of grossular, pyrope and almandine, based on the application of the symmetric regular or assymmetric subregular solid solution models:

(1) Natural Systems

Ganguly and Kennedy (1974) used this "natural laboratory" technique in analysing natural garnet-biotite mineral pairs formed at an assumed temperature of 630 ± 40°C. These authors assumed biotite to behave ideally and accordingly attributed their observed compositional variation in $K_{D_{Fe-Mg}}^{ga-biot}$ to activity coefficients in the garnet. Multiple regression techniques were used to extract the interaction parameters listed in Table 3.1, based on a symmetrical solution model. Dahl (1980) and Saxena (1968, 1969, 1980) have also used this approach. Dahl (1980) has considered garnet-clinopyroxene ± orthopyroxene natural assemblages assumed to have formed at temperatures of 795 ± 50°C and 675 ± 45°C at two localities in Montana. Using this data base, which covers a wide range of composition in terms of X_{Ca}^{ga} and X_{Mn}^{ga}, and assuming that clinopyroxene contributes little to the compositional effects on K_D, multiple regression techniques were used to extract interaction parameters W_{FeMg}^{ga}, $(W_{CaFe}^{ga}-W_{CaMg}^{ga})$, and $(W_{FeMn}^{ga}-W_{MgMn}^{ga})$. These values are listed in Table 3.1.

It is important to note that these natural-rock approaches

suffer from the problems of solution modelling for the other participating phase; the presence of significant amounts of Fe^{3+}; and the large error brackets on any assumed temperature of equilibration relative to temperature errors in experimental or cabrimetric techniques. Nevertheless, this approach provides useful constraints on the sizes of some of the W_{ij}^{ga} terms.

(2) High Pressure experiments

There are two approaches which have been used to extract interaction parameters for garnet solid solutions from experimental studies on simple joins and in the ternary CFMAS system.

(a) Projects have been designed in which it is possible to measure the composition of garnet in equilibrium with an assemblage in which the activities of all other components are fixed. This involves using a simple system assemblage defining a univariant curve in that system, and adding to the system another component which will only enter the garnet phase. Hensen *et al.*(1975) have estimated W_{CaMg}^{ga} from the compositions of garnets in equilibrium with anothite-sillimanite (or kyanite)-quartz at different P and T in the system CMAS. These authors have extracted a W_{CaMg}^{ga} by applying a symmetrical regular solution model to the garnet and estimating $a_{Ca_3Al_2Si_3O_{12}}^{ga}$ using the relation

$$(P_o - P_1)\ \Delta V_o = RT \ln a_{Ca_3Al_2Si_3O_{12}}^{ga},$$

where P_o is the equilibrium pressure of the CAS reaction

3 Anorthite = Grossular + 2Kyanite + Quartz (1)

and P_1 is the run pressure. ΔV_o is the volume change of the CAS reaction at 1 bar, and the possible partial molar volume effects of grossular-pyrope were not considered in the analysis. As a result,

a temperature dependent interaction parameter W^{ga}_{CaMg} has been extracted to account for the observed positive deviations from ideality.

Cressey *et al.* (1978) have applied a similar technique in adding Fe to the simple CAS system and again using reaction (1) above to control $a^{ga}_{Ca_3Al_2Si_3O_{12}}$. These authors, however, also have considered the volume behaviour of grossular-almandine solid solutions at 1 bar, finding a general positive excess volume of mixing in the Alm-Gr join except for a small negative departure in the grossular poor region (Gr 5-20). The P-T-X^{ga}_{gross} data were then analysed in comparison to the breakdown reaction (1) and activity-composition curves constructed for various temperatures. Using the derived partial molar volume data, these a-X relations were then normalised to 1 bar pressure. By these means, it has been found that the excess volumes of mixing in the Alm-Gross join have an important bearing on a-X relations at high pressures. At low grossular contents (< 30%), Fe-Ca garnets are near ideal in the temperature range 850-1200°C at high pressures, but exhibit small negative departures from ideality at 1 bar.

(b) The compositional dependences of $K_D{}^{ga\text{-}mineral}_{Fe\text{-}Mg}$ in series of experimental starting compositions run at the same P and T have been accounted for using various solid solution models for garnet and the coexisting phase, as in the natural rock approach. Here the Fe^{3+} contents of the minerals are negligible and the P-T conditions are much more precise than in the "natural laboratory" technique.

O'Neill and Wood (1979) have studied Fe-Mg exchange between olivine and garnet in FMAS and CFMAS and applied multiple regression techniques to fit model-dependent interaction parameters (W_{ij}) in the olivine and garnet to the experimental data. Using symmetrical regular solution models for both phases, values of $(W^{ol}_{FeMg} - W^{ga}_{FeMg}) =$

800 cal, and $(W^{ga}_{CaMg}-W^{ga}_{CaFe}) \simeq 2{,}670$ cal at 30 k bar have been extracted. O'Neill and Wood (1979) have argued that, because the molar volume curves on the Alm-Gross and Py-Gross joins are very similar, the term $(W^{ga}_{CaMg}-W^{ga}_{CaFe})$ should not be significantly pressure dependent. These authors also estimated a very small W^{ga}_{MgFe} value of 195 cal, indicating near ideality of the pyrope-almandine join in contrast to the results of Ganguly and Kennedy (1979).

Jenkins and Newton (1979), in a study of the reaction $Mg_2Si_2O_6 + CaMgSi_2O_6 + MgAl_2O_4 = Mg_2SiO_4 + CaMg_2Al_2Si_3O_{12}$ have retrieved a value of $(W^{ga}_{CaMg})_{1000°C} = 2000 \pm 350$ cals, assuming a symmetric regular solution model for garnet and "ideal two site" models for orthopyroxene and clinopyroxene. The activity of grossular in the garnet was estimated by considering the reaction:

$$Mg_3Al_2Si_3O_{12} + Ca_3Al_2Si_3O_{12} + 2Mg_2SiO_4 = Mg_2Si_2O_6 + 3CaMgSi_2O_6 + 2MgAl_2O_4,$$

for which the molar volumes change and the ΔS^{o}_{1273} could be calculated from available V^o, S^o, and Cp data.

(3) Calorimetric Techniques

Enthalpy of solution measurements on natural and synthetic garnets on the Py-Gross join have been fitted by Newton *et al.* (1977) and Newton (1978) to a two parameter subregular solution model:

$$\Delta H^{excess} = 3([X^{ga}_{Ca}]^2 X^{ga}_{pyrope}.2000 + [X^{ga}_{pyrope}]^2 X_{gross}.3820)$$

Enthalpy of solution values deviate by up to 2 kcal/mol from an ideal model at 970°K, with the larger deviations occurring at the pyrope-rich end of the series.

The positive excess free energies of mixing indicated by Newton

et al. (1977) are less than those derived from the W^{ga}_{CaMg} value of Hensen *et al.* (1975), but in reasonable agreement with the symmetric regular solution W^{ga}_{CaMg} value of Ganguly and Kennedy (1974) for garnets with less than 30 mol % grossular.

Haselton and Newton (1980) have formulated activity-composition expressions for pyrope-grossular garnets which include excess enthalpy, entropy and volume terms, using the relationship:

$$W_G = W_H - T\,W_S + P\,W_V$$

Excess enthalpies of mixing on the Py-Gross join were obtained from the data of Newton *et al.* (1977) and fitted to an assymmetric regular solution model to yield values of W^{py}_H and W^{gr}_H. The temperature dependence of the non-identity was estimated from calorimetric measurements on Pyrope, Grossular and a $Py_{60}Gr_{20}$ garnet in the temperature range 150-298°K. Excess entropies of the $Py_{60}Gr_{40}$ garnet were fitted to a symmetric function and a value of W_S extracted. This W_S value is only one-third the magnitude of the W_S term found by Hensen *et al.* (1975).

The molar volume data of Newton *et al.* (1977) were fitted to a quadratic plus gaussian curve and the partial molar volumes of pyrope and grossular were then generated from this curve and added to the a-X expression through the relationship:

$$\left(\frac{\partial \ln a_i}{\partial P}\right)_{T,Xj} = (\bar{V}_i - V^o_i)/RT$$

Activity coefficients derived from the combined W^{py}_H, W^{gr}_H, Ws and Wp terms of Haselton and Newton (1980) compare favourably with those derived by Hensen *et al.* (1975) if the latter values are corrected for the partial molar volume terms. The large apparent W_S term

derived by Hensen *et al.* (1975) thus seems to include an excess volume term in addition to a smaller excess entropy effect.

The conclusions which can be drawn from all the work outlined above and summarised in table 3.1 are that Ca-Mg-Fe garnets show substantial positive deviations from ideality on the Ca-Mg join at high pressures, while mixing on the Fe-Mg join may be very close to ideal. Mixing on the Fe-Ca join may be slightly positively non-ideal at high pressures. On the Fe-Ca and Ca-Mg joins the excess partial molar volumes will be important contributions to non-ideality and thus the extent and magnitude of deviations from ideality will be pressure dependent for each join. The similarities of the molar volume curves in the Py-Gross and Alm-Gross joins would suggest that any pressure dependencies, Wp, will largely cancel in multicomponent reactions where the term ($W^{ga}_{CaMg} - W^{ga}_{CaFe}$) arises in the excess free energy or the non-ideal contribution to $\Delta G^{o}_{reaction}$.

It is also evident that, for grossular contents less than 30 mol %, symmetric regular solution models should adequately describe the garnet solid solutions in CFMAS.

In modelling the effects of the addition of Ca on the Al_2O_3 solubility in orthopyroxene coexisting with garnet, the solution properties of Ca-Mg-Fe garnets must be considered. In the light of the above discussion, a symmetric ternary regular solution model has been used for the garnet and a value of (W^{ga}_{CaMg}-W^{ga}_{CaFe}) has been extracted from the experimental data in an approach similar to 2(b) above. This parameter, and the values W^{ga}_{CaMg}, W^{ga}_{CaFe} can be compared with those obtained by other workers (Table 3.1)

Table 3.1 INTERACTION PARAMETERS FOR GARNET SOLID SOLUTIONS IN CFMAS

PARAMETER	MODEL/CONDITION	REFERENCE	VALUE (cal/mol)
W_{CaMg}	SmR ; at 670 °C	Ganguly and Kennedy (1974)	3830 (110)
"	SmR ; at 750 °C	Dahl (1980)	2810 (954)
"	SmR ; at 825 °C	Saxena (1978)	3820
W_{py}	AsmR	Saxena (1980)	2340
W_{gr}		" "	3840
W_{py}	AsmR ; at 700 °C	Newton et. al. (1977)	2000
W_{gr}		" "	3820
W_{py}	AsmR with T depe	Haselton and Newton (1980)	1000
W_{gr}	-ndence ; at	" "	4047
W_s	700 °C	" "	1.5 cal/mol/K
W_{py}	AsmR	Perkins and Essene (1977)	1230 (2390)
W_{gr}		" "	4580 (1620)
W_{CaMg}	SmR, but with T	Hensen et. al. (1975)	7460
W_s	dependence	" "	4.3 cal/mol/K
W_{CaMg}	SmR	Jenkins and Newton (1979)	2020 (370)
"	SmR	Oka (1978)	1334
"	SmR	Wood and Nicholls (1978)	3000
W_{CaMg}	SmR with P-T	Powell (1978)	5671
W_s	dependence	" "	4.3 cal/mol/K
W_p		" "	100
W_{FeCa}	SmR ; at 1000 °C	Cressey et. al. (1978)	0
W_{FeCa}	SmR ; at 670 °C	Ganguly (1979)	678 (340)
"	SmR	Wood and Nicholls (1978)	-1000
"	SmR	Oka (1978)	1666
"	SmR	Ghent (1976)	-460 to 320
"	SmR	Wood (1975)	800
W_{FeMg}	SmR ; at 670 °C	Ganguly and Kennedy (1974)	2979 (369)
"	SmR ; at 670 °C	Ganguly (1979)	2710 (200)
"	SmR ; at 750 °C	Dahl (1980)	1509 (1392)
"	SmR	O'Neill and Wood (1979)	195 (430)
"	SmR ; at 825 °C	Saxena (1978)	2580
"	SmR ; at 550 °C	Oka and Matsumoto (1974)	2600
"	SmR	Wood and Nicholls (1978)	0

Table 3.1 cont.

PARAMETER	MODEL/CONDITION	REFERENCE	VALUE (cal/mol)
W_{FeMg}	SmR ; at 1100 °C and 50 kbar	Kawasaki and Matsui (1977)	2120 (690)
W_{FeMg}	SmR ; at 1100 °C normalised to 1 bar	"	804
$W_{CaMg} - W_{FeCa}$	SmR ; at 750 ° C	Dahl (1980)	2810 (954)
"	SmR ; at 670 ° C	Ganguly and Kennedy (1974)	4603 (2117)
"	SmR ; at 670 ° C	Ganguly (1979)	3152 (720)
"	SmR	O'Neill and Wood (1979)	2676 (201)
$W_{CaMg} - W_{FeCa} + W_{FeMg}$	SmR ; at 975 - 1050 ° C	THIS STUDY	2100 (200)
"	SmR, corrected for volume terms	THIS STUDY	2530 (200)
"	SmR, K_D data assumed	THIS STUDY	2450 (600)
W_{FeMg}		" "	0

Notes : (1) SmR.....symmetrical regular solution model used.
AsmR.....assymmetrical regular solution model used.

(2) figures in parentheses are standard errors in estimated parameter values.

(3) all W_{ij} values are applicable to a 4 Oxygen garnet formula i.e. (Ca,Mg,Fe) $Al_{2/3}Si\ O_4$.

3.3 THERMODYNAMIC CONSIDERATIONS - CFMAS

The introduction of Ca as an extra component in the experimental determination of Al_2O_3 solubility in orthopyroxene necessitates the expansion of activity-composition expressions for garnet and orthopyroxene (equations (5) and (16), Appendix 2).

Using the two-site regular solution modelling for orthopyroxenes (Chapter Two), the introduction of Ca will require the introduction of interaction parameters on the M2 site, W^{M2}_{CaFe} and W^{M2}_{CaMg}, assuming Ca does not occupy the M1 site, by analogy with clinopyroxenes (e.g., Herzberg, 1978). In addition, an exchange reaction of the type

$$MgMg + CaFe = CaMg + MgFe,$$

with a free energy of exchange designated as $\Delta\bar{G}^{o}_{CaMg}$, must be introduced to adequately account for reciprocal terms. In view of the very small quantities of Ca entering the orthopyroxenes under most conditions, all the above adjustments have been ignored in the analysis of CFMAS data.

We may treat garnet as either a ternary symmetric solid solution or a ternary assymmetric regular solution in Ca-Mg-Fe (section 3.2). The range of compositional data obtained in this study is not suitable for evaluation between the more sophisticated assymetric model and the symmetric regular solution model as the two models are virtually indistinguishable for all but very high X^{ga}_{Ca} contents (> .30).

In the CaO-FeO-MgO ternary system, by the regular solution model (Thompson, 1969):

$$3\,RT\ln\gamma^{ga}_{Mg} = 3\,(X^{ga}_{Fe})^2\,W^{ga}_{FeMg} + 3\,(X^{ga}_{Ca})^2\,W^{ga}_{CaMg} + 3\,X^{ga}_{Ca}\,X^{ga}_{Fe}\,(W^{ga}_{FeMg} + W^{ga}_{CaMg} - W^{ga}_{CaFe}) \qquad (1)$$

where $X^{ga}_{Fe} = Fe/Mg + Fe + Ca = (1 - X^{ga}_{Ca})\ (Fe/Fe + Mg)^{ga}$

defining $X^{ga}_{Ca} = Ca/Mg + Fe + Ca$, and $X^{ga}_{Ca} + X^{ga}_{Mg} + X^{ga}_{Fe} = 1$.

As we are considering the change in garnet activity with the addition of Ca to the FMAS system already modelled in Chapter Two, the first term on the right-hand side of equation (1) can be ignored and the Ca-effect on the activity coefficient of pyrope will be

$$\Delta 3\ RT\ \ln \gamma^{ga}_{Mg} = 3(X^{ga}_{Ca})^2\ W^{ga}_{CaMg} + 3\ X^{ga}_{Ca}\ X^{ga}_{Fe}\ (W^{ga}_{FeMg} + W^{ga}_{CaMg} - W^{ga}_{CaFe})$$

$$= 3\ X^{ga}_{Ca}\ (1 - X^{ga}_{Mg})\ W^{ga}_{CaMg} + 3\ X^{ga}_{Ca}\ X^{ga}_{Fe}\ (W^{ga}_{FeMg} - W^{ga}_{CaFe}) \qquad (2)$$

For *small* values of W^{ga}_{FeMg} and W^{ga}_{CaFe}, and if we choose a data set at near constant $(Mg/Mg + Fe)^{ga}$, expression (2) can be approximated by

$$-\Delta 3\ RT\ \ln \gamma^{ga}_{Mg} \simeq -3\ X^{ga}_{Ca}\ (1-X^{ga}_{Mg})[W^{ga}_{CaMg} + W^{ga}_{FeMg} - W^{ga}_{CaFe}]$$

$$\simeq -3\ X^{ga}_{Ca}\ \{1 - (1-X^{ga}_{Ca})(Mg/Mg+Fe)^{ga}\}$$

$$x\ (W^{ga}_{CaMg} - W^{ga}_{CaFe} + W^{ga}_{FeMg}) \qquad (3)$$

In Chapter Two, Fe-Mg garnet was treated as a single component with a mole fraction, X^{garnet}, equal to unity in equation 2(9). With the introduction of Ca into the system, the mole fraction of Fe-Mg garnet will be reduced by dilution:

$$(X^{garnet})^3 = (1 - X^{ga}_{Ca})^3 \qquad (4)$$

Fitting equations (3) and (4) into equation 2(5), with equation (3) being added to the non-ideal terms and expression (4) being incorporated as the denominator in the expression for K, the following condition governing the Al_2O_3 contents of orthopyroxene in equilibrium with garnet

in CFMAS is derived:

$$\Delta G^{o}_{1,T} + P\Delta V_r \simeq RT \ln \left\{ \frac{X^{opx}_{Al}\,(1 - X^{opx}_{Al})}{(1 - X^{ga}_{Ca})^3} \right\} + W^{Ml}_{FeAl}\,(1 - X^{opx}_{Al})(1 - 2X^{opx}_{Al})(1 - X^{opx}_{Mg}) - 3(W^{ga}_{CaMg} - W^{ga}_{CaFe})\,X^{ga}_{Ca}\left\{1 - (1 - X^{ga}_{Ca})\left(\frac{Mg}{Mg+Fe}\right)^{ga}\right\} \quad (5)$$

CFMAS experimental data on Al_2O_3 solubility may thus be analysed by comparison of equation (5) with equations 2(5) and 2(9) in the FMAS system, using W^{Ml}_{FeAl} (= 5157 cals) derived from FMAS experimental data. The parameter $(W^{ga}_{CaMg} - W^{ga}_{CaFe})$, with W^{ga}_{MgFe} assumed to be zero, is extracted from the CFMAS experimental data by a plot of

$$RT \ln \left\{ \frac{X^{opx}_{Al}(1-X^{opx}_{Al})}{(1 - X^{ga}_{Ca})^3} \right\} + 5157\,(1-X^{opx}_{Al})(1-2X^{opx}_{Al})(1-X^{opx}_{Mg}) - P\Delta V_r$$

versus

$$X^{ga}_{Ca}\left\{1 - (1-X^{ga}_{Ca})\left(\frac{Mg}{Mg+Fe}\right)^{ga}\right\} \quad \text{at constant temperature.}$$

CFMAS $K_{D\,Fe-Mg}^{ga-opx}$ CONSIDERATIONS

Assuming a symmetric regular solution model for Ca-Mg-Fe garnets in the compositional range $0 \leq X_{Ca} \leq .20$ we obtain (O'Neill and Wood, 1979):

$$RT \ln \gamma^{ga}_{Mg} = (X^{ga}_{Fe})^2 W^{ga}_{FeMg} + (X^{ga}_{Ca})^2 W^{ga}_{CaMg} + X^{ga}_{Ca} \cdot X^{ga}_{Fe}\,(W_{FeMg} + W_{CaMg} - W_{CaFe})$$

and similarly:

$$RT \ln \gamma_{Fe}^{ga} = (X_{Mg}^{ga})^2 W_{FeMg}^{ga} + (X_{Ca}^{ga})^2 W_{CaFe}^{ga} + X_{Ca}^{ga} \cdot X_{Mg}^{ga} (W_{FeMg} + W_{CaFe} - W_{CaMg}).$$

Thus, in CFMAS

$$RT \ln \left(\frac{\gamma_{Fe}^{ga}}{\gamma_{Mg}^{ga}} \right) = W_{FeMg} (X_{Mg}^{ga} - X_{Fe}^{ga}) + (W_{CaFe} - W_{CaMg}) X_{Ca}^{ga} \qquad (6)$$

where $X_{Mg}^{ga} = \frac{Mg}{Mg+Fe+Ca} = \left(\frac{Mg}{Mg+Fe}\right)(1 - X_{Ca})$,

Previously in FMAS it was found that (Chapter 2):

$$RT \ln \left(\frac{\gamma_{Fe}^{ga}}{\gamma_{Mg}^{ga}} \right) = \left\{ \left(\frac{Mg}{Mg+Fe}\right) - \left(\frac{Fe}{Mg+Fe}\right) \right\} W_{FeMg}^{ga} \qquad (7)$$

Thus, by comparison of (6) with (7):

$$\Delta RT \ln \left(\frac{\gamma_{Fe}^{ga}}{\gamma_{Mg}^{ga}} \right) = (W_{FeMg}^{ga} + W_{CaFe}^{ga} - W_{CaMg}^{ga}) \cdot X_{Ca}^{ga} \qquad (8)$$

At constant P, T and X_{Mg}, if the compositional effects on $K_{D_{Fe-Mg}}^{ga-opx}$ arise solely from interactions in the ternary garnet solid solution, then a plot of ($-RT \ln K_D$) versus X_{Ca}^{ga} will yield a straight line of slope ($W_{FeMg}^{ga} + W_{CaFe}^{ga} - W_{CaMg}^{ga}$).

Orthopyroxenes in equilibrium with Ca-bearing garnets will also contain a small amount of Calcium, largely confined to the M2 site. Experimentally produced orthopyroxenes in this study show a regular increase in $CaMgSi_2O_6$ component with X_{Ca}^{ga}, as there is no other Ca-bearing phase produced (e.g., clinopyroxene, plagioclase). Orthopyroxenes synthesised at 975°C abd 1050°C may contain up to 5 mol % $CaMgSi_2O_6$ (Appendix 2). Thus, the observed $K_{D_{Fe-Mg}}^{ga-opx}$ may be affected by Ca in orthopyroxene. To model this we can apply a ternary regular

solution model to the M2 site of the orthopyroxene:

$$RT \ln(\gamma_{Mg}^{M2}) = (X_{Fe}^{M2})^2 \cdot W_{FeMg}^{M2} + (X_{Ca})^2 W_{CaMg}^{M2} + X_{Fe}^{M2} X_{Ca}^{M2} (W_{FeMg}^{M2} + W_{CaMg}^{M2} - W_{CaFe}^{M2})$$

and

$$RT \ln(\gamma_{Fe}^{M2}) = (X_{Mg}^{M2})^2 \cdot W_{FeMg}^{M2} + (X_{Ca}^{M2})^2 W_{CaFe}^{M2} + X_{Mg}^{M2} \cdot X_{Ca}^{M2} (W_{FeMg}^{M2} + W_{CaMg}^{M2})$$

Thus

$$RT \ln\left(\frac{\gamma_{Mg}^{M2}}{\gamma_{Fe}^{M2}}\right) = W_{FeMg}^{M2} (X_{Fe}^{M2} - X_{Mg}^{M2}) + (W_{CaMg}^{M2} - W_{CaFe}^{M2}) X_{Ca}^{M2} \qquad (9)$$

Where $X_{Mg}^{M2} = (Mg/Mg+Fe+Ca)^{M2}$

The macroscopic orthopyroxene activity-composition relationship may also include a reciprocal term $\Delta\bar{G}^{o}_{CaMg}$ allowing for the cross-site effect of Calcium on the M1 site. The magnitude of this term is unknown.

Comparing equation (9) with the orthopyroxene M2 activity coefficent term in the FMAS system (equation A1.9), it is found that:

$$\Delta\tfrac{1}{2}RT \ln\left(\frac{\gamma_{Mg}^{M2}}{\gamma_{Mg}^{M1}}\right) \simeq \tfrac{1}{2}(W_{FeMg}^{M2} + W_{CaMg}^{M2} - W_{CaFe}^{M2}) X_{Ca}^{opx} \qquad (10)$$

As discussed in Appendix One, W_{MgFe}^{M2} is small, and positive ($\simeq$ 600 cal). Values of W_{CaMg}^{M2} and W_{CaFe}^{M2} have been derived from natural rock data (Saxena, 1976) and calorimetric measurements (Holland, Navrotsky and Newton, 1979). Using the values

$$W_{CaMg}^{M2} \simeq 8000 \text{ cal}$$
$$W_{CaFe}^{M2} \simeq 5000 \text{ cal}$$

(Table A1.2), the coefficient $\frac{1}{2}(W^{M2}_{FeMg} + W^{M2}_{CaMg} + W^{M2}_{CaFe})$ is in the range 1500-1800 cal. The garnet interaction parameter term in equation (8) is at least -2000 cal, derived from the X^{opx}_{Al} data, and in all cases $X^{ga}_{Ca} >> X^{opx}_{Ca}$. Given these values for the non-ideal contributions arising from garnet and orthopyroxene, it can be seen that the net effect of (8) and (10) will be a smaller compositional dependence of $K_D{}^{ga\text{-}opx}_{Fe\text{-}Mg}$ in CFMAS than predicted by considering garnet solid solution properties only. Conversely, in ignoring the orthopyroxene contribution we may derive a value of $(W^{ga}_{CaFe} - W^{ga}_{CaMg})$ which is small in comparison with other workers' data obtained from garnet-olivine exchange (O'Neill and Wood, 1979) or calorimetry. This conclusion, however, ignores the possible effects of $\Delta\bar{G}^{o}_{CaMg}$. This exchange term may cancel out the other orthopyroxene effects, but the size and sign of this term are unknown. For simplicity, the experimental data have been reduced according to euqation (11) below, and the possible effects of Ca in orthopyroxene are ignored:

$$RT \ln K = RT \ln K_D + \tfrac{1}{2}X^{opx}_{Al}(W^{M1}_{MgAl} - W^{M1}_{FeAl}) + (1-2X^{opx}_{Mg})W^{opx}_{FeMg} + (W^{ga}_{FeMg} + W^{ga}_{CaFe} - W^{ga}_{CaMg})\, X^{ga}_{Ca} \qquad (11)$$

where $X_{Mg} = (Mg/Mg+Fe)$, and $W^{opx}_{FeMg} \simeq \frac{1}{2}(W^{M1}_{FeMg} + W^{M2}_{FeMg})$.

The more complete form of this equation is:

$$RT \ln K = RT \ln K_D + W^{ga}_{FeMg}(X^{ga}_{Mg} - X^{ga}_{Fe}) + (W^{ga}_{FeMg} + W^{ga}_{CaFe} - W^{ga}_{CaMg})\, X^{ga}_{Ca} + (1-2X^{opx}_{Mg})\, W^{opx}_{FeMg} + \tfrac{1}{2}X^{M1}_{Al}\,(W^{M1}_{MgAl} - W^{M1}_{FeAl}) + \tfrac{1}{2}X^{opx}_{Ca}(W^{M2}_{CaMg} - W^{M2}_{CaFe}) + \tfrac{1}{2}\Delta\bar{G}^{o}_{CaMg}\, X^{M2}_{Ca}(1-X_{Al})(1-2X^{opx}_{Mg})$$

Thus, we are basically assuming equal site occupancy ratios for Mg-Fe

in orthopyroxenes and the condition

$$W^{M2}_{CaMg} - W^{M2}_{CaFe} + (1-2X^{opx}_{Mg})\,[W^{opx}_{FeMg} + \Delta\bar{G}^{o}_{CaMg}\,(1-X_{Al})] \simeq 0$$

in applying equation (11).

3.4 EXPERIMENTAL TECHNIQUES

Experiments have been performed in a piston cylinder apparatus, as described in Chapter Two. All runs except T779 (975°C, 10 kb) used multibore graphite capsules sealed in noble metal outer capsules (Chapter Two). Run conditions are listed in Table 3.3 and experimental procedures are those outlined in Chapter Two.

(1) STARTING MIXES

Two sets of glasses have been prepared from analytical grade CaO, MgO, Al_2O_3, SiO_2 and Fe_2O_3or Fe_2O_3-Fe reagents. All oxides were ground thoroughly in an agate mortar under acetone and the powders then pelletised and fired in air at 900°C to produce oxidised but anhydrous powders.

(a) High pressure synthesised glasses

Three mixes of constant X_{Mg}^{bulk} =.50 and varying X_{Ca}^{bulk} (= 2, 4 and 8) were prepared and run at 1450°C and 10 kbar in large diameter graphite capsules. Analyses of resultant glasses are presented in Table 3.2. Pale to medium green quench-free glasses resulted. Raman spectra of one of these glasses indicated the presence of dissolved CO_2. This dissolved CO_2 phase has acted as a flux in experiments where these mixes have been used, resulting in minor or extensive melting of some charges at 1150°C and 1050°C.

(b) One atmosphere glasses

Three mixes of nominal X_{Mg}^{bulk} =.50 and X_{Ca}^{bulk} = 2, 4, and 8 respectively, have been prepared using analytical grade oxides and additional Fe^{metal}. Fe_2O_3+ Fe^{metal} have been added in these mixes and the mixes fired in an Argon-atmosphere furnace to produce FeO stoichiometrically:

$$Fe_2O_3 + Fe = 3Fe\ O$$

In this type of preparation pelletised oxides plus Fe powder were loaded into platinum buckets and run in a one atmosphere furnace at 1300°C, under an Argon atmosphere, for up to two hours. Green glasses with minor liquidus quartz crystals resulted. These glasses are essentially anhydrous and free of dissolved CO_2. Runs performed using these mixes are usually free of melt and of much finer grainsize than those performed using mixes of type (a). Analyses of these one-atmosphere glasses are presented in Table 3.2.

Both glass types (a) and (b) were seeded with 7% wt almandine seeds previously synthesised for FMAS experiments (Chapter 2). These seeded glass mixes were then used in the experimental programme to determine Al_2O_3 contents of orthopyroxene in equilibrium with garnet in CFMAS.

Table 3.2 COMPOSITIONS OF GLASS STARTING MIXES USED IN CFMAS

	M50C2 1 atm.	M50C4 1 atm.	M50C8 1 atm.	M50C2 hi. P	M50C4 hi. P	M50C8 hi. P
SiO_2	55.64	54.82	53.40	56.60	55.83	53.84
Al_2O_3	11.00	10.44	10.20	10.08	10.24	10.32
FeO	20.02	20.71	21.29	19.85	20.11	20.95
MgO	12.54	12.62	12.03	12.38	11.97	11.77
CaO	0.80	1.41	2.80	0.65	1.27	2.68
X_{Mg}	52.75	52.07	50.19	52.62	51.44	50.04
Ca/ Ca+Mg+Fe	2.35	4.01	7.73	1.95	3.77	7.56
$\frac{1}{2}$Al/ $\frac{1}{2}$Al+Fe+Mg	15.46	14.55	14.40	14.48	14.82	14.77

3.5 RUN PRODUCTS - CFMAS

Analytical data and comments on products from individual runs are presented in Table 3.3. The analytical data for orthopyroxene and garnet are averaged values, or selected values based on zoning directions established in individual grains where relict seeds remain. Complete experimental data for each run are plotted on Al_2O_3-FeO-MgO and Ca-Mg-Fe diagrams presented in Appendix Two.

Experimental run conditions for the CFMAS experiments are in the P-T range 17.5 - 10 kbar and 1050°C - 975°C. These conditions have been chosen under the constraints that:

(a) Al_2O_3 contents in orthopyroxenes in FMAS are sufficiently high so that any effects of Ca will be detectable and significantly larger than analytical scatter;

(b) melting is avoided or limited;

(c) graphite capsules could be used, to avoid Fe addition into the charges.

These three constraints effectively rule out low temperature runs, where high Al_2O_3 contents are possible only at low pressures where Fe capsules are necessary. Melting, and the consequent loss of garnet, has been found to occur in runs at 1150°C and 12.5 kb in these quartz-bearing compositions, and thus most runs have been performed below this temperature.

(1) PRODUCTS IN HIGH-PRESSURE GLASS TYPE MIXES

(i.e., CO_3^{2-} present in initial glasses)

Generally, coarse (20 μm - 100 μm) subhedral prismatic orthopyroxene and subhedral to euhedral garnet have been produced in runs performed with these mixes. Lobate and ovoid quartz often occurs as

inclusions in strongly poikiloblastic garnets, or as free grains. In all runs, an Fe- and Ca- rich melt fraction has been produced. At high temperatures (T741 - 1150°C, 12.5 kbar; and T740 - 1050°C, 12.5 kb) abundant melting has occurred, garnet has been consumed, and euhedral to subhedral, very coarse (to 200 μm) orthopyroxenes have resulted. Often, these orthopyroxenes form a cumulate area segregated from most of the melt. Quench runs, spikes and feathery orthopyroxenes have grown on the coarse euhedral and form a spinifex textured network in some quenched melts (plate 2.2).

In other runs at 1050°C and at 975°C, garnet remains as coarse grains with orthopyroxene plus quartz in areas with minor melt phase. These crystalline areas are often separated from melt areas which in these runs constitute 10% to 50% of the sample area (Table 3.4).

The presence of abundant melt has important effects on the experimental results. The melts formed are usually very aluminous (A/AFM = 0.27); more iron-rich than the garnet; and, significantly, highly calcic. The production of such melts and segregation of them from the crystallising phases, lowers the maximum possible grossular contents in the garnets at a constant bulk composition. Hence, the spread in X_{Ca}^{ga} contents in different X_{Ca}^{bulk} mixes of this type is only small (X_{Ca}^{ga} = .010 to .040), and as a consequence the Ca-dependence of X_{Al}^{opx} is difficult to ascertain from these data alone.

In addition, the production of a significant melt fraction causes the garnet and orthopyroxene compositions to lie to the Mg-rich side of the hypothetical opx-bulk-garnet tie line of a melt free system. Thus $K_{D_{Fe-Mg}}^{ga-opx}$ cannot be as well constrained in the melt-bearing runs.

Garnets formed in these mixes zone from almandine seed

compositions to Mg-, Ca- richer runs. Broad core regions (≤ 20 μm) are often surrounded by poikiloblastic rims characterised by ovoid quartz inclusions and a sharp increase in X_{Ca}^{ga} and X_{Mg}^{ga}. Some scatter in X_{Ca}^{ga} occurs within these rim regions (see Appendix Two).

Orthopyroxenes show zoning to lower Al_2O_3 contents towards their rims, accompanied by a decrease in CaO contents. Quench rims on orthopyroxene, and quench grains within melt, are highly aluminous and often variable in CaO.

(2) PRODUCTS IN 1-ATMOSPHERE GLASS MIXES

(i.e., glasses without CO_3^{2-})

Apart from runs at 1200°C (T820, T821), where up to 20% of spinifex textured melt fraction occurs, run products from this mix type are homogeneously textured granoblastic polygonal garnet, orthopyroxene and lobate quartz. Grainsizes in these products are usually 10 μm - 20 μm, much finer than produced from the CO_3^{2-}-bearing glasses.

Relict almandine cores are common in all runs. These are rimmed by more Mg- and Ca- rich rims which are often strongly zoned. Fine garnets without almandine cores and without apparent chemical zoning are interstitial to coarser garnet and orthopyroxene.

Orthopyroxenes are usually subhedral to anhedral, and consistently zone from high Al_2O_3 (and often high CaO) cores to lower Al_2O_3 and CaO rims. Zoning in orthopyroxenes in T779 (10 kbar, 975°C) is extreme and renders this run less reliable than other, more homogeneous, runs in the formulation of equations governing X_{Al}^{opx} in CFMAS.

In the absence of melt, the range in X_{Ca}^{ga} achieved using mixes of different X_{Ca}^{bulk} is greatly enhanced (X_{Ca}^{ga} = .030 to .140), and as

a consequence the effects of Ca on X_{Al}^{opx} and $K_{D_{Fe-Mg}}^{ga-opx}$ can be more adequately ascertained. It should still be noted, however, that the parameters derived from these data will strictly apply only to low-grossular garnets. Commonly, garnets in both ultramafic and granulite garnet-orthopyroxene assemblages contain less than 22 mol % grossular. Thus, despite the limited X_{Ca}^{ga} range of the experimental data, the derived parameters are applicable, with very little extrapolation, to all garnet-orthopyroxene assemblages but may not be applicable to grossular-rich garnet of corundum eclogites, kyanite eclogites or grosspydites.

TABLE 3.3 CFMAS EXPERIMENTAL RUN DETAILS

P Equation kbar	Run	P kbar	T °K	Capsule	Mix	X^{opx}_{Al}	X^{opx}_{Mg}	X^{ga}_{Mg}	X^{ga}_{Ca}	Time (hours)	Melt	Texture Comments	General Comments	K_D
23.1	T821	30	1473	C in Pt	mineral mix	.077 (.002)	.5811 (.004)	.4518 (.010)	.0339	53.5	present	coarse subhedral ga and opx, melt common.	elongate deformed bores, melt generated and segregated and contains spinifex textured quench. Cracks between bores allowed passage of Ca.	1.683
22.9					M50C8	.080 (.003)	.5932 (.004)	.4593 (.010)	.0331		present	very coarse, to 100μm subhed. poik. ga and opx.		1.717
22.2	T820	25	1473	C in Pt	M50C8	.082 (.003)	.6080 (.003)	.4843 (.009)	.0684	54.3	present	very coarse granuloblastic ga+opx, some melt.	elongate bore, melt segregated and quench crystals + rims form.	1.652
	T741	12.5	1423	C in $Ag_{50}Pd_{50}$	M50C2 M50C4 M50C8					95.5	present in all, segregated	ga did not form; resorbed in all bores, low Al opx plus melt plus quench crystals present. Strong zoning	Silicic acid added to provide water, resulted in widespread melting so hiCa, Al melt formed at expense of garnet. Bulk composition Fe loss.	
16.8	T749	17.5	1323	C in $Ag_{75}Pd_{25}$	M50C4	.091 (.004)	.635 (.005)	.479 (.008)	.0131	188	present X_{Mg} = .38 X_{Ca} = .08	coarse granuloblastic, opx abundant, ga rare, melt segregated + round qz.	Zoning in opx to lower X_{Al} rims. Half of bore is melt + qz separated from ga+opx+qz.	1.892
15.5	T754	17.5	1323	C in $Ag_{75}Pd_{25}$	M50C2	.097 (.007)	.592 (.004)	.452 (.007)	.010	236	present X_{Mg} = .24	very coarse ga+opx, common melt+qz segregated.	Cracks occur in graphite capsule. Bores elongate, ellipsoidal.	1.758
17.0					M50C8	.082 (.004)	.618 (.003)	.463 (.005)	.037		present X_{Ca} =.23 X_{Mg} =.29	abundant melt separated from coarse granuloblastic ga+opx		1.876
13.5	T774	15	1323	C in $Ag_{75}Pd_{25}$	M50C2 atm glass	.112 (.006)	.5945 (.004)	.4574 (.003)	.029	197.5		homogeneous moderate (10-20μm) grainsize ga+opx+qz polygonal granoblastic in all bores	Two bores (C4 and C2) elongate deformed. No melt. Some Ca occurs in opx in equilibrium with garnet	1.739
13.7					M50C4 atm glass	.100 (.004)	.5810 (.002)	.4362 (.005)	.059					1.792
13.9					M50C8 atm glass	.084 (.004)	.5717 (.007)	.4218 (.005)	.122					1.830
	T740	12.5	1323	C in $Ag_{50}Pd_{50}$	M50C2 M50C4 M50C8					170	abundant	very coarse subhedral opx with melts; Fe loss in bulks	Silicic acid added for water. Very elongate deformed bores. Fe-Ca rich segregated melts abundant	

13.6	T760	15	1248	C in $Ag_{75}Pd_{25}$	M50C4	.086 (.004)	.5959 (.003)	.4330 (.010)	.015	385	X_{Mg} =.35 X_{Ca} =.10	coarse polygonal ga+ opx,ga rare; melt common	Bores deformed into cuspate shapes, melts segregrated from grains	1.854
14.6					M50C8	.074 (.003)	.5963 (.004)	.4250 (.003)	.042		X_{Mg} =.35 X_{Ca} =.155	very coarse euhedral opx, minor ga and abundant melt		1.974
14.0	T785	15	1248	C in $Ag_{75}Pd_{25}$	M50C2 atm glass	.082 (.002)	.6132 (.002)	.4514 (.004)	.035	455		homogeneous granulo-blastic ga+opx+qz fine grained.	Bores slightly deformed (C4 and C8).Relict alm cores common; zoned ga; no melt; late finer garnets; opx zoned in X_{Al} and mostly low X_{Al} ones analysed.	1.927
15.6					M50C4 atm glass	.067 (.003)	.6147 (.002)	.4405 (.005)	.063			"		2.026
15.2					M50C8 atm glass	.058 (.002)	.5981 (.003)	.4097 (.005)	.140			"		2.144
11.2	T743	12.5	1248	C in $Ag_{50}Pd_{50}$	M50C2	.109 (.010)	.5832 (.005)	.4239 (.008)	.011	362	minor	fine granuloblastic, poik.ga	Some silicic acid added. Elongate deformed bores. Mixes have lost Ca to melt in cracks and margins of bores.	1.902
11.6					M50C4	.107 (.005)	.6028 (.005)	.4298 (.007)	.015			fine granuloblastic polyg,subhedral, interstitial ga.		2.015
12.0	T743	12.5	1248	C in $Ag_{50}Pd_{50}$	M50C8	.105 (.003)	.6058 (.008)	.4304 (.011)	.0312			fine granuloblastic opx, poik.ga:to subhedral.		2.034
12.0	T786	12.5	1248	C in $Ag_{75}Pd_{25}$	M50C2 1 atm	.100 (.005)	.6025 (.004)	.4525 (.001)	.029	383		fine grained granulo-blastic homogeneous textures in all mixes.	Elongate deformed bores, no cracks between. Relict Alm cores occur and opx zones high X_{Al} (cores) to low X_{Al} (rims). Ga-opx intergrowths occur	1.834
12.1					M50C4 1 atm	.090 (.008)	.6013 (.004)	.4451 (.003)	.070					1.880
11.6					M50C8 1 atm	.081 (.002)	.5857 (.005)	.4043 (.008)	.134					2.083
9.0	T779	10	1248	Fe in $Ag_{75}Pd_{25}$	M50C2 1 atm	.135 (.008)	.5877 (.003)	.4358 (.009)	.040	362		fine granuloblastic, common relict almandine	Fe globules on edge of bores only. Bores undeformed.Relict ga cores common, ga strongly zoned in X_{Mg}. Opx very strongly zoned in X_{Al}^{opx} and interpre-tation subjective. High Al Ca opx phase common relict. Poor equilibrium, strong zoning in X_{Al}^{opx}.	1.845
10.2					M50C4 1 atm	.109 (.005)	.5792 (.005)	.4150	.060					1.940
11.2					M50C8 1 atm	.088 (.010)	.5555 (.005)	.3726	.091			opx fine equigranular prismatic, ga irregul-ar ragged relict ga seeds in very fine grained ga+opx+qz. Xenoblastic opx.		2.104
8.4	T857	7.5	1173	C in Pt	M50C8 1 atm	.083 (.010)	.545 (.007)	.366	.052	465				2.08

NUMBERS IN PARENTHESES ARE THE STANDARD DEVIATIONS FROM THE LISTED VALUES.

Table 3.4 COMPOSITIONS OF MELTS GENERATED IN CFMAS EXPERIMENTS.

	T821	T820	T749	T753			T760		T743	
SiO_2	54.74	50.52	50.74	53.69	54.21	52.41	55.11	54.46	54.92	54.32
Al_2O_3	10.69	10.88	16.17	16.80	16.77	16.33	16.23	15.72	16.67	16.35
FeO	23.90	24.83	22.44	21.34	18.01	19.64	18.78	19.07	17.35	18.95
MgO	6.62	8.89	7.72	4.56	4.06	5.77	5.45	5.50	5.79	5.82
CaO	3.12	4.10	2.44	2.85	5.95	5.29	3.03	4.26	3.63	2.98
TOTAL	91.77	101.75	83.48	77.58	83.00	84.76	78.34	82.62	80.77	80.48
X_{Mg}	33.06	38.98	38.04	27.52	28.74	34.36	34.10	33.90	37.30	35.40
X_{Ca}	10.07	11.42	7.95	11.04	23.19	18.40	12.00	15.90	14.40	11.50
X_{Al}	17.43	15.87	23.94	28.65	31.90	27.80	28.70	27.70	29.80	28.21

3.6 ANALYSIS OF RESULTS

(1) SOLUBILITY OF Al_2O_3 IN ORTHOPYROXENE COEXISTING WITH GARNET AND QUARTZ IN CFMAS.

The effect of X_{Ca}^{ga} on X_{Al}^{opx} (= Al/2) is illustrated in figure 3.1 (a) and (b), for various pressures at the temperatures 975°C, 1050°C and 1200°C. At approximately constant X_{Mg}^{opx}, an increase in the grossular content of garnet will result in a decrease in X_{Al} of the coexisting orthopyroxene.

This data has been analysed following equation 3(5) above, based on a ternary regular solution model for garnet and ignoring the effects of calcium in orthopyroxene. In figure 3.2, $-\Delta G$ has been plotted against the parameter $X_{Ca}^{ga}\{1 - (1-X_{Ca}^{ga})(Mg/Mg+Fe)\}$ following equation (5), for 975°C and 1050°C data. Within the error of measurement, the data can be fitted to parallel lines of constant slope $3(W_{CaMg}^{ga} - W_{CaFe}^{ga} + W_{FeMg}^{ga})$. Regression fits to the data, honouring the error bars on all points, yield slopes of 6300 ± 300, which yields a value of

$$W_{CaMg}^{ga} - W_{CaFe}^{ga} + W_{FeMg}^{ga} = 2100 \pm 200 \text{ cals}$$

In this fit to the data, $\Delta G_{1,T}^{o}$ is expressed as

$$\Delta G_{1,T}^{o} = RT \ln \left\{ \frac{X_{Al}^{opx}(1 - X_{Al}^{opx})}{(1 - X_{Ca}^{ga})^3} \right\} - P\Delta V_r + 5157\,(1 - X_{Al}^{opx})(1 - 2X_{Al}^{opx})(1 - X_{Mg}^{opx}) \qquad (12)$$

where ΔV_r is the volume change of reaction using partial molar volume expressions for enstatite and Mg-tschermak in orthopyroxene, and $5157 = W_{FeAl}^{opx}$ derived from FMAS data (Chapter 2).

An alternative regression in which ΔV_r is modified to include

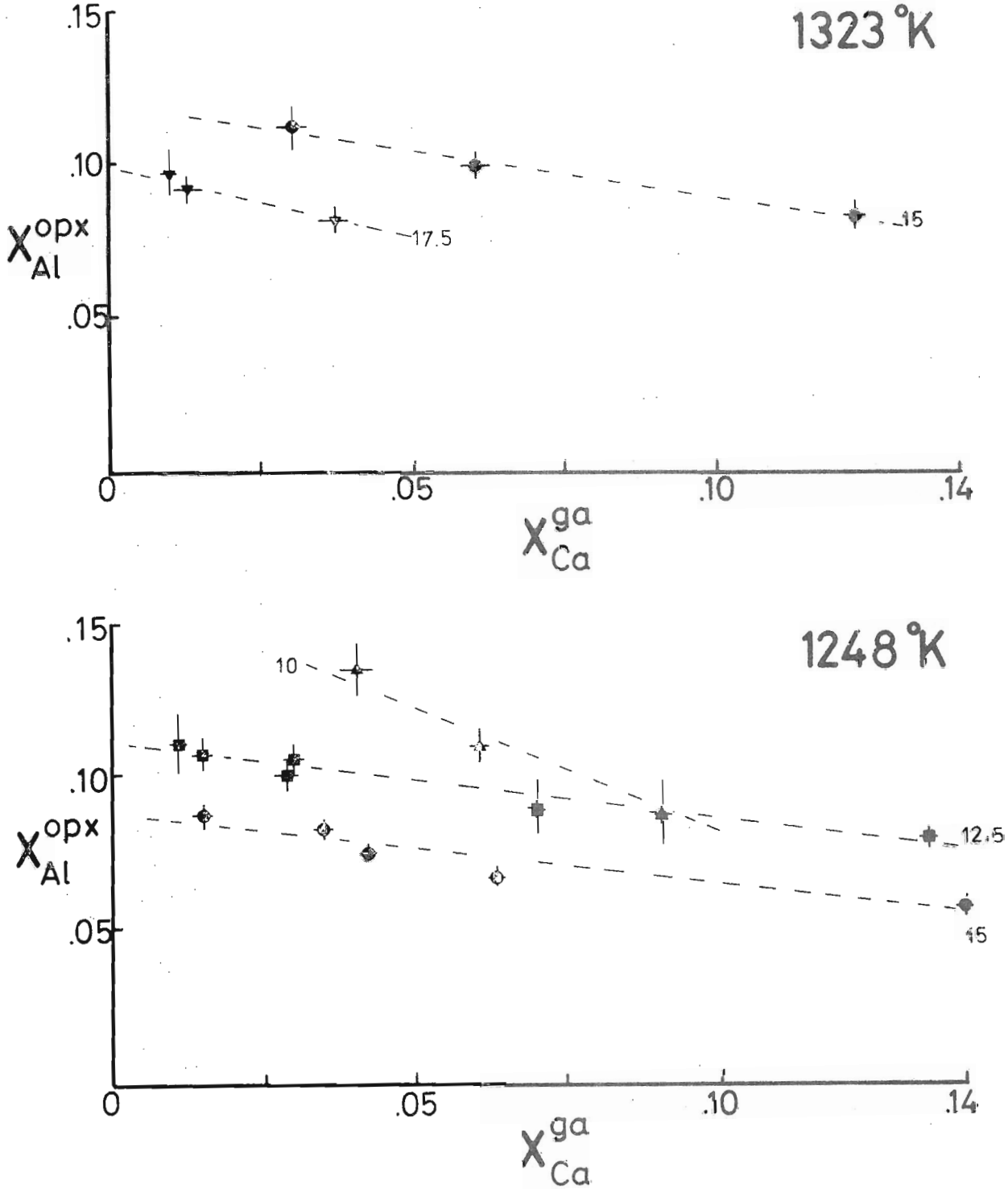

Fig. 3.1 Alumina contents of experimental orthopyroxenes (X^{opx}_{Al} = Al/2) plotted against X^{ga}_{Ca} (Ca/Ca+Mg+Fe) of coexisting garnets for CFMAS data at 1323 °K and 1248 °K. Small numbers refer to pressures in kbar, and dashed lines join isobaric data points. Symbols : ▲ 10 ■ 12.5 ● 15 ▽ 17.5 kbar.

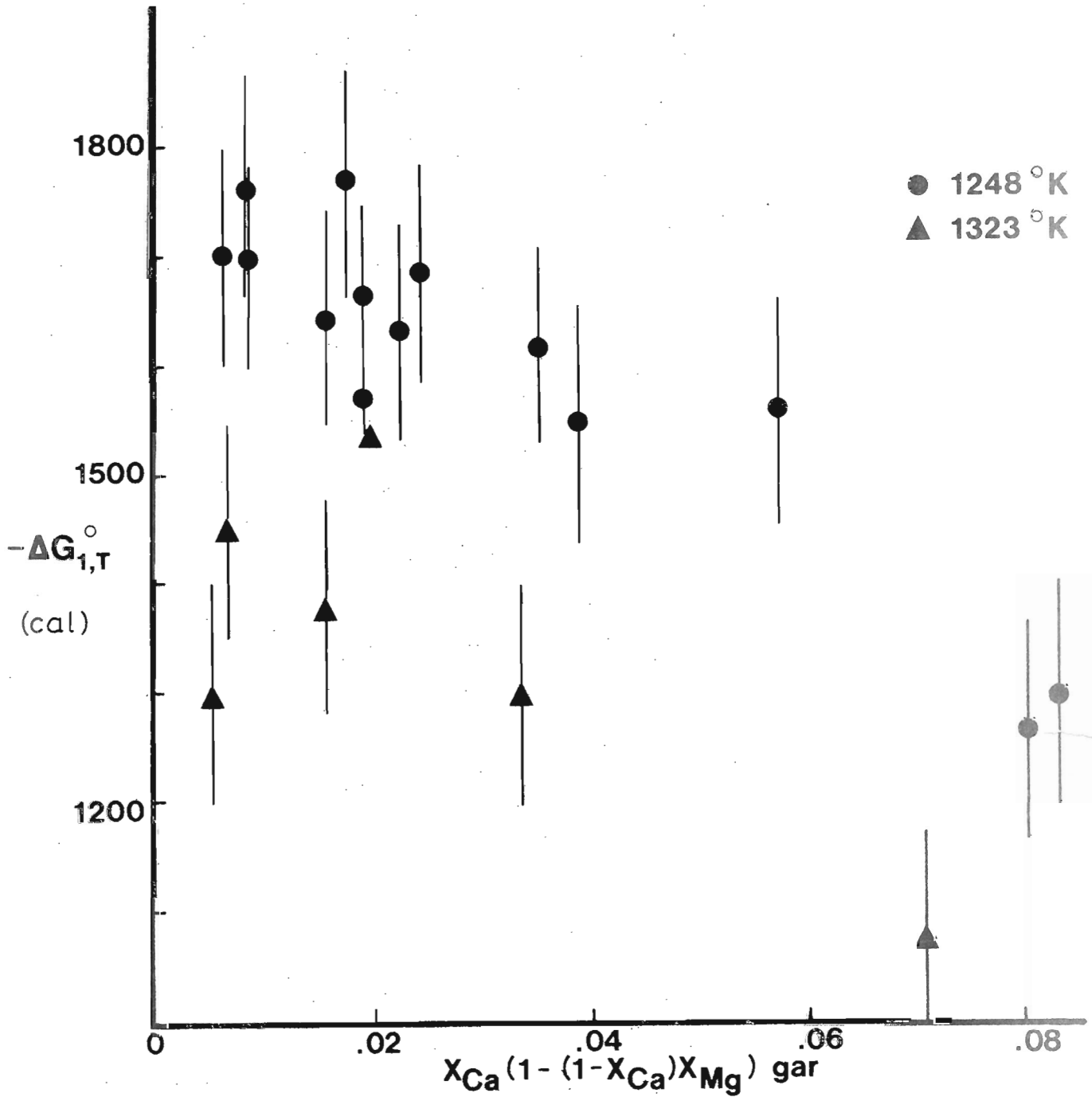

Fig 3.2 Plot of $-\Delta G^{\circ}_{1,T}$ against $X_{Ca}\left\{1-(1-X_{Ca})X_{Mg}\right\}^{ga}$, where $-\Delta G^{\circ}_{1,T}$ is defined as in text (equation 3(12)). Slopes of regression lines to isothermal data sets give values of a net interaction parameter, $W^{ga}_{CaMg} - W^{ga}_{CaFe} + W^{ga}_{FeMg}$.

the partial molar volume of pyrope in grossular-pyrope solid solutions, has been performed to allow comparisons with a-X data of Haselton and Newton (1980). As the molar volume curves on the Py-Gr and the Alm-Gr joins are similar (Cressey *et al.*, 1978), this correction should be applicable to the garnets produced here. Using the volume relation of Haselton and Newton (1980) for py-gr garnets:

$$(\overline{V} - V^{o})_{pyrope} = .765 = .512\ X_{py}^{ga}\ (2-X_{py}) = 5.036$$

$$(.083 - Z + ZX_{py})\ \exp\{\frac{-Z^2}{2}\} \qquad (13)$$

in cm^3, where $Z = (X_{py} - .940)/.083$.

For application to this CFMAS data, we replace X_{py} by $(1-X_{Ca})^{ga}$ and convert the volume change to cals $kbar^{-1}$ (cm^3 x 23.90057).

Inclusion of this volume term produces $\Delta\overline{V}_r = \overline{V}_{py} - \overline{V}_{En} - V_{MgTs}$ such that ΔV_r = function $(X_{Ca}^{ga}, X_{Al}^{opx})$. Recalculated values of $-\Delta G^{o}_{1,T}$ with this term are plotted against the X_{Ca}^{ga} parameter in figure 3.3. The regressed slopes for this recalculated data are -7600 ± 300, giving a value of

$$W_{CaMg}^{ga} - W_{CaFe}^{ga} + W_{FeMg}^{ga} = 2530 \pm 200 \text{ cals}$$

Considering the magnitude of this volume correction on the eventual estimate of $(W_{CaMg} - W_{CaFe} + W_{Fe\ Mg})^{ga}$, the expression for ΔV_r excluding the correction of V_{pyrope}, and the resultant interaction parameter coefficient of 2100 cals will be used in the subsequent development of this geobarometer. The value of 2530 cals for $(W_{CaMg} - W_{CaFe} + W_{Fe\ Mg})$ may more closely approximate the true value of this parameter, and is thus considered to be useful as an input into other reaction equilibria. With the assumption that $W_{FeMg}^{ga} \simeq 0$;

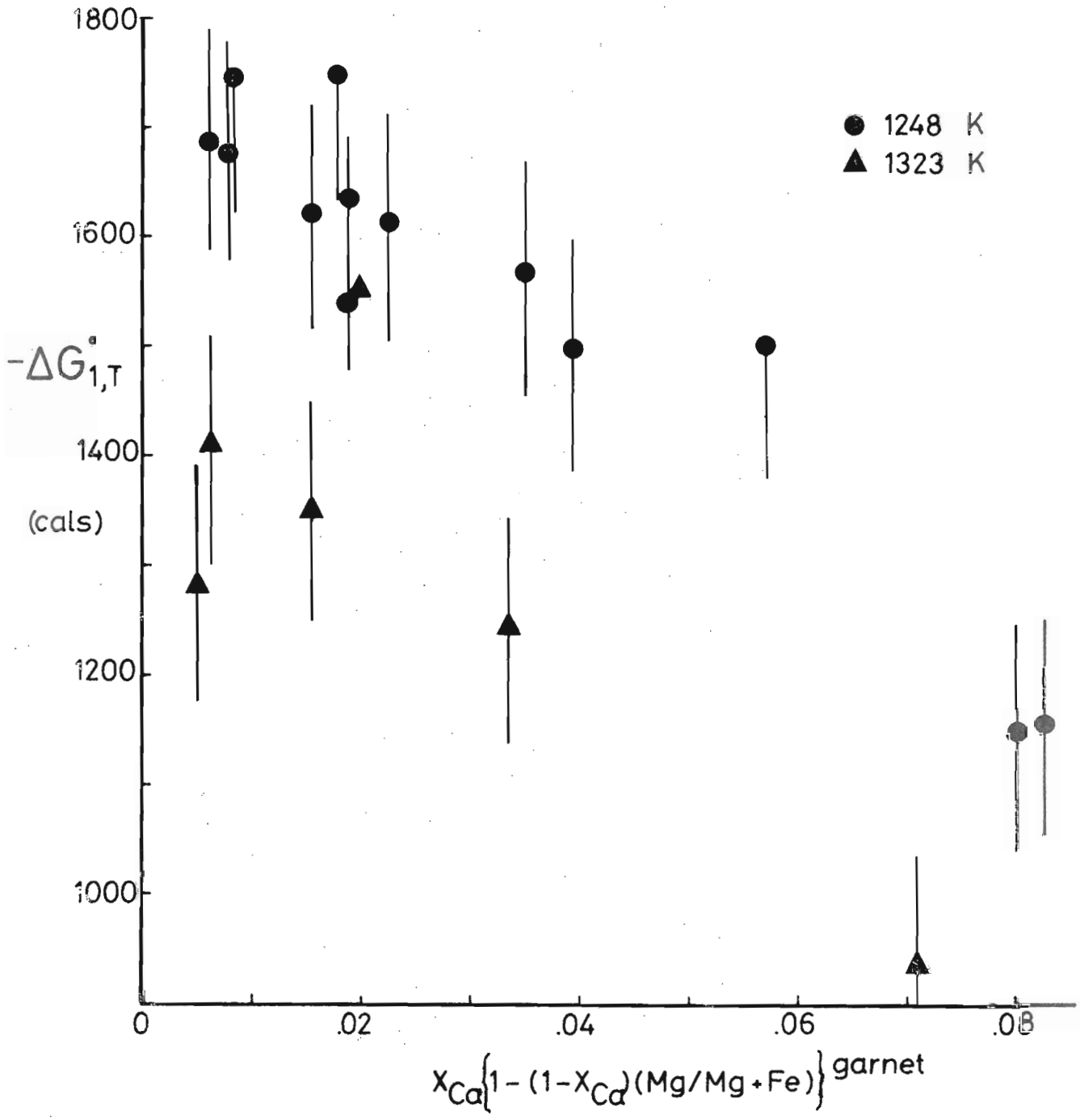

Fig 3.3 As for figure 3.2 except that the $-\Delta G^{\circ}_{1,T}$ term has been adjusted with the partial molar volume terms of Haselton and Newton (1980).

$(W^{ga}_{CaMg} - W^{ga}_{CaFe}) \simeq 2500 \pm 200$, which is in excellent agreement with the data of O'Neill and Wood (1979), Jenkins and Newton (1979) and Dahl (1980); and in good agreement with the value of Ganguly (1979).

Comparison of the best-fit lines to the CFMAS data at 1050°C and 957°C indicates an entropy change of the reaction of about -3.7 ± 1.6 cals K^{-1} mol^{-1}. As a result of the large errors on the data (± 100 cal at least) in relation to the small temperature interval, a more precise ΔS value cannot be obtained. The ΔS value obtained from FMAS experimental data, $-2.93 \pm .30$ cals K^{-1} mol^{-1}, is in agreement with the crude estimate obtainable from the CFMAS data, and thus the agreement between the two data sets is quite good.

In order to develop a geobarometer applicable to garnet-orthopyroxene ± quartz parageneses in the system CaO-MgO-FeO-Al_2O_3-SiO_2, the term

$$-3\, X^{ga}_{Ca} \{1 - (1-X^{ga}_{Ca})(Mg/Mg+Fe)^{ga}\} (W^{ga}_{CaMg} - W^{ga}_{CaFe} + W^{ga}_{FeMg})$$

$$= -6300\ (\pm 300) \times [X^{ga}_{Ca} (1-(1-X^{ga}_{Ca})(Mg/Mg+Fe)^{ga})]$$

is added to the numerator in the FMAS equation (9), where

$$\Delta S = -2.93 \pm .30 \text{ cals } K^{-1} \text{ Mol}^{-1}$$

$$\Delta H = -5650 \pm 250 \text{ cals mol}^{-1}$$

$$W^{opx}_{FeAl} = 5157 \pm 200 \text{ cals mol}^{-1}$$

Thus:

$$P_3(\text{kbar}) = -\frac{1}{\Delta V_r}\Big\{ (R \ln K_3 - 2.93)T + 5650 + 5157\,(1-X^{opx}_{Al})(1-2X^{opx}_{Al})(1-X^{opx}_{Mg}) - 6300\, X^{ga}_{Ca}\,(1 - (1-X^{ga}_{Ca})(\frac{Mg}{Mg+Fe})^{ga})\Big\} \qquad (15)$$

where

$$K = X_{Al}^{opx}\,(1 - X_{Al}^{opx}) / (1 - X_{Ca}^{ga})^3 \qquad \text{from 3(5);}$$

$$-\Delta V_r = 183.3 + 178.98\, X_{Al}^{opx}\,(1 - X_{Al}^{opx})\ ;$$

$$X_{Ca}^{ga} = (Ca/Ca + Mg + Fe)^{ga},\ X_{Mg}^{opx} = (Mg/Mg+Fe)^{opx}$$

$$X_{Al}^{opx} = Al/2 \text{ in low-Cr, } Fe^{3+} \text{ orthopyroxene}$$

and T is in degrees Kelvin.

Major limitations to equation (15) above will arise in the following circumstances:

(a) where Fe^{3+} contents are high in the orthopyroxenes, X_{Al} will no longer be Al/2 as an ($Fe^{3+}Al$) molecule occurs (Arima, 1978). In these cases, the $Fe^{3+}Al$ (ferritschermaks) molecule may be extracted first and then $M^{2+}Al$ (tschermaks) molecule calculated for use in (15):

$$X_{Al}^{opx} = \tfrac{1}{2}(Al^{total} - Fe^{3+})$$

As equation (15) is written, this calculation will result in an increase in P estimate, by reducing the numerator in the ln K term. The occupancy of the Al-site in the garnet by Fe^{3+} must also be considered. Using equation 2.9, the K expression may now be written as

$$K = \frac{X_{Al}^{opx}\,(1 - X_{Al}^{opx})}{(1-X_{Ca}^{ga})^3(1-X_{Fe3+}^{ga})^2}\ ,$$

where $X_{Fe3+}^{ga} = (Fe^{3+}/Fe^{3+} + Al)^{ga}$. With this expression, the denominator is also reduced and hence estimated pressure will be lowered and similar, in many cases where Fe^{3+} is only moderate ($X_{Fe3+}^{ga} < .05$), to P(15). At higher Fe^{3+} contents, other reciprocal and non-ideal on-site mixing terms may arise in the garnet. These terms are, as yet, not constrained by any experimental data.

(b) Where Cr^{3+} contents of garnets and orthopyroxenes are significant, as is the situation in many garnet peridotite inclusions in Kimberlite, the ($Cr^{3+}Al$) molecule in orthopyroxene may need to be accounted for in a similar way to the ($Fe^{3+}Al$) molecule. Garnets with appreciable Cr^{3+} contents must be modelled using more complex multi-site mixing solutions involving reciprocal terms and both $Mg_3Cr_2^{3+}$ and $Ca_3Cr_2^{3+}$ end members (e.g., Wood and Nicholls, 1978). Experimental work being undertaken by colleagues at this institution will hopefully enable the extension of garnet-orthopyroxene barometry/thermometry to the Cr^{3+}-bearing systems.

(c) Equation (15) does not include terms for Mn^{2+} in garnet. In many natural systems Mn^{2+} is low, however in some granulite facies parageneses X_{Mn}^{ga} (= Mn/Mn + Ca + Fe + Mg) ranges up to .10 or in rare cases to .20. From natural rock data Ganguly and Kennedy (1974) and Dahl (1980) have determined interaction parameters W_{MgMn}^{ga} and W_{FeMn}^{ga} which are similar to the MgCa and FeCa parameters obtained in these rocks and from experimental work. Adjustment of equation (15) for cases where X_{Mn}^{ga} is high, while $X_{Mn_2Si_2O_6}^{opx}$ is still low so that orthopyroxene non-idealities can be ignored, can be accomplished by replacing the term

$$(1 - X_{Ca})^3 \qquad \text{by} \qquad (1 - y)^3$$

where y = (Ca + Mn/Ca + Mn + Mg + Fe), and also using the parameter "y" in the garnet interaction term. This adjustment tacitly assumes that the behaviour of Mn and Ca in Pyrope-Almandine rich garnets are identical in the P-T conditions for which (15) is applicable. Experimental data in the system MnFMAS are necessary to allow better estimation of this effect.

(2) EFFECT OF X_{Ca}^{ga} on $K_{D_{Fe-Mg}}^{ga-opx}$ AT $X_{Mg}^{opx} \simeq .60$.

$K_{D_{Fe-Mg}}^{ga-opx}$ data derived from the CFMAS experiments are inherently more reliable than FMAS data because of the avoidance of Fe-addition. In runs where no melting has occurred, K_D is constrained by the ga-opx tie line passing through the bulk composition. Where melt has formed this is no longer the case and $K_{D_{Fe-Mg}}^{ga-opx}$ must be considered less reliable in such runs. The effects of X_{Ca}^{ga} on ln K_D at different pressures are shown in figure 3.4 for temperatures of 1323°K and 1248°K.

Ln K_D, and naturally $K_{D_{Fe-Mg}}^{ga-opx}$, increases at any one temperature with increasing pressure and increasing X_{Ca}^{ga}, for approximately constant X_{Mg}^{opx}.

In order to extract the calcium effect on $K_{D_{Fe-Mg}}^{ga-opx}$ from pressure effects and minor effects resulting from variations in X_{Al}^{opx} and X_{Mg}^{opx}, the experimental data have been analysed using equation 3(11) and plotting the term

$$RT \ln K_D + P\Delta V^o - 2579\, X_{Al}^{opx} + 600\,(1-2X_{Mg}^{opx}) = -\Delta G_{1,T}^{*}$$

against X_{Ca}^{ga} (Figure 3.5). From equation 3(11), the slopes of the regression lines of figure 3.5 will approximate the net interaction parameter W^{ga}, where

$$W^{ga} = (W_{FeMg}^{ga} + W_{CaFe}^{ga} - W_{CaMg}^{ga}).$$

The effects of Ca in orthopyroxene are not considered in this treatment, however as X_{Ca}^{opx} increases with X_{Ca}^{ga} in these runs such effects will not be detectable. The magnitude of the errors in K_D and hence $\Delta G_{1,T}^{*}$ effectively blanket the orthopyroxene terms, and simple linear regressions of the data against X_{Ca}^{ga} sufficiently describe the variations

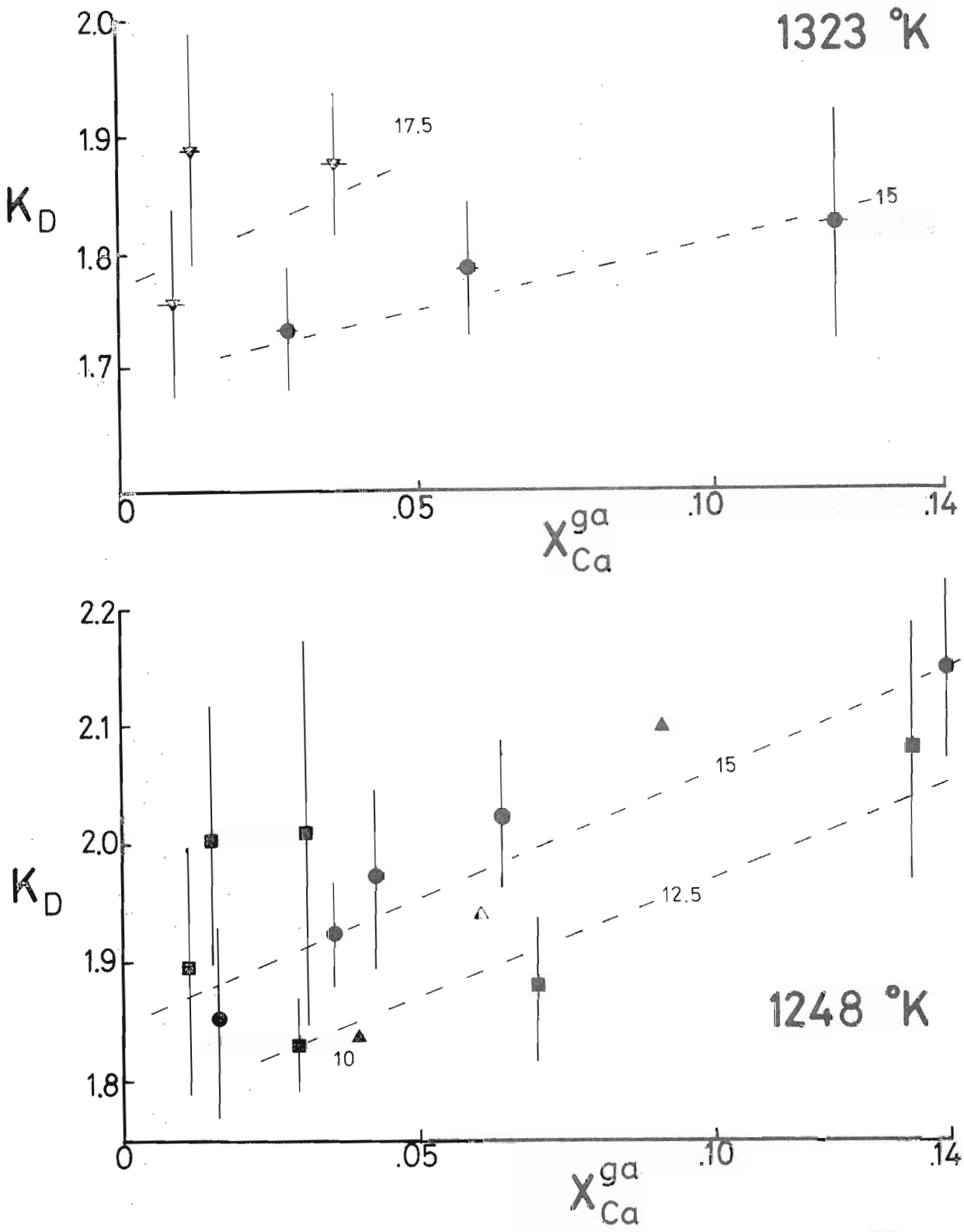

Fig. 3.4 Plots of experimentally determined values of $K_D^{ga\text{-}opx}{}_{Fe\text{-}Mg}$ against X_{Ca}^{ga}, for temperatures of 1323 °K and 1248 °K. Dashed lines join isobaric data sets in each plot. Pressures are indicated on these lines. Note K_D generally increases with increasing X_{Ca}^{ga}, increasing P, and decreasing T.

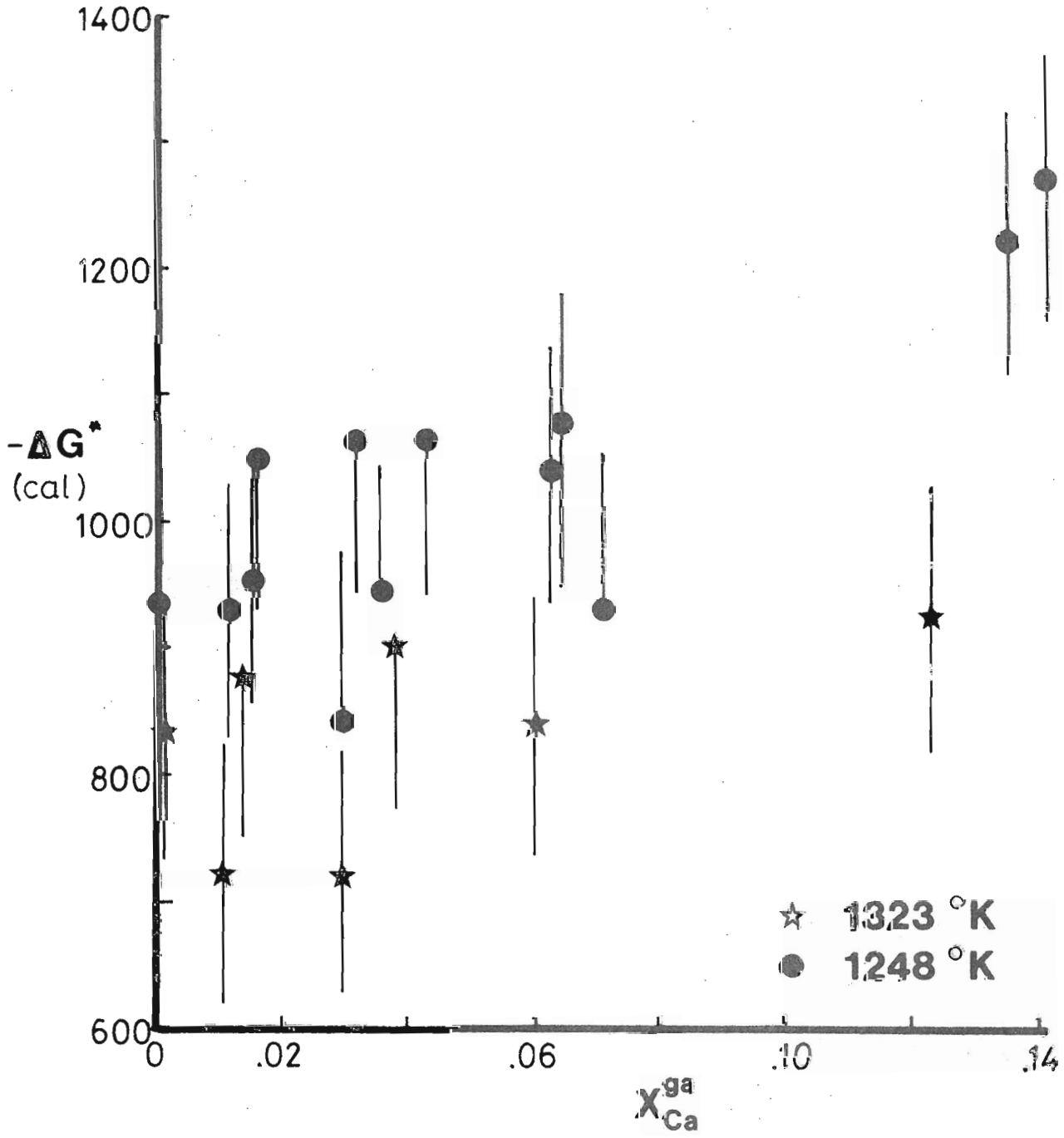

Fig. 3.5 Plot of $-\Delta G^{*}_{1,T}$, as defined in the text, against X_{Ca}^{ga} for experimental K_D data at 1323 °K and 1248 °K.

At 1248°K, the best fit regression line honouring the error brackets gives a slope of

$(W^{ga}_{FeMg} + W^{ga}_{CaFe} - W^{ga}_{CaMg}) = -2450 \pm 600$ cal, in good agreement with the value of 2530 ± 200 cals previously obtained for $(W^{ga}_{CaMg} - W^{ga}_{CaFe} + W^{ga}_{FeMg})$ using volume-adjusted X^{opx}_{Al} data, if $W^{ga}_{FeMg} \simeq 0$ (actually $W^{ga}_{FeMg} \leq 80 \pm 400$ cals).

Data obtained at 1323°K showed marked scatter. However, if the melt-absent 15 kbar run only is considered, this data can be fitted to a regression line of slope - 2450 ± 600 cals, at lower $\Delta G^{*}_{1,T}$ values than the 1248°K data. $\Delta S^{o}_{1,T}$ obtained from comparison of the two temperature-translated regression lines is - 2.5 ± .9 cals K^{-1} mol^{-1}, in agreement with the $\Delta S^{o}_{1,T}$ values obtained from adjusted and selected FMAS experimental data.

At 1248°K, using the value of $\Delta S^{o}_{1,T} = -2.5$ cal K^{-1} and the value of $-\Delta G^{*}_{T} = 915$ mol^{-1}, - 4000 ± 1000 cals is obtained for $\Delta H^{o}_{1,T}$. This is in good agreement with $\Delta H^{o}_{1,T}$ values derived from FMAS data, but is also subject to large uncertainty.

To adjust the approximate (and highly uncertain) $K_{D_{Fe-Mg}}^{ga-opx}$ "thermometer" of the FMAS system for the effects of calcium, the term

$$2450\ (\pm 600)\ [X^{ga}_{Ca}]$$

is simply added to the numerator in equation 2(10) to obtain

$$T\ °K = \frac{4000 + 2576\ X^{opx}_{Al} - 600\ (X^{ga}_{Mg} - X^{opx}_{Mg}) + 2450\ X^{ga}_{Ca} + 22.865P(kbar)}{R \ln K_D + 2.42} \qquad (16)$$

where $K_D = \left(\frac{Fe}{Mg}\right)^{ga} \cdot \left(\frac{Mg}{Fe}\right)^{opx} \geq 1$

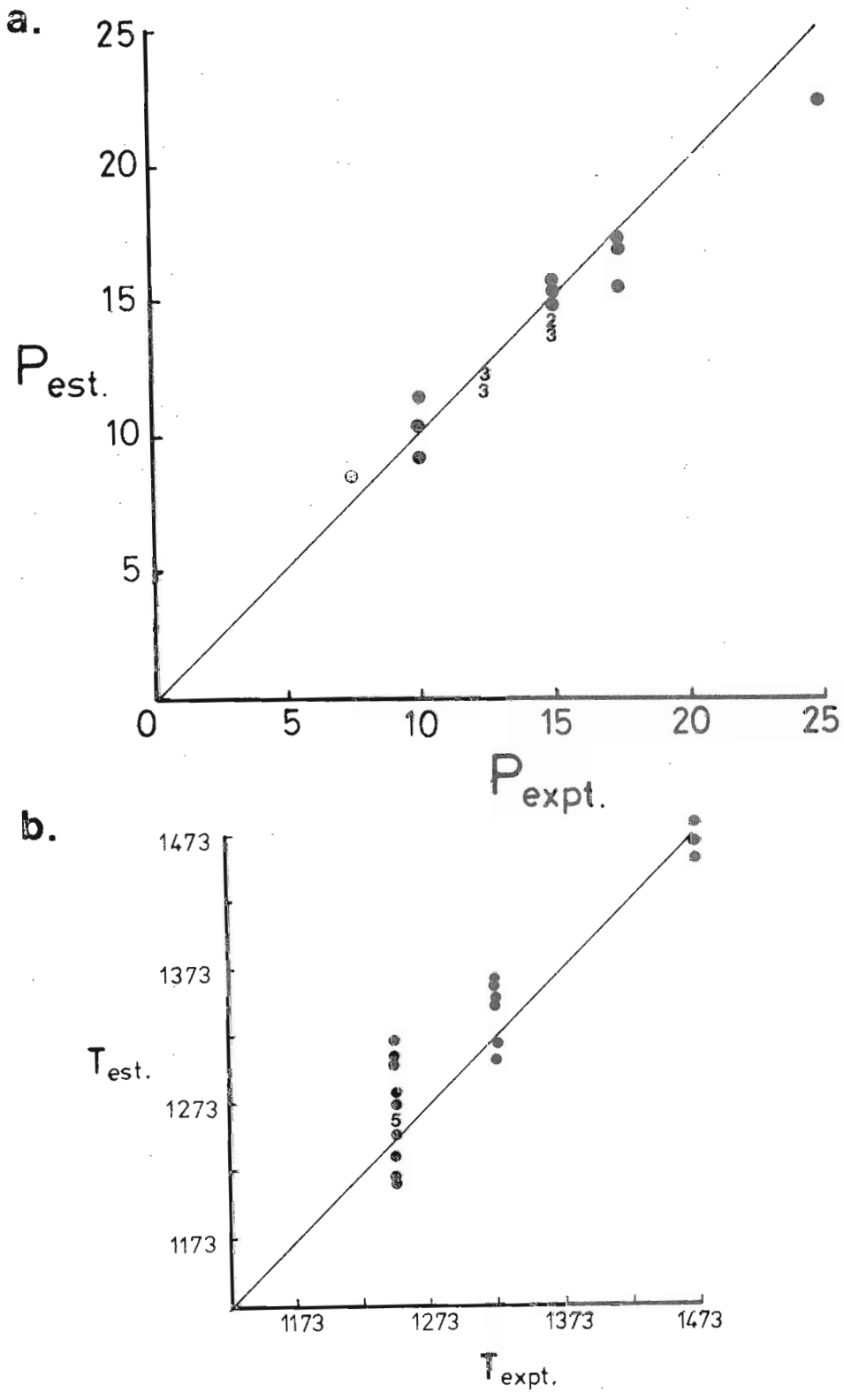

Fig. 3.6 a. Estimated pressures (P_{est}), obtained using equation 3(15), plotted against experimental run pressures (P_{expt}) for CFMAS data. Diagonal line represents a perfect fit. Each data point has an error of ±1 kbar.

b. Estimated temperatures (T_{est}), obtained using equation 3(16), plotted against experimental temperatures (T_{expt}) for K_D data obtained in CFMAS.

As discussed in the previous section (p. 97), the effects of X^{ga}_{Mn} are likely to be similar to those of X^{ga}_{Ca}, that is, increasing Mn contents will lead to higher $K_{D_{Fe-Mg}}^{ga-opx}$ at constant P, T and X^{opx}_{Mg}. Dahl (1980) has considered garnet-orthopyroxene pairs in natural rocks from Montana and has deduced such a dependence for $K_{D_{Fe-Mg}}^{ga-opx}$. The size of the term (W^{ga}_{MnFe} - W^{ga}_{MnMg}) is similar to the calcium term (W^{ga}_{CaFe} - W^{ga}_{CaMg}), although subject to large uncertainty.

As the geothermometer developed here is subject to large uncertainty arising from the experimental data and inadequate knowledge of orthopyroxene solid solution properties, Mn may be treated as identical to Ca in equation (16), so that X_{Ca} = Ca/Ca + Mg + Fe becomes

$$X = Ca + Mn/Ca + Mn + Mg + Fe,$$

without introducing significantly more error.

Chapter 4

THE COMPARISON OF GARNET-ORTHOPYROXENE GEOBAROMETRY WITH PREVIOUS EXPERIMENTAL INVESTIGATIONS AND APPLICATIONS TO NATURALLY OCCURRING GARNET-ORTHOPYROXENE ASSEMBLAGES

4.1 INTRODUCTION

Equations derived from the experimental data of Chapter 2 and Chapter 3 (equations 2.9 and 3.15) are in a form which can be readily applied to the experimental data of other workers in simple systems. In this section, these equations are used to produce calculated pressures from other workers' experimental data in MAS, CMAS and CFMAS. These calculated pressures are compared with the nominal run pressures of the appropriate experiments in order to judge the validity, or otherwise, of equation 2.9 and 3.15.

In $MgO-Al_2O_3-SiO_2$, equation 2. simplifies to:

$$P(kbar) = \frac{1}{\Delta V_r}\left[(R\ ln\ K - 2.93)T + 5650\right] \qquad \ldots 4.1$$

where $K = (X_{Al})(1-X_{Al})^{opx}$.

$\Delta V_r = 183.3 + 178.98\ X_{Al}(1-X_{Al})$

and T is in ^{o} Kelvin.

Experimental data obtained in MAS, presented in the following section, are treated using equation 4.1 and compared through this equation with the FMAS experimental data. It should be made clear that equation 4.1, and equation 4.2 derived later, are obtained from the FMAS and CFMAS experimental results *only*. Hence, new MAS experiments reported below and the data of earlier workers in MAS, FMAS, CMAS and CFMAS form an independent data set. These experiments constitute one test of the compositional factors in the extrapolation of FMAS and CFMAS data in that they provide independent data from limiting end-member systems (MAS, CMAS).

4.2 NEW EXPERIMENTS IN $MgO-Al_2O_3-SiO_2$

A series of experiments in the $MgO-Al_2O_3-SiO_2$ system have been performed in the P-T range 15-40 kbar and 900-1200°C, with the purpose of direct comparison of results obtained in the high pressure laboratory at the University of Tasmania with those obtained elsewhere.

Two starting mixes have been used for these experiments.

(a) pyrope-seeded sintered oxide mixes prepared from analytical grade MgO, Al_2O_3 and SiO_2. The reagents were ground under acetone to achieve homogeneity and sintered using the procedures outlined in Chapter 2, section 3 . Pyrope seeds, synthesised at 1200°C and 30 kbar, were then added to the recrystallised oxide mix. This starting composition represents an initially oversaturated mix, where a lower Al_2O_3 orthopyroxene must exsolve contemporaneously with the nucleation and growth of pyrope or pre-existing seeds.

(b) Pyrope-enstatite mineral mixes prepared by prolonged mixing and grinding of previously synthesised pyrope and enstatite (see section 2.3 for synthesis details). This mix type represents an initially undersaturated medium, in which a higher-Al_2O_3 orthopyroxene must form by the consumption of pyrope.

Most runs have been performed using mix type (a), wherein product enstatites zone to lower-Al_2O_3 rims. These rim compositions, and rim compositions of enstatites formed from mix type (b) at 40 kbar, 1200°C, are reported in table 4.1.

Zoning of Al_2O_3 contents in the enstatites is ubiquitous even in these runs of comparatively long duration (48 hours at 1100°C, 46 hours at 900°C). Such zoning cautions against the use of Xray-diffraction methods to estimate "equilibrium" compositions. Microprobe analysis must also be undertaken with great care to ensure that the position of any analysed point in a grain is known. The combined SEM-EDAX system

Table 4.1 EXPERIMENTAL DATA IN THE SYSTEM $MgO-Al_2O_3-SiO_2$ (MAS)

RUN NO.	T °K	P kbar	TIME hours	CAPSULE	MIX TYPE	X_{Al}^{opx}	P_{est} kbar
T312, T317, T511.	1473	20	48	Pt	$M_{45}A_{10}S_{45}$ sintered oxide	.190	19.6
T372	1423	20	48	Pt	$M_{45}A_{10}S_{45}$ sintered oxide + 5% pyrope	.190	18.0
T395	1373	20	49	Pt	$M_{45}A_{10}S_{45}$ sintered oxide +10% pyrope	.160	18.5
T426	1373	25	48	$Ag_{50}Pd_{50}$	" "	.112	23.2
T547	1373	40	84	$Ag_{50}Pd_{50}$	" "	.030	42.5
T428	1273	16	68	Pt	$M_{45}A_{10}S_{45}$ sintered oxide + 7% pyrope	.164	14.9
T403	1273	25	48	Pt	" "	.112	19.5
T402	1273	30	48	Pt	" "	.060	27.7
T512	1173	15	122	$Ag_{75}Pd_{25}$	Py-En mineral mix	.150	12.5
T520	1173	25	120	$Ag_{75}Pd_{25}$	$M_{45}A_{10}S_{45}$ sintered oxide + 7% pyrope	.060	23.2

at the University of Tasmania allows accurate assessment of the positions of analysed points by direct observation of the secondary electrom image. Grain boundaries can be readily located and rims analysed without contamination arising from the presence of other phases.

The experimentally determined Al_2O_3 contents of product enstatites, selected on the basis of observed and predicted zoning patterns, have been treated using equation 4.1. Estimated and nominal run pressures for these data are presented in figure 4.1. Generally, the fit of equation 4.1 to this data set is quite good (± 2.5 kb). Lower pressure runs, in which seeded oxide mixes were used, plot below the perfect fit line. This indicates that the minimum Al_2O_3 contents determined in these runs are slightly greater than would be expected by extrapolation from FMAS data, although approaching "equilibrium" values closely.

The unreversed data obtained from this set of experiments is thus in reasonable agreement with both the recent reversal data obtained on a variety of materials in MgO-Al_2O_3-SiO_2 (see below), and the FMAS results obtained in this study (Chapter 2).

4.3 COMPARISONS WITH PREVIOUS EXPERIMENTAL WORK IN $MgO-Al_2O_3-SiO_2$

Boyd and England (1964) experimentally determined the Al_2O_3 contents of orthopyroxenes coexisting with pyrope in the system $MgO-Al_2O_3-SiO_2$. These authors found the alumina contents of enstatite to increase with increasing temperature and decreasing pressure, a result confirmed in a general sense in all subsequent experimental work.

In the P-T ranges 20-50 kbar and 1100-1600°C, "equilibrium" alumina contents were determined using a variety of mix types:

(a) aluminous glass mixes,

(b) enstatite-pyrope synthetic mineral mixes, and

(c) highly aluminous single-phase orthopyroxene mixes.

These mix types effectively approach equilibrium Al_2O_3 contents from both high- and low-Al_2O_3 sides. It was found that glass mixes initially formed homogeneous pyroxenes and then pyrope exsolved slowly, with a resultant decrease in Al_2O_3 contents in orthopyroxene. Mineral mix starting compositions were stated to react quickly, at high temperatures, to form aluminous orthopyroxenes. Thus, Boyd and England (1964) inferred that sluggish nucleation of pyrope from glass starting mixes resulted in Al_2O_3 contents in enstatite which were higher than equilibrium values, while mineral mix results were closer to equilibrium Al_2O_3 contents.

Comparison of the Boyd and England (1964) data with subsequent investigations (Macgregor, 1974; Howells and O'hara, 1978; Lane and Ganguly, 1980) indicates that the equilibrium Al_2O_3 contents of enstatite reported by Boyd and England (1964) are too high for any chosen P-T condition. This discrepancy may result from the uncertainties associated with analytical techniques used by Boyd and England (1964). Xray determinations, and partial probe analyses of product

enstatites can indicate illusory high Al_2O_3 contents because rimward zoning is not adequately considered. It has been shown in more recent investigations that orthopyroxenes formed in the enstatite-pyrope system are strongly zoned even at high temperatures (e.g. Howells and O'Hara, 1978; Lane and Ganguly, 1980), and that rim compositions must be used in products formed from both glass and mineral mix starting materials.

Estimated pressures using equation 4.1 are plotted against nominal experimental pressures for the data of Boyd and England (1964) in figure 4.1. These data give calculated pressures consistently below their run pressures by 5-7.5 kbar, except for some runs at 1100°C which show a 2-3 kbar difference. The Al_2O_3 contents reported by Boyd and England (1964) are thus consistently higher than predicted by extrapolation of FMAS data (Chapter 2) to the MAS system.

Macgregor (1974) performed experiments in the MgO-Al_2O_3-SiO_2 system in which Al_2O_3 contents of enstatite coexisting with pyrope were determined in the P-T field 25-40 kbar and 1000-1400°C. Aluminous glasses seeded with pyrope were used exclusively in this study, thus equilibrium Al_2O_3 contents in most runs were approached from the high-Al_2O_3 side. Run times varied from 75 hours (at 1000°C) to only 6 hours (at 1400°C). Considering the nature of these experiments, it may be expected that Al_2O_3 contents reported in product orthopyroxenes will be higher than "equilibrium" values attained for longer run durations.

These experimental data have formed the basis of the geobarometer of Wood and Banno (1973), and part of the data base for the calibration of Wood (1974). The nominal run pressures can be compared with estimated pressures using the data of Macgregor (1974) and equation 4.1 of this study (figure 4.2). The agreement between the pressures estimated

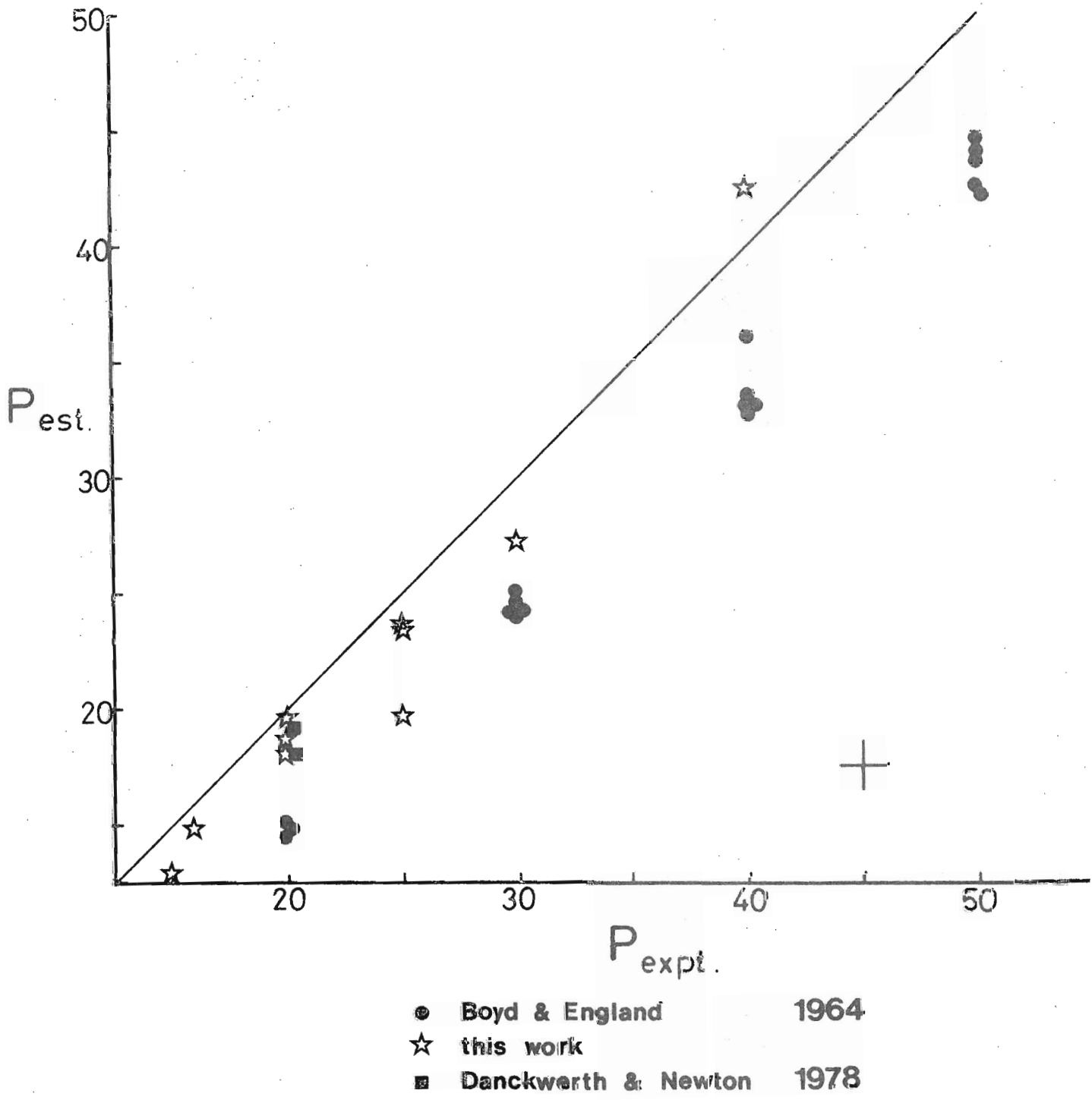

Fig 4.1 Comparison of nominal experimental pressures in the MAS system with pressures estimated via equation 4(1) using published compositional data and data in this work. Error bars in bottom right corner of diagram.

using equation 4.1, derived from an independent data base, and the nominal run pressures of Macgregor (1974) is very good. Data at 35 kbar show the most scatter about the perfect correlation line, with other data being within ±1 kbar of the nominal rin pressures. Given the standard error on equation 4.1 (±1 kbar), and the precision of the pressure calibration for the piston-cylinder apparatus (±.5 to 1 kbar), the data of Macgregor (1974) show an excellent fit to 4.1.

Arima and Onuma (1977) have estimated Al_2O_3 contents of enstatite coexisting with pyrope at 20 and 25 kbar in the temperature range 1150-1450°C. The Al_2O_3 contents of orthopyroxene in this study were estimated by Xray diffraction measurements and the appearance of pyrope in mixes of critical alumina contents. Reduction of the data of Arima and Onuma (1977) using equation 4.1 yields good agreement between estimated and nominal run pressures for their 25 kbar data. Estimated pressures for the 20 kbar data (derived from figure 3c, 1977) are 22.5 kbar, suggesting that the Al_2O_3 contents determined by Arima and Onuma (1977) are lower at 20 kbar than would be predicted from my FMAS data. However, the En/En+Py curve of Arima and Onuma (1977) (depicted in their figure 3c) is poorly constrained, particularly at 1200°C. Thus this 20 kbar data is subject to large uncertainty. In view of this the discrepancy of 2.5 kbar is considered reasonable agreement.

Howells and O'Hara (1978) have determined Al_2O_3 contents of orthopyroxenes in equilibrium with pyrope at 30 kbar and temperatures in the range 1100-1600°C. By conparison of run products obtained in a variety of starting materials (e.g. sintered oxide mixes, gels, synthetic mineral mixes, and glass mixes), these workers have concluded

that gels or recrystallised sintered oxide mixes are better starting materials, yielding lower Al_2O_3 contents in enstatites, than unseeded glass starting materials.

In the temperature range 1200-1500°C, the agreement between equation 4.1 and the data of Howells and O'Hara (1978) is excellent (figure 4.2). Only two data points (1373°K, 1873°K; figure 4.2) are in poor agreement, and may indicate a temperature-dependent discrepancy between equation 4.1 and the 30 kbar data set of Howells and O'Hara (1978). The lowest temperature orthopyroxenes have higher Al_2O_3 contents than predicted by equation 4.1 while the highest temperature orthopyroxenes have lower than predicted Al_2O_3 contents. These discrepancies may suggest a smaller negative ΔS^o value for the garnet-orthopyroxene Al_2O_3 equilibrium in MAS than obtained on the basis of FMAS experiments outlined in Chapter 2.

Three experimental points from the data of Danckwerth and Newton (1978) are plotted in figure 4.1. Estimated pressures using these data and equation 4.1 are in excellent agreement with the nominal pressures reported by Danckwerth and Newton (1978). The Al_2O_3 contents given by these authors are best-fit or overlap values obtained from reversal experiments using both high-Al_2O_3 enstatite-bearing, and low-Al_2O_3 enstatite-bearing mineral mixes. The authors noted complex zoning within individual grains in each mix type, and were able to show overlapping or similar Al_2O_3 contents in rims of orthopyroxenes grown from each mix type.

In the most recent epxerimental study within the $MgO-Al_2O_3-SiO_2$ system, Lane and Ganguly (1980) have determined Al_2O_3 contents of orthopyroxenes coexisting with pyrope in the P-T range 26-40 kbar and 960-1330°C. Equilibrium Al_2O_3 contents were approached from both the high-alumina and low-alumina sides using synthetic mineral mixes

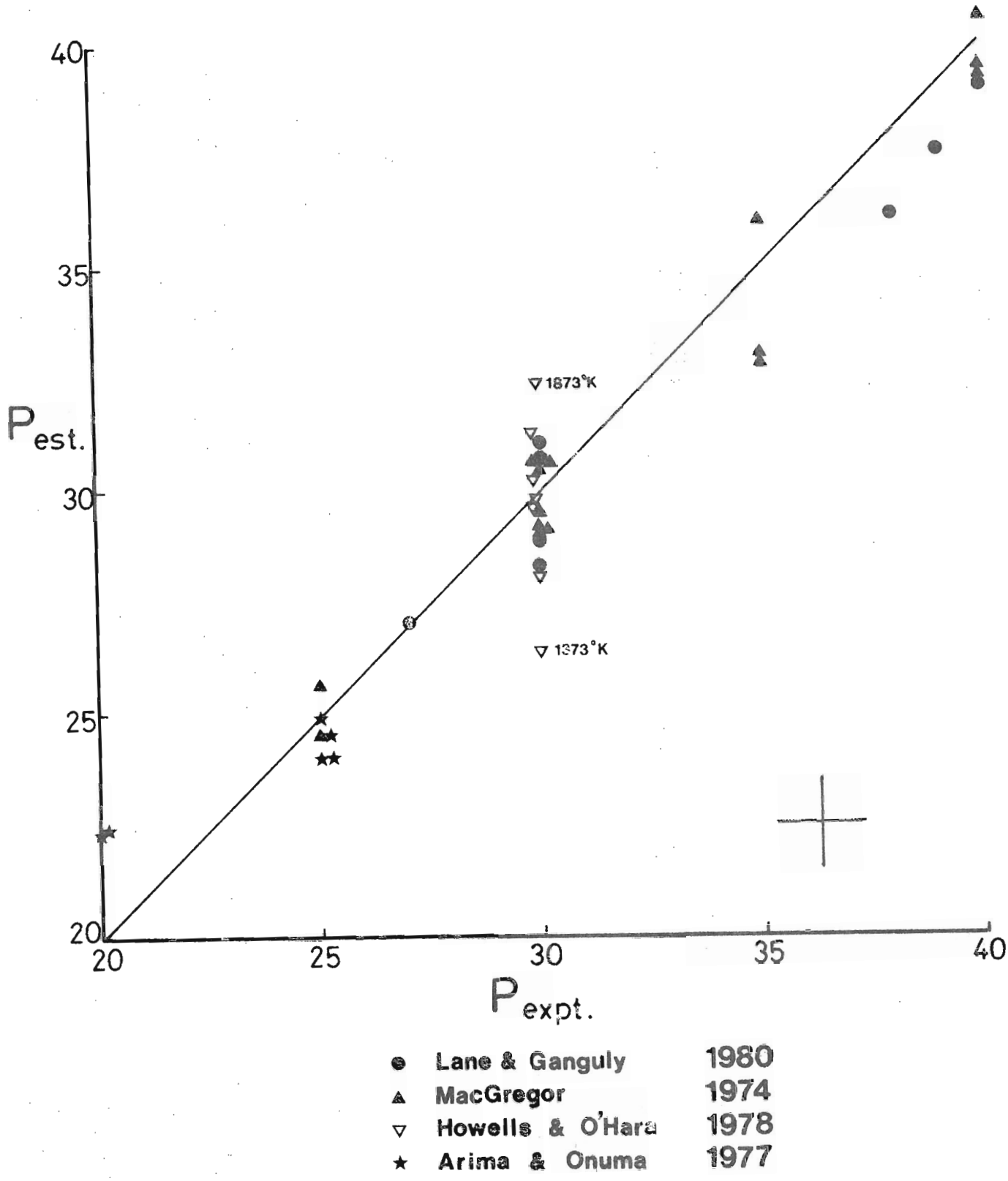

Fig 4.2 Comparison of nominal experimental pressures in MAS with pressures estimated using equation 4(1) and published compositional data . Error bars in bottom right corner.

(aluminous enstatite + pyrope, and pure enstatite plus pyrope respectively). The data reported by Lane and Ganguly (1980) are based on overlap values of Al_2O_3 in orthopyroxenes grown from both mix types, and constitute good reversals. Reduction of this reversal data using equation 4.1 results in estimated pressures which are in good agreement (±1.5 kbar) with the nominal run pressures reported by Lane and Ganguly (1980).

Figures 4.1 and 4.2 generally indicate very good agreement between pressures calculated using equation 4.1 and nominal run pressures for most recent experimental data in the MgO-Al_2O_3-SiO_2 system. The data of Boyd and England (1964) are shown to be inconsistent with subsequent experimental work, erring in the direction of high Al_2O_3 contents at any given P-T condition. The later results (post-1974) are in very good agreement with the FMAS data obtained in this study (Chapter 2). In particular, a number of well-reversed experimental data points in MAS are consistent with equation 4.1. Thus, the separate data base of MAS experimental work provides support for the FMAS experimental results reported herein (Chapter 2). Equations formulated on the basis of FMAS experiments reported in Chapter 3 can be extrapolated to the MAS system with confidence and without significant disagreement arising with existing MAS data.

4.4 COMPARISONS WITH PREVIOUS INVESTIGATIONS IN FMAS

Wood (1974) performed experiments in the FeO-MgO-Al_2O_3-SiO_2 system in which alumina contents of orthopyroxenes coexisting with garnet were determined by microprobe analysis. Starting mixes used in the study were aluminous glasses seeded with aluminous orthopyroxene and natural pyrope-almandine garnet. In such mixes, orthopyroxenes approach equilibrium Al_2O_3 contents from an oversaturated direction, and it would be expected that the Al_2O_3 contents reported may be higher than reversed values.

The data of Wood (1974) in the range 800-1300°C and 8-30 kbar are plotted in figure 4.3. Calculated pressures, obtained from the application of equation 2.9. to the data of Wood (1974), are consistently higher (by 1 to 10 kbar) than the nominal run pressures. The average discrepancy between the data presented herein and the data of Wood (1974) is 4 kbar, much greater than would be expected to result from differences in apparatus calibration. The present experiments indicate that, at any chosen P-T condition, orthopyroxenes coexisting with garnet in FMAS will contain more alumina than predicted from the data of Wood (1974).

Wood (1974) also performed a number of experiments in CaO-MgO-FeO-Al_2O_3-SiO_2. Calculated pressures using equation 3.15 are usually 5 kbar greater than nominal run pressures for this data. Thus, pressures calculated based on the calibration of Wood (1974) for both Ca-poor and Ca-richer orthopyroxene-garnet assemblages will be too low compared with results obtained using equations 2.9 and 3.15. Recent experimental work in MAS (Lane and Ganguly, 1980; Howells and O'Hara, 1978) and CMAS (Howells and O'Hara, 1978a), and data obtained from some natural assemblages (O'Hara and Yarwood, 1978) also suggest that the equation of Wood (1974) underestimates pressures of formation.

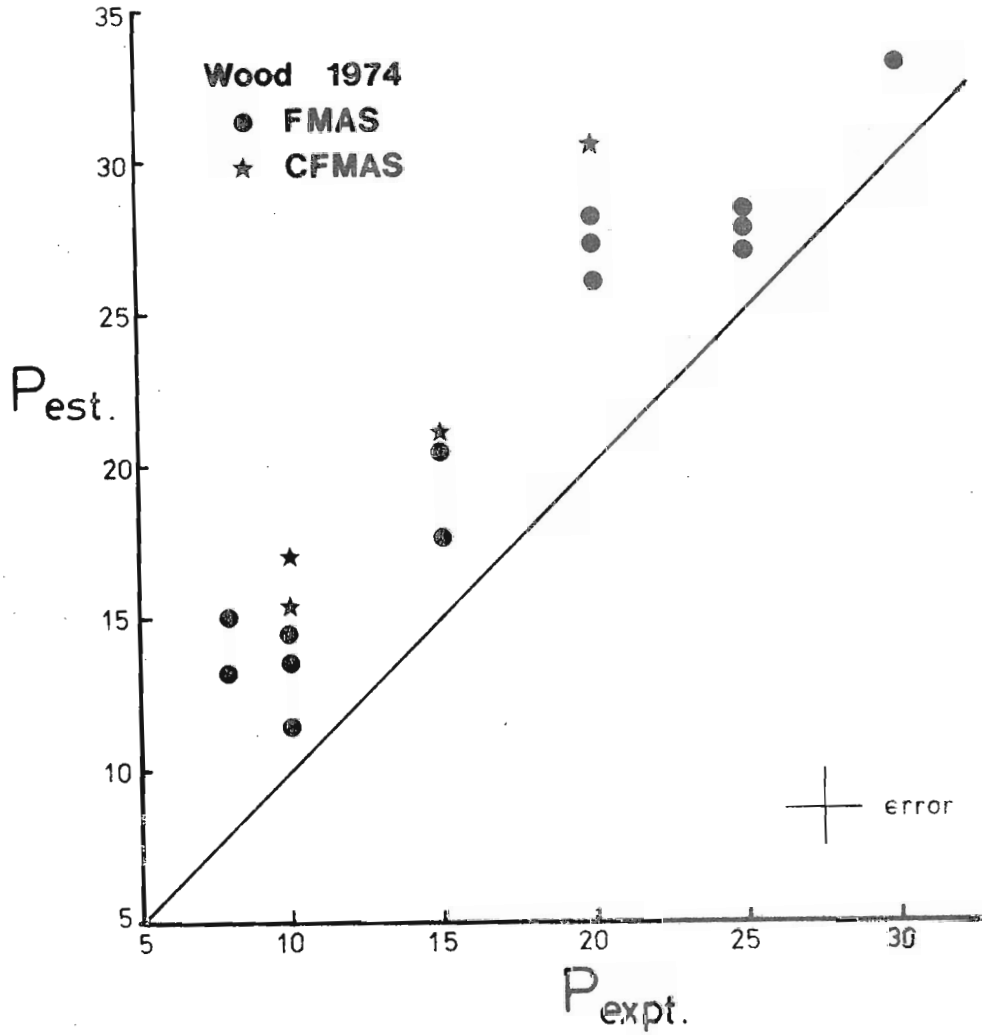

Fig 4.3 Comparison of the experimental data of Wood (1974) with equation 3(15) derived in this study. Data of Wood (1974) generally indicates less Al in orthopyroxene at any P and T than suggested by equation 3(15).

This is particularly apparent in pressures calculated for some Fe- and Ca-rich granulite facies parageneses, where application of the barometer of Wood (1974) sometimes yields negative pressures.

4.5 COMPARISONS WITH PREVIOUS INVESTIGATIONS IN CaO-MgO-Al_2O_3-SiO_2 (CMAS) AND CaO-MgO-FeO-Al_2O_3-SiO_2 (CFMAS)

Previous experimental data obtained for the solubility of alumina in orthopyroxene coexisting with garnet in CMAS and CFMAS can be compared with the present results using equation 3.15 to estimate pressures for the run products given in these studies.

In CMAS, equation 3.15 reduces to the relation:

$$P = \frac{1}{\Delta V_r}\left[(R\ \ln K - 2.93)T + 5650 - 6300(X_{Ca}^{ga})^2\right] \text{kbar} \qquad \ldots 4.2$$

where $K = \dfrac{X_{Al}^{opx}(1-X_{Al}^{opx})}{(1-X_{Ca}^{ga})^3}$

$X_{Al}^{opx} = Al/2$

$X_{Ca}^{ga} = Ca/Ca+Mg+Fe$

and $\Delta V_r = 183.2 + 178.98\ X_{Al}^{opx}(1-X_{Al}^{opx})$ cals $kbar^{-1}$

Pressures have been estimated for various CMAS data sets using equation 4.2 and for CFMAS experimental data sets using equation 3.15. These calculated pressures are plotted against nominal run pressures reported by previous workers in figures 4.4, 4.5 and 4.6.

Akella (1973), Akella and Boyd (1974) and Akella (1976) have determined Al_2O_3 contents of orthopyroxenes equilibrated with garnet and clinopyroxene in CMAS and CFMAS in the range 26-44 kbar and 1000-1500°C. Starting compositions used in CMAS experiments included glass mixes, recycled lower pressure opx-cpx-garnet assemblages, and low Al_2O_3-pyroxene+garnet mineral mixes. In the CFMAS system two

mineral mixes of variable X_{Mg}^{bulk} were used.

Calculated pressures for all this experimental data are well below the nominal run pressures, by up to 15 kbar (figure 4.4).

In CMAS experiments, where glass mixes were most often those used, calculated pressures are usually 5-10 kbar below nominal run pressures, suggesting that the Al_2O_3 contents in orthopyroxene which are reported in these experiments are consistently too high at any chosen P-T condition, a conclusion also reached by Howells and O'Hara (1978).

The CFMAS data of Akella (1976) and Akella and Boyd (1974) show convergence between calculated and nominal pressures at 30 kbar, but large deviations at higher pressures. Again, accepting equation 3.15, equilibrium Al_2O_3 contents in orthopyroxenes coexisting with garnet are lower than those obtained in the experiments of Akella (1976) and Akella and Boyd (1974). This discrepancy may well result from the short run durations (30 hours at 1000°C) used by these workers, or failure to analyse rim compositions.

Data obtained by Hensen (1974) for orthopyroxenes in CFMAS are plotted in figure 4.4. Calculated pressures are in good agreement with nominal run pressures for three of the four data points. Hensen (1974) reported widespread zoning and scatter in compositions of pyroxenes and garnets in these experiments, but could estimate preferred Al_2O_3 contents based on the established direction of reaction from natural mineral seeds to final product rims. The long durations of the runs (2-3 weeks at 1100°C) give some confidence that "equilibrium" compositions may have been closely approached at least on grain boundaries.

The reasonable agreement of these long-duration experiments with the equations derived herein provides some support for the

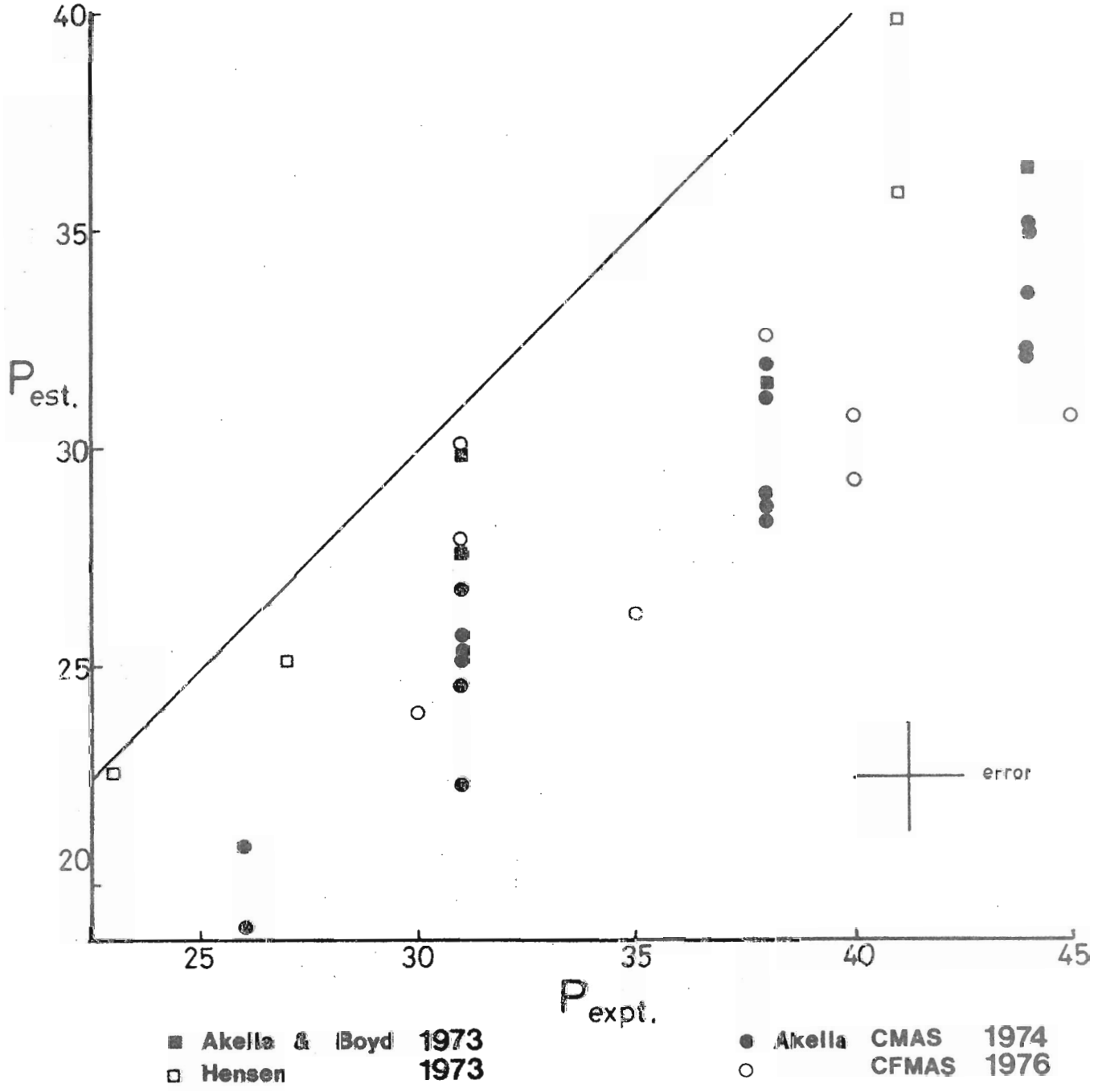

Fig. 4.4 Comparison of experimental pressures in CMAS and CFMAS systems with pressures estimated via application of equation 3(15) to published compositional data of previous workers.

application of equation 3.15 to ultramafic compositions.

Howells and O'Hara (1978) have performed experiments in CMAS over the range 25-35 kbar and 1100-1600°C, in which Al_2O_3 contents of orthopyroxene coexisting with garnet and clinopyroxene have been determined. Data obtained by these workers using longer run times and a variety of starting mixes designed to approach equilibrium from different directions are in very good agreement with the present results extrapolated to CMAS. Pressures calculated by the application of equation 4.2 to the data of Howells and O'Hara (1978a) are within ±2.5 kbar of their nominal run pressures at 30 and 35 kbar (figure 4.5a).

The present work supports lower Al_2O_3 in orthopyroxene coexisting with garnet and clinopyroxene than found by Akella (1976) but similar Al_2O_3 contents to those determined by Howells and O'Hara (1978) in CMAS.

Perkins and Newton (1981) have recently determined Al_2O_3 contents of orthopyroxene coexisting with garnet and clinopyroxene in CMAS in the P-T range 15-40 kbar and 900-1100°C. All these Al_2O_3 contents have been determined from reversed data using two contrasting mineral mix starting materials. The agreement between these well-reversed data and equation 4.2 is extremely good (figure 4.5b). Calculated pressures are all within 2.5 kbar of nominal run pressures over the whole P-T range. When the analytical error bars given by Perkins and Newton (1981) are included, this independent data set is in perfect agreement with equation 4.2 extrapolated from FMAS and CFMAS data obtained herein (Chapter 2 and Chapter 3).

Mori and Green (1978) have determined Al_2O_3 contents of orthopyroxenes crystallised with garnet, clinopyroxene, olivine, and additional ilmenite and phlogopite in a pyrolite-40% olivine multi-

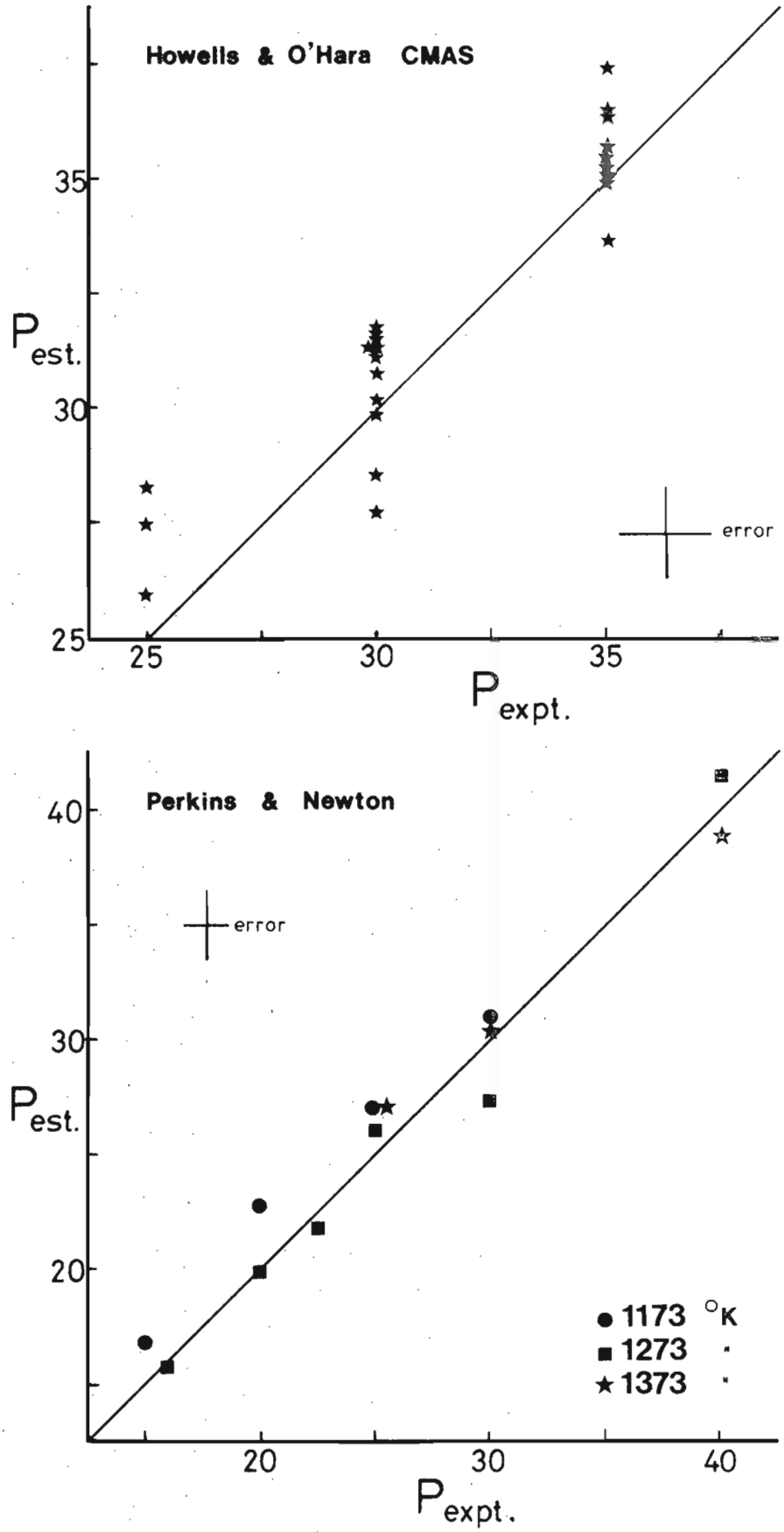

Fig. 4.5 Comparison of experimental run pressures with pressures estimated via equation 4(2) using the compositional data of

a. Howells and O'Hara (1978)

b. Perkins and Newton (1981).

component mineral mix. For a few experiments alternative mineral mix starting compositions were used. In all experiments, TiO_2 and Cr_2O_3 are minor but important constituents which complicate the application of equation 3.15 to these experiments. Pressures calculated assuming $X_{Al}^{opx} = Al/2$ (i.e. by ignoring the presence of Cr^{3+} in orthopyroxene) are plotted against nominal run pressures in figure 4.6. The considerable scatter which occurs in the estimated pressures at 30 and 40 kbar is not consistently related to temperature. At 30 kbar, calculated pressures range from 35 kbar to 22 kbar with the majority of points plotting below the best-fit line. Most of this data, and the data obtained at 40 kbar, would indicate greater alumina contents in multicomponent orthopyroxene coexisting with Cr-bearing garnets than would be predicted from equation 3.15.

Given the large scatter in calculated pressures which results mainly from original non-systematic scatter in the data of Mori and Green (1978), it is difficult to evaluate the fit of equation 3.15 to this "natural rock" experimental data.

Summary

Equations based on experimental studies presented in Chapter 2 and Chapter 3 are in excellent agreement with the most recent CMAS experimental data (Perkins and Newton, 1981; Howells and O'Hara, 1978). This result provides support for the application of equations 2.9 and 3.15 to rock compositions which approach the CMAS simple system. Previous experimental data in the CFMAS system show a wide and often non-systematic scatter of results which are ambiguous in testing the applicability of equation 3.15 to "natural rock" peridotite compositions.

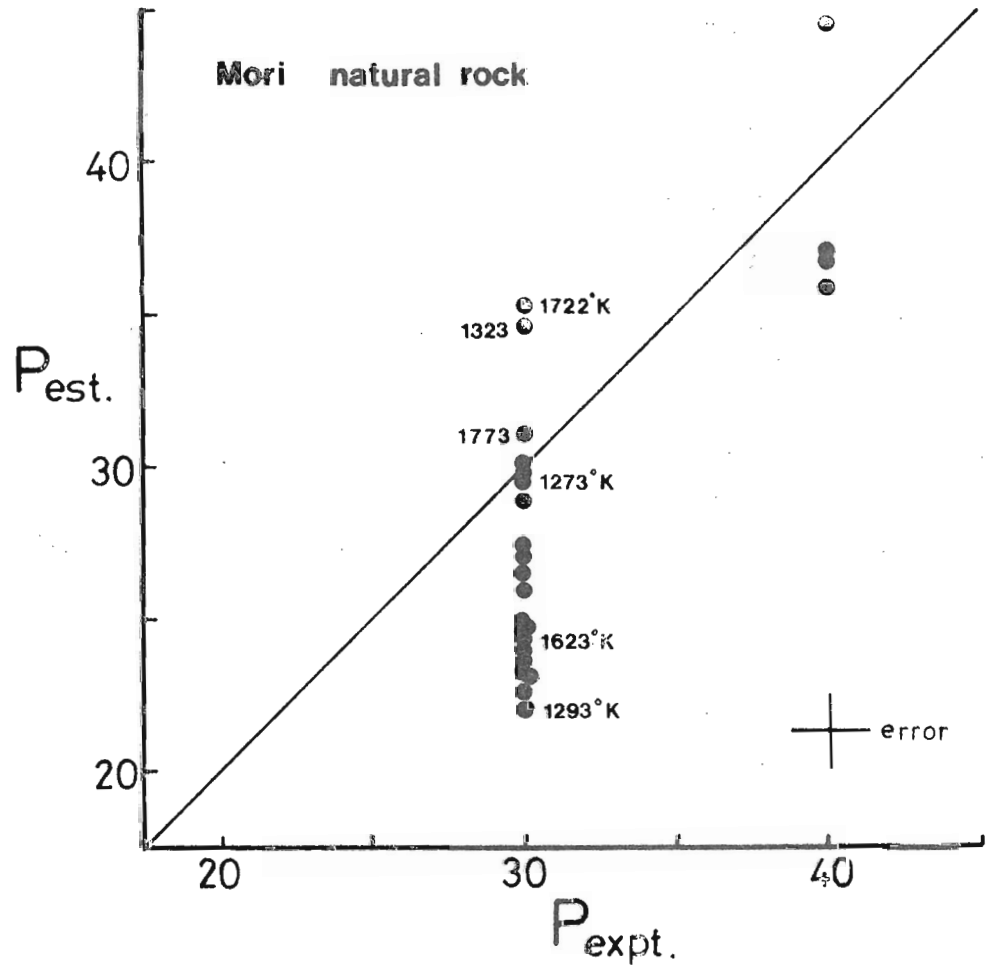

Fig. 4.6 Comparison of run pressures of Mori and Green (1978) with pressures calculated via equation 3(15) using their compositional data.

X_{Al}^{opx} is not corrected for the presence of variable Cr contents.

In subsequent sections of this chapter, the barometry and thermometry equations derived in Chapter 3 (3.15 and 3.16) are applied to natural garnet-orthopyroxene parageneses from well-documented occurrences including kimberlite xenoliths, garnet-peridotite and orthopyroxene-eclogite bodies, and crustal granulites. Such natrual occurrences provide a test of the precision and consistency of the garnet-orthopyroxene barometry developed in Chapter 2 and Chapter 3.

4.6 APPLICATIONS OF GARNET-ORTHOPYROXENE BAROMETRY TO NATURAL ASSEMBLAGES

I. GARNET-PERIDOTITE AND GARNET-PYROXENITE XENOLITHS IN KIMBERLITIC AND BASALTIC DIATREMES

The estimation of the physical conditions of formation (P-T) of garnet-peridotite xenoliths in kimberlites was pioneered by Boyd (1973). On the basis of geothermometry and barometry techniques available at the time, Boyd (1973) constructed a "paleogeotherm", the Lesotho geotherm, from the P-T estimates obtained for suites of granular and sheared (porphyroclastic) xenoliths from various kimberlite pipes. In recent years, much more information has accumulated on xenolith suites from kimberlites from South Africa, Russia, North America, and Australia. The estimation of the P-T conditions of formation of such xenolith suites by the application of updated or new barometer/thermometer calibrations has resulted in some revision of the earlier estimates inferred by Boyd (1973) and other workers (e.g. Eggler and MacCallum, 1974; Nixon and Boyd, 1973; Boyd and Nixon, 1975; Dawson *et al.*, 1975; Danchin and Boyd, 1976; Danchin, 1979; Carswell *et al.*, 1979; Sobolev, 1977; Boyd and Finger, 1975; Harte *et al.*, 1975).

The P-T conditions of formation of garnet-peridotite xenolith suites from kimberlites, estimated using a variety of geothermometers and the barometer of Wood (1974), have recently been summarised by Carswell and Gibb (1980). These authors present a revised best-fit geotherm for xenoliths from southern Africa based on a large sample set. Arguments concerning the possible significance of the P-T paths mapped out by the xenoliths, and interpretations of the nature of the "perturbed geotherms" which the xenoliths are suggested to define, are presented in Carswell (1978), Mitchell *et al.* (1980), Dawson *et al.* (1975), Harte *et al.* (1981), and Fraser and Lawless (1978), and will not be discussed here.

P-T estimates for garnet peridotite and garnet-pyroxenite xenoliths reported in the literature are presented in figures 4.7 and 4.8. The samples plotted in these diagrams have been selected on the arbitrary criterion that the garnets contain less than 2 wt.% Cr_2O_3. Thus, only low-Cr assemblages have been considered so that equations derived in Chapter 2 and Chapter 3 can be applied to compositions not far removed from the CFMAS system.

Pressures have been estimated by application of equation 3.15 to reported compositions of orthopyroxene and garnet, using $X_{Al}^{opx} = Al/2$. Temperatures for the selected xenoliths have been estimated in two distinct ways:

(a) using the measured value of $K_{D_{Fe-Mg}}^{ga-opx}$ and applying the garnet-clinopyroxene thermometer of Ellis and Green (1979), and

(b) using the two-pyroxene thermometer of Wells (1977).

P-T estimates for individual samples have been obtained from intersections of the orthopyroxene Al_2O_3 isopleths with the constant K_D lines (Ellis and Green, 1979) or with the two-pyroxene temperature (Wells, 1977). Alternative geotherms obtained by these methods are

Fig. 4.7 P-T estimates for garnet lherzolite nodules from kimberlites of South Africa. P estimated via equation 3(15). T estimated via :

a. ga-cpx Fe-Mg distribution thermometry (Ellis and Green,1979)

b. two-pyroxene thermometry (Wells,1977)

Curve a. - Lesotho geotherm of Boyd (1973)

Curve b. - Lesotho geotherm of Carswell and Gibb (1980a)

Sources of data :

Boyd (1974), Boyd and Nixon (1975,1976), Boyd and Finger (1975), Cox et. al. (1973), Carswell et. al. (1979), Danchin (1979), Dawson et. al. (1970), Dawson et. al. (1978), Griffin et. al. (1979), MacGregor (1979), Mori (1978), Nixon (1973), Nixon and Boyd (1973), Reid and Dawson (1972), Rolfe et. al. (1973).

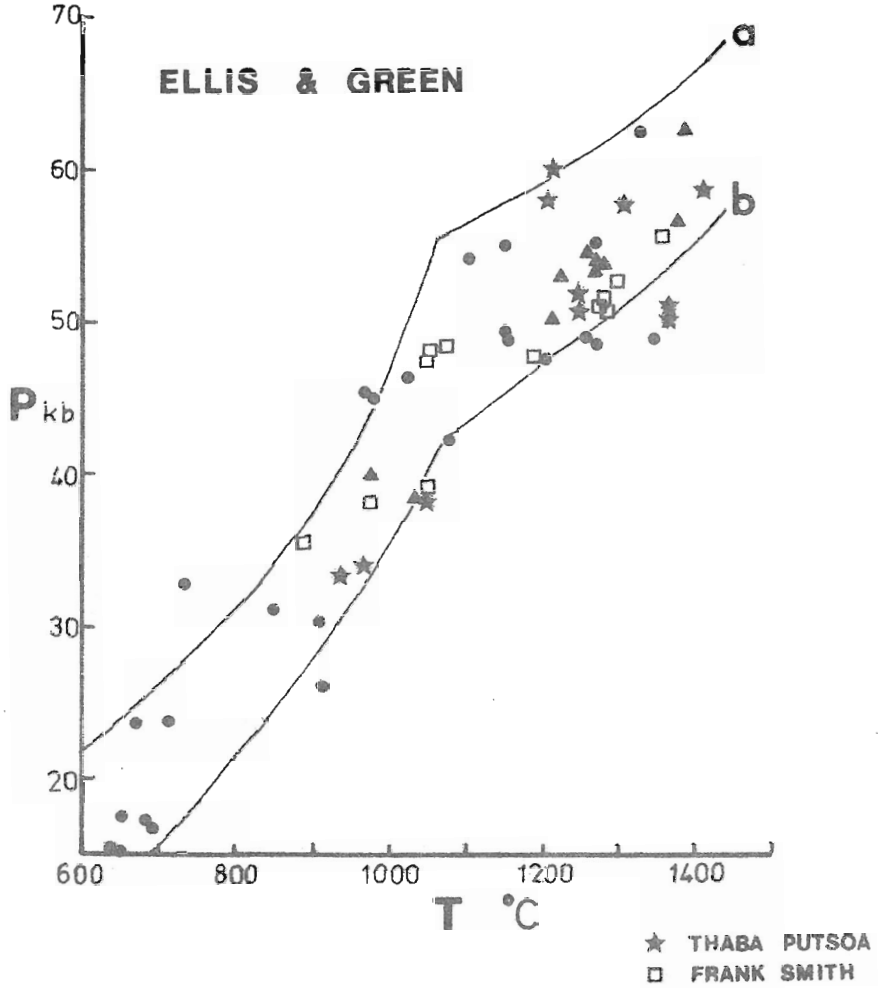
ELLIS & GREEN
a
b
70
60
50
40
30
20
P kb
600
800
1000
1200
1400
T °C
THABA PUTSOA
FRANK SMITH

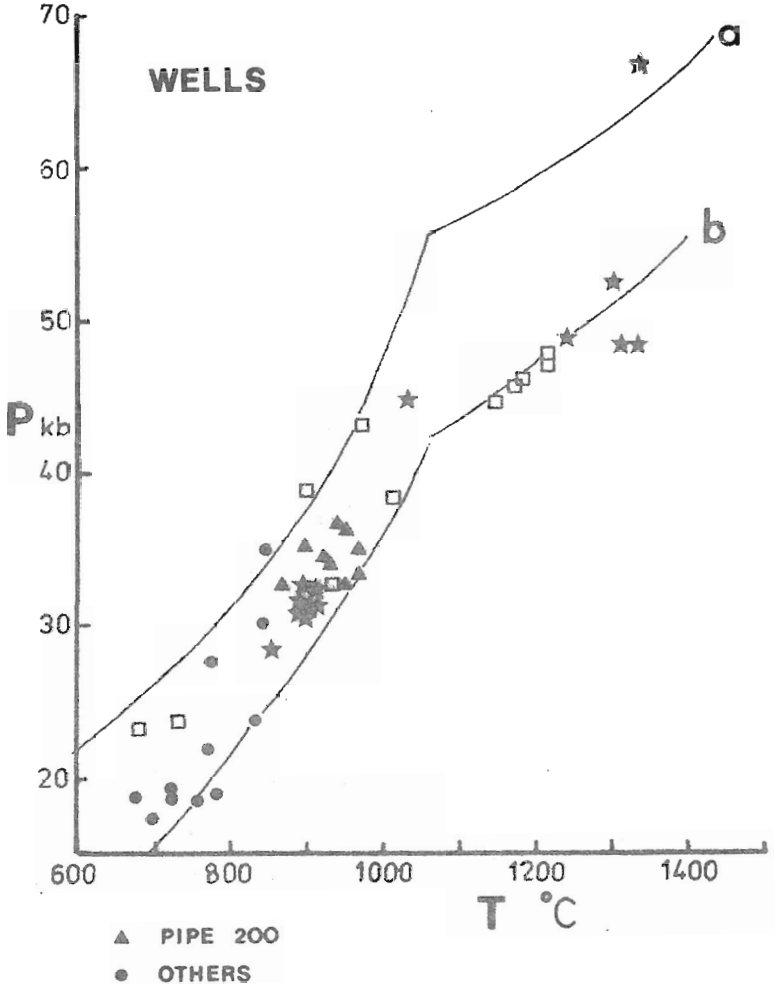
WELLS
a
b
70
60
50
40
30
20
P kb
600
800
1000
1200
1400
T °C
PIPE 200
OTHERS

only (e.g. figure 4.7, Pipe 200). Comparison of the data of Mori and Green (1978) with the thermometer of Wells (1977) suggests that the latter may underestimate temperatures of equilibration of the higher-T xenoliths (> 1100°C) by up to 100°C. If the data of Mori and Green (1978) are accepted, the P-T conditions inferred for xenoliths from Frank Smith pipe and Pipe 200 using the Wells (1977) thermometer may be too low. On the other hand, the Ellis and Green (1979) thermometer may give unrealistically high temperatures (and consequently unrealistic pressures via equation 3.15) for the highest-T xenoliths (Carswell and Gibbs, 1980).

(c) P-T data from different pipes may show clustering into lower P-T and higher P-T groups or may show a range of P-T conditions of formation (compare Frank Smith pipe, Pipe 200) for the xenoliths. The presence and extent of clustering is again thermometer dependent.

(d) kinked geotherms are not necessary to describe the P-T array for the xenoliths (figures 4.7 and 4.8). Xenoliths from individual pipes (e.g. Frank Smith) may define a kinked P-T curve, but the presence of this kink is dependent on the thermometer used.

In contrast to the data from kimerlitic pipes from South Africa, USSR, and North America, xenolith data from the Solomon Islands (Nixon and Boyd, 1979) and from diatremes in southeastern Australia (Lovering and White, 1969; Irving, 1973; Ferguson and Sheraton, 1979) define hot thermal regimes at shallow depths (figure 4.8a and b). Calculated equilibration pressures of 20-24 kbar (at 1100°C) for a spinel-garnet lherzolite from New South Wales (Ferguson *et al.*, 1977) are consistent with the presence of both spinel and garnet in this rock, and are in good agreement with previous P-T estimates. Pressures calculated for garnet-websterite xenoliths from southeastern Australia are dependent on the thermometer used (figure 4.8a and b), but are

Fig. 4.8 P-T estimates for garnet lherzolite nodules from kimberlites in the U.S.S.R. and North America, and from alkali basalts, kimberlites, or breccia pipes in other areas. Pestimated via equation 3(15); T estimated via:

a. ga-cpx Fe-Mg distribution thermometry (Ellis andGreen,1979)

b. two-pyroxene thermometry (Wells,1977)

Curve a. - Lesotho geotherm (Boyd,1973)

Curve b. - Lesotho geotherm (Carswell and Gibb,1980a)

Sources of data:

Boyd et. al. (1976), Eggler and McCallum (1974,1976), Ehrenberg (1979), Ferguson and Sheraton (1979), Ferguson et. al. (1977), Garrison and Taylor (1980), Irving (1973), Lovering and White (1964), McCallum et. al. (1975), Mitchell (1977,1978), Nixon and Boyd (1979), Sobolev (1977), Wilkinson (1974), Smith and Levy (1976).

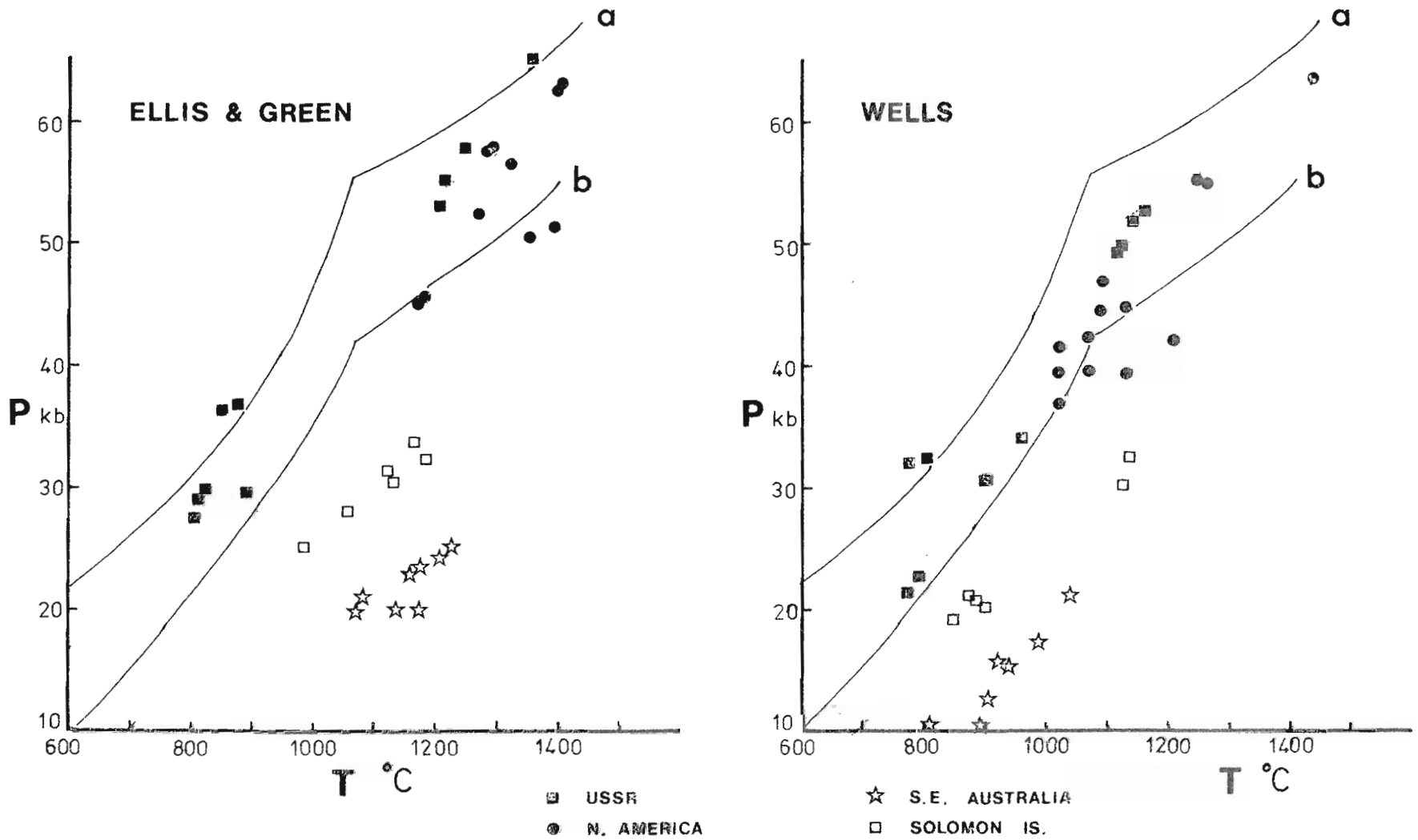
ELLIS & GREEN
a
b
60
50
40
30
20
10
P kb
600
800
1000
1200
1400
T °C
USSR
N. AMERICA
WELLS
a
b
60
50
40
30
20
10
P kb
600
800
1000
1200
1400
T °C
S.E. AUSTRALIA
SOLOMON IS.

not unreasonable estimates (10-20 kbar) in either case.

It must be stressed that the application of the orthopyroxene-Al_2O_3 barometer to garnet peridotite xenoliths is subject to large uncertainty arising both from error in temperature estimation, as discussed above, and from analytical uncertainty. As Al_2O_3 contents in the orthopyroxenes contained in garnet peridotites are very low, the problems of analytical uncertainty will be greatly magnified in calculation of equilibrium pressures. Thus, for the higher P-T xenolith samples the cumulative error in calculated pressures may be ±10 kbar.

II. ALPINE AND NORWEGIAN GARNET PERIDOTITES AND ORTHOPYROXENE ECLOGITES

P-T estimates obtained for published examples of garnet peridotite bodies in gneiss terraines (Ernst, 1978; Evans and Trommsdorff, 1978; O'Hara and Mercy, 1966; Medaris, 1980; Obata, 1980) and Norwegian orthopyroxene eclogites (Lappin and Smith, 1978; Green, 1969; Lappin, 1977; Carswell and Gibb, 1980) are presented in figure 4.9a and b. Pressures have been calculated using equation 3.15 and temperatures obtained using either garnet-clinopyroxene Fe-Mg exchange thermometry (Ellis and Green, 1979) or two-pyroxene thermometry (Wells, 1977).

Alpine and Norwegian garnet-peridotite-bearing ultramafic bodies (figure 4.9a and b) yield P-T estimates which lie between the low-pressure limbs of the Lesotho geotherms generated by Boyd (1973) (curve a) and Carswell and Gibb (1980) (curve b). Core and rim mineral composition data (Evans and Trommsdorff, 1978; Medaris, 1980), connected by arrows in figure 4.9a, clearly indicate retrograde equilibration of the garnet-peridotites enclosed in ultramafic bodies.

Fig. 4.9 P-T estimates for garnet peridotite-bearing ultramafic bodies in crustal gneisses in the Alps and Norway, the Ronda peridotite massif, and Norwegian orthopyroxene eclogites. P estimated via equation 3(15); T estimated via :

a. ga-cpx Fe-Mg distribution thermometry (Ellis and Green,1979)

b. two-pyroxene thermometry (Wells, 1977)

Curve a. - Lesotho geotherm (Boyd, 1973)

Curve b. - Lesotho geotherm (Carswell and Gibb, 1980a)

Sources of data :

Carswell (1973,1978), Ernst (1978), Evans and Trommsdorff (1978), Green (1969), Lappin (1974), Lappin and Smith (1978), Medaris (1980), Mysen and Heier (1972), Obata (1980), O'Hara and Mercy (1966).

Core to rim zoning data obtained by Medaris (1980) and Evans and Trommsdorff (1978) for minerals in garnet peridotite bodies are shown by arrows.

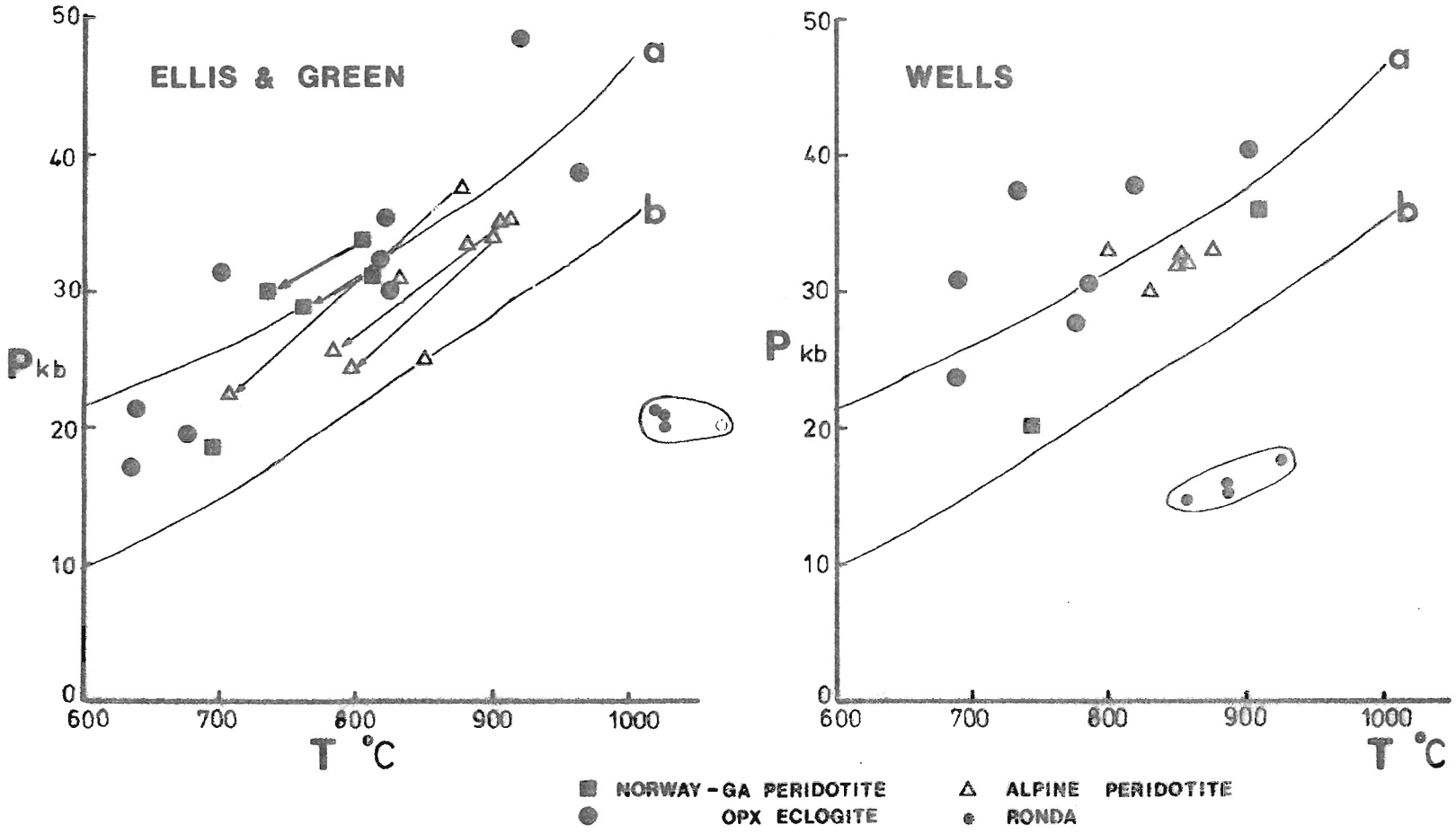
ELLIS & GREEN
WELLS
a
b
P kb
T °C
50
40
30
20
10
0
600
700
800
900
1000
NORWAY - GA PERIDOTITE
OPX ECLOGITE
ALPINE PERIDOTITE
RONDA

The new P-T estimates obtained here support an upper mantle origin of these garnet peridotite bodies, and indicate emplacement and upward tectonic transport of pre-existing garnet-peridotite assemblages into crustal rocks, consistent with the interpretations of previous workers.

The Ronda garnet-peridotite mass (Obata, 1980) is an example of a contrasting garnet-peridotite association in that this body equilibrated at much higher temperatures and at lower pressures than the ultramafic bodies discussed above (figure 4.9a and b). P-T estimates obtained for the Ronda massif are related to a subsolidus recrystallisation event, rather than to the P-T conditions of formation of original aluminous pyroxene porphyroblasts (Obata, 1980). The distinct P-T regime and field relationships (Obata, 1980) of the Ronda peridotite mass suggest that the mode of emplacement of this body was different to the tectonic interleaving processes apparently responsible for emplacement of the garnet-bearing peridotite bodies considered above.

Orthopyroxene eclogites or garnet pyroxenites occur in the gneiss terrain of Norway in isolated eclogitic boudins which may also contain quartz-eclogite, kyanite-eclogite, and zoisite-eclogite layers (country-rock eclogites). These eclogites have been interpreted in two distinct ways:

(a) as *in situ* prograde metamorphic assemblages. The eclogites have formed from deep-seated metamorphism of basaltic rock types previously emplaced as dykes in a crustal sequence (Brynhi *et al.*, 1977; Mysen and Heier, 1972; Griffin, 1971; Green, 1969; Krogh *et al.*, 1976; Carswell, 1974; Carswell and Gibb, 1980a). A model of subduction and continental collision has been developed to account for the

eclogite-gneiss terrane (Krogh, 1977);

(b) as tectonically emplaced bodies which were metamorphosed *prior to* emplacement in surrounding gneisses (Lappin, 1977; Lappin and Smith, 1978). The eclogites and surrounding gneisses are thus not isofacial in this model. Eclogites formed under upper mantle conditions are suggested to have been emplaced into the gneisses during a continent-continent collision event.

The essential argument in denying an *in situ* model for the origin of the country-rock eclogites is the P-T conditions of formation of these eclogites in relation to the enclosing gneisses. P-T estimates for such eclogites, based on equation 3.15 and garnet-clinopyroxene (Ellis and Green, 1979) or two-pyroxene (Wells, 1977) thermometry are presented in figure 4.9a and b.

These estimates show a broad region of overlap with pressures calculated for Norwegian and Alpine garnet-pyroxenite-bearing ultramafic bodies. The lower P-T data derived from published mineral composition data (Green, 1969; Carswell, 1968; Krogh and Griffin, 1981) for country-rock eclogites are also in the upper range of the P-T path proposed by Krogh (1977) for Norwegian eclogites and may be continuous with that path. Higher P-T estimates obtained from the data of Lappin and Smith (1978) are inconsistent with the presence of plagioclase in surrounding gneisses and would argue against an *in situ* origin for the orthopyroxene eclogites.

The range of P-T estimates obtained for these country-rock eclogites (650^{o}C, 17 kb to 950^{o}C, 40 kb) is considered to be too large in comparison to the overall similarities of the various orthopyroxene eclogites. At present, the P-T information gained from published data must be considered ambiguous in any interpretation of an *in situ* or foreign origin of these eclogites, for the following reasons:

(a) in most published work, the nature and direction of compositional zoning in coexisting phases in the orthopyroxene eclogites has not been reported or considered. In view of the importance of the P-T estimates, it is essential that coexisting *rim* analyses be available and that zoning relationships are well known so that the rim data may be evaluated critically.

(b) the 4 kbar/100°C slope of the orthopyroxene-garnet Al_2O_3 barometer applied herein (equation 3.15) means that estimated pressure is critically dependent on the calculated or assumed temperature of equilibration. At low temperatures (650-1000°C) the $K_D^{ga-opx}_{Fe-Mg}$ thermometer (Ellis and Green, 1979) is more sensitive and hence more applicable than the two-pyroxene thermometer, but still is considered to have an accuracy of only ±50°C. This error alone results in a ±2 kbar uncertainty on calculated pressures, even before analytical uncertainties and the problems outlined in (a) above are considered.

III. CRUSTAL GRANULITES

P-T estimates for published examples of garnet-orthopyroxene-bearing granulite facies assemblages are presented in figure 4.10. In these examples, pressures are calculated using equation 3.15 and temperatures obtained using the published estimates or the following thermometers:

(a) in clinopyroxene-bearing assemblages, the $K_D^{ga-cpx}_{Fe-Mg}$ thermometer (Ellis and Green, 1979) - e.g. Griffin *et al.* (1980); Wells (1979); O'Hara and Yarwood (1978); Savage and Sills (1980); Griffin and Raheim (1973); McLelland and Whitney (1977).

(b) in other assemblages (e.g. ga + opx + cd + qz; ga + opx + sill ± qz; ga + opx + qz), the $K_D^{ga-opx}_{Fe-Mg}$ thermometer developed in

Chapter 2 and Chapter 3 has been used - e.g. Nixon *et al.* (1973; Berg (1977a,b); Krylova and Priyatkina (1976); Davidson and Mathison (1974), Howie and Subramaniam (1957); Weaver *et al.* (1978); Karsakov (1973); Kitsul and Kopylov (1974).

As noted in previous sections, the temperature estimate is a critical factor in the estimation of pressures of equilibration because of the 4 kbar/100^{o}C slope of the Al_2O_3 barometer.

In general, pressures estimated using equation 3.15 are reasonable in that excessively high (> 15 kbar) pressures or negative pressures are not calculated for any granulite facies samples. In addition, P-T estimates are in good agreement with the favoured estimates of the original workers. For example, all but two samples from the Nain complex, Labrador (Berg, 1977a,b), are in the P-T field 1-7 kbar and 675-850^{o}C, with most samples indicating pressures below 4 kbar (figure 4.10b), in good agreement with the general range of P-T conditions inferred by Berg (1977a,b) using other barometry-thermometry techniques.

The extensive P-T field embraced by the granulite facies is indicated in figure 4.10. The orthopyroxene-bearing parageneses occur over a pressure range of 2-12 kbar (and possibly 15 kbar) and in the temperature interval 650-1000^{o}C.

Suites of granulites or garnet-orthopyroxene-bearing meta-igneous rocks from selected areas show good clustering of P-T estimates. Archaean granulite facies relics from southwestern Greenland (Griffin *et al.*, 1980) are inferred to have equilibrated at 10 ± 2 kbar and 660 ± 50^{o}C (figure 4.10a), in contrast to the scattered pressure estimates obtained by Griffin *et al.* (1980) using the barometer of Wood (1974). Ultramafic and mafic granulites from the Lewisian province of Scotland (O'Hara and Yarwood, 1978; Savage and Sills, 1980)

Fig. 4.10 P-T estimates for published examples of ga-opx bearing granulites. P estimated via equation 3(15) ; T estimated via equation 3(16), or using the ga-cpx thermometer of Ellis and Green (1979). Sources of data :

a. □ Greenland (Griffin et. al.,1980);
■ Scourie (O'Hara and Yarwood, 1978)
○ Stanovik, U.S.S.R. (Karsakov, 1973)
▲ Kola Peninsula (Krylova and Priyatkina, 1976)
△ W. Australia (Davidson and Mathison, 1974)
● Vredefort, S. Africa (Schreyer and Abraham, 1978)
• Greenland and Scotland (Wells, 1979 ; Savage and Sills, 1980)

b. ■ Nain, Labrador (Berg, 1977a,1977b)
▼ Norway (Griffin and Raheim, 1973)
● Adirondacks (McLelland and Whitney, 1977)
□ India (Howie and Subramaniam, 1957 ; Jan and Howie, 1980 ; Weaver et. al.,1978)
▽ Uganda (Nixon et. al.,1973)

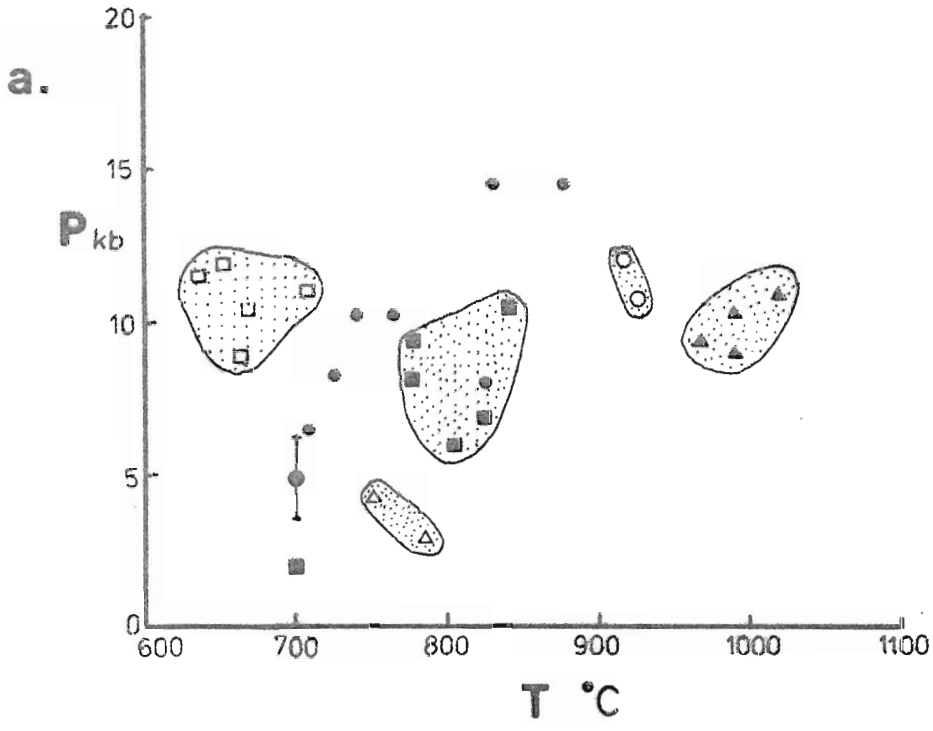
a.
20
15
10
5
0
Pkb
600
700
800
900
1000
1100
T °C

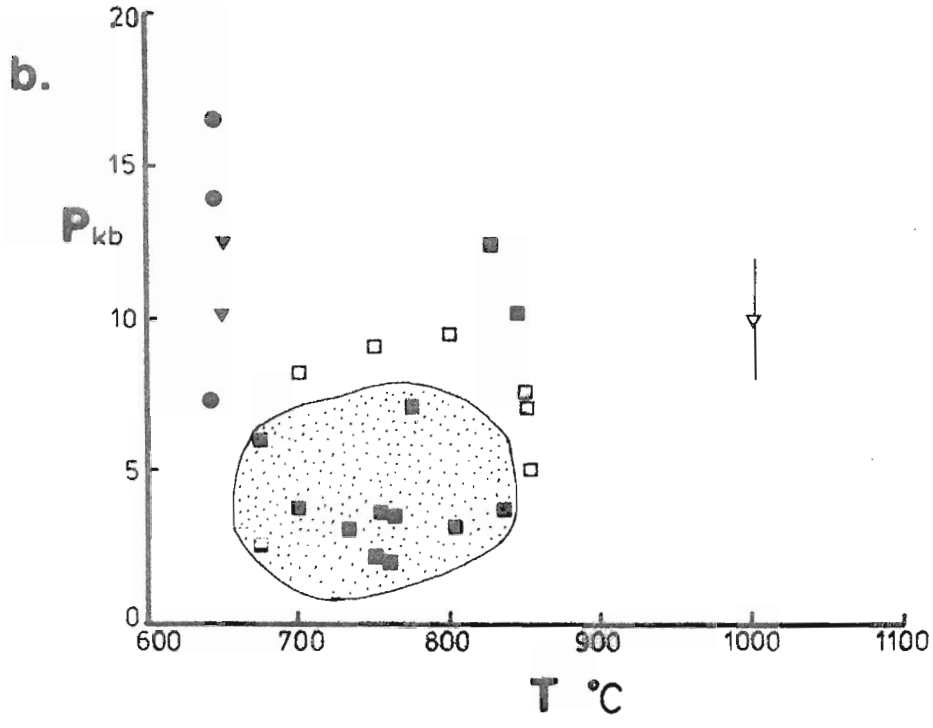
b.
20
15
10
5
0
Pkb
600
700
800
900
1000
1100
T °C

are estimated to have re-equilibrated at 8 ± 2 kbar and at temperatures of 800 ± 50°C (figure 4.10a). These temperatures are higher than those estimated by O'Hara and Yarwood (1978) but are in agreement with the estimates of Savage and Sills (1980), and the calculated pressures are reasonable for all but one sample of O'Hara and Yarwood (1978) which yields a pressure of only 2 kbar. Combined use of the garnet-clinopyroxene thermometer (Ellis and Green, 1979) and equation 3.15 thus yields positive and, usually, reasonable P-T estimates for the data of O'Hara and Yarwood (1978), in contrast to the *negative* pressures these authors have calculated for the same samples using the barometer of Wood (1974).

Sillimanite- or sapphirine-bearing garnet-orthopyroxene assemblages reported from the USSR (Krylova and Priyatkina, 1976; Lutts and Kopaneva, 1968) and from Uganda (Nixon *et al.*, 1973) yield P-T estimates, based on the garnet-orthopyroxene barometry and thermometry developed in Chapter 2 and Chapter 3, which are consistent with the phase topology constraints and the experimental work of Hensen and Green (1973) (figure 4.10).

Retrograde garnet-bearing coronas in meta-igneous rocks from Norway (Griffin and Råheim, 1973) and the Adirondacks (McLelland and Whitney, 1977) are estimated to have formed at 600-650°C and 7-17 kbar. The coronas in metamorphosed dolerites from Norway, are inferred to have formed at 10-12 kbar, consistent with the partial eclogitisation undergone by these dolerites (Griffin and Råheim, 1973). On the other hand, the data of McLelland and Whitney (1977) yield unrealistically high pressures of 14 and 16.5 kbar for two magnesian samples. In view of the strong compositional zoning likely to be present in the coronas, there is a strong possibility that reported Al_2O_3 contents are not those of orthopyroxenes coexisting with garnet in such

assemblages. These results indicate that geothermobarometry must be applied with great caution to assemblages displaying disequilibrium textures. It is essential to obtain analyses of *adjacent rim* compositions of constituent minerals.

The granulites considered in figure 4.10 include a wide range of compositions in terms of X_{Ca}^{ga} and X_{Mg}^{opx}. In general, the garnet-orthopyroxene barometer can be used over this compositional range without apparent systematic errors arising except in some Mg-rich parageneses. The barometer is less reliable and has large uncertainty when X_{Al}^{opx} is very low, for example in high-Ca, high-Fe assemblages formed at low temperatures (600-700°C). In such cases analytical uncertainty in determination of Al_2O_3 is responsible for large uncertainties in pressure calculation.

For all applications, the following points must be recognised:

(a) Fe^{3+} calculation will alter X_{Al}^{opx}, and thus $P_{calculated}$. Fe^{3+} corrections must be applied to garnet as well as orthopyroxene, and these corrections should probably only be applied in obviously oxidised assemblages or where Fe_2O_3 contents have been directly determined.

(b) it is necessary to obtain, if possible, analyses of *coexisting* garnet and orthopyroxene rims. If core compositions are to be used it is vital to clearly define the nature and direction of zoning, if any occurs, within the minerals. Such careful attention to analytical techniques will enhance the reliability of this barometer and the independent thermometers used to derive P-T conditions.

Chapter 5

PYROXENE GRANULITES FROM THE NAPIER PROVINCE, ENDERBY LAND, ANTARCTICA : PETROGRAPHY, MINERAL REACTIONS, AND P-T METAMORPHIC HISTORY.

5.1 INTRODUCTION

The purpose of this and subsequent chapters is to obtain a reconstruction of the physical conditions of metamorphism and the metamorphic evolution of granulites from the Napier Complex, Enderby Land, based on the application of experimentally determined geothermometers and geobarometers to common mineral assemblages.

This chapter documents the occurrence and petrography of two-pyroxene bearing granulites from the Napier Complex. Widely used semi-empirical thermometers are applied to estimate temperatures of formation of the primary metamorphic assemblages. Retrograde equilibria leading to the formation of garnet in these rocks during a later metamorphic event and shearing are discussed, and P-T conditions of these events are established using garnet-clinopyroxene thermometry (Ellis and Green, 1979) and garnet-orthopyroxene thermometry-barometry developed in previous chapters.

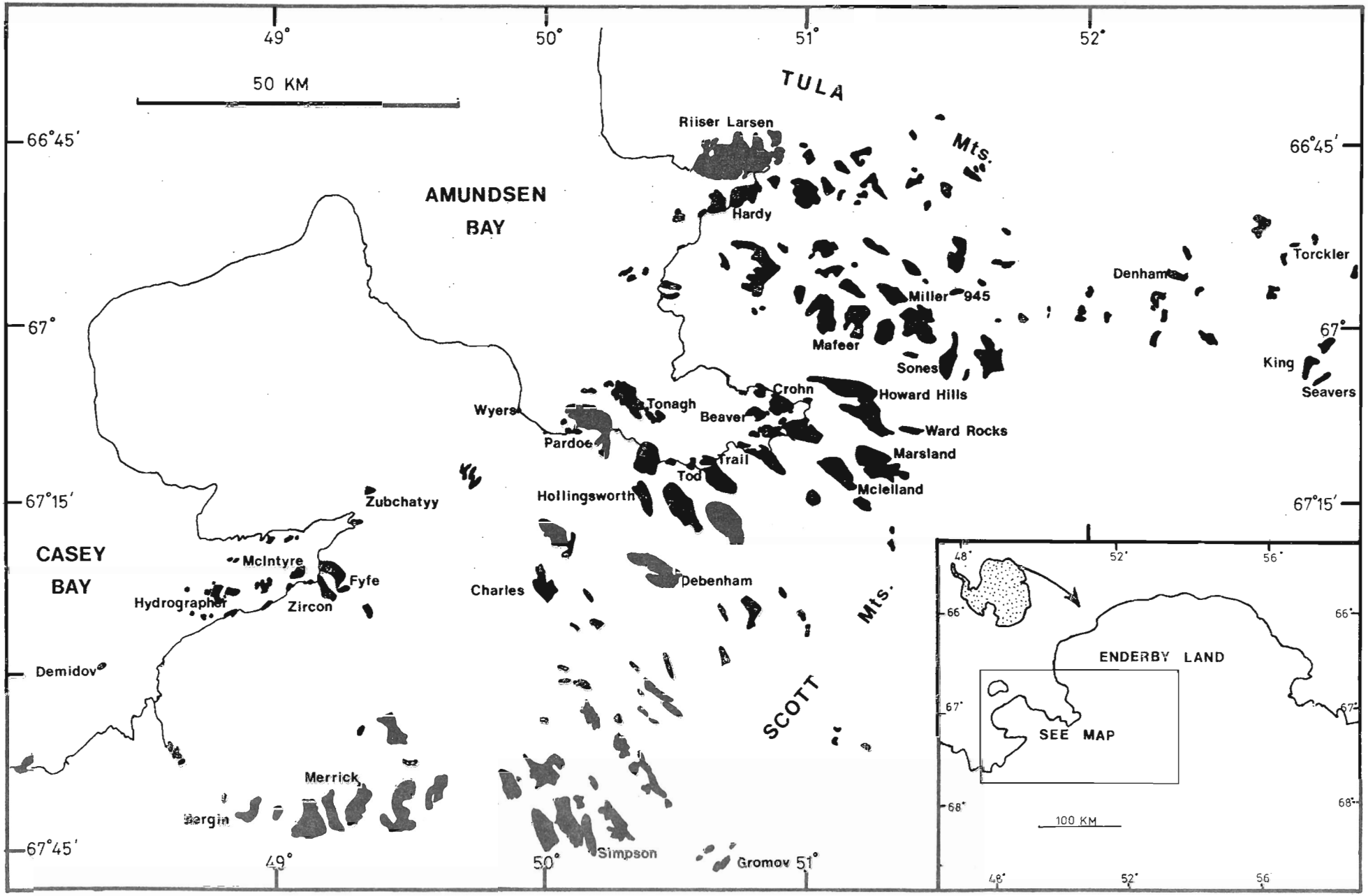

FIG. 5.1 LOCALITY MAP OF ENDERBY LAND, ANTARCTICA

5.2 REGIONAL GEOLOGICAL SETTING OF THE NAPIER COMPLEX

The Napier Complex (Kamenev, 1975) is an Archaean granulite facies terrain of some 100,000 km^2 area, making up most of Enderby Land, Antarctica (figure 5.1). This polymetamorphic complex is bounded by the Proterozoic Rayner Complex (Kamenev, 1975). Early investigations by Russian workers (Kamenev, 1972; Ravich & Kamenev, 1975) established these two separate provinces, and regions of overlap of the younger metamorphic terrain (Rayner Complex) onto the Archaean Napier Complex.

The Rayner Complex consists of upper amphibolite to granulite facies metamorphics, charnockitic and anorthositic (?) intrusives and boudinaged metamorphosed basic dykes which are interpreted to be metamorphosed relics of basic dykes occurring in the Napier Complex (Amunsden Dykes, Sheraton *et al*, 1980). Metamorphism in the Rayner Complex is dated at 1000 m.a. (m.a. = million years) on the basis of U/Pb and Rb/Sr isotopics (Black, in prep.; Grew, 1978).

The Napier province is unusual among granulite facies terraines in the preservation on a regional scale of the high grade aluminous and pelitic assemblages sapphirine-quartz (Dallwitz, 1968, Sheraton *et al.*, 1980; Ellis *et al.*, 1980; Grew, 1980), hypersthene-sillimanite-quartz, and osumilite bearing assemblages (Ellis *et al.*, 1980). Over a large area including the Scott and Tula mountains (figure 5.1) primary garnet-cordierite assemblages were unstable during M1-M2 (3100 m.a.). These observations place broad constraints on the P,T conditions of the first metamorphic events in the Napier province, and indicate metamorphism at 7-9 kbar and 900-980°C (Ellis, 1980; Grew, 1980; Sheraton *et al.*, 1980).

The unusual mineral assemblages referred to above have attracted a great deal of interest, and previous detailed petrological studies

have concentrated in particular on the sapphirine-quartz and osumilite-bearing assemblages. Such rocktypes occur as rare thin (1cm-1 metre) layers within a much more extensive well-layered granulite sequence. The well layered sequence has been termed the Tula Series (Kamenev, 1975). This consists predominantly of garnet-quartz feldspar gneisses and two pyroxene-feldspar-quartz granulites, subordinate layers of aluminous and siliceous metasediments (Sheraton *et al.*, 1980), with ultramafic pyroxenite boudins locally developed. As well as the exotic mineral assemblages referred to above, the aluminous rocktypes include garnet-sillimanite- and garnet-orthopyroxene-bearing feldspathic gneisses which locally may comprise up to thirty percent of the layered sequence (e.g., Mt. Sones, Tonagh Island East).

A separate, poorly layered to massive gneiss group, the Raggatt Series (Kamenev, 1975) has been recognised in the Napier province. This series consists of pyroxene-feldspar-quartz gneisses with minor mafic and ultramafic layers (Sheraton *et al.*, 1980). The major rocktype in this series is orthopyroxene-quartz-feldspar gneiss which occasionally contains garnet. Two-pyroxene gneisses and granulites are also common. These consist of orthopyroxene-clinopyroxene-plagioclase ± Kfeldspar ± quartz with additional ilmenite, magnetite, apatite and hornblende or biotite. Orthopyroxene-clinopyroxene websterite boudins also occur in this group.

Pyroxene granulites and orthopyroxene-garnet parageneses thus occur in both the well layered granulite gneiss sequence (Tula Series) and in the more massive series (Raggatt Series). The widespread occurrence of these assemblages throughout Enderby Land renders them useful in delineating regional metamorphic patterns and in determining (P,T) histories at individual sites or outcrops. Such P-T information

provides a framework into which information obtained from the exotic sapphirine and osumilite-bearing assemblages referred to above may be integrated.

5.3 STRUCTURAL GEOLOGY AND GEOCHRONOLOGY OF THE NAPIER COMPLEX

Following earlier reconnaisance by Russian workers (Kamenev, 1972; Ravich and Kamenev, 1975), a detailed and comprehensive programme of geological investigation has been undertaken in the Napier Complex over the last decade by Australian scientific expeditions.

The current understanding of the regional geological history of the Napier province has been summarised by Sheraton *et al.*(1980) and James and Black (1981). A table summarising the sequence of geological events with time, modified after Sheraton *et al* (1980), is presented in Table 5.1

Three distinct major deformation episodes have been recognised in the Napier province (Sheraton *et al.*, 1980; James and Black, 1981). The first deformation, D1, produced recumbent symmetric isoclinal folds on all scales. This deformation was characterised by intense flattening, a horizontal style, and marked thickening of fold hinges (James and Black, 1981). Axial plane fabrics defined by quartz ribbons, lensoidal pyroxene aggregates, and sillimanite orientations in the paragneisses of the very well layered gneissic sequence (James and Black, 1981), are preserved occasionally in F1 minor fold hinges. Generally, however, uniform equigranular to inequigranular granoblastic textures, with some streaky layer-parallel foliation or mineral elongation, are developed in most rocktypes (James and Black, 1981).

The second deformation, D2, has produced common mesoscopic to moderate scale (amplitudes 100's metres) assymmetric, tight to isoclinal folds (Sheraton *et al.*, 1980; James and Black, 1981; Griffin, 1979). These folds are characterised by inclined axial planes, the abundance of parasitic assymmetric folds, the absence of marked hinge thickening, and the general absence of any penetrative S2 planar

Table 5.1 DEFORMATION / METAMORPHIC HISTORY OF THE NAPIER PROVINCE

EVENT	AGE (m.a.)	DEFORMATION FEATURES	METAMORPHISM & TEXTURES
D1	3100 to 3000	flat lying isoclinal folds; layer-parallel foliation ; strong elongation lineation; symmetric folds ; ribbon textures in axial; regions ; sillimanite lineations .	GRANULITE FACIES PEAK 950°C, 7-10 KB * coarse elongate textures, or polygonal granoblastic
D2	3000 to 2700 ?	assymmetric tight folds; parasitic folds common ; inclined axial planes ; no penetrative S_2 ; rodding lineation ; sillimanite lineation ; boudinage .	COOLING TO 700°C, 4-7 KB * coarse granoblastic textures, some pretectonic elongate porphyroblasts. garnet coronas, exsolutions.
D3	2500	upright open-close folds ; large scale dome and basin; weak vertical S_3 ; localised intense deformation and contemporaneous shearing	AMPHIBOLITE TO GRANULITE FACIES TO 600-700°C, 5-9 KB * very variable recrystallisation to fine grain-sizes. Development of garnet coronas, biotite (?) amphibole.
		Mylonite zones	
		Unmetamorphosed dykes	
		Mylonite zones	
	1100	Overprinting by Rayner metamorphism in south	* development of biotite, amphibole

Sources : Sheraton et. al. (1980) ; Black and James (1979); James and Black (1981) ; Black et. al. (in prep) ; this study.

structures (James and Black, 1981).

Original elongate fabrics developed during D1 are often randomised to more equigranular polygonal fabrics by static recrystallisation accompanying and post-dating D2 (James and Black, 1981). The textures resulting from superposed D1 and D2 events are often granoblastic equigranular and polygonal, with no clear tectonite fabrics preserved within individual layers. This general feature has been interpreted to indicate that the early high grade granulite assemblages, herein ascribed to metamorphic "events" M1-M2, reached a final state of textural equilibrium at the culmination of D2 (James and Black, 1981; Black *et al.* (in press)).

The third major deformation, D3, is largely responsible for the current macroscopic and regional orientations of layering in the Napier province (Sheraton *et al.*, 1980; James and Black, 1981; Black and James, 1979). D3 has resulted in the formation of large scale upright, open to close, non-cylindrical and cylindrical folds. These folds have amplitudes of $\simeq$ 1 kilometre and wavelengths in the order of kilometres to tens of kilometres. D3 folding of the earlier recumbent gneiss-granulite sequence has produced a dome-and-basin structural style (James and Black, 1981). Further effects sometimes correlated with D3 are the production of the earliest discrete shear zones and mylonite-ultramylonite zones.

Microscopically, textural effects resulting from the superposition of D3 deformation upon pre-existing granulite fabrics include the development of deformation bands, subgrain structures and marginal recrystallisation in quartz grains. Deformation twins, kinked twins, grainboundary recrystallisation and total recrystallisation to polygonal aggregates may be developed in plagioclase. Orthopyroxenes may be

kinked, and both orthopyroxene and clinopyroxene may recrystallise to finer polygonal aggregates (James and Black, 1981). The intensity of development of these fine grained recrystallised D3 textures is very heterogeneous, and both strongly recrystallised and relatively unaffected zones may occur within one thin section (James and Black, 1981; Black *et al.* (in press)).

In addition to the recrystallisation effects outlined above, the D3 deformation and subsequent recovery has resulted in the production of a variety of reaction coronas involving the formation of garnet along with recrystallisation of quartz-feldspar masses (Sheraton *et al.*, 1980; Black *et al.* (in press)). Such retrograde metamorphic effects are also related to D3- and post-D3 shearing (Sheraton *et al.*, 1980), where amphibolite facies assemblages may develop. The metamorphic effects associated clearly with D3 recrystallisation are termed M3 in this thesis. Some metamorphic indicators such as zoning in minerals may be distinguished from M3 effects on the basis of a lack of recrystallisation. In the absence of unambiguous textural information on the age of retrogressive reaction coronas with respect to D3, these coronas or secondary assemblages can only be dated as post-D2, or, in some cases, post-D1. The formation of these latter secondary assemblages may not be time-synchonous with M3 as defined above.

U/Pb, Pb/Pb and Rb/Sr geochronological studies (Black and James, 1979; James and Black, 1981; Black *et al.* (in press); Grew, 1978) have established the existence of a major metamorphic event, correlated with D3 and M3, at 2480 m.a. The geochronological work of James and Black (1981) indicates an age of 3000-3100 m.a. for cooling following the major deformation - metamorphic episodes which produced the granulite mineral assemblages and pervasive microstructures in the Napier

province (D1-D2 and M1-M2). Further isotopic age dating (Black *et al.*, in press) supports this 3000 m.a. age for early high grade events at Fyfe Hills (figure 5.1), although recent results from Mt. Riiser Larsen may suggest a younger age of 2700 m.a. for D2. (Black, pers. comm.).

5.4 FIELD OCCURENCE AND GENERAL FEATURES OF PYROXENE GRANULITES

The two-pyroxene granulites considered in this chapter occur in two major field associations:

(1) Widespread concordant two pyroxene + plagioclase ± kfeldspar ± quartz + ilmenite gneisses which occur both in the massive sequence (Raggatt Series) and interlayered with aluminous and quartzitic metasediments (Sheraton *et al.*, 1980; James and Black, 1981) of the Tula Series. These two-pyroxene gneisses are clearly an integral, syngenetic, part of the enclosing sequences. Such gneissic layers may be hundreds of metres thick. These two-pyroxene gneiss layers may be massive but often some fine-layering into pyroxene richer- and pyroxene-poorer (plagioclase rich)-bands is developed on scales of 1cm to 10cm. Occasionally pyroxenitic layers (< 3cm) or coarse aggregates occur. Elongation of these aggregates define a poorly developed lineation which is parallel to sillimanite and other mineral elongation lineations developed in metapelites. Mesoscopic tight and isoclinal F2 folds are also developed within the layered two pyroxene granulites (e.g., Tonagh Island, Hydrographer Island, Mt. Charles). These features indicate that these two-pyroxene granulites have shared the same structural history as the metapelities.

In the field, distinct two-pyroxene-feldspar granulite lithologies may be recognised on the basis of the overall modal abundances of pyroxenes compared with feldspar ± quartz. Thus, these granulites may range from mafic two-pyroxene granulites, where pyroxenes comprise most of the rock, to felsic (leucocratic) two-pyroxene granulites whose pyroxenes occur as scattered grains in essentially quartz-feldspathic rocktypes. Intermediate pyroxene granulites with near equal modal abundances of pyroxenes and feldspars also occur.

(2) Locally common but usually minor ultramafic pyroxenitic or websteritic (± minor plagioclase) boudins, layers and lenses occurring mostly within the layered sequences. These bodies rarely exceed 2 metres in thickness and may be up to 10 metres in length. Such boudins are often characterised by very coarse grainsizes (pegmatitic varieties 1cm-10cm grains) in the cores of the bodies. On boudin margins and in "pressure shadows", extensive recrystallisation of the coarse pyroxenes to finer grained (.5cm - 1mm) websteritic granular gneiss is common.

These pyroxenite bodies include both diopsidic, bronzitic and websteritic magnesian rocktypes, and iron-rich rocktypes which may contain primary Fe-augite, Fe-hypersthene or Fe-pigeonite. Evidence has been presented elsewhere (Ellis, 1979) for the pre-metamorphic origin of at least some of the magnesian pyroxenites as cumulate ultramafic bodies.

(3) In addition, two-pyroxene granulites have developed from some cross-cutting basaltic dykes which have intruded prior to or during D3. Such dykes (e.g. at Tonagh Is., Hydrographer Is., and Fyfe Hills) have suffered extensive recrystallisation to very fine (< .1mm) 2 pyroxene + plagioclase ± hornblende ± quartz assemblages during M3 or a later overprinting metamorphism.

Olivine-bearing websteritic granulites have formed from the metamorphism of early magnesian ultramafic dykes in the Mount King area (sample 4095) and at Zircon Point (sample 49408). These metamorphosed dykes (?) have been termed B1 dykes by Sheraton *et al.* (1980).

5.5 PRIMARY METAMORPHIC ASSEMBLAGES

I. PETROGRAPHIC AND TEXTURAL FEATURES

(a) Two-Pyroxene + plagioclase (± qz ± kspar ± hbl ± ilm) granulites

Primary mineral assemblages in these rocktypes range from quartz-absent to quartz bearing types, with quartz bearing types being more feldspathic. Characteristic primary mineral assemblages include:

opx + cpx + plag ± ilm ± hbl (mt may occur)

opx + cpx + plag + ilm ± kspar + quartz

opx + cpx + hbl

opx + cpx + plag

cpx + plag ± minor opx.

These mineral assemblages are believed to reflect, in general, different initial bulk rock compositions in terms of X_{Mg}^{bulk}, Ca contents, and silica saturation.

Coarse grained (.5 to 2mm) lobate and polygonal granuloblastic equigranular textures are typical of most samples. In some cases (e.g., 3508, 3593), particularly in well layered samples, pyroxenes and feldspars may show some dimensional orientation parallel to layering. In leucocratic varieties, which may contain quartz and K-feldspar, primary elongate textures may be preserved in the feldspathic layers. Such elongate textures are, however, often overprinted by later fine recrystallisation attributed to D3. These effects will be discussed in section 5.6.

Pyroxenes are usually anhedral to subhedral with lobate to polygonal grainboundaries. Orthopyroxenes are pleochroic from pink and brown to yellow-green or pale green. Clinopyroxenes are usually pale-green to medium green, and may be pleochroic to yellow-green.

Clinopyroxenes in a metagabbro at Fyfe Hills (49464) are deep green and strongly pleochroic to medium green.

Exsolution lamellae are often strongly developed particularly in clinopyroxenes. Apart from the common pyroxene lamellae, rutile or ilmenite exsolutions may also be developed. Pyroxene exsolution lamellae are typically elongate blebs or thin (10 m) continous lamellae mainly restricted to cores of individual grains.

Plagioclase is usually granoblastic polygonal to lobate where primary textures have not been affected by later recrystallistation. Multiple twinning and optical zoning are common features. In the leucocratic granulites, lobate Kfeldspar and quartz occur with the plagioclase. In most samples, Kfeldspar and quartz are recrystallised (section 5.6) and have sutured grain boundaries.

The granoblastic textures characteristic of primary assemblages indicate textural equilibrium, attained largely during a period of post-deformational crystallisation. This static recrystallisation may be correlated with a thermal peak closely postdating D2 (James and Black, 1981). Earlier (D1?) textures are rare, however strongly poikiloblastic coarse (4mm-6mm) clinopyroxene in 4510 from Fyfe Hills may represent an earlier pre-tectonic (pre-D2) porphyroblast which has partially survived the static recrystallisation event.

(b) Pyroxenitic granulites from boudinaged layers

Primary mineral assemblages in these rocktypes include:

bronzite + diopside ± minor plag + mt

Fe-pigeonite ± plag ± qz + mt

subcalcic Fe-augite ± plag

cpx + garnet ± quartz ± plagioclase + mt

opx + cpx + garnet ± hornblende ± plagioclase ± mt

Assemblages in which primary garnet is absent range from granuloblastic polygonal coarse (1mm-4mm) grained websterites to very coarse grained (5cm-10cm) single pyroxene rocks. These latter rocks consist almost entirely of subhedral to euhedral primsatic pyroxene grains which may become anhedral and form a granuloblastic texture in some rocks. Interstitial plagioclase, lobate magnetite and sometimes quartz occur with the primary pyroxene.

Original pigeonite or subcalcic clinopyroxene in the iron-rich, garnet-absent, primary assemblages contain an early generation of pyroxene exsolution lamellae which are kinked by later deformation and cut by garnet lamellae which appear to have formed during this later deformation. These textures are described in section 5.6.

Primary metamorphic garnet occurs with orthopyroxene, clinopyroxene, magnetite and sometimes hornblende, and plagioclase in garnet pyroxenites from Gromov Nunataks (4818), Demidov Island (4598) and from other localities south of Amundsen Bay (Sheraton *et al.*, 1980; Ellis (in press); (e.g., Wyers ice shelf, Edward Is., 4596). Primary metamorphic textures in these rocks are granuloblastic polygonal and equigranular. Superimposed upon these textures are a variety of later exsolution features resulting in the formation of second generation garnet, orthopyroxene, clinopyroxene and magnetite. Further corona textures involving hornblende and plagioclase are developed in 4598. (section 5.6).

Iron and manganese rich garnet-clinopyroxene (or pigeonite)-quartz -magnetite primary metamorphic assemblages occur associated with the more magnesian pyroxenitic layers in some boudins. Primary metamorphic textures in these ga + cpx + qz rocks are generally polygonal to lobate granuloblastic. Clinopyroxenes usually contain abundant exsolution

lamellae, which may be kinked by later a deformation responsible for the production of recrystallised ga + opx + qz assemblages (e.g., 49461, 3929).

II. MINERAL CHEMISTRY

Chemical data for coexisting orthopyroxene and clinopyroxene from the two pyroxene granulites are presented in Table 5.2. In addition, compositional data for primary metamorphic and secondary recrystallised garnets in the pyroxene granulites is summarised in Table 5.3.

All chemical analyses have been obtained by energy dispersive electron microprobe microanalysis, performed using a JEOL-50A electron microscope attached to an EDAX energy dispersive system. All phases were simultaneously analysed for ten elements (Na, Mg, Al, Si, K, Ca, Ti, Cr. Mn, Fe). All corrections were performed by the TAS-SUEDS data reduction programme (Griffin, 1980).

In each sample, between six and twenty analyses have been performed on each phase. Both cores and rims, as well as internal zones and exsolution lamellae, of individual grains and coexisting grains have been analysed. Data presented in Tables 5.2 and 5.3 for core and rim compositions are based on a number of chemical analyses of the cores or rims, and represent the averages of clusters of analyses (in the case of rims) or end-points in rim to core compositional zoning patterns. In samples showing recrystallisation textures (see below, 5.6), particular attention has been focused upon the delineation of zoning in the individual phases (e.g., 49464). Area scans ($\leq 500\mu m^2$) using a defocused electron beam, have been performed on pyroxenes

where exsolution has been extensive in order to estimate the pre-exsolution compositions of the pryoxenes.

Coexisting pyroxenes, and both primary (4818, 4598) and secondary (in 4818, 4598, 4510, 4509, 4520, 4704, 4359, 4092) garnets are plotted in the Ca:Mg:Fe diagrams of figures 5.2 to 5.7. Localities corresponding to the sample numbers are listed in Table 5.2. In these diagrams, pyroxenes have been adjusted by the extraction of non-quadrilateral components or end-members (e.g., CaTs, MgTs, $Mn_2Si_2O_6$, jadeite, $CaTiAl_2O_6$) and then plotted. Thus, for pyroxenes, these diagrams are equivalent to Wo:En:Fs diagrams. For garnets, the diagrams are analogous to grossular:pyrope:almandine plots. The variable spessartine contents of garnets are thus not represented.

The two-pyroxene primary assemblages span a range of X_{Mg}^{bulk} from .90 to .60, based on the compositions of the coexisting pyroxenes (Figures 5.2 to 5.5). Single pyroxene pigeonite or subcalcic clinopyroxene initial metamorphic assemblages are restricted to iron rich rocktypes (figure 5.3, 5.4) with X_{Mg}^{bulk} less than .50, or to highly calcic or manganiferous rocktypes (see below).

(a) Two-Pyroxene ± plagioclase ± quartz granulites

(1) clinopyroxenes.

Clinopyroxene compositions from both the two-pyroxene + plagioclase gneisses and the websteritic boudins lie almost wholly within the pyroxene quadrilateral, with only minor contents of Al, Ti, Na, Mn and Cr present.

Clinopyroxenes consist of >80% diopside-hedenbergite solid solutions (e.g., figures 5.2 to 5.7). X_{Mg}^{cpx} varies from 93 in plagioclase-free websteritic boudins (3578), to 55 in a quartz-ilmenite-plagioclase bearing feldspathic pyroxene granulite (49412). Most

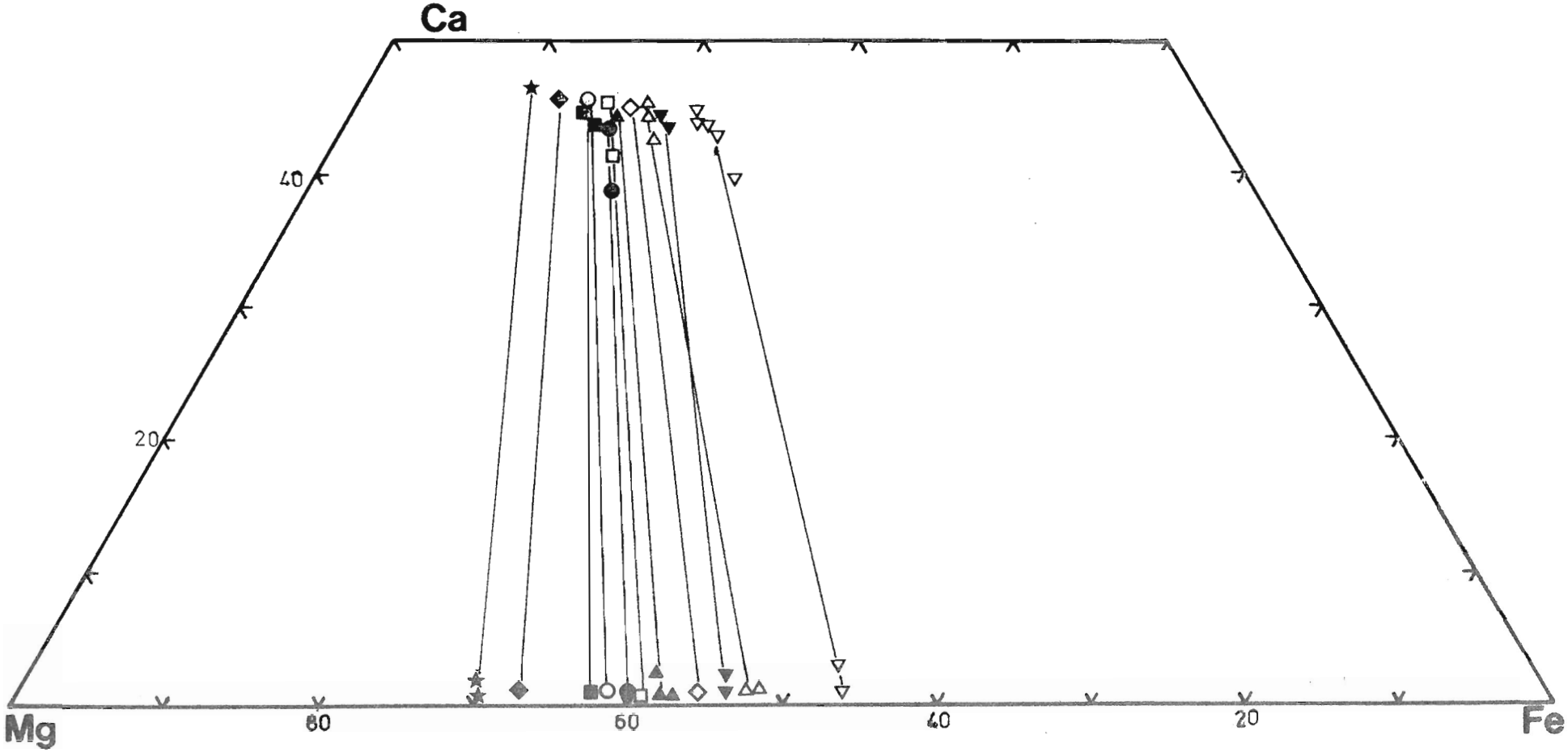

Fig 5.2 Pyroxene quadrilateral (Ca-Mg-Fe diagram with non-quadrilateral components subtracted from pyroxene compositions) illustrating compositions of coexisting pyroxenes from the Napier province. Cores and rims are shown for each sample. Cores plot along opx-cpx rim tielines. Key to symbols :

★ 4095, ◆ 4099, ■ 3577, ○ 3566, ● 3596, □ 3593, ▲ 3508, ◇ 4539, △ 3565, ▼ 3515, ▽ 4509.

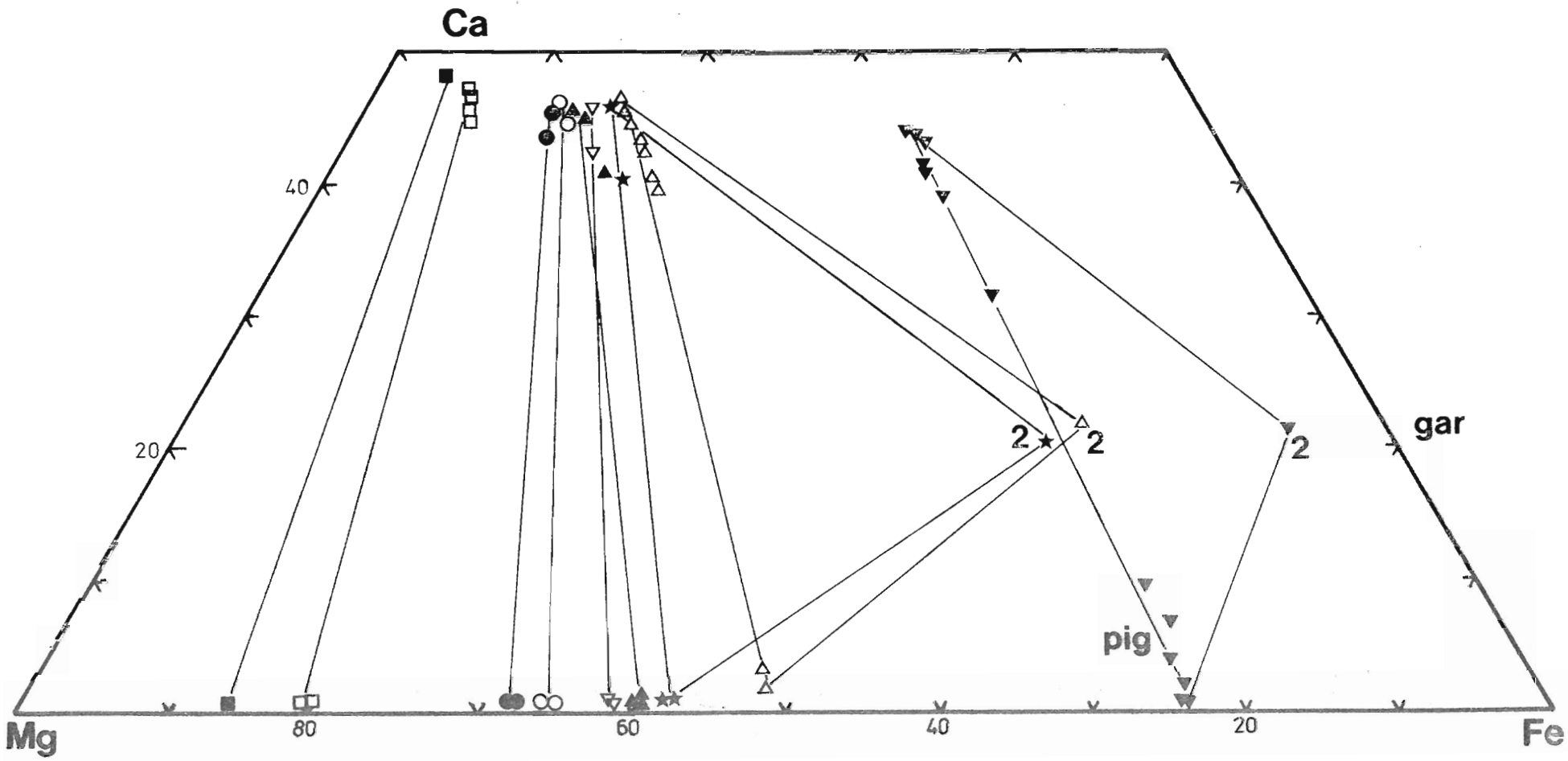

Fig 5.3 Compositions of coexisting pyroxenes and garnets from two-pyroxene granulites from the Napier province , plotted on a partial Ca-Mg-Fe diagram. Non-quadrilateral pyroxene components have been extracted from pyroxene compositions. Cpx cores plot along opx-cpx rim tielines or within opx-cpx-gar triangles. Garnets are secondary (labelled "2"). Symbols : pig...pigeonite ; gar...garnet

■ 3578, □ 4091, ● 4004, ○ 4008, ▲ 3517, ▽ 4545, ★ 4094, △ 4093, ▼ 4092

two-pyroxenes-plagioclase granulites contain clinopyroxenes with X_{Mg}^{cpx} in the range .80 to .60, with the more feldspathic varieties generally containing less magnesian clinopyroxene. Quartz-bearing two-pyroxene granulites contain the most Fe-rich clinopyroxenes (e.g. 4942) but X_{Mg}^{cpx} values in these quartz-bearing rocks overlap with those of the quartz-absent pyroxene granulites (e.g., quartz bearing types 3508, 3565, 3593, 4008, 4521, 4525). Cr and Mn contents are low ($CaCr_2SiO_6 \leq .8$ mol%; $Mn_2Si_2O_6 \leq 1$ mol%; or $Cr_2O_2 \leq .6$ wt%, $MnO \leq .6$ wt%). TiO_2, and hence $CaTiAl_2O_6$ molecule, are also only minor except in some clinopyroxene cores where exsolution has not been marked ($CaTiAl_2O_6 < 1$ mol% but up to 2 mol%, .6 wt%, in some cores).

Na contents of clinopyroxenes are negligible, often below EDAX detection limits or only up to .5 wt% Na_2O (Jd < 4 mol%). On the other hand, the clinopyroxenes contain between 2 and 9 mol% Ca Al_2SiO_5 (Calcium-tschermaks) molecule. The CaTs content of clinopyroxene in equilibrium with plagioclase and quartz is a useful geobarometer (e.g., Ellis, 1980; Wells, 1979; Wood, 1976), and may be applied to the quartz bearing assemblages in this study. In plagioclase bearing assemblages, the CaTs contents of clinopyroxenes tends to increase with increasing anorthite in the plagioclase (Figure 5.13).

Orthopyroxene exsolution lamellae are common within clinopyroxenes from many samples. Analyses presented as end points on orthopyroxene-clinopyroxene tie lines in Fig. 5.2 -5.7 are actually exsolved clinopyroxenes, while less calcic clinopyroxenes are plotted along such tie lines. Cores, area scans, and unexsolved clinopyroxenes are generally more Fe-rich and less calcic than exsolved or rim clinopyroxenes, the latter also often containing lower CaTs contents. In samples where secondary garnet has not formed and no evidence of a discrete lower temperature event is present, clinopyroxenes may show marked

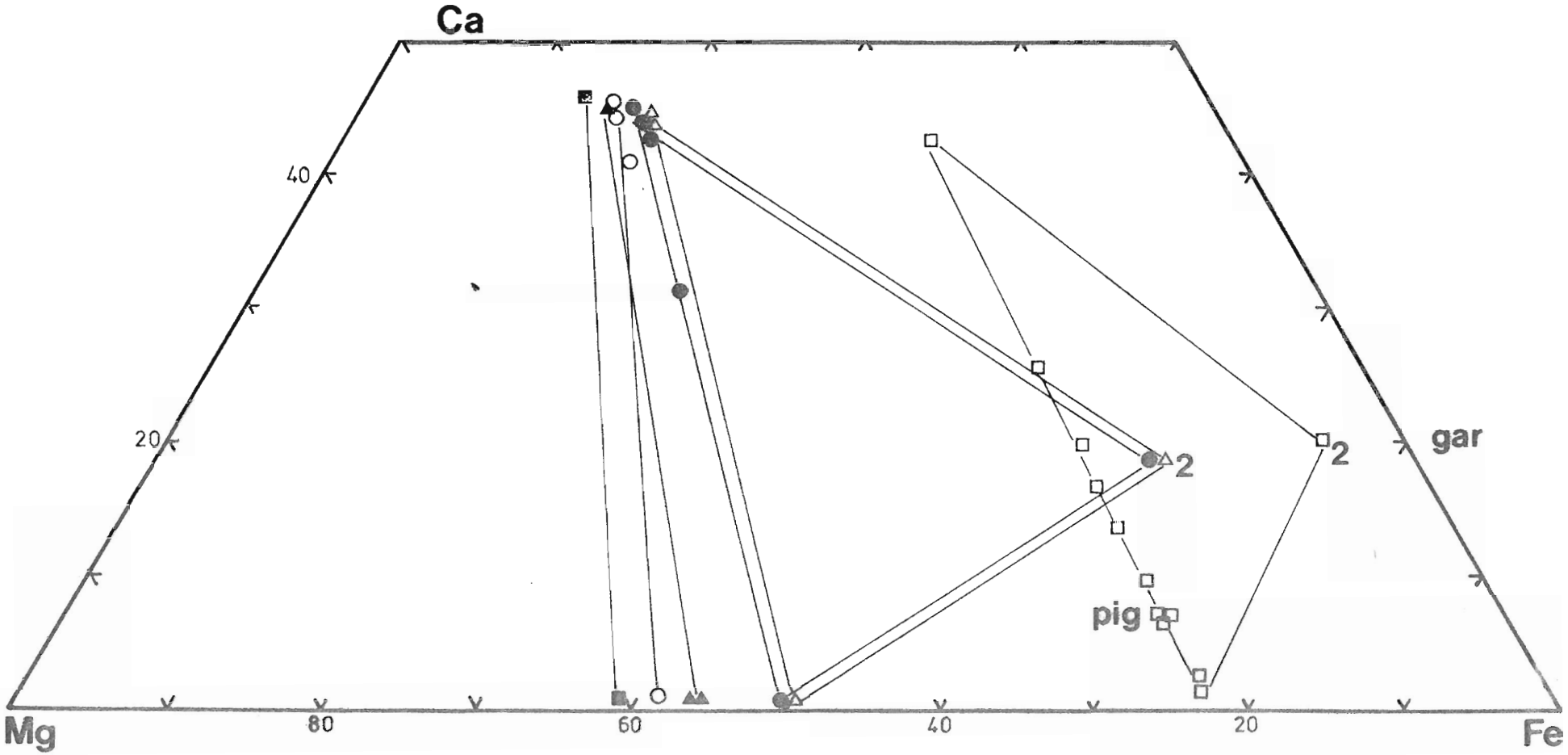

Fig 5.4 Compositions of pyroxenes and garnets (labelled "2") in samples of pyroxene granulites from the Napier province, Enderby Land. Pyroxene are Di-Hd-En-Fs end members only. pig...primary metamorphic pigeonite in 4359, other pyroxenes and garnet inthis sample are secondary (retrograde) products. Symbols :

■ 4525, ○ 4521, ▲ 4319, □ 4359, △ 4520, ● 4704.

zoning and exsolution as evidence of higher metamorphic temperatures followed by prolonged cooling [e.g., 3593, 3596, 4505 (Fig. 5.2); 3517, 4545 (fig. 5.3); 4521 (fig. 5.4); 49458 (fig. 5.7(a)] The increase in calcium content of clinopyroxene coexisting with orthopyroxene, due to mutual exsolution represents a widening of the two-pyroxene "solvus" gap and thus, qualitatively, indicates cooling. Temperature estimates for the highest T cores and area scans, as well as the lower T rims and exsolved clinopyroxenes, will be presented in section 5.7. These estimates are based on various calibrations of the two-pyroxene thermometer (Wood and Banno, 1973; Wells, 1977; Mori and Green, 1978; Henry and Medaris, 1980).

Exsolution lamellae and zoning to more calcic rims is also common in samples where secondary garnet has formed (e.g., 4093, 4094 (fig. 5.3); 4704 (fig. 5.4); 4510 (fig. 5.7(b)). In these samples, however, it is necessary to distinguish recrystallised clinopyroxenes from earlier clinopyroxene porphyroblasts. The lines connecting second generation clinopyroxenes and orthopyroxenes do not necessarily pass through the earlier, less calcic, clinopyroxene compositions as garnet has formed along with the secondary pyroxenes. The formation of secondary garnet in these basic to intermediate pyroxene granulites will be discussed in section 5.6.

(2) Orthopyroxenes

Orthopyroxenes from the two-pyroxene granulites are essentially enstatite-ferrosilite solid solutions ranging in X_{Mg}^{opx} from .86 (bronzite) to .45 (hypersthene). Most samples contain orthopyroxenes with X_{Mg}^{opx} between .70 and .50. X_{Mg}^{opx} is invariably less than the magnesium number of the coexisting clinopyroxene.

The only non-quadrilateral components calculated in the ortho-

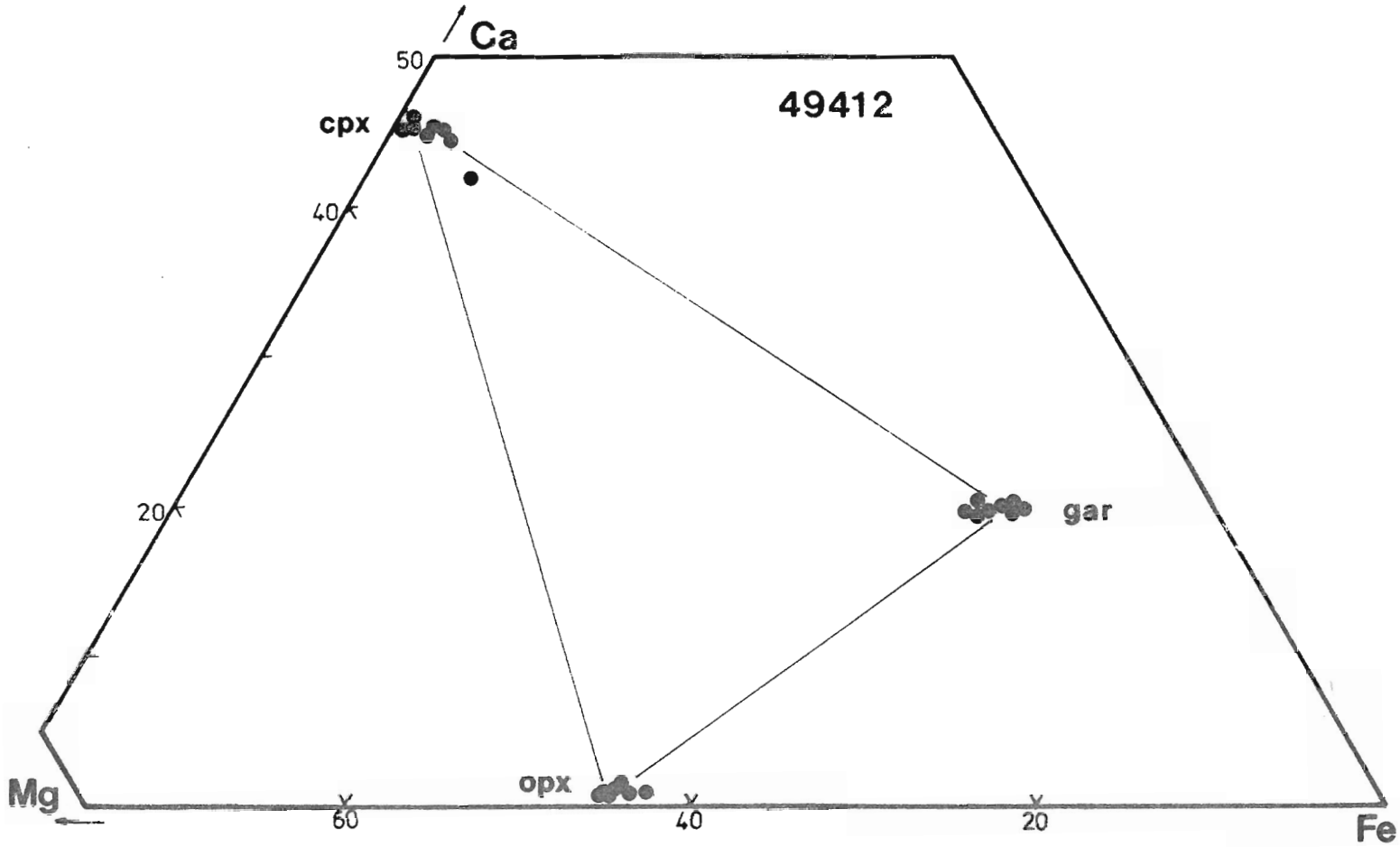

Fig 5.5 Partial Ca-Mg-Fe diagram showing compositions of pyroxenes (quadrilateral components only) and garnets (secondary) in sample 49412 from Zircon Point. Cpx and opx compositions in equilibrium with garnet are indicated by tie lines.

pyroxenes are $Mn_2Si_2O_6$ and $MgAl_2SiO_6$ (MgTs). $Mn_2Si_2O_6$ ranges up to 2 mol% (= 1.3 wt% MnO), while MgTs is in the range 1-6 mol% (≈ .5 to 3 wt% Al_2O_3). Al_2O_3 contents of orthpyroxene increase with increasing Anorthite in coexisting plagioclase, and increasing Al_2O_3 in clinopyroxene.

All orthopyroxenes are low in Ca (< 2 mol% Wo), although orthopyroxene cores and area scans of exsolved grains have higher wollastonite contents (e.g., 4505, 3515, 3508, 4095). These more calcic orthopyroxenes are inferred to have coexisted with the lowest calcium clinopyroxenes in their respective samples, at higher temperatures than would be calculated for coexisting rim compositions.

(3) Other phases

Fine spinel (X_{Mg}^{sp} =.27, Cr_2O_3 = 14 wt%) and interstitial lobate olivine (X_{Mg}^{ol} =.64) occur with clinopyroxene and orthopyroxene in the magnesian, feldspar free pyroxenitic sample 4095.

Early or primary metamorphic hornblende coexists with two pyroxenes in a number of samples (Table 5.2). These amphiboles are aluminous (A/AFM=20), and contain appreciable Na_2O and K_2O (Na_2O up to 3 wt%, K_2O up to 1.2 wt%). Most amphiboles plot between hornblende and pargasite on the diagrams of Figure 5.8. The samples in which primary amphibole is important are mainly restricted to localities occurring in the Rayner Complex.

Compositions of plagioclase coexisting with pyroxenes in individual samples are given in Table 5.2. All feldspars are plotted on the CaNaK (An:Ab:Or) diagram of Figure 5.9 , from which the wide compositional range is obvious.

(b) Garnet + clinopyroxene + orthopyroxene ± plagioclase assemblages (4817, 4818, 4596, 4598)

Compositions of coexisting primary metamorphic phases and secondary or recrystallised phases in these assemblages are plotted in Figure 5.6 (a) and (b).

Early metamorphic clinopyroxenes exhibit marked exsolution of orthopyroxene, garnet, opaque and plagioclase. Compositions of these clinopyroxenes which correspond to the highest metamorphic grades are based on integrated area-scans of individual grains. Such reconstructed primary metamorphic clinopyroxenes are aluminous (X_{CaTs} = .08 to .12 mol%, Al_2O_3 up to 6 wt%), low in Na_2O, and may contain up to .70 wt% TiO_2. X_{Mg}^{opx} is in the range .65-.70, and wollastonite contents are usually 40 mol%. These primary clinopyroxenes are essentially diopsidic, with appreciable solid solution of Calcium Tschermaks molecule and $CaTiAl_2O_6$.

Clinopyroxenes are strongly zoned rimwards to higher wollastonite contents and more magnesian compositions (Fig. 5.6). The rim compositions of clinopyroxenes are discussed in section 5.6(4). It should be noted here that exsolved clinopyroxene lamellae within individual grains approach the rim compositions and secondary clinopyroxene compositions depicted in Figure 5.6.

Early orthopyroxenes have lower Mg-numbers than coexisting clinopyroxene (X_{Mg}^{opx} = .59-.67), but lie essentially on the pyroxene quadrilateral as other end-member molecules are virtually absent. Exsolution lamellae of clinopyroxene and magnetite are developed.

Orthopyroxene coexisting with early clinopyroxene in 4818 is considerably more magnesian than that in 4598, resulting in significantly lower $K_{D_{Fe-Mg}}^{opx-cpx}$ for the former sample. This contrast may be

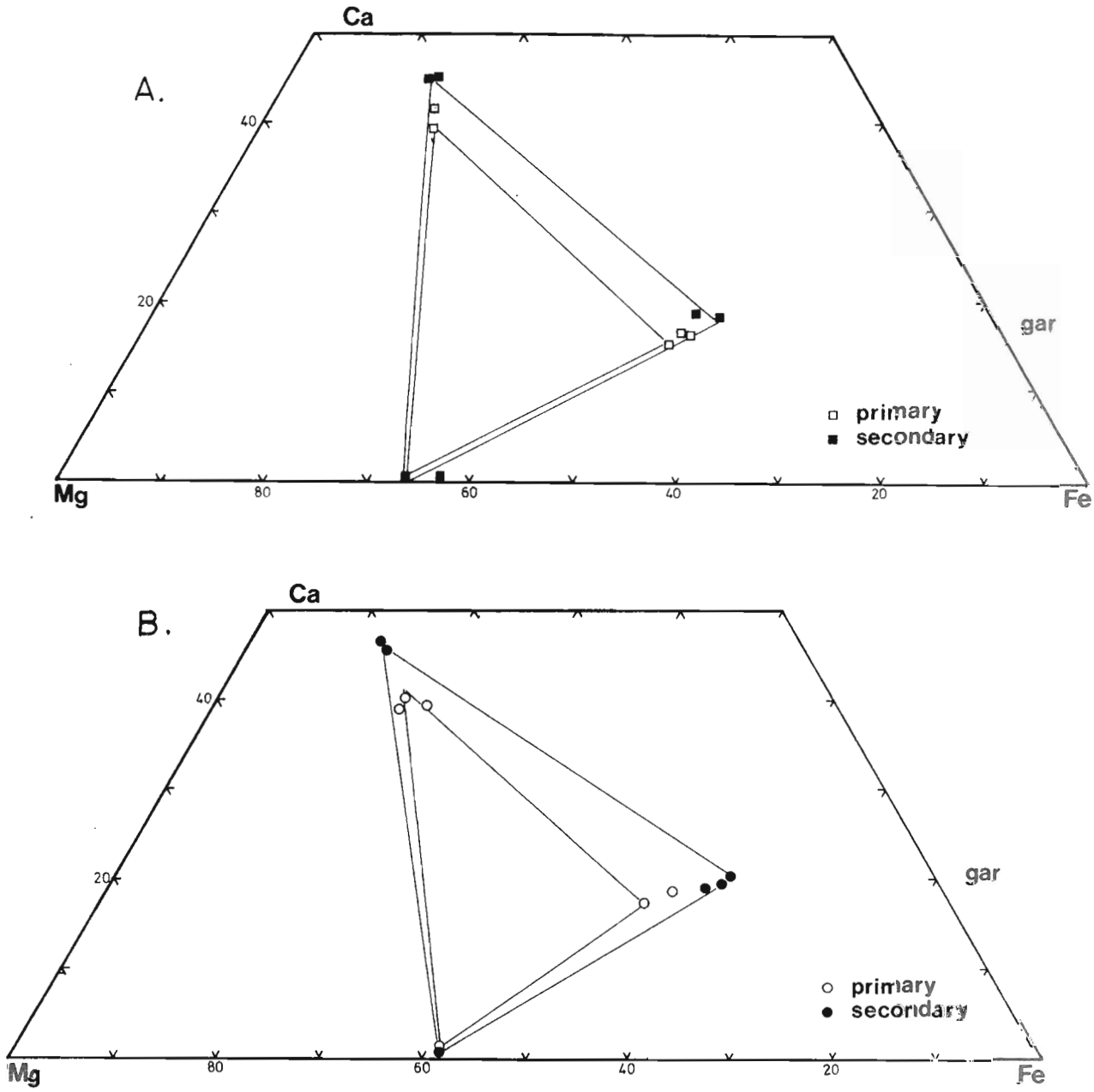

FIG. 5.6 Ca-Mg-Fe diagrams of pyroxenes (quadrilateral components only) and garnets in primary and secondary assemblages in garnet pyroxenites from the Napier province.

A. 4818 Gromov Nunataks
B. 4598 Demidov Island

related to higher temperatures of equilibration for the primary ga + cpx + opx assemblages in 4818. Early-formed or primary metamorphic garnets in each sample are essentially almandine-pyrope-grossular solid solutions with spessartine contents below 1.5%. Grossular contents are in the range X_{Ca}^{ga} = .16 to .18, while X_{Mg}^{ga} ranges from .39 in 4818 to .30-.36 in 4598. Strong rimward zoning to higher X_{Ca}^{ga} and lower X_{Mg}^{ga} accompanies the growth of new garnet as recrystallised grains and exsolved blebs.

Minimum $K_{D_{Fe-Mg}}^{ga-cpx}$ values derived from core compositions of garnet and clinopyroxenes are in the range 3.45-3.64 for 4598 and 4818, indicating similar temperatures of formation in contrast to the $K_{D_{Fe-Mg}}^{opx-cpx}$ values for the same rocks. Temperature estimates based on $K_{D_{Fe-Mg}}^{ga-cpx}$, and on $K_{D_{Fe-Mg}}^{ga-opx}$ (= 3.2 to 2.6) will be presented in section 5.7.

Additional primary phases include plagioclase (An_{80} cores), ilmenite (X_{Mg}^{ilm} = .11), and pargasitic amphibole (figure 5.8). Amphiboles are intermediate in Mg number between clinopyroxene and orthopyoxene (X_{Mg}^{amph} = .63 - .67), and are titaniferous (TiO_2 = 2 - 2.6 wt%).

(c) Iron-rich pyroxene ± plag ± qz assemblages

Two samples, 4092 (Ward Rocks) and 4359 (Zubchatyy) consist mainly of primary metamorphic Fe-rich pyroxene (X_{Mg} = .24-.25) coexisting with quartz, plagioclase (X_{An} = 67 in 4359) and ilmenite (X_{Mg} =.04). Original metamorphic pyroxenes are pigeonites now inverted to orthopyroxene, with Wo contents of 7-9 mol%, and very low Mn, and Al contents. These pyroxenes contain abundant thin exsolution lamellae (10-20μm) of clinopyroxene in a low-Ca orthopyroxene host (figures 5.3 and 5.4). Exsolved clinopyroxenes are Fe-rich (X_{Mg} = .35-.34)

diopside-hedenbergite solid solutions with Wo contents of 40-43%. Orthopyroxene hosts are very Fe-rich (X_{Mg} =.23-.25), containing negligible Mn and Al. The compositions of original metamorphic pigeonite lie on the tie lines connecting exsolved clinopyroxenes and orthopyroxenes in 4092 and 4359. In addition, analyses representing clinopyroxene - orthopyroxene mixtures on edges of exsolution lamellae (particularly 4359) lie on tie lines from the original pigeonite composition.

Temperature estimates for these samples, based on two-pyroxene thermometry, are presented in section 5.7. As exsolution compositions are used in these estimates, the reported temperatures are minima and do not correspond to the temperature at which pigeonite was stable prior to cooling.

(d) Fe-Mn rich garnet-clinopyroxene - quartz - magnetite samples (49461)

Coarse grained (to 5mm) polygonal to lobate granuloblastic ga + cpx + mt + qz form the primary metamorphic assemblage in 49461. This texture is overprinted by a number of subsequent effects including recrystallisation, discussed in section 5.6(1).

Original coarse clinopyroxenes are very subcalcic (Wo = 30-25) iron rich (X_{Mg} =.57), and rich in manganese (MnO - 3 wt%). Analyses of these pyroxenes, obtained by area scans (400μm^2) to incorporate the extensively developed orthopyroxene exsolution lamellae, are illustrated in Figure 5.7(a). These clinopyroxenes coexist with iron- (X^{ga}_{Mg} = .19) and manganese-rich (MnO = 10.5 wt%, $X^{ga}_{spessartine}$ = .24) garnets which also contain appreciable grossular (X^{ga}_{Ca} = .20). $K_{D\,Fe-Mg}^{ga-cpx}$ values of 5.6 are obtained from the compositions of clinopyroxene areas and garnet cores, in contrast to the higher values of

Fig. 5.7 Ca-Mg-Fe diagram illustrating compositions of pyroxenes (quadrilateral components only) and secondary garnets in samples from the Fyfe Hills. Compositions of subcalcic (Mn-rich) primary metamorphic clinopyroxene in 49461 are indicated by area scan analyses. Calcic samples 49464 and 4509 do not contain orthopyroxene.

a. samples from the Fyfe Hills Russian geochronological site.

b. samples from other sites in the Fyfe Hills.

Symbols : Di...diopside

Hy...hypersthene

Ga...garnet

A.

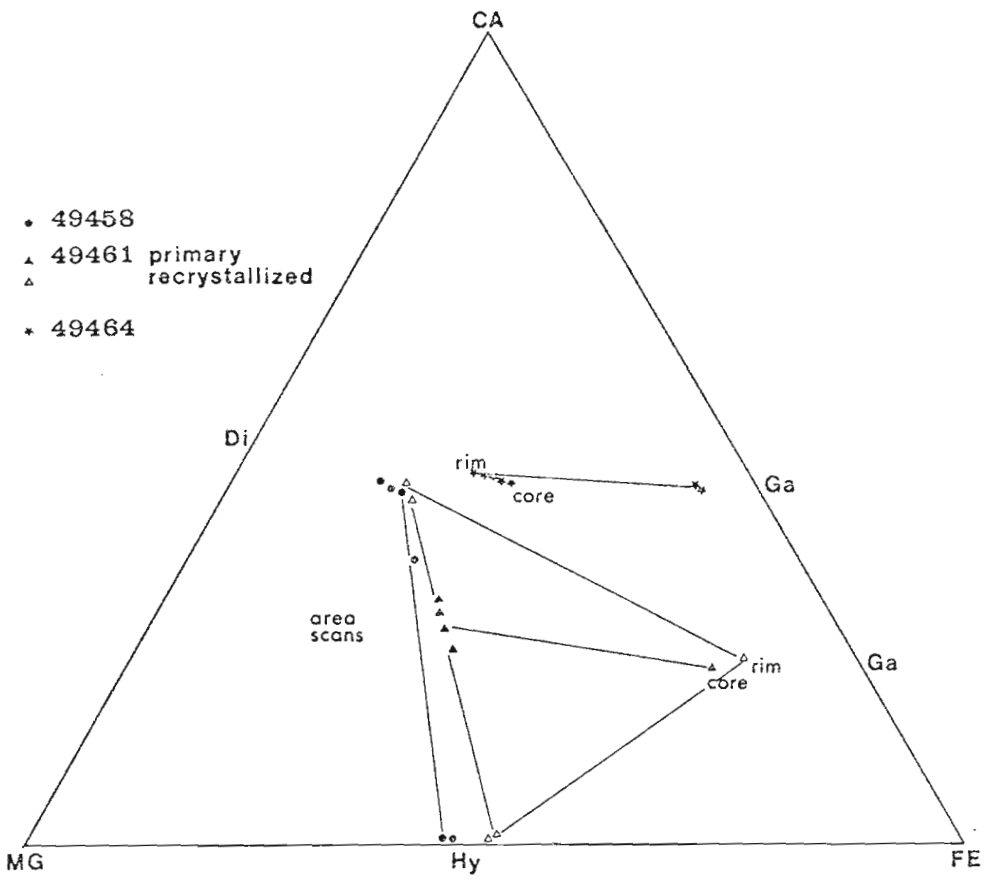

• 49458
▲ 49461 primary
△ recrystallized
* 49464

B.

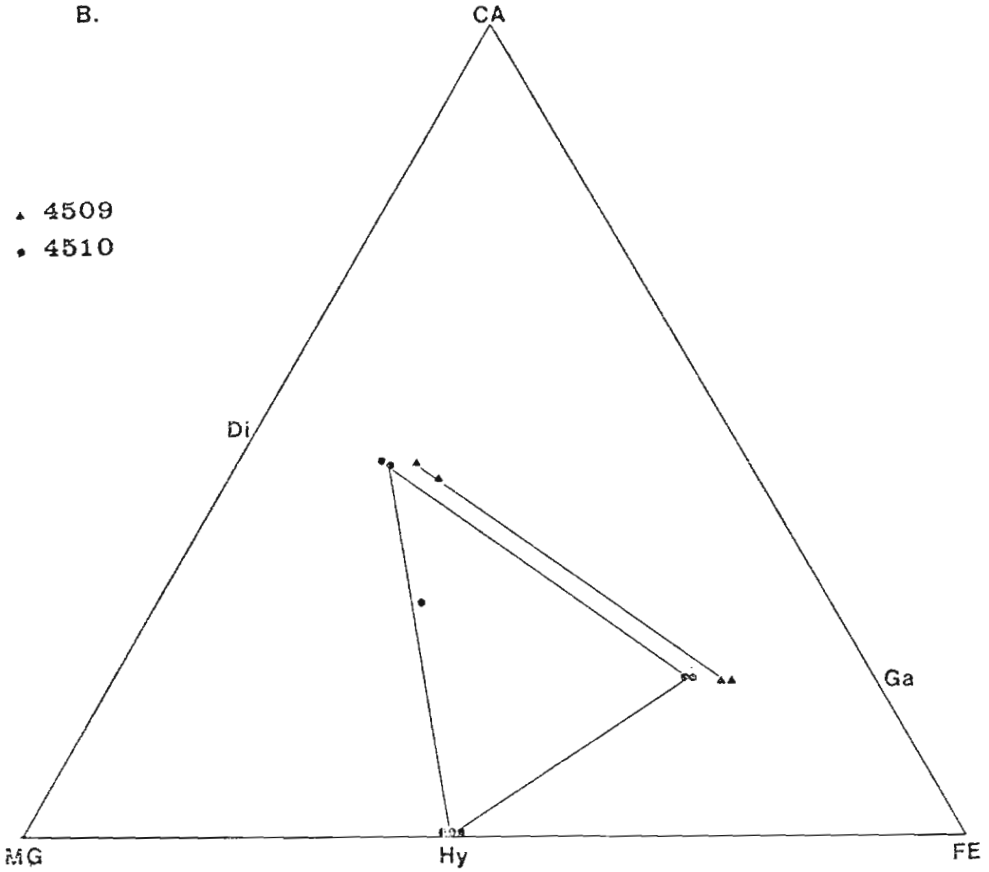

▲ 4509
• 4510

$K_D^{ga\text{-}cpx}{}_{Fe\text{-}Mg}$ (10.4) obtained from rims and recrystallised grains in this sample.

(e) 49464 Metagabbro (cpx-plag primary metamorphic)

Clinopyroxene occurs as elongate, rodlike aggregates of granular polygonal grains in a well layered cpx-plag metagabbro from Fyfe Hills (Black *et al.*, in prep.). The excellent layering and lens shaped cross sections of numerous clinopyroxene areas have been interpreted as deformed cumulate structures, and are similar to textures described in metagabbros from Fiskanneasett, Greenland.

Primary metamorphic clinopyroxene, which coexists with calcic plagioclase (An 72), is iron-rich (X_{Mg}^{cpx} =.47) and contains up to 9.5% $CaAl_2SiO_6$ component (≤ 5 wt% Al_2O_3). (Figure 5.7(a) and 5.12) In addition,clinopyoxene cores may contain minor (≤ .7 wt%) Na_2O, TiO_2 and MnO.

The coexistence of primary aluminous clinopyroxene and plagioclase in this sample allows estimation of maximum pressures of formation of primary metamorphic assemblages.

III. GENERAL FEATURES

Combining the mineral chemistry data from primary metamorphic assemblages of all associations (section 5.5II), the two pyroxene assemblages span a wide range in X_{Mg}^{bulk}. In general, tie line orientations between opx and cpx are consistent, forming a fanning pattern with few cases of crossing tie lines. The geographically distinct samples 3565 and 3566, which are from a locality within the Rayner Complex, and the sample 4319, contain coexisting pyroxenes on tie lines which cut across the general pattern. This discordance is probably

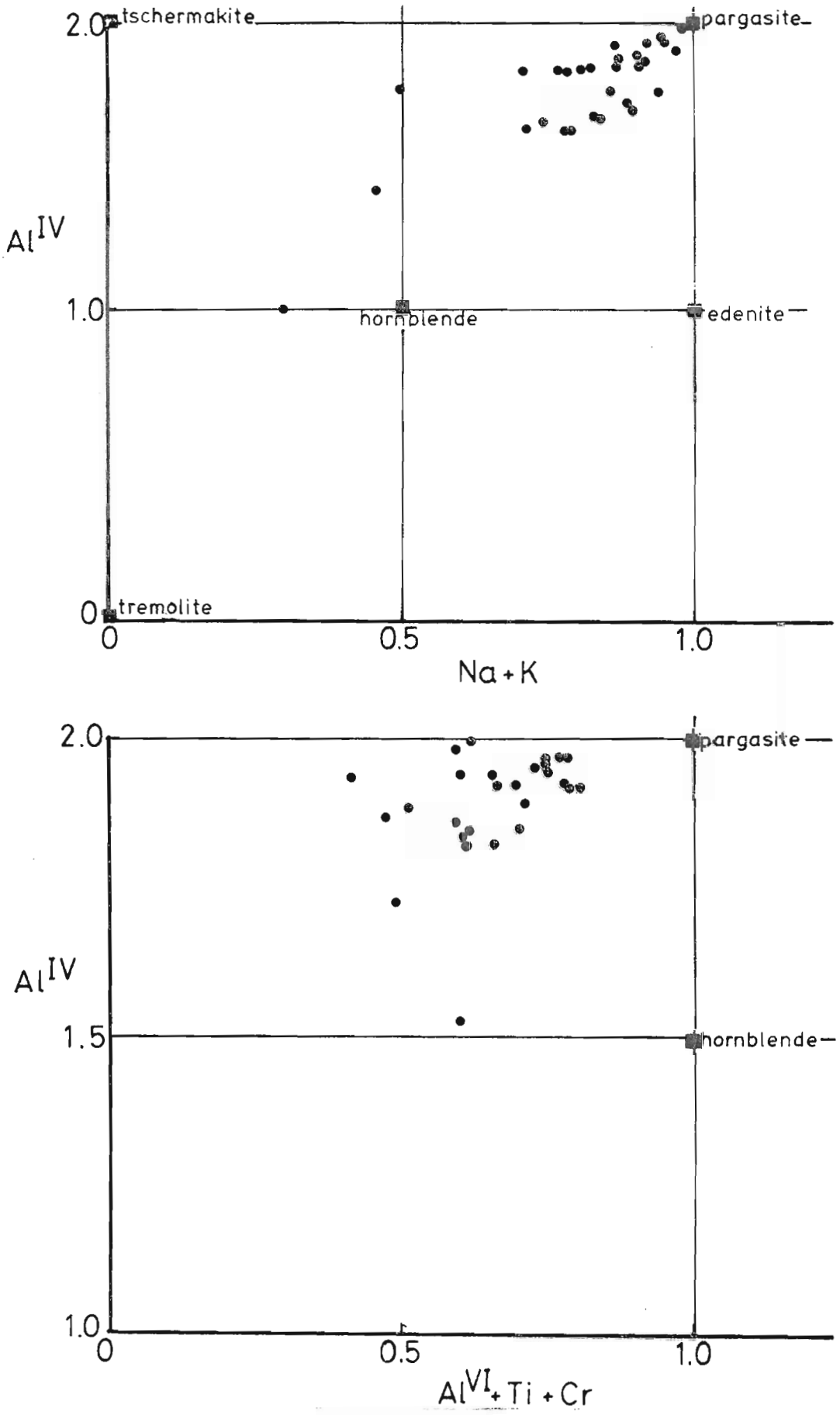

Fig. 5.8 Compositions of metamorphic amphiboles in pyroxene granulites from Enderby Land.

a. Al^{IV} versus Na + K

b. Al^{IV} versus Al^{VI} + Ti + Cr.

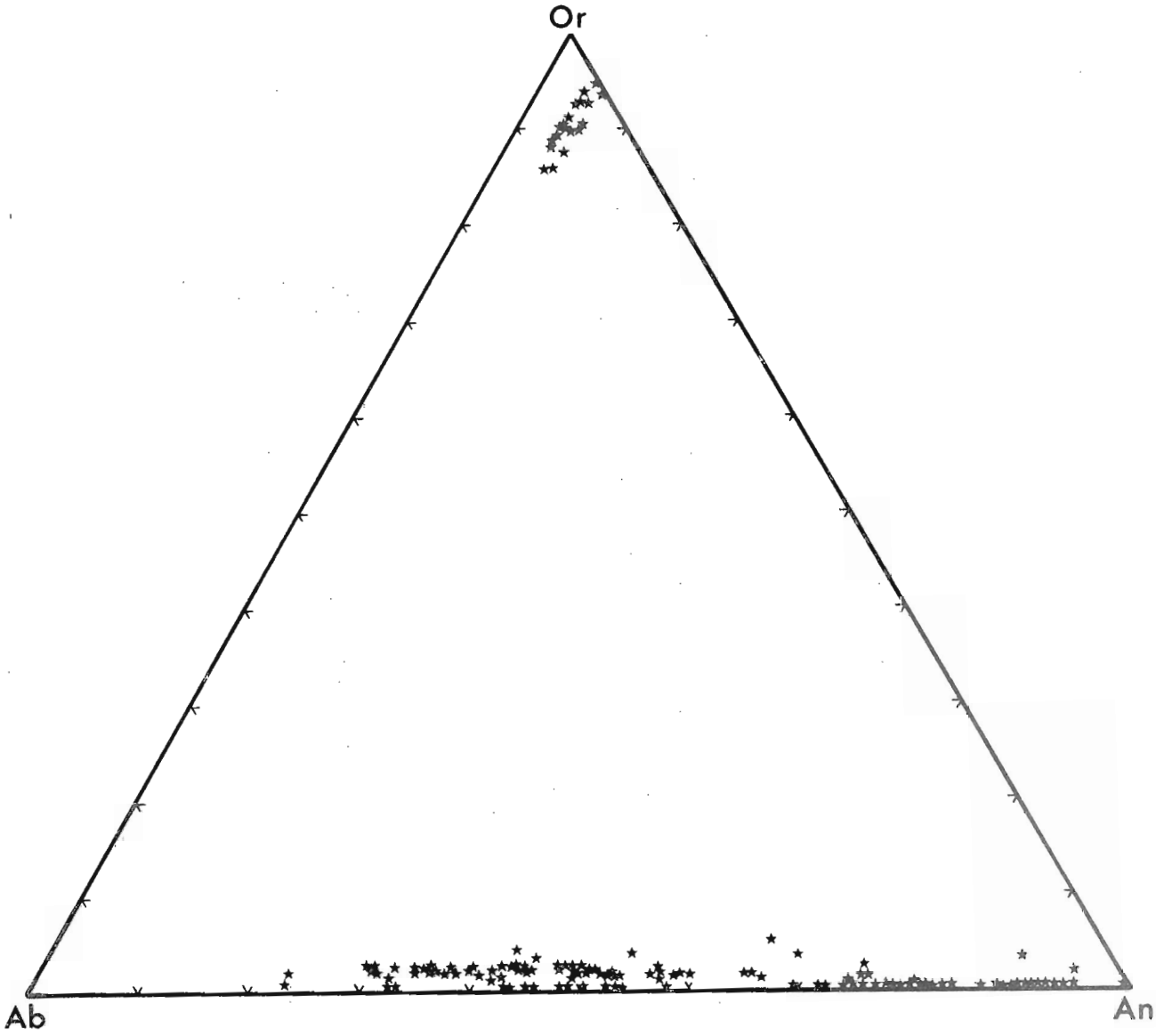

Fig. 5.9 Ca-Na-K (An-Ab-Or) diagram illustrating compositions of feldspars coexisting with pyroxenes in pyroxene granulites from the Napier province.

related to different P-T conditions of formation.

In all assemblages, X_{Mg}^{cpx} is greater than X_{Mg}^{opx}, and a consistent distribution of Fe and Mg between coexisting pyroxenes in most samples is indicated (figure 5.10). In figure 5.10 X_{Fe}^{opx} is plotted against X_{Fe}^{cpx} for all samples and compared with the data of Davidson (1968) for two pyroxene granulites from Western Australia. The data from Enderby Land lie, in general, between the envelope of Davidson's data (800°C ?) and the $X_{Fe}^{opx} = X_{Fe}^{cpx}$ line. This result can be interpreted to indicate, qualitatively, higher temperatures of formation for the two pyroxene assemblages from Enderby Land (e.g., Kretz, 1963).

$K_{D_{Fe-Mg}}^{opx-cpx}$ is plotted against X_{Mg}^{opx} for the garnet-absent primary metamorphic two-pyroxene assemblages in figure 5.11. Most K_D data, with error brackets included, are in the range 1.5-2.0. K_D data from Fyfe Hills and some localities marginal to the Rayner Complex are among the higher K_D values, while samples from the Amundsen Bay-Mount King area generally have lower K_D values (1.5-1.8) and thus may indicate slightly higher temperatures of formation (Kretz, 1963). For the majority of samples, a $K_{D_{Fe-Mg}}^{opx-cpx}$ value of 1.65 ± .2 may be extracted which is not *singificantly* dependent upon X_{Mg}^{opx}. Previous investigators (Binns, 1962; Davidson, 1968; Scharbert and Kurat, 1974) have found that $K_{D_{Fe-Mg}}^{opx-cpx}$ increases with increasing X_{Mg}^{opx} above a value of X_{Mg}^{opx} of .6. These investigations were based on a comparatively large number of samples from small areas where P-T conditions could be assumed to be constant. Data obtained over a wider area studied herein do not permit the isolation of such X_{Mg}^{opx} dependencies. The $K_{D_{Fe-Mg}}^{opx-cpx}$ range and average value falls within the range of granulite facies K_D values summarized by Kretz (1963) and Saxena (1968).

Core and rim or exsolution analyses of primary pyroxenes from all

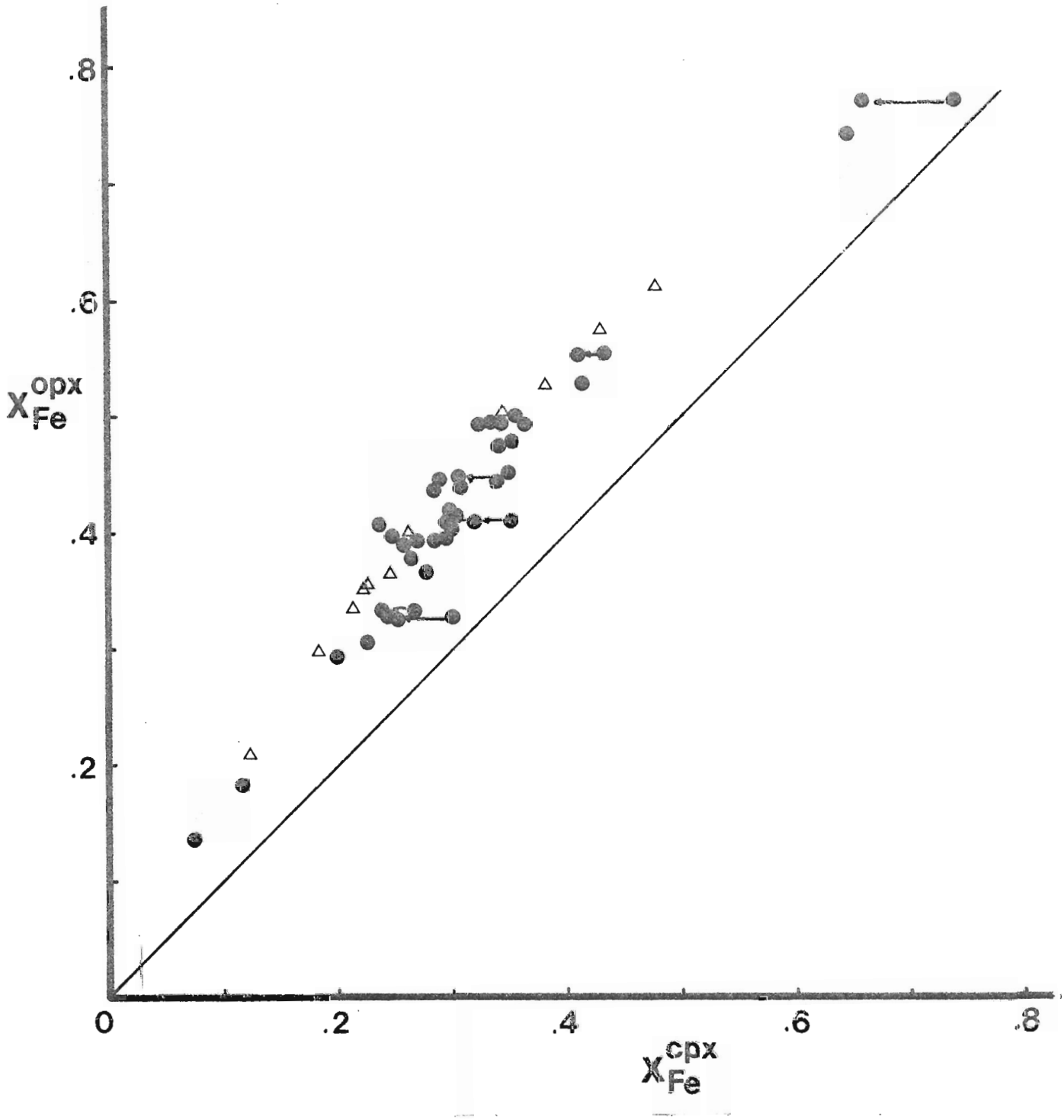

Fig. 5.10 Distribution of Fe-Mg between coexisting pyroxenes in two-pyroxene granulites from Enderby Land, Antarctica. (solid circles). Arrows indicate core to rim variations in X_{Fe}^{cpx}. Open triangles are the two-pyroxene data of Davidson (1968) for granulites from Western Australia.

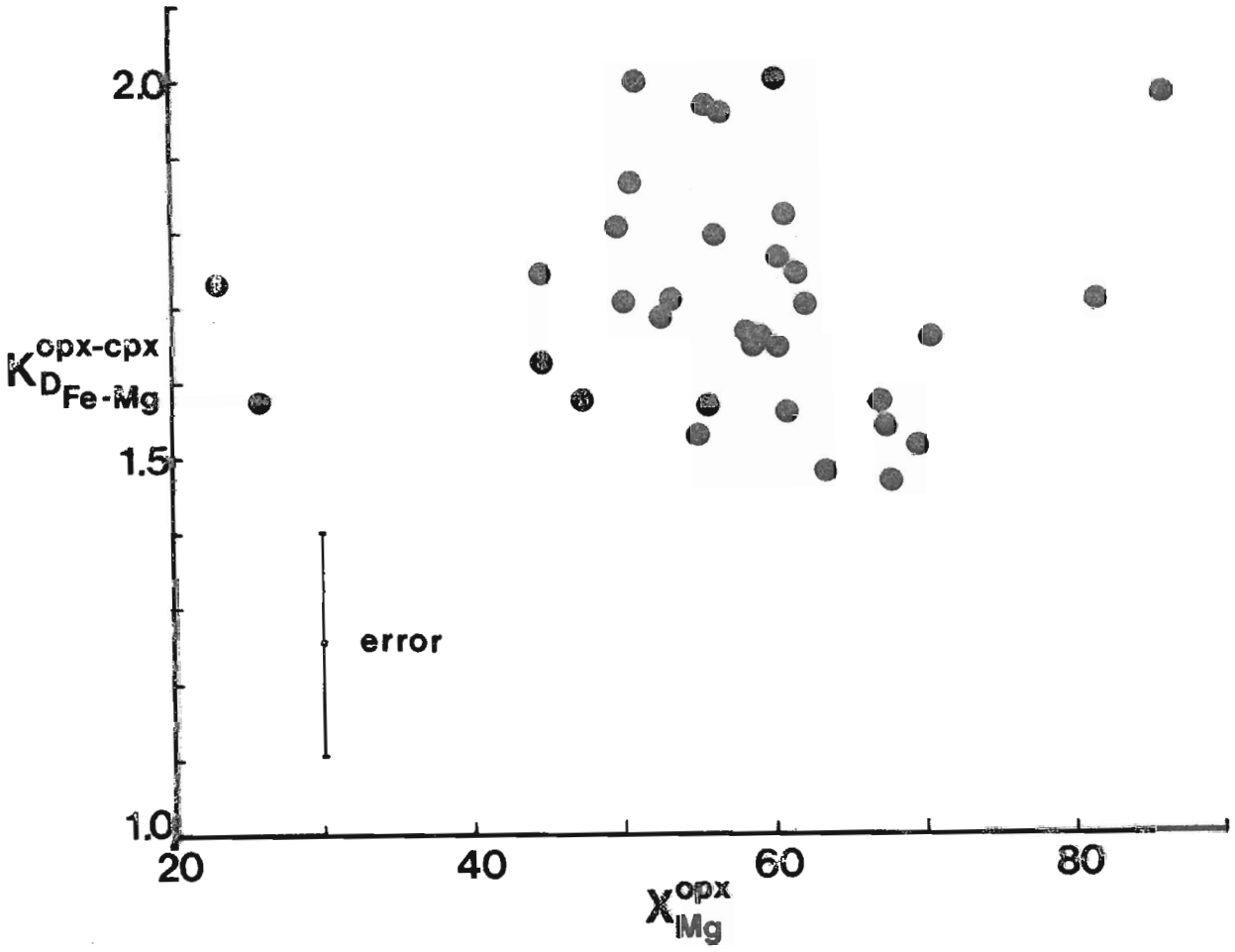

Fig. 5.11 Variation of $K_{D_{Fe-Mg}}^{opx-cpx}$ with X_{Mg}^{opx} for two-pyroxene granulite samples from the Napier province. Average error bars for each K_D value indicated in bottom left corner of diagram.

associations are distinguished in the quadrilateral plot of figure 5.21, which shows the widening of the diopside-orthopyroxene "solvus" gap with cooling from T_{max} and the consistency of this result between samples from a broad area.

The distribution of Al_2O_3 between pyroxenes is shown in figure 5.12. In plagioclase (± quartz) bearing, garnet absent assemblages, alumina favours clinopyoxene over orthopyroxene. Despite scatter probably resulting from variation in other components and from real P-T differences between samples, X^{cpx}_{CaTs} is consistently greater than X^{opx}_{MgTs} ($X^{cpx}_{CaTs} \simeq 1.4\ X^{opx}_{MgTs}$) in contrast to the results of experimental work in garnet-bearing peridotite systems where $X_{CaTs} \simeq X_{MgTs}$ (e.g., Perkins and Newton, 1981; Obata, 1976). Wilson (1976) reports higher Al_2O_3 and Al^{IV} in clinopyroxenes, than in coexisting orthopyroxene in two-pyroxene granulites from Fraser Range, Western Australia. Wilson's results, and analyses of pyroxenes from two-pyroxene granulites from other areas (e.g., Jan and Howie, 1981; Scharbert and Kurat, 1974; Davidson, 1968), are in agreement with the Al_2O_3 distribution shown in figure 5.12. Generally, the MgTs and CaTs contents of the respective pyroxenes increase with increasing anorthite content in plagioclase, despite significant scatter in the data and the dependence of this result upon a few high-An Samples (figure 5.13(a) and (b)). These effects and correlations can be explained by the reactions

$$\underset{\text{CaTs in clinopyroxene}}{CaAl_2SiO_6} + \underset{\text{qz}}{SiO_2} = \underset{\text{anorthite in plagioclase}}{CaAl_2Si_2O_8} \qquad (1)$$

and

$$Mg_2Si_2O_6 + CaAl_2SiO_6 = CaMgSi_2O_6 + MgAl_2SiO_6 \qquad (2)$$

operating at constant P and T but at variable X^{plag}_{An}. As X^{plag}_{An} increases,

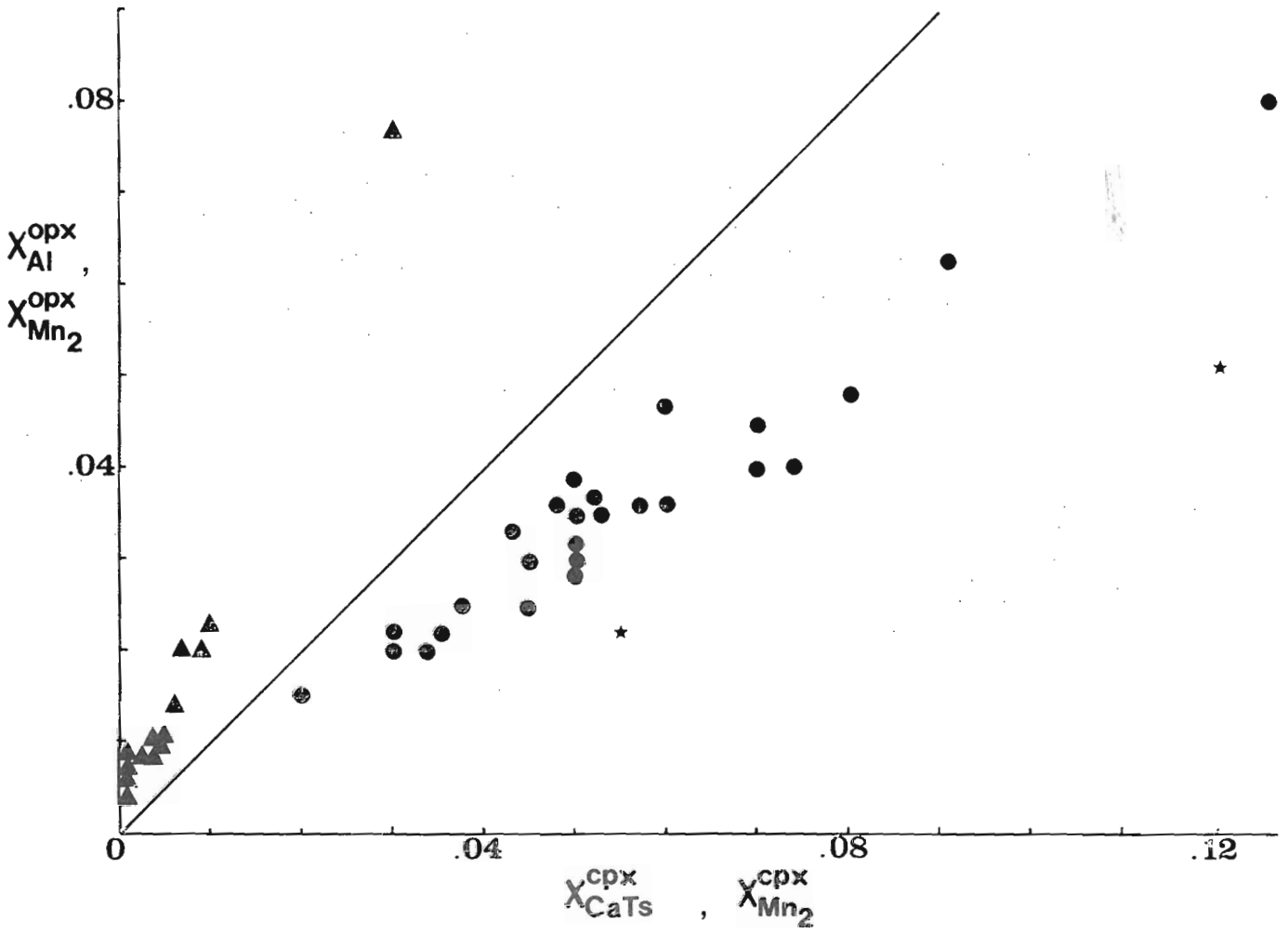

FIG. 5.12 Distribution of Al and Mn between coexisting pyroxenes in pyroxene granulites from the Napier province.

- ● X_{Al} distribution in two pyroxene granulites
- ★ " " " in garnet pyroxenites
- ▲ Mn distribution

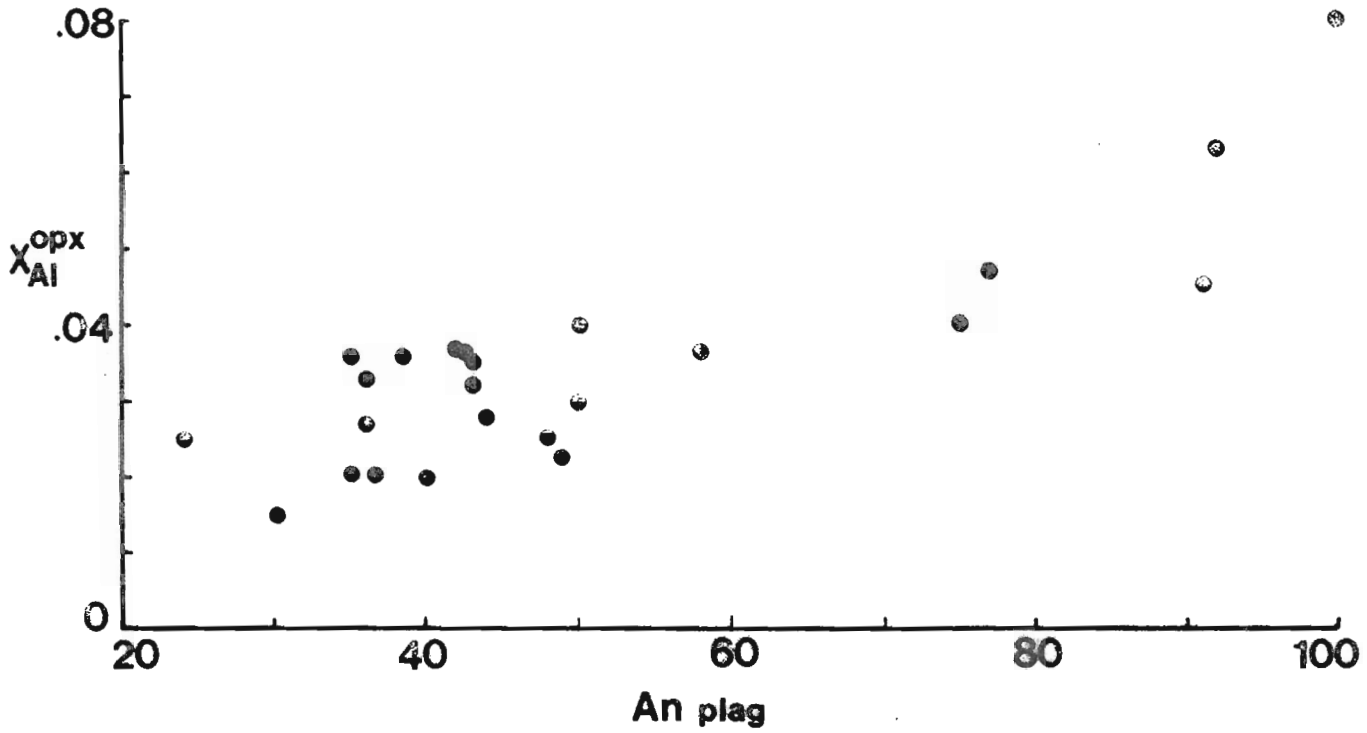

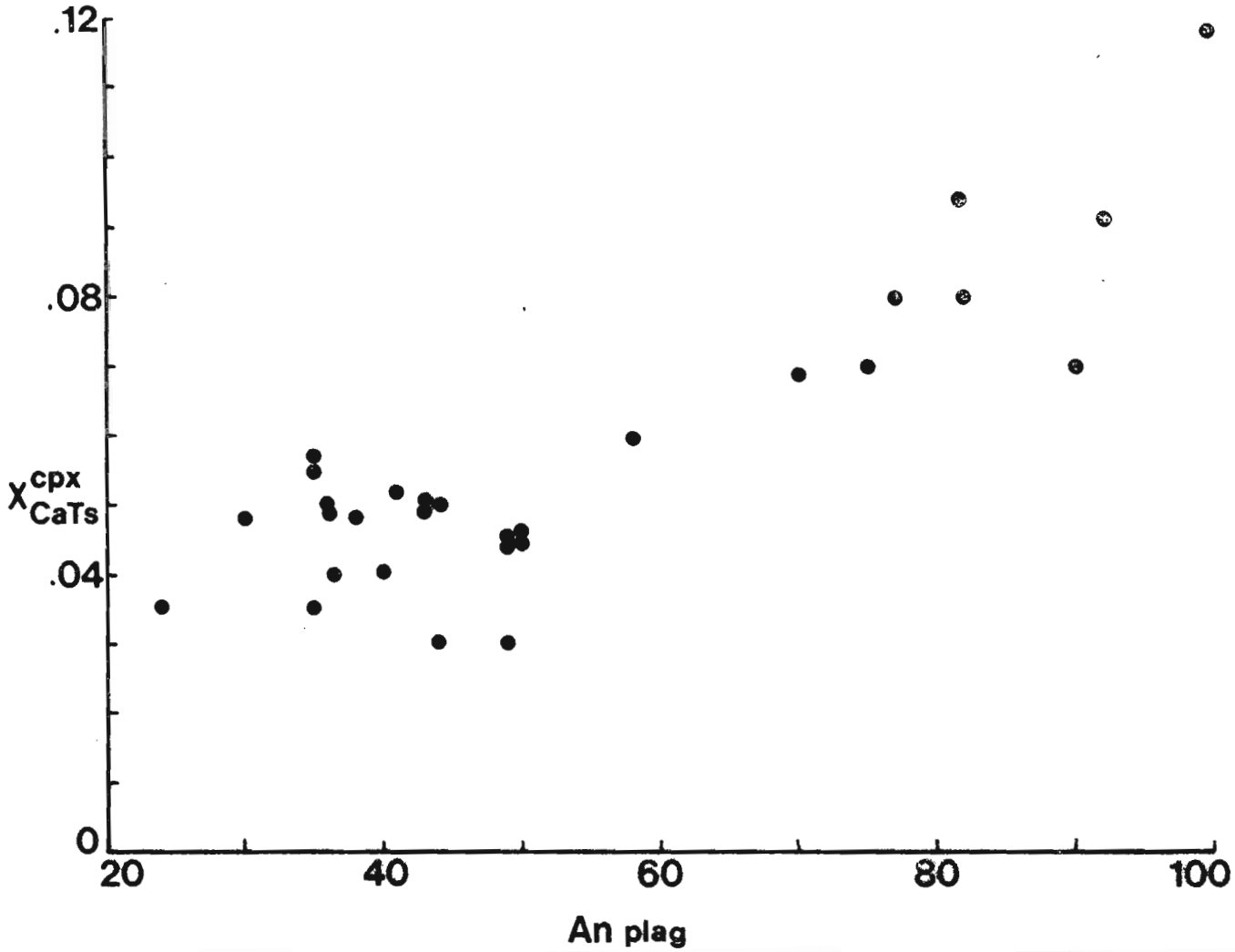

Fig. 5.13 Variation in $X_{Al}^{pyroxene}$ with An content of coexisting plagioclase in pyroxene granulites from the Napier province

a. orthopyroxenes

b. clinopyroxenes

then by reaction (1) at constant silica values X_{CaTs}^{cpx} will increase. The increase in X_{CaTs}^{cpx} leads to a correlated increase in X_{MgTs}^{opx} through reaction (2).

As reported by previous workers on pyroxene granulites (e.g., Wilson, 1976; Jan and Howie, 1980; Scharbert and Kurat, 1974) Mn strongly favours orthopyoxene (figure 5.12), to the extent that $\frac{Mn^{opx}}{Mn^{cpx}} \simeq 2.5$ for pyroxene granulites from Enderby Land.

5.6 RECRYSTALLISED OR SECONDARY METAMORPHIC ASSEMBLAGES

The various pyroxene granulites described above (section 5.5I) all show some form of P-T evolution,be it in the form of exsolution lamellae or minor zoning within primary pyroxene grains which indicate some cooling from metamorphic peak conditions; or in the form of reaction coronas or recrystallised textures. This section deals principally with assemblages formed by recrystallisation or reconstruction of the original metamorphic fabric, and hence the term "secondary metamorphic assemblage" refers to those mineral assemblages typical of coronas on earlier phases or of recrystallised polygonal masses. In many instances (Black *et al.*, in prep; Black and James, 1981), recrystallisation and corona formation can be linked with D3 recrystallised textures (section 5.3) in other rocktypes. Thus, many of the textures to be described below and many of the newly formed assemblages are regarded as D3 and post-D3 (≃ 2500 m.a.) in age, although some may be related to still younger shearing events. This age-structure (deformational) constraint on the timing of formation of the secondary assemblages (= M3 during and after D3) allows the regional P-T conditions in the Napier province to be assessed for an event occurring some 500 m.a.-300 m.a. after peak granulite facies metamorphic conditions, and allows the possible rates of uplift of the Napier "shield" region to be inferred.

TYPES OF REACTION TEXTURES AND ASSEMBLAGES

(1) 49461 - Fyfe Hills

The primary iron- and manganese-rich metamorphic assemblage opx + ga + qz + magnetite has been partially recrystallised to much finer grained (<.2mm) cpx + opx + qz + magnetite ± garnet with the growth of polygonal masses of cpx and opx. Textural evidence indicates a complex history for this rock.

(i) primary coarse granuloblastic ga-cpx-qz-mt;

(ii) exsolution of coarse abundant pyroxene lamellae;

(iii) deformation of the coarse garnet + exsolution pyroxenes resulting in the kinking of lamellae, undulose extinction, and breaking up of grains with subsequent migration of magnetite;

(iv) partial recrystallisation of the assemblage to finer grained polygonal granoblastic pyroxene-quartz+garnet masses along grainboundaries and in broken up areas;

(v) further minor cataclasis, with the formation of undulose extinction in recrystallised grains.

The recrystallised event (iv) is correlated with syn- and post-deformational recovery during D3.

Compositions of secondary garnet, clinopyoxene and orthopyroxene are plotted in figure 5.7(a). Recrystallised pyroxenes have high MnO contents distributed favourably towards orthopyroxenes. Typically, orthopyroxene contains 4.5 wt% MnO ($M^{opx}_{Mn_2Si_2O_6}$ = .077), while clinopyroxene contains 1.7 wt% MnO ($X^{cpx}_{Mn_2Si_2O_6}$ = .030). It is evident from a plot of $X^{pyroxene}_{Mn}$ against Wo contents or $X^{pyroxene}_{Mg}$ (figure 5.14), that the original subcalcic clinopyroxenes have recrystallised to the

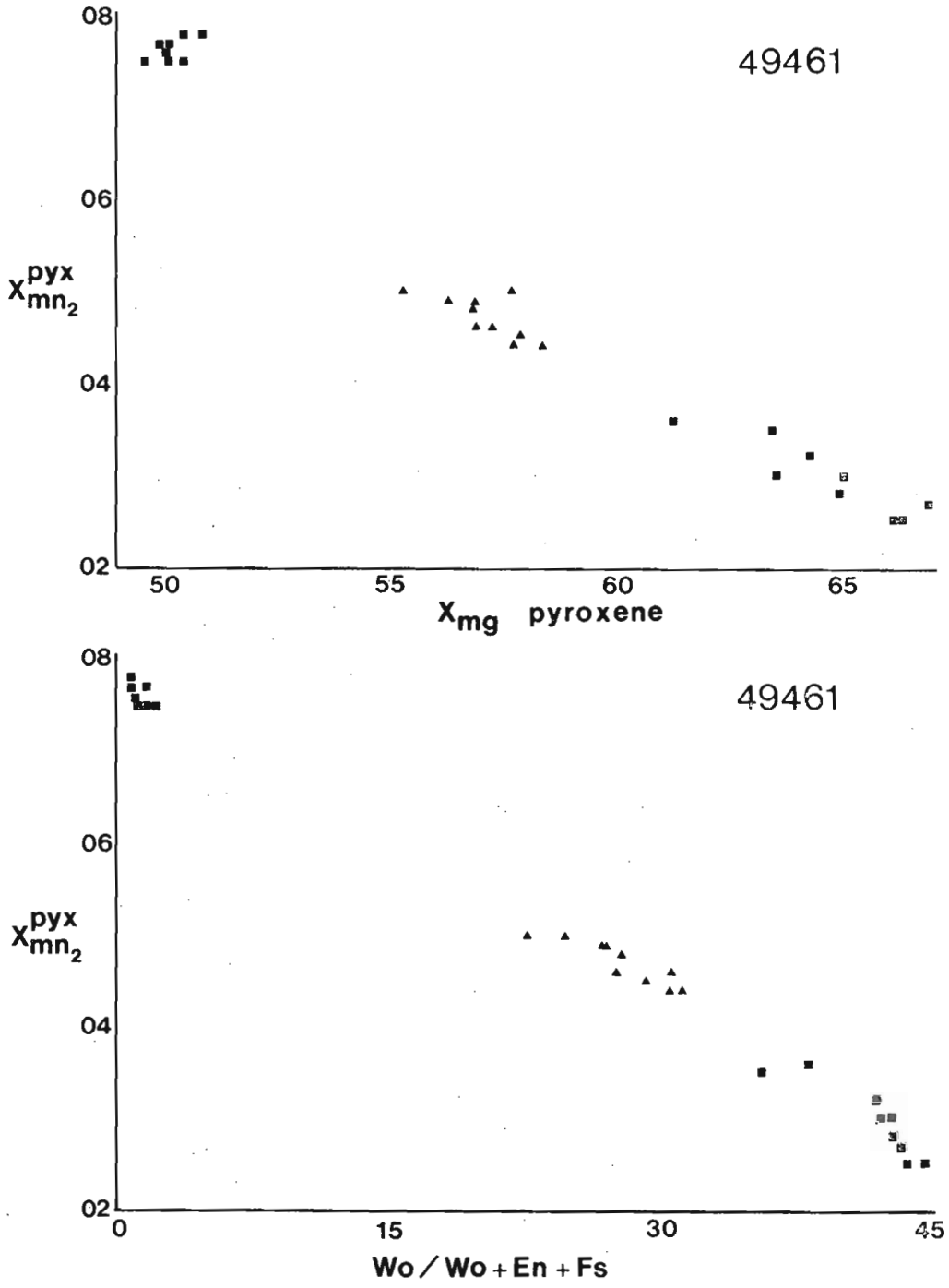

Fig. 5.14 Manganese contents of pyroxenes, expressed in mol% $Mn_2Si_2O_6$, in 49461 from Fyfe Hills.

▲ area scan compositions of primary cpx

■ compositions of secondary exsolved and recrystallised pyroxenes.

a. variation of Mn with $X^{pyroxene}_{Mg}$

b. variation of Mn with calcium contents of pyroxene

secondary opx-cpx assemblage essentially by exsolution and further re-equilibration of the exsolved species, without significant participation of Mn-rich primary garnet. Secondary clinopyroxene is calcic (Wo44), and has maximum X_{Mg}^{cpx} values of .65-.67. Coexisting orthopyroxene is less magnesian (X_{Mg}^{opx} = 50), producing quite high $K_{D_{Fe-Mg}}^{opx-cpx}$ values of 1.9 ± .1. These high K_D values are in accord with lower temperatures of formation. Garnet rims and rare fine recrystallised garnets, are more Fe- and Ca-rich than primary metamorphic garnet (X_{Mg}^{ga} = .15-.16, X_{Ca}^{ga} = .22) while still being rich in MnO (10.6 wt%, X_{Mn}^{ga} = .25). Resultant values of $K_{D_{Fe-Mg}}^{ga-cpx}$ for the secondary assemblage are 10-11, also indicating a marked decrease in temperature (at constant X_{Ca}^{ga} and X_{Mn}^{ga}) from that of the primary assemblage.

Zoning relationships and the expansion of the three phase triangle in figure 5.7(a) indicate the general reaction:

cpx 1	+ ga 1	→	cpx 2	+ opx 2	+ ga 2
low Ca, hi Mn	Mn, Ca rich Fe rich		hi Ca, low Mn Mg richer	hi Mn Fe-Mg opx	Mn,Ca rich, Fe richer

leading to the formation of the observed assemblages. The P-T conditions of the recrystallisation estimated from mineral compositions, will be presented in section 5.7.

(2) Coronas in 49464

Clinopyroxene-plagioclase is rimmed by almost continuous coronas of lathlike subhedral garnet (.05 mm wide), polygonal and subhedral sphene, and rod-like quartz (figure 5.16). Clinopyroxene is conspicuously zoned adjacent to these rims (figure 5.15, figure 5.7(a)), becoming more magnesian (X_{Mg}^{cpx} = .53 maximum), and less aluminous

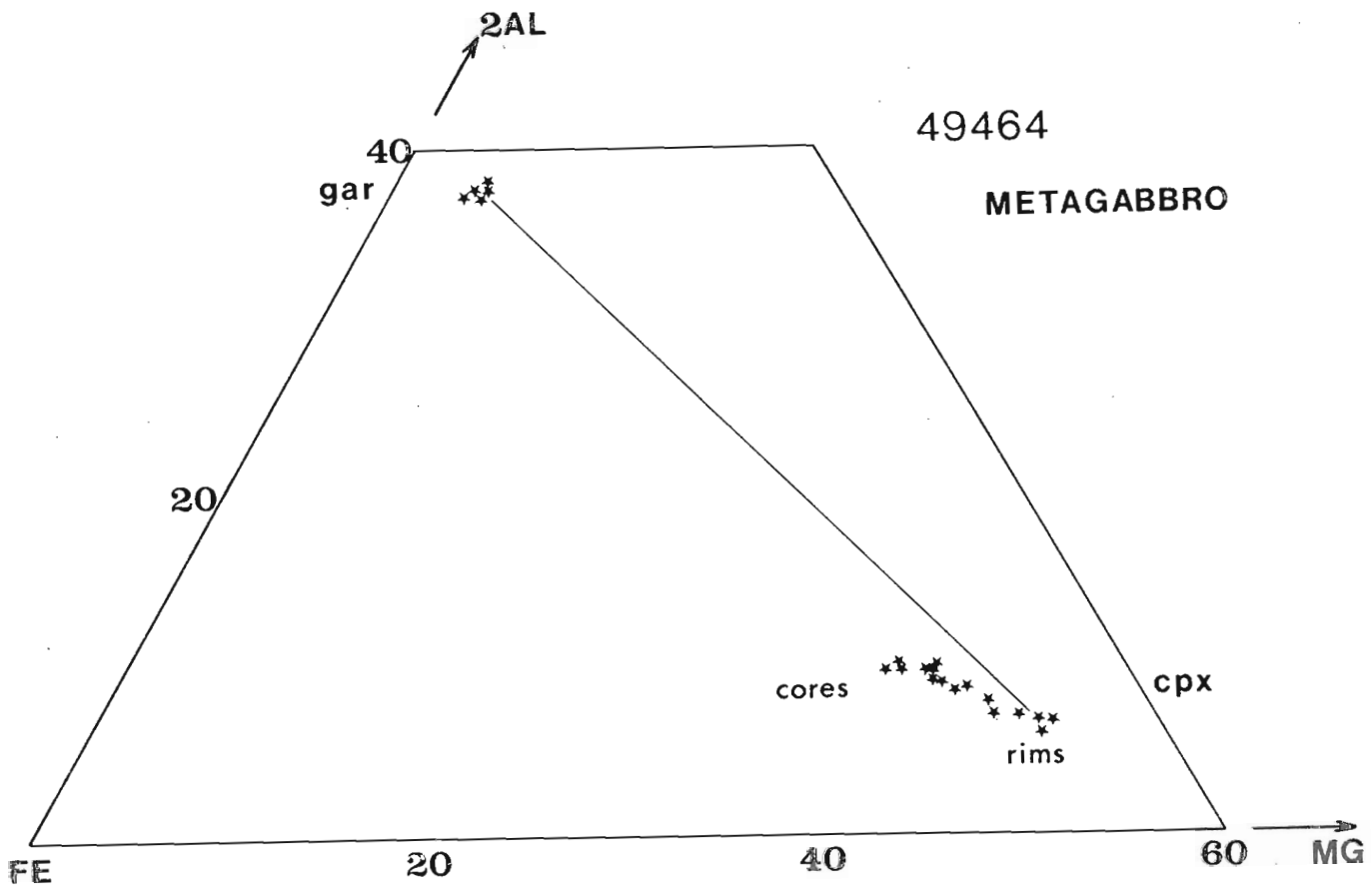

Fig. 5.15 Partial 2Al-Fe-Mg diagram illustrating compositions of primary metamorphic Al-cpx and secondary lower-Al cpx and garnet in 49464 from Fyfe Hills.

(X^{cpx}_{CaTs} = .069), but retaining a similar jadeite content to that in the cores. Thus Jd/CaTs is higher in the rim compositions than in unexsolved cores. TiO_2 contents of the clinopyroxene also decrease on the rims.

Plagioclase is weakly zoned to less anorthite rich rims (An 72).

The garnet, formed as discrete coronas on zoned clinopyroxene, is very grossular-(X^{ga}_{Ca} = .44) and spessartine-rich (X^{ga}_{Mn} = .111), and has a low Mg number (X^{ga}_{Mg} = .105). The compositions of this secondary garnet and coexisting clinopyroxene rims yield a $K_{D_{FeMg}}^{ga\text{-}cpx}$ of 10 ± .5.

The textural and mineral zoning evidence indicate the formation of garnet in this rock by the following reaction:

cpx 1	+ plag	=	cpx 2	+ ga	+ Sphene + qz.
hi Al, hi Ca, hi Ti	Anorthite		low Al low Ti hi Ca	hi Ca, Mn	

inferred to progress from left to right with a decrease in temperature. Plagioclase is inferred to participate in this reaction as clinopyroxene core compositions lie below the garnet-rim-clinopyroxene tieline of figure 5.15.

(3) Fe-rich pyroxene ± quartz ± plagioclase rocks 4092 and 4359

Very coarse polygonal to subhedral Fe-pigeonite grains described in section 5.5. have undergone a complex subsequent deformation and recrystallisation history:

(a) initial extensive exsolution of calcic clinopyroxenes (Wo 40-43, X^{cpx}_{Mg} = .35) and iron rich orthopyroxene (X^{opx}_{Mg} = .24) has resulted in abundant tabular or continuous lamellae which traverse

Fig. 5.16 EXSOLUTION AND RECRYSTALLISATION TEXTURES IN PYROXENE GRANULITES FROM THE NAPIER PROVINCE.

cp = clinopyroxene
op = orthopyroxene
ga = garnet
pl = plagioclase
sph = sphene

Horizontal bars.....scales as indicated

A. Coronas of elongate, lathlike garnet, subhedral sphene, and lamellar quartz formed between earlier Al-cpx and calcic plagioclase. Sample 49464, Fyfe Hills Russian site.

B. Very coarse polygonal-subhedral grain of inverted pigeonite with pyroxene exsolution lamellae (horizontal lines) and cross-cutting elongate garnet exsolved from the pyroxene (pyx). Plagioclase also develops in the pyroxene, and garnet may rim pyx-plag. Garnet post-dates pyroxene exsolution. Sample 4092, Ward Rocks.

C. Similar to 5.16B. Coarse inverted pigeonite with pyroxene lamellae (vertical lines) cut by later garnet lamellae which form on kink-band boundaries and adjacent to plagioclase. Magnetite (black) and minor recrystallised cpx occurs with the garnet. Sample 4359, Zubchatyy Ice Shelf.

D. Multiple exsolution products in primary aluminous cpx in garnet pyroxenite.

black...ilmenite ; stippled...garnet
vertical lines...opx; clear.....host cpx.

Sample 4598, Demidov Island.

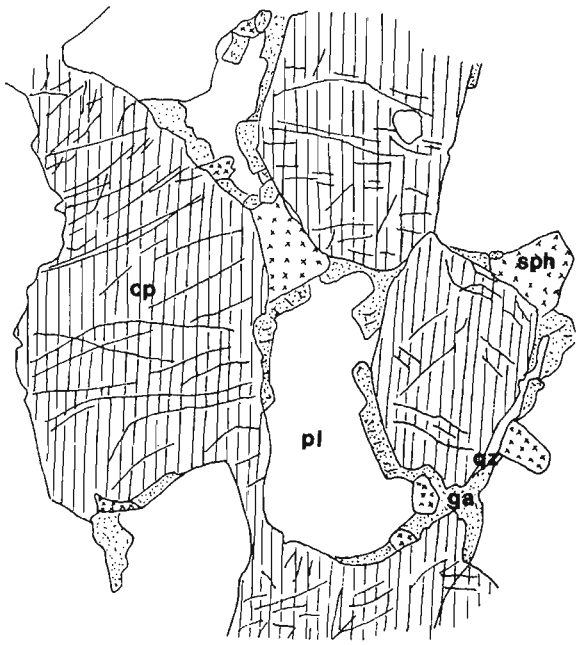
cp
sph
pl
qz
ga
A
0.2mm

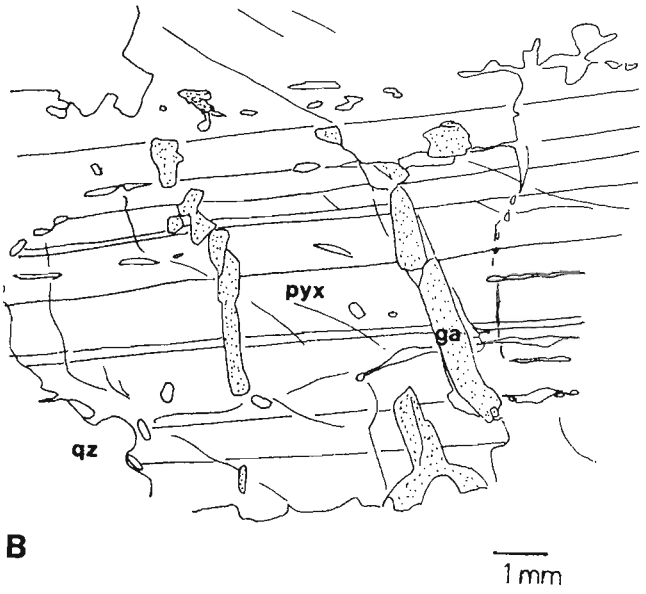
pyx
ga
qz
B
1 mm

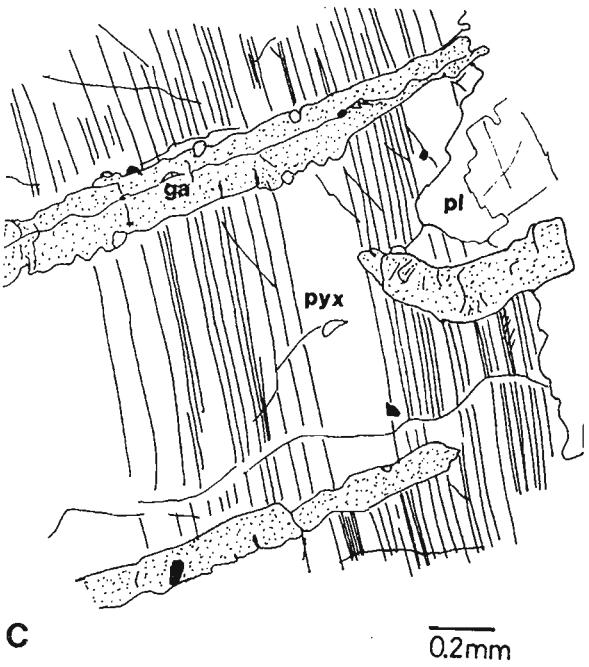
ga
pl
pyx
C
0.2mm

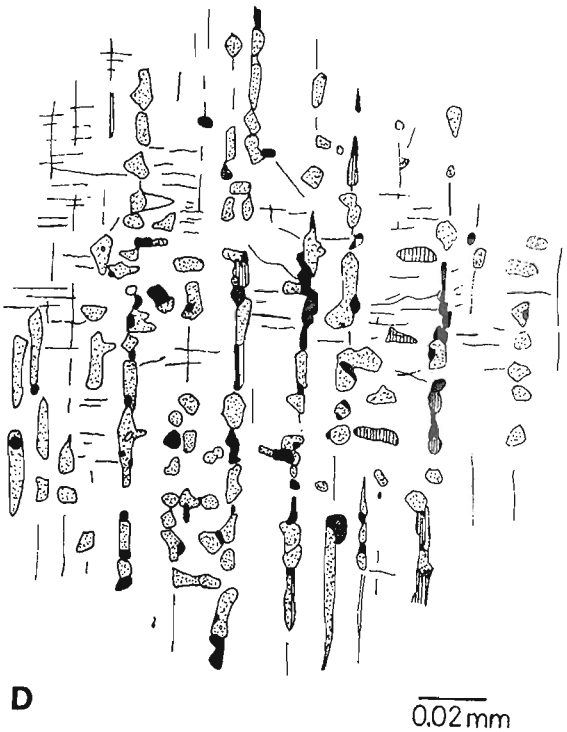
D
0.02 mm

whole pyroxene grains. Compositions of exsolved pyroxenes are indicated in figures 5.3 and 5.4.

(b) cataclasis and deformation of exsolved pyroxenes has produced kinked lamellae, *en echelon* polygonal quartz veins, and undulose extinction within the coarse pyroxenes. Large pryoxene grains have disaggregated, while quartz becomes undulose and has recrystallised to fine polygonal masses;

(c) following the deformation (b), garnet has developed along grain boundaries: as finger-like lamellae cutting across earlier pyroxene exsolution lamellae; as subhedral grains with lobate ilmenite; or as curved and irregular lamellae forming along cracks or kink-band boundaries (figure 5.16(b) and (c)). Fine polygonal quartz, clinopyroxene and plagioclase, may develop with this garnet.

(d) further cataclasis in 4092 has disrupted some garnet lamellae or rods (figure 5.16(b)).

The secondary garnets, formed exclusively on pyroxene, are essentially almandine-grossular garnets (X_{Mg} =.06 or.08, X_{gross} = .2 - .21) with minor spessartine (.2 mol% spessartine) and pyrope, $K_D{}^{ga\text{-}cpx}_{Fe\text{-}Mg}$, based on compositions of the most highly exsolved rim clinopyroxenes (i.e., X_{Mg}^{cpx} maximum) and the average garnet compositions, are 6.6 ± .2 for 4092 and 7.9 ± .1 for 4359.

Zoning within the pyroxenes and the textural relationships between garnet and pyroxene indicate that garnet formation is later than and distinct from the exsolution of two-pyroxenes from the initial homogeneous pyroxenes. Garnet generally has preferentially developed along discontinuities but is always associated with pyroxenes. This suggests that garnet has formed principally by exsolution and preferential nucleating from the bulk pyroxene:

inverted pigeonite → garnet + (lower Ca Higher Mg lower Al)pyroxene
subcalcic, FeRich some Al_2O_3 — calcic, Fe rich
+ calcic cpx

Al_2O_3 contents of the exsolved pyroxenes are slightly less than those of the early pigeonite, in support of the above reaction, however plagioclase may be involved to provide the necessary calcium and alumina. The close proximity of the original pyroxene bulk compositions to the secondary clinopyroxene-orthopyroxene tie lines indicate that little secondary garnet could form from the original pyroxene alone.

The secondary garnet is suggested to form in M3, during or post-D3. The deformation-kinking event (b) is regarded as being synchronous with the time of boudinage, while later deformation (d) may be related to post-D3 shearing.

(4) Garnet Pyroxenites

Coarse polygonal-granular primary metamorphic ga + cpx + opx ± hbl + plag + magnetite assemblages (4818, 4598) in these rocktypes have been modified by a number of subsequent effects:

(a) Strong rimward zoning in clinopyroxene and abundant exsolution lamellae (opx) in clinopyroxene cores results in secondary clinopyroxenes which are much more calcic (Wo 45-46), more magnesian (X_{Mg} = .75-.76) and less aluminous (X_{CaTs} = .030 - .060) than primary metamorphic clinopyroxene (figures 5.6(a) and (b)). Accompanying this strong zoning and exsolution are the exsolution of ilmenite from both clinopyroxene and primary hornblendes.

(b) Garnets also zone to more calcic (X_{Ca} = .2) and more iron-rich rims (X_{Mg} = .30-.28). In some cases these garnet rims re-grow on margins of earlier coarse pyroxenes, along with saccharoidal ilmenite

grains.

In 4598, garnet of lower X_{Mg}^{ga} (=.24) is exsolved along with ilmenite and orthopyroxenes from a primary aluminous clinopyroxene (figure 5.16 (d)). Garnet of this composition also forms as rims on earlier pyroxenes and as symplectites with ilmenite, suggesting multiple growth of garnet. Two late generations of garnet may thus be recognised in 4598: an earlier garnet formed by rimward zoning of pre-existing grains and some overgrowth on these grains; and a garnet formed as discrete exsolution blebs and trails in *cores* of clinopyroxene and as fine grains on pyroxene rims.

(c) Plagioclase is zoned to more sodic compositions (An 50) rimwards. In 4598, this zoning is marked (An 80 cores to An 50 rims), but restricted to optically distinct plagioclase zones on the rims of grains, suggesting regrowth of plagioclase as a result of discontinuous reactions (see page 189).

These textural observations, and zoning data for the phases (e.g., expansion of the ga-cpx-opx triangles in figure 5.6) indicate the following reactions leading to the formation or readjustment of garnet in these rocks:

(1)	opx 1	+	cpx 1	+	gal	±	plag	=	cpx 2	+ ga 2 + opx 2
			hi Al, subcalcic		Mg richer calcic		An rich		low Al, calcic	lower Mg hi calcic

, a reaction leading to the zoning in garnets and regrowth of some garnet rims.

(2)	cpx 1	=	cpx 2	+	opx 2	+	ga 2 + ilmenite
	hi Al, subcalcic hi TiO_2		low Al, calcic low TiO_2 hi Mg		low Al		Fe-rich calcic

a generalised reaction describing the formation of the exsolution product present in clinopyroxenes of 4598 and the garnet-ilmenite simplectites.

As a result of the rimward zoning in clinopyroxenes and garnets, $K_D{}^{ga\text{-}cpx}_{Fe\text{-}Mg}$ increases rimwards in these assemblages (K_D = 8 for rims). Exsolved garnet compositions in 4598 yield still higher K_D values (10). These increases in $K_D{}^{ga\text{-}cpx}_{Fe\text{-}Mg}$ indicate a progressive *decrease* in temperatures of equilibration, consistent with the decrease in Al_2O_3 contents of clinopyroxenes towards rims (Ellis, 1979; Herzberg, 1978).

Similar textures and zoning patterns to these described above are described for a garnet-clinopyroxene from Wyers Ice Shelf, Amundsen Bay (Ellis, 1979), with the additional observation of plagioclase as an exsolution product from clinopyroxene. The apparent absence of plagioclase exsolution lamellae from clinopyroxenes in 4598 may be a result of the lower Ca- and Al-contents in these clinopyroxenes compared with the pyroxenes of Ellis (1979).

Discontinuous zoning to very sodic rims (An 50) which occurs in 4598 plagiocalse, is strongly associated with the formation of pargasitic hornblende coronas on occasional biotites in this sample. These coronas appear to post-date the garnet forming reactions in this rock. Strongly zoned plagioclase occurs on pyroxenes, ilmenite and biotite, indicating the growth of an amphibolite facies amphibole-plagioclase assemblage:

cpx 2	+ opx 2	+ An plag	→	amphibole	+	lower Ca
	+ biotite (Ti bearing)			hi Mg, Al, Na and K bearing; calcic		(3)
	± ilm					

Hornblende is restricted to rims on biotite and ilmenite.

This spatial association is inferred to be controlled by the availability of TiO_2 and OH^-.

Temperature of formation of the secondary garnet-bearing assemblages, which are tentatively correlated with M3 (during D3), are estimated in section 5.7. The hornblende-plagioclase coronas developed in 4598 are believed to have formed during later uplift, shearing, or the superposition of Rayner Complex metamorphism at 1100 m.a.

(5) Two Pyroxene Granulites without primary garnet

A variety of reactions have led to the development of garnet in both quartz-bearing and quartz-absent two pyroxene granulites. Textural and compositional evidence from a range of samples indicate that such reactions have progressed at lower temperatures than the temperature of formation of the precursor metamorphic assemblages, with garnet being formed as a retrograde mineral, i.e., during cooling and/or a late deformation. The range of corona textures and specific zoning patterns are discussed below and related to various garnet-forming reactions. Compositional data for the secondary garnets and pyroxenes are presented in Appendix 4, and are illustrated in figures 5.3, 5.5 and 5.7(b). Examples of the variety of corona textures are depicted in figures 5.17 (a) - (d) and 5.18(a) and (b).

(a) Clinopyroxene-Orthopyroxene-Magnetite (Plagioclase)
Samples 4093 and 4094.

Lobate magnetite is concentrated into layers within these dominantly granoblastic pyroxenitic samples. Pale pink, lobate garnet is almost exclusively restricted in occurrence to rims on magnetite (fig. 5.17(a)). Such coronas are continuous between magnetite and clino-

Fig. 5.17 CORONA TEXTURES IN TWO-PYROXENE GRANULITES FROM THE NAPIER PROVINCE

cp = clinopyroxene
op = orthopyroxene
ga = garnet
pl = plagioclase
hbl = hornblende

Horizontal bars = .2 mm

A. Corona of garnet formed around magnetite (black) in contact with clinopyroxene and orthopyroxene. Note that no garnet is formed between cpx and opx only.
Sample 4094, Wyers Ice Shelf

B. Euhedral garnet forming coronas, with clinopyroxene, between orthopyroxene, plagioclase and ilmenite. Note that cpx+plag are still partly in contact, and that opx+cpx are in contact in the absence of ilmenite. Sample 4510, Fyfe Hills.

C. Saccharoidal subhedral-polygonal garnet and cpx, and lamellar cpx, forming corona between opx and plagioclase. A second polygonal plagioclase (pl2) is developed as a moat between garnet and opx. Note garnet corona on hornblende. Sample 4704, Hydrographer Island.

D. As for 5.17C, saccharoidal garnet and lamellar cpx forming rims on opx+plag. Sample 4704, Hydrographer Island.

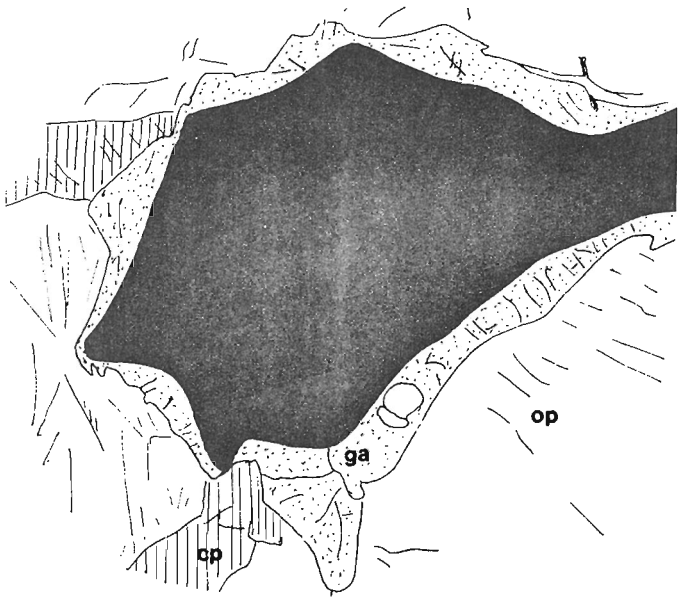

A

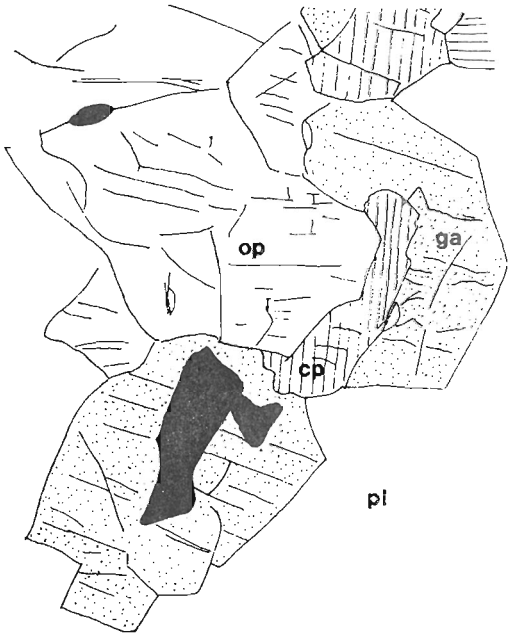

B

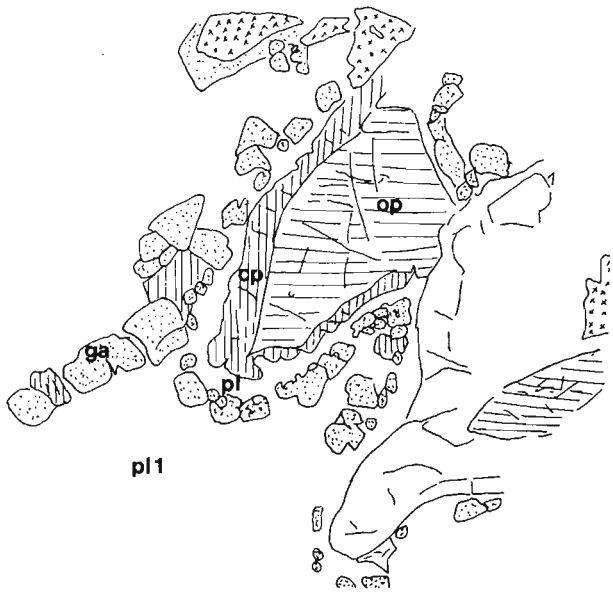

C

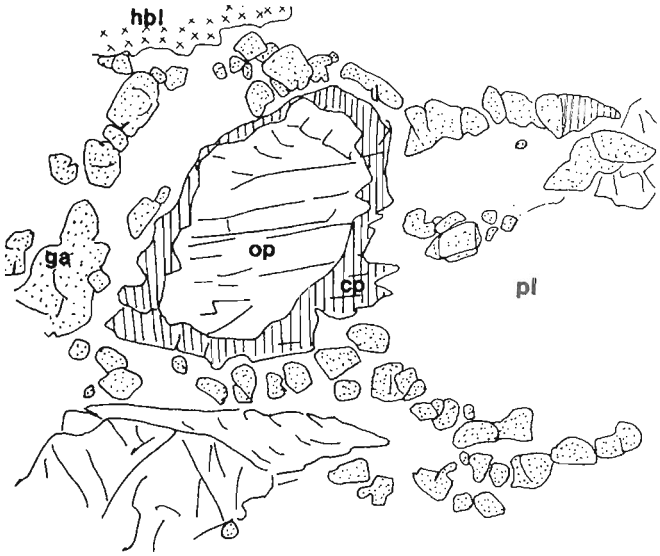

D

pyroxene or orthopyroxene, and only rarely between pyroxenes in the absence of magnetite. These features suggest that formation of garnet in these samples is controlled by the presence of magnetite, and hence that the garnet-forming reaction involved a decrease in fO_2.

Clinopyroxene, which has exsolved orthopyroxene prior to the formation of garnet, is strongly zoned to more calcic and magnesian compositions adjacent to garnet (X_{Mg}^{cpx} = .65-.70, Wo 45)(figure 5.3). This zoning is accompanied by a decrease in Al_2O_3 contents. Orthopyroxene zones to lower Ca and Al_2O_3 contents, and may become more magnesian (figure 5.3). Plagioclase, present in 4094, zones to rims richer in albite.

The corona garnets are almandine-rich (X_{Mg}^{ga} = .26-.29), with moderate grossular contents (X_{Ca}^{ga} = .20 - .22) and low MnO (1.6 wt% - 2.5 wt%).

Zoning relationships in the pyroxenes, the association of garnet with magnetite, and the composition of the garnet, indicate the formation of garnet in these samples by the general reaction:

$$2\ CaAl_2SiO_6 + MgFeSi_2O_6 + Fe_3O_4 + 3SiO_2$$

in cpx, or cpx + opx

$$= \underset{\text{garnet}}{(CaMgFe_4)Al_4Si_6O_{24}} + \underset{\text{in cpx}}{CaSiO_3} + \tfrac{1}{2}O_2 \qquad (4)$$

As written, this reaction indicates that the formation of garnet in these rocks is a function of P,T and fO_2. The reaction also involves the consumption of silica. In both 4093 and 4094 free quartz does not occur, so the reaction above is not a completely adequate description of the formation of garnet. The involvement of plagioclase in the reaction above reduces the requirement of free silica for reaction (4)

to proceed.

Temperature estimates based on Fe-Mg partitioning between garnet and coexisting pyroxene rims or recrystallised grains are presented in section 5.7. These estimates will relate to the temperature of formation, or equilibration, of the ga + opx + cpx + mt assemblages providing that the pyroxene rims are in equilibrium with the secondary garnets.

(b) Two pyroxene-plagioclase-quartz free granulites (*4704* and *4510*).

In these quartz-free samples, plagioclase may comprise up to 30% of the assemblage. These plagioclases are polygonal (*4510*) or lobate, well twinned, and optically zoned. Coexisting primary pyroxenes (section 5.4) are extensively exsolved and zoned rimwards.

Clinopyroxene contains abundant, closely spaced (50μm) orthopyroxene exsolution lamellae, opaque blebs (ilmenite) and occasionally plagioclase lamellae (up to 50μm wide). Orthopyroxenes also contain some clinopyroxene lamellae. In both samples, finer (<.5-1mm) green polygonal or finger-like clinopyroxene may rim orthopyroxene or form polygonal aggregates (figure 5.17(b),(c),(d)). These secondary clinopyroxenes are free of exsolution lamellae, and are more calcic (Wo44) magnesian (X_{Mg}^{cpx} = .69-.71), and less aluminous than earlier clinopyroxene (figure 5.4 and 5.5).

Pale pink garnet is developed as euhedral to lobate granular bead-like grains (≤ .2mm diameter) in *4704*. These grains form trails along plagioclase and orthopyroxene-plagioclase grain boundaries, producing a necklace-like network. Frequently garnet occurs as coronas with finely recrystallised plagioclase (± quartz) around orthopyroxene which is rimmed by thin overgrowths of clinopyroxene (fig. 5.17(a)).

Garnet and clinopyroxene also develop on ilmenite grains, although the involvement of opaque does not appear to be necessary in the development of the coronas in general.

Garnet is developed in *4510* as euhedral rims or overgrowths on ilmenite and pyroxenes adjacent to plagioclase. New clinopyoxene may develop with this garnet (figure 5.17(b)).

The secondary garnets are essentially Ca-Mg-Fe solid solutions with up to 2 mol% spessartine. Grossular contents are moderate (X_{Ca}^{ga} = .19), and the garnets are iron rich (X_{Mg}^{ga} = .245 and .21 in *4510* and *4704* respectively). Values of $K_D{}_{Fe-Mg}^{ga-cpx}$ derived from compositions of adjacent corona garnets and clinopyroxenes are 7.8-7.6, while $K_D{}_{Fe-Mg}^{ga-opx}$ values are 3.9 ± .1. The similar K_D values from each sample indicate qualitatively similar conditions of formation of garnet.

Recrystallised plagioclase grains, and plagioclase rims adjacent to garnet are more sodic than plagioclase cores. In *4704* plagioclase zones from An50 (cores) to An42 (rims), while plagioclase zone from An54 (cores) to An44 (rims) in *4510*.

The textural and mineral zoning characteristics outlined above, suggest the formation of garnet in these rocks by the following reactions:

(1) in the absence of opaque:

$$\underset{\text{in opx}}{3\ MgFeSi_2O_6} + \underset{\text{plag 1}}{2\ CaAl_2Si_2O_8} = \underset{\text{garnet}}{(CaMg_2Fe_3)\ Al_4Si_6O_{24}} + \underset{\text{cpx}}{CaMgSi_2O_6} + 2\ SiO_2$$

and (2) in the presence of ilmenite:

$$2\ MgFeSi_2O_6 + 2\ CaAl_2Si_2O_8 + Fe_2O_3 = (CaMgFe_4)Al_4Si_8O_{24}$$

opx; plag; in ilmenite (by stoichiometry); garnet

$$+ CaMgSi_2O_6 + \tfrac{1}{2}O_2$$

cpx

Rutile appears as exsolution blebs in pyroxenes in 4704, and with garnet in 4510, although not developed extensively on ilmenite grains. If TiO_2 is involved, the corona-forming reaction may be written as:

$$(2a)\quad 2\ MgFeSi_2O_6 + 2\ CaAl_2Si_2O_8 + 2\ FeTiO_3$$

opx; plag; ilmenite

$$= (CaMgFe_4)\ Al_4Si_6O_{24} + CaMgSi_2O_6 + 2\ TiO_2\ ,$$

garnet; cpx; rutile

and formation of coronas in these rocks would not be dependent on fO_2 (reaction (2) above).

Depending upon the relative amounts of clinopyroxene and orthopyroxene reacting, the compositions of the pyroxenes, and the abundance of opaque, quartz may be produced or consumed in the net reaction resulting from combinations of (1), (2) and (2a) above.

(c) Two Pyroxene-plagioclase-quartz ± kfeldspar ± apatite -ilmenite granulites (*49412* and *4509*)

Based on modal proportions of the phases and their compositions, these samples are similar to sample 77284029 of Ellis (1979), which approaches a quartz-tholeiite composition.

Feldspar-quartz rich layers in these samples have suffered partial recrystallisation from coarse (1-2mm) lobate granular textures to fine masses of polygonal grains. Relict quartz and feldspars are sutured,

show subgrains, deformation lamellae and undulose extinction. Extensive perthitic and antiperthitic exsolution may be developed. Fine (< .1mm) polygonal recrystallised grains occur on relict grain boundaries or as fine trails and lenses defining S3. The deformation-recrystallisation features described here can be correlated with D3 (James and Black, 1981).

Subhedral to ragged pyroxenes occur with lobate ilmenite in the inequigranular quartzofeldspathic mosaic. Clinopyroxenes in particular show exsolution lamellae, deformation bands, and may be recrystallised marginally to fine polygonal grains (.1-.2mm) associated with fine garnet. In some areas green hornblende is developed with or without brown biotite, on lobate ilmenite and clinopyroxene (fig. 5.18(a)).

Garnet is developed in these rocks principally as:

(a) elongate lens-shaped coronas of saccharoidal grains formed on pyroxenes and opaque in contact with plagioclase (fig. 5.18(a)). Polygonal quartz often forms a second corona inside garnet, adjacent to pyroxenes. These elongate coronas develop into "clots" which define an S3 foliation parallel to the S3 feldspar fabric in *4509*;

(b) coarse (≤ 5mm) lobate-subhedral garnet-quartz (± clinopyroxene) vermicular symplectites forming near-continuous rims between plagioclase and orthopyroxene - clinopyroxene-ilmenite (fig. 5.18(b));

(c) lobate garnet-quartz symplectites on ilmenite alone;

(d) thin garnet-quartz rims on plagioclase;

(e) lobate garnet-quartz intergrowths which corrode and embay primary orthopyroxene or clinopyroxene grains;

(f) lobate grains with polygonal clinopyroxene on orthopyroxene and ilmenite.

Fig. 5.18 CORONA TEXTURES IN QUARTZ-BEARING PYROXENE GRANULITES

cp = clinopyroxene
op = orthopyroxene
pl = plagioclase
ga = garnet
qz = quartz
hbl = hornblende
apat=apatite

Horizontal bars = .2 mm

A. Aggregates of polygonal-saccharoidal garnet forming corona between clinopyroxene and plagioclase. Clinopyroxene and quartz remain in contact. Amphibole (crosses) forms thin rims between clinopyroxene and ilmenite, or occurs as alterations on clinopyroxene rims. Sample 4509, Fyfe Hills.

B. Euhedral-subhedral corona of symplectitic garnet-quartz (±cpx) forming between pyroxenes +ilmenite and plagioclase. Sample 49412, Zircon Point.

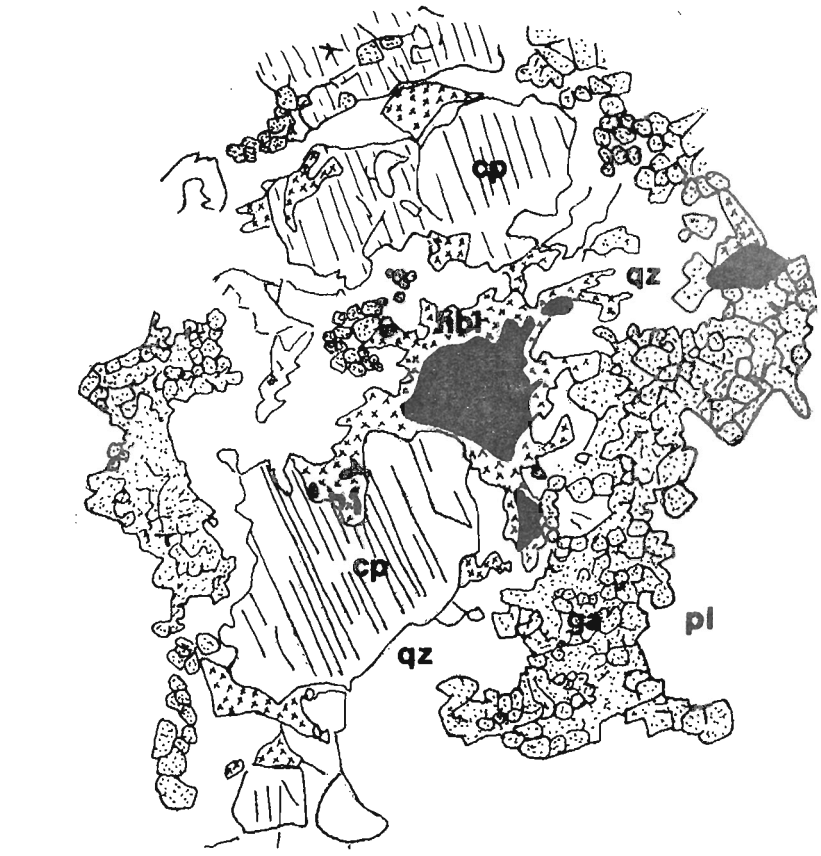

A

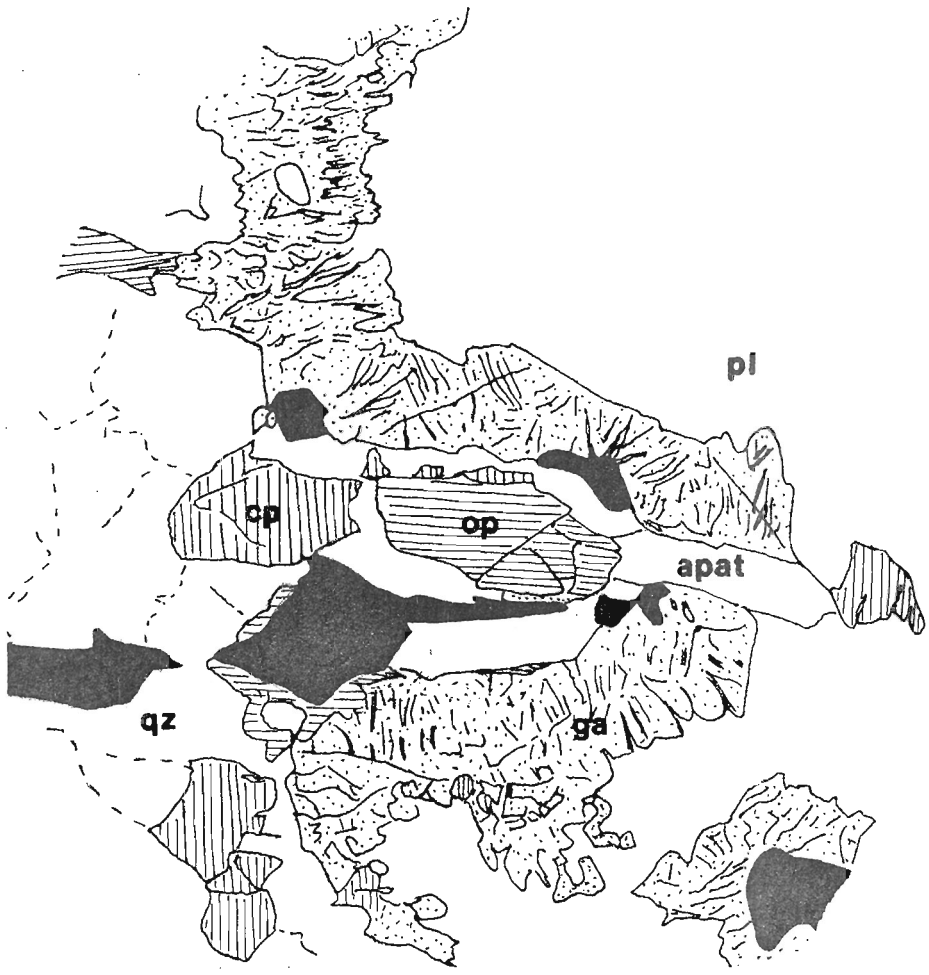

B

Orthopyroxene and clinopyroxene remain in contact without the development of garnet, in the absence of plagioclase and ilmenite. Spatially, the development of garnet-bearing coronas is very strongly controlled by the presence of ilmenite.

Relict orthopyroxenes zone to more magnesian and less aluminous rims adjacent to garnet (X_{Al} = .020, X_{Mg}^{opx} = .448), while recrystallised clinopyroxenes are more magnesian (X_{Mg}^{cpx} = .64-.62), and have higher calcium contents (Wo45) than primary metamorphic clinopyroxene (figure 5.5). Plagioclase zones to slightly more sodic compositions adjacent to garnet (An 32).

Symplectite or corona garnet is iron-rich and calcic (X_{Mg}^{ga} = .14-.20, X_{Ca}^{ga} = .19-.20), with low MnO contents (1.5-3 mol% spessartine). This garnet is irregularly zoned in X_{Mg}, however the lower X_{Mg}^{ga} compositions appear to coexist with recrystallised clinopyroxene. These compositions give $K_{D_{Fe-Mg}}^{ga-cpx}$ values of 9.6-10.4, while K_D values obtained using maximum X_{Mg}^{ga} data are 6.2-6.9. The latter values have not been derived from adjacent analyses however, and in view of the very strong compositional gradients within these symplectites are not considered reliable.

The textural and compositional observations indicate the formation of garnet in these assemblages by reactions involving opaque as well as pyroxenes and plagioclase:

(1) $3\ CaAl_2Si_2O_8 + 3\ Fe_2O_3 + 3\ SiO_2 = 3\ CaFe_2Si_3O_{12} + O_2$,
plag in ilm qz garnet

a partial reaction leading to garnet coronas on ilmenite, in the absence of any development of rutile in these rocks.

(2) $3\ MgFeSi_2O_6 + 2\ CaAl_2Si_2O_8 = (CaMg_2Fe_3)\ Al_4Si_6O_{24}$
opx plag garnet
$+ CaMgSi_2O_6 + 2\ SiO_2$,

a reaction leading to garnet-clinopyroxene-quartz symplectites on orthopyroxene.

(3) $\underbrace{CaMgSi_2O_6 + CaAl_2SiO_6 + 4\ FeSiO_3}_{\text{in cpx}} = (CaMgFe_4)Al_4Si_6O_{24} + 2\ CaSiO_3 + SiO_2$,

a possible reaction leading to zoning in original clinopyroxene, and the garnet coronas on clinopyroxene in *4509*.

The actual continuous reaction leading to the formation of these coronas will be a more complex combination of the three reactions given above. The exact balance of this reaction will depend on the compositions of the pyroxenes, the amount and type of opaque present, and the presence of quartz (McLelland and Whitney, 1977).

In *4509*, additional hydration and oxidation reactions have produced Ca-Ti-Al amphibole and occasional biotite as coronas on ilmenite (figure 18(a)) close to garnet, plagioclase or clinopyroxene. These textures suggest further retrogression with the development of hornblende after garnet, by such reactions as

$$Ilm + ga + cpx = hbl + plag$$

and

$$Ilm + ga + cpx + kspar = Biot + hbl \pm plag.$$

Discussion:

Garnet-bearing coronas on pyroxene and opaque, similar in many respects to those described above, have been reported previously from other metamorphic provinces (Gjelsvik, 1952; de Waard, 1965; Griffin and Heier, 1969, 1973; Griffin, 1971, McLelland and Whitney, 1977). In these cases, the formation of garnet coronas has been inferred to result from overstepping of reaction boundaries during a retrogressive (lower T) event or during cooling (e.g., Griffin and Råheim, 1973).

The transition from medium-pressure granulites facies conditions (2 pyroxene + plagioclase) to a high-pressure (garnet-clinopyroxene) granulite facies regime has been accomplished by near-isobaric cooling, with garnet forming as the P-T path crosses to the high pressure side of reactions such as

$$An + opx + Fe\ oxide + quartz = ga + cpx + O_2,$$

which have positive dP/dT slopes (Griffin and Råheim, 1973; McLelland and Whitney, 1977).

In the samples considered here, and in those of Ellis (1979), secondary clinopyroxenes are still poor in jadeite and acmite, and retain high CaTs/Jd ratios. Hence, reactions involving the albite component of plagioclase, which lead to the formation of eclogitic assemblages (ga + high Jd-Ac clinopyroxene), did not proceed at the P-T conditions under which *49412* and *4509* recrystallised.

McLelland and Whitney (180) have produced an expression for a generalised garnet-forming reaction for metaigneous rocks from the Adirondacks. The exact form of this reaction, which assumes limited mobility of Al_2O_3, is dependent on compositional variables including the An content of plagioclase, silica mobility, and the presence or absence of olivine. For silica saturated rocks, McLelland and Whitney (1977) have given a simplified garnet-forming reaction

$$2\ CaAl_2Si_2O_8 + (6 - \alpha)(MgFe)SiO_3 + \alpha\ Fe\text{-oxide} + (\alpha - 2)\ SiO_2$$
$$= Ca(FeMg)_5Al_4Si_6O_{24} + Ca(MgFe)Si_2O_6 + O_2,$$
$$Gr_{18}\ garnet$$

where α is a compositional variable:

$$\alpha = 6 - 5\left(\frac{X^{ga}_{Mg}}{X^{opx}_{Mg}}\right) - \left(\frac{X^{cpx}_{Mg}}{X^{opx}_{Mg}}\right)$$

Substitution of the measured values of X^{opx}_{Mg}, X^{cpx}_{Mg} and X^{ga}_{Mg} in *49412*

yield an approximate value of 3 for α. Substitution of this α value into the equation above gives good balance of Fe and Mg on both sides of the equation, indicating that the generalised garnet forming reaction of McLelland and Whitney (1977) is a reasonable approximation to the corona forming reaction in *49412*.

TABLE 5.2 PYROXENE MINERAL CHEMISTRY AND THERMOMETRY -BAROMETRY OF PYROXENE GRANULITES FROM ENDERBY LAND.

Rock	Locality	X^{opx}_{Mg}	X^{cpx}_{Mg}	comment	X^{plag}_{An}	X^{cpx}_{CaTs}	X^{opx}_{MgTs}	a^{opx}	a^{cpx}		Pellis 1980	$K_D^{opx-cpx}$ Fe-Mg	T Wood-Banno	T Wells	T Lindsley-Dixon	T Nehru-Wyllie
4598	DEMIDOV I.	.592	.763		82 49 rim	.08	.022	.339	.046 .088 .110	exsolution rims cores	<11 < 7	2.22 (.2)	851 938 971	883 1015 1068	792 1019 1124	742 895 962
4505	DENHAM	.473	.589		91	.07	.045	.198	.034	average	<10.2	1.57 (.12)	821	873	807	742
4525	SIMPSON PEAK	.609	.739	cores	38	.048	.036	.347	.075 .047 .030	core rim exsolution	<12.3	1.82 (.15)	923 861 805	985 891 811	959 803 681	858 750 661
4095	SEAVERS RIDGE	.705	.799		-	.059	.060	.462	.039	average	-	1.66 (.12)	862	849	725	703
4091	AMUNDSEN BAY	.816	.883		35	.057	.036	.635	.063 .045 .034	core rim exsolution	<14.3	1.70 (.12)	973 924 884	927 865 816	838 742 672	801 730 674
4092	AMUNDSEN BAY	.257	.352	primary pigeonite	35	.034	.015	.057 .048	.018 .031 .012	rim core exsolution	10.2	1.57 (.10)	824 916 777	888 1036 816	933 1269 796	812 1011 722
4093	WARD ROCKS	.526	.650		-	.050	.050	.245	.058	rim low rims core	-	1.68 (.10)	886 829 944	959 872	938 791 1036	835 734 899
4094	WARD ROCKS	.586	.699		100	.130core .050 rim	.080core .030rim	.311	.033	average	<15 < 7	1.64 (.26)	818	837	723	690
3508	MT. McLENNAN	.584	.700		43	.050	.032	.318	.046	average	<11.9	1.66 (.10)	855	892	810	752
3566	MT. DENHOLM	.621	.736		36	.040	.020	.364	.046	average	11.1	1.69 (.08)	859	884	788	742
3515	MT.MAFEER	.549	.650		77	.080	.048	.262	.037	average	<12.2	1.52 (.11)	833	871	783	731
3565	MT.DENHOLM	.527	.655		49	.045	.025	.256	.044	average	10.1	1.70 (.09)	847	898	833	764
3593	MT.TOP	.605	.730 .715		44	.050	.035	.338	.044 .030 .070	rims exsolution cores	<11.7	1.77 1.64 -	854 809 914	882 817 972	788 691 939	740 668 845
3596	CROHN I.	.606	.705		75	.070	.040	.341	.048	average cores	<11.3	1.55 (.04)	864	897	811	756
4545	MT. MERRICK	.620	.739		41	.052	.037	.362	.051	average	<12.5	1.73 (.11)	870	900	814	760
3517	MT.MAFEER	.603	.753		43	.053	.035	.336	.049	average	<12.3	2.01 (.16)	865	899	816	760
4004	BEAVER I.	.694	.774		93	.091	.063	.434	.042	average	<12.4	1.51 (.10)	872	868	753	723

Rock	Locality	X^{opx}_{Mg}	X^{cpx}_{Mg}	comment	X^{plag}_{An}	X^{cpx}_{CaTs}	X^{opx}_{MgTs}	a^{opx}	a^{cpx}		Pellis 1980	$K_D{}^{opx-cpx}_{Fe-Mg}$	T Wood-Banno	T Wells	T Lindsley Dixon	T Nehru-Wyllie
4008	BEAVER I.	.669	.760		58	.070	.036	.413	.042	rims	13	1.57	881	896	752	720
									.055	average	to 10	(.10)	918	929	830	777
									.060	areas			930	950	880	798
4319	MT.CHARLES	.564	.716		88	.043	.033	.299	.045	recryst.	6.5	1.95	847	887		
									.061	relict		(.15)	888	949		
4818	GROMOV	.673	.750		-	.120	.056core	.428	.049	exsolved	-	1.46	881	891		
	NNK		.691	area					.085	areas		1.09	955	999		
4359	ZUBCHATYY	.231	.342		67	.020	.010	.050	.043	exsolutions	2.2	1.73	949	1089		
	ICE SHELF								.036	exsolutions			925	1048		
4539	MT.BERGIN	.558	.693		44	.050	.033	.293	.045	rims	<11.7	1.79	831	865		
		.537	.637	cores					.098	cores		(.10)	952	1062		
4099	SEAVERS	.673	.760		36	.050	.040	.422	.042	rims	<13	1.54	861	863		
	RIDGE		.730	core					.080	cores		1.32	949	989		
4510	FYFE HILLS	.557	.711	rim	50	.045	.030	.293	.043		<10.1	1.96 (.22)	843	884	801	745
4509	FYFE HILLS	-	.646	rim	35	.055	-	-	-		14	-				
		-	.605	core												
49464	FYFE HILLS	-	.530	rim	70	.069	-	-	-			-				
		-	.467	core	80	.094	-	-	-							
49461	FYFE HILLS	.500	.644		-	.030	.020ex	.203	.057	exsolution		1.81	896	982	990	867
		.507	.664			.015	.011rext.	.214	.049	recryst		1.92	871	941	913	817
49458	FYFE HILLS	.554	.696		50	.074	.040core	.279	.050	rims	<14-11	1.85	865	917	857	783
			.659	areas		.045 rim			.088	cores		1.56	942	1038	1077	927
4704	FIELD IS.	.510	.674		49	.045	.022	.250	.025	exsolution	<10.2	1.99	777	799	682	654
						.020rim			.048	rims	4	(.11)	853	912	861	782
									.090	areas			935	1044	1106	940
4520	HYDRO-	.508	.657	areas	40	.035	.020	.245	.043	areas	<10.6	1.86	857	919	874	790
	GRAPHER IS.		.665	rims					.025	rims		1.92	779	802	687	658
4521	HYDRO-	.588	.701	exsol.	24	.040	.025	.324	.036	exsolution	<13	1.65	825	846	/36	700
	GRAPHER IS.		.680	rims					.065	rims			900	958	918	829
			.649						.099	cores		1.49	958	1049	1086	938
49412	ZIRCON	.448	.585		30	.040cores	.020	.191	.039	rims	10.3	1.74	831	892	848	768
	POINT		.567	core		.030	.014	.168	.042	cores		1.61	850	921	899	802

NUMBERS IN PARENTHESES - STANDARD DEVIATIONS IN K_D VALUES.

TABLE 5.3 GARNET-BEARING PYROXENE GRANULITE ASSEMBLAGES

Number	Locality	X_{Mg}^{opx}	X_{Mg}^{cpx}	X_{Mg}^{ga}	X_{Ca}^{ga}	$K_D^{ga\text{-}cpx}{}_{Fe\text{-}Mg}$	$K_D^{ga\text{-}opx}{}_{Fe\text{-}Mg}$	Tga-cpx Ellis & Green (1979)	Tga-opx This work		P ga-opx
(1) PRIMARY ASSEMBLAGES											
49461	FYFE HILLS	-	.571	.192	.214	5.33	-	769			-
4818	GROMOV	.673	.691	.381	.162	3.64	2.90	860	837		12
4598	DEMIDOV	.592	.660	.360	.176	3.45	2.51	867	899		>10
(2) CORONA ASSEMBLAGES											
49464	FYFE	-	.530	.105	.438	9.65	-	750	-		-
4509	FYFE	-	.646	.150	.195	10.35	-	606	-		-
4510	FYFE	.557	.711	.245	.193	7.61	3.89	677	675		8.0
49461	FYFE	.506	.664	.159	.222	10.43	5.40	628	660	hiMngar.	7.0
49412	ZIRCON PT.	.448	.619	.144	.198	9.65	4.83	619	560		
				.169	.198	6.94	3.99	696	624		7.0
4520	HYDROGRAPHER	.508	.680	.200	.190	8.89	4.13	634	640		7.6
4359	ZUBCHATYY	.231	.342	.062	.202	7.87	4.55	671	600		6.2
4092	AMUNDSEN BAY	.257	.352	.080	.214	6.56	3.97	700	665		6.6
4093	WARD ROCKS	.526	.650	.263	.220	7.91	3.12	689	800		8.0 at 800° 4.0 at 700°
4094	WARD ROCKS	.586	.699	.286	.200	5.79	3.53	718	738		
							4.20		670		7.6
4598	DEMIDOV	.592	.763	.240	.190	7.39	4.50	660	647		-
						10.21		577			-
4818	GROMOV	.673	.750	.316	.189	7.92	4.47	659	660		4.6
4704	FIELD IS.	.510	.695	.210	.187	8.92	3.92	667	660		9.4

5.7 PRESSURE-TEMPERATURE CONDITIONS OF FORMATION

I. PRIMARY METAMORPHIC ASSEMBLAGES

(A) TEMPERATURES

(1) Stability of Pigeonite.

The presence of primary metamorphic pigeonite, now inverted and exsolved, in 4359 and 4092 indicate high maximum temperatures of metamorphism (O'Hara and Yarwood, 1978; Smith, 1974; O'Hara and Barnicoat, 1980). Comparison of the reconstructed compositions of primary pigeonites (X_{Mg} =.25, Wo = 8%) with the experimental data of Ross and Huebner (1975) suggests minimum temperatures of 970°C for equilibration of the metamorphic pigeonites. Minimum temperatures of 962°C ± 20°C are obtained from the application of the pigeonite stability curve of Ishii (1975), at an assumed pressure of 8 kbar. Peak metamorphic temperatures in the first recognisable major granulite facies event (M1-M2) are thus inferred to be in excess of 950°C on the basis of the stability of Fe-rich pigeonite.

(2) Garnet-Clinopyroxene-Orthopyroxene assemblages

$K_D^{ga\text{-}cpx}{}_{Fe\text{-}Mg}$ and $K_D^{ga\text{-}opx}{}_{Fe\text{-}Mg}$ data obtained from the compositions of primary garnet-clinopyroxene-orthopyroxene in 4598 and 4818 (Table 5.3) have been used to estimate equilibration temperatures for these assemblages in M1-M2.

Application of the garnet-clinopyroxene Fe-Mg distribution thermometer (Ellis and Green, 1979) to these samples yields temperatures of 870-890°C at an assumed pressure of 10 kbar. Garnet-clinopyroxene thermometry (Ellis and Green, 1979) for the Mn-rich sample 49461 yields a temperature of only 780°C, however. The garnet-clinopyroxene thermometer of Ganguly (1979), which otherwise yields anomalously high

temperatures for garnet-clinopyroxene bearing assemblages in granulites from Enderby Land, gives a calculated temperature of 870°C for *49461*. A similar estimate is given by the Ellis-Green (1979) thermometer if Mn in garnet is treated as identical to Ca in increasing $K_{D_{Fe-Mg}}^{ga-cpx}$ at constant P and T. Clearly, and as considered by Dahl (1980), the effects of spessartine component in garnet upon Fe-Mg distribution between garnet and other phases may be considerable. Experimental determination of the magnitude of these effects is necessary before garnet-clinopyroxene Fe-Mg distribution thermometry can be reliably applied to Mn-rich compositions or assemblages such as *49461* (see Table 5.3, figure 5.7a).

The garnet-orthopyroxene Fe-Mg distribution thermometer (Chapter 2 and 3) yields temperatures of 840-900°C for primary garnet-orthopyroxene compositions in *4598* and *4818* at an assumed pressure of 10 kbar. These estimates are in good agreement with the garnet-clinopyroxene temperatures derived for these samples, although the garnet-orthopyroxene thermometry must be considered less precise as a result of the problems involved in the experimental calibration (Chapter 2) and the relatively small changes in $K_{D_{Fe-Mg}}^{ga-opx}$ with temperature.

(3) Pyroxene Miscibility Gap

In recent years, considerable use has been made of the mutual solubility of orthopyroxene and clinopyroxene as a geothermometer both in lherzolites and granulites. Most experimental data pertaining to the two-pyroxene solvus have been obtained in the CMS system (Davis and Boyd, 1966; Mori and Green, 1975, 1976; Lindsley and Dixon, 1976; Warner and Luth, 1974; Nehru and Wyllie, 1974) or in more complex systems applicable directly to garnet lherzolites (Mori and Green, 1978). Data on the hedenbergite-ferrosilite join have been obtained by

LIndsley and Munoz (1969), while the two-pyroxene miscibility gap has been determined for a range of bulk X_{Mg} values at one atmosphere by Ross and Huebner (1975, 1979).

Practical geothermometers for application to a wide range of bulk compositions in terms of X_{Mg} have been developed by Wood and Banno (1973), Wells (1977), and Henry and Medaris (1980). These thermometers depend on two separate experimentally determined data sets - the CMS pyroxene "solvi" (see above), and the CFS hedenbergite-ferrosilite miscibility gap of Lindsley and Munoz (1969).

The practical thermometers applied to the two-pyroxene granulites of Enderby Land differ mainly in two aspects:

(a) the particular CMS data set used to construct the calibration. All CMS solvi have been determined at higher pressures than appropriate for crustal granulites;

(b) the method of interpolation between CMS end-member system and the CFS data of Lindsley and Munoz (1969). The thermometers of Wood and Banno (1973) and Henry and Medaris (1980) are based on a quadratic interpolation scheme (using terms in X_{Fe}^{opx} and $(X_{Fe}^{opx})^2$), while a linear interpolation is used by Wells (1977).

The two differences outlined above give rise to the discrepancies between the various thermometers when applied to these granulites. In all cases, however, there may be some error introduced by the application of simple system experimental data in CMS and CFS to more complex natural systems.

Recent experimental data in CMS are in reasonable agreement on the mutual solubility limits of enstatite-diopside (Mori and Green, 1975; Lindsley and Dixon, 1975). These results, however, are in marked disagreement with the solvus data of Davis and Boyd (1966) upon which the Wood-Banno (1973) thermometer is based. Comparison of the

respective solvi data indicates that the Wood-Banno thermometer may overestimate T by up to 60°C at low temperatures (< 1000°C) in magnesian ($X_{Mg}^{opx} \geq 60$) compositions (Mori and Green, 1978) and in crustal granulites (Wood, 1975; Hewins, 1975; Ellis, 1980).

Two-pyroxene activity data and temperatures estimated using the available semi-empirical thermometers are presented in Table 5.2. In all cases, average estimated temperatures have been calculated based upon averaged rim compositions of coexisting pyroxenes or on averages of all $a_{Mg_2Si_2O_6}^{pyx}$ values obtained in relatively unzoned samples. In those samples where exsolution and compositional zoning are abundant, temperatures have also been calculated from compositions of exsolution lamellae and rims (minimum T) and compositions of unexsolved pyroxene cores or integrated area scans of exsolved grains (maximum T).

In all calculations, the ideal multisite solid solution model of Wood and Banno (1973) has been used:

$$a_{Mg_2Si_2O_6}^{pyroxene} = X_{Mg}^{M1} \cdot X_{Mg}^{M2} = X_{Mg_2Si_2O_6}^{pyroxene}$$

In addition, non-random distribution of Fe-Mg between sites has been neglected and thus values of $X_{Mg_2Si_2O_6}^{pyroxene}$ have been calculated using the algorithm:

$$X_{Mg_2Si_2O_6}^{pyroxene} = (X_{Mg}^{pyroxene})^2[(1 - Ca - Na - Mn) \times (1 - Na - Cr/2 - Ti - Mn - (Al - Na - 2Ti)/2]$$

to correct for non-quadrilateral pyroxene components. The ignoring of Fe-Mg site preferences is considered to introduce no significant error in the temperature estimates, compared with analytical errors and errors inherent in the various calibrations.

The four two-pyroxene geothermometers used in this study are

compared in figures 5.19 and 5.20. The major features to emerge from these comparisonsare:

(a) X_{Mg}^{opx} dependence of T estimates:

The Wells (1977) and Henry and Medaris (1980) thermometers show marked compositional dependence of calculated T, with higher X_{Mg}^{opx} parageneses yielding lower T even at adjacent localities (figure 5.19). Maximum T data derived from core and area-scan analyses (figure 5.20) show considerable scatter correlated with X_{Mg}^{opx}, with Fe-rich samples yielding unreasonably high calculated temperatures of 1050-1100°C by these thermometers.

On the other hand, the Wood-Banno (1973) thermometer displays only minor X_{Mg}^{opx} dependence, with slightly higher temperatures estimated for more magnesian samples (figure 5.19). This results in the lower degree of scatter in core-, rim-, and average-temperatures obtained using the Wood-Banno thermometer in comparison to the other calibrations (figure 5.20).

(b) Absolute values of estimated Temperatures:

Peak metamorphic conditions, based on pre-exsolution pyroxene compositions, are indicated to be 915-980°C by the Wood-Banno (1973) thermometer, while other thermometers show a considerable range of peak T estimates resulting from compositionally dependent scatter. Adopting a downward revision of the Wood-Banno temperature by 60°C (p.), peak metamorphic temperatures are inferred to have been as high as 920°C. This estimate is consistent with the stability of pigeonite in some Fe-rich rocktypes (see above).

On the basis of average and rim temperature data, the Wood-Banno (1973) thermometer appears the most reliable in that it has less

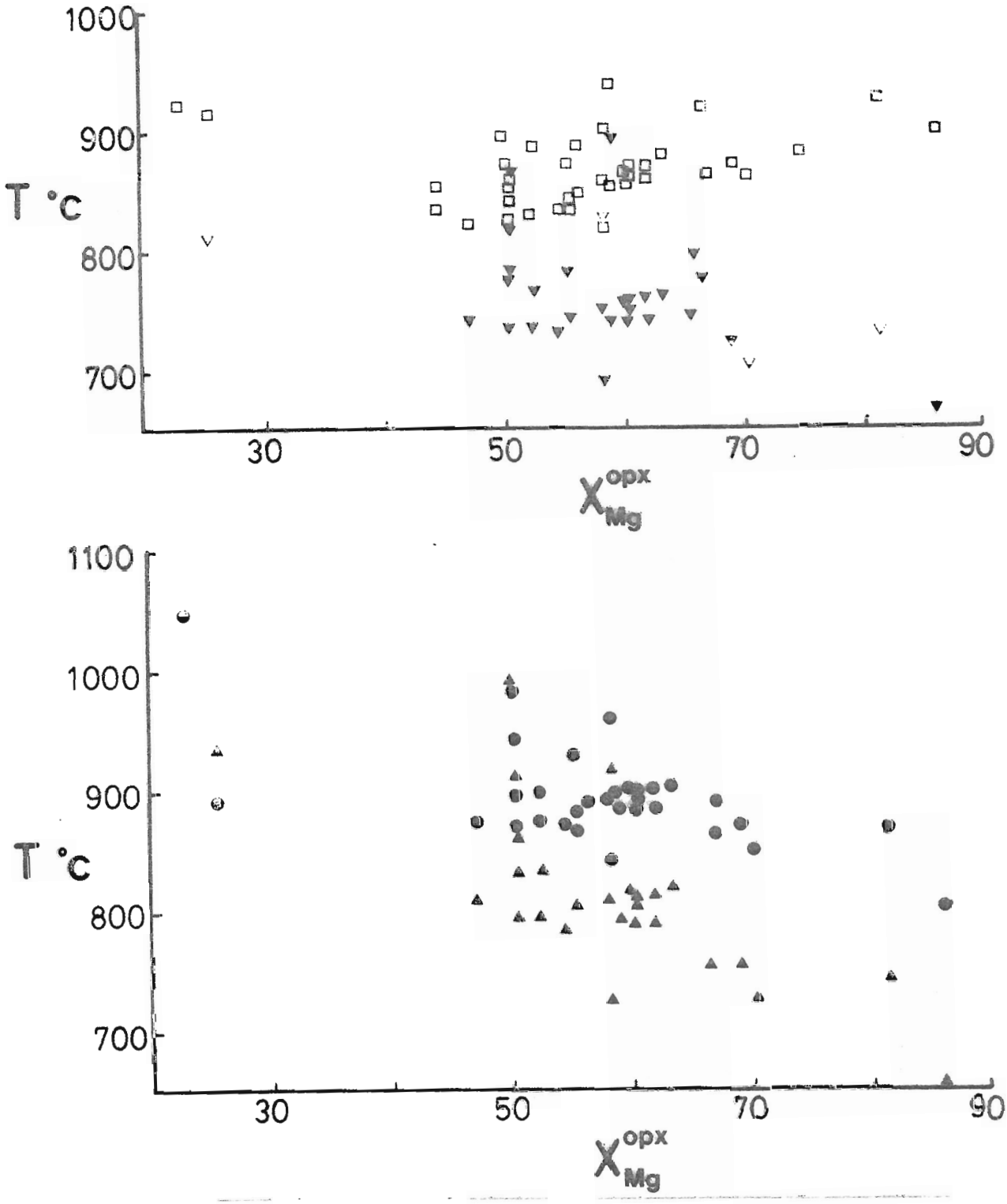

Fig. 5.19 Variation of estimated temperature with X_{Mg}^{opx} for average and rim data, using various two-pyroxene thermometer calibrations:

a. □ Wood and Banno (1973)

▽ based on Nehru and Wyllie (1974)*

b. ● Wells (1977)

▲ based on Lindsley and Dixon (1976)*

* In Stormer and Whitney (1977)

inherent compositionally dependent scatter than other calibrations, although its absolute accuracy may be open to question. Inferred rim temperatures of 815-900°C (figure 5.20), with a main clustering in the range 840-860°C, are in reasonable agreement with temperatures obtained using the Lindsley-Dixon solvus (figure 5.20, cluster at 800 ± 20°C) if a downward adjustment of 60°C is applied to the Wood-Banno (1973) based temperatures.

For the dominantly Fe-rich granulites studied here, the Wells (1977) thermometer gives the highest average temperatures (figure 5.20), with considerable compositionally dependent scatter (800-1025°C) and a main cluster in the range 860-900°C. The Nehru-Wyllie based thermometer gives low average temperatures (700-800°C) with marked scatter in estimated temperature resulting from variations in X_{Mg}^{opx} (figure 5.20).

Two-pyroxene compositional data from Enderby Land are compared to the one-atmosphere pyroxene solvus data of Ross and Huebner (1975) in figure 5.21. In view of the uncertainties in the experimental and natural rock data, maximum metamorphic temperatures in excess of 900°C are suggested by this comparison, in agreement with the thermometry based on Wood and Banno (1973) with a -60°C adjustment. Average and rim temperature data plot mainly near the 800°C isotherm of figure 5.21, in good agreement with temperatures suggested above for the equilibration of pyroxene rims.

The insensitivity of the two-pyroxene solvus gap below even 900°C prohibits any interpretation of real temperature differences between separate localities within granulite facies terrains (e.g., Bohlen and Essene, 1980; Bohlem *et al.*, 1980), and makes the determination of absolute temperatures of equilibration of two-pyroxene granulite assemblages an uncertain procedure. Further uncertainty is introduced by

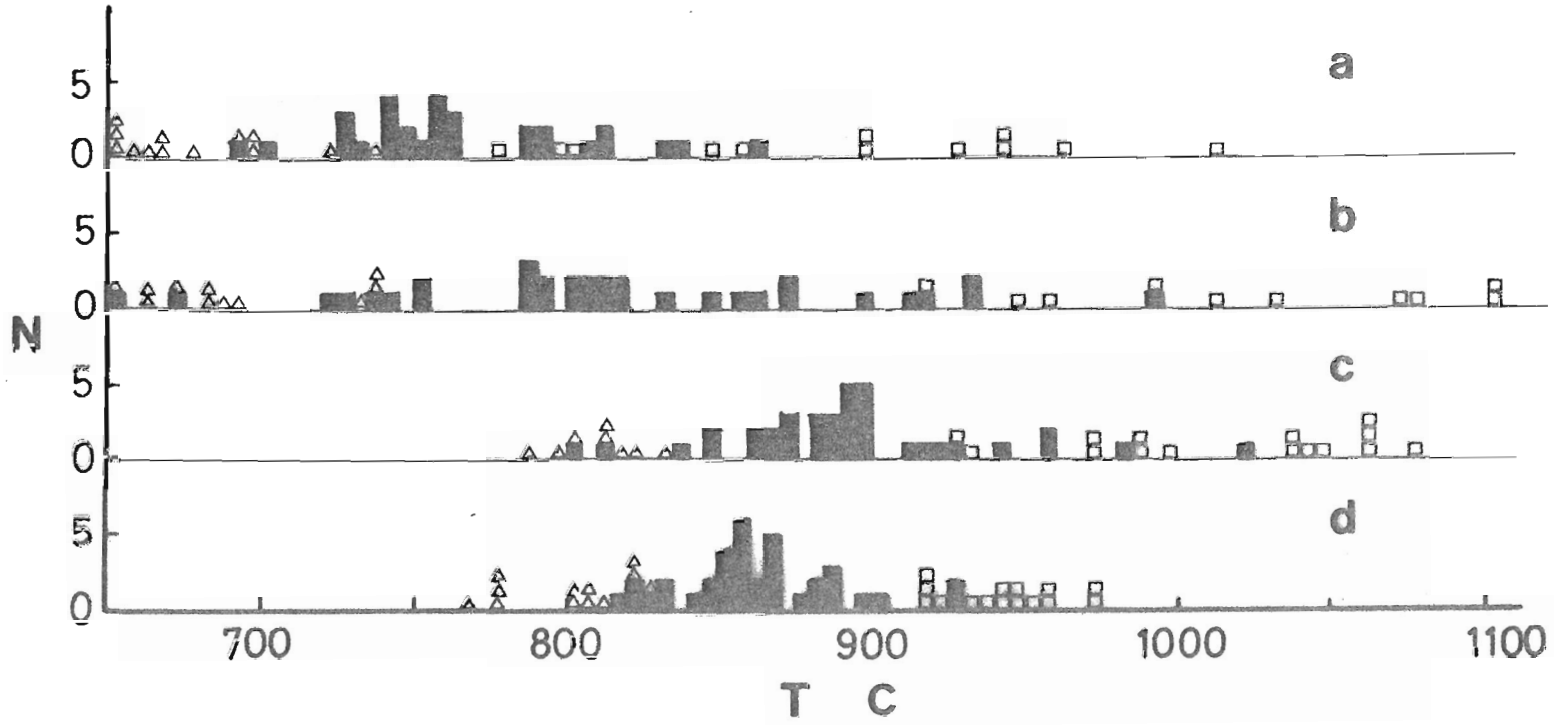

Fig. 5.20 Two-pyroxene temperature-histograms for granulites from the Napier province.
N...number of samples giving similar T estimates (within a 5°C range)

□ core or maximum T data

■ rim or average T data

△ exsolutions and recrystallised grain T data.

a. based on Nehru and Wyllie (1974) b. based on Lindsley and Dixon (1976)

c. Wells (1977) d. Wood and Banno (1973)

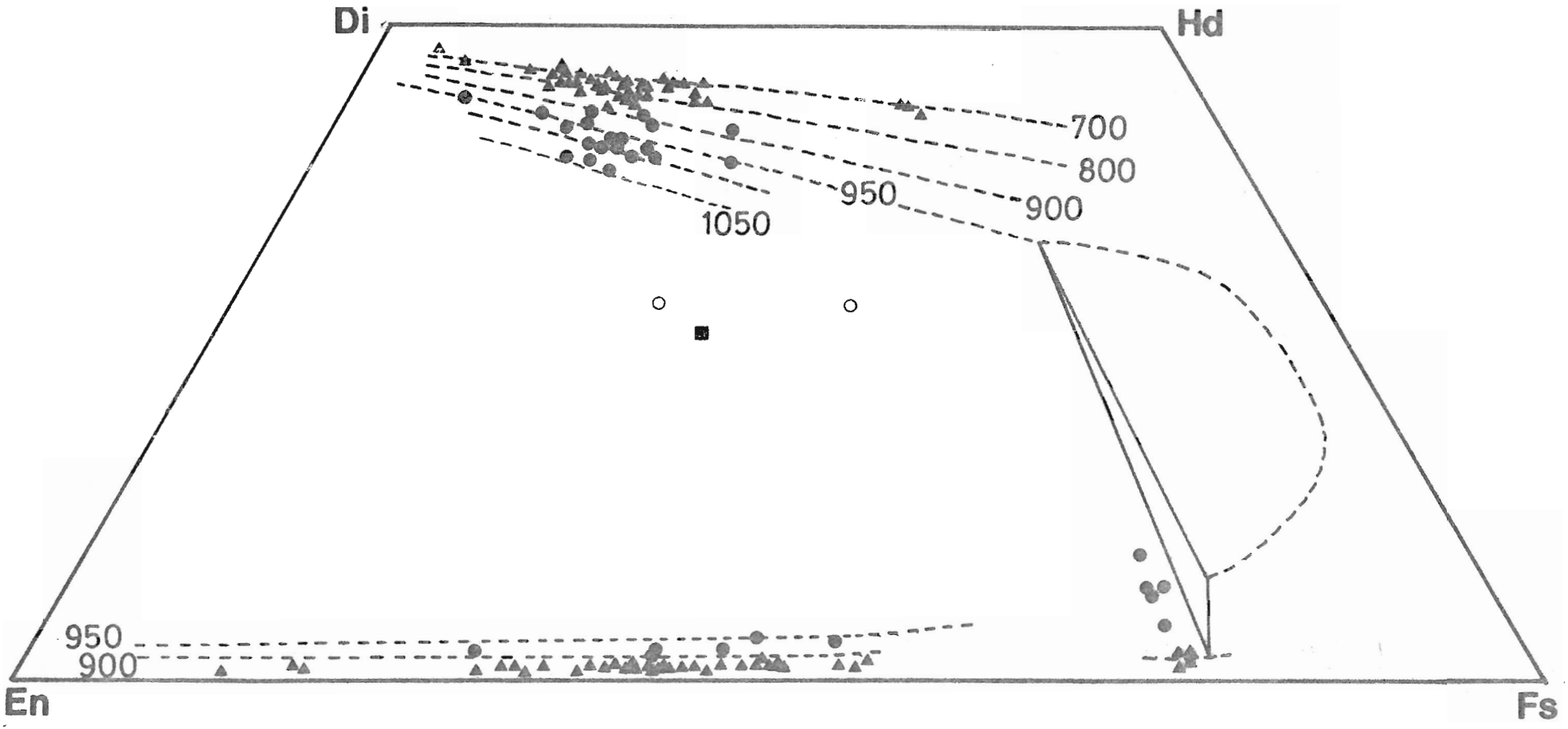

Fig. 5.21 Pyroxene quadrilateral illustrating compositions of pyroxenes in pyroxene granulites from the Napier province, superimposed on the isotherms of Ross and Huebner (1975) for pyroxenes coexisting at 1 atm. Numbers refer to temperatures corresponding to particular isotherms (°C).

- ● core compositions of clino- and orthopyroxenes or primary metamorphic pigeonite.
- ▲ rim and exsolution or recrystallised grain compositions.
- ■ cpx core composition in 49461.

the choice of thermometer, as shown above. Nevertheless, the Wood-Banno (1973) thermometer data in particular (figure 5.20) indicate consistent differences in temperatures estimated for cores, rims or average grain analyses, or recrystallised grains and exsolution lamellae.

It is suggested that the two-pyroxene granulites initially equilibrated at temperatures in excess of 900°C, in a thermal episode (M1-M2) correlated with D1 or D2. The assemblages re-equilibrated in D2 or subsequent to D2 at temperatures of ≈800°C, with further cooling resulting in exsolution lamellae and rim compositions which yield temperatures less than 800°C.

(B) PRESSURES

(1) The geobarometer of Ellis (1980) has been used to estimate the pressures of formation of the two-pyroxene-plagioclase ± quartz granulites. This barometer is based on a thermodynamic treatment of the reaction:

$$\underset{\text{in clinopyoxene}}{CaAl_2SiO_6} + \underset{\text{quartz}}{SiO_2} = \underset{\text{plagioclase}}{CaAl_2Si_2O_8}$$

In the absence of quartz, $CaAl_2SiO_6$ can persist to lower pressures than in the assemblage CaTs + Qz. Thus, for quartz absent two-pyroxene-plagioclase granulites pressures calculated using the barometer derived from the reaction above will be maximum pressures.

Pressures calculated for the two pyroxene granulites are given in Table 5.2. Several problems are apparent in applying this geobarometer to these particular rocks:

(a) from figure 5.12 it can be seen that X^{cpx}_{CaTs} is often quite low (generally 3-6 mol%), as would be expected for lower-pressure clinopyro-

xene bearing assemblages. At low alumina contents the presence of other minor components (e.g., Na, Ti) can lead to large relative errors in calculated X^{cpx}_{CaTs}, and hence considerable errors in calculated pressures. In most samples studied, maximum Al/2 values have been used in pressure calculations and hence pressure overestimates may be expected;

(b) plagioclase is often moderately zoned. In most samples studied, plagioclase has not been analysed exhaustively for the delineation of such zoning, whereas clinopyroxenes have been more extensively analysed. The poorer constraints on plagioclase composition lead to some uncertainty in pressure estimates. A further problem lies in the interpretation of which plagioclase composition is in equilibrium with the measured X^{cpx}_{CaTs}, particularly in those samples affected by later recrystallisation.

Bearing in mind the problems outlined above, and the implication that the derived pressures are in general *maximum* pressures, the CaTs-An-Qz data are internally consistent. Maximum pressures of formation of the 2 pyroxene granulites are in the range 10-14 kbars, with most samples yielding pressures of 10-12 kbar at 900°C. There is no apparent regional variation in the maximum pressures obtained from these assemblages (Table 5.2).

The two-pyroxene granulites of the Napier province occur interlayered with sillimanite-bearing pelitic gneisses. At 900°C, the stability of sillimanite suggests maximum pressure conditions of 11 kbar (Day and Kumin, 1980). Thus, maximum pressures of 10-11 kbar at 900°C are indicated for the peak metamorphic conditions suffered by these two pyroxene granulites.

Garnet-orthopyroxene barometry developed in Chapter 2 and Chapter 3

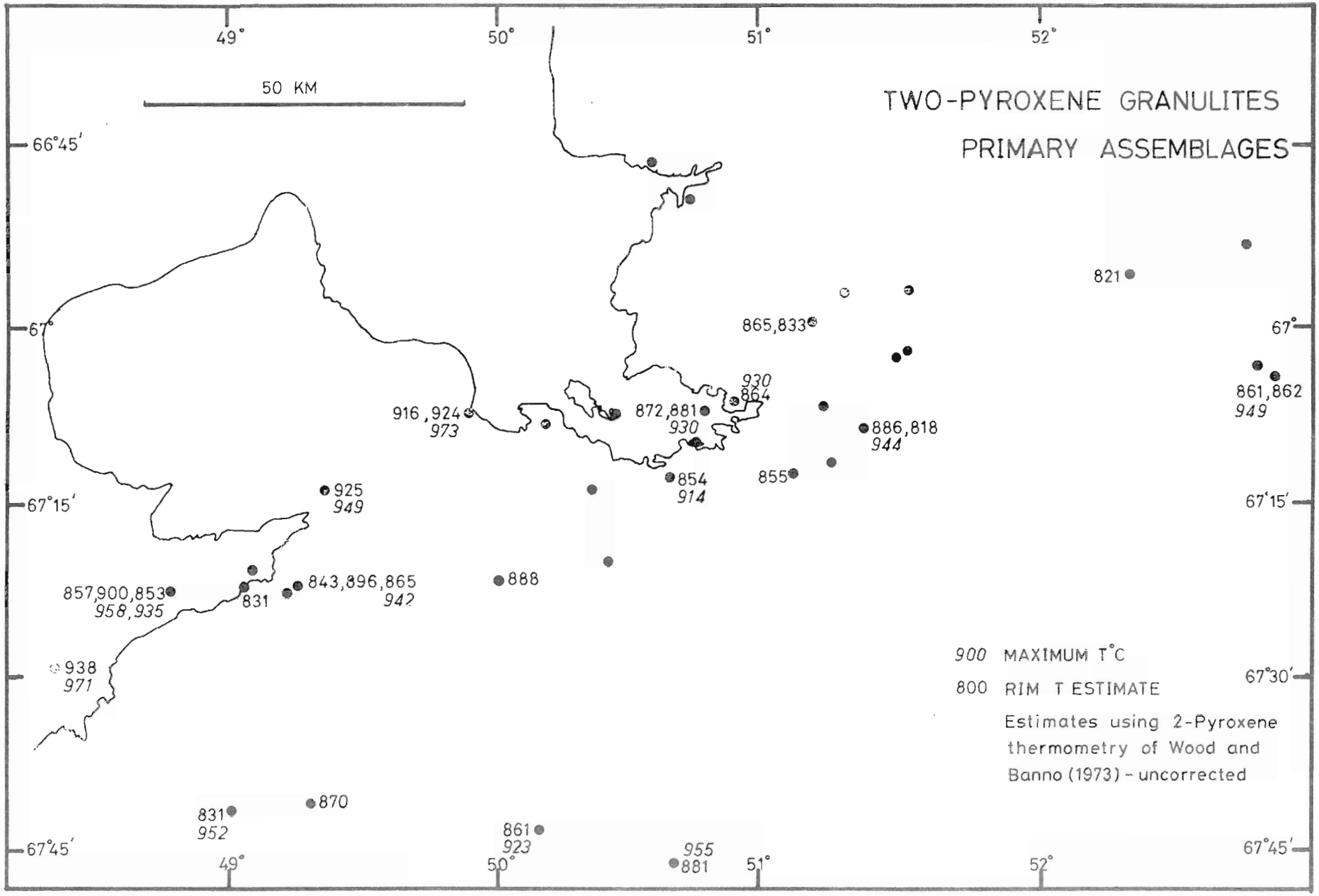

FIG 5.22 REGIONAL DISTRIBUTION OF T ESTIMATES FOR PRIMARY ASSEMBLAGES

herein yields pressures of 12.6 kbar ± 1 for the garnet-clinopyroxene-orthopyroxene sample *4818*, in reasonable agreement with the maximum pressure estimates obtained above.

(C) SUMMARY

The application of various geothermometers and geobarometers to the primary metamorphic assemblages of the pyroxene granulites studied herein indicates peak metamorphic temperatures of ≥ 900-950°C at pressures less than 10-11 kbar. These peak metamorphic conditions were achieved prior to final grain boundary equilibration.

From average pyroxene compositional data for a wide range of samples in which partial recrystallisation of the primary, peak metamorphism assemblages is observed, a high degree of recrystallisation, including textural equilibrium, appears to have been achieved at 800-860°C during or after D2.

Further re-equilibration at temperatures below 800°C, and possibly as low as 700°C has resulted in the formation of pyroxene exsolution lamellae in most two-pyroxene granulites.

II. PRESSURE AND TEMPERATURE CONDITIONS OF FORMATION OF SECONDARY GARNET-BEARING ASSEMBLAGES

Simultaneous P-T estimates for recrystallised garnet-bearing assemblages have been obtained from intersections of $K_D^{ga\text{-}cpx}{}_{Fe\text{-}Mg}$ and $K_D^{ga\text{-}opx}{}_{Fe\text{-}Mg}$ lines with Al_2O_3 isopleths for orthopyroxene coexisting with garnet. In these calculations, the garnet-clinopyroxene thermometer of Ellis and Green (1979) has been combined with the garnet-orthopyroxene Fe-Mg thermometer and the garnet-orthopyroxene Al_2O_3 barometer developed in Chapter two and three.

P-T estimates for corona-bearing secondary assemblages are listed in Table 5.3 and are plotted on the regional map of figure 5.23. Most data is confined to the southern part of the Napier province (Scott Mts.), where D3 is considered to be most strongly developed (James and Black, 1981).

In the Fyfe-Hills-Casey Bay region, consistent P-T estimates of 650 ± 70°C and 7-9 kbar are obtained for the secondary garnet coronas in quartz-bearing and quartz-absent rocks. There is some evidence that garnet formation occurred at higher temperature (700-750°C) in the quartz absent pyroxene granulites *49464* and *4510*, although still at pressures of 7-8 kbar.

Garnet rods and rims developed in the original pigeonitic samples *4359* and *4092* have formed under estimated conditions of 670-690°C and 6-9 kbars, with the higher pressures obtained for *4359* from the Zubchatyy Ice Shelf.

The formation of garnet rims on pyroxene-magnetite in *4093* and *4094* from Ward Rocks has occurred at ca ≈ 700°C and 9 kbar, although garnet-orthopyroxene thermometry indicates higher temperatures (740-800°C) for this corona formation.

Secondary garnet assemblages have formed in the garnet pyroxenites *4818* and *4598* at temperatures of 650°C and pressures of 6-7.5 kbar. In *4818*, garnet rims suggest earlier P-T conditions of 760°C and 9 kbar ± 1 possibly related to cooling from the peak metamorphic conditions described earlier. *4598*, from Demidov island, shows further garnet exsolution from pyroxene to temperatures of ca. 580°C. These temperatures may correspond to the temperature of formation of hornblende-plagioclase coronas in this sample.

The diverse garnet-bearing secondary retrograde metamorphic

assemblages from a range of localities indicate a regional event(s) occurring in the cooling history of the complex, at P-T conditions of 650-700°C and 6-9 kbar. These conditions are consistent with the incoming of garnet in rocks of quartz-tholeiite (Mg60) composition (650°C ≃ 7 kb), based on the linear extrapolation of the curve of Green and Ringwood (1967). The P-T estimates are also consistent with the continued stability of the assemblage ga-opx-cpx in *4818* and *4598* throughout cooling from ca. 850°C to 650°C.

The correlation of these corona textures (M3) and their associated P-T estimates with time and deformational history of the Napier Complex is a major problem. On the basis of the textural characteristics described above, garnet formation in quartz-bearing pyroxene granulites can be correlated with D3 recrystallisation. This recrystallisation event is termed M3, and is dated at 2500 ma. (Black and James, 1979; James and Black, 1981). Some textural features of these and the other rocktypes include discrete zones of intense deformation and recrystallisation or broader areas of less intense deformation giving rise to kink bands, deformation lamellae, and disaggregated grains. Such textural features are characteristic of D3 and of post-D3 shearing. Thus, the P-T conditions estimated for the diverse secondary assemblages described here may also relate to post-D3 shearing (< 2500 ma.) rather than recrystallisation solely in D3 (M3).

At localities from Fyfe Hills and Hydrographer Island, the presence of cross-cutting metamorphosed dykes enables the following time-relationships to be established.

(1) D3 deformation producing open folds;

(2) intrusion of basaltic dyke and metamorphism under granulite facies conditions syn- or post-D3;

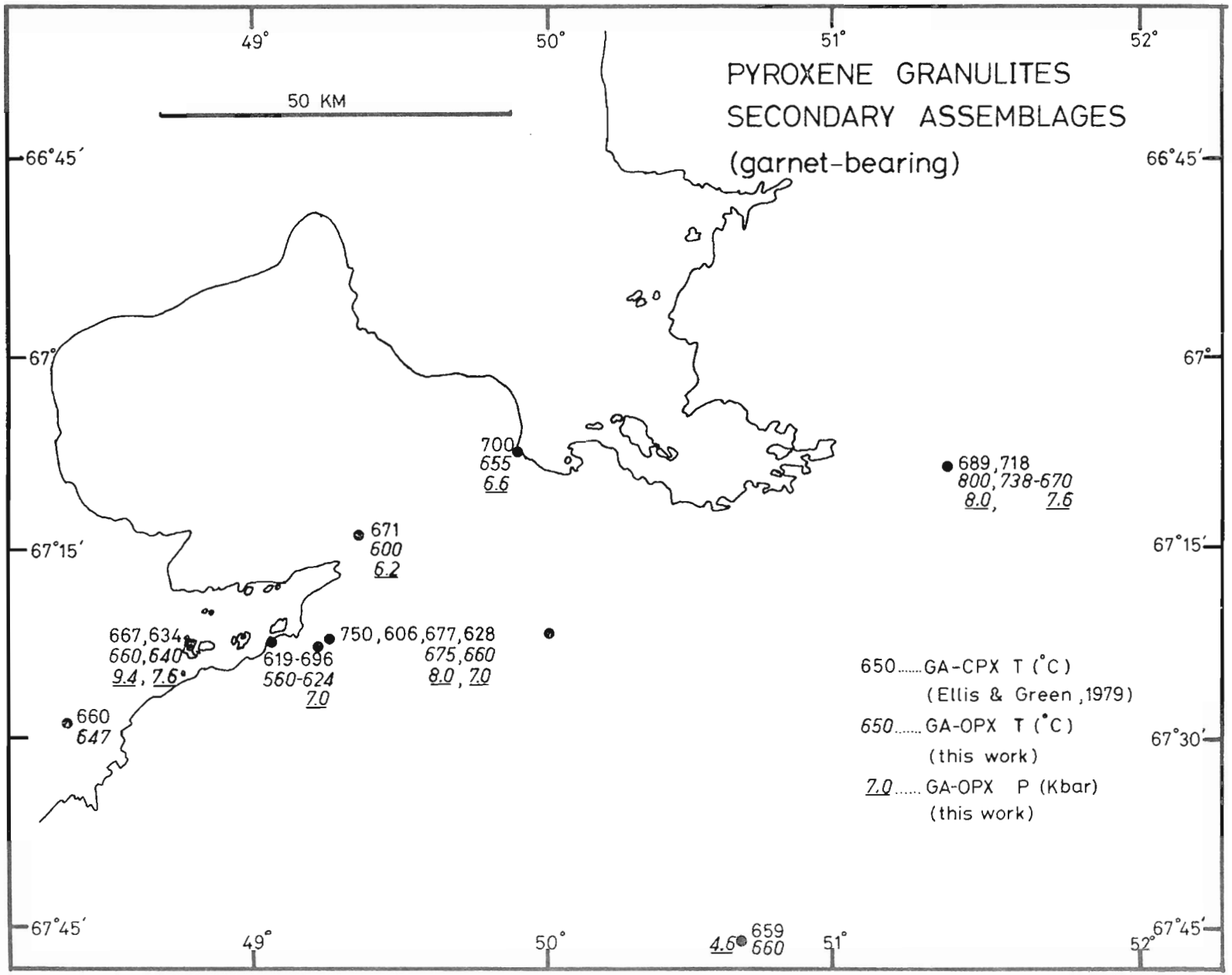

FIG 5.23 REGIONAL DISTRIBUTION OF P-T ESTIMATES FOR SECONDARY ASSEMBLAGES

(3) formation of discrete shear zones which cut across D3 structures and the metamorphosed dykes.

Such field evidence indicating the timing of M3 in relation to shearing is not available in most localities, however, and thus the timing of formation of many of the coronas described above must remain uncertain.

III. P-T METAMORPHIC HISTORY

A generalised P-T path obtained for these two-pyroxene granulites, constructed between the P-T conditions specified for primary metamorphic assemblages and later lower temperature garnet-bearing recrystallised assemblages, is presented in figure 5.24. The position of the P-T path is, strictly, not constrained at conditions between the various P-T boxes, however a linear path is constructed for simplicity and to be consistent with the continued stability of garnet in garnet pyroxenite from Gromov Nunataks, Demidov Island, and Edwards Island; and the stability of sillimanite in interlayered metapelites.

The P-T path so generated is believed to represent a time from up to 3100 ma. (D1) to at least 2500 ma. (D3), a span of up to 600 million years.

The formation of garnet-bearing retrograde assemblages has occurred under conditions of near-isobaric cooling, or under conditions of slow uplift from a maximum of 30 kilometres to 20-24 kilometres depth over the D1 (or D2) to D3 period. An alternative scheme may include a loop or back-bending in the P-T path at the time of D3 to include some minor increase in temperature (or thermal pulse) at this time. In any case, slow uplift rates during cooling are indicated by the P-T estimates, in contrast to many other metamorphic terrains where near-

Fig. 5.24 P-T-time path deduced for pyroxene granulites from the Napier province, Enderby Land. Stippled areas are P-T fields for peak metamorphic conditions and for conditions relating to the equilibration of rim compositions, based on adjusted two-pyroxene thermometry.

● P-T conditions for garnet-bearing primary and secondary assemblages, estimated using ga-opx barometry (this study) and ga-cpx Fe-Mg distribution thermometry (Ellis and Green, 1979).

1 = Sillimanite-Kyanite inversion (Day and Kumin, 1980 ; Holdaway - Weill data).

2 = first appearance of garnet in a quartz tholeiite composition (X_{Mg} =.61), extrapolated from Green and Ringwood (1967).

3 = first appearance of garnet in a tholeiite composition, extrapolated from Ito and Kennedy (1971).

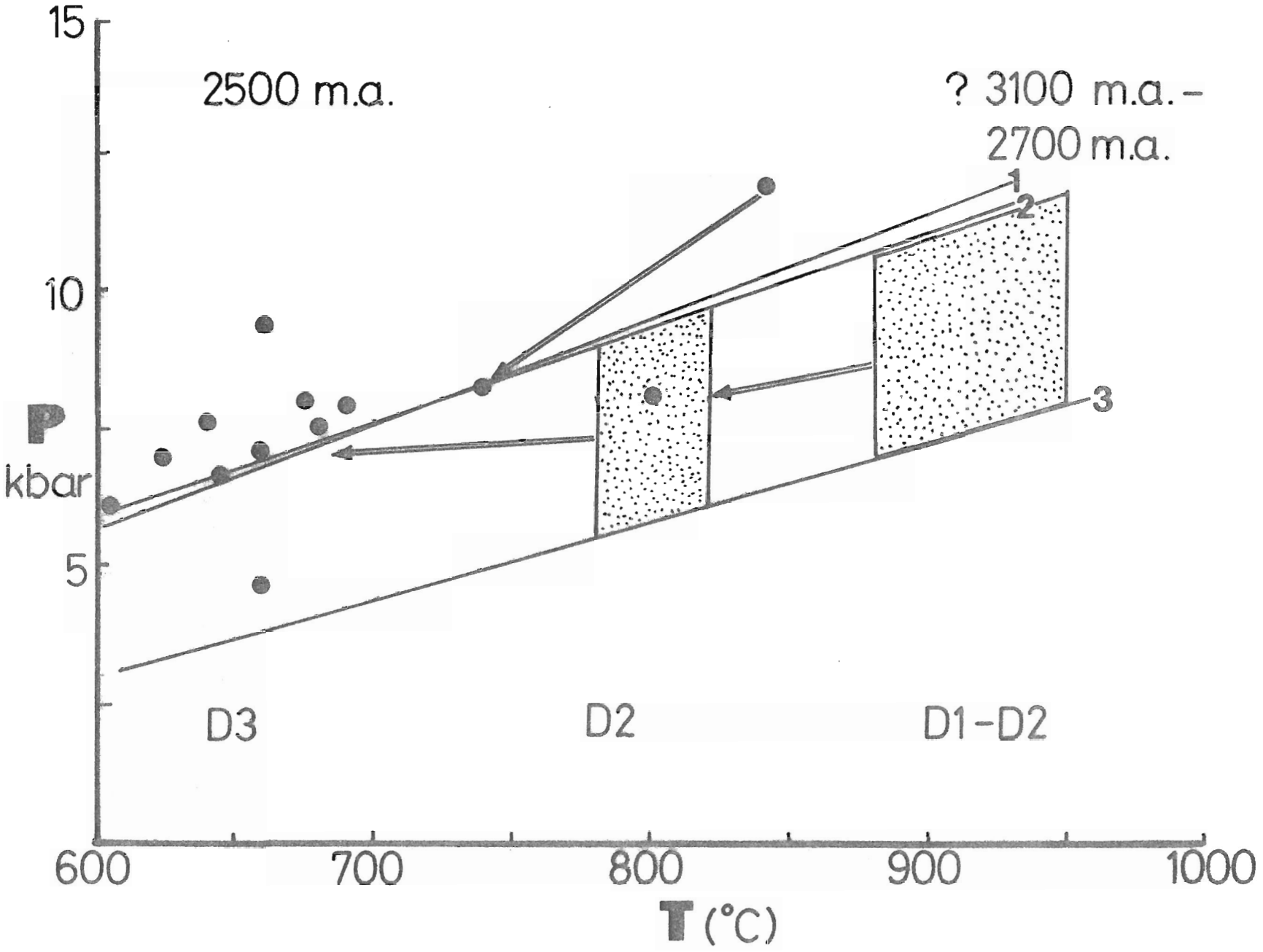
15
10
5
P
kbar
2500 m.a.
? 3100 m.a.-
2700 m.a.
1
2
3
D3
D2
D1-D2
600
700
800
900
1000
T (°C)

isothermal uplift has occurred subsequent to high grade metamorphism (e.g., Norway - Griffin, 1971; Scourie - O'Hara and Yarwood, 1978; Savage and Sills, 1980; Discussion by Ellis (1980)).

Isobaric cooling of dolerite dykes intruded into the basal gneiss of Norway has given rise to corona textures similar to those described here (Griffin and Råheim, 1973), while a similar history of slow cooling at depth has been inferred for coronites from the Adirondacks by McLelland and Whitney (1977). Thus, there exist examples of other metamorphic terrains where a near-isobaric P-T cooling path has controlled the development of secondary mineral assemblages. The path obtained here, however, is constrained in age and duration, as well as in P-T conditions. The presence of widely spaced multiple deformation episodes is also a distinctive feature of the Napier province P-T history. The implications of the P-T estimates and a general discussion of the metamorphic history of the Napier Complex will be presented in Chapter Seven, following the consideration of garnet-orthopyroxene bearing metapelitic assemblages from the Napier Complex.

Chapter 6

GARNET-ORTHOPYROXENE BEARING GRANULITES FROM THE NAPIER PROVINCE, ENDERBY LAND, ANTARCTICA, AND THE P-T METAMORPHIC EVOLUTION OF THE NAPIER COMPLEX

6.1 INTRODUCTION

Garnet-orthopyroxene geothermometry and geobarometry developed in previous chapters are applied in this chapter to garnet-orthopyroxene quartzitic and pelitic granulites from the Napier province, Enderby Land, Antarctica. The general geology and regional setting of these granulites have been summarized in Chapter 5.

The assemblage garnet-orthopyroxene is stable over a wide geographical area in Enderby Land, in a broad range of bulk rock compositions and in equilibrium with a range of other phases including quartz, feldspars, and various Fe-Mg-Al minerals. Thus, regional P-T estimates for Enderby Land may be obtained from a study of the garnet-orthopyroxene bearing parageneses. In addition, P-T - Time evolutionary paths for the Napier province at a number of localities may be obtained from consideration of primary metamorphic and retrograde recrystallised garnet-orthopyroxene assemblages.

In addition to the garnet-orthopyroxene-clinopyroxene assemblages developed in metabasic rock types, considered in Chapter 5, garnet-orthopyroxene occurs as a common primary metamorphic (M1) assemblage in metapelitic granulites from the well-layered sequence (Tula Series) and as occasional lenses or layers in the dominantly pyroxene-granulite sequence (Raggatt Series). Within the Raggatt Series, the typical garnet-orthopyroxene bearing assemblages include

Ga - Hy - Kspar - Qz

and Ga - Hy - Kspar - Plag - Qz

with accessory ilmenite and occasional biotite.

Within the well-layered metasedimentary granulite sequences typical garnet-orthopyroxene parageneses considered in this study are:

(a) in the Napier Mountains

1. Ga - Hy - Kspar - Qz ± Plag ± Biot
2. Ga - Hy - Cd - Kspar - Qz ± Plag ± Biot

(b) in the Tula Mountains

3. Ga - Hy ± Qz ± Kspar ± Plag ± Rutile or Ilm
4. Ga - Hy - Sa (± Kspar and Rutile)
5. Ga - Hy - Sa - Plag

(c) in the Scott Mountains and at Tonagh Island

6. Ga - Hy - Sill ± Sa
7. Ga - Hy - Sill - Qz (± Kspar)
8. Ga - Hy - Osu.

In the absence of quartz, the four phase assemblage ga-hy-sa-sill may be stable in the system FMAS (Hensen and Green, 1973; Ellis *et al.*, 1980). This assemblage has been found at localities on McIntyre Island and Tonagh Island in western Enderby Land.

The P-T significance of the various garnet-orthopyroxene parageneses outlined above, based upon topological relationships of phases in FMAS, is discussed along with the garnet-orthopyroxene thermometry and barometry in section 6.4 . Assemblages listed above are schematically illustrated in figure 6.1.

In the following sections, the textural features, mineral chemistry and zoning relationships of coexisting garnets and hypersthenes in granulites from the Napier province are described. This information is subsequently used to derive P-T estimates and paths for metamorphism in Enderby Land.

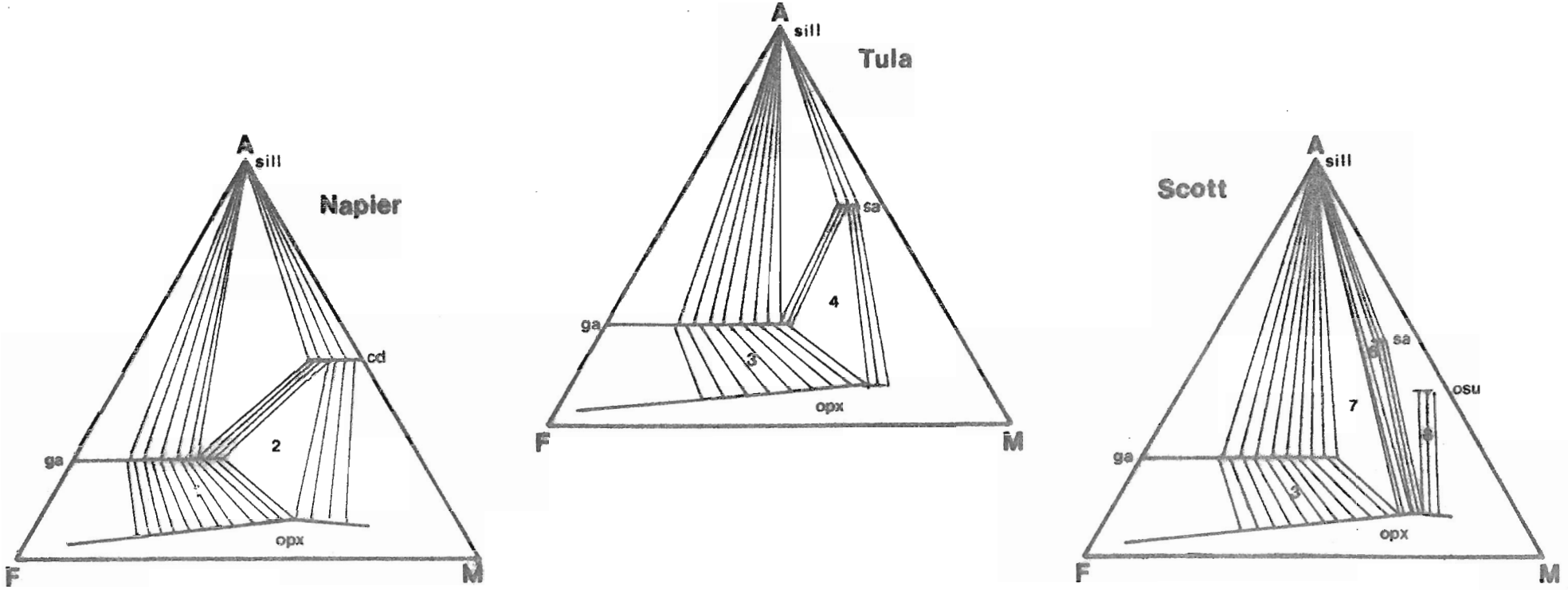

Fig. 6.1 Schematic AFM diagrams of orthopyroxene-bearing assemblages present in metapelites of the Napier province. Assemblages numbered as in text. All assemblages may contain additional quartz and feldspars. Ga-Cd, stable in the Napier Mts, is not stable in the Tula and Scott Mts. .

6.2 TEXTURAL FEATURES

Relevant textural information for individual samples is presented in table 6.1. Most samples show the overprinting of early coarse grained (2 mm - 10 mm) textures by a number of subsequent finer-grained recrystallisation and corona textures. These features will be discussed following consideration of the general characteristics of the primary metamorphic granulite facies textures ascribed to equilibration of garnet-orthopyroxene during M1-M2.

I. PRIMARY METAMORPHIC FEATURES

Typical garnet-orthopyroxene samples consist of variable modal abundances of garnet and orthopyroxene in quartzofeldspathic gneisses. In such gneisses, garnet and orthopyroxene may comprise from 5 to 90% of the sample. Near pure garnet-orthopyroxene bimineralic segregations or layers occur in more typical feldspathic gneisses, while garnet + orthopyroxene ± sapphirine or sillimanite rocks may occur as lenses or discrete layers in otherwise quartzofeldspathic granulites.

The gneisses have typically granuloblastic polygonal to lobate textures, which range from equigranular and polygonal in ga-opx rich types to inequigranular and lobate-subhedral in quartzofeldspathic varieties. Most samples show no preferred orientation of orthopyroxene or quartz, however strong ribbon-like elongate quartz textures are exhibited in 49786 and 4549. In these cases, where elongate D1 quartz textures are preserved, lobate garnet and subhedral-lobate orthopyroxene are elongate parallel to this quartz ribbon texture, and are thus inferred to have formed during D1.

Quartzofeldspathic gneisses usually show granoblastic lobate quartz-feldspar textures. Both quartz and mesoperthitic K-feldspar are coarse (1 mm - 3 mm), lobate or sutured, and sometimes elongate parallel to compositional layering. Quartz often shows extinction, deformation bands, and marginal recrystallisation to finer polygonal aggregates. Elongate quartz ribbons in 49786 are partially recrystallised to coarse equidimensional subgrains which may result from deformation during D2. Further recrystallisation to fine aggregates is possibly related to D3.

K-feldspar is usually mesoperthitic, with coarse string- and filament mesoperthite commonly developed (Ellis, 1979 ; Sheraton *et al.*, 1980). Both K-feldspar and plagioclase may show marginal recrystallisation to fine polygonal aggregates (0.1 mm - 0.01 mm diameter) which may form elongate trails (S3) when well developed. In samples affected by recrystallisation correlated with D3, mesoperthitic K-feldspar may develop further irregular bead- and bleb-like exsolution features cross-cutting earlier string exsolution lamellae, and plagioclase may develop deformation bands, deformation twins, and exsolution blebs.

Garnet occurs as lobate to polygonal anhedral grains. Grain-sizes are commonly 1 mm - 3 mm, however garnet porphyroblasts are often 5 mm - 2 cm in diameter. In hand specimen, garnets are pink to mauve, while in thin section most are pale pink to colourless.

Coarse garnet porphyroblasts are often poikiloblastic, containing lobate and ovoid inclusions of quartz, rutile, hypersthene, zircon, occasional feldspar, and, in samples from the Napier Mountains (4528), cordierite. Sillimanite occurs as coarse rhombs included in garnet, or as very fine aggregates and clusters of fibrous grains which may form an internal foliation within the garnet grains.

In 49657 and 49891, separate fibrous sillimanite clusters occur within individual garnet porphyroblasts. Within each cluster the sillimanites are oriented to form one or more consistent internal foliation directions, but the orientations of the sillimanites vary between separate clusters. It is inferred from these observations that the garnet porphyroblasts have formed from the coalescence of a number of separate, finer grained garnet poikiloblasts which had enclosed fine sillimanite growing in the early stages of D1. Thus, the separate sillimanite clusters represent separate cores, and garnet growth in these cases appears to be synkinematic with D1 (poikiloblastic cores), postkinematic to D1 (coalescing of separate rotated garnets), and possibly synkinematic with D2 (presence of coarse rhombic sillimanite inclusions on garnet rims).

Orthopyroxene is lobate to polygonal and anhedral in ga-opx rich samples, and is subhedral prismatic to lobate in quartzofeldspathic rock types. Generally, primary metamorphic orthopyroxenes are coarse grained (0.5 mm - 2 mm) and form even-grained layers with garnet in the quartzofeldspathic granulites. Orthopyroxene porphyroblasts (3 mm - 5 cm) occur as subhedral grains in some granulites. These porphyroblasts usually show kink bands, undulose extinction, and elongate augen structure.

Fe-richer orthopyroxenes (X_{Mg} =.50, hypersthenes) show pronounced pleochroism from yellow-green and green to pink, pink-brown, and red-brown or orange. More magnesian orthopyroxenes (X_{Mg} =.70) are pleochroic from pale green and yellow-green to pale pink or yellow. All orthopyroxenes may exhibit rutile exsolutions or intergrowths as fine needles which form criss-cross patterns particularly in cores of orthopyroxene grains. In some samples abundant rutile appears to have exsolved as coarse prisms and blebs in hypersthene cores.

Orthopyroxene occurs as polygonal grains with polygonal or prismatic subhedral sillimanite, and occasional garnet, in samples from Tonagh Island, McIntyre Island, and Mt. Charles (49834, 49817, 19607, 3971). In these samples, particularly the bimineralic samples 49607 and 49834, primary metamorphic orthopyroxene and sillimanite are clearly in textural equilibrium. It is inferred that orthopyroxene + sillimanite ± ga (without quartz) was stable at or near the peak metamorphic conditions experienced in these particular localities.

II. SECONDARY OR RETROGRADE METAMORPHIC TEXTURES

Primary metamorphic garnet-orthopyroxene textures have been overprinted in many samples by a variety of later recrystallisation and corona textures. Such secondary textures are described for individual samples in table 6.1. On the basis of the presence of D3 recrystallisation textures in quartz-feldspar layers adjacent to garnet-orthopyroxene layers, many of the textures to be described below can be correlated with the overprinting of earlier structures by D3 (≈ 2500 m.a.). However, in many samples there is no definite textural evidence for the correlation of secondary garnet-orthopyroxene recrystallisation with D3. It is possible that a number of the textures described below are a result of cooling from the thermal peak of M1 or M2 and do not reflect the further overprinting by a separate M3 event correlated with D3.

In any case, combination of textural information, which indicates several generations of garnet and orthopyroxene in any one sample, with mineral chemistry and mineral zoning information for the different generations can yield P-T data which are interpreted as points on a P-T - Time evolutionary path for any particular sample.

Fig. 6.2 Recrystallisation textures present in garnet-orthopyroxene assemblages from the Napier province.

In all cases : op = orthopyroxene
ga = garnet
pl = plagioclase
qz = quartz
ru = rutile

Horizontal bars 0.2 mm

a. Second euhedral garnet forming rims on earlier coarse garnet adjacent to plagioclase and orthopyroxene. Sample 49868, Mt. Hollingsworth.

b. Fine euhedral, saccharoidal garnet rimming earlier coarse lobate garnet and orthopyroxene adjacent to plagioclase. Note orthopyroxene in top left which has rim of second garnet on one edge. Sample 49657, McIntyre Island.

c. Coarse subhedral garnet rimming earlier, very coarse orthopyroxene porphyroblast adjacent to plagioclase. X_{Al}^{opx} decreases markedly adjacent to the secondary garnet. Sample 49834, island at the N.E. end of Mt. Trail.

d. Symplectitic garnet-quartz rimming coarse lobate garnet, and fine polygonal orthopyroxene recrystallising on earlier orthopyroxene near garnet. Sample 3410, Mt. Marsland.

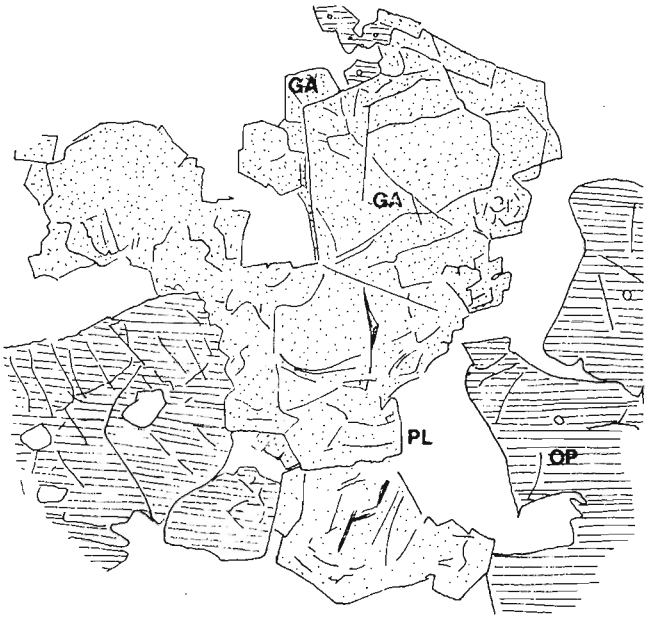

A

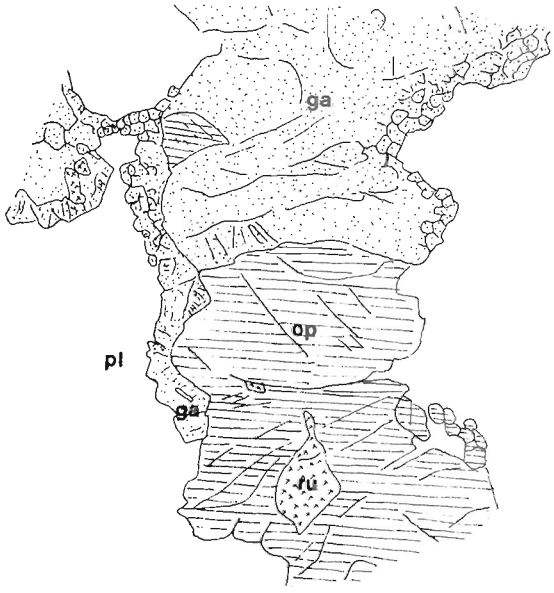

B

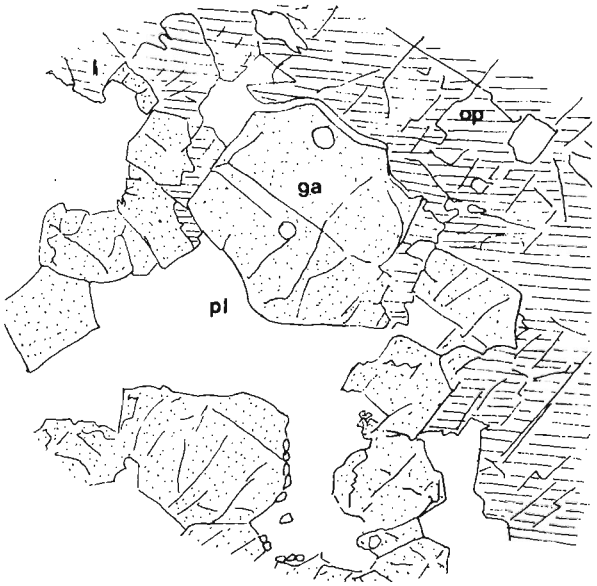

C

D

(a) Recrystallisation textures

In quartzofeldspathic gneisses where garnet and orthopyroxene comprise less than 50% of the modal mineralogy, typical secondary textures involve the recrystallisation of both garnet and orthopyroxene to finer grainsized aggregates, trails and overgrowths on ragged or resorbed primary metamorphic grains.

(1) Fine euhedral garnet and garnet-quartz intergrowths occur on earlier garnet and orthopyroxene (49868, 49657, 49891, 3970). Original coarse garnet may be rimmed by well formed, fine grained (0.1-0.2 mm diameter) garnet euhedra adjacent to plagioclase and orthopyroxene (figure 6.2a). In other cases, fine polygonal and euhedral garnet-quartz intergrowths (0.05 mm diameter) rim earlier coarse, lobate garnet and form borders on adjacent primary metamorphic orthopyroxene grains (figure 6.2b). Often these fine recrystallised garnets are associated with fine polygonal aggregates of recrystallised quartz and feldspars, and thus may be correlated with D3 deformation. In 49657, the fine granular garnet forms trails off coarser orthopyroxene adjacent to recrystallised feldspathic masses, in addition to euhedral overgrowths on earlier garnet.

(2) Coarser euhedral-subhedral garnet (0.3-0.8 mm diameter) occurs as grains rimming a very coarse (1 cm diameter) hypersthene porphyroblast in 49834 (figure 6.2c). In this sample, polygonal granoblastic garnet and orthopyroxene form an even grained ($\simeq$ 1 mm) mosaic in which the very coarse hypersthene is set. The garnets which rim this orthopyroxene are similar in composition to garnets from elsewhere in the sample, but appear to have formed from the hypersthene porphyroblast which is strongly zoned rimwards to lower X_{Al}^{opx} and higher X_{Mg}^{opx} values. These rim compositions for the porphyroblast are, however, similar to orthopyroxene compositions in the equigranular

ga-opx layers. Thus, the formation of the garnets rimming the orthopyroxene porphyroblast in this sample is regarded as being contemporaneous with the attainment of general textural equilibrium in the sample, possibly during or post-D2. The coarse hypersthene grain thus represents a pre-D2 porphyroblast.

In 49834, further textural and mineral compositional modification has taken place with the development of thin lamellar garnet rims between polygonal orthopyroxenes (D2) of the equigranular areas (see below).

(3) Kinked and disaggregated coarse orthopyroxenes are traversed by trails of fine granular euhedral garnet (0.05-0.1 mm diameter). Such garnet trails may cut across earlier kink band boundaries, or may form partial rims around broken and ragged orthopyroxene (figure 6.2d). Garnet formation in these cases clearly postdates deformation features which are characteristic of D3 and post-D3 shearing (see section 5.1).

(4) In some samples (3410 Mt Marsland, 49657 McIntyre Is., 3918) orthopyroxene suffers partial recrystallisation, along with garnet, to very fine grained polygonal aggregates and trails of saccharoidal grains (0.02-0.05 mm diameter). Such aggregates may rim earlier ragged orthopyroxenes and garnets displaying symplectitic ga-qz overgrowths (figure 6.3a).

(5) In 4319 from Mt Charles, original coarser (1 mm diameter) orthopyroxenes have suffered complete recrystallisation to polygonal aggregates and trails of fine grains (0.01 mm diameter). Feldspars and quartz are also nearly completely recrystallised to very fine grained aggregates, with only rare relict mesoperthite and ragged quartz grains present. Euhedral, fine grained (0.3-0.5 mm diameter) garnet also occurs as aggregates and random grains within the

Fig. 6.3 Recrystallisation and corona textures in garnet-orthopyroxene assemblages. In all cases :

op = orthopyroxene
ga = garnet
pl = plagioclase
qz = quartz

Horizontal bars 0.2 mm

a. Polygonal-subhedral aggregates of fine garnet forming partial rims around lobate, resorbed, early orthopyroxene. Sample 3970, Mt. Charles

b. Finely and almost totally recrystallised orthopyroxene forming polygonal aggregates, and occurring with fine euhedral secondary garnets in a fine mosaic of plagioclase and quartz. Sample 4319, Mt. Charles.

c. Garnet occurring as exsolution lamellae and as thin continuous rims around primary orthopyroxene grains. Note some lamellae are continuous with the garnet rims. Sample 49576, Hydrographer Island.

d. Garnet (±orthopyroxene ±quartz) forming thick elongate and granular rims on earlier coarse and polygonal-lobate orthopyroxene. Sample 49406, Zircon Point.

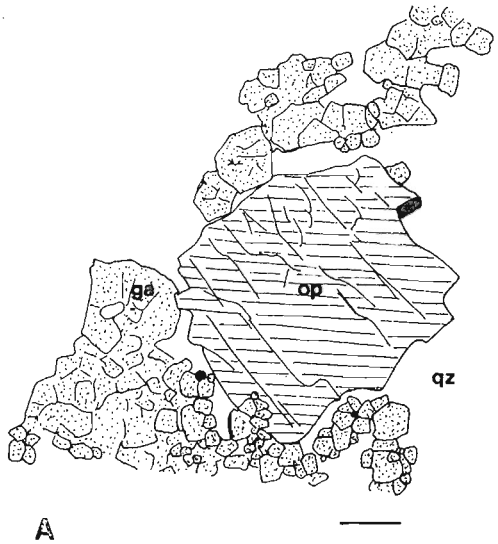

A

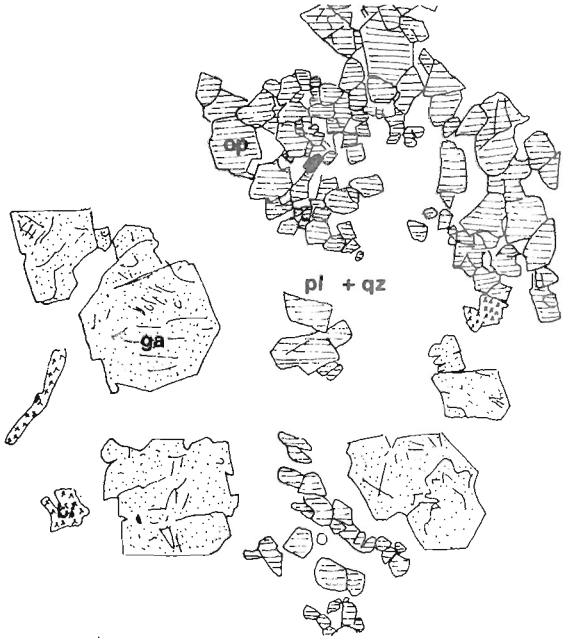

B

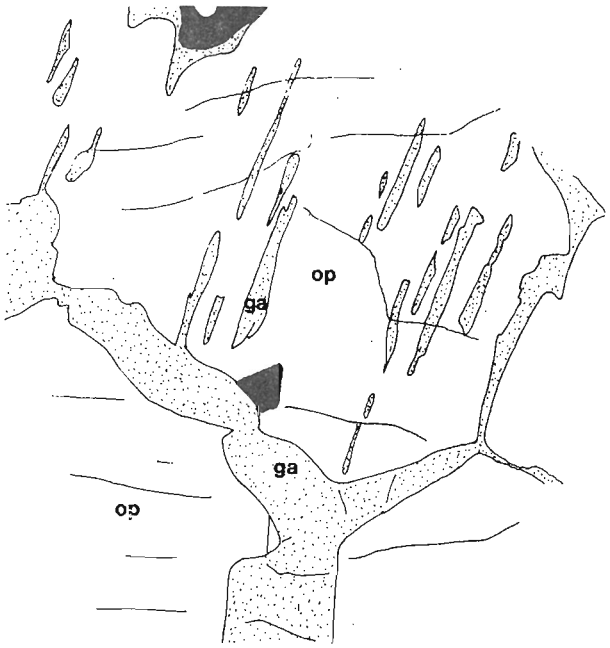

C

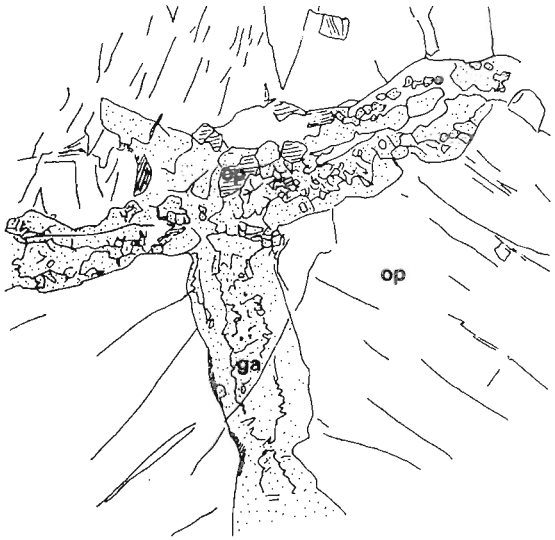

D

recrystallised masses (figure 6.3b). The marked reduction in grainsize and wholesale recrystallisation in this sample is attributed to D3 deformation. Biotite, developed within the recrystallised areas, forms a foliation which is axial planar to a microfold present in thin section and is highly discordant to compositional layering. These features also provide support for the formation of recrystallised orthopyroxene and garnet in 4319 during D3 (2500 m.a.).

(b) Corona, Rim, and Exsolution Textures.

Secondary reaction textures described below occur in samples where garnet and orthopyroxene dominate over quartz and feldspars in the modal mineralogy. In some cases, primary metamorphic garnet is not present, and garnet only occurs as rims and coronas on pre-existing orthopyroxene or orthopyroxene and plagioclase. In these samples, recrystallised quartz-feldspar textures characteristic of D3 are not developed because of the relative paucity of quartz and K-feldspar. Thus, the relationship of garnet-orthopyroxene textures described below to D3 is uncertain, and much regrowth of garnet may be related to post-D2 cooling rather than to a D3 episode. Despite this ambiguity, the corona and exsolution features are considered to be at least post-D2 in age, and therefore give information on P,T conditions in the Napier province at some time after peak metamorphic conditions were established.

(1) Garnet exsolution lamellae are developed within orthopyroxenes from orthopyroxene rich samples, particularly in the Field Islands and at Tonagh Island (49576, 49856, 49891). In some cases, garnet lamellae may be up to 0.05 mm wide (figure 6.3c) and may be continuous with garnet rims developed between orthopyroxene grains.

(2) Garnet is developed as thin (0.05-0.3 mm wide) lamellar rims between polygonal-lobate earlier orthopyroxene grains in many

Fig. 6.4 Corona textures in garnet-orthopyroxene assemblages from the Napier province. In all cases :

op = orthopyroxene
ga = garnet
pl = plagioclase
qz = quartz
sa = sapphirine
hbl = hornblende

Horizontal bars 0.2 mm

a. Euhedral-subhedral thick garnet forming as rims or coronas between orthopyroxene and plagioclase. Orthopyroxene recrystallises to fine polygonal grains adjacent to garnet Quartz usually forms between garnet and orthopyroxene. Sample 49404, Zircon Point.

b. Saccharoidal-subhedral fine garnet forming coronas, with quartz, which enclose early lobate orthopyroxene adjacent to plagioclase. Note development of hornblende on ilmenite and the presence of a quartz "moat" between garnet and orthopyroxene. Sample 4523, Hydrographer Island.

c. Sapphirine-orthopyroxene (±garnet) exsolution lamellar symplectite after garnet, sample 49817, Tonagh Island.

d. As for 6.4c, showing relict garnet breaking down to sa + opx + ga symplectite. Sample 49817, Tonagh Island.

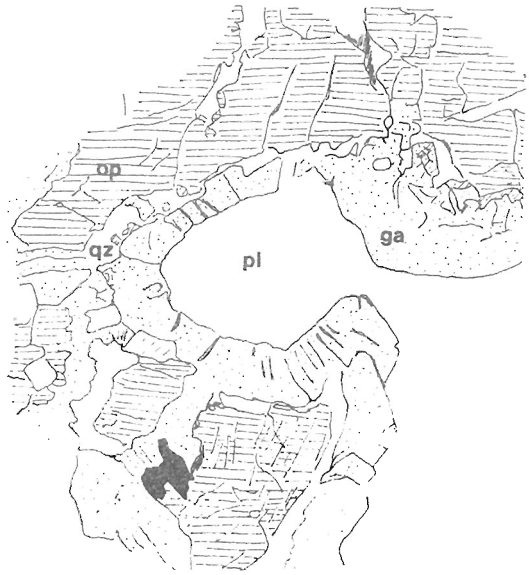

A

B

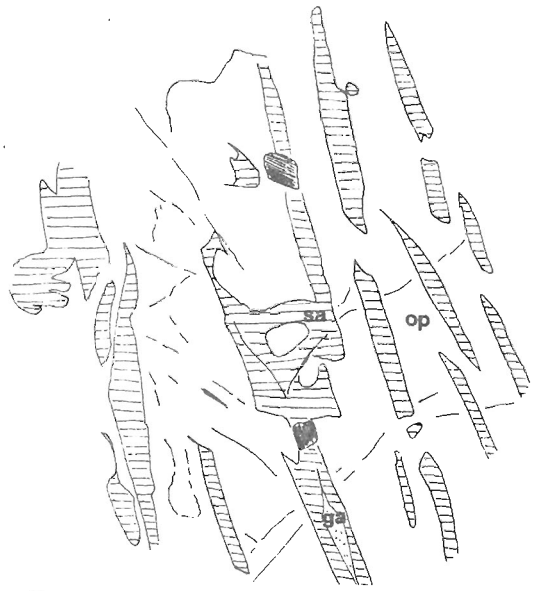

C

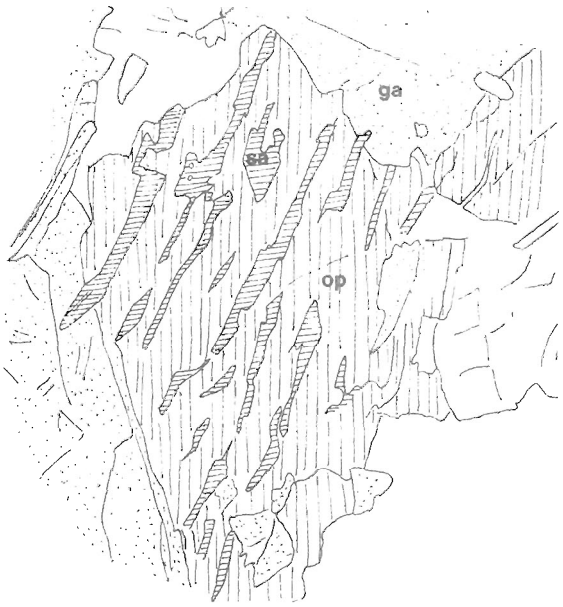

D

samples (49576, 49406, 49434, 49786, 49856, 49657, 49659, 4354). These rims follow original orthopyroxene grain boundaries and occasionally fill cracks developed within orthopyroxene, illustrating clearly the late, post D1-D2 timing of secondary garnet development in these cases. In some samples (figure 6.3d), fine polygonal orthopyroxene, quartz and minor rutile may be developed with the garnet in the late rims.

(3) Garnet is developed as rims between primary metamorphic orthopyroxene and plagioclase in 4523 and 49404 (figure 6.4a and 6.4b). In 4523, granular polygonal garnets (0.05-0.1 mm diameter) from near continuous coronas and trails around orthopyroxene in contact with plagioclase. Fine polygonal quartz, and occasional plagioclase, are developed with this secondary garnet, usually adjacent to the orthopyroxene (figure 6.4b). In 49404, garnet forms near-continuous subhedral rims (0.2 mm wide) around orthopyroxene (figure 6.4a). Adjacent to plagioclase grains the secondary garnet has euhedral outlines, while the rims are more ragged adjacent to orthopyroxene, where garnet + quartz symplectites and fine polygonal recrystallised orthopyroxene may develop (figure 6.4a).

(4) In magnesian, orthopyroxene rich samples (e.g. 4833, 49817) pale blue sapphirines may be developed as fine (0.02 mm wide) finger-like grain boundary lamellae on orthopyroxene which also exhibits rutile exsolution.

(5) In the presence of quartz and mesoperthite, primary metamorphic hypersthene and sillimanite may be rimmed by fine grained ($\leq$0.1 mm) granular aggregates of secondary orthopyroxene, fibrous sillimanite, and occasional garnet (e.g. 3971 Mt Charles, 49831 and 49817 Tonagh Island). These coronas occur in samples which also show D3 recrystallisation features in feldspars, and garnet overgrowths on earlier garnet grains.

(6) In 49817, from Tonagh Island, one sapphirine-orthopyroxene-garnet layer exhibits the growth of orthopyroxene rims between sapphirine and garnet, and lamellar symplectites of orthopyroxene, sapphirine and minor garnet after earlier garnet porphyroblasts (figures 6.4c and 6.4d). These textures can be interpreted to result from a continuous Fe-Mg-Al reaction involving the movement of the three phase Ga-Opx-Sa triangle to lower X_{Mg} values with changing (P,T) conditions. Garnet zones rimwards to lower X_{Mg}^{ga}, while sapphirine zones to higher X_{Al}^{sa} and higher X_{Mg}^{sa} values, consistent with the continuous reactions

$$3(Mg,Fe)_3Al_2Si_3O_{12} = (Fe,Mg)_2Al_4SiO_{10} + [(Fe,Mg)Al_2SiO_6 + 3Mg_2Si_2O_6]$$

garnet — sapphirine — orthopyroxene

$$+ SiO_2$$

and

$$(Fe,Mg)_3Al_2Si_3O_{12} + (Fe,Mg)_2Al_4SiO_{10} = (Mg,Fe)_2Si_2O_6 + SiO_2 + 3(Mg,Fe)Al_2SiO_6.$$

As sapphirine involved in these reactions is peraluminous (section 6.3), the reactions in the actual rock may not require the presence of quartz. Under conditions of decreasing temperature, $K_D^{ga\text{-}sa}{}_{Fe\text{-}Mg}$ will increase as observed in these coronas and symplectites.

6.3 MINERAL CHEMISTRY

I. PRIMARY METAMORPHIC COMPOSITIONS

In most samples studied, both orthopyroxenes and garnet showed some rimward zoning in composition. The features of these zoning patterns will be described in section 6.3 II. Compositions of garnet and orthopyroxene considered in this section refer to cores of analysed grains or to homogeneous areas of grains where zoning is not strongly developed.

(a) Orthopyroxene

In the assemblages studied, orthopyroxenes are essentially solid solutions in FMAS, with only very minor CaO and MnO present. In most cases, Fe_2O_3 calculated from stoichiometry considerations imposed on microprobe analyses is also very low.

Orthopyroxenes are aluminous hypersthenes and Mg-hypersthenes which range in X_{Mg}^{opx} from .33 to .76 and in X_{Al}^{opx} from 0.02 to 0.25 (12.5 wt.%). Orthopyroxenes from quartzofeldspathic pelitic gneisses alone are more restricted in composition (X_{Mg}^{opx} = .45- .76, X_{Al}^{opx} = 0.05-0.25), while more Fe-rich orthopyroxenes occur in equilibrium with primary metamorphic garnet in more pyroxene-rich samples (3918, 4085). Compositions of orthopyroxene cores are illustrated in figures 6.5-6.10.

(b) Garnet

Compositions of primary metamorphic garnets are illustrated on the AFM diagrams of figures 6.5-6.10.

Fig. 6.5 Partial AFM (½Al-Fe-Mg) diagrams of coexisting garnets and orthopyroxenes for granulites from the Napier province.
In cases where both open and solid symbols are given :
open symbols...rim or recrysyallised grain compositions
solid symbols..core compositions.
Sample localities corresponding to numbers in the diagrams are given in Table 6.1 .

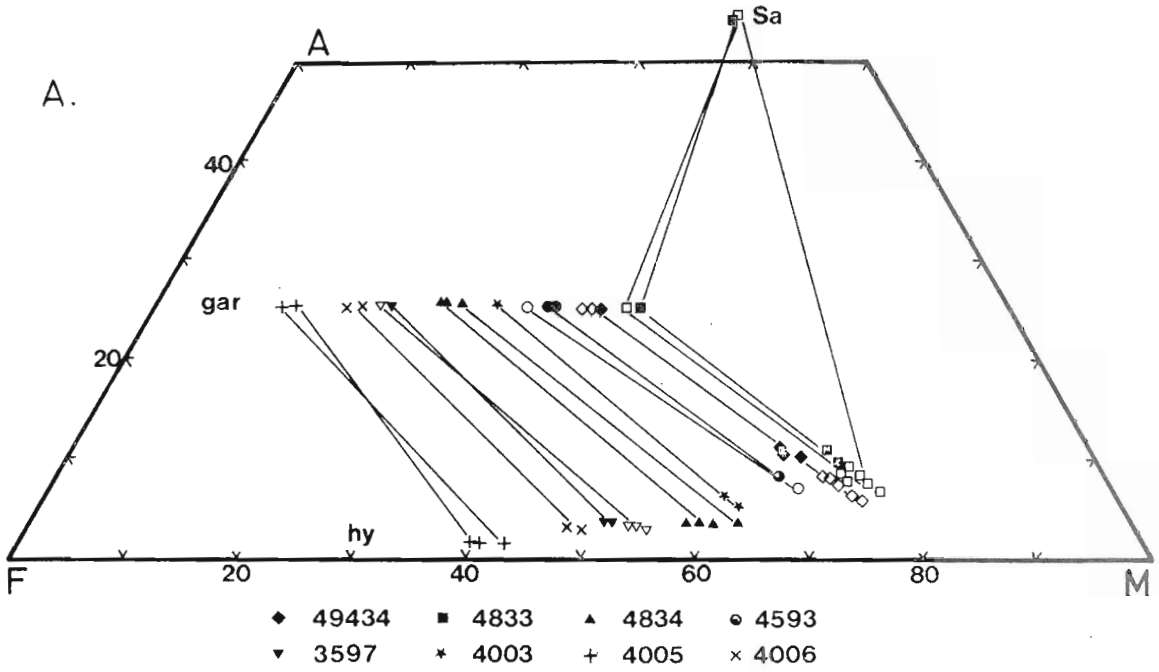
A.
A
Sa
40
20
gar
hy
F
20
40
60
80
M
49434
4833
4834
4593
3597
4003
4005
4006

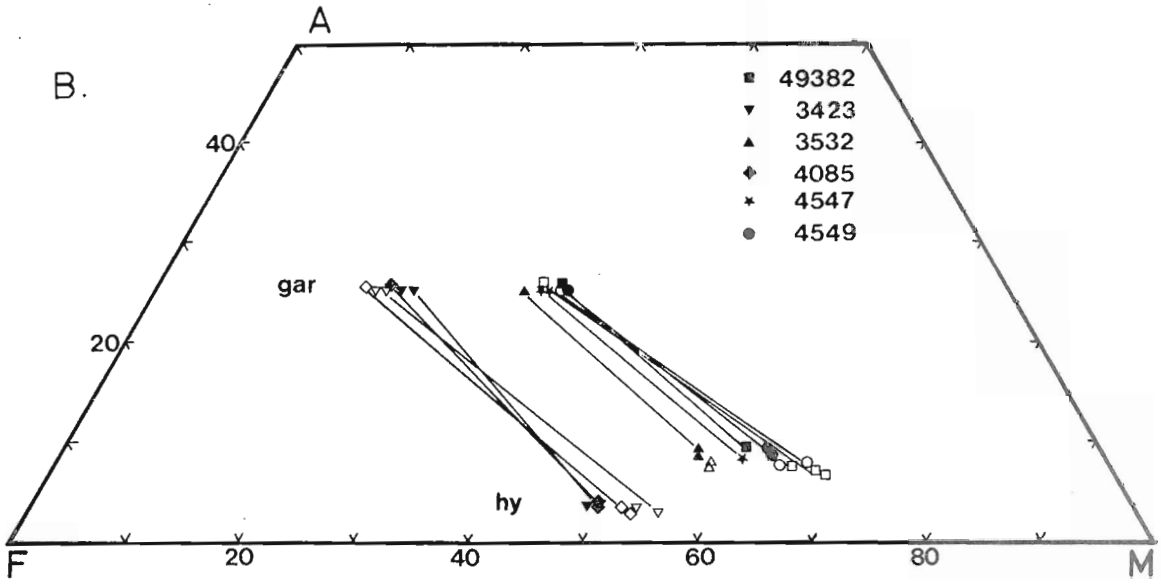
B.
A
49382
3423
3532
4085
4547
4549
40
20
gar
hy
F
20
40
60
80
M

Fig. 6.6 Partial AFM (½Al-Fe-Mg) diagrams of coexisting garnets and orthopyroxenes for samples from the Napier province. Compositional data and localities for particular samples are given in Table 6.1 .

a. Open symbols....rim or recrystallised grain compositions

b. Solid symbols...core compositions

b. Open symbols for 49607 and 49657 represent recrystallised grain compositions ; other open symbols are for averaged rim data obtainedin ga-opx-cpx assemblages.

sa = sapphirine.

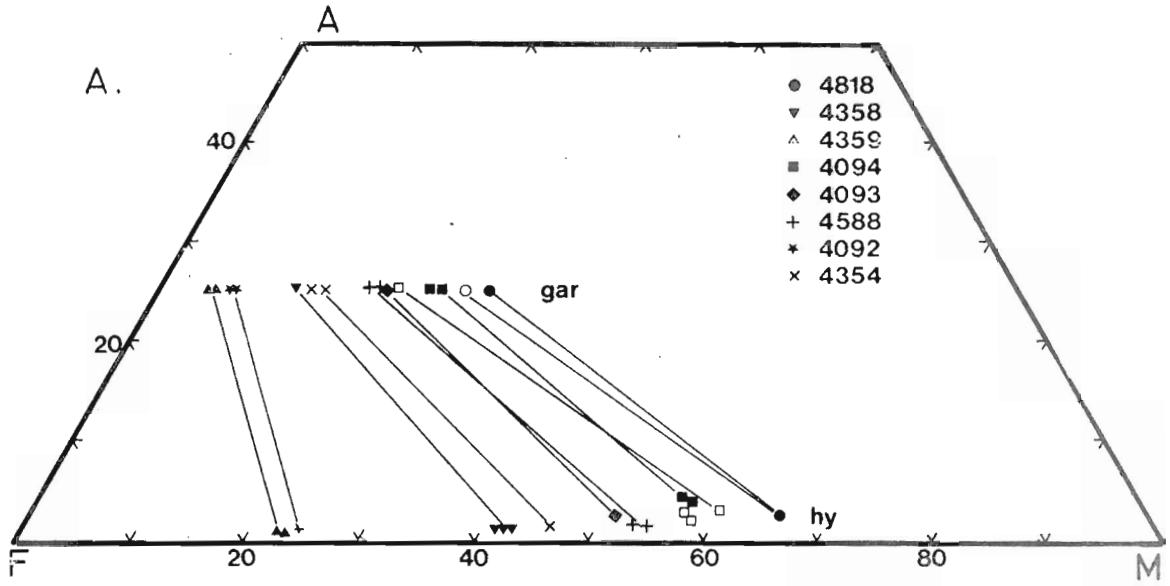
A.
A
40
20
F
20
40
60
80
M
4818
4358
4359
4094
4093
4588
4092
4354
gar
hy

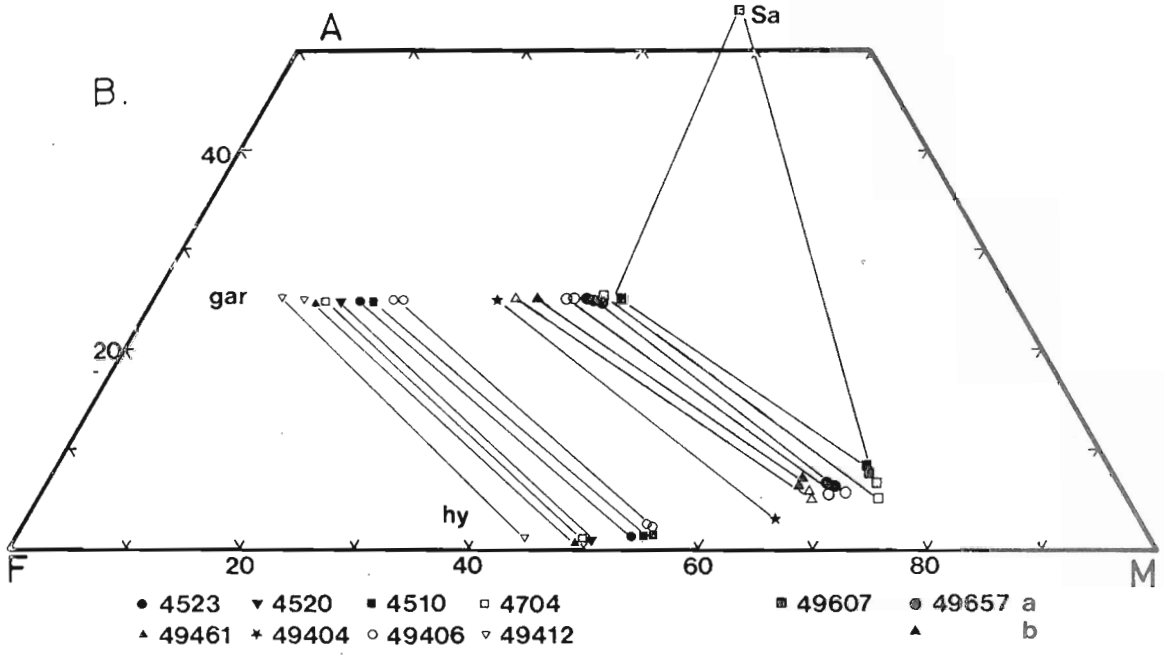
B.
A
Sa
40
20
gar
hy
F
20
40
60
80
M
4523
4520
4510
4704
49607
49657 a
49461
49404
49406
49412
b

Fig. 6.7 AFM (½Al-Fe-Mg) diagrams for garnet-orthopyroxene bearing samples from Tonagh Island. Sample numbers as given in Table 6.1, along with compositional data.

Open symbols....rim and recrystallised grain compositions

Solid symbols...core compositions.

Tie lines join compositions of coexisting early and retrograde or recrystallised phases.

Note :

(1) Fe-Mg tie line rotation in garnet-orthopyroxene assemblages.

(2) tie line lengthening by a decrease in X_{Al}^{opx} in rims and recrystallised grains

(3) peraluminous sapphirine zones to higher Al, X_{Mg} values rimwards.

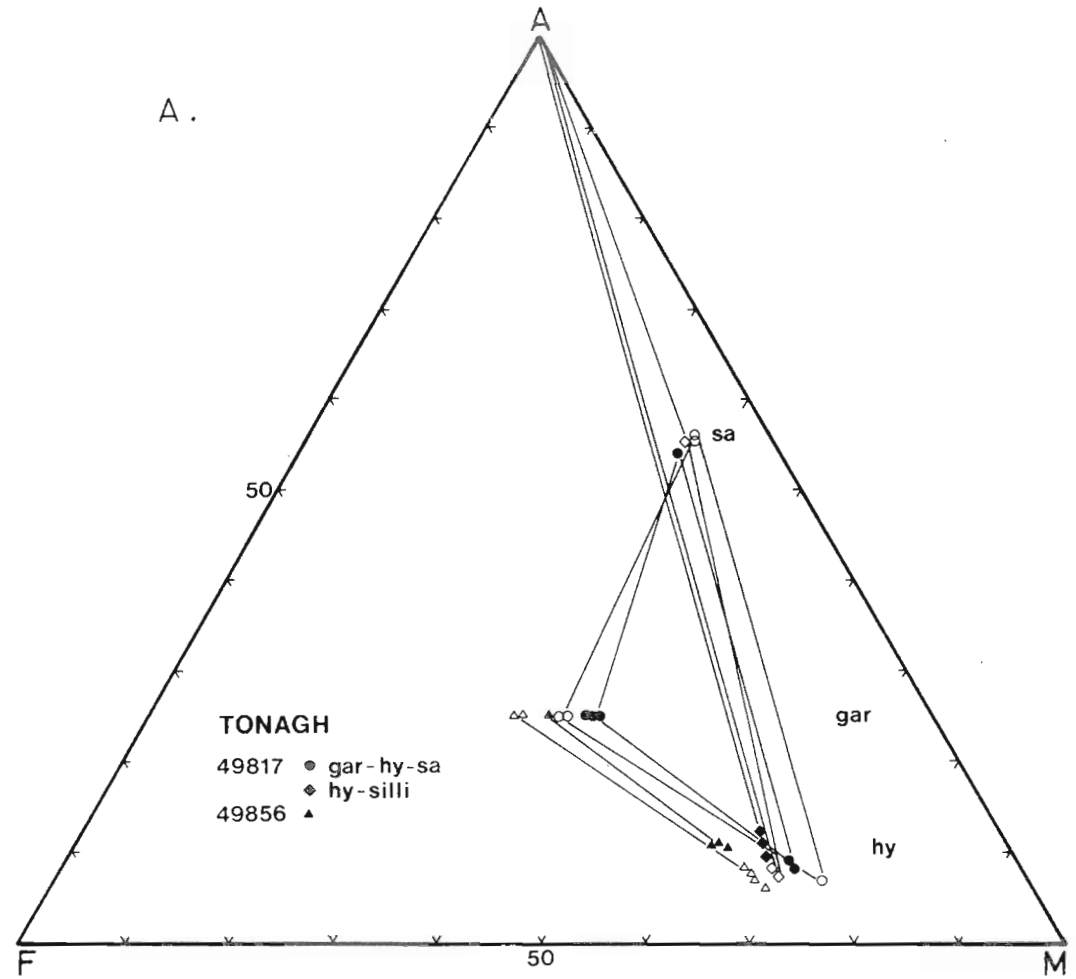
A.
A
50
sa
gar
hy
TONAGH
49817 gar-hy-sa
hy-silli
49856
F
50
M

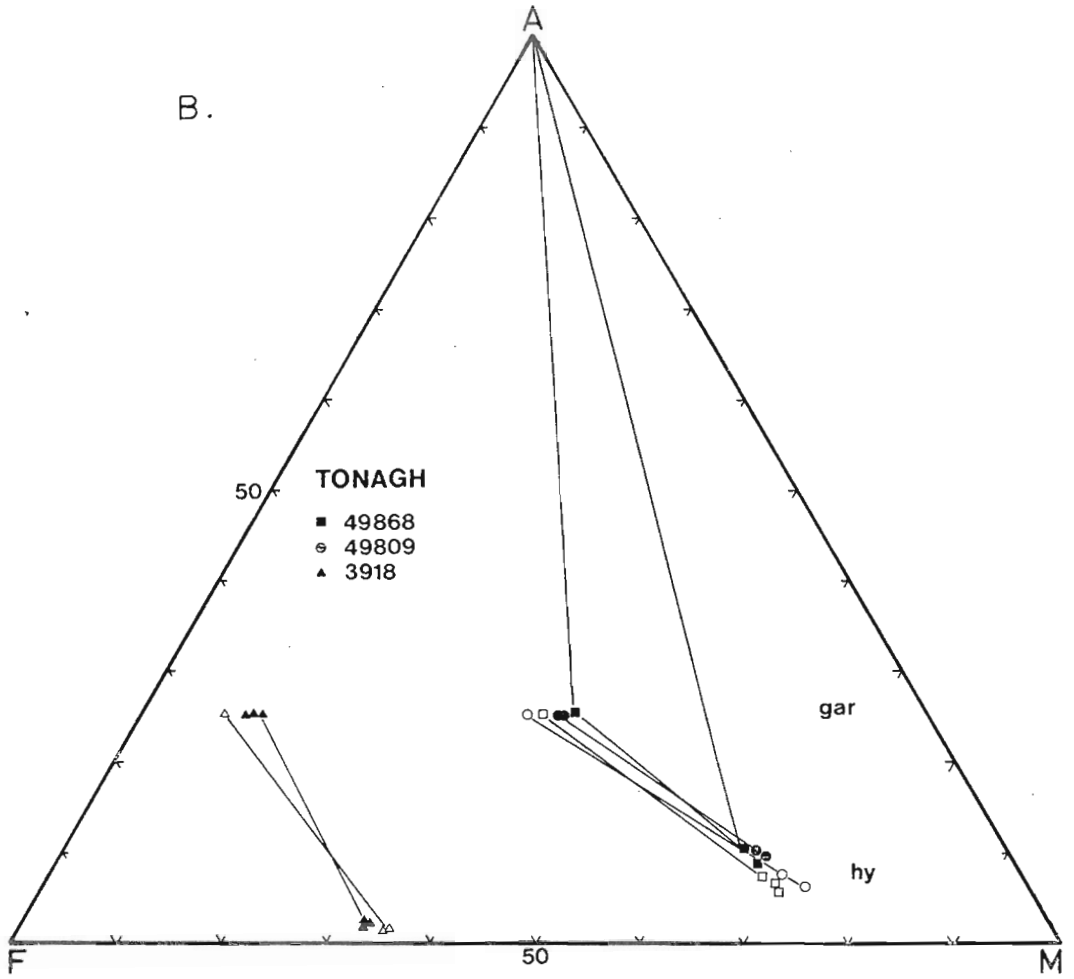
B.
A
50
TONAGH
49868
49809
3918
gar
hy
F
50
M

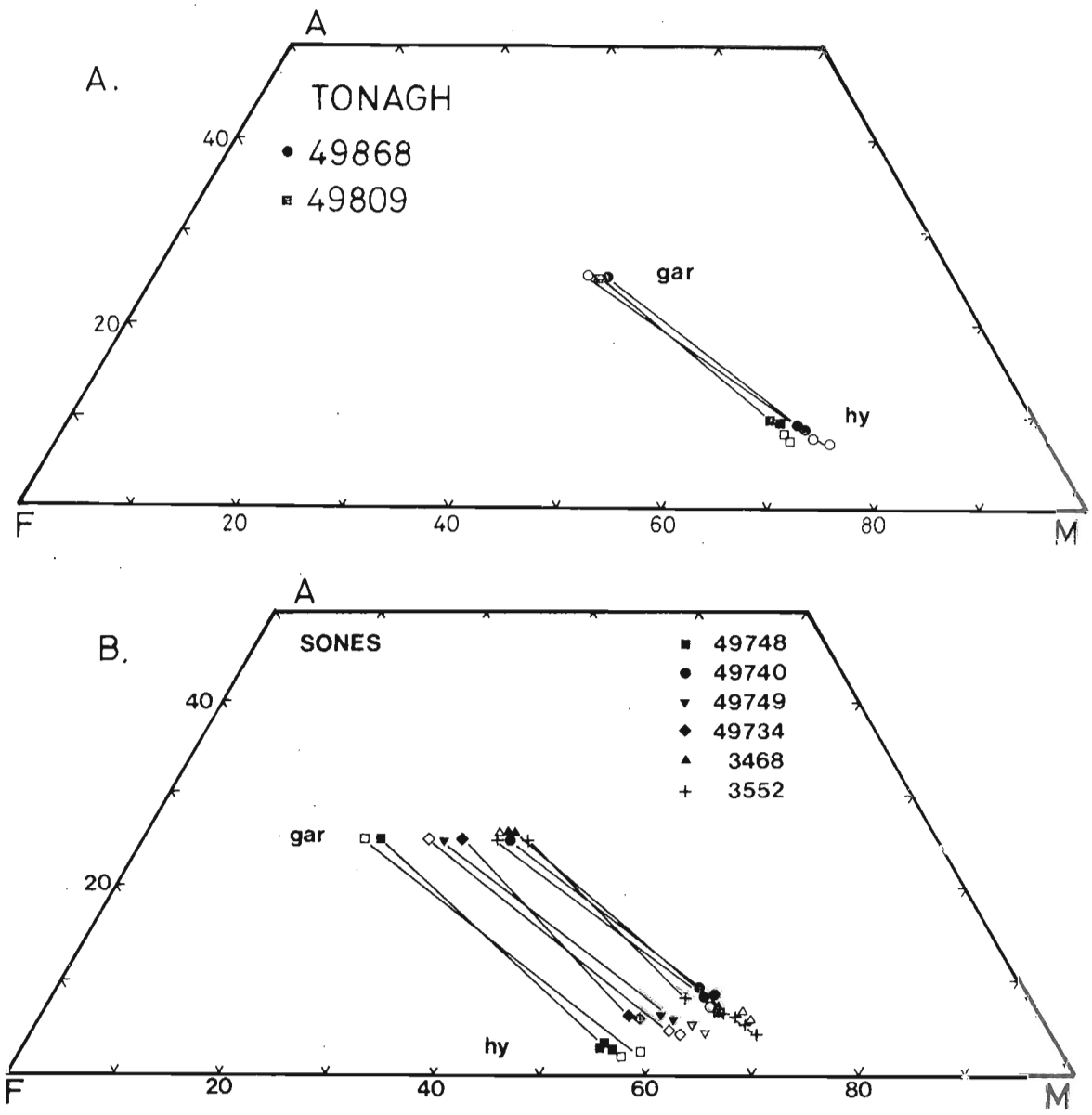

FIG. 6.8 Partial AFM (½Al-Fe-Mg) diagrams for ga-opx samples from Tonagh Island (a.) and Mt. Sones (b.).
open symbols = rims and recrystallised grains
solid symbols = cores

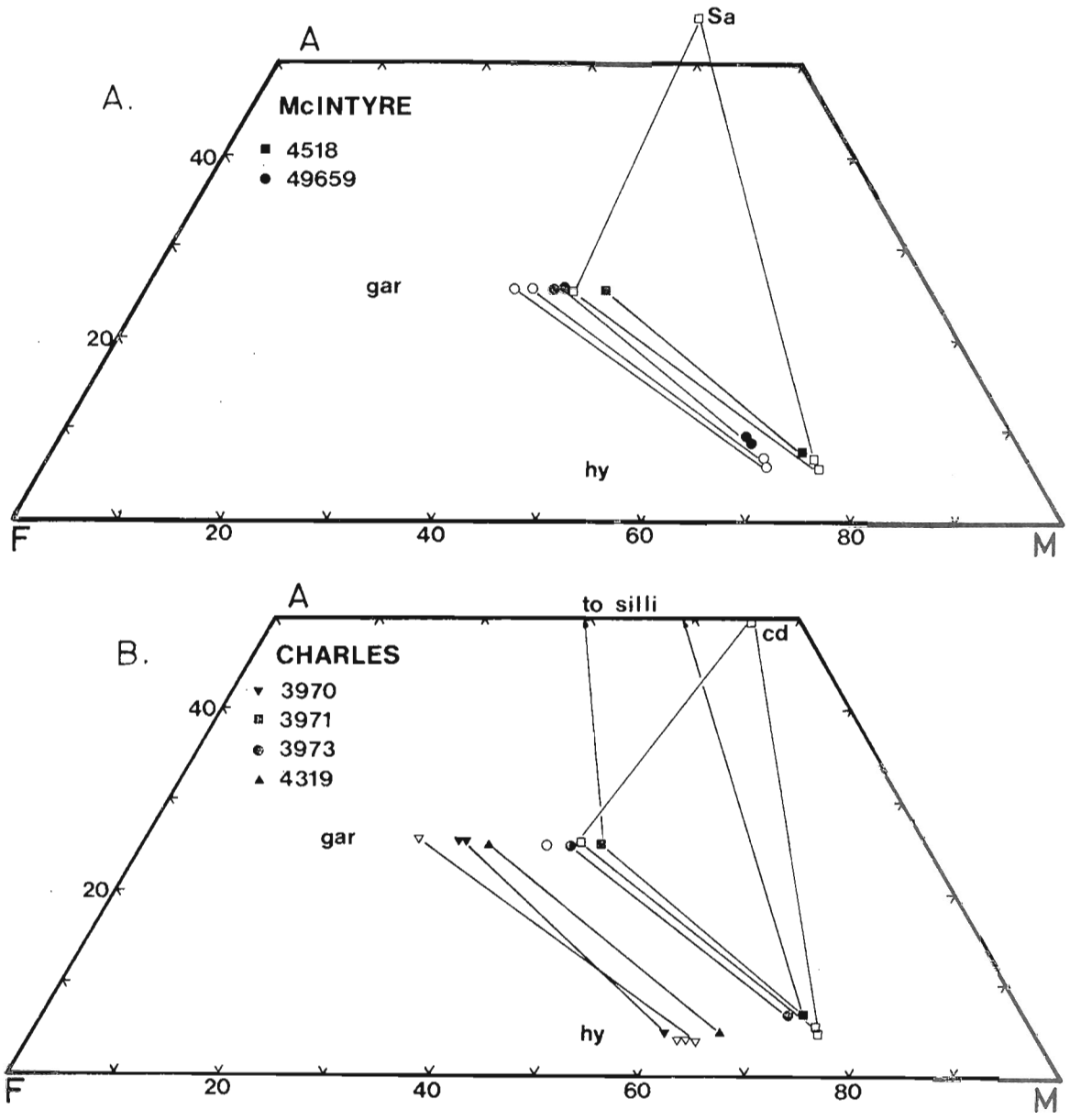

FIG. 6.9 Partial AFM (½Al-Fe-Mg) diagrams for ga-opx samples from Mc Intyre Island (a.) and Mt. Charles (b.).
open symbols = rims and recrystallised grains
solid symbols = cores

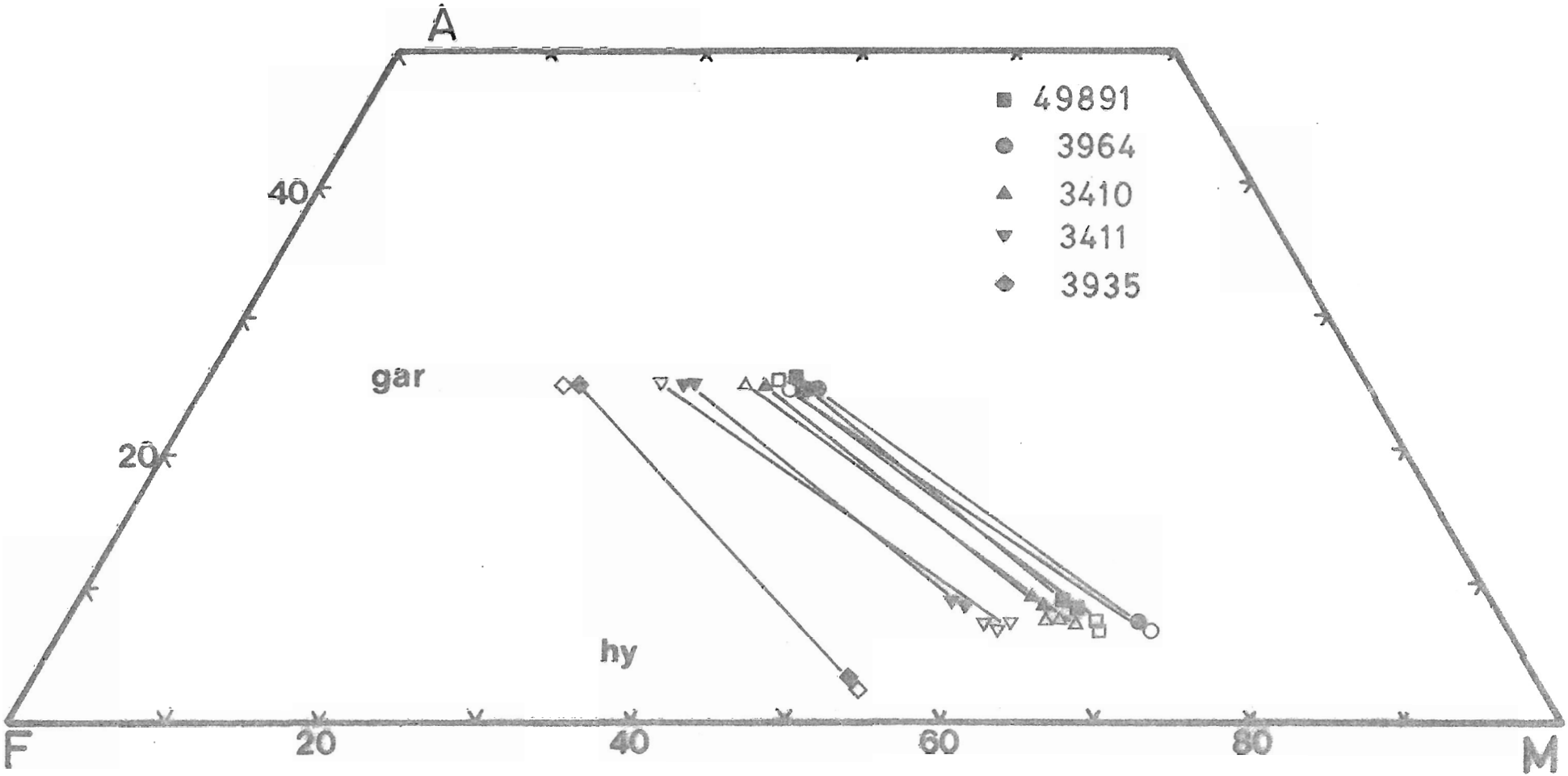

Fig. 6.10 Partial AFM (½Al-Fe-Mg) diagram for garnet-orthopyroxene samples from Amundsen Bay area.. Localities as given in Table 6.1.

open symbols...rims and recrystallised grains
solid symbols..cores

In most cases, garnets are essentially pyrope-almandine-grossular solid solutions, with low or negligible MnO present ($\leq$ 3 wt.%). In metapelites, garnets are essentially pyrope-almandine solid solutions with only minor grossular contents (X_{Ca}^{ga} up to 0.16 but usually less than 0.06. In these samples X_{Mg}^{ga} ranges from 0.20 to 0.60, always less than X_{Mg}^{opx} of the coexisting orthopyroxene ($K_{D\,Fe-Mg}^{ga-opx} > 1$). There is a general increase in X_{Ca}^{ga} with decreasing X_{Mg}^{ga} in garnets from metapelitic ga-opx assemblages (figure 6.11b). The most magnesian garnets coexisting with orthopyroxene (X_{Mg}^{ga} = .55- .60) occur in metapelitic rocks where sapphirine or sillimanite may be additional phases, and where plagioclase is absent or very sodic if present.

Garnet-orthopyroxene rich rock types contain more Fe-rich garnets (X_{Mg}^{ga} = .14- .30) which contain significant grossular component (X_{Ca}^{ga} = 0.03 -0.12). These garnets contrast with those from clinopyroxene-bearing metabasic rock types (Chapter 5) where X_{Ca}^{ga} is in the range 0.20-0.22 over a wide range of X_{Mg}^{ga} (.06- .32).

(c) Sapphirine

In some highly magnesian garnet-orthopyroxene- and orthopyroxene-sillimanite-bearing samples, sapphirine is present as primary subhedral prismatic grains or as secondary rims between grains (49607, 4518, 4833, 49817). Excess cations over 7 for each 10 oxygens indicates the presence of minor Fe^{3+} in these sapphirines.

All sapphirines analysed are Mg-rich (X_{Mg} = .78- .84) and depart from the theoretical end-member sapphirine composition (R^{2+}:Al:Si = 2:2:1) because of the substitution $R^{2+}Si = 2(Al+Cr+Fe^{3+})$. Analysed sapphirines are thus similar to those reported by Ellis *et al.* (1980) from Spot Height 945 and by Grew (1980) from sapphirine+quartz assemblages throughout Enderby Land.

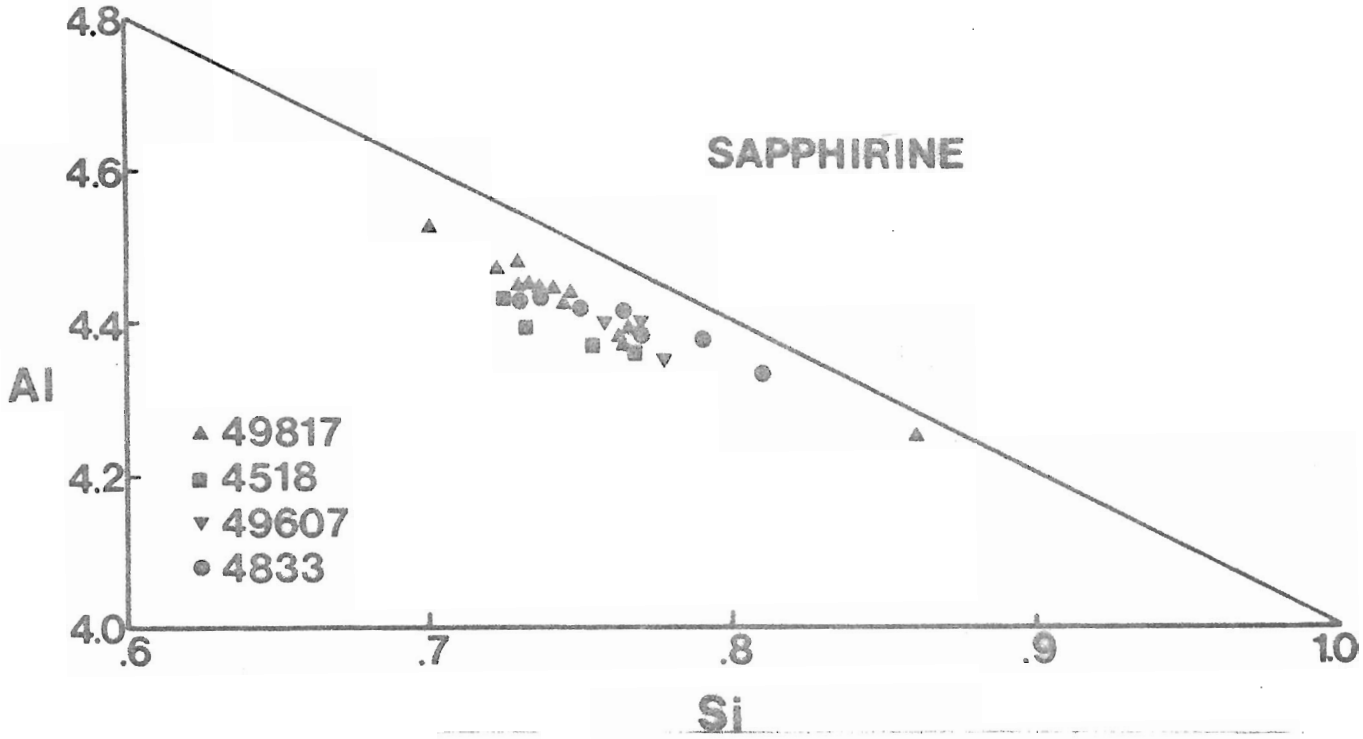

Fig. 6.11 a. Molecular proportions of Al vs Si (per 10 Oxygens) in sapphirines from various ga-opx rocks. Sample localities in Table 6.1. Diagonal line represents ideal substitution $2Al = M^{2+}Si$

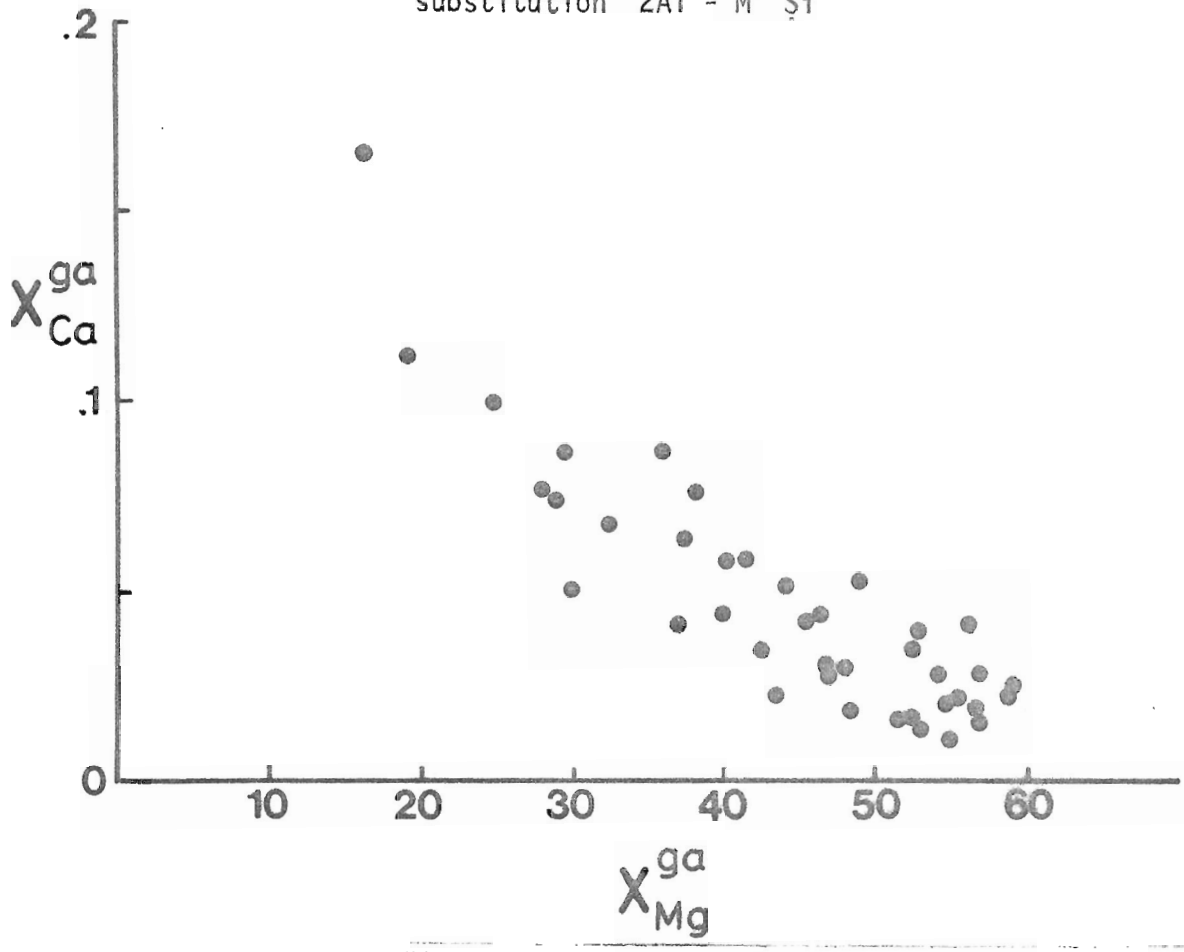

b. X^{ga}_{Ca} (Ca/Ca+Mg+Fe) plotted against X^{ga}_{Mg} (cores) for ga-opx assemblages from the Napier province.

Sapphirine compositions are plotted in Figure 6.11a. The analytical points depart from the ideal $R^{2+}Si = 2Al$ substitution line because of the presence of small amounts of Fe^{3+} which are not considered in constructing the diagram. These sapphirines are more aluminous than those of Grew (1980), but lie in the higher-Al_2O_3 range of sapphirines reported by Ellis *et al.* (1980) (figure 7) from Enderby Land.

Sapphirines coexisting with garnet and orthopyroxene in 49817 show zoning with an increase in X^{sa}_{Mg} and X^{sa}_{Al} rimwards, while garnet shows a decrease in X^{ga}_{Mg} rimwards and hypersthene an increase in X^{opx}_{Mg} and a decrease in X^{opx}_{Al}. This suggests a general expansion of the Sa-ga-hy three phase field (no quartz) with decreasing temperature or increasing pressure. A temperature decrease is inferred from the increase in $K_{D\,Fe-Mg}^{ga-opx}$ and the decrease in X^{opx}_{Al} observed in the zoning patterns. In the same sample, sapphirine coexisting with garnet alone shows an increase in X_{Mg} from cores to rims while X^{ga}_{Mg} decreases. A wide (0.1 mm) orthopyroxene rim (X^{opx}_{Mg} = .75, Al_2O_3 = 7-9 wt.%) has formed between sapphirine and garnet, indicating the overall movement of the Ga-Sa tieline to the Al- and Fe-rich side of the initial Ga-Sa join.(figure 6.7a).

(d) Feldspars

Plagioclase and K-feldspars coexisting with garnet and orthopyroxene are plotted in figure 6.12. Plagioclase shows a wide range of composition from An_{15} to An_{70}, depending on the sample. More anorthite-rich plagioclase generally coexists with more grossular- and iron-rich garnets, and with orthopyroxenes of lower alumina content. These correlations are in accord with the reaction (Wells, 1979):

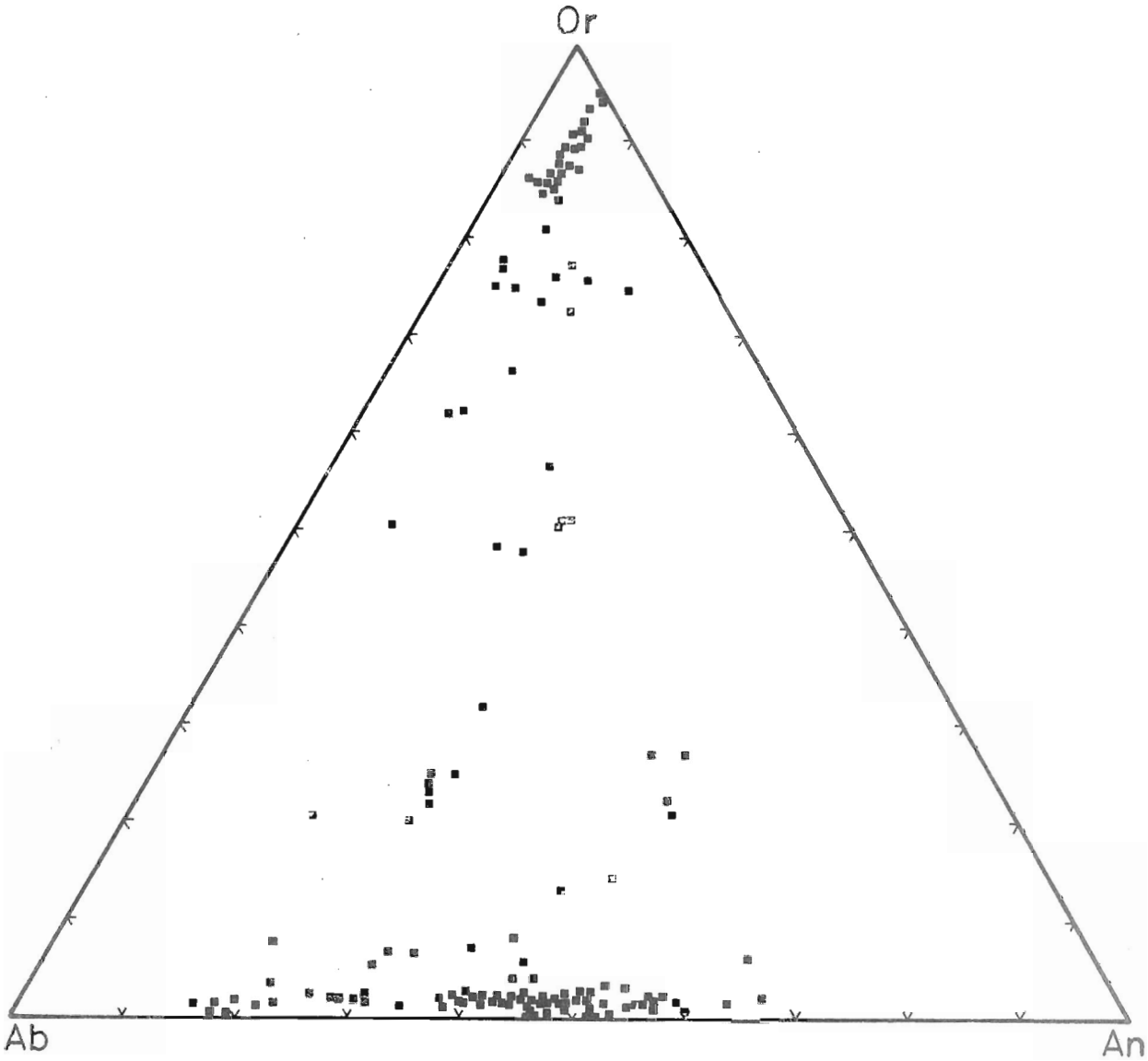

Fig. 6.12 Ca-Na-K diagram (An-Ab-Or) of feldspars from ga-opx assemblages from the Napier province. Note the highly Calcic pre-exsolution alkali feldspar compositions.

$$Mg_2Si_2O_6 + CaAl_2Si_2O_8 = CaMg_2Al_2Si_3O_{12} + SiO_2$$

ortho-pyroxene — plagioclase — garnet — quartz

which can be applied as a geomarometer for the plagioclase-bearing assemblages.

Mesoperthite K-feldspar analyses have been obtained from area scans using a defocussed electron beam. Strongly developed exsolution lamellae have been accounted for by averaging several area scans (500 μm^2) on single grains. An important feature of these mesoperthites from a number of samples (49740, 3935, 3411) is the very Na- and Ca-rich composition of the pre-exsolution alkali feldspars.

(e) General Compositional Relationships between Garnet and Orthopyroxene.

(i) Variation of $K_D^{ga\text{-}opx}_{Fe\text{-}Mg}$ with X^{ga}_{Ca}

Values of $K_D^{ga\text{-}opx}_{Fe\text{-}Mg}$ for primary metamorphic garnet-orthopyroxene pairs (cores and rims) and recrystallised grains or coronas are presented in table 6.1 . K_D values obtained from core compositions are in the range 1.8-3, with $K_D^{ga\text{-}opx}_{Fe\text{-}Mg}$ increasing with X^{ga}_{Ca} (Figure 6.13). K_D data for rim compositions and for secondary garnet-orthopyroxene assemblages are higher than core K_D values, and range from 2.8-3.6 for low X^{ga}_{Ca} samples to 3.4-4.8 for higher X^{ga}_{Ca} samples (figure 6.13).

In any one sample, reversed Fe-Mg zoning patterns in garnets and orthopyroxenes leads to an increase in $K_D^{ga\text{-}opx}_{Fe\text{-}Mg}$ towards rims and in secondary assemblages, at near constant X^{ga}_{Ca}. In typical magnesian metapelites, K_D increases from core values of 2-2.6 to 2.8-3.6 on rims and recrystallised grains, indicating a general decrease in temperature with the formation of the rims and secondary assemblages.

The generalised increase in $K_D^{ga\text{-}opx}_{Fe\text{-}Mg}$ with X^{ga}_{Ca} for both core compositions and maximum K_D values (figure 6.13) is in agreement with

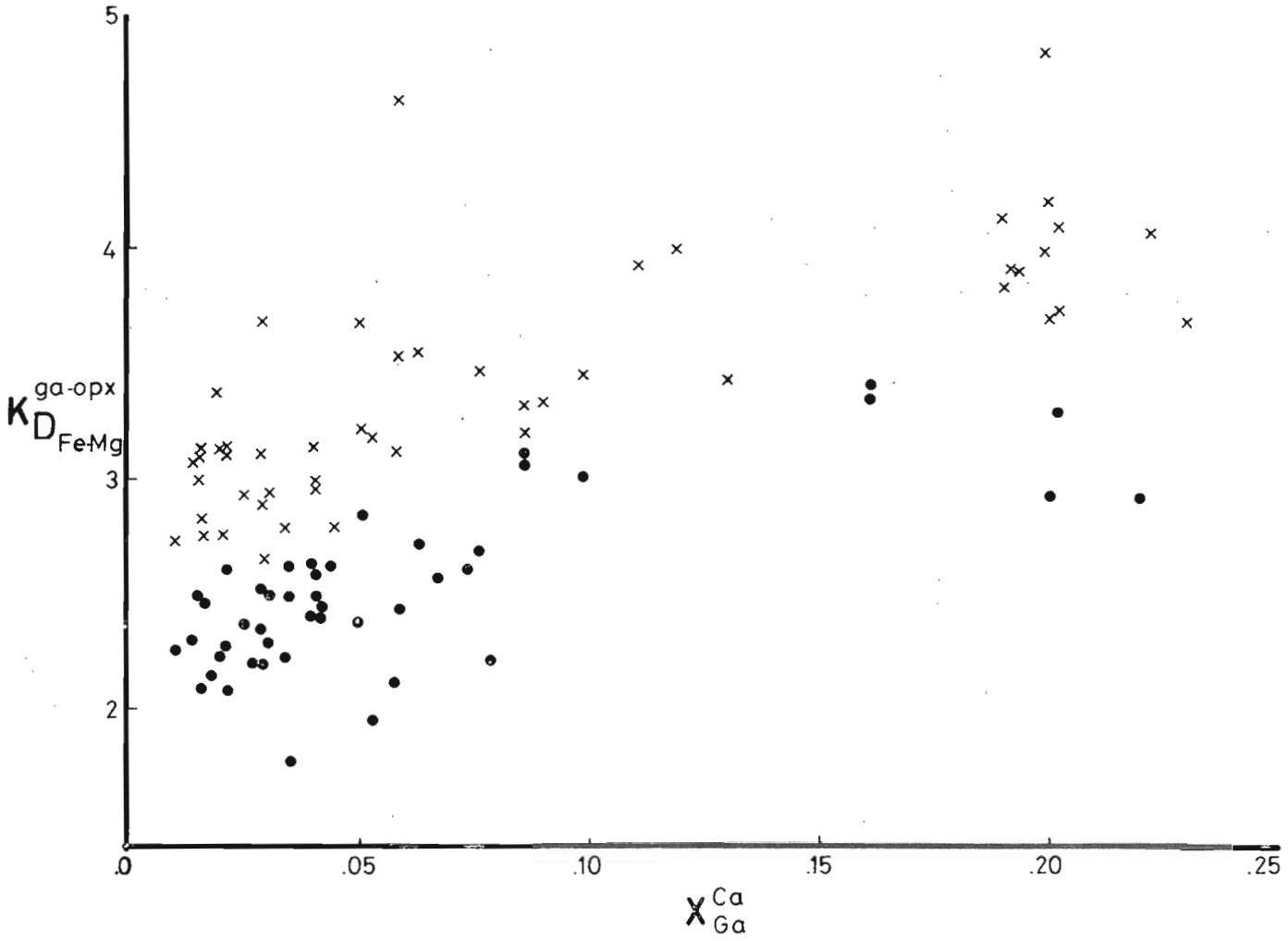

Fig. 6.13 $K_{D_{Fe-Mg}}^{ga-opx}$ plotted against X_{Ca}^{ga} for ga-opx pairs from the Napier province, showing the general increase in K_D with increasing Ca- content of the garnet for both core (peak) compositions (filled circles) and rims or recrystallised assemblages (crosses)

experimental observations on the effect of X_{Ca}^{ga} on K_D at constant X_{Mg}^{opx} (Chapter 3). However, the natural rock data show considerable scatter and are thus not directly comparable with the experimentally determined Ca effect. This scatter results from the influence of a number of other variables, for example:

(1) Variations in X_{Mg}^{opx} between samples plotted on Figure 6.13. Samples from a restricted range of X_{Mg}^{opx} values only exhibit a very restricted range in X_{Ca}^{ga}, so that data with a broad range in X_{Ca}^{ga} can cover a broad range in X_{Mg}^{opx}. As $K_{D_{Fe-Mg}}^{ga-opx}$ decreases with decreasing X_{Mg}^{opx} at constant T and P (Chapter 2; also Davidson and Mathison, 1968), the apparent Ca-effect on K_D in the natural rocks will be lowered as the more Ca-rich samples are generally more Fe-rich.

(2) The compositional data have been extracted from samples obtained from a number of separate sites over a wide geographic area (figure 5.1). Thus it is unlikely that core or rim-recrystallised grain values represent constant P,T data. Scatter in $K_{D_{Fe-Mg}}^{ga-opx}$ may be a result of real P-T differences between samples.

Suites of samples which cover some range in X_{Ca}^{ga} have been obtained from Beaver Island (three samples), Mt Sones (seven samples) and Tonagh Island (seven samples). At these localities the samples have been collected from adjacent layers or from sites which are only separated by up to 1 km, and thus relatively constant P,T conditions may be assumed and $K_{D_{Fe-Mg}}^{ga-opx}$ variations attributed solely to compositional variations.

In these cases, particularly in the Beaver Island samples, minimum or core K_D values consistently increase with increasing X_{Ca}^{ga}, in agreement with experimental observations although not directly comparable to experimental data because of variations in X_{Mg}^{opx} and other compositional parameters (e.g. Mn, Ti).

This effect of Ca on $K_{D_{Fe-Mg}}^{ga-opx}$ (figure 6.13) is very important for the samples considered here in that rim K_D values obtained for low X_{Ca}^{ga} samples, which are considered to represent lower temperatures than core K_D data, are similar to core-K_D data for higher X_{Ca}^{ga} samples (K_D = 3). Failure to account for X_{Ca}^{ga} would thus lead to erroneous conclusions regarding the peak metamorphic conditions experienced by Ca-richer samples and the timing of thermal peaks recorded by different samples.

(ii) Variation of X_{Al}^{cpx} with X_{Ca}^{ga}

Values of $(X_{Al}^{opx})^{cores}$ and $(X_{Al}^{opx})^{rims\ or\ secondary}$ for the garnet-orthopyroxene assemblages are plotted against X_{Ca}^{ga} in figure 6.14a and 6.14b. In any one sample, there is usually some zoning to lower X_{Al}^{opx} adjacent to orthopyroxene rims, and in samples with secondary recrystallised orthopyroxenes and garnets the latter orthopyroxenes also have lower X_{Al}^{opx} than primary core compositions (section 6.2 II). Using either the core or rim Al-populations, there is a general decrease in X_{Al}^{opx} with increase in X_{Ca}^{ga} between samples. As in the case of $K_{D_{Fe-Mg}}^{ga-opx}$ variations, other compositional factors (X_{Mg}^{opx}, Mn contents) and *real* variations in (P,T) between samples lead to scatter in the X_{Al}^{opx} data. Isofacial samples collected from single sites (e.g. Beaver Island, Tonagh Island, McIntyre Island, Mt Sones) exhibit rapid decrease in X_{Al}^{opx} with X_{Ca}^{ga} for low values of X_{Ca}^{ga}. At larger X_{Ca}^{ga} values (0.10-0.20), the decrease in X_{Al}^{opx} with X_{Ca}^{ga} is reduced. The general exponential form of the X_{Al}^{opx} vs X_{Ca}^{ga} data is in agreement with the Ca effect determined experimentally in Chapter 3, wherein a general decrease in X_{Al}^{opx} with increase in X_{Ca}^{ga} was described in terms of a linear variation of $ln\ X_{Al}^{opx}.(1-X_{Al}^{opx})$ with a function involving X_{Ca}^{ga}.

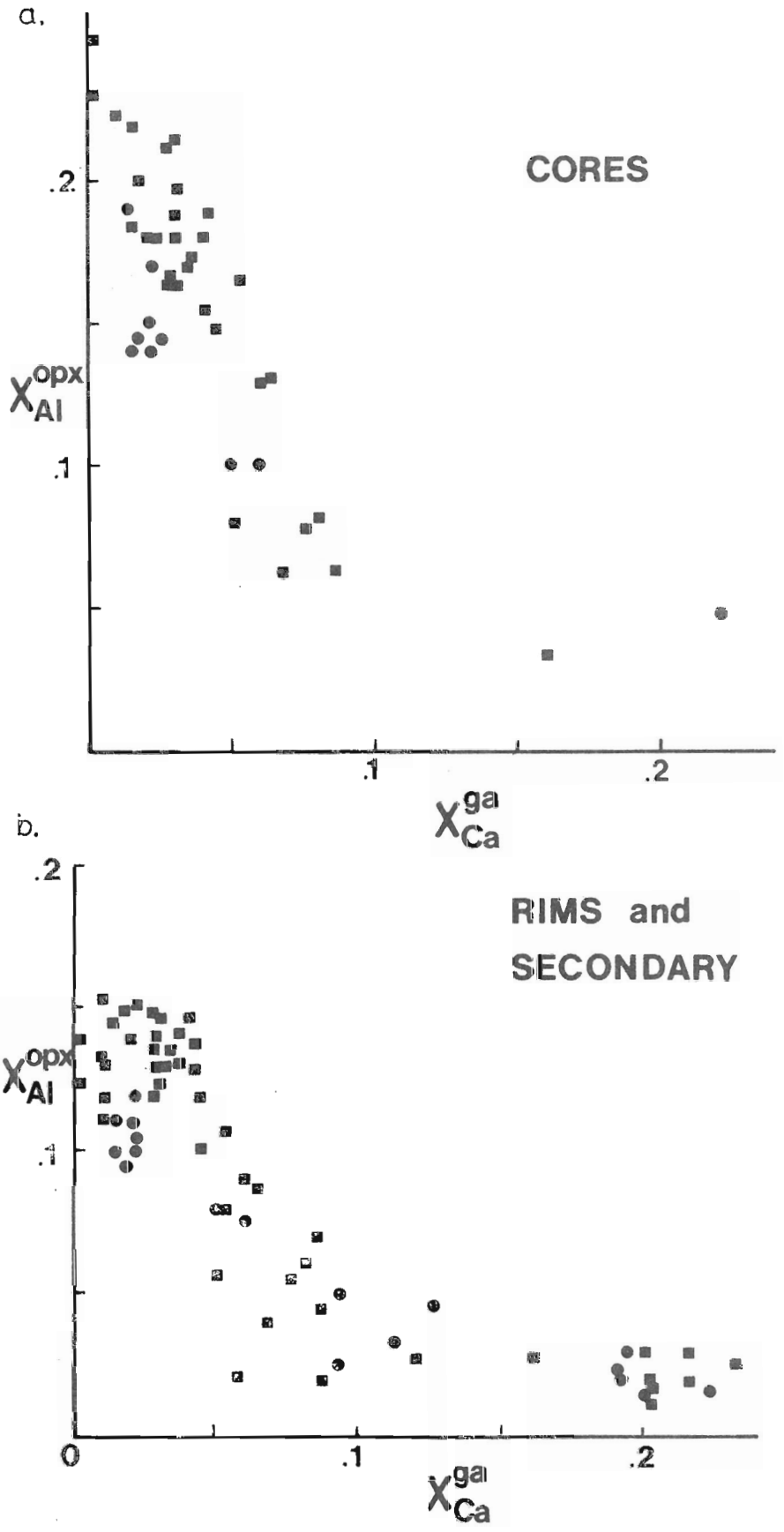

Fig. 6.14 Alumina contents of orthopyroxenes ($X_{Al}^{opx} = Al/2$) plotted against X_{Ca}^{ga} for ga-opx pairs from the Napier province. Highest Ca assemblages also contain clinopyroxene.

a. core compositions ; filled circles for samples from the Casey Bay area.

b. rim and recrystallised grain compositions.

II. ZONING RELATIONSHIPS IN COEXISTING GARNET AND ORTHOPYROXENE

(a) Garnet and Orthopyroxene Assemblages

In assemblages containing only garnet and orthopyroxene, with additional feldspars and quartz, both minerals usually exhibit zoning from cores to rims which is consistent with ga-opx tie line rotation under conditions of decreasing temperature (figures 6.5-6.10). This anticlockwise tie line rotation is further accentuated in those samples where recrystallised ga-opx rims and coronas also occur.

Garnet is usually homogeneous throughout most of the bulk of any grain, but develops zoning to lower X_{Mg}^{ga} values near rims adjacent to orthopyroxene. In most cases there is no significant change in X_{Ca}^{ga} accompanying this Fe-Mg zoning. In recrystallised assemblages, where garnet regrowth has occurred (section 6.2), the new garnets have lower X_{Mg}^{ga}, and sometimes higher X_{Ca}^{ga} than the primary grains. Some samples show a consistent change in garnet composition:

$$(X_{Mg}^{ga})\text{core} > (X_{Mg}^{ga})\text{rim} > (X_{Mg}^{ga})\text{recrystallised}$$

correlated with a decrease in T between earlier and later events (see below).

Orthopyroxene coexisting with garnet displays zoning to greater X_{Mg}^{opx} and lower X_{Al}^{opx} adjacent to zoned garnet rims (figures 6.5-6.10). Near orthopyroxene rims, a continuous change in X_{Al}^{opx} and X_{Mg}^{opx} from a compositional plateau, (X_{Al}^{opx})core, to (X_{Al}^{opx})rim and (X_{Mg}^{opx})maximum occurs, resulting in a series of orthopyroxene compositions which plot along a tie line directly away from garnet.

Recrystallised orthopyroxene grains show higher X_{Mg}^{opx} and lower X_{Al}^{opx} than the primary metamorphic orthopyroxenes.

Orthopyroxene adjacent to recrystallised garnet euhedra, garnet grain boundary lamellae, garnet exsolution lamellae, and garnet quartz coronas on opx-plag, also shows a marked decrease in X_{Al}^{opx} and increase in X_{Mg}^{opx}.

These zoning patterns, coupled with compositional data and textural information from the garnet-orthopyroxene parageneses, indicate the operation of two coupled reactions proceeding from left to right with decreasing temperature, at near constant pressure:

$$Fe_2Si_2O_6 + Mg_3Al_2Si_3O_{12} = Mg_2Si_2O_6 + Fe_3Al_2Si_3O_{12} \quad \ldots 6(1)$$

$$(Fe,Mg)_2Si_2O_6 + (Fe,Mg)Al_2O_6 = (Fe,Mg)_3Al_2Si_3O_{12} \quad \ldots 6(2)$$

in opx garnet

Reaction (1) is the equation describing Fe-Mg exchange between garnet and orthopyroxene, and results in the increase in observed $K_D^{ga\text{-}opx}{}_{Fe\text{-}Mg}$ with decreasing T.

Reaction (2) describes Al exchange between garnet and orthopyroxene (Chapter 2), leading to a decrease in X_{Al}^{opx} with decreasing T and to the formation of secondary garnet rims and grains between orthopyroxenes or on garnet-orthopyroxene (section 6.2 , part II)

In those samples where no primary garnet is present (49406, 49404, 4523), the zoning patterns in orthopyroxenes and the formation of Ca-bearing garnet coronas on opx-plag, are consistent with the general reaction:

opx 1	+	plag	=	ga	+	opx 2	+	qz	... 6(3)
high Al, low Mg		Ca component		Fe,Ca bearing		low Al, high Mg			

which proceeds from left to right with decreasing T (Green and Ringwood, 1967; Wells, 1979).

(b) Opx-Sill Assemblages

In the absence of garnet, orthopyroxene in equilibrium with sillimanite zones to lower X_{Al}^{opx} rimwards (figure 6.7a and b) without significant increase in X_{Mg}^{opx}. Orthopyroxene compositions lie essentially on a tie line connecting the rims with sillimanite on AFM diagrams. These zoning features indicate the reaction

$$\underset{\text{in opx}}{MgAl_2SiO_6} + \underset{\text{qz}}{SiO_2} = \underset{\text{in opx}}{MgSiO_3} + \underset{\text{sill}}{Al_2SiO_5} \quad \ldots 6(4)$$

In the absence of quartz, orthopyroxene in equilibrium with sillimanite will contain more Al_2O_3 than that in the assemblage opx-sill-qz.

Reaction (4) above also describes the formation of second orthopyroxene-sillimanite aggregates and coronas on earlier orthopyroxene and sillimanite or garnet in 49831, 3970 and 3971.

(c) Opx ± Ga ± Sapphirine Assemblages

In the presence of sapphirine, primary metamorphic orthopyroxene grains zone to lower X_{Al}^{opx} rimwards, often with only minor change in X_{Mg}^{opx} (X_{Mg}^{opx} = .72-.75). Al_2O_3 in orthopyroxene decreases from 9-11 wt.% (cores) to 6-7 wt.% on rims adjacent to sapphirine grains or to secondary (retrograde) sapphirine lamellae (49607, 49817), with a correlated decrease in X_{Mg}^{opx}. These zoning features, and zoning of coexisting garnet to more Fe-rich compositions, can be explained by the continuous reaction:

$$\underset{\text{opx 1}}{(Fe,Mg)Al_2SiO_6} + \underset{\text{garnet}}{(Fe,Mg)_3Al_2Si_3O_{12}} \quad \ldots 6(5)$$

$$= \underset{\text{sapphirine}}{(Fe,Mg)_2Al_4SiO_{10}} + \underset{\text{low Al opx}}{(Fe,Mg)_2Si_2O_6} + \underset{\text{qz}}{SiO_2}$$

which corresponds to a movement of the three-phase triangle ga-opx-sa to more Fe-rich compositions on an AFM diagram such that the original ga-opx tie line lies within the three-phase field stable at lower T (figure 6.7a).

In 49817, sapphirine rims orthopyroxene which has also exsolved rutile and zones to lower X_{Al}^{opx} and TiO_2. In this case, sapphirine may have formed by the reaction:

$$(Fe,Mg)Al_2SiO_6 + MgTiAl_2O_6 = (Fe,Mg)_2Al_4SiO_{10} + TiO_2 \quad \ldots 6.6$$

orthopyroxene sapphirine rutile

on a decrease in temperature at high pressure.

TABLE 6.1 GARNET - ORTHOPYROXENE PAIRS

ROCK	LOCALITY	X^{opx}_{Al}	X^{opx}_{Mg}	X^{ga}_{Mg}	X^{ga}_{Ca}	$K_{D\ Fe-Mg}^{ga-opx}$	Comments	X^{plag}_{An}	P_1 at 900°C	P ga-opx	T ga-opx	TEXTURAL COMMENTS
4518	McINTYRE I.	.150	.768	.594	.022	2.26	cores	-	-	10.6	960	primary layer of lobate ga-opx-felds-silli. Recrystallisation to finer opx-felds and ga common. In one layer primary Sapph. has cornonas cd-sill-ga or opx-silli-ga.
				.584		2.56	"			8.6	900	
		.110	.785	.540		3.11	rims			4.3	692	
49659	"	.190	.720	.530	.014	2.28	cores	.18	8.2	8.6	963	mutally resorbed v. coarse opx+ga with plagioclase.
		.110	.730	.470		3.05	rims			4.5	727	Second ga along opx grainboundaries and exsolved from opx.
49607	"	.175	.770	.549	.021	2.81	cores	-	-	7.5	900	Subhedral opx-silli, with lobate Sapph in one part.
		.100	.775	.525	.036	3.12	rims			5.5	713	Garnet qz + opx in one part, fine recrystallised ga.
49657 layer 1	"	140	.734	.527	.015	2.48	cores	.21	7.7	8.8	905	coarse (5mm) ga porphyroblasts with trails of silli inclusions.
		100	.740	.480	.018	3.08	rims			4.7	706	Recrystallised finer ga on rims of blasts. Opx polygonal-lobate. Fine granular ga+.
49757 layer 2	"	.145	.710	.450	.015	2.99	rims	.21	6.4	8.3	900	opx rim and wrap around earlier coarse grains. Feldspars
		.095	.710	.420	.018	3.38	recryst.			4.6	713	recrystallised to fine polygonal grains.
3973	MT.CHARLES	.140	.760	.550	.022	2.59	cores & rims	.28	8.2	10.7	943	primary lobate ga with subhedral opx. Common symplectite
		.120	.765	.510		3.13	recryst			5.0	742	areas of sill + cd on garnet. Fine recryst.ga also.
3971	"	.144	.772	.589	.025	2.36	cores & rims	.32	8.8	10.5	940	primary ragged opx, lobate ga blasts. Abundant recryst. fine
		.105	.785	.556		2.92	recryst	.20	10.	6.3	740	ga, and fine symplectites sill + cd or cd + opx on ga.
3970	"	.100	.630	.414	.058	2.41	cores	.41	9.	11.	940	early coarse lobate ga-opx. Opx kinked, some recrystallised.
		.076	.655	.350		3.53	recryst			5.4	721	Second fine ga developed on early ga and on opx grains.
4319	"	.100	.688	.440	.051	2.81	core	.42	8.3	8.5	810	euhedral ga and polygonal opx developed with finely
		080	.692	.413		3.19	rim			6.6	740	recryst. feldspars.
49891	MT.HOLLINGS-WORTH	.175	.695	.523	.035	2.08	cores	.40	9.5	7.7	955	polygonal-lobate ga-opx-plag. Euhedral ga overgrowths
		.142	.720	.510	.037	2.47	rims	.47	7.9	8.2	895	on earlier ga; also ga-qz symplectite on ga. Ga occurs
		.132	.715	.490		2.61	recryst			7.0	850	as lamellae symplectites with qz in opx.
3964	DEBENHAM	.155	.746	.528	.039	2.63	cores	.49	8.1	9.6	955	layered into ga-sill-plag and ga-opx-plag layers. Some
		.132	.754	.508		2.97	rims			8.	900	recrystallised opx; biotite present on opx.
										6.	800	
3410	MARSLAND	.180	.676	.485	.019	2.22	core	-	-	7.9	955	layered opx-ga-qz lobate granoblastic. Recrystallised
		.140	.705	.465		2.75	rims+rext			5.4	814	fine grained subhedral ga and fine opx. Primary osumilite broken down to symplectite.
3411	"	.170	.620	.425	.034	2.21	cores	.47	7.1	6.7	938	ga prophyroblasts in lobate ga-opx-felds-qz. Symplectite
		136	.644	.395		2.77	rims			5.2	800	fine ga overgrowths on ga with opx.
3935	PARDOE	.062	.543	.323	.067	2.50	cores	.30	9.6	8.2	815	resorbed poikiloblastic ga. Biotite alteration of lobate
		.040	.555			2.62	rims			9.1	740	opx. Extensive multipe exsolution lamellae in feldspars.
										to 10.8	780	
49786	TONAGH I.	.215	.735	.542	.028	2.34	cores	-	-	7.4	959	elongate platy qz+opx+ga. Dl flattening fabric. Coarse
		.125	.780	.490		3.69	rims			4.0	720	elongate ga and opx are finely recrystallised, with fine rare ga along cracks in opx.
49817		.250	.742	-			cores+silli					strongly layered into opx+sill polygonal layer, with Sapph
		140	.745	-			rims+sa					forming on grain boundaries; also ga+sapph+opx layers
		.125	.756	-			recryst.+silli					with formation of opx+Sa symplectites on earlier garnets.
		.184	765	.570	.016	2.46	cores	.30	7.2	7.0	950	A second recrystallised garnet forms with opx+sa in places.
		.146	760	.530		2.81	rims and symplectite			7.7	916	Opx with sill (no qz) is strongly zoned in Al_2O_3, and 2nd opx
										5.8	755	forms.
49809	"	.200	.723	.568	.018	1.99	cores	-	-	9.2	1000	coarse ga-opx-qz plus Osumilite; secondary formation of ga-opx
		.150	.740	.555		2.28	rims			8.3	900	granules, aggregates of opx-ga recrystallised with quartz. Osu breakdown to variable symplectites.
49856	"	.220	.688	.514	.016	2.09	core	-	-	7.7	980	coarse polygonal ga+opx; ga blast to 1cm; Second finger-
		.135	.721	.484	.010	2.76	recryst.					like ga as rims on opx and as lamellae in opx.
		.120	.729	.463		3.12	recryst			5.0	758	
49868	"	.210max	.747	.535	.028	2.57	core	-	-	6.7	900	primary granuloblastic poly-lobate ga-opx-plag-qz. Secondary
		.157		.511		2.83	rim			5.5	818	euhedral ga overgrowth on ga blasts, also fine opx with this
		.126	.780	.492		3.67	recryst			4.1	725	ga. Opx zones to lower X_{Al}, higher X_{Mg}.
3918	"	.050	.331	.141	.034	3.04	core hiMn	-	-	6.2	820	coarse granuloblastic opx+ga, minor kinking and recrystal-
		.022	.355	.106	(+.023Mn)	4.65	recryst			5.0	650	lisation with fine garnets formed.
49831	TONAGH I.	.224	.730	.584	.010	2.37	cores	-	-	7.5	960	well layered gneiss, kspar+qz+opx+ga and euhedral Sillimanite.
		.155					rim			8.0	900	Ga as blasts, usually separate from opx. Both types are ragged
		.132	.745	.516	.010	2.74	recryst.			5.7	760	and broken, with finer subhedral ga grains formed on ga or in
		.115					minimum					cracks in opx. Silli grains have finely recrystallised fibrolite ± opx ± ga on them. Also on opx.

ROCK	LOCALITY	X^{opx}_{Al}	X^{opx}_{Mg}	X^{ga}_{Mg}	X^{ga}_{Ca}	$K_{D_{Fe-Mg}}^{ga-opx}$	Comments	X^{plag}_{An}	P_1 900°C	P ga-opx	T ga-opx	TEXTURAL COMMENTS
4003	BEAVER IS.	.102	.650	.400	.044	2.79	rims	.43	7.2	9.2- 6.7 6.0	900- 830 800	coarse granuloblastic lobate ga+opx.
4006	"	.051	.500	.250 .225	.100 .100	3.00 3.44	rims	-		7.2	775	granoblastic lobate-polygonal ga + opx.
4005	"	.034 .028	.405	.167	.162	3.40	rims	-		8.0	770	granulobastic lobate-polygonal ga+opx, opague common mylonite - streakyand flaser textures occur.
3597	CROHN I.	.078 .055	.524 .558	.282 .264	.076	2.80 3.50	cores rims	.42	10.8	9. 8.8	900 805	granuloblastic polygonal-lobate ga+opx. Some recryst. opx rims. 1cm porphyroblast ga.
4593	HOWARD HILLS	.165 .140	.690 .708	.470 .440	.028	2.51 3.09	cores rims	.27	8.6	7.2 6.0	920 780	coarse granoblastic ga+opx; no qz and rare plag.
4833	MT. TRAIL	.215 .130	.744 .781	.570 .552	.029	2.19 2.89	cores rims + sa	.60	7.2	8.5 6.3	995 800	polygonal granulobastic opx+ga and occasional sapph+phlogopite. Opx zoned, with finger-like Sapphirine on opx rims.
4834	TRAIL	.072	.646	.363	.086	3.20	average	.57	8.1	5.5	754	polygonal-lobate elongate opx+ga in strongly exsolved feldspars. Marginal fine recrystallised ga+opx on earlier grains.
49434	TRAIL	.230 .150 .120	.700 .753 .765	- .516 .500	.028 "	2.70 3.26	early opx rims with ga recryst	.40	-	8.5 5.0 3.6	1000 770 710	very coarse(5mm) opx porphyroblast zoned near rims to lower Al. Euhedral garnet on rims of this opx. Also general opx-ga polygonal granoblastic with even later ga as lamellar rims on opx.
49748	MT.SONES	.064 .045 .020	.565 .570 .580	.294 .295 .294	.086	3.12 3.17 3.32	cores average rims	.57	7.2	5.6 6.3	750 700	granuloblastic, coarse polygonal ga-opx-ilm-qz-plag. minor second fine euhedra.
49740	SONES	.190 .130	.676 .685	.456	.042	2.49 2.59	core rim	.37 .45	9. 7.8	5.5 6.1	905 840	layered, coarse lobate elongate ga+opx with minor recrystal-lised grains of opx. Kfelds strongly exsolved, common feldspar recrystallisation.
49734	"	.128 .092	.589 .637	.405 .360	.058 .063	2.11 3.12	cores rims	.50 .66	8.9 5.9	7.9 4.0	940 740	polygonal granoblastic opx-ga-felds-qz.
49749	"	.130 .088	.620 .662	.376 .356	.063	2.71 3.54	cores rims	.52	8.	6.9 5.5	900 760	elongate ribbon quartz layers; recrystallised qz+felds. common. Elongate lobate anhedral-subhedral opx+ga.
3468	"	.148 .120	.678	.465	.044	2.42	rims and cores	.52	7.6	7.2 7.2	858 905	coarse lobate granoblastic opx+garnet: second fine garnet occurs as thin rims and grains between opx+plag. Garnet also as symplectite with quartz.
3552	"	.165 .108 .080	.650 .714	.489 .440	.053	1.94 3.18	cores rims	.58	9.2	7.4 5.0	955 760	polygonal granuloblastic ga+opx in felds+qz.
3423	RIISER LARSEN	.080 .056	.510 .570	.304 .265	.050 .048	2.38 3.68	cores rims	.27	9.	7.0 3.3	848 660	coarse lobate granoblastic opx+lobate poikiloblastic ga. Strongly exsolved feldspars.
49382	"	.148 .132	.720	.467	.029	2.62 2.93	cores recryst	.341	8.2	5.2 5.7 4.3	880 827 770	well layered coarse opx+kspar layer and polygonal ga+sp+opx layer. Spinel breaks down to Cor+Ilm+mt. Biotite (later) between layers.
4549	HARDY	.190 .140	.678 .700	.480 .470	.029	2.28 2.63	cores rims	.40	7.7	7.0 5.4	940 822	well layered elongate granoblastic texture, alternate layers ga and opx rich. Intergrowth ga+qz on opx in some grains.
4547	"	.164	.652	.460	.029	2.20	average	.36	7.9	7.0	920	lobate, resorbed and disaggregated ga, subhedral nematoblastic opx forming foliation discordant to layering.
3532	945	.190 .152	.612 .620	.433	.022	2.07 2.14	cores rims	.31 .24	7.4 8.2	7.2 7.2	962 922	well layered into ga-spinel-feldspar and opx-qz rich layer.
4092	AMUNDSEN	.030 .020 .011 min	.245	.085	.216	3.49	secondary ga	-	-	6.6	668	garnet occurs as lamellae, finger-like rims, and fracture fillings in coarse, subhedral pyroxene. The pyroxene was pigeonite, now exsolved and inverted as well as deformed and disaggregated.
4588	WARD HOCKS	.026	.554 .530	.260 .234	.112 (.120Mn)	3.53 3.67	secondary ga;hi MnO	-	-	8.0	670	coarse polygonal ga-opx-qz, some marginal fine recrystallised opx. Garnet associated with ilmenite.
4093	"	.048	.525	.275 .242	.220 (.060Mn)	2.91 3.41	secondary ga	-	-	8.1	810	ga as rims on pyroxenes with opaque, or as lobate symplectite areas with magnetite and minor quartz.
4094	"	.090 .030	.585 .590	.320 .280 .255	.200	2.93 3.70 4.20	primary exsolved ga	1.	9.9	9.5 7.6	708 670	ga as coronas between polygonal-lobate pyroxenes and magnetite.
4354	MYERS ICE SHELF	.029	.465	.179	.118	3.99	secondary ga	-	-	5.7	650	granoblastic polygonal to coarse subhedral opx. Lobate ga or gas as finger-like rims on opx or lamellae in opx, with opaque.
4359	ZUBCHATYY	.018	.230	.068	.202	4.09 4.55	secondary ga	.38	8.1 (at800°C)	9.9 6.0	670 600	coarse subhedral-euhedral pigeonite, with ga lamellae and ga thin rims with qz. Pigeonite exsolved to cpx-opx. Deformed plag.
4358	"	.020	.435 .408	.190 .155	.202	3.28 3.74	early recryst	.52	9.6 (at800°C)	12.0 6.2	740 626	well layered, subhedral to polygonal elongate opx with lobate ga and lobate mesoperthite.

ROCK	LOCALITY	X^{opx}_{Al}	X^{opx}_{Mg}	X^{ga}_{Mg}	X^{ga}_{Ca}	K_D	COMMENT	X^{plag}_{An}	P_1	P ga-opx	T ga-opx
4085	MILLER	.082	.510	.280	.076	2.68	cores	-	-	6.0	822
		.062	.538	.252		3.46	rims			3.3	700
4528	WILKINSONS PEAKS	.198	.585	.370	.040	2.40	cores	.49	7.	4.0	890
		.166	.615	.337		3.14	rims		(at700°C)	2.0	788
		.154					Cd present			2.5	788
161279/19	FYFE	.038	.483	.192	.115	3.92	secondary ga	-	-	4.7	645
		.033									
4510	"	.030	.557	.245	.193	3.89	secondary ga	.49	9.5 (at700°C)	8.0	675
										7.2	660
49461	"	.020	.500	.198	.222	4.06	hi Mn garnet	-	-	9.1	658
		.011	.507	.150	.222	5.83	recryst			to 7.0	640
4523	HYDROGRAPHER	.031	.544	.239	.193	3.81	secondary ga	.45	9.8 (at700°C)	9.5	680
4520	"	.023	.508	.200	.190	4.13	secondary ga	.40	9.3 (700°C)	7.6	640
4704	FIELD IS.	.021	.510	.208	.191	3.92	secondary ga	.50	8.9 (700°C)	9.4	660
49404	ZIRCON PT.	.055	.690	.394	.125	3.197	cores	.70	8.8	7.2	730
		.036	.675	.386		3.421	rims	.87	8.4	9.5	680
49406	"	.025	.561	.264	.092	3.57	recryst.rims	-	-	7.3	720
		.045		.293		3.09				8.5	640
49412	"	.020	.448	.144	.198	4.828-	recryst	.32	8.7	7.9	650
		.014				3.99					
4818	GROMOV	.048	.673	.381	.162	3.34	core			12.	850
				.362	.189	3.62	rim			9.	770
							secondary			4.5	650

TEXTURAL COMMENTS
coarse granoblastic polygonal-lobate opx-ga with interstitial qz. Ga often interstitial and may have exsolved from opx.
primary ga-opx-cd lobate granoblastic grains. Later symplectite cd-qz, and some symplectite opx-ga.
finger-like and lobate ga occurs on opx-opaque contacts as rims and coarser areas.
garnet developed as euhedral secondary rims on opx+cpx+plag or on plag-ilmenite contacts.
primary coarse lobate ga+cpx+mt+qz. Strong fine recrystallisation to cpx+opx+ga in areas between original grains.
fine garnet as bead-like grains on polygonal-lobate opx and plag.
fine polygonal-lobate granuloblastic ga+opx+cpx recystallised from earlier pyroxenes.
ga occurs as bead-like rims and coronas with cpx on earlier opx+cpx+plag.
garnet occurs as euhedral,thick rims between opx and plag
garnet (+quartz+second opx) occurs as lamellae and rims between early coarse opx grains.
garnet developed as euhedral-subhedral coronas in symplectite intergrowth with qz, on earlier cpx, opx, ilm and plag.
polygonal-lobate granuloblastic ga-opx-hbl-plag-cpx; also some second ga growth as rims on earlier pyroxenes.
polygonal-lobate granoblastic ga-opx-plag, recrystallised ga lamellae on pyroxene rims and as exsolved grains in cpx.

6.4 TEMPERATURES AND PRESSURES OF METAMORPHISM

Temperature and pressure conditions of initial metamorphism and cooling or recrystallisation of the garnet-orthopyroxene samples from Enderby Land have been estimated based on the mineral composition data listed in table 6.1 and the textural characteristics described above and listed in table 6.1 . For any particular sample, a number of P,T estimates have been obtained, based on the recognised zoning patterns and recrystallisation features.

(1) Peak P-T conditions are obtained from analyses of cores of garnets and cores of adjacent orthopyroxene grains, where primary metamorphic garnet porphyroblasts are present. Such analyses usually give the minimum $K_{D_{Fe-Mg}}^{ga-opx}$ values and the highest values of X_{Al}^{opx}. Thus, the conditions obtained from these compositions will be T_{max} and a corresponding P_{min} at that temperature.

(2) Averaged core data for garnet and orthopyroxene are assumed to avoid the problem of possible existence of highly Al-rich orthopyroxene prior to garnet formation and thus may yield more realistic estimates of P-T conditions attained in prograde metamorphism - inferred to be M1 correlated with deformation episodes D1-D2. Generally, pressures estimated using averaged data will be higher than P_{min} from (1) above, and temperatures may be lower than T_{max}.

(3) P-T estimates for post-D2 (or D1) cooling have been obtained from rim analyses of coexisting primary metamorphic garnet-orthopyroxene grains. As outlined above, such analyses yield higher $K_{D_{Fe-Mg}}^{ga-opx}$ and lower X_{Al}^{opx} values than core analyses, indicating a decrease in temperature rimwards. Analyses of coexisting garnet and orthopyroxene in some coronas where a second garnet rims orthopyroxene yield P-T conditions which in some cases may refer to post-D2 cooling.

(4) Analyses of coexisting recrystallised garnet and orthopyroxene or of orthopyroxene rims adjacent to garnet coronas (section 6.2 II above) yield maximum $K_{D_{Fe-Mg}}^{ga-opx}$ values, and usually minimum X_{Al}^{opx} data, for any particular sample. Minimum T and P data obtained for these cases may relate to cooling or to D3 recrystallisation (see Chapter 5, and section 6.1 above).

I. PEAK M1-M2 METAMORPHIC CONDITIONS

Application of garnet-orthopyroxene Fe-Mg exchange geothermometry and garnet-orthopyroxene Al_2O_3 geobarometry, developed in Chapters 2 and 3, to core analyses of primary metamorphic garnet-orthopyroxene pairs enables the simultaneous estimation of peak, or prograde, P-T conditions. These estimates will be subject to uncertainty derived from the large experimental errors inherent in the geothermometry ($K_{D_{Fe-Mg}}^{ga-opx}$), experimental errors in the Al_2O_3 barometer, and analytical errors. In addition, the P-T conditions indicated by different samples may not necessarily be time-synchronous. In samples where D1 ribbon textures are preserved or other D1 textures are present, the peak P-T conditions most probably relate to a D1 or post-D1 age. In other granuloblastic samples, core analyses may indicate P-T conditions prevalent just after D2 (see Chapter 5).

P-T estimates for peak metamorphic conditions are presented along with P-T paths obtained from rim and recrystallised grain data in figures 6.16 and 6.15. In spite of broad compositional variations in orthopyroxenes and garnets, from different samples, there is marked consistency in the P-T estimates for specific localities and between most localities. The regional distribution of peak P-T estimates is presented in figure 6.17 .

Five different samples from Mount Sones, in the Tula Mountains, yield peak metamorphic conditions of 900-950°C and 7.5-8.3 kbar. These P-T conditions are in good agreement with peak metamorphic conditions of 910-970°C and 6.2-7.5 kbar estimated for Spot Height 945 from data of Ellis (1979).

Other localities in the Tula Mountains and around Amundsen Bay (e.g. Mt Riiser Larsen, Mt Hardy, Mt Marsland, Mt Torckler, Howard Hills, Mt Hollingsworth) also exhibit evidence of an early metamorphic peak at temperatures of 900-960°C and minimum pressures of 7-8 kbar. These P-T estimates are based on analyses of cores of zoned garnets and hypersthenes in each sample.

Higher pressures of 9-10 kbar, or even up to 12 kbar, at 900°C , are indicated for the initial metamorphic event or peak at Beaver Island and Crohn Island in the Amundsen Bay area. Minerals in samples from these localities are not obviously well zoned rimwards but rather show more random inhomogeneity. Thus, the P-T intersections obtained from data in some of these samples may not be realistic due to different closure temperatures of Fe-Mg exchange and Al_2O_3 redistribution. It must be stressed that adequate knowledge of the direction and nature of zoning in the orthopyroxenes and garnets is an essential pre-requisite to accurate P-T estimation.

Samples from Mount Trail indicate peak metamorphic conditions of 990°C and 8.5 kbar. These estimates are relevant to the conditions of initial equilibration of the aluminous hypersthene porphyroblast in 49434.

The diverse suite of samples from Tonagh Island yield P-T estimates of 1000-900°C and 9.2-7 kbar for the peak of metamorphism in D1 or D2. Strongly zoned assemblages, some with D1 ribbon textures, yield the highest temperature estimates (> 950°C) and pressures usually

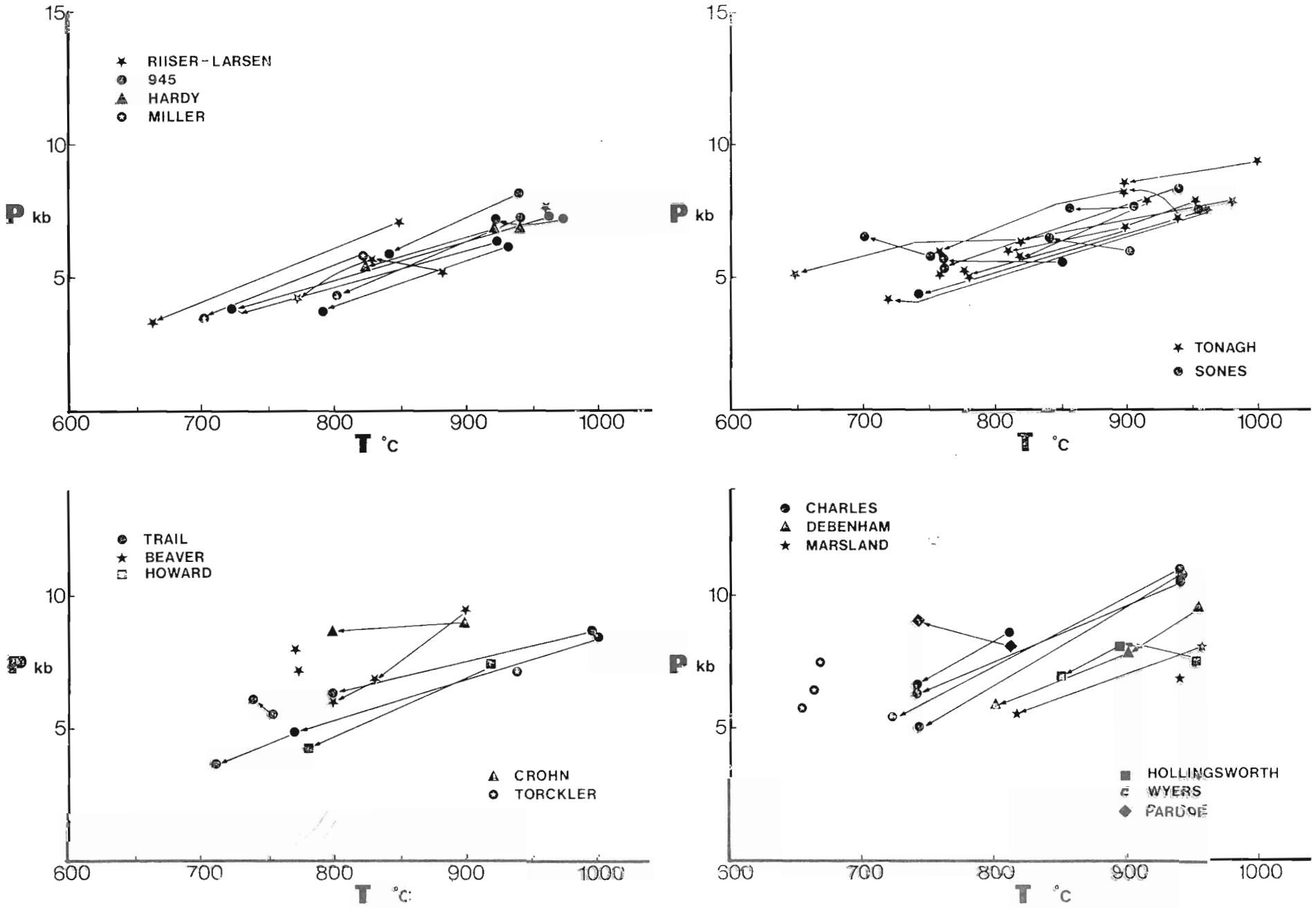

FIG. 6.15 P-T trajectories for ga-opx samples from the Napier province. Data given in Table 6.1 Specific P-T points based on core, rim, and recrystallised grain analyses.

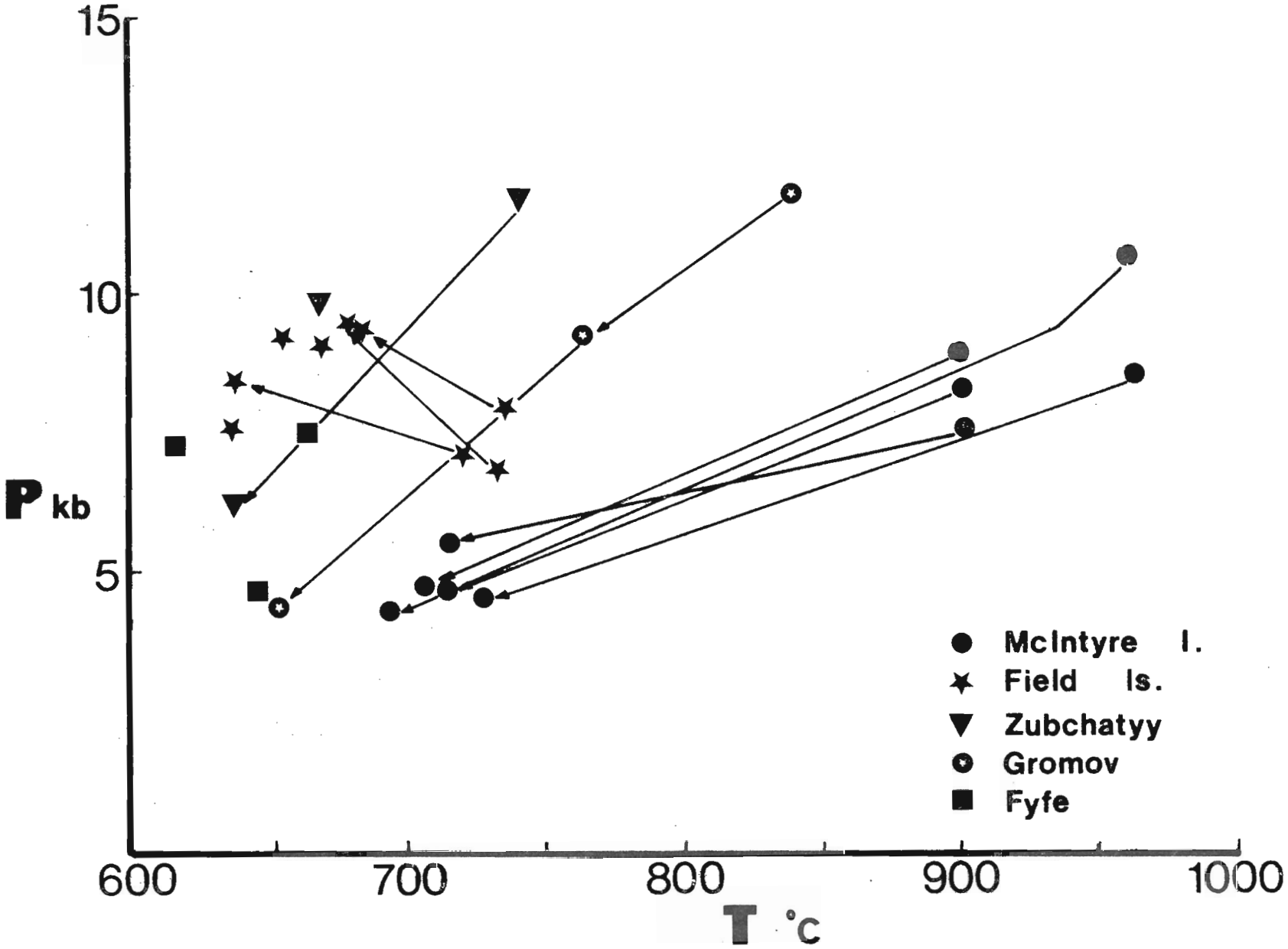

Fig. 6.16 P-T-time trajectories for ga-opx (±cpx) samples from the Casey Bay area and Gromov Nunatak. P-T points are based on core, rim, and recrystallised grain analyses.

in the range 7-8 kbar. The opx-sill assemblage in 49817 yields a minimum pressure of 7 kbar at 950°C.

In the Scott Mountains further south of Amundsen Bay, and in the Casey Bay area, pressures during the peak of M1 may have been greater than those further north in the granulite terrain. Samples from Debenham Peak and Mount Charles, where primary opx-sill-qz was a stable M1 assemblage, indicate pressures of 9.5-11 kbar at 950 ± 30°C. Peak M1 conditions at McIntyre Island and Hydrographer Island, where coexisting opx-sill and opx-sill-qz are recorded, are estimated to have been 9-11 kbar at 950-980°C.

P-T data obtained using garnet-orthopyroxene thermometry and barometry developed in earlier chapters would thus suggest a metamorphic peak at temperatures of 950°C, recorded in the cores of coexisting garnets and orthopyroxenes. Pressures in the Tula Mountains and around Amundsen Bay during this peak are estimated to have been 7-9 kbar, while the pressures may have been greater further south (9-11 kbar). These conclusions are in agreement with those of Sheraton *et al.* (1980) who suggest an increase in pressure to the southwest of Amundsen Bay. Grew (1980) has estimated P-T conditions of 7 ± 1 kbar and 900 ± 30°C for the formation of sapphirine-quartz assemblages in the Tula Mountains, in reasonable agreement with the peak M1 conditions suggested here for that region.

Ellis (1980) has estimated peak metamorphic conditions of 8-10 kbar at 900-980°C for osumilite-sapphirine-quartz bearing granulites from Spot Height 945 in the Tula Mountains. Garnet-orthopyroxene Fe-Mg distribution thermometry applied herein yields maximum temperatures of 910-970°C for samples from this locality (3532; and Ellis, 1979a), in good agreement with the estimates of Ellis (1980). Pressures estimated using the Al_2O_3 contents of orthopyroxene as a geobarometer

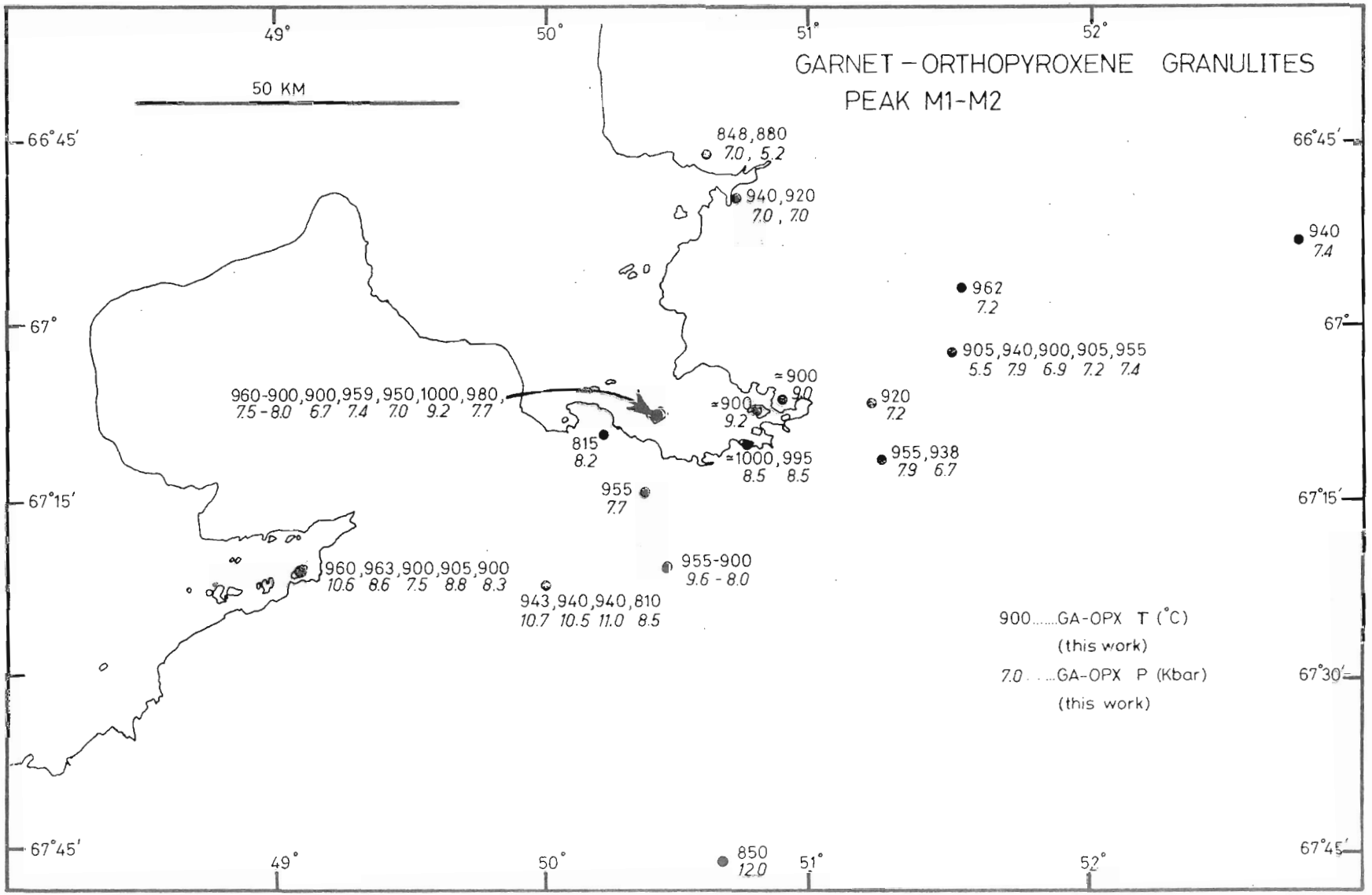

FIG. 6.17 REGIONAL DISTRIBUTION OF PEAK P-T CONDIONS BASED ON GA-OPX CORES

(Chapters 2 and 3) are 6.2-7.5 kbar at these temperatures, some 2 kbar below the estimates of Ellis (1980). These calculated pressures are minima however, as Fe^{3+} in both orthopyroxene and garnet has not been considered in the estimation of X_{Al}^{opx}, X_{Mg}^{opx} and X_{Mg}^{ga}. Allowing for these errors, garnet-orthopyroxene geobarometry (Chapters 2 and 3) would indicate pressures of 7-9 kbar at this locality during the metamorphic peak.

In plagioclase-bearing garnet-orthopyroxene-quartz assemblages pressures can be estimated using the barometer of Wells (1979) with activity coefficients for the various phases included (Appendix 3). Pressures estimated by this technique are in the range 7-10 kbar at 900°C for samples from both the Tula and Scott Mountains. These estimates are in very good agreement with the range of pressures obtained from garnet-orthopyroxene barometry.

One layered sample (3964) from Debenham Peak contains the assemblage garnet-sillimanite-plagioclase-quartz. Application of the barometer of Ghent (1976) with suitable activity coefficients included for garnet and plagioclase yields a pressure of 7 kbar at 950°C for this sample, compared with 9.5 kbar estimated from garnet-orthopyroxene barometry.

II. P-T CONDITIONS ESTIMATED FROM RIM COMPOSITIONS

Rim compositions of primary metamorphic garnet and orthopyroxenes yield P-T conditions which may relate to grain boundary re-equilibration during D2 or to post-D2 cooling. In samples where polygonal granuloblastic D2 textures are strongly developed, core analyses may be identical to rim analyses and no earlier higher-T peak may be estimated.

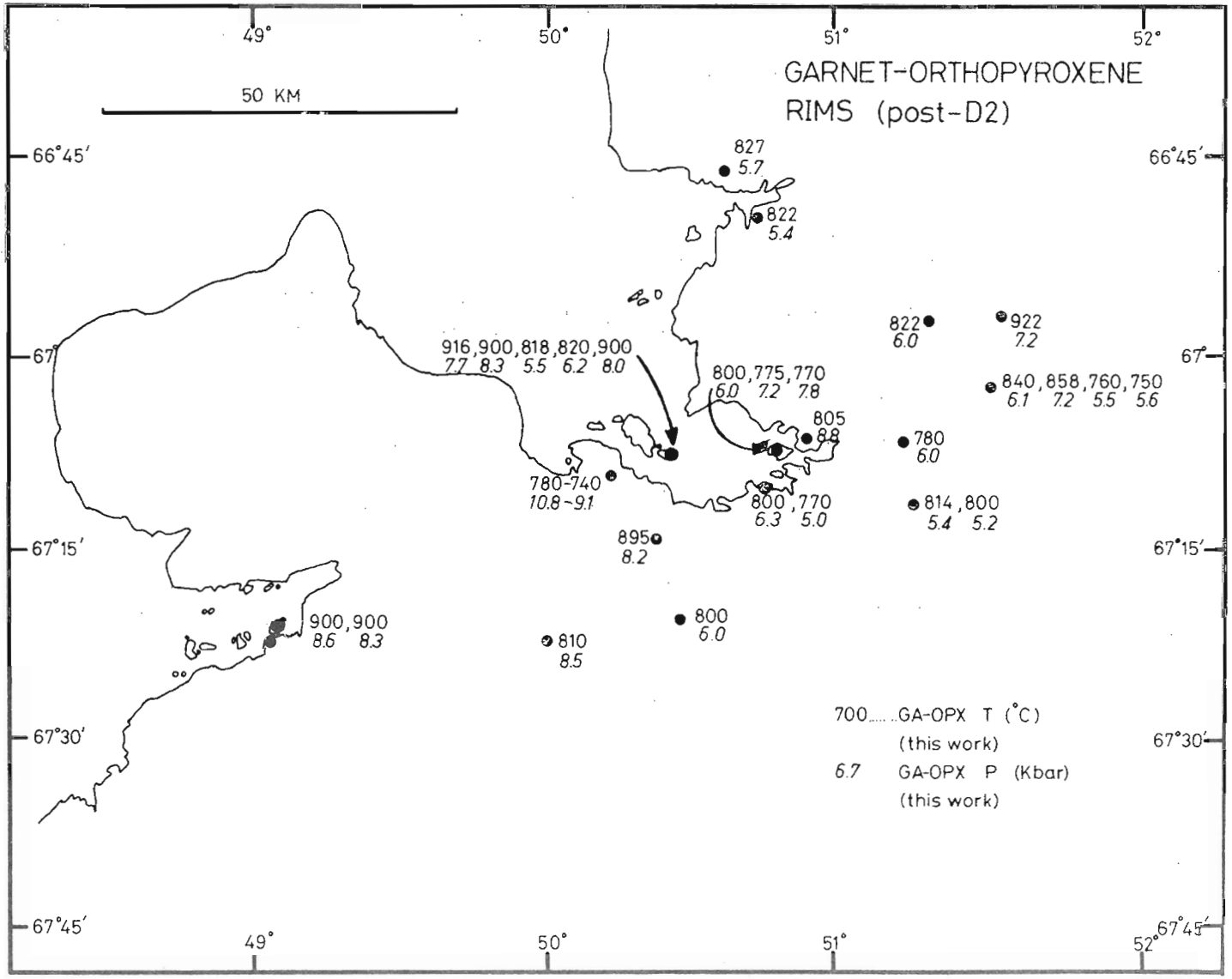

FIG. 6.18 REGIONAL DISTRIBUTION OF P-T CONDITIONS BASED ON GA-OPX RIM ANALYSES

Temperatures estimated from ($K_{D_{Fe-Mg}}^{ga-opx}$) rims are in the range 800-850°C for most samples where later recrystallisation is not evident (figures 6.16 and 6.15; table 6.1).

In the Tula Mountains (e.g. Mts Sones, Hardy, Miller, Riiser Larsen, Marsland, Howard Hills, Tonagh Island, Mt Trail, Hollingsworth, Beaver Island), pressures deduced from rim analyses of primary orthopyroxene grains coexisting with garnet are in the range 5-7 kbar, at 800-850°C. Specific localities where a number of samples are available show excellent clustering of P-T estimates for equilibration of rims (e.g. Mount Sones, 5.5-6.5 kbar; Tonagh Island, 5.5-6.2 kbar). Such clustering may be a record of a separate thermal event related to D2 or may be a result of the crossing of blocking temperatures of intergrain diffusion on cooling, in the absence of recrystallisation.

Samples from Crohn Island and Mount Pardoe, in the Amundsen Bay area, indicate greater pressures (8-8.5 kbar) at 800°C. Similar pressures are estimated for coexisting garnet-orthopyroxene rims from samples at Mount Charles in the Scott Mountains.

III. P-T CONDITIONS OF FORMATION OF CORONAS AND RECRYSTALLISED GA-OPX PAIRS

Pertinent compositional data and P-T estimates for the secondary (retrograde) assemblages described in section 6.2 are presented in table 6.1 . These P-T estimates are plotted on the P-T paths of figures 6.16 and 6.15, and a regional map of the distribution of P-T estimates is presented in figure 6.19.

Recrystallised ga-opx assemblages in metapelitic rocks from the Tulo Mountains give P-T conditions of 4-6 kbar and 700-750°C. A suite of samples from Mount Sones suggests recrystallisation at 4.2-5.6 kbar

and 740-760°C, while strongly recrystallised samples from Tonagh Island yield P-T estimates of 5-6 kbar and 740-780°C for the recrystallisation. At some other localities, recrystallisation of secondary garnet appears to have taken place at higher pressures (9-7 kbar, Mt Pardoe) or lower pressures (3.5 kbar, Mt Trail) in the same temperature range (700-750°C).

Recrystallised ga-opx and ga-opx-sill assemblages inferred to have developed in D3 at Mount Charles give P-T estimates of 5-6.5 kbar at 740-720°C. Extensive recrystallised ga-opx assemblages at McIntyre Island, also possibly developed during D3, are suggested to have formed at 4.5-5.5 kbar at 700-730°C. Just south of this locality, at Zircon Point (informal name), garnet-bearing coronas formed on primary orthopyroxene-plagioclase assemblages at 7-8 kbar and 720-740°C. Further compositional zoning in these coronas indicates continued equilibration to lower temperatures of 640-680°C at pressures of 8-9 kbar. The latter P-T conditions are in good agreement with conditions prevalent after D3 at Fyfe Hills (650°C, 5-7.5 kbar; see Chapter 5) and Hydrographer Island (640-670°C, 7.7-9.2 kbar).

Post-D2 recrystallisation and corona formation appear to have progressed at P-T conditions of 700-750°C and 4-7 kbar over much of the Tula Mountains-Scott Mountains area. Lower temperatures of 650°C and pressures of 5-9 kbar are indicated for corona formation in assemblages where garnet was not a primary metamorphic phase. In some cases the correlation of the P-T estimates with D3 time can be demonstrated on the basis of textural information, however many recrystallised assemblages may only be recording a post-D2 cooling history rather than the overprinting of earlier assemblages by D3 deformation.

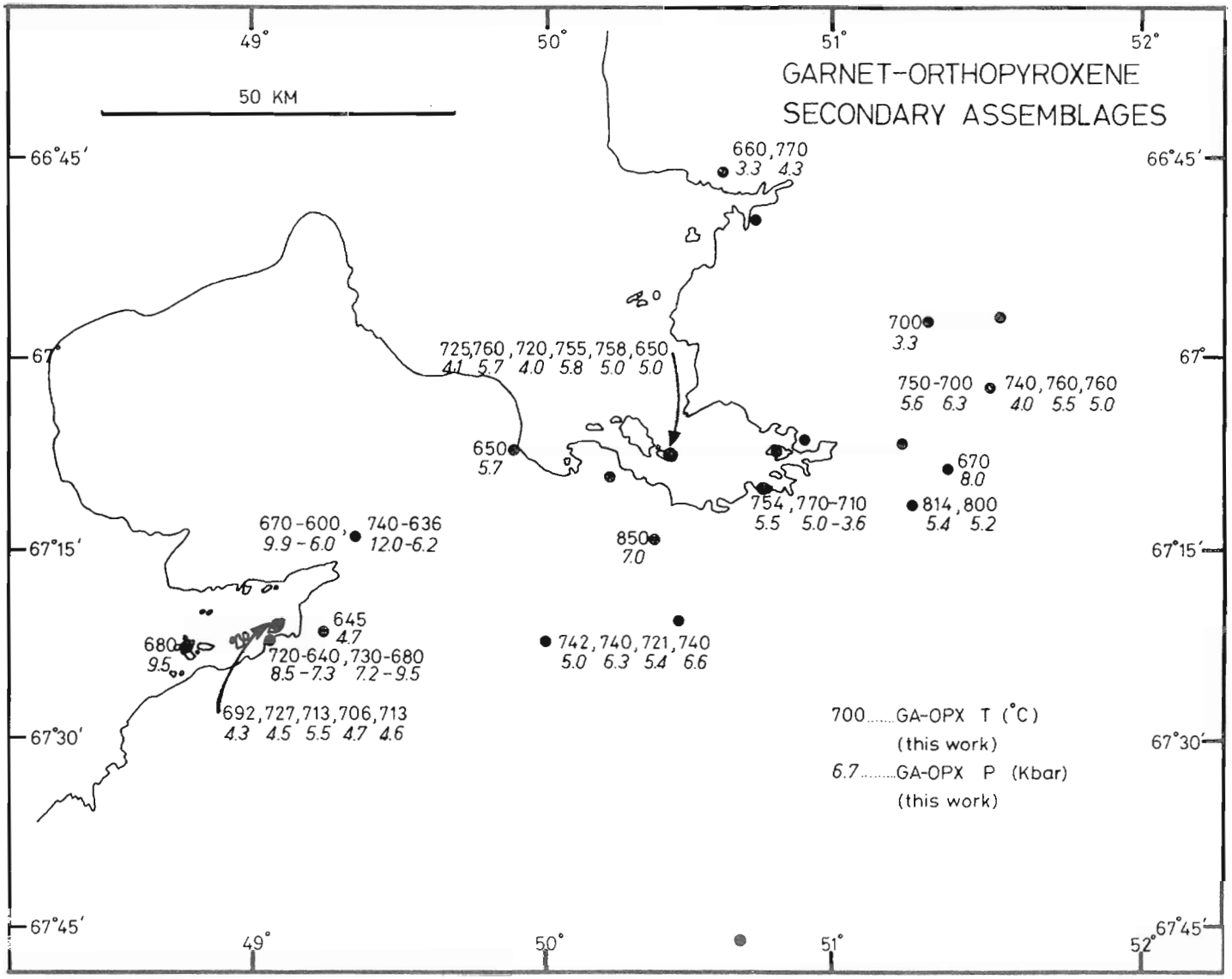

FIG. 6.19 REGIONAL DISTRIBUTION OF P-T CONDITIONS INFERRED FOR THE FORMATION OF SECONDARY GA-OPX ASSEMBLAGES.

IV. P-T TRAJECTORIES BASED ON GARNET-ORTHOPYROXENE THERMOMETRY AND BAROMETRY

P-T paths for individual samples and groups of samples are presented in figures 6.16 and 6.15. The recognition of several generations of garnet and orthopyroxene has enabled the construction of these paths, which record the P-T evolution of the southwestern part of Enderby Land through time from D1-D2 to D3. The most prominent feature of these P-T - time paths is the near-isobaric cooling path demonstrated for western Enderby Land over the time span 3100 m.a. (D1) to 2500 m.a. (D3). This feature, and other features of these P-T trajectories, will be discussed along with P-T information recorded in Chapter 5, in a general review of the metamorphic evolution of granulites from Enderby Land presented in the following chapter.

Chapter 7

THE METAMORPHIC EVOLUTION OF THE NAPIER PROVINCE AND IT'S IMPLICATIONS FOR ARCHAEAN TECTONICS

7.1 METAMORPHIC EVOLUTION OF THE NAPIER PROVINCE

A summary of the P-T estimates obtained in Chapters Five and Six and by other workers for granulites from the Napier province is presented in Table 7.1. The constraints of mineral equilibria have enabled the elucidation of peak metamorphic conditions inferred to be related to D1 or D2 deformation episodes, cooling paths from this peak, and P-T conditions prevalent during D3 (2500 m.a.). Such P-T estimates, based on differed thermometers and barometers, are distinguished in Table 7.1.

(a) Comparison of the thermometers/barometers

This comparison is made for the data from southwestern Enderby Land (figures 5.22, 5.23 and 6.17-6.19). The sensitivity of the various thermometers and barometers and some indication of their closure temperatures (e.g. Ellis, 1980), can be judged from the data obtained in Chapter 5 and 6 and summarized in Table 7.1. Consistent T estimates for peak metamorphic conditions are obtained using a range of techniques (Table 7.1). In general, over a large area (10,000 km^2) temperatures of greater than 900°C, and probably as high as 950°C, were attained during or after D1 and perhaps in D2 (~3000 m.a.). A variety of geobarometers, in particular the garnet-orthopyroxene Al_2O_3 barometer developed herein, indicate pressures of 6-10 kbar corresponding to crustal depths of ≈20-30 kilometres during this metamorphic peak. These pressures are suggested to have been sustained during post-D2 cooling to temperatures of 800-700°C.

Metamorphic temperatures prevalent during D3 are estimated at 620-720°C by garnet-clinopyroxene Fe-Mg exchange thermometry (Ellis and Green, 1979) and garnet-orthopyroxene Fe-Mg exchange thermometry

Table 7.1 P-T ESTIMATES FOR THE NAPIER PROVINCE, ENDERBY LAND

THERMOMETER / BAROMETER	M1-M2 PEAK IN D1-D2 3000 M.A.	COOLING/ EXSOLUTION	SYN- AND POST-D3 2500 M.A.
TEMPERATURES °C			
Gar-cpx Fe-Mg K_D	890 -850	—	720 - 620
Gar-opx Fe-Mg K_D	1000 - 860	800 - 700	700 - 640
Fe pigeonite stable	960 - 925	—	—
Sa-qz stable (Ellis, 1980)	950	—	—
Gar-biot Fe-Mg K_D	—	—	650 - 600
Two-pyroxene solvus	950 - 900	800 ± 30	750
PRESSURES (KBAR)			
Cpx-plag-qz (Ellis,1980)	12 - 10	—	—
Gar-opx Al_2O_3	6 - 8 Tula 7 - 10 Scott	7 - 5	9 - 7 and to 5
Gar-sill-plag-qz	7 ± 1	—	—
Gar-opx-plag-qz	10 - 7		10 - 8.5
Gar-cd-sill-qz	6 ± 1 Napier	—	—
Sillimanite stable	11 at 950 °C	8 at 750 °C	7 at 650 °C

(Chapter 2 and 3). In comparison, garnet-biotite Fe-Mg exchange (Ferry and Spear, 1978) suggest temperatures of 600-650°C for the formation of secondary biotite in D3 or after D3. The two-pyroxene solvus thermometers yield minimum temperatures for recrystallised pyroxene assemblages which are higher than suggested by Fe-Mg exchange thermometers. At low temperatures (< 800°C), the two-pyroxene thermometry is unreliable as it is rather insensitive to large changes in temperature and because of the possibility that the recrystallisation reactions in D3 proceed at temperatures below the blocking temperature of the two-pyroxene miscibility gap (Ellis, 1979).

Pressures attained during D3 are suggested to be 7-8 kbar, based on the continued stability of sillimanite in most metapelites but sporadic occurrence of kyanite in some localities (e.g., Sheraton *et al.*, 1980) and the stability of garnet in rocks approaching a quartz-tholeiite bulk composition (Chapter 5, figure 5.24). Garnet-orthopyroxene Al_2O_3 barometry suggests pressures of 7-9 kbar, just within the kyanite stability field (fig. 5.24), for the formation of garnet-bearing coronas in *clinopyroxene-bearing* samples (Chapter 5, figure 5.23). Recrystallised garnet-bearing assemblages and garnet-coronas, possibly formed during D3, which occur in metapelites and *clinopyroxene-absent* orthopyroxene + plagioclase rocks (Chapter 6), suggest pressures of 5-8 kbar over a broad area of southwestern Enderby Land at this time (fig. 6.19). These latter pressures are consistent with the observation that secondary garnet-clinopyoxene-qz assemblages are only sporadically and locally developed in the metaigneous two-pyroxene granulites of the Napier province, and are mainly restricted to the Scott Mts/Casey Bay area (fig. 5.23).

(b) Regional distribution of P-T conditions at peak (M1)

A synthesis of P-T estimates obtained in Chapter 5 and 6 for primary metamorphic mineral assemblages based upon core analyses, is presented in figure 7.1. Temperature estimates recorded in this figure are based on maximum 2-pyroxene temperatures, the stability of pigeonite, and $K_{D_{Fe-Mg}}^{ga-opx}$ thermometry. Pressures indicated in Figure 7.1 are based on garnet-orthopyroxene Al_2O_3 barometry of samples considered in Chapter 6. Pressures calculated from CaTs-An-Qz equilibria (Chapter 5) are generally greater (by $\simeq$ 2 kbar) than those reported on figure 7.1, but are not considered reliable for reasons discussed in Chapter 5.

In the Tula Mountains-Amundsen Bay-Scott Mountains region, peak metamorphic temperatures attained at perhaps 3000 ma.(in D1-D2) consistently reach 950°C. A regional pressure gradient is indicated, however, by comparison of the P-T paths depicted in figure 7.1a and 7.1b. In the Tula Mts-Amundsen Bay region M1 pressures are 6-8 kbar, while southwards in the Scott Mts. (Mt. Charles) and in the Casey Bay-Fyfe Hills areas pressures of 7.5-11 kbar are suggested by the garnet-orthopyroxene Al_2O_3 barometer. Al_2O_3 contents in orthopyroxenes from garnet-orthopyroxene samples from the Tula Mts-Amundsen Bay area are in the range 9-11 wt%, while in the Scott Mts-Casey Bay region Al_2O_3 contents are 6-8 wt%.

(c) Regional distribution of P-T conditions post-D2 and during D3 (2500 ma)

The regional pattern of P-T conditions attained subsequent to D2, in a period of post-deformational cooling, is indicated in figures 6.18, 6.19 and 7.1. These diagrams are based on data obtained from zoning relationships in minerals and rim or recrystallised grain compositions

Fig. 7.1 Summary of P-T estimates and P-T-time paths constructed for granulites from the Napier province from the data of Chapter 5 and Chapter 6. Diamond shaped boxes cover P-T estimates for peak, cooling, and D3 episodes as indicated. Slopes of upper and lower lines bounding these diamonds are the slopes of Al_2O_3 isopleths (opx). Arrows connect P-T data obtained from individual samples and groups of samples from adjacent or nearby localities.

a. Tula Mts. and Amundsen Bay localities. Sample from Crohn Island indicated by sloping lines at 12 kbar, 900-940 °C

b. Scott Mts. and Casey Bay area. Open diamonds for sample from Mt. Hollingsworth. Separate arrow joins P-T data secondary ga-opx assemblages from Fyfe Hills and Zircon Point. (low T diamonds).

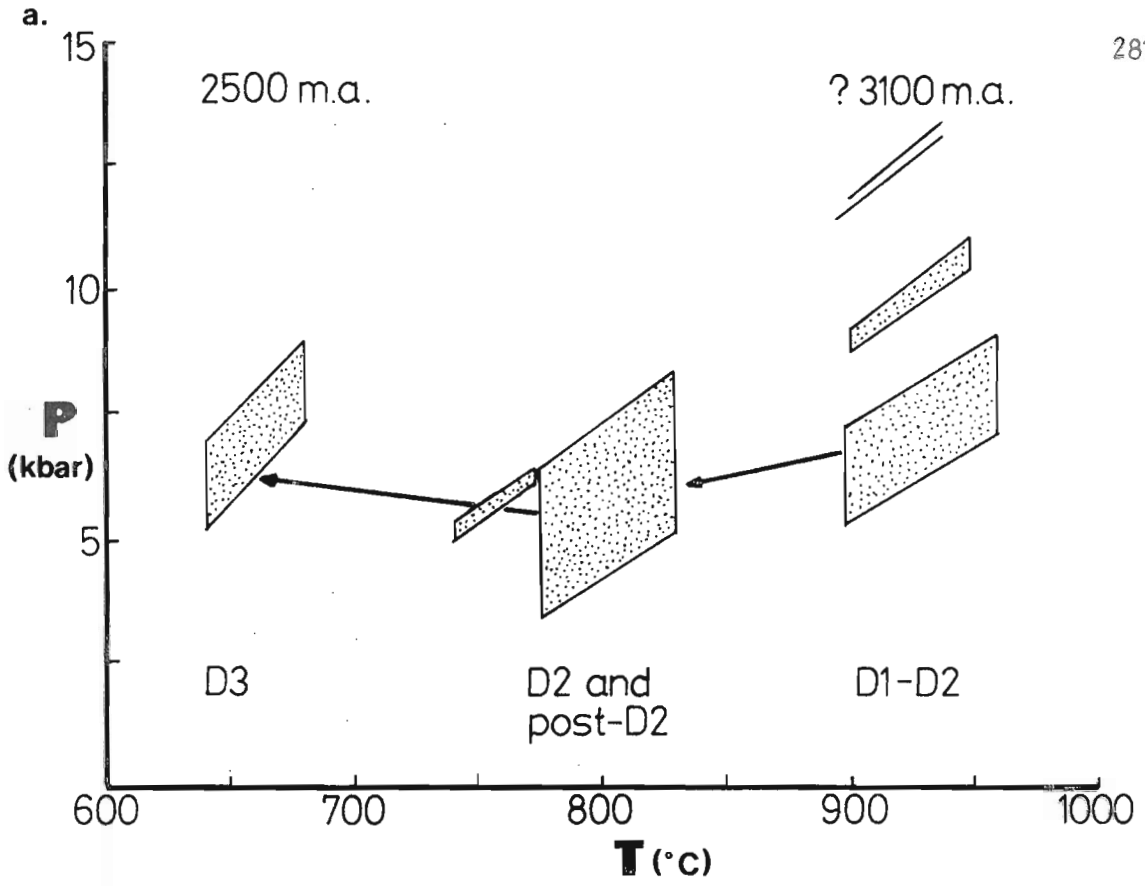
a.
15
10
5
P
(kbar)
2500 m.a.
? 3100 m.a.
D3
D2 and
post-D2
D1-D2
600
700
800
900
1000
T (°C)

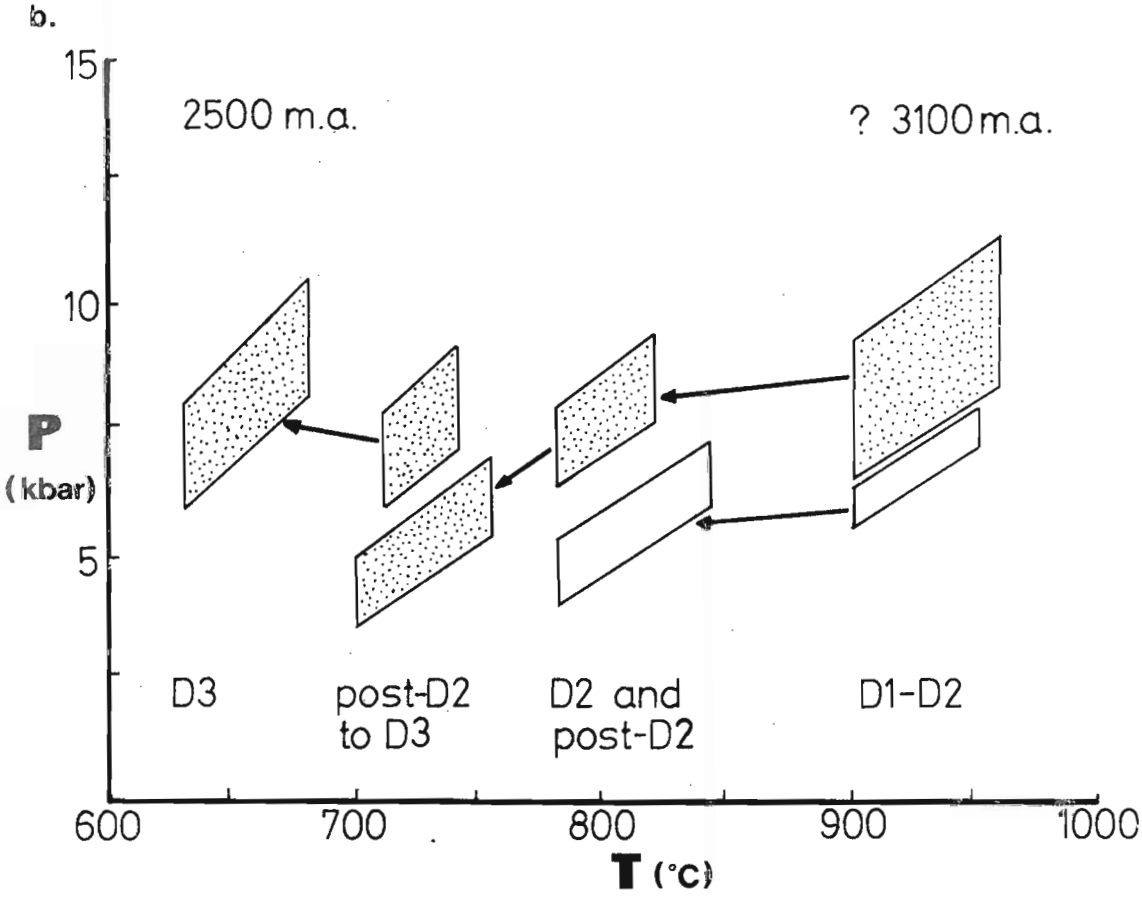
b.
15
10
5
P
(kbar)
2500 m.a.
? 3100 m.a.
D3
post-D2
to D3
D2 and
post-D2
D1-D2
600
700
800
900
1000
T (°C)

documented in Chapter 6. The data may not necessarily represent P-T conditions prevailing in the Napier province at one point of time because of the lack of adequate knowledge of the timing of recrystallisation or rim-composition adjustment in different samples in relation to D3 and because of the long time span (300-500 ma) between D2 and D3, inferred from geochronological data (James and Black, 1981).

P-T estimates over the whole Tula Mts-Scott Mts area for the D2-D3 interval are consistently in the range 5-7 kbar and 800-600°C. P-T conditions deduced specifically to relate to D3 recrystallisation are also illustrated in Figure 7.1, and indicate lower temperatures during this deformation episode than were prevalent during post-D2 cooling. Orthopyroxene Al_2O_3 barometry of Ca-rich garnet + clinopyroxene + orthopyroxene assemblages discussed in Chapter 5 indicate pressures of 7-9 kbar during the D3 event south of Amundsen Bay. These pressures are somewhat higher than those estimated in Chapter 6 for recrystallised Ca-poor garnet + opx assemblages thought to have formed during D3 (5-7 kbar) in the same geographic area. This discrepancy may be a real pressure difference of up to 2 kbar, linked with different timing of the garnet-forming reactions in relation to D3 deformation and post-D3 shearing, or the 2 kbar discrepancy may be an artifact of the geobarometer calibration. The cpx-opx-ga assemblages of Chapter 5, for which the higher D3-event pressures are obtained, are the most Fe- and Ca-rich garnet-orthopyroxene assemblages studied from the Napier complex. As the garnet-orthopyroxene barometer applied to these rocks was calibrated in the Ca-bearing system only for more magnesian compositions ($X_{Mg}^{opx} \simeq 60$) (Chapter 3), and as symmetrical regular solution behaviour in Ca-Mg-Fe was assumed for garnet in the thermodynamic treatment of the experimental data, any deviations from the

assumptions in Chapter 3 may lead to an overcorrection for the effect of Ca on Al_2O_3 solubility in orthopyroxene in the Fe-rich systems where the X_{Ca}^{ga} compositional term of equation 3(15) is larger.

Notwithstanding these possible errors in the geobarometry, the P-T conditions inferred for the period around D3 (2500 ma) in the Napier province are consistent with the observed mineral assemblages formed during that period and the apparent continued stability, in most areas, of sillimanite. The estimated pressures for ga-cpx-opx assemblages (see figure 5.24) lie within the kyanite stability field (Day and Kumin, 1980) but kyanite is only rarely observed in metapelites affected by D3. The P-T estimates are, in general, within 1 kbar of the kyanite-sillimanite inversion, and there is sufficient error in the barometry-thermometry ($\pm$ 1 kbar, and $\pm$ 50°C minimum errors) to allow the stability of sillimanite *or* kyanite in aluminous metapelites during D3.

(d) Retrograde (cooling) P-T paths for the Napier Complex in the interval 3000-2500 ma.

The P-T information given in Chapters 5 and 6 is summarized in the two regional P-T trajectories given in Figure 7.1a and b. In the Tula Mts-Amundsen Bay region (figure 7.1a), the thermometry-barometry techniques indicate a cooling history, or an episodic P-T evolution, over a temperature range of $\simeq$ 300°C in the period 3000(?)-2500 ma. During this interval, pressures decreased from 6-8 or 9 kbar at $\simeq$ 3000 ma, to 4-6 or 7 kbar after D2 and possibly near D3 time. In the Scott Mts-Casey Bay region, initial peak metamorphic pressures were greater (8-11 kbar) but a similar parallel P-T-time trajectory can be constructed.

In a strict sense, the P-T trajectories illustrated in Figures 7.1a

and b, and previously depicted in Figures 5.24, 5.15 and 6.16, are not continuous P-T paths as the data on which they are based is necessarily of a discrete or episodic nature. The actual P-T-time path of a particular sample between any two P-T datum points, such as obtained from core analyses and contrasting rim analyses, cannot be determined. The fact that garnet does not break down between cores and rims (or recrystallised grains), and that sillimanite does not invert to kyanite during growth, constrains the possible path between any two P-T datums obtained for a particular rock and indicates that wild fluctuations of pressure did not occur between P-T points. Thus, arrows drawn directly between the separate P-T boxes of Figure 7.1 are considered to be reasonable mean P-T-time paths.

The trajections drawn in Figure 7.1(a) and (b) may be interpreted in two contrasting ways:

(1) The P-t-time paths are *cooling paths*, i.e., a continuous cooling from peak metamorphic conditions down to temperatures where reaction kinetics are so sluggish that no further textural and compositional adjustment occurs. In this interpretation, reaction coronas and recrystallised secondary assemblages are considered to be formed by the gradual "overstepping" of reaction boundaries or by the continuous movement of 3-phase fields across bulk compositions during cooling. The euhedral shapes of secondary garnets, the formation of garnet both as exsolution lamellae and thin rims along pyroxene grain boundaries, the presence of randomly oriented reaction coronas in some samples, and the continuous near-rim zoning in some coexisting minerals are all consistent with such an interpretation.

(2) The P-T-time data points record separate, distinct metamorphic-deformational (tectonothermal) *episodes*, i.e., each P-T data point for

a sample records an actual "event". In this interpretation, the corona and recrystallisation textures are related to definite thermal peaks or jumps which punctuate the general P-T-time evolutionary path. Such an interpretation allows loops, jumps and gaps in the P-T path. The association of many coronas and secondary recrystallised assemblages with D3 textural features, the alignment of coronas and recrystallised trails in some samples, and the distinct higher-pressure regime indicated for some corona assemblages are evidence in favour of this interpretation for at least the lower temperature part of the P-T path (D3 tectonothermal event).

The generalised P-T-time trajectory for these granulites from the Napier Complex is one of near-isobaric cooling over an, apparently, prolonged period of time. This P-T trajectory is consistent with the isobaric cooling history of Enderby Land proposed by Ellis *et al.* (1980) and Ellis (1980), based on studies of aluminous metapelites. Cooling through 300°C has occurred over a time span of some 200-500 ma, with uplift during this interval of only 6-9 kilometres from original crustal depths of 21-30 kilometres. The (dP/dT) path of the granulites now exposed in Enderby Land was only 10 bar/°C in the D1-D3 interval (2-3 km uplift per 100°C), a shallow evolutionary path in contrast to the near-isothermal uplift trajectories inferred for many other metamorphic terrains (e.g., Norway - Griffin, 1971; Scotland - O'Hara, 1977). Using a time span of 500 ma. to 200 ma. for the interval between D1-D2 and D3, and the P-T estimates of Table 7.1 and Figure 7.1, calculated uplift rates are very slow indeed (2-6 cm/1000 years). Such uplift rates, and related erosion rates, correspond to a tectonically stable crustal environment but may be unrealistically low as the combined effects of more rapid uplift-cooling and prolonged periods of stability

at near P-T conditions are smeared out.

P-T data suggest some crustal thickening and deepening at the time of D3 (Figure 7.1), in the southern part of the area studied.

7.2 TECTONIC IMPLICATIONS OF P-T-TIME EVOLUTIONARY PATHS

The recognition of near-isobaric cooling over an extended time interval (200-500 ma) for the Napier province granulites provides a constraint on the possible tectonic models applicable to the metamorphism and evolution of this region of Archaean lower crust.

An isobaric or near-isobaric cooling path for a metamorphic province is a product of the interaction between erosion rates of tectonically thickened crust and thermal relaxation of the crust to the steady-state geothermal gradient. England and Richardson (1977) have shown that near-isothermal uplift paths will be characteristic of metamorphic belts formed by continental collision or overthrusting processes, where rapid erosion rates of the tectonically thickened pile predominate. In contrast, moderate to isobaric cooling paths may be developed in metamorphic belts formed in crust thickened by magma addition if conductive relaxation dominates over erosion rates. Wells (1980) has developed magma-accretion models for the metamorphism of Archaean crust dominated by metaigneous rocks, wherein near-isobaric cooling paths may be generated given sufficiently long periods of accretion of large quantities of magma and slow erosion rates (e.g. accretion times of 20 ma.)

Two major problems with magmatic-accretion models for the tectonic evolution of the Napier complex in the Archaean are:

(1) The time-span of the near-isobaric cooling path for the Napier complex is extremely long.

(2) The multiple-deformation history cannot be correlated with successive magma-additions, in fact intrusive magmatic bodies are rare in the Napier province. Definite evidence of large scale magmatic additions to the crust prior to or during M1 is very limited as intrusive charnockites are only rarely observed. The ultimate origin

(i.e., volcanic/crustal or intrusive) of the layered pyroxene granulites and the widespread charnockite-pyroxene granulite sequence is not known.

On the basis of a large positive modified free air gravity anomaly under the granulites of the Napier province (Wellman and Tingey, 1977), Ellis (1980) has postulated the presence of a mantle diapir (i.e., "hotspot") or mantle derived magmas under the granulites. Such a diapir or magmatic accumulation may have acted as a heat source responsible for the high temperature peak metamorphism.

It is generally agreed that the metamorphism of the Enderby Land granulites, and the subseqeunt near-isobaric cooling history, has been produced by some magmatic or diapric (mantle "hotspot") disturbance in the basal heat flux into the lower crust (Ellis, 1980; Sheraton *et al.*, 1980; Grew, 1980). Grew (1980) proposes further that the apparent regional metamorphic terrain of the Napier province may be a regional-scale aureole overlying deeper anorthositic (or magmatic) massifs, analogous to the granulites of the Nain Complex (Berg, 1977a). However, anorthosites have not been observed in the Napier province (except for very minor, local anorthositic layers), nor have other intrusives commonly associated with anorthositic complexes (e.g., syenites).

An alternative model for the metamorphic evolution of the Napier province involves a change in conductive basal heat-flux into the lower crust resulting from movements of the thickened crust over a laterally heterogeneous mantle.

It is envisaged that the thickened crust may have moved across underlying mantle and become resident upon a relatively fertile,

undepleted, radioactive-element enriched area of upper mantle which provided a greater basal heat flux into the crust over a prolonged period of time. Migration of the Archaean craton over such an enriched lateral heterogeneity in the mantle would lead, eventually, to a broad scale regional heating of the lower crust to temperatures above the steady-state Archaean geotherm. Continued migration of the deformed and heated crust back onto more differentiated and depleted mantle would result in slow thermal relaxation with low erosion rates as the heat source is removed.

The model outlined above requires two major characteristics in the Archaean crust-mantle system:

(1) An incompletely differentiated, laterally heterogeneous upper mantle in the Archaean (cf. Green, 1981).

(2) This upper mantle is virtually decoupled from the overlying crust, i.e. the continental crust comprised most of the continental lithosphere and did not drag a thick layer of mantle along with it. This characteristic is suggested by estimates of heat-production from radioactive elements present in the Archaean earth. Higher average heat-flow at 3000 ma. (e.g., Green, 1975, 1981; Davies, 1979; Tarney and Windley, 1977; Baer, 1977, 1981; Hargraves, 1978) may have resulted in thinner continental lithosphere than exists today. Several authors (Baer, 1981; Chapman and Pollack, 1977; Davies, 1979; Hargraves, 1978; Jordan, 1978) suggest that present day continental shield areas have thickened root zones corresponding to a lithosphere of chemically distinctive, "sub-continental" mantle up to 200-400 kilometres, such root-zones coupled to continental slabs would not be possible (e.g., Baer, 1981) until after the depression of steady-state geotherms in the sub-continental lithosphere was accomplished by depletion of this

mantle in radioactive elements through differentiation processes such as melting, formation of thickened crust, and granulite metamorphism (Baer, 1981). Prolonged crustal stability (as suggested by uplift rates determined from P-T paths) in the Napier province in the period after 3000 ma. and 2500 ma. may have been brought about by thickening of the sub-continental lithosphere which remained coupled to the continental crust.

The very slow uplift rates and apparent prolonged period of lower crustal residency for the Napier granulites (≃ 500 ma.) indicate that this area became an essentially stabilised craton after 3000 ma., with further deformations and tectonothermal events possibly representing adjustments of this stabilized and unified crustal area. The slow uplift rates have analogies in some Archaean-Proterozoic shield areas exposed in continental nucleii today. For example, the Gawler Block of South Australia is partly covered by undeformed shallow shelf sediments and flat lying volcanics of mid-late Proterozoic age (≃ 1100 ma.) (Gawler Range Volcanics). The present elevation of these sediments suggest uplift of the Gawler block of only 1 km over at least 900 ma. Lower crustal gneisses or granulites which underly the Gawler Block would thus have a prolonged history of development with negligible uplift rates.

Table 7.2 P-T ESTIMATES FOR ARCHAEAN HIGH GRADE TERRANES.

AREA	P(kbar)	T (°C)	REFERENCE
Greenland :			
Buksefjorden	7	630	Wells (1976),
	10.5	810	Wells (1979)
Fiskenaesset	5 - 6	650 - 700	Bickle (1978)
	7	800 - 900	
Ameralik	9 - 11	700 - 800	Griffin et. al. (1980)
Scotland :			
Scourie	15	1250	O'Hara (1977)
	12	1000	Savage and Sills (1980)
South Harris	10 - 13	800 - 860	Wood (1975)
	9 - 11	700 - 800	
U.S.S.R. :			
Aldan shield	11 - 12	925	Kitsul & Kopylov (1974)
Kola Peninsula	9 - 10.5	960 - 1020	Krylova & Priyatkina(1976)
Stanovik	4 - 5	835 - 875	Karsakov (1973)
Anabar massif	8	830	Lutts & Kopaneva (1968)
Limpopo Belt, Africa	10	800	Nixon et.al. (1973)
India :			
Sittampundi	7 - 8	850	Bickle (1978)
	9 - 10	800	
Western Australia :			
Quairading	5	800	Davidson & Mathison(1974)
Antarctica :			
Enderby Land	10	970	Ellis et. al. (1980)
	7	900 - 950	Grew (1980)
	7 - 11	950	this study

7.3 IMPLICATIONS FOR ARCHAEAN TECTONIC MODELS

Any thermal-tectonic models of crustal evolution in the Archaean, for instance, models deducing the intensity and importance of plate-tectonic processes, must fit the constraints of the extrapolated thermal budget of the earth (Bickle, 1978; Chapman and Pollack, 1977; Baer, 1981; Hargraves, 1978) and the geological constraints provided by studies of Archaean high-grade gneiss-granulite terrains and greenstone belts.

The P-T estimates obtained for Archaean metamorphic belts provide constraints on the thickness of continental crust, and on the maximum geothermal gradients in that crust, in the Archaean. As discussed previously and as considered by many workers (Turner and Verhoogen, 1960; Ellis, 1980; Bickle, 1978; Watson, 1978; England and Richardson, 1977), the metamorphic geothermal gradients obtained from studies of granulites will be higher than steady-state geotherms as the metamorphic geotherm is a disturbance of the steady-state condition.

The geobarometry of the Napier province granulites from southwest Enderby Land indicates that crustal thicknesses of at least 21-30 km were attained in the region by 3000 ma. These estimates are applicable to rocks now exposed at the surface and themselves underlain by $\leq$ 35-45 km of crustal material (Grew, in press).

Thus, crustal thicknesses of up to 60 km may have been developed in the Napier province by 3000 ma., or alternatively the present underlying crust may have been developed by underplating processes since the Archaean. The relative crustal stability inferred from estimated uplift rates for the Napier province in the period 3000 ma-2500 ma. suggests that substantial additions to the crust were accomplished before 3000 ma. and that the Napier province then acted as a stabilised continental

nucleus, with a crustal thickness similar to present-day shield areas. P-T data for other Archaean high-grade metamorphic provinces (e.g., Chapter 4) also indicate substantial crustal thicknesses, similar to present-day shield areas, attained by the end of the Archaean.

Geothermal gradients for the Napier province granulites are moderate and comparable with those obtained from other Archaean and younger metamorphic belts. A gradient of 53-35 °C/km is calculated for the peak metamorphic conditions. Between ≈ 3000 ma. and 2500 ma. these geothermal gradients decayed to 47-31 °C/km (at 800-700°C) and 31-27 °C/km (at 650°C). These values are not higher than gradients estimated from most younger metamorphic belts. It is therefore suggested that the greater amounts of heat generated by decay of more abundant radioactive nuclides present in the Archaean earth must have been dissipated by faster or more intense crustal creation/destruction and convective processes operating in Archaean oceanic lithosphere, as proposed by many recent workers on Archaean thermal regimes (e.g., Bickle, 1978; Baer, 1981; Green, 1975, 1981; Hargraves, 1978).

Appendix 1

THERMODYNAMIC CONSIDERATIONS IN GARNET-ORTHOPYROXENE EQUILIBRIA

APPENDIX ONE

THERMODYNAMIC CONSIDERATIONS IN GARNET-ORTHOPYROXENE EQUILIBRIA

A1.1 INTRODUCTION

The reaction governing the Al_2O_3 content of orthopyroxene in equilibrium with garnet may be written as

$$Mg_2Si_2O_6 + MgAl_2SiO_6 = Mg_3Al_2Si_3O_{12} \quad (1)$$

orthopyroxene solid solution — garnet

(Boyd and England, 1964; MacGregor, 1974; Wood and Banno, 1973; Wood, 1974), for which the condition of equilibrium is

$$\mu_{Mg_2Si_2O_6} + \mu_{MgAl_2SiO_6} = \mu_{Mg_3Al_2Si_3O_{12}} \quad (2)$$

where μ refers to the chemical potential of the components in the phases. With the standard states taken as the pure phase at the T and P of interest, (2) becomes

$$\mu^{o}_{Mg_2Si_2O_6} + RT \ln a^{opx}_{Mg_2Si_2O_6} + \mu^{o}_{MgAl_2SiO_6} + RT \ln a^{opx}_{MgAl_2SiO_6} = \mu^{o}_{Mg_3Al_2Si_3O_{12}} + RT \ln a^{ga}_{Mg_3Al_2Si_3O_{12}} \quad (3)$$

(Wood and Banno, 1973)

μ^{o} = chemical potential of component in standard state

a^{i}_{j} = activity of component i in phase j.

Rearranging (3):

$$(\Delta G^{o})_{P,T} = -RT \ln \left(\frac{a^{ga}_{Mg_3Al_2Si_3O_{12}}}{a^{opx}_{Mg_2Si_2O_6} \cdot a^{opx}_{MgAl_2SiO_6}} \right) \quad (4)$$

that is, $(\Delta G^{o})_{P,T} = -RT \ln K$

Generally, $(\Delta G^{o})_{P,T} = (\Delta G^{o})_{1,T} + \int_{1}^{P} \Delta V^{o}\, dP$

$$= \Delta H^{o}_{1,T} - T\Delta S^{o}_{1,T} + \int_{1}^{P} \Delta V^{o}\, dP$$

$$\simeq \Delta H^{o}_{1,T} - T\Delta S^{o}_{1,T} + P\,\Delta V^{o}$$

where P is in kilobars, T in ^{o}Kelvin, and

$$\Delta V^{o} = V^{o}_{Mg_3Al_2Si_3O_{12}} - V^{o}_{Mg_2Si_2O_6} - V^{o}_{MgAl_2SiO_6}$$

Wood and Banno (1973) and Wood (1974) have previously established the use of both an ideal multisite solid solution model and a regular solution model for orthopyroxene. Before obtaining a final expression for equation (4), I will review the data and modelling of activity-composition relations in both garnet and orthopyroxene.

A1.2 GARNET SOLID SOLUTIONS

Garnets can be treated as two-site multicomponent solid solutions (Ganguly, 1979; Wood, 1974; Haselton and Newton, 1981), with three essentially equivalent 8-coordinated sites and two equivalent octahedral sites:

$$\infty_3\beta_2Si_3O_{12}$$

where ∞ = Ca, Fe, Mg, Fe^{3+}

β = Cr, Al, Fe^{3+}

in most important garnet compositions coexisting with orthopyroxenes. We will not consider Fe^{3+} in this treatment as most analyses are obtained from microprobe techniques. It must be recognised that Fe^{3+} will be important in some compositions and introduces one limitation to the applicability of the final barometry equation.

The general form of the garnet solid solution can be written as:

$$(Ca, Mg, Fe)_3\ (Al, Cr)_2\ Si_3O_{12}$$

and the activity of pyrope, $a^{ga}_{Mg_3Al_2Si_3O_{12}}$, is related to composition by the

the expression:

$$a^{ga}_{Mg_3Al_2Si_3O_{12}} = (X^{ga}_{Mg})^3 \ (X^{ga}_{Al})^2 \cdot \gamma_{Mg}{}^3 \cdot \gamma_{Al}{}^2$$

where γ_{Mg}, γ_{Al} are activity coefficients on each site. Wood and Nicholls (1978) have pointed out the possibility of reciprocal, or cross-site, interactions in Cr-rich garnets. These interactions are of the type Ca-Cr and Ca-Al, where the properties of one lattice site is partly dependent on the constitution of the other site. My experimental data applies to non-Cr bearing garnets, so reciprocal effects may be neglected, although they may become important in natural systems.

In FMAS, the garnet solid solution is essentially only a one-site mineral, $(X_{Al}) = 1$, and

$$a^{ga}_{Mg_3Al_2Si_3O_{12}} = (X^{ga}_{Mg})^3 \cdot \gamma_{Mg}{}^3$$

To evaluate $\gamma_{Mg}{}^3$, I have adopted a binary regular solution model for garnet in FMAS (Thompson, 1968; Ganguly, 1979; O'Neill and Wood, 1979), where:

$$RT \ln \gamma^{ga}_{Mg} = (1 - X^{ga}_{Mg})^2 \cdot W^{ga}_{FeMg} \qquad (5)$$

Hence

$$RT \ln a^{ga}_{Mg_3Al_2Si_3O_{12}} = 3RT(\ X^{ga}_{Mg}) + 3W^{ga}_{FEMg} \cdot (1 - X^{ga}_{Mg})^2 \qquad (6)$$

Previous estimates of W^{ga}_{FeMg} range from 2580 cal (Oka, 1978) and 3000 cal (Ganguly and Kennedy 1974) to 195 ± 215 cal (O'Neill and Wood, 1979) or zero (Wood and Nicholls, 1979).

$W^{ga}_{FeMg} = 0$ has been adopted in this treatment, based on the experimental work of O'Neill and Wood (1979) on garnet-olivine Fe-Mg partitioning. Hence,

$$RT \ln a^{ga}_{Mg_3Al_2Si_3O_{12}} = 3 \ln X^{ga}_{Mg}$$

in FMAS.

Table A1.1 MOLAR VOLUME DATA FOR ORTHOPYROXENES AND GARNETS IN FMAS

ENSTATITE	
V°_{298} (cm^3)	reference
62.88	Hensen and Essene (1971)
62.70	Matsui et. al. (1968)
62.69	Ganguly and Ghose (1979)
62.62	Danckwerth & Newton (1978)
62.6 *	Newton et. al. (1979)
62.52	Turnock et. al. (1973)
62.31	Arima and Onuma (1977)

FERROSILITE	
66.03	Matsui et. al. (1968)
66.02	Akaogi and Akimoto (1977)
66.00 *	Turnock et. al. (1973)

Al-ENSTATITE		
	mol% MgTs	reference
62.49	5.0	SB
62.53	5.0	AO
62.28	8.21	DN
62.15	8.80	GG
62.27	10.0	SB
61.96	10.0	C
62.18	10.0	AO
62.09	15.0	SB
61.99	15.0	AO
62.06	16.14	DN
61.92	20.0	SB
61.96	20.0	AO
61.80	24.25	DN
61.80	25.0	SB
61.89	25.0	AO
61.71	30.0	SB
61.78	30.0	AO
61.74	30.0	HE
61.42	50 extrap.	GG
60.29	100 extrap.	AO

PYROPE	
V°_{298} (cm^3)	reference
113.38	Ganguly and Kennedy (1974)
113.29	Skinner and Boyd (1964)
113.27	Hensen and Essene (1971)
113.24	Oka (1978)
113.23	Akaogi and Akimoto (1977)
	Newton et. al. (1977)
113.22	O'Neill and Wood (1979)
113.2	Cressey et. al. (1978)
113.13 *	Charlu et. al. (1975)
113.12	Takahashi and Liu (1970)

ALMANDINE	
115.45	Takahashi and Liu (1970)
115.37 *	Oka (1978)
115.35	Kawasaki and Matsui (1977)
115.34	Hsu (1968)
115.33	O'Neill and Wood (1979)
115.3	Cressey et. al. (1978)
115.29	Akaogi and Akimoto (1977)

abbreviations :

SB	Skinner and Boyd (1964)
AO	Arima and Onuma (1977)
DN	Danckwerth and Newton (1978)
GG	Ganguly and Ghose (1979)
C	Charlu et. al. (1975)
HE	Hensen and Essene (1971)

A1.3 ORTHOPYROXENE ACTIVITY-COMPOSITION RELATIONS

Following the work of Saxena and Ghose (1969), Virgo and Hafner (1970) and Wood and Banno (1973), the orthopyroxene solid solution is described in terms of a multi-site mixing model. The orthopyroxene contains two tetrahedral sites, A and B, and two non-equivalent octahedral sites, M1 and M2. It has been found (Takeda, 1972) that Al only enters the Si-B site and essentially is restricted to the M1 octahedral site (Ganguly and Ghose, 1980). Wood and Banno (1973) used a two-site mixing model thus:

$$a^{opx}_{Mg_2Si_2O_6} = X^{M2}_{Mg} \cdot X^{M1}_{Mg} \cdot \gamma^{opx}_{Mg_2Si_2O_6} \; (=\gamma^{M2}_{Mg} \cdot \gamma^{M1}_{Mg}) \qquad (7)$$

and $$a^{opx}_{MgAl_2SiO_6} = X^{M2}_{Mg} \cdot X^{M1}_{Al} \cdot \gamma^{opx}_{MgAl_2SiO_6} \; (\gamma^{M2}_{Mg} \cdot \gamma^{M1}_{Al}) \qquad (8)$$

, which assumes no contribution of the tetrahedral site to the entropy of mixing. Powell (1978) proposed a more complete a-X model based on the statistical models of Kerrick and Darken (1975):

$$a_{Mg_2Si_2O_6} = X^{M1}_{Mg} \cdot X^{M2}_{Mg} \cdot (X^{T}_{Si})^2$$

$$a_{MgAl_2SiO_6} = 4X^{M2}_{Mg} \cdot X^{M1}_{Al} \cdot X^{T}_{Al} \cdot X^{T}_{Si}$$

While these expressions allow more fully for the possibility of Al-Si disorder in the tetrahedral sites, in practice they are unwieldy and subject to large errors resulting from analytical errors.

In FMAS, orthopyroxene may be regarded as multisite regular solution (Thompson, 1968), with each sublattice behaving as a regular solution. Assuming Al in the M2 site is negligible, the M2 site can be treated as a binary regular solution in Fe-Mg; thus

$$RT\ln \gamma^{M2}_{Mg} = (X^{M2}_{Fe})^2 \cdot W^{M2}_{FeMg} \qquad (9)$$

Mixing of Fe-Mg-Al will occur on the M1 site, which can be treated as a ternary symmetric regular solution (Thompson, 1968). Expressions for the activity coefficients may be written as follows (Sack, 1980; Wood, 1974):

$$RT\ln \gamma_{Mg}^{M1} = (X_{Fe}^{M1})^2 \cdot W_{FeMg}^{M1} + (X_{Al}^{M1})^2 \cdot W_{MgAl}^{M1} + (X_{Fe}^{M1} \cdot X_{Al}^{M1})\ (W_{FeMg}^{M1} + W_{MgAl}^{M1} - W_{FeAl}^{M1}) \quad (10)$$

$$RT\ln \gamma_{Al}^{M1} = (X_{Fe}^{M1})^2 \cdot W_{FeAl}^{M1} + (X_{Mg}^{M1})^2 \cdot W_{MgAl}^{M1} + (X_{Mg}^{M1} \cdot X_{Fe}^{M1})\ (W_{FeAl}^{M1} + W_{MgAl}^{M1} - W_{FeMg}^{M1}) \quad (11)$$

It must be noted that these expressions represent on-site terms only, that is the non-ideal contribution to the macroscopic activity of a component in the multisite solid solution which arises only from interactions on one type of site. As shown by Oka (1977), Wood and Nicholls (1978), and Sack (1980), interactions across the sites may be important contributors to the macroscopic activities observed in site-distribution experiments. Oka (1977) and Sack (1980) considered Fe-Mg mixing in orthopyroxenes using reciprocal solid solution models to explain the site distribution data of Saxena and Ghose (1969) and Virgo and Hafner (1970). Sack (1980) formulated Fe-Mg exchange between olivine and orthopyroxene using both on-site regular solution terms and a reciprocal exchange term for Fe-Mg distribution in orthopyroxene. It was shown that the value of $\Delta\bar{G}_X^o$, the free energy of the exchange reaction

$$Mg(M1)Mg(M2) + Fe(M1)Fe(M2) = Mg(M1)Fe(M2) + Fe(M1)Mg(M2),$$

has an important effect on the apparent macroscopic activities of $Mg_2Si_2O_6$ and $Fe_2Si_2O_6$ in orthopyroxenes.

Failure to include this term in analysis of site-distribution data, results in apparent values of (W_{FeMg}^{M1})opx and (e.g. Saxena, 1976; Virgo and Hafner, 1970; Navrotsky, 1971) (W_{FeMg}^{M2})opx which are inconsistent with data obtained on $K_{D\ FeMg}^{opx-ol}$. On this basis, it may be warranted to use a reciprocal approach for $(Mg,Fe)_{M2}\ (Mg,Fe,Al)_{M1}$ orthopyroxenes. Following the methods of Sack (1980) and Wood and Nicholls (1978), two exchange reactions will be required to relate the components FeAl and FeMg to the minimum four

components (MgMg, FeFe, MgAl and MgFe) required to define the solid solution:

$Mg(M1)Mg(M2) + Fe(M1)Fe(M2) = Mg(M1)Fe(M2) + Fe(M1)Mg(M2)$ for which we have $\Delta\bar{G}^{o}_{X}$ given by Sack (1980), and,

$Fe(M1)Fe(M2) + Mg(M2)Al(M1) = Fe(M2)Al(M1) + Mg(M1)Fe(M2)$,

the free energy of this exchange being designated as $\Delta\bar{G}^{o}_{FeAl}$.

Then,

$$RT\ln \gamma^{opx}_{Mg_2Si_2O_6} = \Delta\bar{G}^{o}_{X}\,(X^{M1}_{Fe} \cdot X^{M2}_{Fe}) + \Delta\bar{G}^{o}_{FeAl}\,(X^{M2}_{Fe} \cdot X^{M1}_{Al}) + \text{site terms (eqns. (9) and (10))} \quad (12)$$

$$\text{and } RT\ln \gamma^{opx}_{MgAl_2SiO_6} = \Delta\bar{G}^{o}_{X}\,(X^{M1}_{Fe} \cdot X^{M2}_{Fe}) + \Delta\bar{G}^{o}_{FeAl}\,(X^{M1}_{Mg} \cdot X^{M2}_{Fe}) + \text{site terms (eqns. (9) and (11))} \quad (13)$$

Substituting (9), (10) and (12) into equation (7), and (9), (11) and (13) into equation (8) we derive:

$$RT\ln a^{opx}_{Mg_2Si_2O_6} = RT\ln\,(X^{M2}_{Mg} \cdot X^{M1}_{Al}) + \Delta\bar{G}^{o}_{X}\,(X^{M1}_{Fe} \cdot X^{M2}_{Fe}) + \Delta\bar{G}^{o}_{FeAl}\,(X^{M2}_{Fe} \cdot X^{M1}_{Al}) + (X^{M1}_{Fe})^2\,W^{M1}_{FeMg} + (X^{M1}_{Al})^2\,W^{M1}_{MgAl} + (X^{M2}_{Fe})^2 \cdot W^{M2}_{FeMg} + (X^{M1}_{Fe} \cdot X^{M1}_{Al})\,(W^{M1}_{FeMg} + W^{M1}_{MgAl} - W^{M1}_{FeAl}) \quad (14)$$

and,

$$RT\ln a^{opx}_{MgAl_2SiO_6} = RT\ln(X^{M2}_{Mg} \cdot X^{M1}_{Al}) + \Delta\bar{G}^{o}_{X}\,(X^{M1}_{Fe} \cdot X^{M2}_{Fe}) + \Delta\bar{G}^{o}_{FeAl}\,(X^{M1}_{Mg} \cdot X^{M2}_{Fe}) + (X^{M1}_{Fe})^2 \cdot W^{M1}_{FeAl} + (X^{M1}_{Mg})^2\,W^{M1}_{MgAl} + (X^{M2}_{Fe})^2\,W^{M2}_{FeMg} + (X^{M1}_{Mg} \cdot X^{M1}_{Fe})\,(W^{M1}_{FeAl} + W^{M1}_{gAl} - W^{M1}_{FeMg}) \quad (15)$$

From (14) and (15) it follows that

$$RT\ln\,(a^{opx}_{Mg_2Si_2O_6} \cdot a^{opx}_{MgAl_2SiO_6}) = RT\ln\,((X^{M2}_{Mg})^2\,X^{M1}_{Mg} \cdot X^{M1}_{Al})$$

Table A1.2 INTERACTION PARAMETERS FOR ORTHOPYROXENE SOLID SOLUTIONS

PARAMETER	DEFINITION/MODEL	REFERENCE	VALUE (cal/mol)
W^{M1}_{FeMg}	SmR Fe-Mg opx on M1 and M2 sites	Saxena (1976)	$3525\left(\frac{10^3}{T}\right) - 1667$
W^{M2}_{FeMg}	" "	" "	$2458\left(\frac{10^3}{T}\right) - 1261$
W^{opx}_{FeMg}	SmR bulk opx apparent parameter	Kawasaki and Matsui (1977)	1570 (110C)
W^{M2}_{FeMg}	SmR multisite Fe-Mg-Al opx	Powell (1978)	0
W^{M1}_{FeMg}	SmR multisite Fe-Mg opx with reciprocal terms	Sack (1980)	900 (110)
W^{M2}_{FeMg}		" "	640
$W^{M1}_{FeMg}-W^{M2}_{FeMg}$		" "	$1067\left(\frac{10^3}{T}\right) - 406$
$\Delta\bar{G}^{\circ}_{x}$	reciprocal exchange term	" "	$-6680 \sim 4.75(T)$
$W^{M1}_{FeMg}+W^{M2}_{FeMg} - \Delta\bar{G}^{\circ}_{x}$	net non-ideal term due to on-site and cross-site effects	" "	$5983\left(\frac{10^3}{T}\right) - 2928$
$W^{M1}_{FeMg}-W^{M2}_{FeMg}$	SmR multisite Fe-Mg opx with reciprocal terms	Oka (1977)	420 at 800 °C 910 at 500 °C
$\Delta\bar{G}^{\circ}_{x}$	reciprocal term	" "	-1290 at 800 °C
W^{M1}_{FeAl}	SmR, Fe-Mg-Al mixing on M1 site of opx	Powell (1978)	3775
$W^{M1}_{FeAl}/\Delta V_r$	SmR, Fe-Mg-Al mixing on M1 site of opx	Wood (1974)	10450 bars
W^{M2}_{CaMg}	SmR, Ca-Mg-Fe mixing on M2 site of opx	Saxena (1976)	7184
W^{M2}_{CaFe}		" "	5000
W^{M2}_{CaMg}		Holland et. al (1979)	8120
$W^{M2}_{CaFe}-W^{M2}_{FeMg}$		Powell (1978)	3788

$$+ 2(X_{Fe}^{M2})^2 \cdot W_{FeMg}^{M2} + X_{Fe}^{M2}\,\Delta\bar{G}_{FeAl}^{O} + W_{FeMg}^{M1}\,((1-2X^{M1})\,X_{Fe}^{M1})$$
$$+ X_{Fe}^{M2} \cdot X_{Fe}^{M1}\,(2\Delta\bar{G}_{X}^{O} - \Delta\bar{G}_{FeAl}^{O})$$
$$+ W_{MgAl}^{M1}\,(X_{Mg}^{M1} - 2X_{Mg}^{M1} + X_{Mg}^{M1})$$
$$+ W_{FeAl}^{M1}\,(1-2X_{Al}^{M1}) \cdot X_{Fe}^{M1} \qquad (16)$$

This is the complete and rigorous formulation of the orthopyroxene solid solution consistent with a multisite regular solution with cross-site interactions.

A1.4 GARNET-ORTHOPYROXENE Al_2O_3 REACTION IN FMAS

Substituting (15) and (6) into equation (4), we derive the equilibrium relation of reaction (1) in terms of compositional variables and a number of non-ideal energy terms:

$$+ (\Delta G^{O})_{P,T} = -RT \ln \left(\frac{(X_{Mg}^{ga})^3}{(X_{Mg}^{M2})^2\, X_{Mg}^{M1}\, X_{Al}^{M1}} \right) - 3(X_{Fe}^{ga})^2\, W_{FeMg}^{ga}$$
$$+ 2(X_{Fe}^{M2})^2\, W_{eMg}^{M2} + X_{Fe}^{M2}\,\Delta\bar{G}_{FeAl}^{O} + W_{FeMg}^{M1}\,((1-2X_{Mg}^{M1}) + X_{Fe}^{M1})$$
$$+ X_{Fe}^{M2} \cdot X_{Fe}^{M1}\,(2\Delta\bar{G}_{X}^{O} - \Delta\bar{G}_{FeAl}^{O})$$
$$+ W_{MgAl}^{M1}\,(X_{Al}^{M1} + X_{Mg}^{M1} - 2X_{Mg}^{M1}\,X_{Al}^{M1})$$
$$+ W_{FeAl}^{M1}\,(1-2X_{Al}^{M1}) \cdot X_{Fe}^{M1}$$
$$= \Delta H_{I,T}^{O} - T\Delta S_{1,T}^{O} + \int_{.001}^{P} \Delta V^{O} dP \qquad (17)$$

In the MAS system $X_{Mg}^{M2} = 1$, $X_{Fe}^{M2} = 0$, $X_{Mg}^{M1} = (1-X_{Al}^{M1})$, $X_{Fe}^{M1} = 0$, and $X_{Mg}^{ga} = 1$. Thus (17) may be simplified to

$$(\Delta G_{I}^{O})_{P,T} = + RT \ln \left(X_{Al}^{M1}(1-X_{Al}^{M1}) \right) + W_{MgAl}^{M1}(1-2X_{Al}^{M1})(1-X_{Al}^{M1})$$
$$= \Delta H_{1,T}^{O} - T\Delta S_{1,T}^{O} + \int_{.001}^{P} \Delta V^{O}\, dP \qquad (18)$$

Following the method of Wood and Banno (1973), we assume that Mg-Al interactions on the M1 site are ideal at 1 bar. Noting that

$$RT\left(\frac{d \ln \gamma_i}{dp}\right)_{T,X} = \bar{V}_i - V_i^o$$

where $\bar{V}_i$ is the partial molar volume of component i in a phase, then

$$RT \ln \gamma_i = \int_{.001}^{P} (\bar{V}_i - V_i^o)\, dP$$

and thus,

$$RT \ln (\gamma_{MgAl_2SiO_6} \cdot \gamma_{Mg_2Si_2O_6}) = \int_{.001}^{P} (\bar{V}_{MgAl_2SiO_6} + \bar{V}_{Mg_2Si_2O_6} - V^o_{MgAl_2SiO_6} - V^o_{Mg_2Si_2O_6})dP$$

but in MAS, via equation (18)

$$RT\ln(\gamma_{MgAl_2SiO_6} \cdot \gamma_{Mg_2Si_2O_6}) = W^{M1}_{MgAl}(1-2X^{M1}_{Al})(1-X^{M1}_{Al})$$

Hence:

$$W^{M1}_{MgAl}\,(1-2X^{M1}_{Al}\,(1-X^{M1}_{Al})) = \int_{.001}^{P} (\bar{V}_{MgAl_2SiO_6} + \bar{V}_{Mg_2Si_2O_6} - V^o_{MgAl_2SiO_6} - V^o_{Mg_2Si_2O_6})dP \qquad (19)$$

Substituting this pressure term into (18) we derive similar expressions to Wood and Banno (1973) and find:

$$\Delta G^o_{1,T} + \int_{.001}^{P} \Delta Vr\, dP = RT \ln (X^{M1}_{Al}\,(1 - X^{M1}_{Al}))_{P,T}$$

where ΔVr is now $V^o_{Mg_3Al_2Si_3O_{12}} - \bar{V}_{Mg_2Si_2O_6} - \bar{V}_{MgAl_2SiO_6}$.

We will approximate by neglecting the effects of thermal expansion and compressibility, thus

$$\int_{.001}^{P} \Delta V_r\, dP \simeq P\Delta V_r \text{ where P is in kbar}$$

In the MAS system, then, we arrive at the condition of Wood and Banno (1973):

$$\Delta H^o_{1,T} - T\Delta S^o_{1,T} + P\Delta V_r = RT \ln (X^{M1}_{Al}\,(1 - X^{M1}_{Al}))$$

where ΔV_r is calculated from molar volume data of Skinner and Boyd (1964), Arima and Onuma (1977), and Danckwerth and Newton (1978). Following the procedures of Wood and Banno (1973) and Danckwerth and Newton (1978), the ΔV_r can be finally expressed as

$$\Delta V_r = -(183.3 + 178.98\ X_{Al}\ (1-X_{Al}))\ \text{cals/kbar}$$

The molar volume data on which this equation is based is summarised in table A1.1

In the FMAS system (eqn. (17)), the ΔV° term may also be adjusted, using partial molar volume data, so that the W^{M1}_{MgAl} terms are accounted for (i.e. replace ΔV° by ΔV_r). This assumes that the volume behaviour of Fe-Al orthopyroxenes is similar to behaviour on the Mg-Al join, and hence that the pressure dependence of any non-ideality in Mg-Fe-Al pyroxenes will be similar to that of the Mg-Al pyroxenes.

To further simplify (17) we may consider the term

$$(X^{M2}_{Mg})^2\ (X^{M1}_{Mg})$$

which appears in the denominator of the lnK expression. From the site occupancy data of Virgo and Hafner (1970) and Saxena and Ghose (1969) we know that Fe^{2+} favours the M2 site in the orthopyroxene, thus

$$\left(\frac{Mg}{Mg+Fe}\right)^{M2} \leq \left(\frac{Mg}{Mg+Fe}\right)^{opx} \leq \left(\frac{Mg}{Mg+Fe}\right)^{M1}$$

and as all values of $\left(\frac{Mg}{Mg+Fe}\right)_i$ are less than unity,

$$\left\{\left(\frac{Mg}{Mg+Fe}\right)^{M2}\right\}^2 \cdot \left(\frac{Mg}{Mg+Fe}\right)^{M1} \leq \left\{\left(\frac{Mg}{Mg+Fe}\right)^{opx}\right\}^2 \cdot \left(\frac{Mg}{Mg+Fe}\right)^{M2}$$

but $\left(\frac{Mg}{Mg+Fe}\right)^{M2} \leq \left(\frac{Mg}{Mg+Fe}\right)^{opx}$

therefore, replacing this term in the R.H.S. of the equation above

$$\left\{\left(\frac{Mg}{Mg+Fe}\right)^{M2}\right\}^2 \cdot \left(\frac{Mg}{Mg+Fe}\right)^{M1} \leq \left\{\left(\frac{Mg}{Mg+Fe}\right)^{opx}\right\}^3$$

Now, $(Mg/Mg+Fe)^{M1} \times (1-X_{Al}^{M1}) = X_{Mg}^{M1}$

and $(Mg/Mg+Fe)^{M2} = X_{Mg}^{M2}$

$(Mg/Mg+Fe)^{opx} = X_{Mg}^{opx}$

So we have:

$$(X_{Mg}^{M2})^2 \; (X_{Mg}^{M1}) \leq (X_{Mg}^{opx})^3 \cdot (1-X_{Al}^{M1}) \qquad (20)$$

Substituting (20) into the lnK expression in (17) we find

$$\left(\frac{X_{Mg}^{ga}}{X_{Mg}^{opx}}\right)^3 \frac{1}{(1-X_{Al}^{1})} \leq \frac{(X_{Mg}^{ga})^3}{(X_{Mg}^{M2})^2 \; (X_{Mg}^{M1})}$$

and hence that

$$RT \ln\left(\frac{(X_{Mg}^{ga})^3}{(X_{Mg}^{M2})^2 \; X_{Mg}^{M1} \cdot X_{Al}^{M1}}\right) \geq 3 \; RT \ln \left(\frac{X_{Mg}^{ga}}{X_{Mg}^{opx}}\right) - RT \ln (X_{Al}(1-X_{Al})) \qquad (21)$$

Substituting equation (21) into (17), and using the volume correction derived in MAS, we can now simplify and approximate equation (17) by the expression:

$$\Delta H^{o}_{1,T} - T\Delta S^{o}_{1,T} + P\Delta V_r \geq -3RT \ln \left(\frac{X_{Mg}^{ga}}{X_{Mg}^{opx}}\right)$$

$$+RT \ln (X_{Al}^{M1}(1-X_{Al}^{M1}))$$
$$+ 2(X_{Fe}^{M2})^2 \; W_{FeMg}^{M2} + X_{Fe}^{M2} \; \Delta\bar{G}^{o}_{FeAl}$$
$$+ W_{FeMg}^{M1} \; ((1-2X_{Fe}^{M1}) \; X_{Fe}^{M1})$$
$$+ X_{Fe}^{M2} \; X_{Fe}^{M1} \; (2\Delta\bar{G}^{o}_{X} - \Delta\bar{G}^{o}_{FeAl})$$
$$+ W_{FeAl}^{M1} \; (1-2X_{Al}^{M1}) \; X_{Fe}^{M1}$$
$$- 3(X_{Fe}^{ga})^2 \; W_{FeMg}^{ga} \qquad (22)$$

noting that $-3RT \ln \left(\frac{X_{Mg}^{ga}}{X_{Mg}^{opx}}\right)$ will be positive and larger than the true term it replaces. At high temperature, as K_D approaches unity, this term

approaches zero and hence the term $-3RT \ln \left(\frac{(X_{Mg}^{ga})^3}{(X_{Mg}^{M2})^2 \, (Mg/Mg+Fe)^{M1}}\right)$ must approach zero also. Thus $\Delta G^{o}_{1,T} + P\Delta V_r \leq$ expression R.H.S. (22), and $\Delta G^{o}_{1,T} + P\Delta V_r >$ R.H.S. (22) + $3RT \ln \left(\frac{X_{Mg}^{ga}}{X_{Mg}^{opx}}\right)$. If we ignore the $(X_{Mg}^{ga}/X_{Mg}^{opx})$ term entirely, our extracted values of W_{ij} will be adjusted to slightly high values, and $\Delta S^{o}_{1,T}$ will be an apparent entropy of reaction with a value slightly different from that obtained if we could apply equation (17). In view of the lack of knowledge on Fe-Mg site distributions in aluminous orthopyroxenes, and the uncertainties in garnet compositions in equilibrium with orthopyroxenes in these experiments (see Chapter 2), ignoring the $(X_{Mg}^{ga}/X_{Mg}^{opx})$ term is justified in the development of a practical barometer.

(Note that this term can contribute 1826-3270 cals to the result, depending upon T, representing a change in $\Delta S^{o}_{1,T}$ of .5 cals; $\Delta S^{o}_{1,T}$ will be more negative than $\Delta S^{*}_{1,T}$ found by ignoring this term).

Now we have the relation

$$\begin{aligned}\Delta H^{o}_{1,T} - T\Delta S^{*}_{1,T} + P\Delta V_r = RT \ln \left(X_{Al}^{M1} \, (1-X_{Al}^{M1})\right) \\ + 2(X_{Fe}^{M2})^2 \, W_{FeMg}^{M2} + X_{Fe}^{M2} \, \Delta\bar{G}^{o}_{FeAl} \\ + W_{FeMg}^{M1} \left((1-2X_{Fe}^{M1}) \, X_{Fe}^{M1}\right) \\ + X_{Fe}^{M2} \, X_{Fe}^{M1} \, (2\Delta\bar{G}^{o}_{X} - \Delta\bar{G}^{o}_{FeAl}) \\ + W_{FeAl}^{M1} \, (1-2X_{Al}^{M1}) \, X_{Fe}^{M1} \\ - 3(X_{Fe}^{ga})^2 \, W_{FeMg}^{ga}\end{aligned} \qquad (23)$$

This can be further simplified for the practical analysis of the experimental data by substituting X_{Mg}^{opx} for the site terms related to the interaction parameters (W_{ij}).

Noting: $X_{Fe}^{M2} \geq X_{Fe}^{opx}$, $X_{Fe}^{M1} \leq X_{Fe}^{opx}\ (1-X_{Al})$, and $X_{Fe}^{M1} \leq X_{Fe}^{opx}$, we can make the following approximations:

(a) $W_{FeAl}^{M1}\ (1-2X_{Al}^{M1})\ (1-X_{Al})\ X_{Fe}^{opx} \geq W_{FeAl}^{M1}\ (1-2X_{Al}^{M1})\ X_{Fe}^{M1}$

(b) $(X_{Fe}^{opx})\ \ (2\Delta\bar{G}_X^{o} - \Delta G_{FeAl}^{o})\ \ X_{Fe}^{M2} \cdot X_{Fe}^{M1}\ (2\Delta\bar{G}_X^{o} - \Delta G_{FeAl}^{o})$

(c) $(1-X_{Al}^{M1})\ X_{Fe}^{opx}\ (1-2(1-X_{Al})X_{Fe}^{opx})\ W_{FeMg}^{M1} \leq ((1-2X_{Fe}^{M1})\ X_{Fe}^{M1})\ W_{FeMg}^{M1}$

(d) $2(X_{Fe}^{opx})^2\ W_{FeMg}^{M2} + X_{Fe}^{opx}\ \Delta\bar{G}_{FeAl}^{o} \leq 2(X_{Fe}^{M2})^2\ W_{FeMg}^{M2} + X_{Fe}^{M2}\ \Delta\bar{G}_{FeAl}^{o}$

It can be seen that the approximations act in opposite directions, and will balance out to some extent. It is considered that the approximations are valid within the errors of the experimental technique, and the level of sophistication of equations (17)-(23) not allowed by the data collected.

Equation (23) is now simplified to:

$$\begin{aligned}\Delta H_{1,T}^{o} - T\Delta S_{1,T}^{*} + P\Delta V_r &= RT \ln (X_{Al}\ (1-X_{Al})) \\ &+ 2(1-X_{Mg}^{opx})^2\ W_{FeMg}^{M2} + (1-X_{Al})\ X_{Fe}^{opx}\ W_{FeMg}^{M1} \\ &- 2\ ((1-X_{Al})\ (X_{Fe}^{opx}))^2\ W_{FeMg}^{M1} + (X_{Fe}^{opx})^2\ (2\Delta\bar{G}_X - \Delta G_{FeAl}^{o}) \\ &+ X_{Fe}^{opx}\Delta\bar{G}_{FeAl}^{o} + (1-2X_{Al}^{M1})\ (1-X_{Al})\ X_{Fe}^{opx}W_{FeAl}^{M1} \\ &- 3(X_{Fe}^{ga})^2\ W_{FeMg}^{ga}\end{aligned}$$

which can be rearranged to:

$$\begin{aligned}\Delta H_{1,T}^{o} - T\Delta S_{1,T}^{o} + P\Delta V_r &= RT \ln K_{Al} \\ &+ (X_{Fe}^{opx})^2\ (2W_{FeMg}^{M2} - 2(1-X_{Al}^{M1})^2\ W_{FeMg}^{M1} + 2\Delta\bar{G}_X^{o} - \Delta\bar{G}_{FeAl}^{o}) \\ &+ (X_{Fe}^{opx})\ (W_{MgFe}^{M1}\ (1-X_{Al}^{M1}) + \Delta\bar{G}_{FeAl}^{o}) \\ &+ W_{FeAl}^{M1}\ ((1-2X_{Al}^{M1})\ (1-X_{Al}^{M1})\ (X_{Fe}^{opx})) \\ &- 3(X_{Fe}^{ga})^2\ W_{FeMg}^{ga}\end{aligned} \qquad (24)$$

With this equation we are in a position to evaluate the contribution of various terms in the solid solutions to $\Delta G_{1,T}^{o}$. Wood (1974) assumed that most of the (Mg/Mg+Fe) dependence of X_{Al} in orthopyroxene arises solely from

non-ideal Fe-Al interactions, a situation which may be valid when we consider the sizes of the other terms.

Sack (1980) obtained an expression for $\Delta\bar{G}^{O}_{X}$, consistent with olivine -opx K_D data, where $\Delta\bar{S}^{opx}_{X} = -4.4$ cal K^{-1} mol^{-1} and $\Delta H^{O}_{X} = -6.68$ kcal. These parameters give the condition:

$$\Delta\bar{G}^{O}_{X} = -6.68 + 4.75\ (\frac{T}{10^3}) \qquad \text{kcal}$$

Sack (1980) also obtained an expression for $W^{M1}_{FeMg} - W^{M2}_{FeMg}$

$$W^{M1}_{FeMg} - W^{M2}_{FeMg} = 1.067\ (\frac{10^3}{T}) - .406 \quad \text{kcal}$$

Using these data, we can consider the size and contribution of the term

$$(X^{opx}_{Fe})^2\ (2(W^{M2}_{FeMg} - (1-X_{Al})^2\ W^{M1}_{FeMg} + \Delta\bar{G}^{O}_{X}))$$

This will be negative, as $W^{M2} < W^{M1}$ and $\Delta\bar{G}^{O}_{X}$ is negative, and can be approximated by

$$(X^{opx}_{Fe})^2\ (2(W^{M2}_{FeMg} - W^{M1}_{FeMg} + \Delta\bar{G}^{O}_{X})) \qquad (24(a))$$

Using the equations of Sack (1980) above, we find that $2(W^{M2}_{FeMg} - W^{M1}_{FeMg} + \Delta\bar{G}^{O}_{X})$ is negative and very temperature sensitive, ranging from -4.2 kcal at 800°C to only -0.4 kcal at 1150°C. Thus, this term will only be significant at low T and in the same T range where the positive term $-3RT \ln (\frac{X^{ga}_{Mg}}{X^{opx}_{Mg}})$ is significant. To evaluate the full effect of (24(a)), the $(X^{opx}_{Fe})^2$ term must be considered. In ultramafic compositions, $X^{opx}_{Fe} \simeq .10$, so the contribution will be insignificant:

$$-(.01) \times (.7) = -.07 \text{ kcal at } 1050^{O}C.$$

In granulites, where $.3 \leq X^{opx}_{Fe} \leq .7$, then

$$.09 \leq (X_{Fe})^2 \leq .49$$

Thus the negative energy contribution of the term (24(a)) will be most significant at high X^{opx}_{Fe} (.7) and low T (700-900°C). Under these conditions values of -2 kcal may be approached, which balances the

positive $-3RT \ln \left(\frac{X_{Mg}^{ga}}{X_{Mg}^{opx}}\right)$ term that has been ignored. Thus for these conditions we should ignore (24(a)) also.

Values, in kcal, of (21(a)) for various T-X_{Mg}^{opx} combinations are given in the table below (Table A2):

T \ X_{Mg}^{opx}	.50	.60	.70
800°C	-1.05	-.67	-.38
900°C	- .54	-.35	-.19
975°C	- .28	-.18	-.10
1050°C	- .18	-.11	-.06

We can now consider the contribution of the term

$$(1-X_{Al}) \ (X_{Fe}^{opx}) \ W_{FeMg}^{Ml} \qquad (24(b))$$

Values of W_{FeMg}^{Ml} decrease with increasing temperature from 900 cal at 800°C to 700 cal at 1000°C (Sack (1980), Oka (1977)). Thus this term can only be significant at high values of X_{Fe}^{opx} and low values of X_{Al}^{opx} i.e. at low T. With X_{Al}^{opx} = .10, and .3 < X_{Fe}^{opx} < .7, then 190 cal ≤ (24(b)) ≤ 450 cal. Thus this term makes a small positive contribution, particularly in iron rich compositions.

The term

$$\Delta\bar{G}_{FeAl}^{o} \ (1-X_{Fe}^{opx}) \ (X_{Fe}^{opx}) \qquad (24(c))$$

will give a symmetrical contribution to the $\Delta G_{1,T}^{o}$ with respect to X_{Fe}^{opx}. In ultramafic compositions and Fe-end member systems $0 \leq (1-X_{Fe})(X_{Fe}) \leq .13$, and thus the contribution of (24(c)) will be rather small (depending on the size of $\Delta\bar{G}_{FeAl}^{o}$). In granulites, and in the X_{Mg}^{opx} ranges of these experiments:

$$.21 \leq (1-X_{Fe}^{opx}) \ (X_{Fe}^{opx}) \leq .25$$

hence $\Delta\bar{G}_{FeAl}^{o} \ (1-X_{Fe}^{opx}) \ (X_{Fe}^{opx}) \simeq (.23) \ \Delta\bar{G}_{FeAl}^{o}$

The size and sign of $\Delta\bar{G}^{o}_{FeAl}$ are unknown and must be estimated, if possible, from experimental data.

The last term to consider is the W^{Ml}_{FeAl} term:

$$W^{Ml}_{FeAl}\ ((1-2X^{Ml}_{Al})\ (1-X_{Al}\ (X^{opx}_{Fe})) \qquad (24(d))$$

Powell (1978) estimated W^{Ml}_{FeAl} = 3775 cal, while Wood (1974), in attributing all the X_{Mg} dependence of X^{opx}_{Al} to this term, derived a value which can be extracted from his parameter C:

$$C = -(W^{Ml}_{FeAl}/\Delta V_r) = 10450 \text{ bar}$$

where $\Delta V_r \simeq -.200$ cal/bar. Thus $W^{Ml}_{FeAl} \simeq 2090$ cal. Thus it is to be expected that (24(d)) will make a large positive contribution to $\Delta G^{o}_{1,T}$, particularly at low X^{opx}_{Al} and high X^{opx}_{Fe}, or low T-high X_{Fe} conditions. These conditions are precisely those where (24(a)) is strongly negative, (24(b)) is positive ($\simeq$ 400 cal), (24(c)) is small, and the term $-3RT \ln \left(\frac{X^{ga}_{Mg}}{X^{opx}_{Mg}}\right)$ is strongly positive and balances (24(a)). The net result is that at low T and high X^{opx}_{Fe}, (24(d)) will be the only term that needs to be considered.

Under higher T, moderate X^{opx}_{Fe} conditions the term (24(a)) will be negative but small (> -400 cal), (24(b)) will be positive but small (< 200 cal), and (24(c)) will be more important and probably strongly positive. The term $-3RT\ln \left(\frac{X^{ga}_{Mg}}{X^{opx}_{Mg}}\right)$ will also be positive and large (1000-2000 cal). The positive contribution of (24(d)) to $\Delta G^{o}_{1,T}$ will be smaller but still significant. Under these conditions, if we ignore all other terms than the W^{Ml}_{FeAl} term (24(d)), then our apparent W^{Ml}_{FeAl} will be too large (and positive) as it will include the overall positive value resulting from the other terms, particularly the unknown $\Delta\bar{G}^{o}_{FeAl}$.

Acknowledging this source of error, we can simplify equation (24) to an expression which will be useful for the analysis of the experimental data in FMAS. This is now a semi-empirical fit similar to the Wood (1974) equation:

$$\Delta H^{o}_{1,T} - T\Delta S^{o}_{1,T} + P\Delta V_r \simeq RT\ln K_{Al} + W^{Ml}_{FeAl}\ ((1-2X^{Ml}_{Al})\ (1-X^{Ml}_{Al})\ (1-X^{opx}_{Mg}) \qquad (25)$$

This equation has been applied as a first approximation to the data. A more sophisticated treatment could then include $\Delta\bar{G}^{o}_{FeAl}$:

$$\Delta H^{o}_{1,T} - T\Delta S^{o}_{1,T} + P\Delta V^{o}_{r} = RT\ \ln K_{Al} + W^{Ml}_{FeAl}\ ((1-2X^{Ml}_{Al})\ (1-X^{Ml}_{Al})\ (1-X^{opx}_{Mg}))$$
$$+ \Delta\bar{G}^{o}_{FeAl}\ (1-X^{opx}_{Fe})\ (X^{opx}_{Fe}) \qquad (26)$$

with the value of W^{Ml}_{FeAl} adjusted accordingly. As a result of all the approximations implicit in eqn. (25), significant deviations from a good fit of natural and experimental data to (25) may occur under the following conditions:

(a) at low T in high X^{opx}_{Fe} assemblages

(b) at high P -T where K_D's and hence $-3RT\ \ln\left(\frac{X^{ga}_{Mg}}{X^{opx}_{Mg}}\right)$ are still large, in moderate X^{opx}_{Fe} compositions.

(c) where $\Delta\bar{G}^{o}_{FeAl}$ is large (> 5000 cal) and not balanced out by other terms.

In summary, the critical assumptions introduced in arriving at (25) are:

(a) the site occupancies of Fe and Mg on M1 and M2 can be ignored and X^{opx}_{Mg} or X^{opx}_{Fe} used where appropriate. Major errors in estimated P using (25) may occur where the site distributions are widely different from X^{opx}_{Mg} and X^{opx}_{Fe}. This problem is somewhat avoided by incorporating assumption (b) below.

(b) $-3RT \ln \left(\frac{X_{Mg}^{ga}}{X_{Mg}^{opx}}\right)$ can be ignored and instead incorporated into an apparent W_{FeAl}^{Ml} or $W_{S_{FeAl}}^{Ml}$ term, or balanced off by other energy terms which are also ignored (24(a)).

(c) $\Delta\bar{G}^{o}_{FeAl}$ is not large enough to be an important factor in the analysis, and may be incorporated into the apparent W_{FeAl}^{Ml} term.

(d) $W_{FeMg}^{ga} = 0$, as found by recent workers.

(O'Neill and Wood, 1979; Wood and Nicholls, 1978)

The equation (25) which we have finally arrived at essentially treats the reaction

$$En + MgTs = Py \qquad (1)$$

as an alternate reaction of the form:

$$M^{2+}_2 Si_2O_6 + M^{2+}Al_2SiO_6 = M^{2+}_3Al_2Si_3O_{12}$$

where M^{2+} = Mg, Fe. No entropy of mixing results from the presence of these two cations in the garnet or the orthopyroxenes. The variation of X_{Al}^{opx} with X_{Mg} is attributed only to mixing of Mg-Al and Fe-Al on the orthopyroxene M1 site. Thus, the addition of Fe^{2+} to the MAS system is not regarded as a dilution effect but as a result of different mixing properties between the $(MgAl)_{Ml}$ and $(FeAl)_{Ml}$ components in a simplified orthopyroxene. This is a rather simplified view of the macroscopic activities of the garnet and orthopyroxene solid solutions arising from a number of complicated effects in the orthopyroxene solid solution. In this regard, the W_{FeAl}^{Ml} value derived from the experimental data should be viewed solely as a regression parameter. Is is not a value to be used unquestioningly as an input to other quite different reactions involving orthopyroxene and other aluminous phases. The more realistic value of W_{FeAl}^{Ml} will be smaller, by up to 2000 cals.

A1.5 GARNET-ORTHOPYROXENE Fe-Mg EXCHANGE - FMAS

The distribution of Fe^{2+} and Mg between coexisting orthopyroxene and garnet is governed by the following reaction:

$$^1/_3\ Mg_3Al_2Si_3O_{12} + {}^1/_2\ Fe_2Si_2O_6 = {}^1/_2\ Mg_2Si_2O_6 + {}^1/_3\ Fe_3Al_2Si_3O_{12} \quad (27)$$

pyrope ferrosilite enstatite almandine

for which the condition of equilibrium is given by

$$\Delta G^{O}_{1,T} + \int_{.001}^{P} \Delta V^{O} dP = -RT \ln \left(\frac{(a^{ga}_{Fe_3Al_2Si_3O_{12}})^{1/3} \cdot (a^{opx}_{Mg_2Si_2O_6})^{1/2}}{(a^{ga}_{Mg_3Al_2Si_3O_{12}})^{1/3} \cdot (a^{opx}_{Fe_2Si_2O_6})^{1/2}} \right) \quad (28)$$

ΔV^{O}_{298} for this reaction is -22.86 cal $kbar^{-1}$, calculated from molar volume data given in table A1, using the relation

$$\Delta V^{O} = \Sigma V^{O} \text{ products} - \Sigma V^{O} \text{ reactants}$$

$$= {}^1/_2\ (V^{O}_{Mg_2Si_2O_6} - V^{O}_{Fe_2Si_2O_6}) + {}^1/_3\ (V^{O}_{Fe_3Al_2Si_3O_{12}} - V^{O}_{Mg_3Al_2Si_3O_{12}})$$

Activity-composition relationships of garnet in FMAS are as given in section A1.2, thus

$$a_{Mg_3Al_2Si_3O_{12}} = (X^{ga}_{Mg})^3\ \gamma^3_{Mg_3Al_2Si_3O_{12}}$$

and $a_{Fe_3Al_2Si_3O_{12}} = (X^{ga}_{Fe})^3\ \gamma^3_{Fe_3Al_2Si_3O_{12}}$

Using a binary regular solution model for garnet in FMAS, as before, we have

$$RT\ln \gamma_{PY} = (X^{ga}_{Fe})^2 \cdot W^{ga}_{FeMg}$$

and $RT\ln \gamma_{ALM} = (X^{ga}_{Mg})^2 \cdot W^{ga}_{FeMg}$

thus $RT \ln \left(\frac{\gamma^{ga}_{Fe}}{\gamma^{ga}_{Mg}}\right) = (1-2X^{ga}_{Fe})\ W^{ga}_{FeMg}$ in FMAS

From equation (14) we have

$$RT \ln a^{opx}_{Mg_2Si_2O_6} = RT \ln (X^{M2}_{Mg} \cdot X^{M1}_{Mg}) + \Delta\bar{G}^{o}_{X} (X^{M1}_{Fe} \cdot X^{M2}_{Fe})$$
$$+ \Delta\bar{G}^{o}_{FeAl} (X^{M2}_{Fe} \cdot X^{M1}_{Al}) + (X^{M1}_{Fe})^2 W^{M1}_{FeMg} + (X^{M1}_{1}) W^{M1}_{MgAl}$$
$$+ (X^{M2}_{Fe})^2 \cdot W^{M2}_{FeMg} + (X^{M1}_{Fe} \cdot X^{M1}_{Al}) (W^{M1}_{FeMg} + W^{M1}_{MgAl} - W^{M1}_{FeAl}) \quad (29)$$

and similarly

$$RT \ln a^{opx}_{Fe_2Si_2O_6} = RT \ln (X^{M2}_{Fe} \cdot X^{M1}_{Fe}) + \Delta\bar{G}^{o}_{X} (X^{M1}_{Mg} \cdot X^{M2}_{Mg})$$
$$+ \Delta\bar{G}^{o}_{FeAl} (X^{M2}_{Mg} \cdot X^{M1}_{Al}) + (X^{M1}_{Mg})^2 W^{M1}_{FeMg} + (X^{M1}_{Al})^2 W^{M1}_{FeAl}$$
$$+ (X^{M2}_{Mg})^2 W^{M2}_{FeMg} + X^{M1}_{Mg} \cdot X^{M1}_{Al} (W^{M1}_{FeMg} + W^{M1}_{FeAl} - W^{M1}_{MgAl}) \quad (30)$$

Substituting the garnet a-x terms and orthopyroxene activites given by equations (29) and (30) into equation (28) we obtain

$$\Delta G^{o}_{1,T} + \int_{.001}^{P} \Delta V^{o} dP = -RT \ln K$$
$$= -RT \ln \left\{ \left(\frac{X^{ga}_{Fe}}{X^{ga}_{Mg}} \right) \cdot \left(\frac{X^{M2}_{Mg} X^{M1}_{Mg}}{X^{M2}_{Fe} \cdot X^{M1}_{Fe}} \right)^{\frac{1}{2}} \right\} - (1-2X^{ga}_{Fe}) W^{ga}_{FeMg}$$
$$- \tfrac{1}{2}(1-2X^{M2}_{Mg}) W^{M2}_{FeMg} - \tfrac{1}{2}(X^{M1}_{Fe} - X^{M1}_{Mg}) W^{M1}_{FeMg}$$
$$- \tfrac{1}{2}(X^{M1}_{Al}) (W^{M1}_{MgAl} - W^{M1}_{FeAl}) - X^{M1}_{Fe} \Delta\bar{G}^{o}_{X}$$
$$- X^{M2}_{Fe} (\Delta\bar{G}^{o}_{FeAl} (X^{M1}_{Mg} - X^{M1}_{Al}) - \Delta\bar{G}^{o}_{X} (1-X^{M1}_{Al})) \quad (31)$$

To simplify equation (31) we make the following approximations:

(1) $(X^{M2}_{Mg} \cdot X^{M1}_{Mg} / X^{M2}_{Fe} \cdot X^{M1}_{Fe})^{\frac{1}{2}} \simeq X^{opx}_{Mg} / X^{opx}_{Fe}$

(2) $X^{M1}_{Fe} \simeq (1-X_{Al}) X^{opx}_{Fe}$

(3) $X^{M2}_{Fe} \simeq X^{opx}_{Fe}$

resulting in the following relation:

$$-Rt\ \ln K \simeq -Rt \ln K_D - (1-2X_{Fe}^{ga})\ W_{FeMg}^{ga} - \tfrac{1}{2}(1-2X_{Mg}^{opx})\ W_{FeMg}^{M2}$$
$$- \tfrac{1}{2}(1-2X_{Mg}^{opx})\ (1-X_{Al})\ W_{FeMg}^{M1}$$
$$- \tfrac{1}{2}X_{Al}^{M1}(W_{MgAl}^{M1} - W_{FeAl}^{M1})$$
$$- \tfrac{1}{2}X_{Fe}(X_{Mg}(1-X_{Al}) - X_{Al})\ \Delta\bar{G}_{FeAl}^{o} \qquad (32)$$

In this expression $\Delta\bar{G}_{FeAl}^{o}$ is unknown, $W_{FeMg}^{ga} \simeq 0$ (O'Neill & Wood, 1979), W_{MgFe}^{M1} and W_{MgFe}^{M2} can be obtained from Oka (1977) and Sack (1980), and $W_{FeAl}^{M1} >> W_{MgAl}^{M1}$ and is known to be large. We can make the following observations on the relative contributions of the various terms:

(a) for reasonable values of X_{Fe}^{opx}, X_{Al}^{opx} the coefficient of $\Delta\bar{G}_{FeAl}^{o}$ will be in the order .07 to .10
i.e. $\tfrac{1}{2}\ X_{Fe}(X_{Mg}(1-X_{Al}) - X_{Al})$ is in the range .07 to .10

(b) $\tfrac{1}{2}(1-2X_{Mg}^{opx})$ will be in the range 0 ± .20 for most granulite facies parageneses, and around -.40 for ultramafic rocks. W_{MgFe}^{M2} is only .400 kcal (table A1), so the contribution from this term is only 0 ± 80 cal in granulites, and -160 cal in ultramafic compositions.

(c) The coefficient for W_{FeMg}^{M1}, $\tfrac{1}{2}(1-2X_{Mg}^{opx})\ (1-X_{Al})$, for similar reasons to (b) above will vary 0 ± .16. W_{MgFe}^{M1} is approximately 900 cal, and decreases with increasing temperature. Thus the contribution from this term will be 0 ± 144 cal for granulite parageneses.

Considering the size of these various energy terms, we can approximate W_{FeMg}^{M1} and W_{FeMg}^{M2} with an apparent interaction term, W_{FeMg}^{opx}:

$$\tfrac{1}{2}(1-2X_{Mg}^{opx})\ W_{MgFe}^{M2} + \tfrac{1}{2}(1-2X_{Mg}^{opx})\ (1-X_{Al})\ W_{MgFe}^{M1}$$
$$= W_{FeMg}^{opx}\ (1-2X_{Mg}^{opx})$$

with $W_{FeMg}^{opx} \simeq \dfrac{W_{FeMg}^{M1} + W_{FeMg}^{M2}}{2} \leq 600$ cal.

This combined term will give a contribution of 0 ± 200 cal to -RTlnK, the contribution being positive at $X_{Mg}^{opx} < .5$, and negative where $X_{Mg}^{opx} > .5$.

(32) now reduces to

$$-RT\ln K = -RT\ln K_D - (1-2X_{Mg}^{opx}) W_{FeMg}^{opx} - \tfrac{1}{2}X_{Al} (W_{MgAl}^{opx} - W_{FeAl}^{opx})$$

$$- \tfrac{1}{2}((X_{Mg} (1-X_{Al}) - X_{Al})) X_{Fe} \cdot \Delta\bar{G}_{FeAl}^{o} \qquad (33)$$

Fitting adjusted experimental data to this equation, where we know ΔV^o, W_{FeMg}^{opx}, and can set upper bounds on $(W_{MgAl}^{opx} - W_{FeAl}^{opx})$, will allow the estimation of $\Delta H_{1,T}^{o}$, $\Delta S_{1,T}^{o}$ and a lower bound on $\Delta\bar{G}_{FeAl}^{o}$.

If we ignore $\Delta\bar{G}_{FeAl}^{o}$, the reciprocal exchange term, equation (33) becomes

$$-RT\ln K = -RT\ln K_D - (1-2X_{Mg}^{opx}) W_{FeMg}^{opx} - \tfrac{1}{2}X_{Al} (W_{MgAl}^{opx} - W_{FeAl}^{opx}) \qquad (34)$$

This equation is used in the analysis of the adjusted Fe-Mg experimental data of Chapter 2.

Appendix 2

EXPERIMENTAL RUN PRODUCTS IN FMAS AND CFMAS

APPENDIX TWO

EXPERIMENTAL RUN PRODUCTS IN FMAS AND CFMAS

All garnet-orthopyroxene (±melt) compositional data obtained in FMAS and CFMAS experiments is presented in the following diagrams, in order of decreasing T (experimental) and with decreasing P at each temperature. All FMAS data is presented first, followed by the CFMAS experimental data.

In the case of FMAS data, compositional information is presented in partial $\frac{1}{2}$Al-Fe-Mg diagrams. Run numbers are indicated in the upper right hand corners of these diagrams, and run conditions (°C, kbar) are given outside the right hand corners of the diagrams.

In each FMAS (and CFMAS) $\frac{1}{2}$Al-Fe-Mg diagram :

(a) horizontal arrows above garnet compositions (gar) indicate direction of zoning from seeds to rims. Arrows between garnet data points indicate progressive rimward zoning in one grain. Garnet zoning is from Fe- to Mg-richer rimwards unless otherwise shown.

(b) diagonal (to greater or lesser Al-contents) arrows adjacent to orthopyroxene analyses indicate direction of zoning from seed compositions or glass bulk composition. Arrows pointing to higher Al-contents refer to mineral mix starting materials , while downward pointing arrows refer to glass starting materials. No arrow indicates approach from higher Al-contents also (glass starting materials).

(c) tie lines join compositions of garnet rims and orthopyroxene rims or average analyses. Tie lines also join orthopyroxene with compositions of olivine (T720) or melt, when present.

Experimental data in CFMAS is presented, for each P-T condition, in two types of diagram :

1. partial $\frac{1}{2}$Al-Fe-Mg diagrams illustrating Al-contents and Mg-numbers of orthopyroxene and garnet (±melt). These diagrams are offset to enable easy visualisation of separate Ca-mix data (labelled C2, C4, and C8 respectively).
2. partial Ca-Mg-Fe diagrams illustrating X_{Ca} values of garnet and orthopyroxene, Ca-Mg zoning in each mineral, and compositions of melts. In these diagrams :
   (a) symbols : solid circles.....C2 mix (X_{Ca}^{mix} 0.02)
   crosses.....C4 mix (" 0.04)
   open circles.....C8 mix (" 0.08)
   (b) garnet compositional zoning to more Ca-Mg rich rims is indicated by arrows from the Fe apex.
   (c) theoretical bulk compositions are shown by filled triangles.

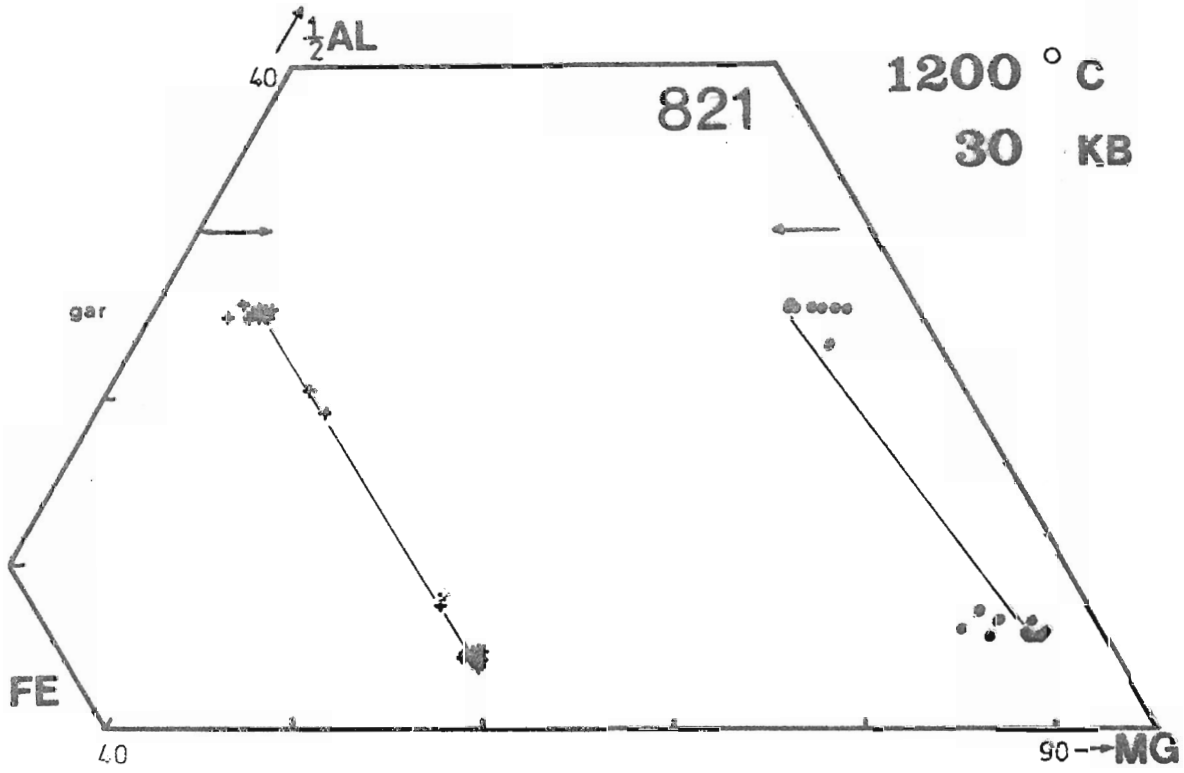
½AL
40
821
1200 °C
30 KB
gar
FE
40
90
MG

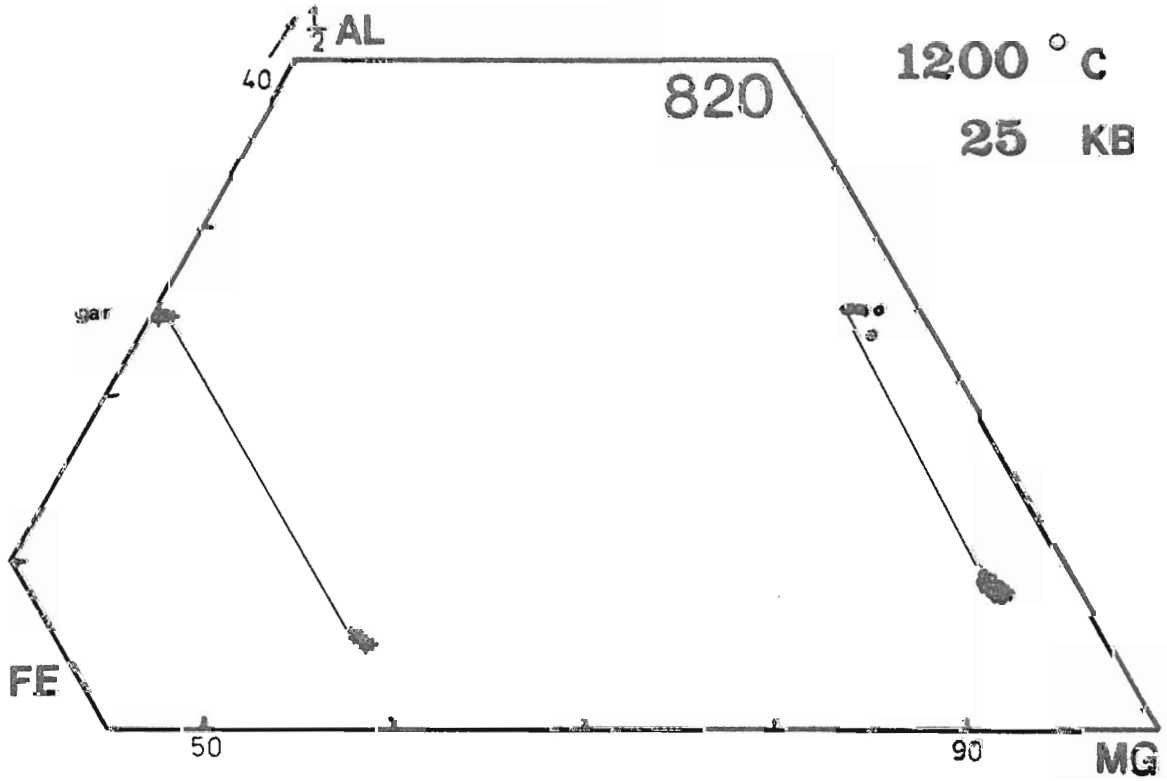
½AL
40
820
1200 °C
25 KB
gar
FE
50
90
MG

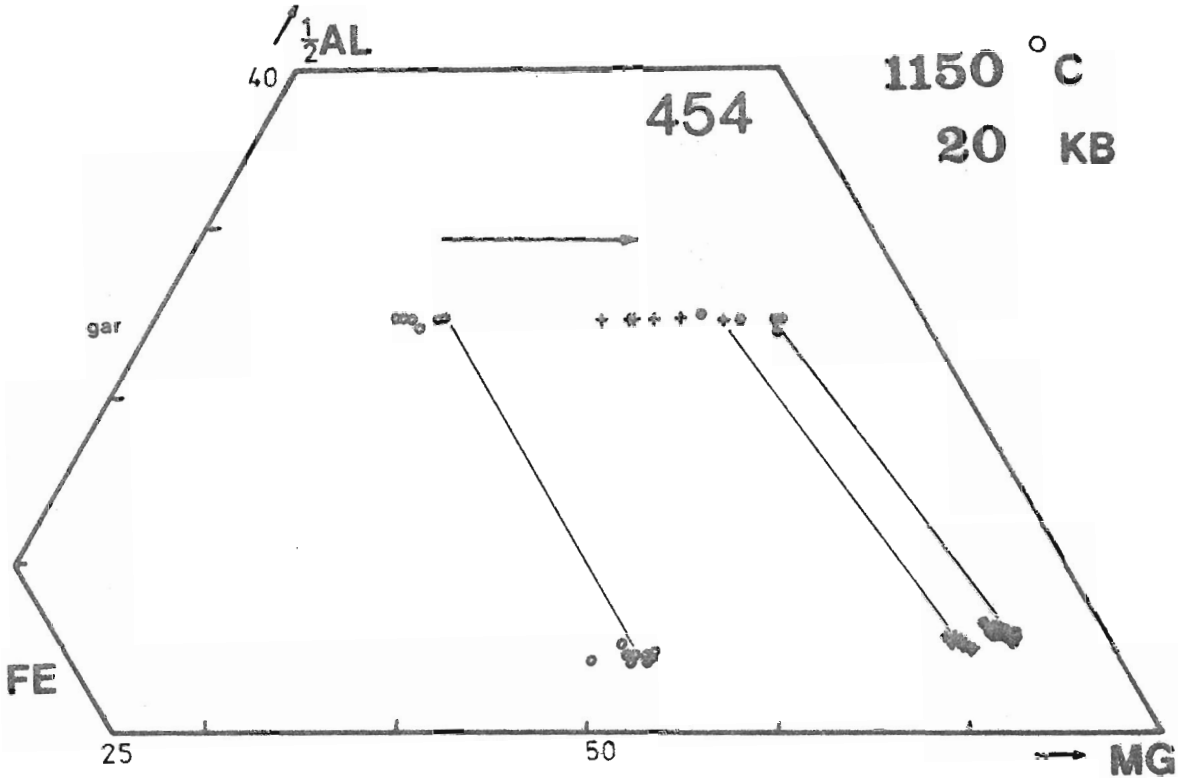
½AL
40
454
1150 °C
20 KB
gar
FE
25
50
MG

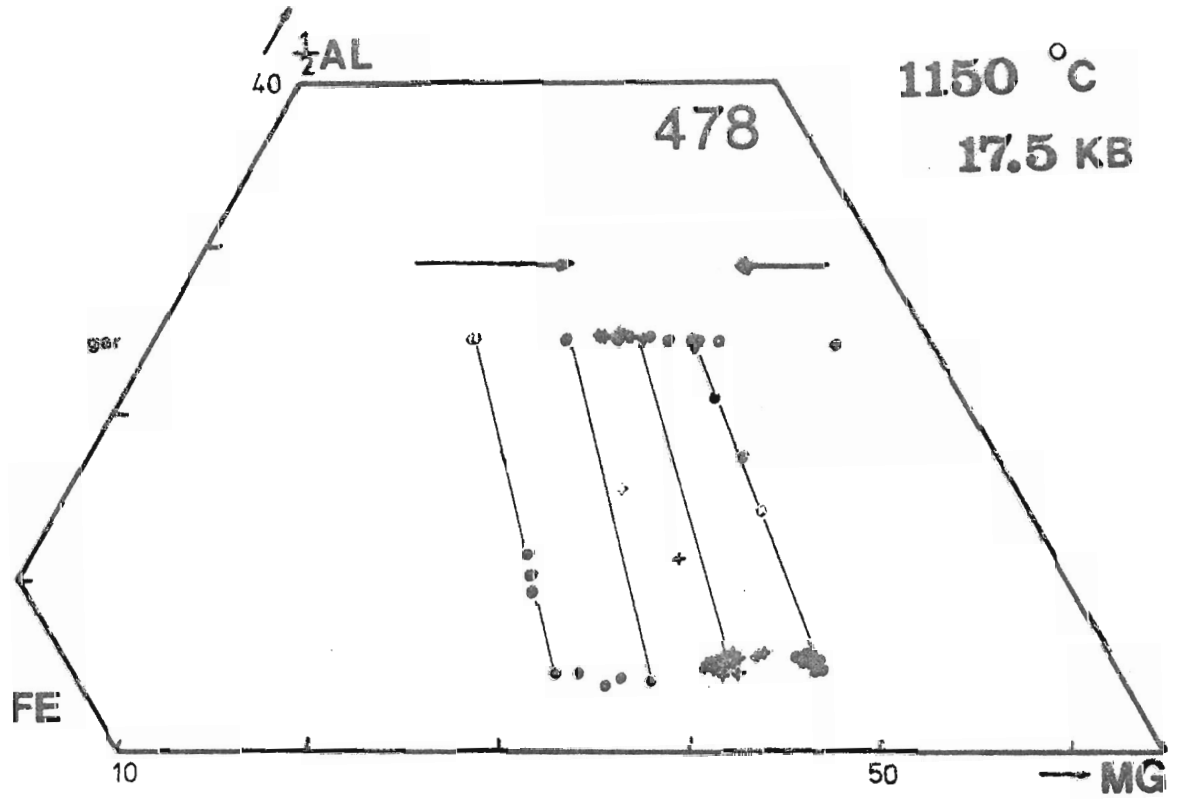
½AL
40
478
1150 °C
17.5 KB
gar
FE
10
50
MG

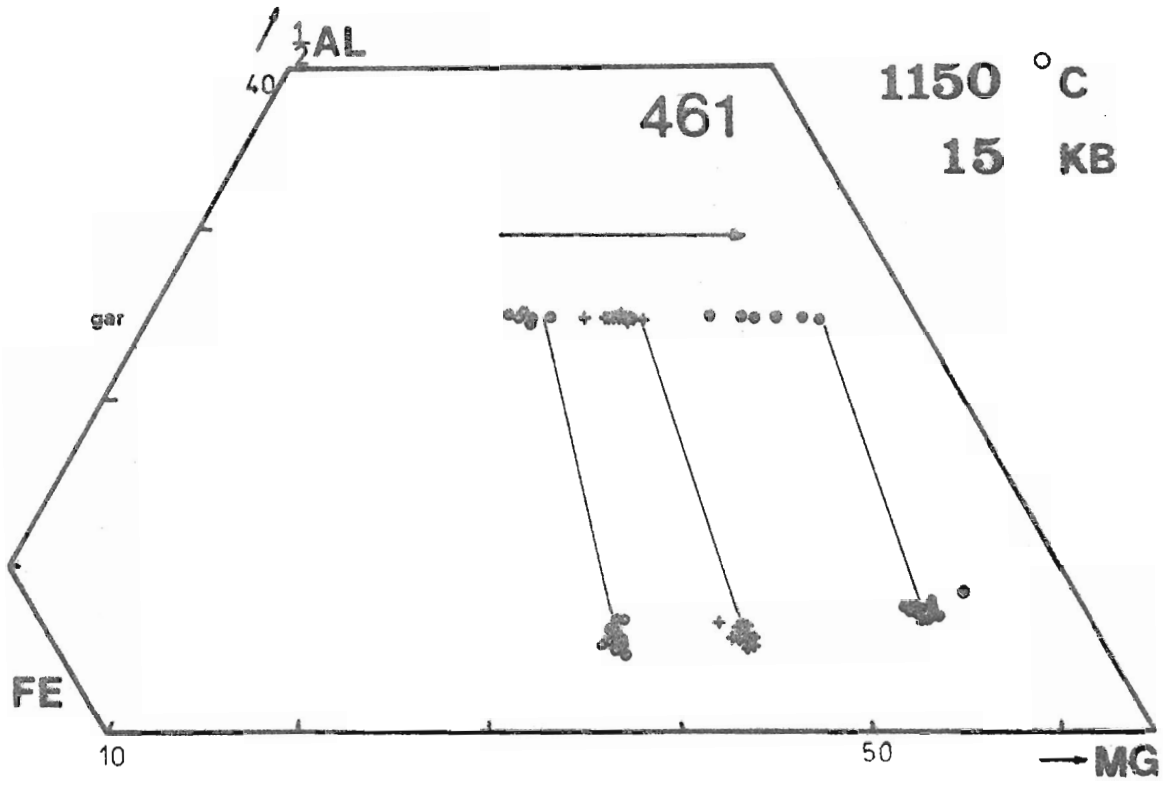
½AL
40
461
1150 °C
15 KB
gar
FE
10
50
MG

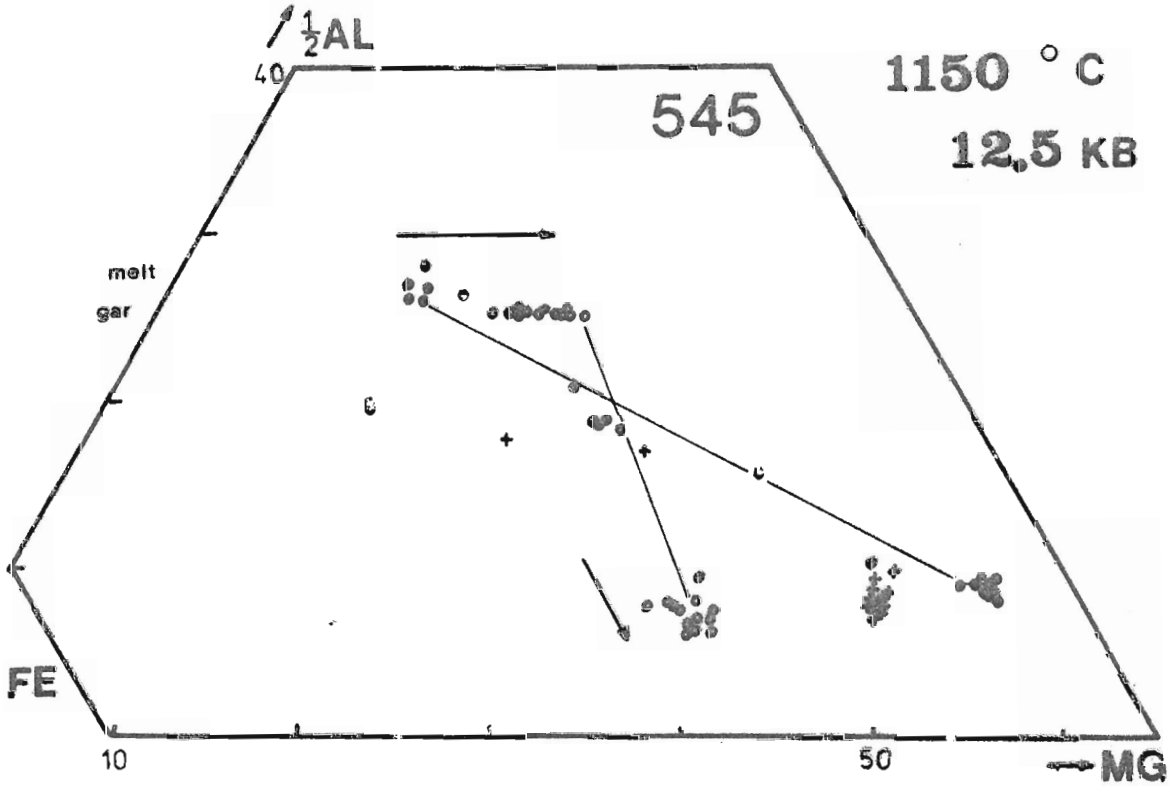
½AL
40
545
1150 °C
12.5 KB
melt
gar
FE
10
50
MG

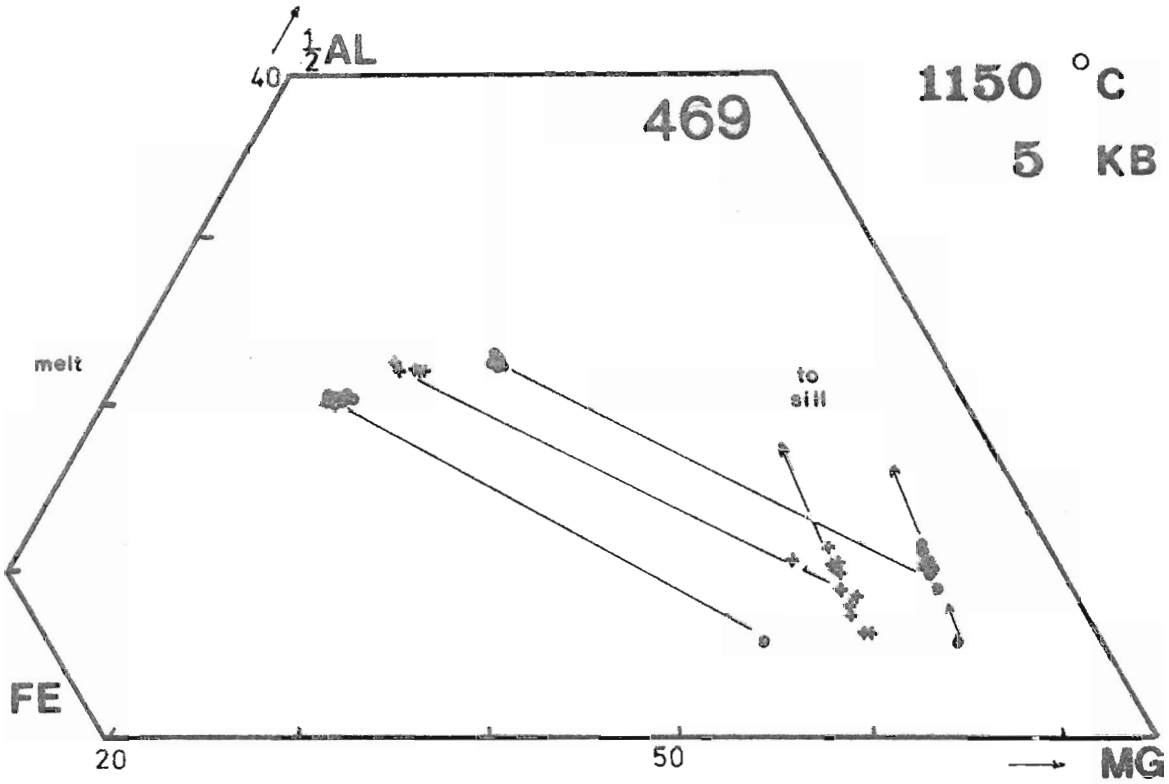
½AL
40
469
1150 °C
5 KB
melt
to sill
FE
20
50
MG

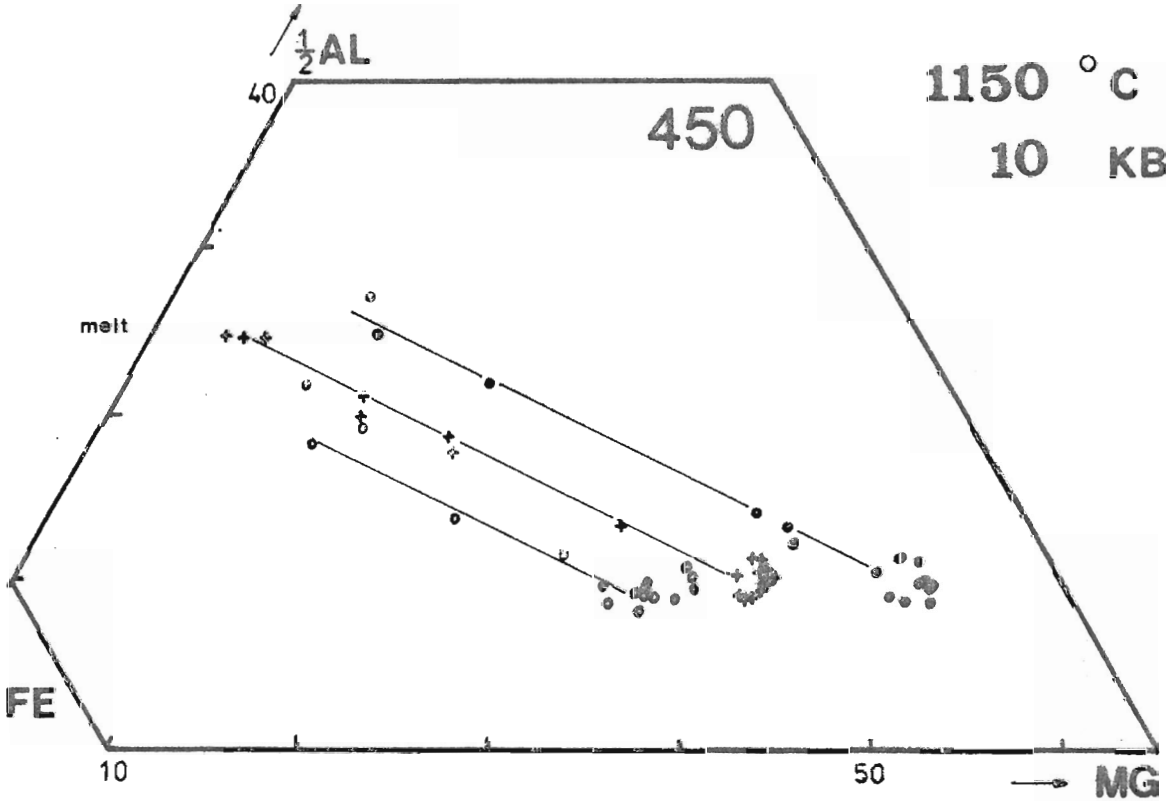
½AL
40
450
1150 °C
10 KB
melt
FE
10
50
MG

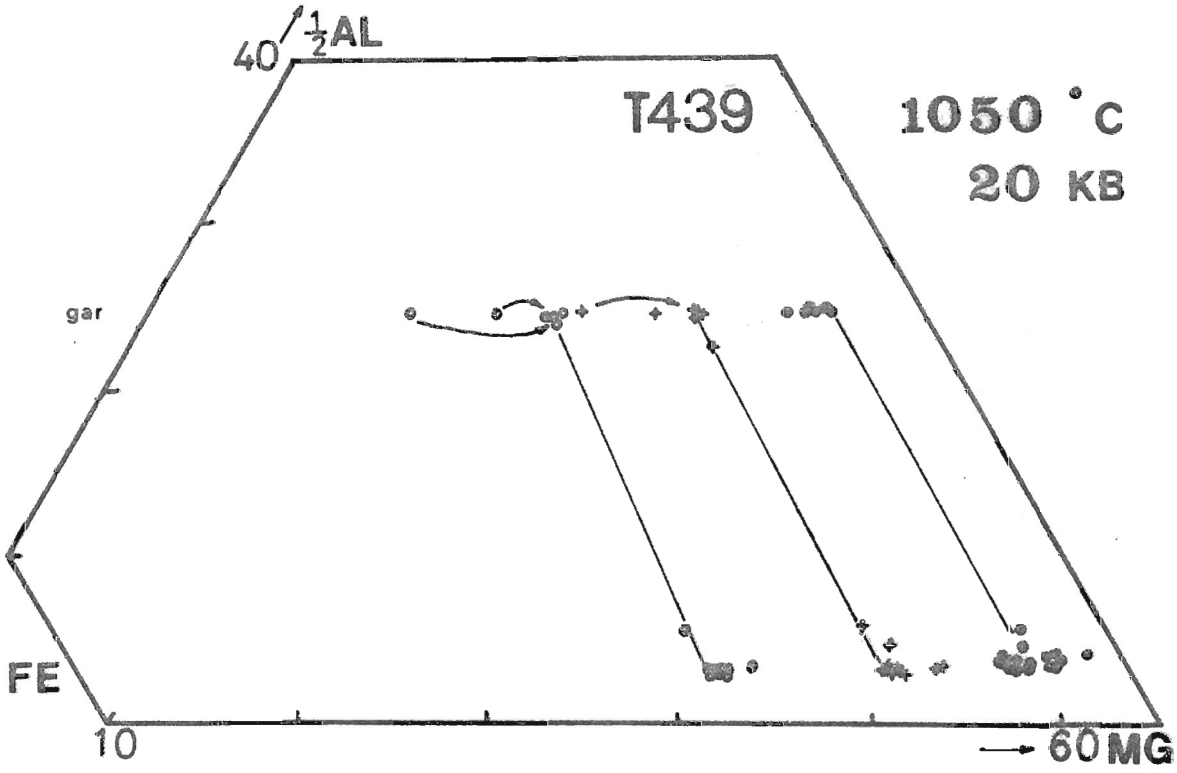
40
½AL
T439
1050 °C
20 KB
gar
FE
10
60 MG

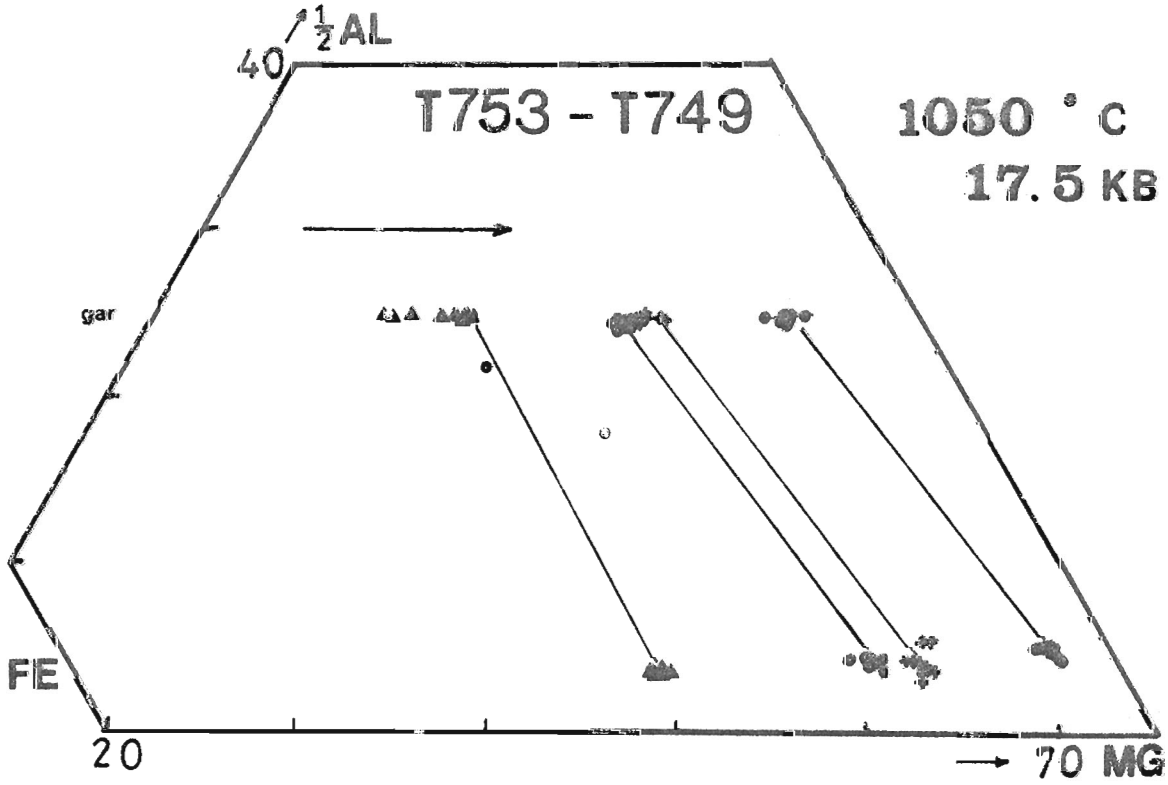
40
½AL
T753 - T749
1050 °C
17.5 KB
gar
FE
20
70 MG

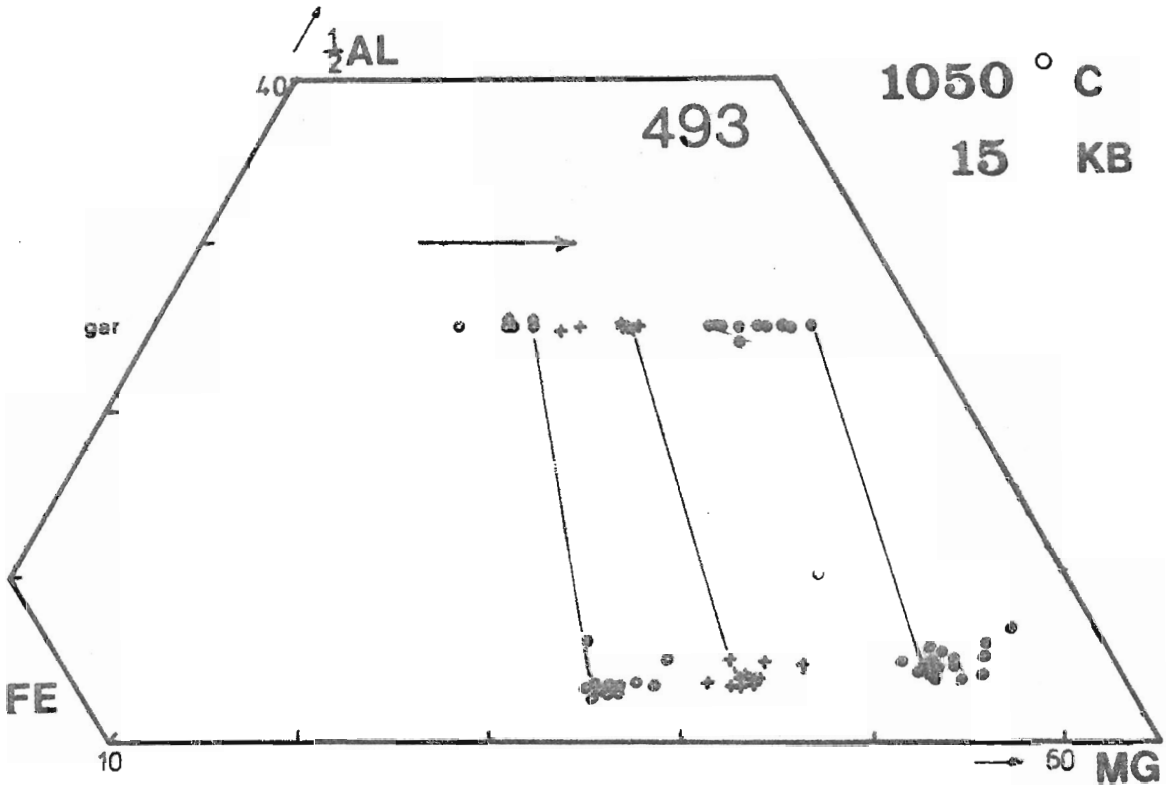
½AL
40
493
1050 ° C
15 KB
gar
FE
10
50
MG

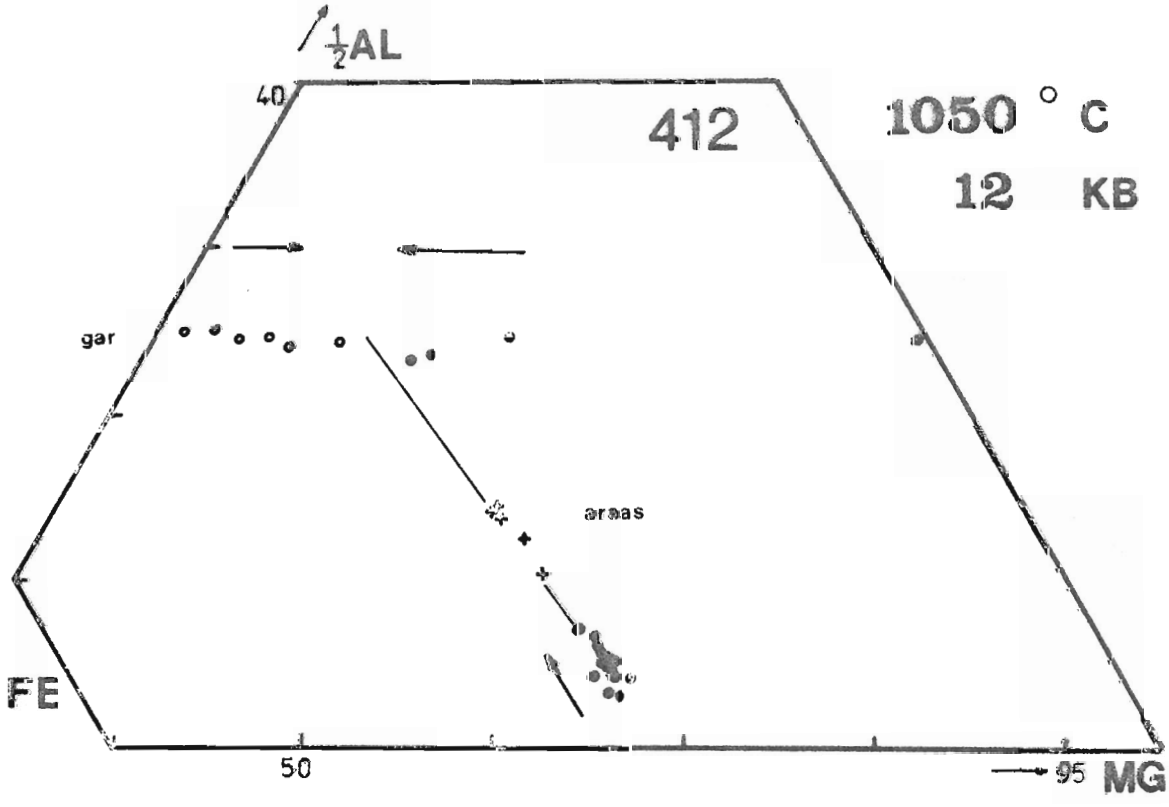
½AL
40
412
1050 ° C
12 KB
gar
arsas
FE
50
95
MG

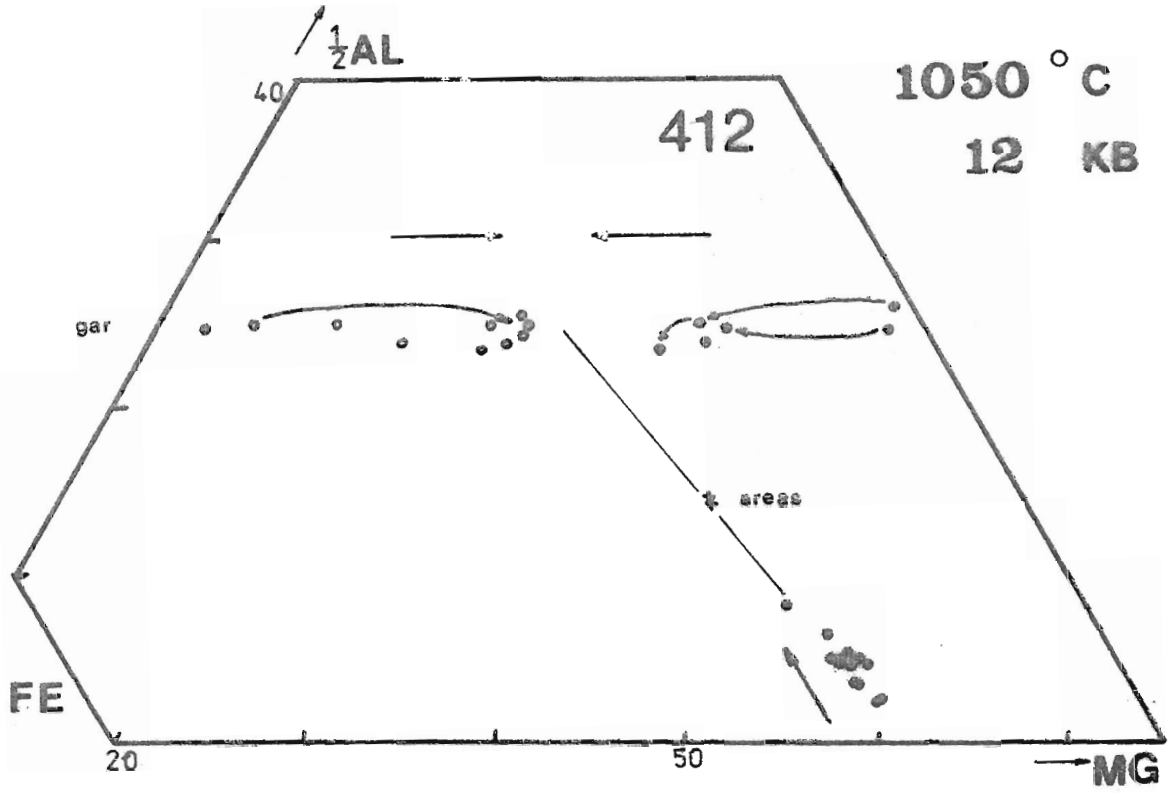
½AL
40
412
1050 °C
12 KB
gar
areas
FE
20
50
MG

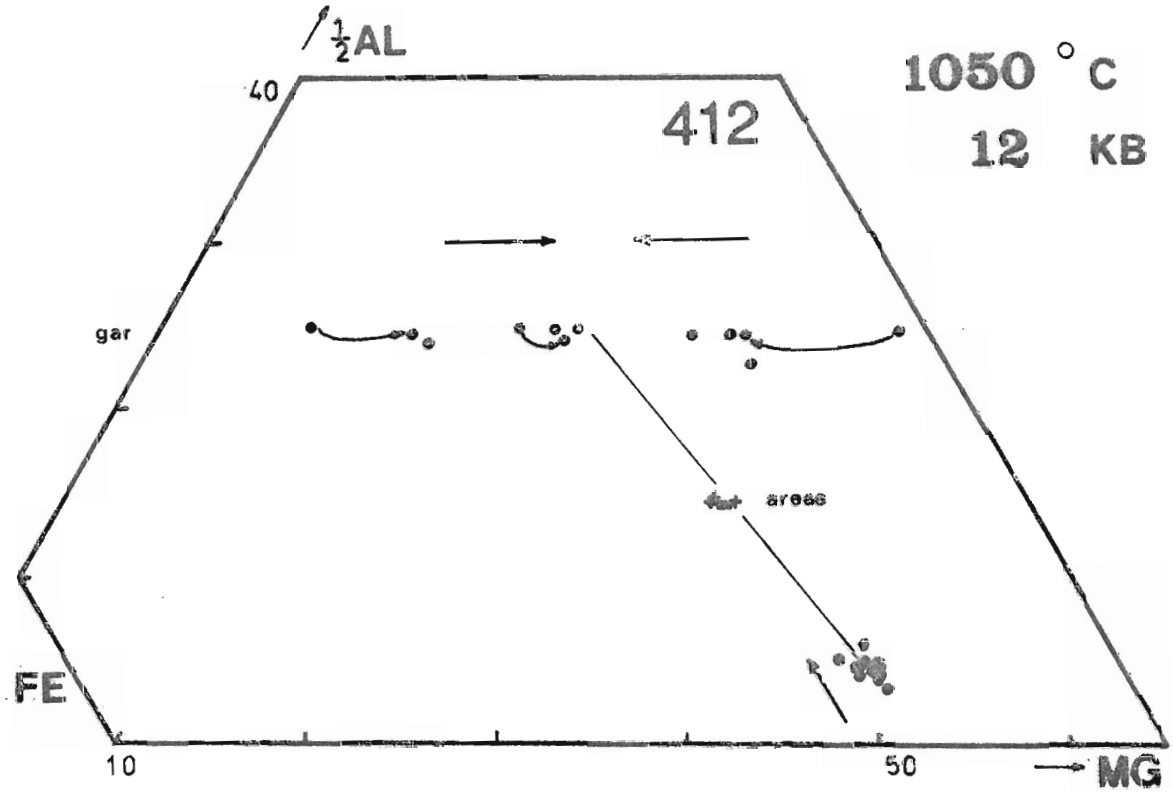
½AL
40
412
1050 °C
12 KB
gar
areas
FE
10
50
MG

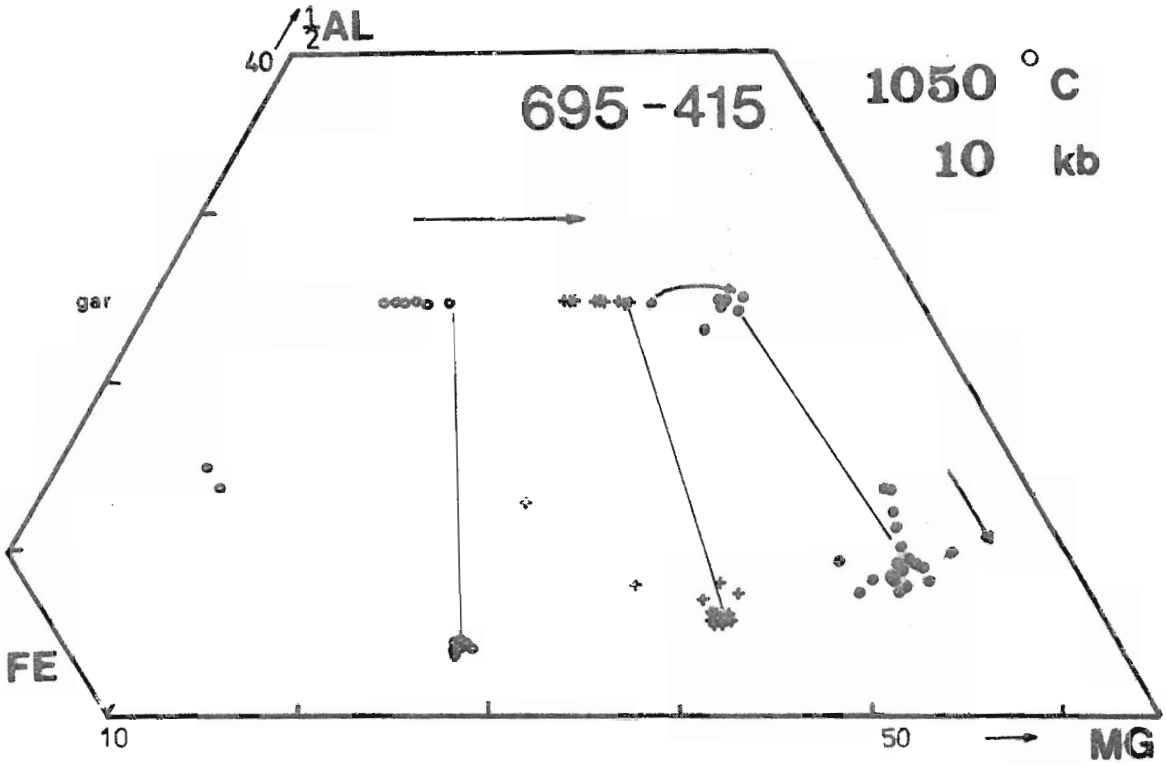
½AL
40
695 - 415
1050 °C
10 kb
gar
FE
10
50
MG

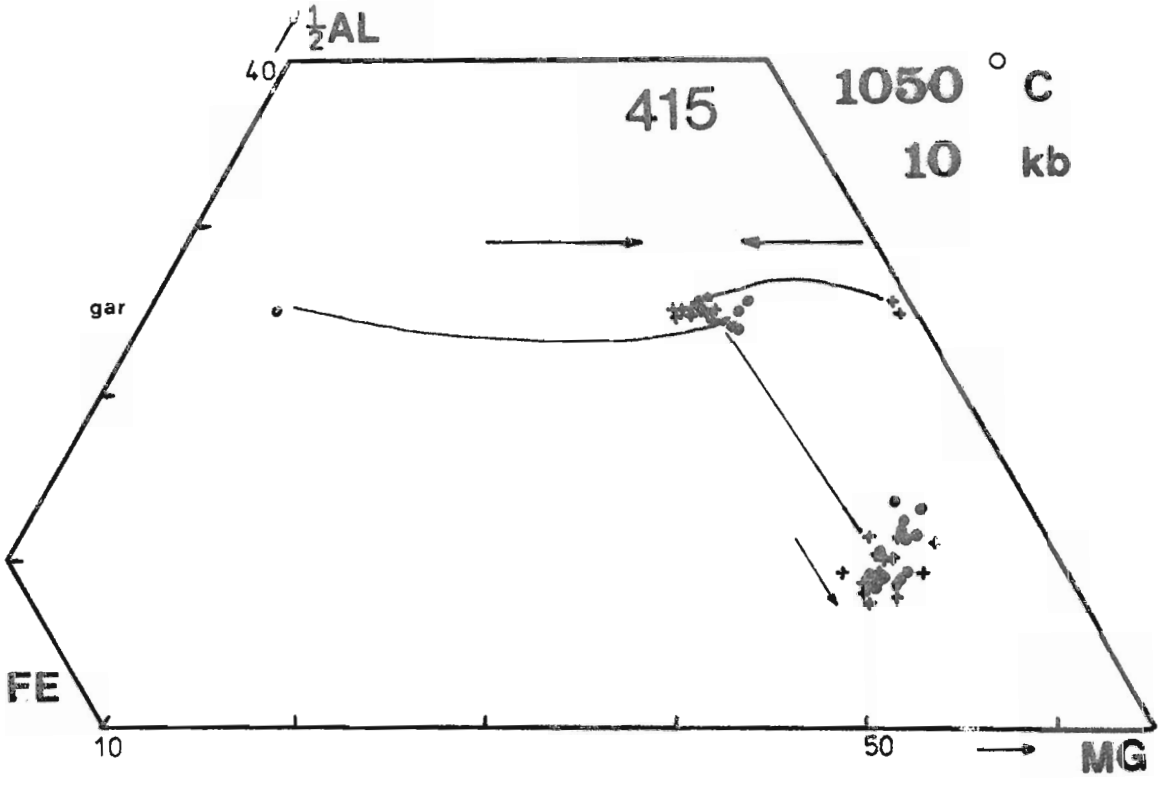
½AL
40
415
1050 °C
10 kb
gar
FE
10
50
MG

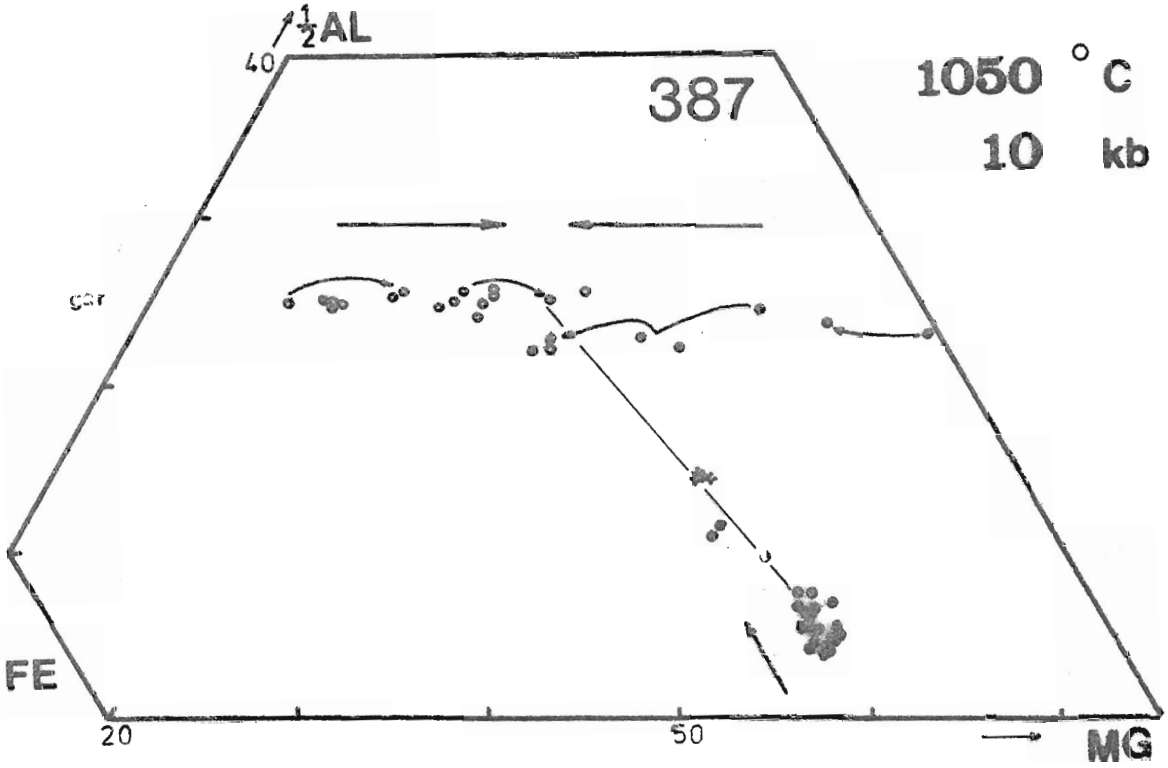
½AL
40
387
1050 °C
10 kb
gar
FE
20
50
MG

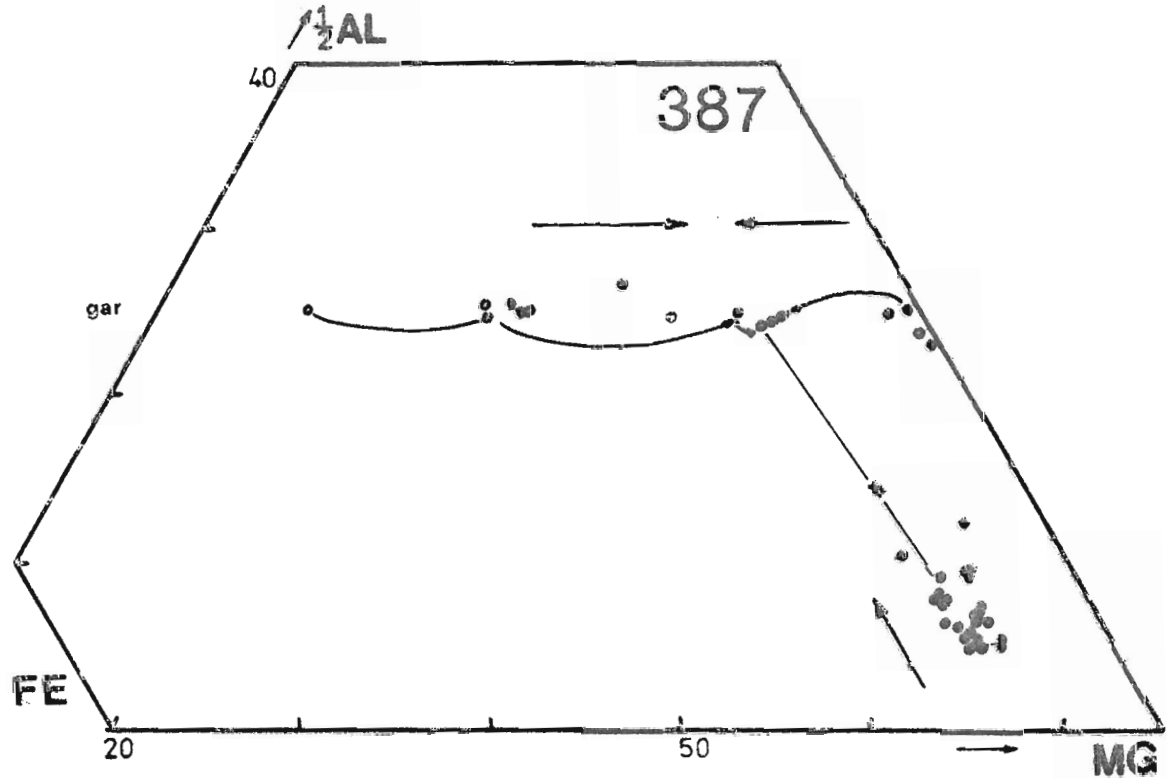
½AL
40
387
gar
FE
20
50
MG

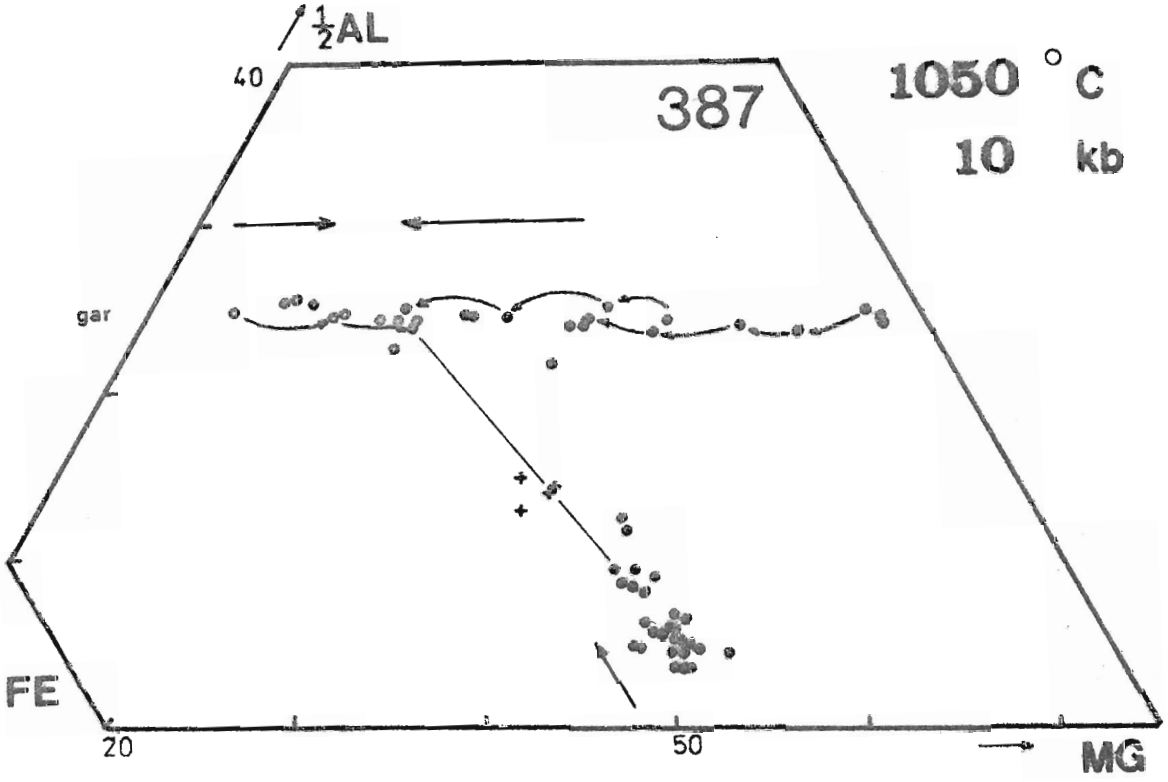
½AL
40
387
1050 °C
10 kb
gar
FE
20
50
MG

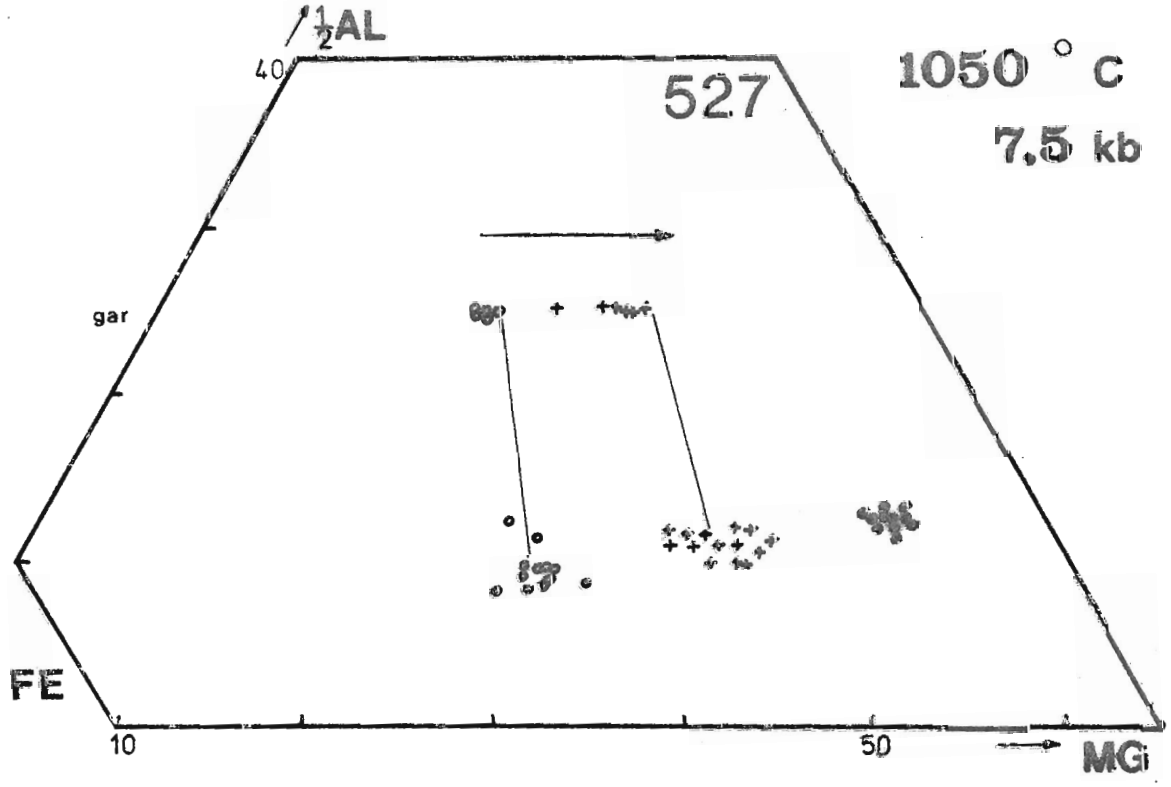
½AL
40
527
1050 °C
7,5 kb
gar
FE
10
50
MG

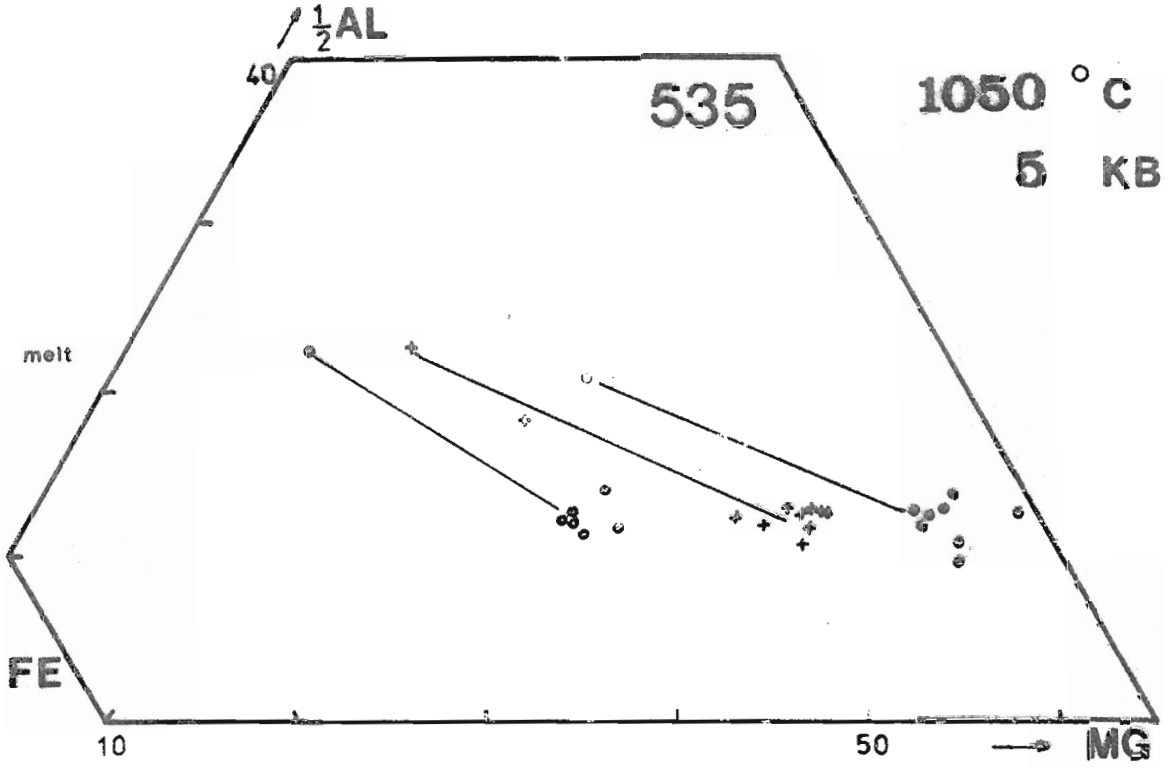
½AL
40
535
1050 °C
5 KB
melt
FE
10
50
MG

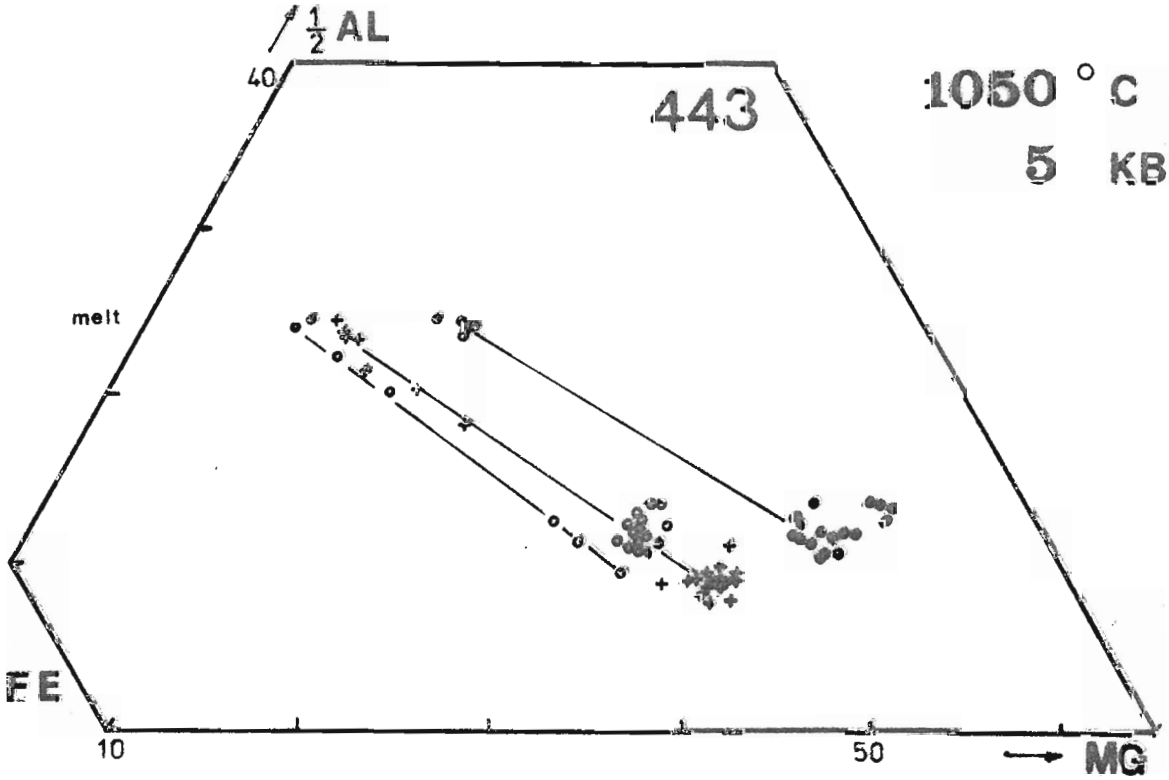
½AL
40
443
1050 °C
5 KB
melt
FE
10
50
MG

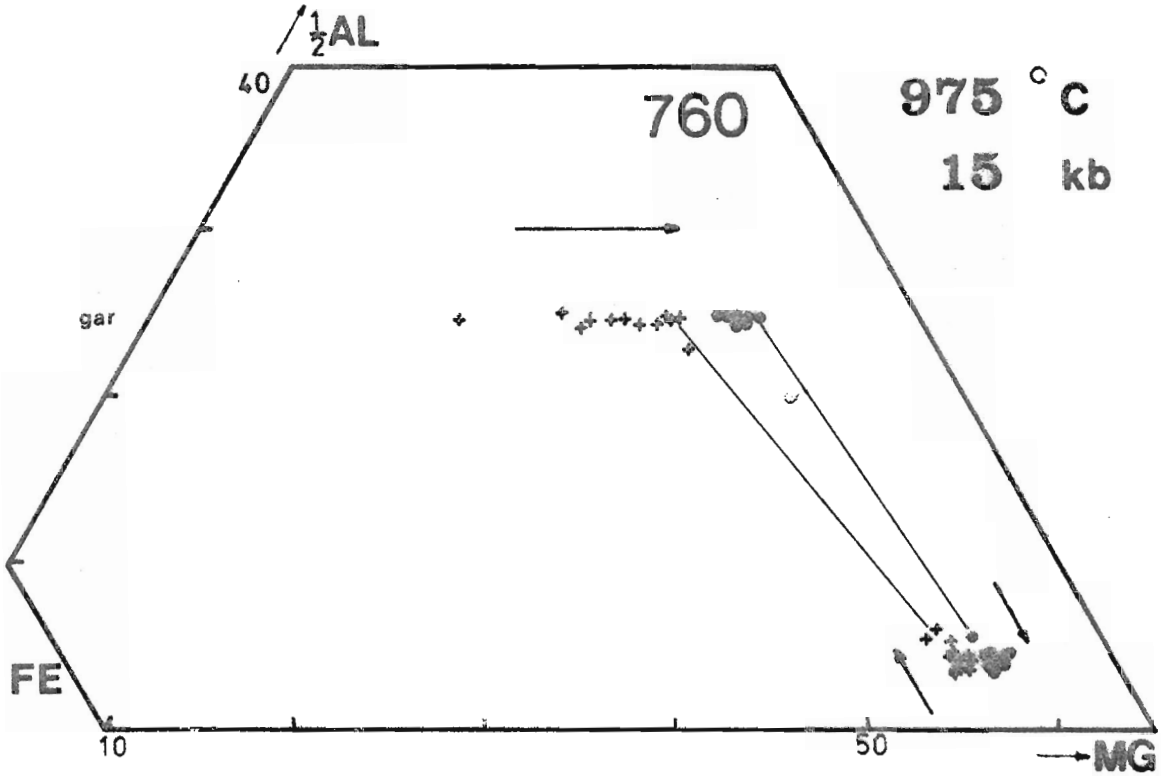
½AL
40
760
975 °C
15 kb
gar
FE
10
50
MG

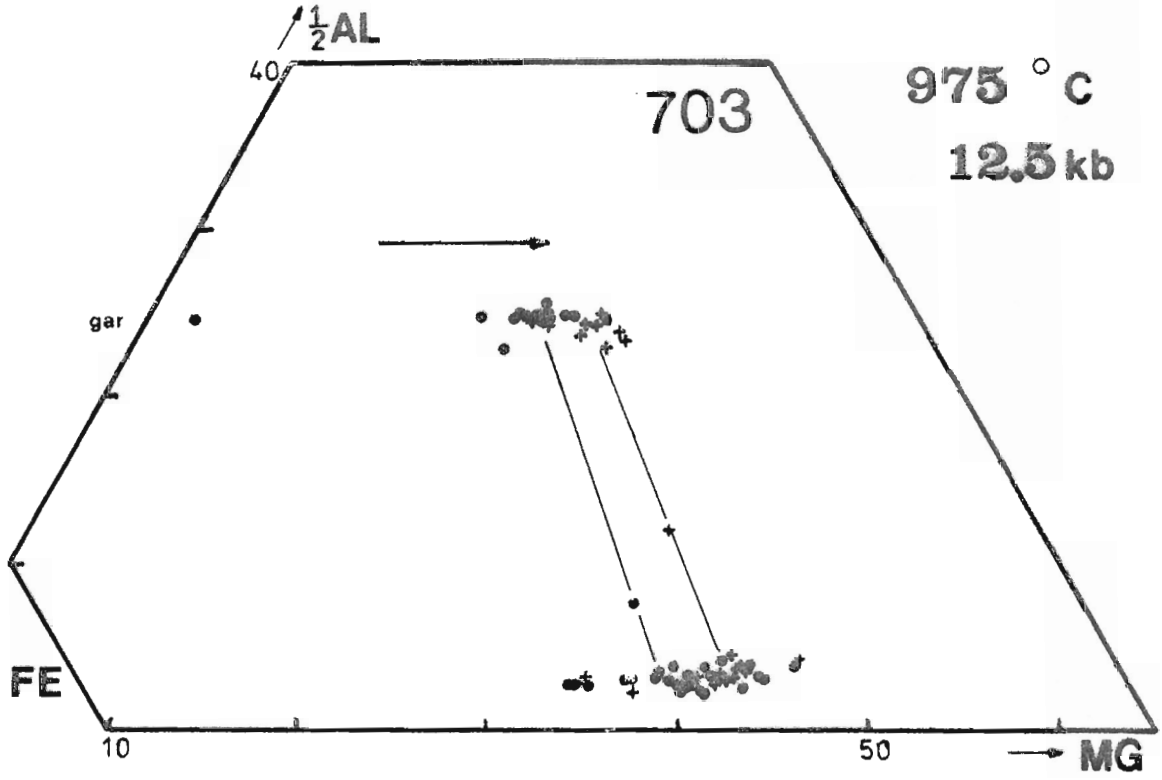
½AL
40
703
975 °C
12.5 kb
gar
FE
10
50
MG

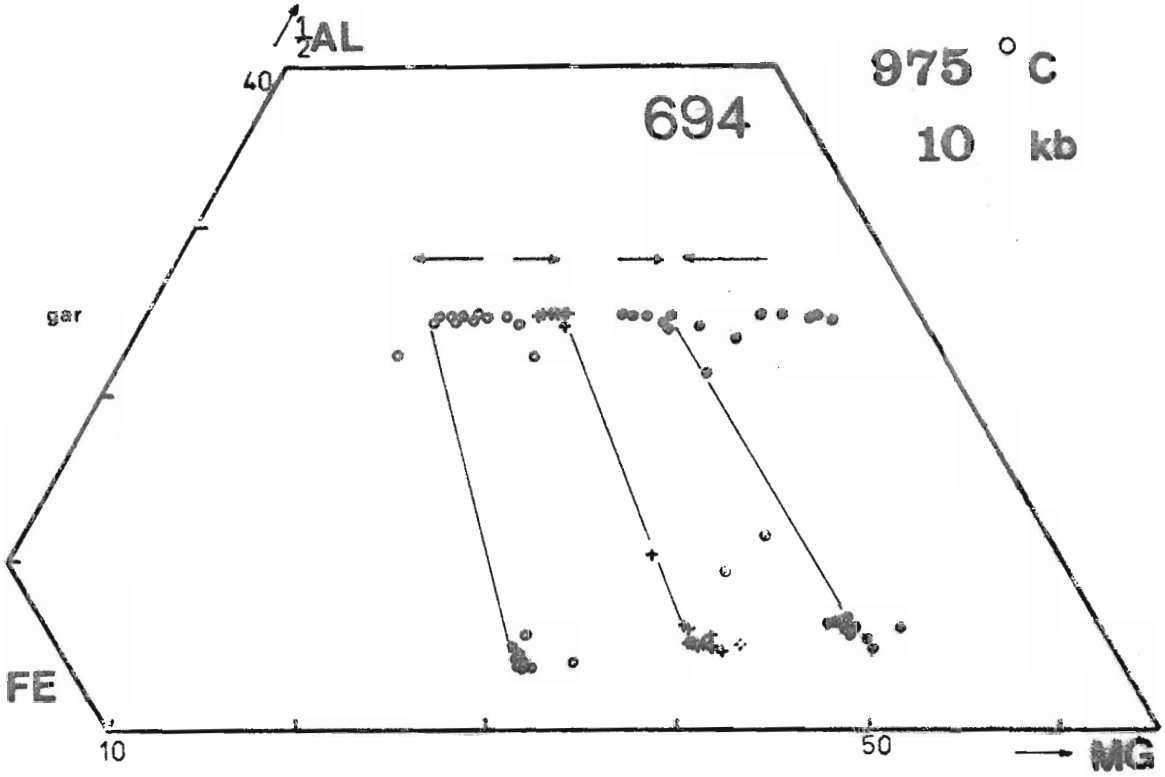
½AL
40
694
975 °C
10 kb
gar
FE
10
50
MG

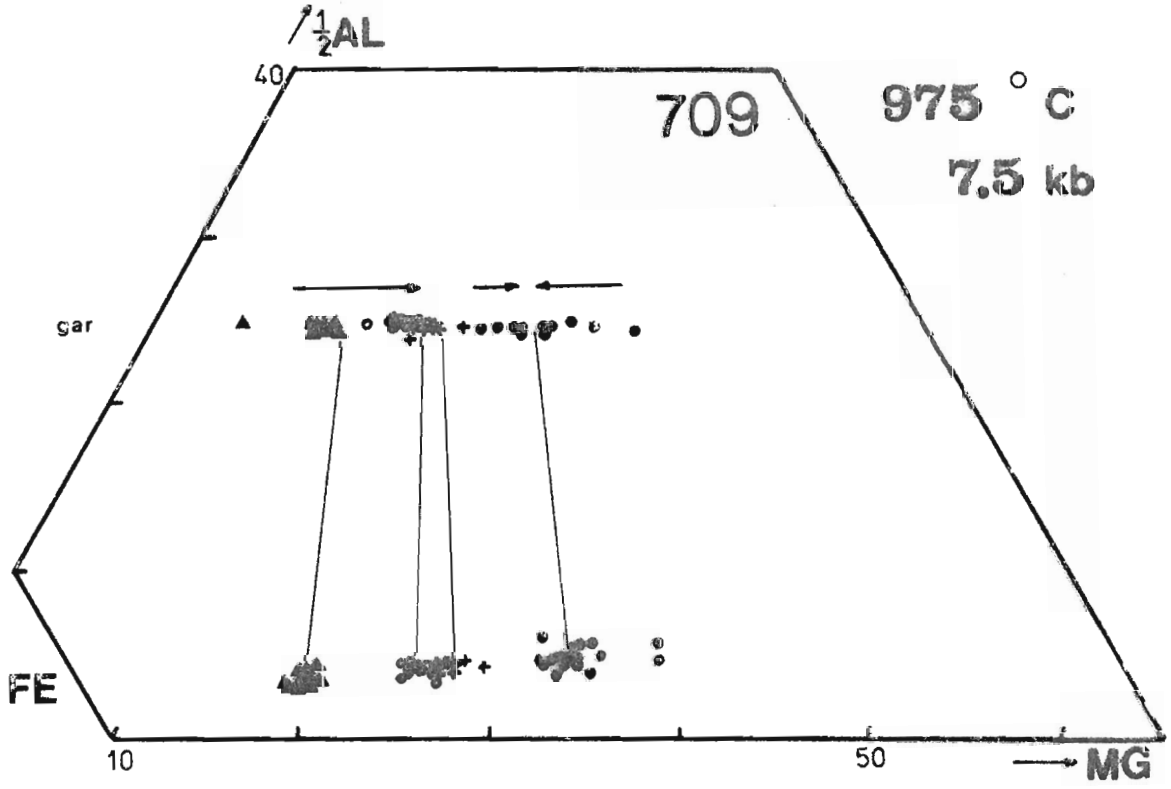
½AL
40
709
975 °C
7.5 kb
gar
FE
10
50
MG

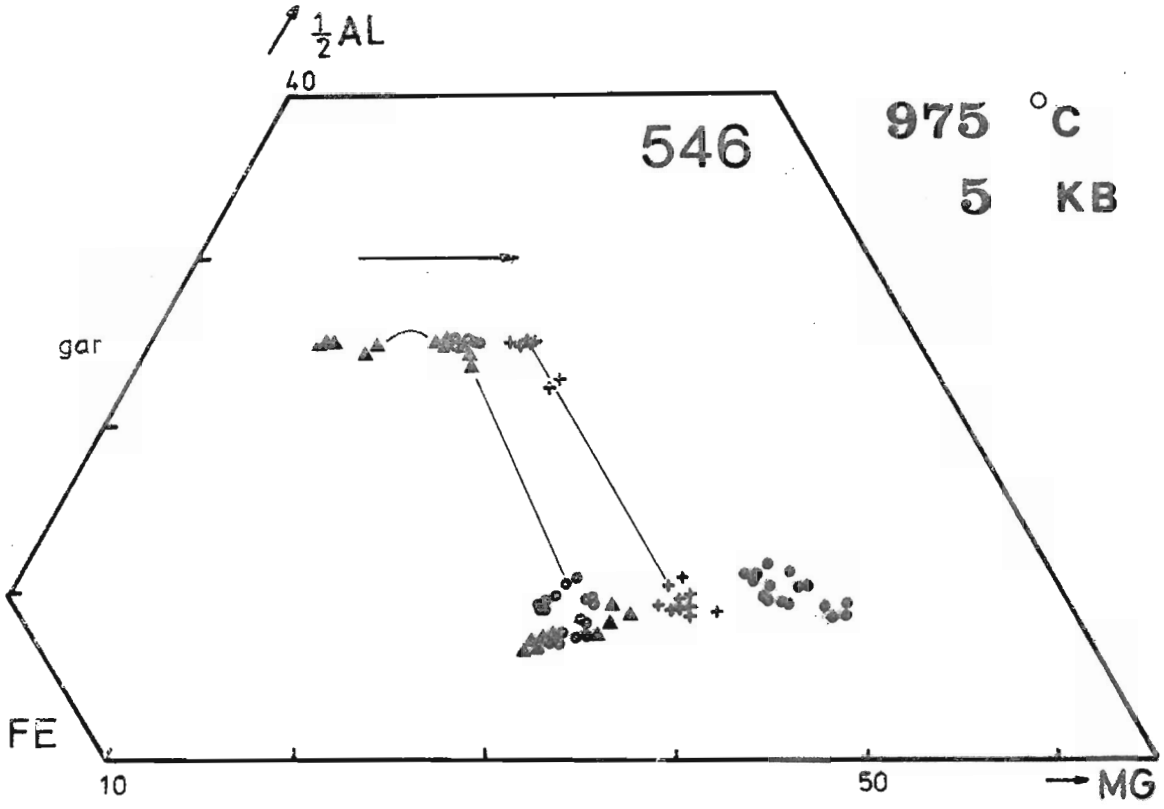
½AL
40
546
975 °C
5 KB
gar
FE
10
50
MG

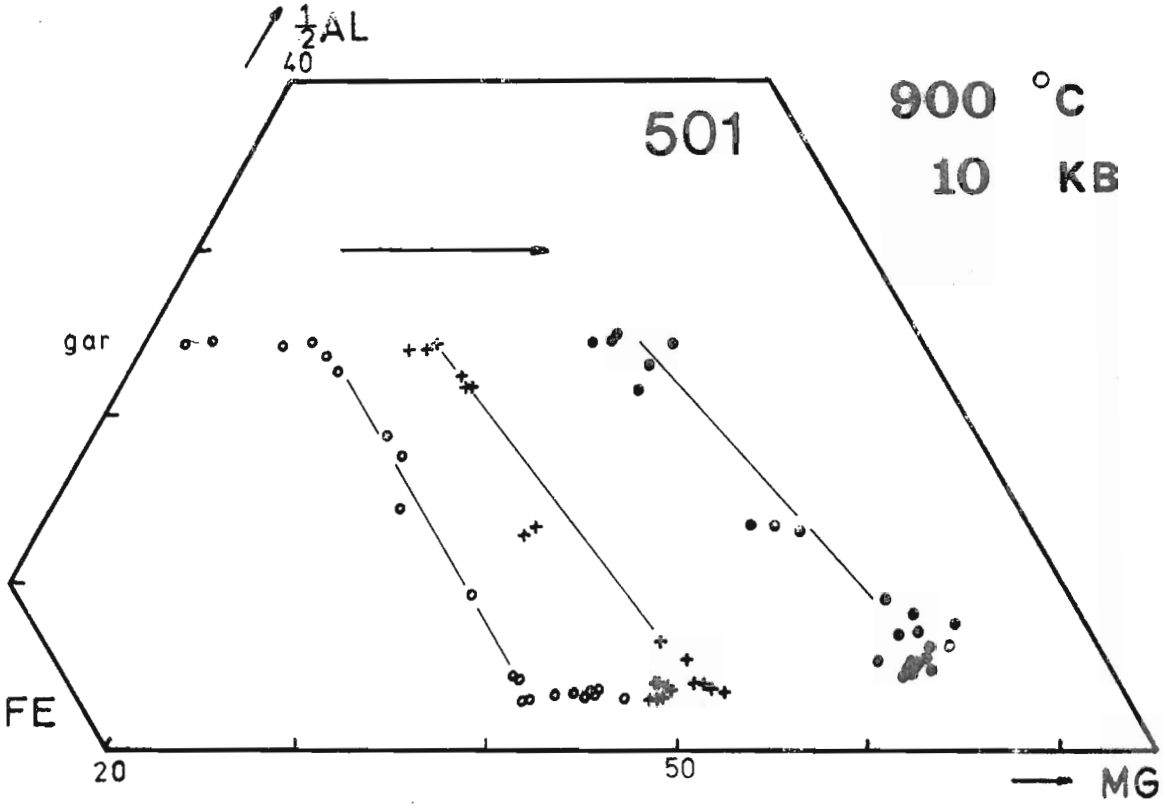
½AL
40
501
900 °C
10 KB
gar
FE
20
50
MG

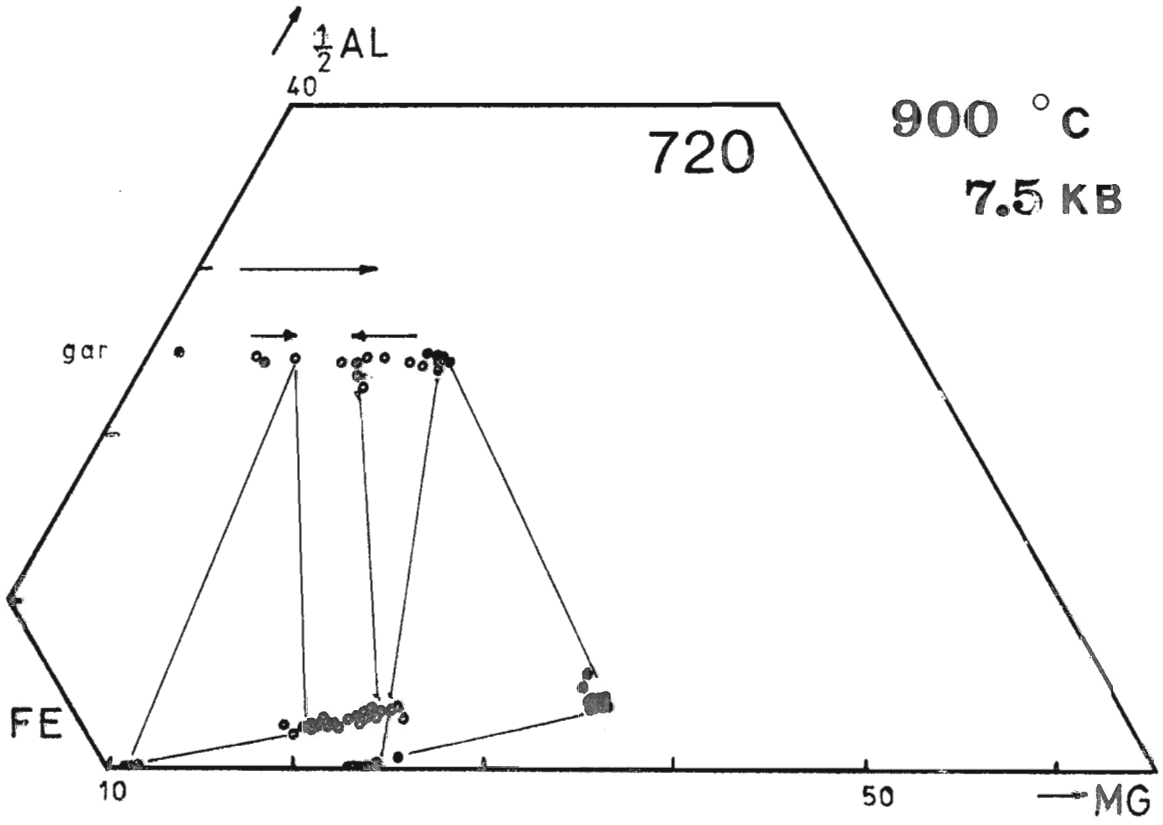
½AL
40
720
900 °C
7.5 KB
gar
FE
10
50
MG

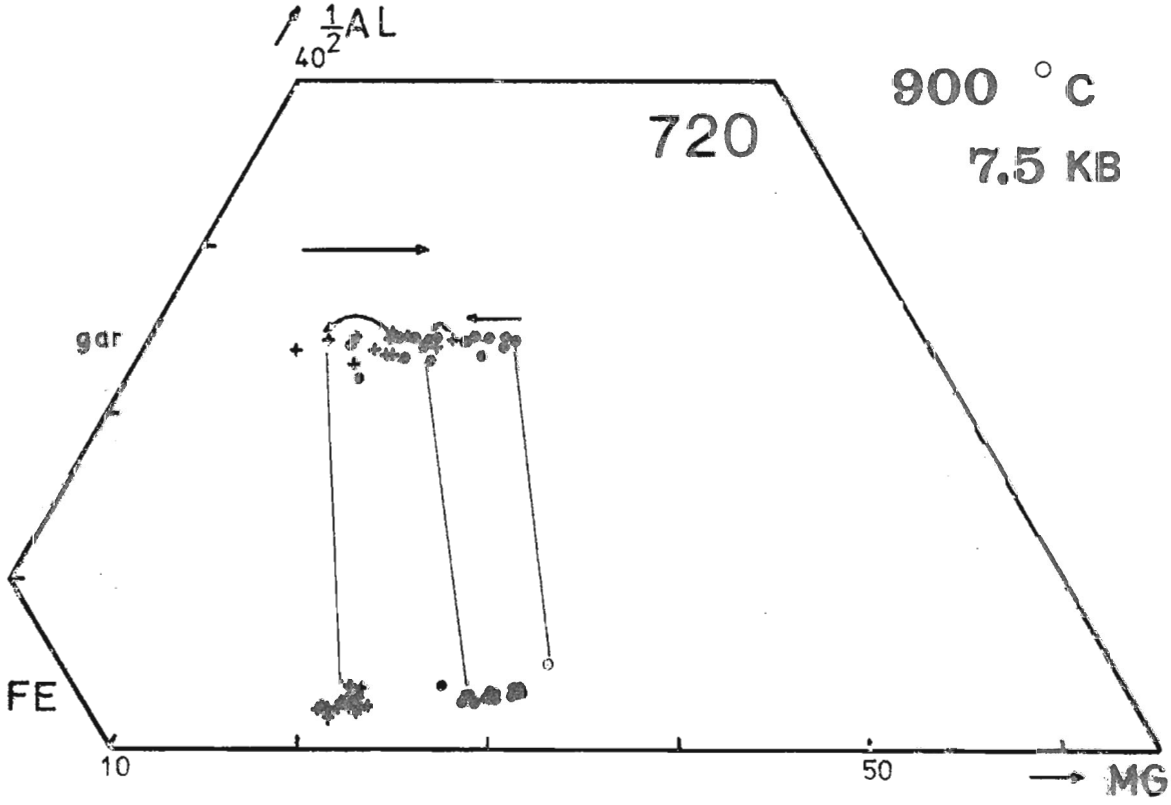
½AL
40
720
900 °C
7.5 KB
gar
FE
10
50
MG

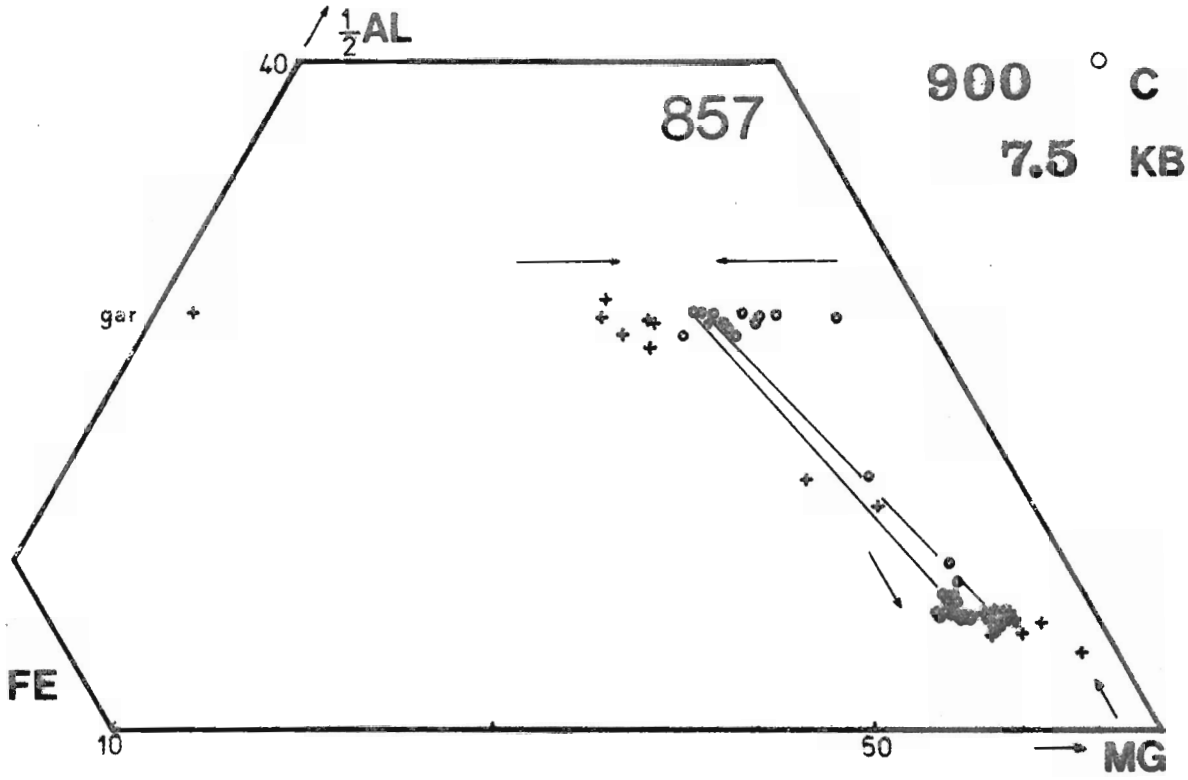
½AL
40
857
900 °C
7.5 KB
gar
FE
10
50
MG

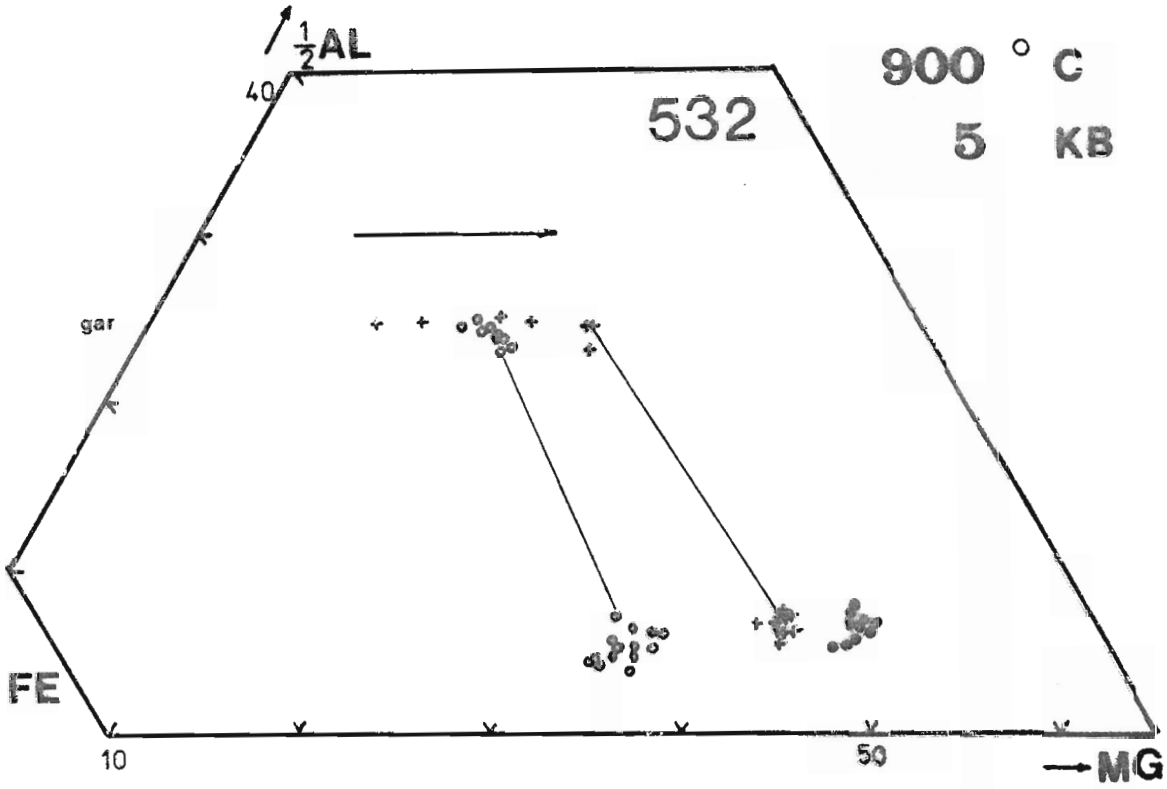
½AL
40
532
900 °C
5 KB
gar
FE
10
50
MG

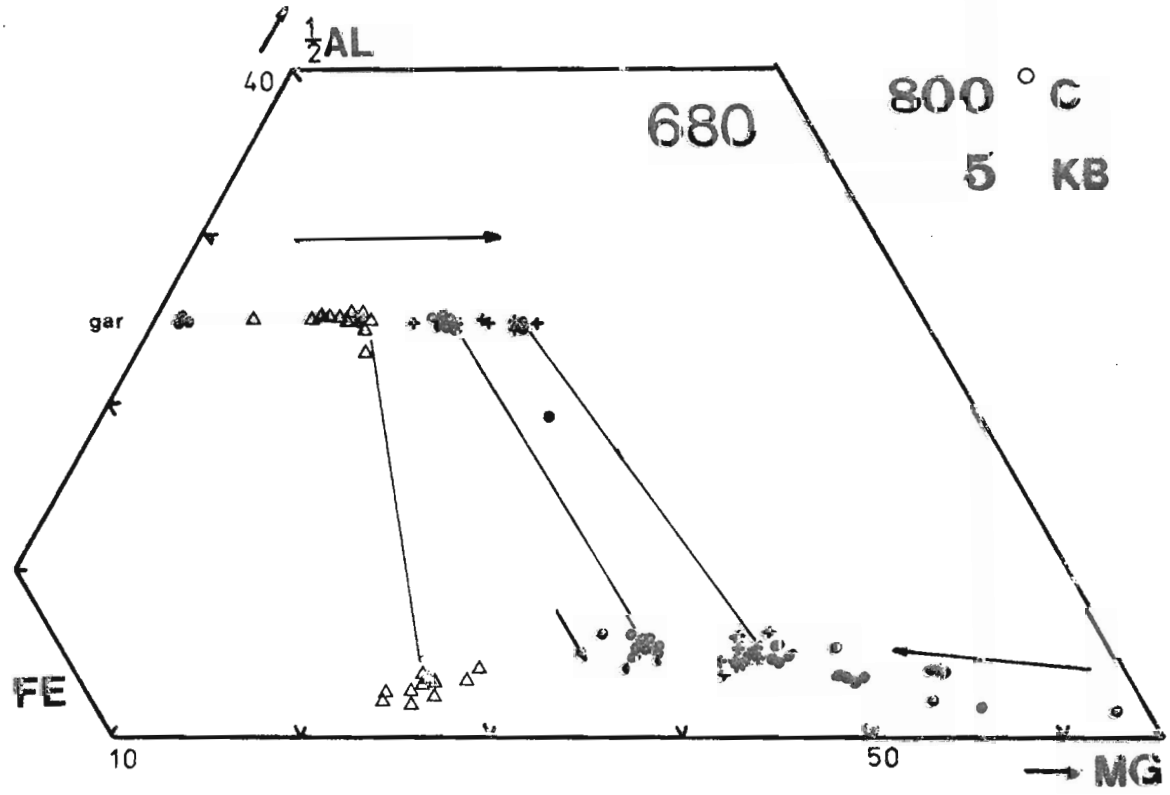
½AL
40
680
800 °C
5 KB
gar
FE
10
50
MG

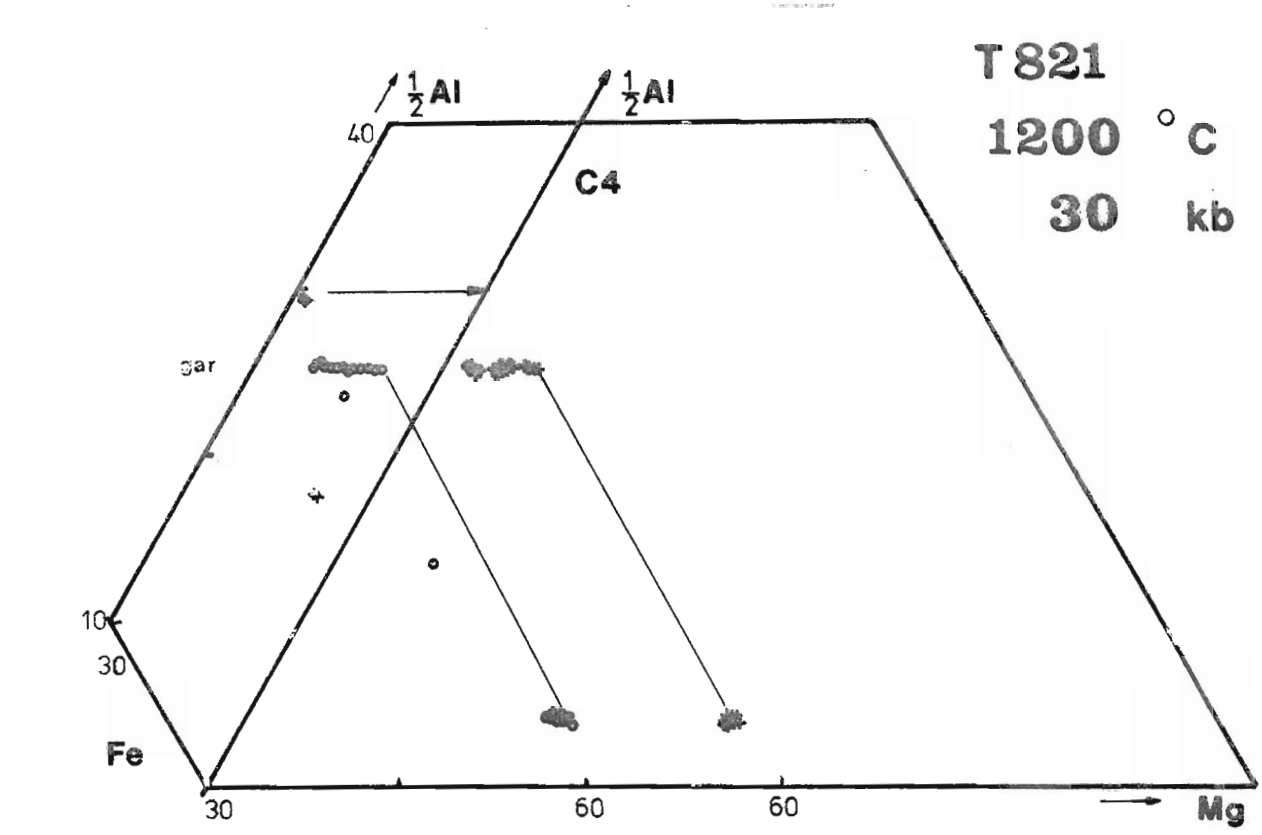
T 821
1200 °C
30 kb
½Al
½Al
C4
gar
40
10
30
Fe
30
60
60
Mg

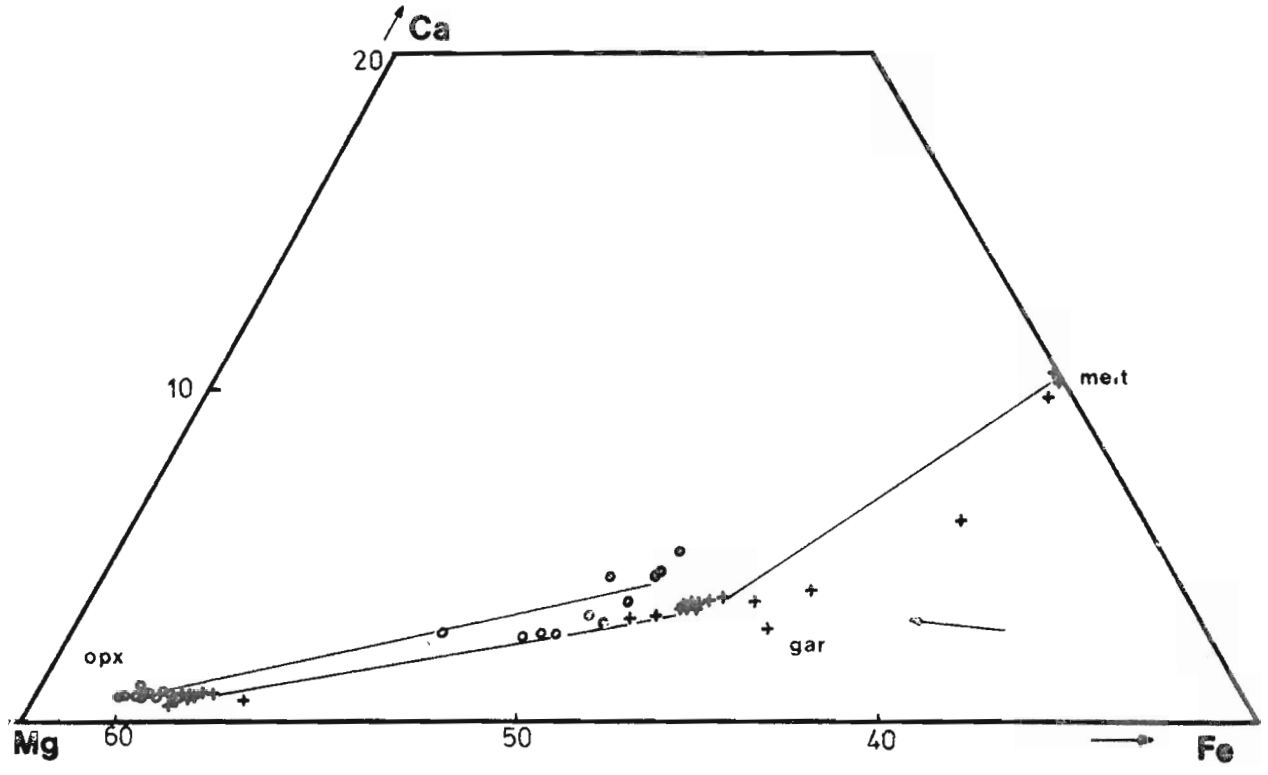
Ca
20
10
melt
gar
opx
Mg
60
50
40
Fe

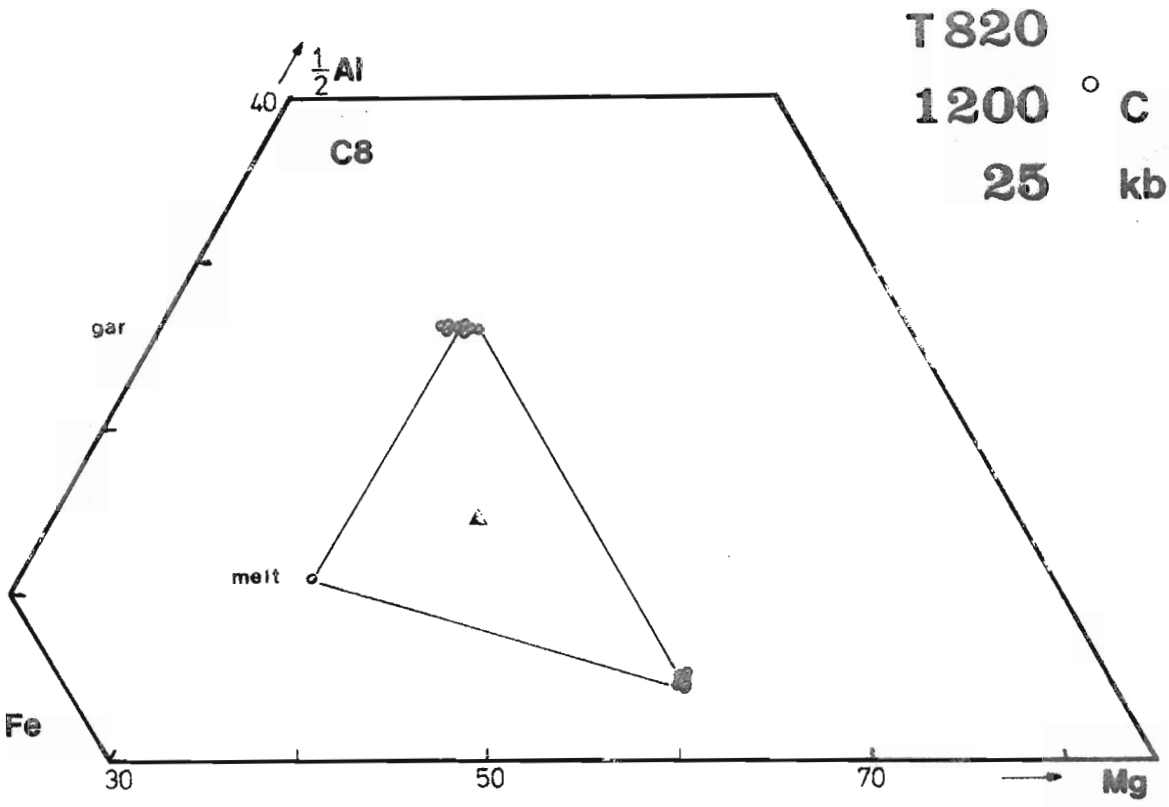
T 820
1200 °C
25 kb
½ Al
40
C8
gar
melt
Fe
30
50
70
Mg

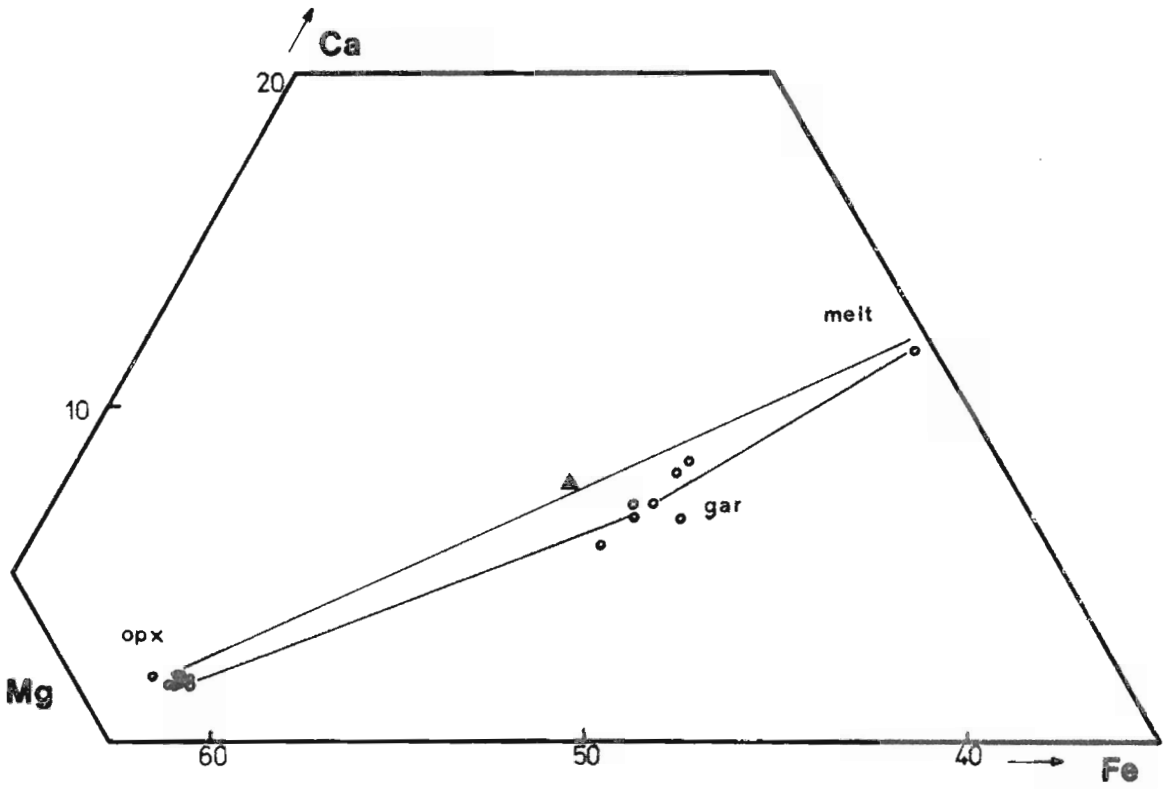
Ca
20
melt
10
gar
opx
Mg
60
50
40
Fe

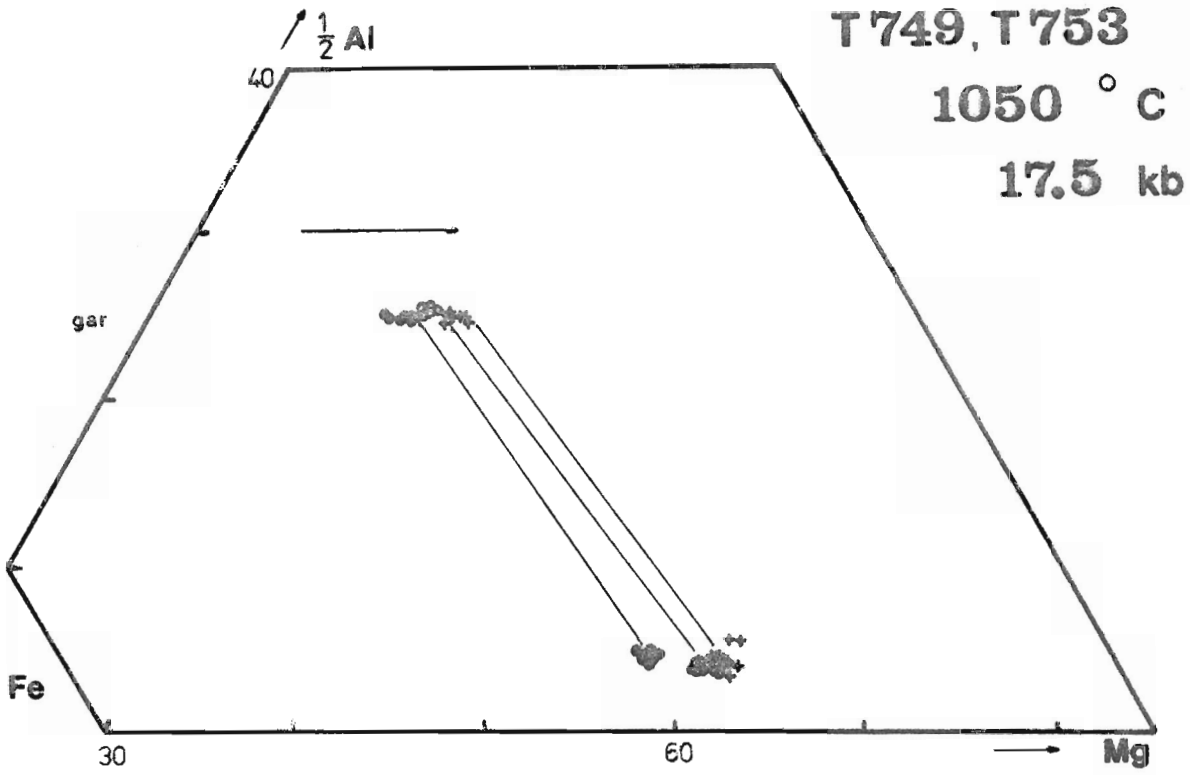
½ Al
40
gar
Fe
30
60
Mg
T749, T753
1050 °C
17.5 kb

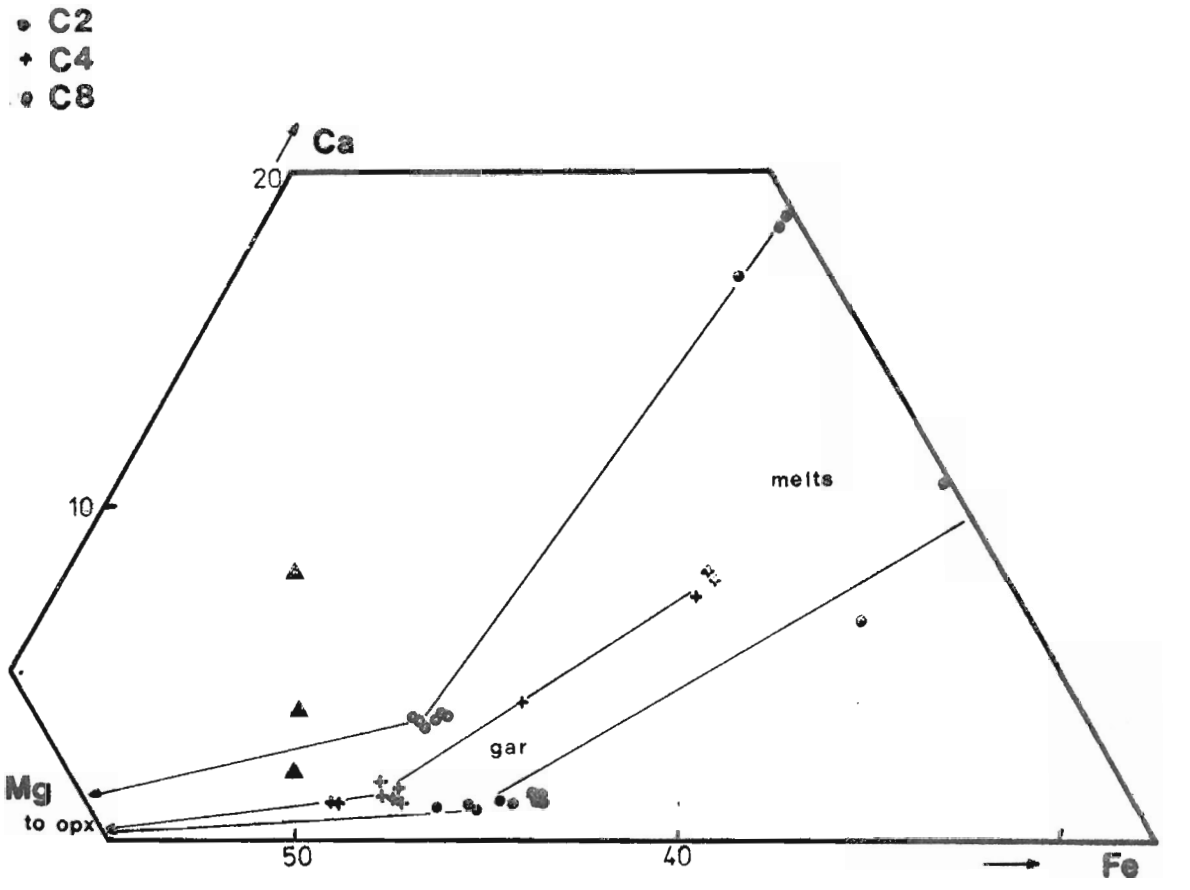
C2
C4
C8
Ca
20
10
melts
gar
Mg
to opx
50
40
Fe

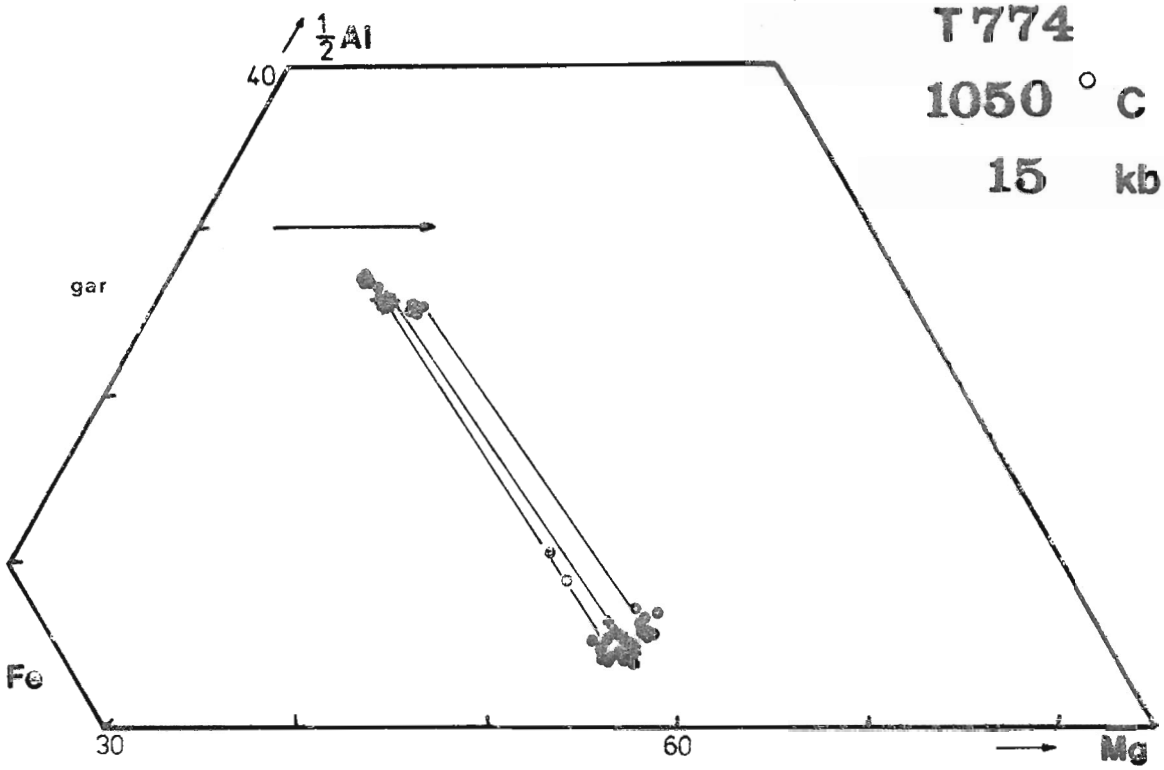
T774
1050 °C
15 kb
½Al
40
gar
Fe
30
60
Mg

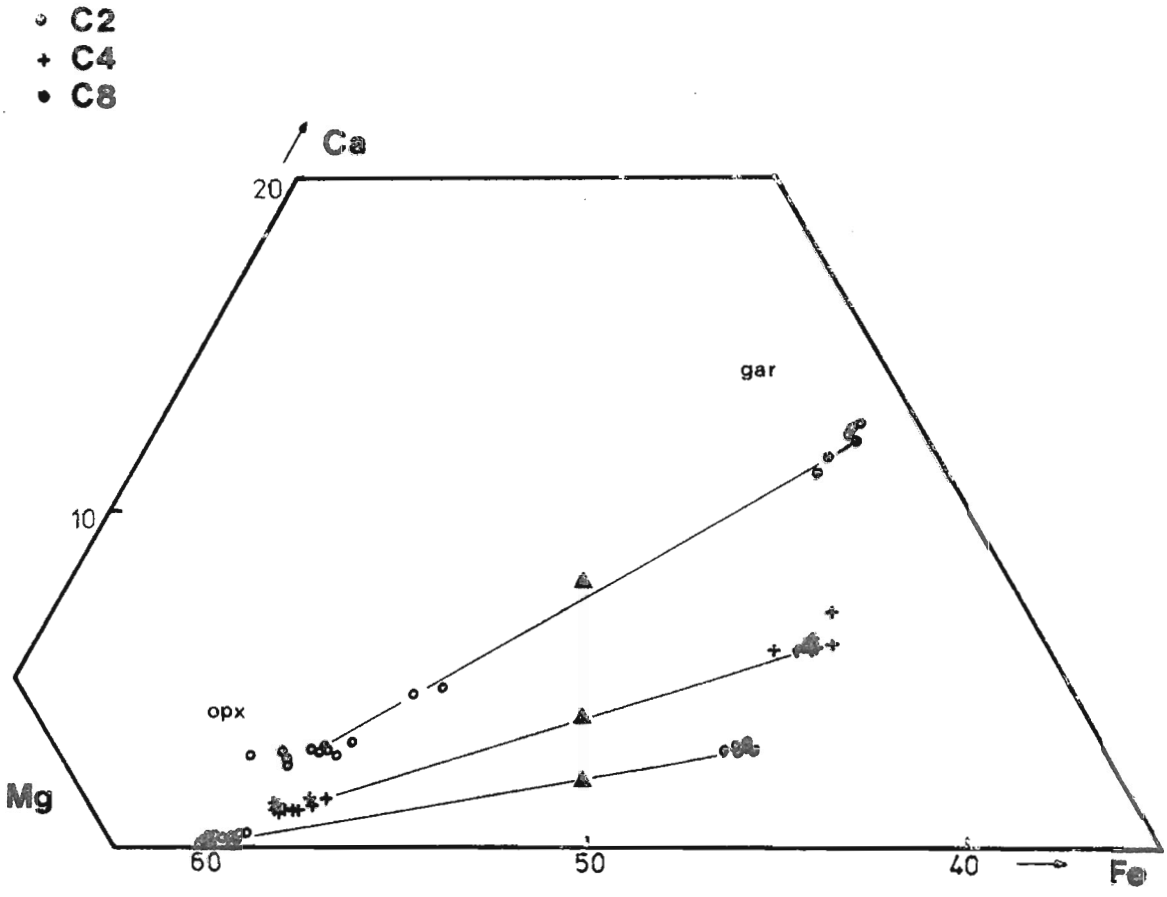
C2
C4
C8
Ca
20
10
gar
opx
Mg
60
50
40
Fe

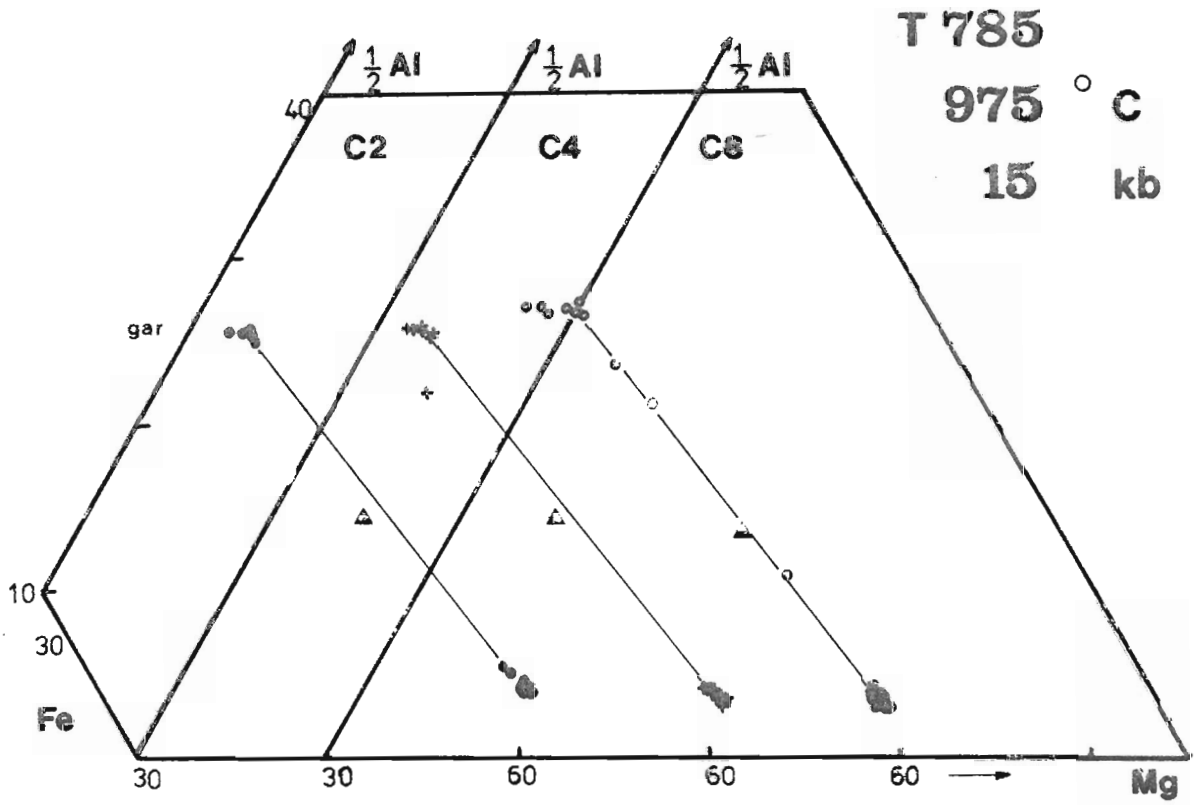
T 785
975 °C
15 kb
½ Al
½ Al
½ Al
40
C2
C4
C8
gar
10
30
Fe
30
30
60
60
60
Mg

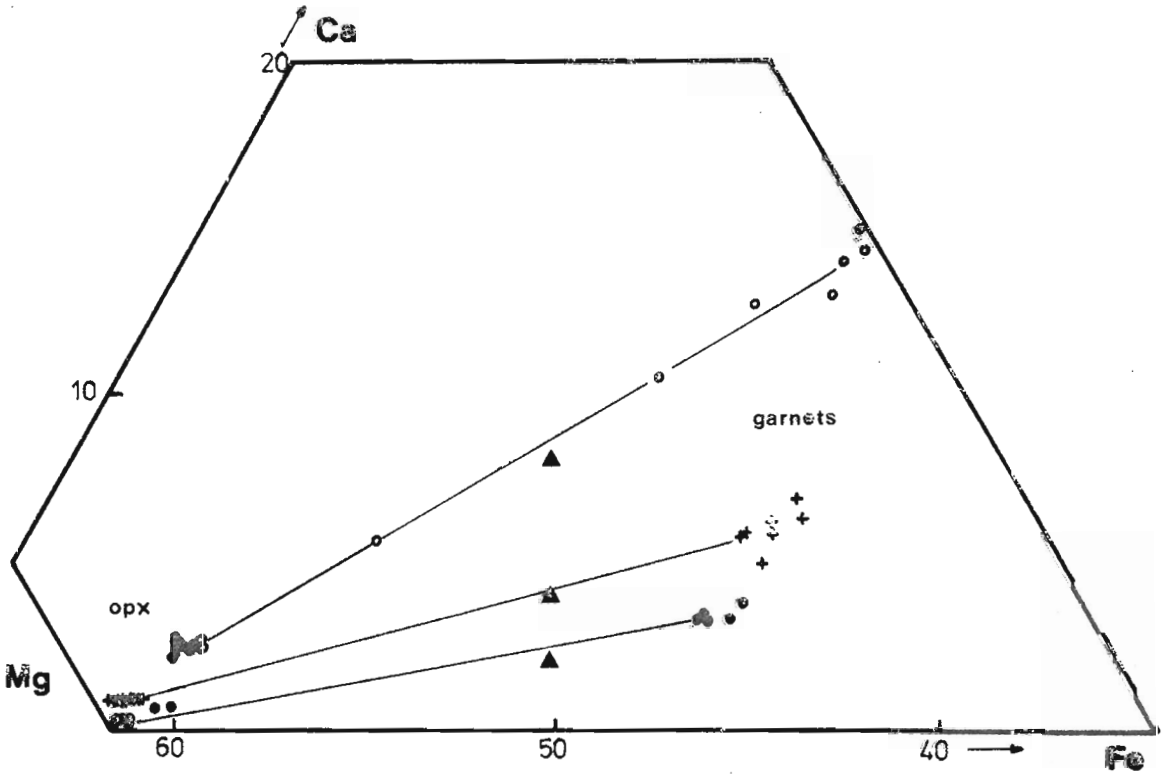
Ca
20
10
garnets
opx
Mg
60
50
40
Fe

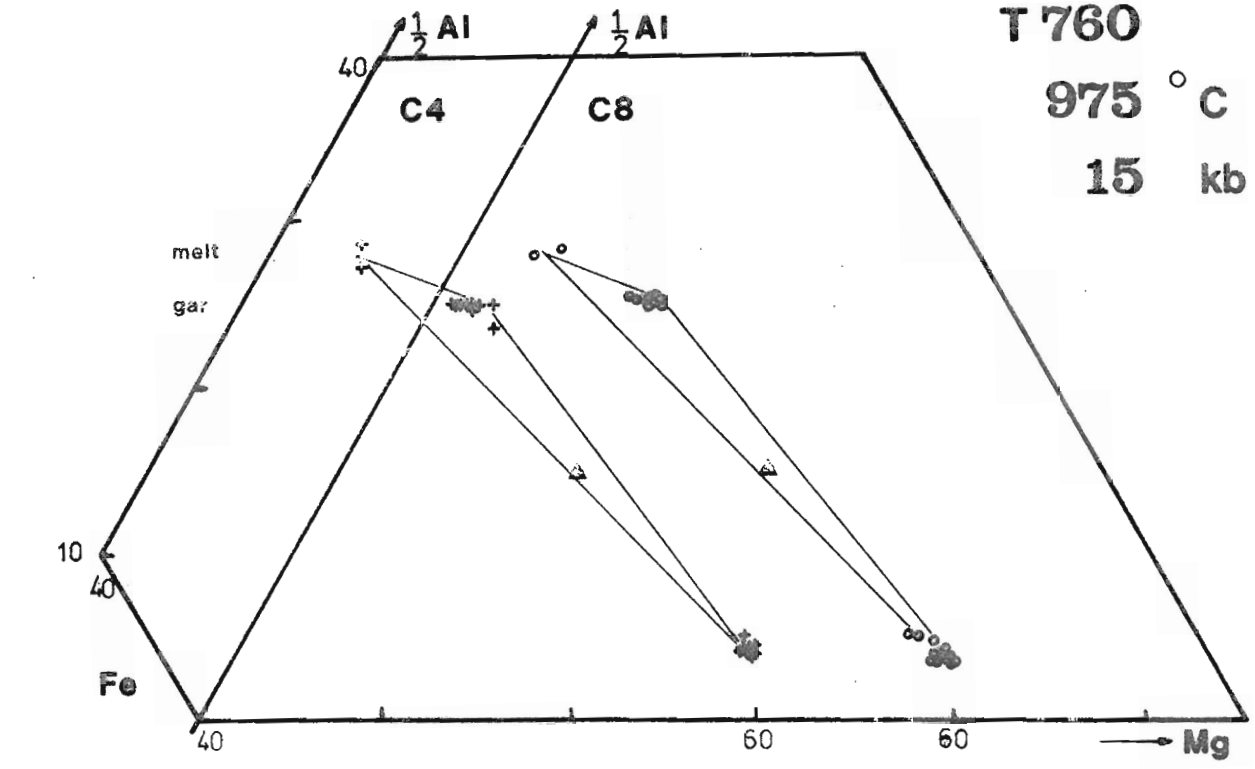
T 760
975 °C
15 kb
½ Al
½ Al
40
C4
C8
melt
gar
10
40
Fe
40
60
60
Mg

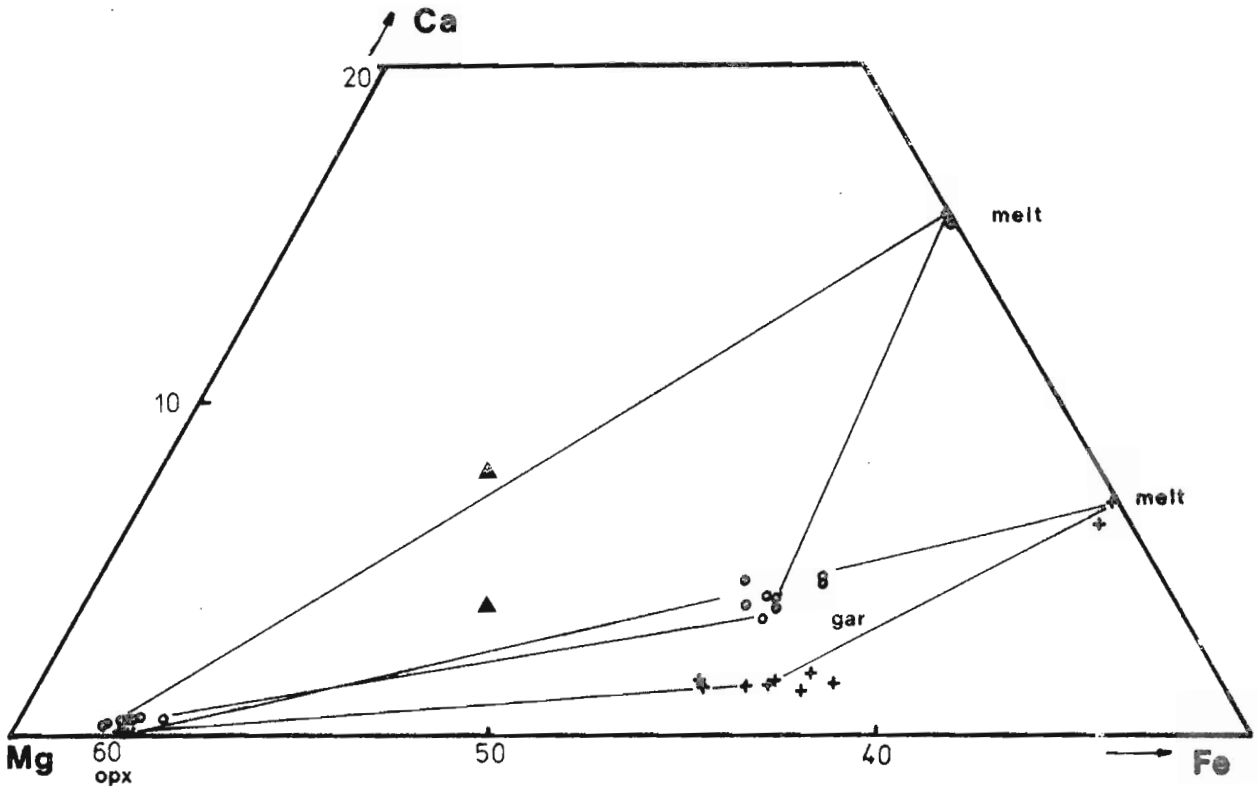
Ca
20
10
melt
melt
B
gar
Mg
60
opx
50
40
Fe

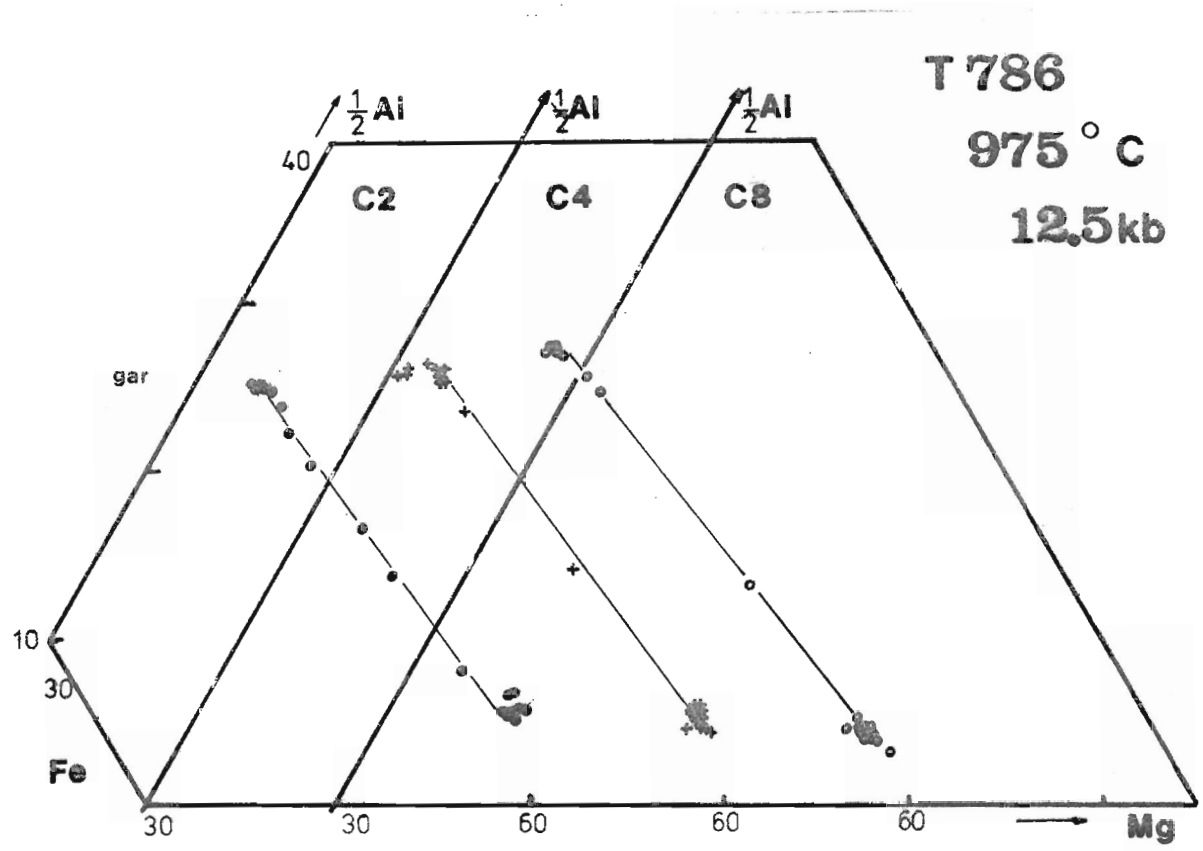
T 786
975 ° C
12.5kb
½ Al
½ Al
½ Al
C2
C4
C8
gar
40
10
30
Fe
30
30
60
60
60
Mg

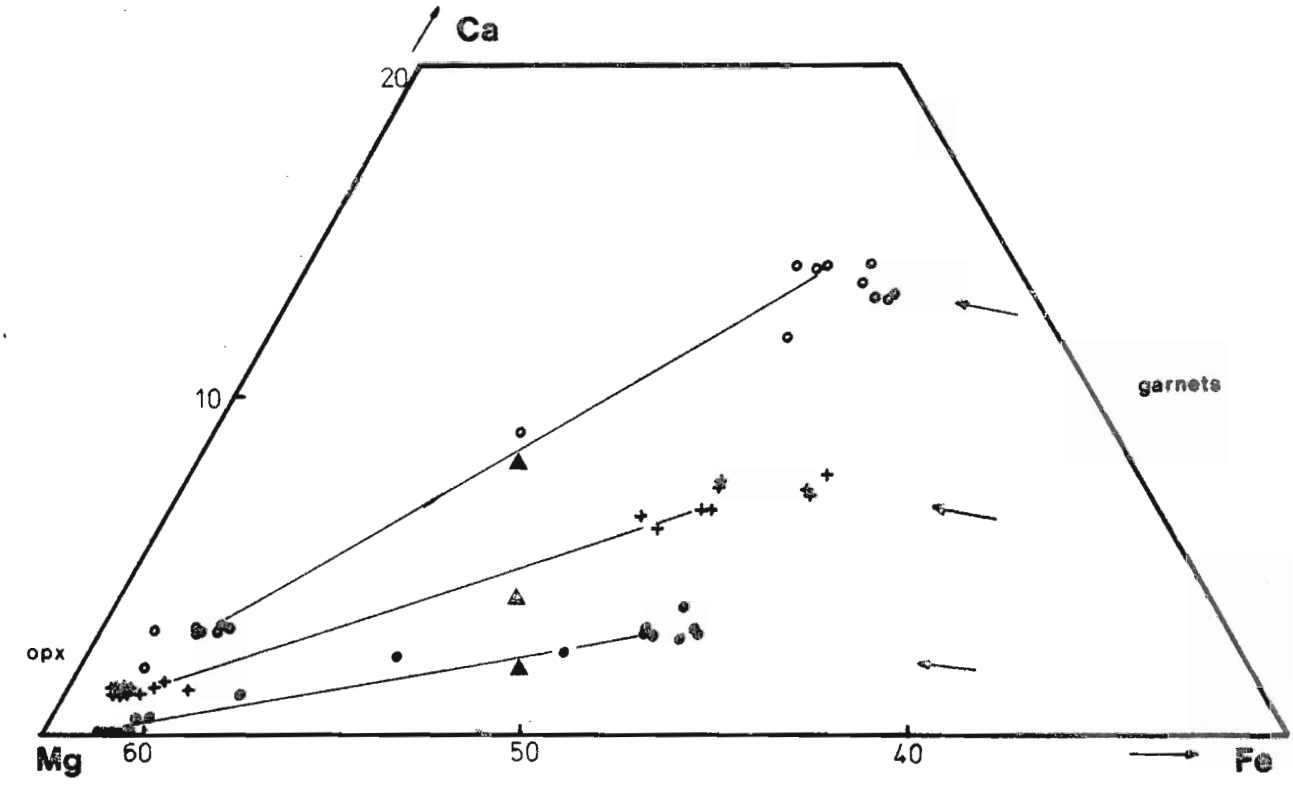
Ca
20
10
garnets
opx
Mg
60
50
40
Fe

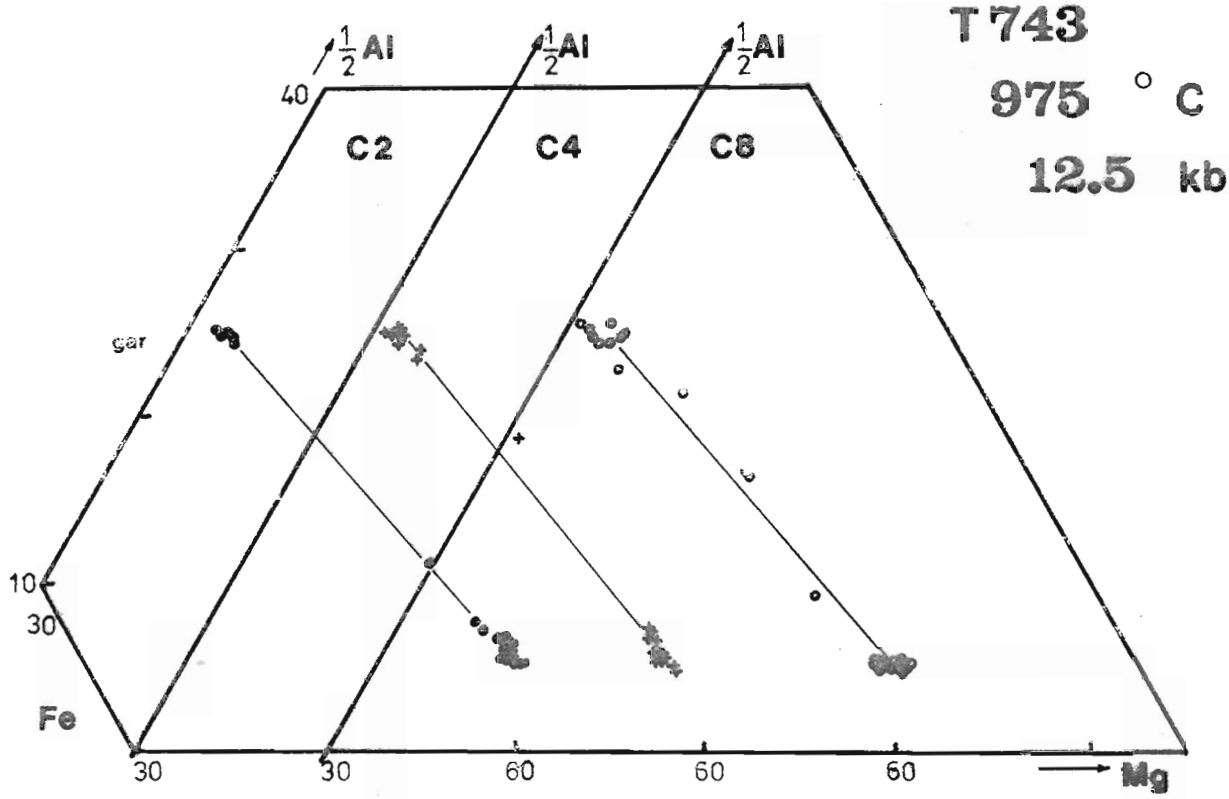
T 743
975 °C
12.5 kb
½Al
½Al
½Al
40
C2
C4
C8
gar
10
30
Fe
30
30
60
60
60
Mg

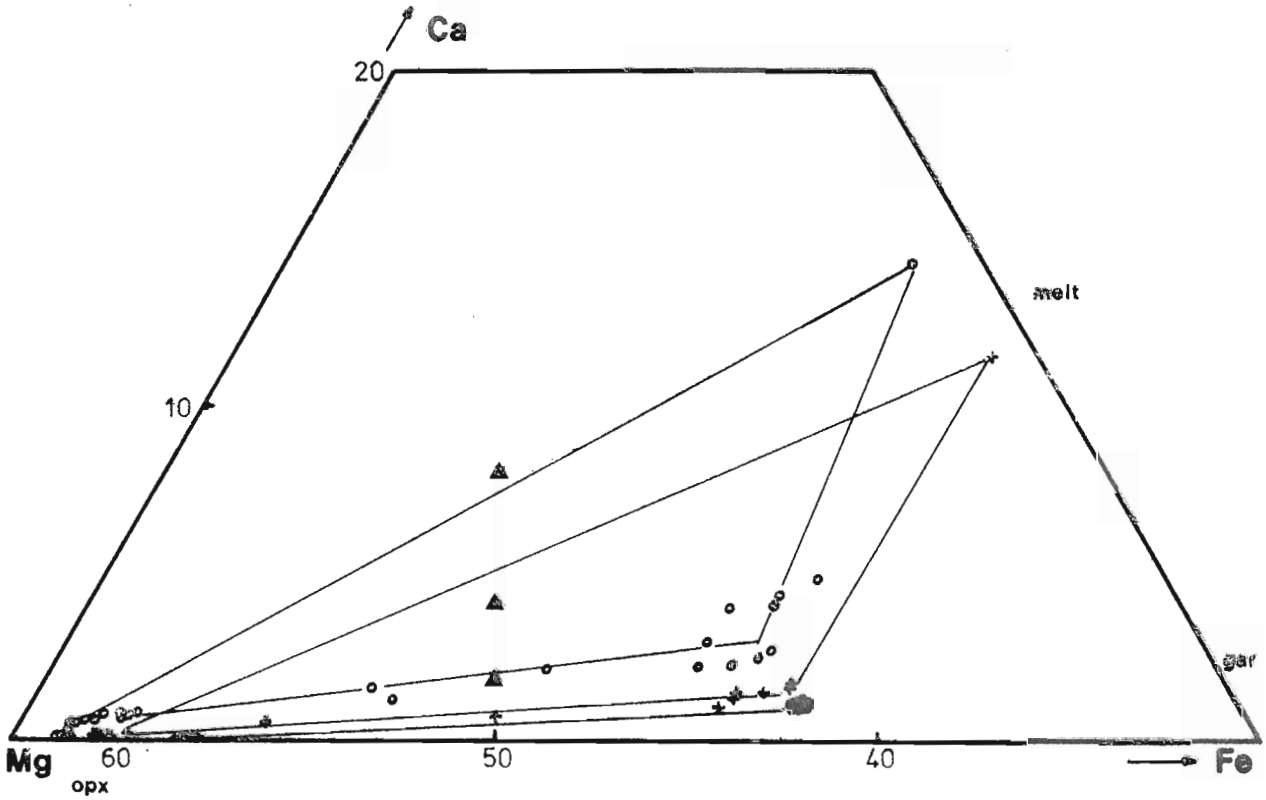
Ca
20
10
melt
gar
Mg
60
50
40
Fe
opx

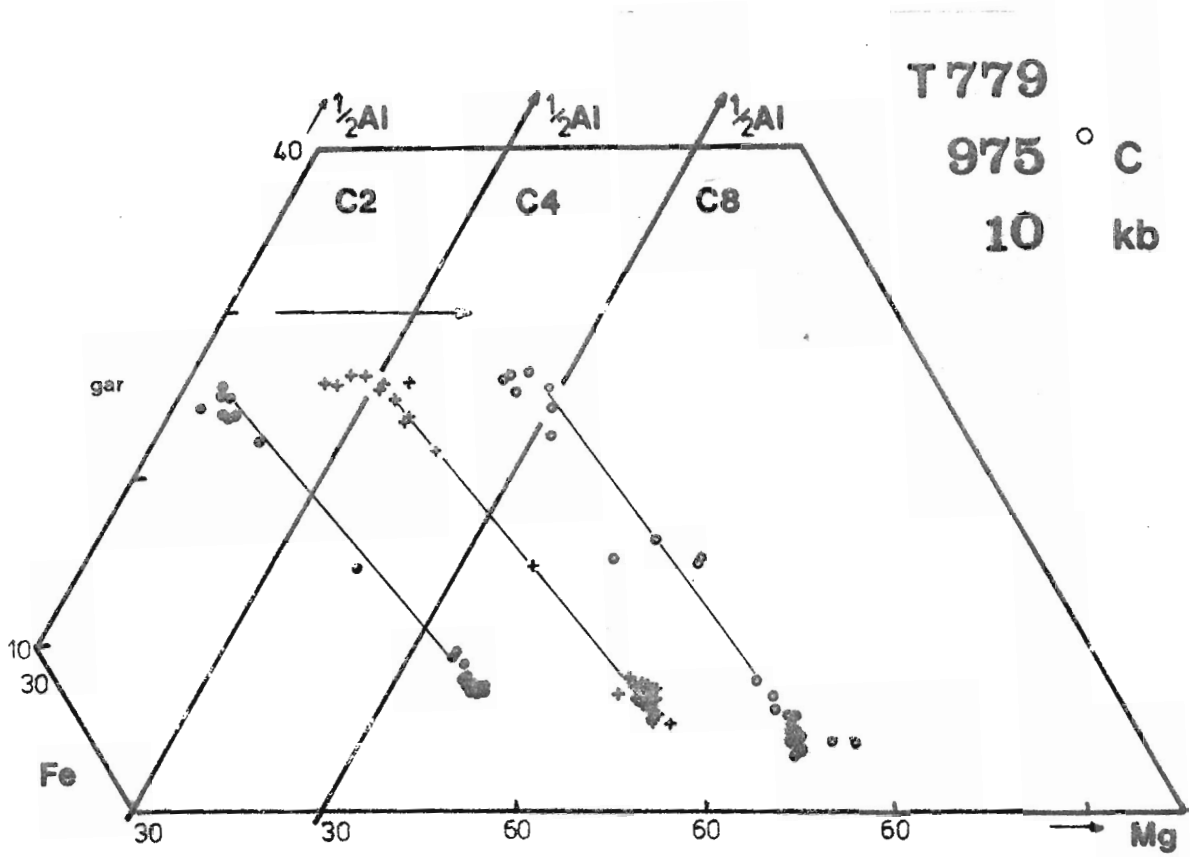
T 779
975 °C
10 kb
½Al
½Al
½Al
40
C2
C4
C8
gar
10
30
Fe
30
30
60
60
60
Mg

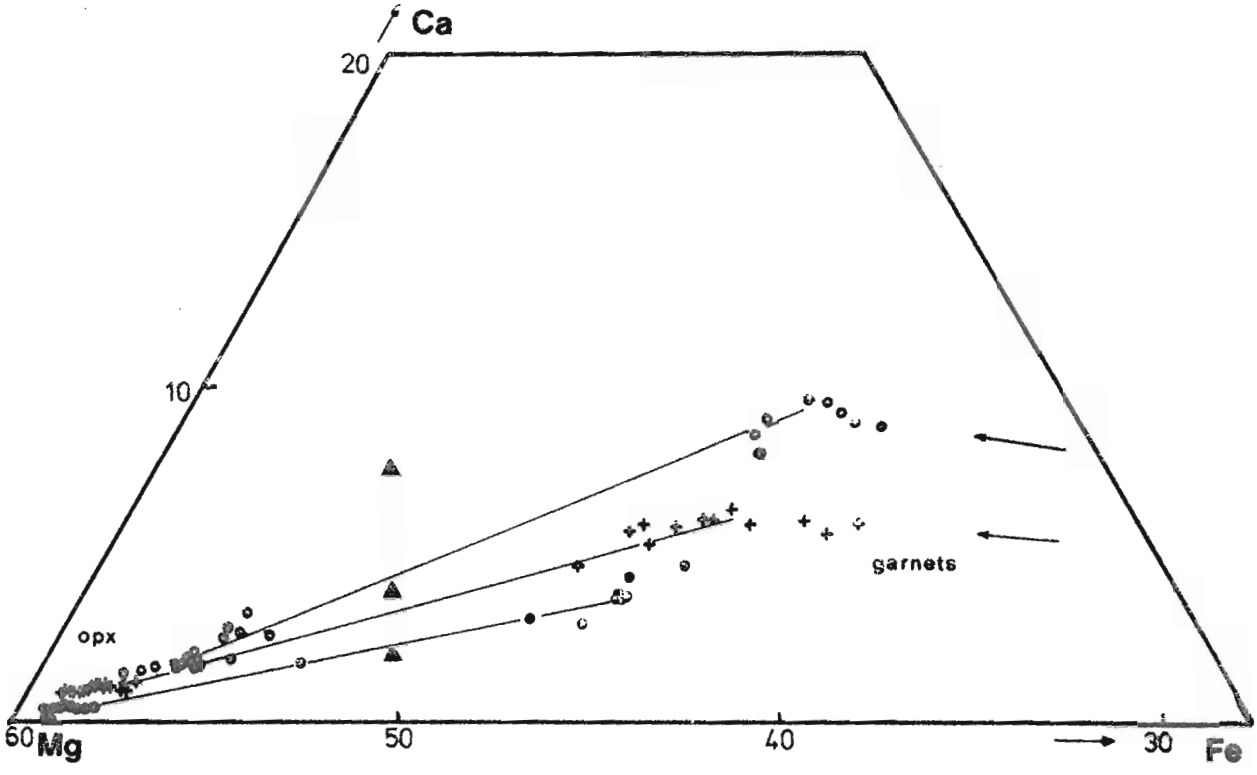
Ca
20
10
opx
garnets
60 Mg
50
40
30
Fe

Appendix 3

THE GARNET-ORTHOPYROXENE-PLAGIOCLASE-QUARTZ GEOBAROMETER

APPENDIX 3

THE GARNET-ORTHOPYROXENE-PLAGIOCLASE-QUARTZ GEOBAROMETER.

For the reaction :

$Mg_2Si_2O_6$ + $CaAl_2Si_2O_8$ = $(Mg_2Ca)Al_2Si_3O_{12}$ + SiO_2

orthopyroxene plagioclase garnet quartz

Wells (1979) gives the following geobarometer relation :

$$P = \frac{1}{567.7}\left\{3300 + 6.26T + RT\ln\left(\frac{X^{ga}_{Ca}.(X^{ga}_{Mg})^2}{X^{M1}_{Mg}.X^{M2}_{Mg}.X^{plag}_{An}}\right) + RT\ln\left(\frac{\gamma^{ga}_{Ca}(\gamma^{ga}_{Mg})^2}{\gamma^{M1}_{Mg}.\gamma^{M2}_{Mg}.\gamma^{plag}_{An}}\right)\right\} \quad \ldots\ldots\ldots\ldots\ldots(1)$$

The following a - X relations have been used in this study for the activity coefficient terms (γ) in equation (1) for each phase :

(a) For <u>garnet</u> solid solutions in Fe-Mg-Ca, a ternary symmetrical regular solution model with the following values of the interaction parameters (as defined in Appendix 1) :

$$W^{ga}_{FeMg} = W^{ga}_{CaFe} = 0$$

W^{ga}_{CaMg} = 2500 cal per 4 oxygen garnet formula.

These values yield the following a - X relation :

$$RT\ln\gamma^{ga}_{ca}(\gamma^{ga}_{Mg})^2 = 2500 \cdot X^{ga}_{Mg}(1-X^{ga}_{Ca})^2 + 5000X^{ga}_{Ca}\left[1-(1-X^{ga}_{Ca})X^{ga}_{Mg}\right]$$

, where X^{ga}_{Mg} = (Mg/Mg Fe) of garnet.

(b) For <u>plagioclase</u> solid solutions, the non-ideal term derived by Saxena and Ribbe (1972) is adopted :

$$\Delta G^{ex} = X_{Ab}X_{An}\left[967+715(X_{Ab}-X_{An})\right] \quad \text{cal/mol}$$

(c) <u>Orthopyroxene</u> solid solutions in Fe-Mg-Al-Ca are assumed to be ideal and Fe-Mg site occupancies are ignored , so that :

$$(X^{M1}_{Mg}.X^{M2}_{Mg}).(\gamma^{M1}_{Mg}.\gamma^{M2}_{Mg}) = (X^{opx}_{Mg})^2.(1-X^{opx}_{Al})$$

, where X_{Al}^{opx} = Al/2 and X_{Mg}^{opx} = Mg/Mg Fe

Substitution of the relations given in (a), (b), and (c) above into equation (1) yields the following equation which has been used to estimate pressures for the garnet-orthopyroxene-plagioclase - quartz assenblages considered in Chapter 6. :

$$P\ (kbar) = \frac{1}{567.7}\left\{ 3300 + 6.26T + RT\ln\left(\frac{X_{Ca}^{ga}.(X_{Mg}^{ga})^2}{(X_{Mg}^{op})^2.(1-X_{Al}^{op}).X_{An}^{plag}}\right) + 2500X_{Mg}^{ga}(1-X_{Ca}^{ga})^2 + 5000X_{Ca}^{ga}\left(1-(1-X_{Ca}^{ga})X_{Mg}^{ga}\right) - X_{Ab}X_{An}\left[967 + 715(X_{Ab}-X_{An})\right] \right\} \quad \ldots\ldots\ldots\ldots(2)$$

REFERENCES

Akaogi, M. and Akimoto, S., 1977: Pyroxene-garnet solid solution equilibria in the systems $Mg_4Si_4O_{12}$-$Mg_3Al_2Si_3O_{12}$ and $Fe_4Si_4O_{12}$-$Fe_3Al_2Si_3O_{12}$ at hi P & T. *Phys.Earth Planet Int.*, 15; 90-106.

Akella, J., 1976: Garnet pyroxene equilibria in the system $CaSiO_3$-$MgSiO_3$-Al_2O_3 and in a natural mineral mixture. *Amer.Mineral*, 61, 589-598.

Akella, J., 1974: Solubility of Al_2O_3 in orthopyroxene coexisting with Garnet and Clinopyroxene for compositions on the Diopside-pyrope join in the system $CaSiO_3$-$MgSiO_3$-Al_2O_3, *Carnegie Inst.Wash.Yearbook*, 73, 273-278.

Akella, J. and Boyd, F.R., 1973: Effect of Pressure on the Composition of Coexisting Pyroxenes and Garnets in the System $CaSiO_3$-$MgSiO_3$-$FeSiO_3$-$CaAlTi_2O_6$. *Carnegie Inst.Wash. Yearbook*, 72, 523-527.

Akella, J. and Boyd, F.R., 1974: Petrogenetic Grid for Garnet Peridotites. *Carnegie Inst.Wash.Yearbook*, 73, 269-273.

Anastasiou, P. and Seifert, F., 1972: Solid solubility of Al_2O_3 in enstatite at high temperatures and 1-5 kbar water pressure. *Contrib.Mineral.petrol.*, 34, 272-287.

Arima, M., 1978: Phase equilibria in the system $MgSiO_3$-Al_2O_3-Fe_2O_3 at high temperatures and pressures, with special reference to the solubility of Al_2O_3 and Fe_2O_3 in enstatite. *Jour.Fac.Sci.Hokkaido Univ.*, Ser.IV, 18(3), 305-338.

Arima, M. and Onuma, K., 1977: The Solubility of Alumina in Enstatite and the Phase Equilibria in the Join $MgSiO_3$-$MgAl_2SiO_6$ at 10-25 kbar. *Contrib.Mineral.Petrol.*, 61, 251-265.

Baer, A.J., 1977: Speculations on the evolution of the lithosphere. *Precamb.Res.*, 5, 249-260.

Baer, A.J., 1981: Geotherms, evolution of the lithosphere and plate tectonics. *Tectonophysics*, 72, 203-227.

Barnicoat, A.C. and O'Hara, M.J., 1979: High temperature pyroxenes from an ironstone at Scourie, Sutherland, *Min.Mag.*, 43, 371-375.

Berg, J.H., 1977a: Regional Geobarometry in the Contact Aureoles of the Anorthositic Nain Complex, Labrador. *J.Petrol.*, V18, pt 3, 399-430.

Berg, J.H., 1977b: Dry Granulite Mineral Assemblages in the Contact Aureoles of the Nain Complex, Labrador. *Contrib. Mineral.Petrol.*, 64, 33-52.

Bickle, M.J., 1978: Heat loss from the earth: a constraint on Archaean tectonics from the relation between geothermal gradients and the rate of plate production. *Earth Planet Sci.Lett.*, 40, 301-315.

Binns, R.A., 1962: Metamorphic pyroxenes from the Broken Hill district, New South Wales, *Min.Mag.*, 33, 320-338.

Bishop, F.C., 1980: The distribution of Fe^{2+} and Mg between coexisting ilmenite and pyroxene with applications to geothermometry. *Am.J.Sci.*, 280, 46-77.

Black, L.P. and James. P.R., 1979: Preliminary isotopic ages from Endery Land, Antarctica (abstr.). *J.Geol.Soc.Aust.*, 26, 266-267.

Black, L.J., James, P.R. and Harley, S.L.:
The geology and geochronology of reputedly ancient rocks at Fyfe Hills, Enderby Land, Antarctica. (in prep.).

Bohlen, S.R. and Essene, E.J.,1977: Feldspar and Oxide Thermometry of Granulites in the Adirondack Highlands. *Contrib. Mineral.Petrol.*, 62, 153-169.

Bohlen, S.R. and Essene, E.J.,1980: Evaluation of coexisting garnet-biotite, garnet-clinopyroxene, and other Mg-Fe exchange thermometers in Adirondack granulites: summary. *Geol.Soc.Amer.Bull.*, 91, 1, 107-109.

Bohlen, S.R., Essene, E.J. and Hoffman, K.S., 1980:
Update on feldspar and oxide thermometry in the Adirondack mountains, New York. *Geol.Soc.Amer.Bull.*, 91, Pt 1, 110-113.

Boyd, F.R., 1973: A Pyroxene Geotherm. *Geochim. et Cosmochim. Acta*, 37, 2533-2546.

Boyd, F.R., 1974: Ultramafic nodules from the Frank Smith Kimberlite Pipe, South Africa. *Carnegie Inst.Wash.Yearbook*, 73, 285-294.

Boyd, F.R. and England, J.L., 1964: The system Enstatite-pyrope. *Carnegie Inst.Wash.Yearbook*, 63, 157-161.

Boyd, F.R. and Finger, L.W., 1975: Homogeneity of minerals in mantle rocks from Lesotho. *Carnegie Inst.Wash.Yearbook*, 74, 519-525.

Boyd, F.R. and Nixon, P.H., 1975: Origin of the ultramafic nodules from some Kimberlites of Northern Lesotho and the Monastery Mine, South Africa, *Phys.Chem.Earth*, 9, 431-454.

Boyd, F.R. and Nixon, P.H., 1976: Ultramafic Nodules from the Kimberly pipes, South Africa. *Carnegie Inst.Wash. Yearbook*, 75, 544-546.

Boyd, F.R., Fujii, T. and Danchin, R.V., 1976: A non inflected geotherm for the Udachnaya Kimberlite Pipe, USSR. *Carnegie Inst.Wash.Yearbook*, 75, 523-531.

Boyd, F.R., 1976: Inflected and non-inflected geotherms. *Carnegie Inst.Wash.Yearbook*, 75, 521-523.

Boyd, F.R. and Meyer, H.O.A., 1979: The Mantle Sample: Inclusions in Kimberlites and other volcanics. *American Geophysical Union*, Washington, D.C.

Brey, G. and Green, D.H., 1975: The role of CO_2 in the genesis of Olivine Melilite. *Contrib.Mineral.Petrol.*,49, 93-103.

Bryhni,I., Green, D.H., Heier, K.S. and Fyfe, W.S., 1970: On the occurrence of eclogite in Western Norway. *Contrib.Mineral.Petrol.*, 26, 12-19.

Bryhni, I., Krogh, E. and Griffin, W.L., 1977: Crustal derivation of Norwegian eclogites: a review. *N.Jbh.f.Miner. Abh.*, 130, 49-68.

Caporuscio, F.A. and Morse, S.A., 1978: Occurrence of sapphirine plus quartz at Peekskill, New York. *Am.J.Sci.*, 278, 1334-1342.

Carswell, D.A., 1968: Possible primary upper mantle peridotite in Norwegian basal gneiss. *Lithos*, 1, 322-355.

Carswell, D.A., 1973: Garnet pyroxenite lens within Ugelvik layered garnet peridotite. *Earth.Planet.Sci.Lett.*, 20, 347-352.

Carswell, D.A., 1974: Comparative equilibration temperatures and pressures of garnet lherzolites in Norwegain gneisses and in Kimberlite. *Lithos*, 7, 113-121.

Carswell, D.A., 1978: Paleogeotherms: implications of disequilibrium in garnet lherzolite xenoliths. *Nature*, 276, 737.

Carswell, D.A., Clarke, D.B., and Mitchell, R.H., 1979: The petrology and geochemistry of ultramafic nodules from Pipe 200, Northern Lesotho, pp. 127-143. *In The Mantle Sample*, (F.R. Boyd and H.O.A. Meyer, eds.), A.G.U., 1979.

Carswell, D.A. and Gibb, F.G.F., 1980: The equilibration conditions and petrogenesis of European crustal garnet lherzolites. *Lithos*, 13, 1, 19-30.

Carswell, D.A. and Gibb, F.G.F., 1980a: Geothermometry of Garnet lherzolite with special reference to those from the Kimberlites of Northern Lesotho. *Contrib.Mineral.Petrol.*,74, 403-416.

Chapman, D.S. and Pollack, H.N., 1977: Regional geotherms and lithospheric thickness. *Geology*, 5, 265-268.

Charlu, T.V., Newton, R.C. and Kleppa, O.J., 1975: Enthalpies of formation at 970K of compounds in the system MgO-Al_2O_3-SiO_3 from high temperature solution calorimetry. *Geochim.et Cosmochim.Acta.*, 39, 1487-1497.

Charlu, T.V., Newton, R.C. and Kleppa, O.J., 1978: Enthalpy of formation of some lime silicates by high-temperature solution calorimetry, with discussion of high pressure phase equilibria. *Geochim. et Cosmochim.Acta.*, 42, 367-375.

Chatterjee, N.D., and Schreyer, W., 1972: The reaction enstatite + sillimanite = sapphirine + quartz in the system MgO-Al_2O_3 -SiO_2. *Contrib.Mineral.Petrol.*, 36, 49-62.

Cox, K.G., Gurney. J.J. and Harte, B., 1973: Xenoliths from the Matsoku pipe, pp. 76-100. *In Lesotho Kimberlites* (P.H.Nixon, ed.), Cape and Transvaal printers, Capetown.

Cressey, G., Schmid, R., Wood, B.J., 1978: Thermodynamic properties of Almandine - Grossular garnet solid solutions. *Contrib.Mineral.Petrol.*, 67, 397-404.

Dahl, P.S., 1980: The thermal-compositional dependence of Fe^{2+}-Mg distributions between coexisting garnet and pyroxene: applications to geothermometry. *Amer.Mineral.*, 65, 854-866.

Dallwitz, W.B., 1968: Coexisting Sapphirine and Quartz in granulite from Enderby Land, Antarctica. *Nature*,219, 476-477.

Danchin, R.V., 1979: Mineral and bulk chemistry of Garnet lherzolite and garnet harzburgite xenoliths from the Premier mine, South Africa. pp. 104-126. *In The Mantle Sample* (F.R. Boyd and H.O.A. Meyer, eds.), A.G.U., 1979.

Danchin, R.V. and Boyd, F.R., 1976: Ultramafic Nodules from the premier Kimberlite pipe, South Africa. *Carnegie Inst. Wash.Yearbook*, 75, 531-538.

Danckwerth, P.A. and Newton, R.C., 1978: Experimental determination of the spinel peridotite to garnet peridotite reaction in the system MgO-Al_2O_3-SiO_2 in the range 900-1100°C and Al_2O_3 isopleths of enstatite in the spinel field. *Contrib.Mineral.Petrol.*, 66, 189-201.

Davidson, L.R., Variation in Ferrous Iron-Magnesium distribution coefficients of metamorphic pyroxenes from Quairading, Western Australia. *Contrib.Mineral.Petrol.*, 19, 239-259.

Davidson, L.R. and Mathison, C.I., 1974: Aluminous orthopyroxenes and associated cordierites garnets and biotites from granulites in the Quairading district, Western Australia, *N.Jb.Miner.Mh.*, H6, 272-287.

Davies, G.F., 1979: Thickness and thermal history of continental crust and root zones. *Earth Planet.Sci.Lett.*, 44, 231-238.

Davis, B.T.C. and Boyd, F.R., 1966: The join $Mg_2Si_2O_6$- $CaMgSi_2O_6$ at 30 kilobars pressure and its application to pyroxenes from Kimberlites. *J.Geophys.Res.*, 71, 3567-3576.

Dawson, J.B., Powell, D.G. and Reid, A.M., 1970: Ultrabasic xenoliths and lava from the Lashaine Volcano, Northern Tanzania. *J. Petrol.*, 11, 3, 519-548.

Dawson, J.B., Gurney, J.J. and Lawless, P.J., 1975: Paleogeothermal gradients derived from xenoliths in Kimberlite. *Nature*, 257, 299-300.

Day, H.W. and Kumin, H.J., 1980: Thermodynamic Analysis of the Aluminium silicate triple point. *Am.J.Sci.*, 280, 265-287.

Eggler, D.H. and McCallum, M.E., 1974: Xenoliths in Diatremes of the Western United States. *Carnegie Inst.Wash.Yearbook*, 73, 294-300.

Eggler, D.H. and McCallum, M.E., 1976: A geotherm from Megacrysts in the Sloan Kimberlite pipes, Colorado. *Carnegie Inst.Wash. Yearbook*, 75, 538-542.

Ehrenberg, S.N., 1979: Garnetiferous ultramafic inclusions in minette from the Navajo volcanic field, pp. 330-344 *in The Mantle Sample*, AGU, 1979.

Ellis, D.J., 1979: Granulites from Enderby Land, Antarctica, the application of experimentally determined cation partition data to estimation of pressures and temperatures of metamorphism. Univ.of Tasmania. Unpubl.PhD Thesis.

Ellis, D.J., 1980: Osumilite-sapphirine-quartz granulites from Enderby Land, Antarctica: P-T conditions of metamorphism, implications for garnet-cordierite equilibria and the evolution of the deep crust. *Contrib.Miner. Petrol.*, 74, 201-210.

Ellis, D.J. and Green, D.H., 1979: An experimental study of the effect of Ca upon garnet-clinopyroxene Fe-Mg exchange equilibria. *Contrib.Mineral.Petrol.*, 71, 13-22.

Ellis, D.J., Sheraton, J.W., England, R.N., and Dallwitz, W.B., 1980: Osumilite-sapphirine-quartz granulites from Enderby Land, Antarctica: mineral assemblages and reactions. *Contrib.Mineral.Petrol.*, 72, 123-143.

England, P.C. and Richardson, S.W., 1977: The influence of erosion upon the mineral facies of rocks from different metamorphic environments. *J.Geol.Soc.Lond.*, 134, 201-213.

Ernst, W.G., 1978: Petrochemical study of lherzolitic rocks from the western Alps. *J.Petrol.*, 19, 3, 341-392.

Evans, B.W. and Trommsdorff, V., 1978: Petrogenesis of garnet lherzolite, Cima Di Gagnone, Lepontine alps. *Earth.Planet.Sci.Lett.*, 40, 333-348.

Ferguson, J., Ellis, D.J. and England, R.N., 1977: Unique spinel-garnet lherzolite inclusion in kimberlite from Australia. *Geology*, 5, 278-280.

Ferguson, J. and Sheraton, J.W., 1979: Petrogenesis of kimberlitic rocks and associated xenoliths of southeastern Australia. *in Kimberlites, diatremes and diamonds: their geology, petrology and geochemistry.* A.G.U. Washington, 1979.

Ferry, J.M. and Spear, F.S., 1978: Experimental Calibration of the partitioning of Fe and Mg between Biotite and Garnet. *Contrib.Mineral.Petrol.*, 66, 113-117.

Fraser, D.G. and Lawless, P.J., 1978: Paleogeotherms: implications of disequilibrium in garnet lherzolite xenoliths. *Nature*, 273, 220-221.

Ganguly, J., 1979: Garnet and clinopyroxene solid solutions, and geothermometry based on Fe-Mg distribution coefficient. *Geochim. et Cosmochim.Acta.*, 43, 1021-1029.

Ganguly, J. and Kennedy, G.C., 1974: The energetics of natural garnet solid solution. I. Mixing of the Aluminosilicate end members. *Contrib.Mineral.Petrol.*, 48, 135-148.

Ganguly, J. and Ghose, S., 1979: Aluminous orthopyroxene: order-disorder, thermodynamic properties and petrologic implications. *Contrib.Mineral.Petrol.*,69, 375-385.

Garrison, J.R. Jr. and Taylor, L.A., 1980: Megacrysts and xenoliths in Kimberlites, Elliott country, Kentucky: A mantle sample beneath the Permian Appalachian plateau. *Contrib.Mineral.Petrol.*, 75, 1, 27-43.

Ghent, E.D., 1976: Plagioclase-garnet-Al_2SiO_5-quartz: a potential geobarometer-geothermometer. *Amer.Mineral.*, 61, 710-714.

Gjelsvik, T., 1952: Metamorphosed dolerites in the gneiss area of Sunnmøre on the west coast of southern Norway. *Norsk.geol.Tidsskr.*, 30, 33-134.

Green, D.H., 1969: Mineralogy of two Norwegian Eclogites. Contributions to Physico-chemical petrology, 1, (Korzhinskii Volume) pp. 37-44.

Green, D.H., 1975: Genesis of Archaean peridotitic magmas and contraints on Archaean geothermal gradients and tectonics. *Geology*, 3, 15-18.

Green, D.H., 1981: Petrogenesis of Archaean ultramafic magmas and implications for Archaean tectonics, Ch.19, 469-489 in A. Kroner (ed.), *Precambrian Plate Tectonics*, Elsevier, Amsterdam, 1981.

Green, D.H. and Ringwood, A.E., 1967: An experimental investigation of the gabbro to eclogite transformation and its petrological applications. *Geochim. et Cosmochim.Acta.*, 31, 767-833.

Green, T.H., 1977: Garnet in Silicic Liquids and its possible use as a P,T indicator. *Contrib.Mineral.Petrol.*, 65, 59-67.

Grew, E.S., 1979: Reactions involving sapphirine and sillimanite + orthopyroxene in quartz-bearing rocks of the 2.5 b.y. Napier complex, Enderby Land, East Antarctica (abstr.). *Geol.Soc.Am. abstracts with programs*, 11, 435-436.

Grew, E.S., 1980: Sapphirine + quartz association from Archean rocks in Enderby Land, Antarctica. *Amer.Mineral.*, 65, 821-836.

Grew, E.S. (in press): The Antarctic Margin.

Griffin, A.C., 1979: Structural evolution of Archaean supracrustal rocks at Amundsen Bay, East Antarctica (abstr.). *J.Geol.Soc.Aust.*, 26, 271.

Griffin, B.J., 1979: Energy dispersive analysis system calibration and operation with TAS-SUEDS, an advanced interactive data reduction package. Univ. of Tasmania, Dept. of Geology, publication no. 343.

Griffin, W.L., 1971: Mineral reactions at a peridotite-gneiss contact, Jotunheimen, Norway. *Min.Mag.*, 38, 435-445.

Griffin, W.L. and Heier, K.S., 1969: Paragenesis of garnet in granulite-facies rocks, Lofoten-Vesteraalen, Norway. *Contrib.Mineral.Petrol.*, 23, 89-116.

Griffin, W.L. and Heier, K.S., 1973: Petrological implications of some corona structures. *Lithos*, 6, 315-335.

Griffin, W.L. and Råheim, A., 1973: Convergent metamorphism of eclogites and dolerites, Kristiansund area, Norway. *Lithos*, 6, 21-40.

Griffin, W.L., Carswell, D.A. and Nixon, P.H., 1979: Lower crustal granulites and eclogites from Lesotho, South Africa. pp. 59-86. *In The Mantle Sample* (Boyd, F.R. and H.O.A. Meyer, eds.) A.G.U., 1979.

Griffin, W.L., McGregor, V.R., Nutman, A., Taylor, P.N. and Bridgwater, D., 1980: Early Archaean granulite-facies metamorphism south of Ameralik, west Greenland. *Earth.Planet.Sci.lett.*, 50, 59-74.

Grover, J., 1974: On calculating activity coefficients and other excess functions from the intracrystalline exchange properties of a double site phase. *Geochim. et Cosmochim.Acta.*, 38, 1527-1548.

Grover, J.E. and Orville, P.M., 1969: The partitioning of Cations between coexisting single and multi-site phases with application to the assemblages: orthopyroxene-clinopyroxene and orthopyroxene-olivine. *Geochim. et Cosmochim.Acta.*, 33, 205-226.

Haselton, H.T. and Newton, R.C. 1980: Thermodynamics of pyrope-grossular garnets and their stabilities at high temperatures and high pressures. *J.Geophys.Res.*, 85,B12, 6973-6982.

Haselton, H.T. and Westrum, E.G. 1980: Low temperature heat capacities of synthetic pyrope, grossular, and pyrope$_{60}$grossular$_{40}$, *Geochim. et Cosmochim.Acta.*, 44, 701-709.

Hargaves, R.B., 1978: Punctuated evolution of tectonic style, *Nature*, 276, 459-461.

Harte, B., 1978: Kimberlite nodules, upper mantle petrology, and geotherms. *Phil.Trans.Roy.Soc.Lond.*, A, 288, 487-500.

Harte, B., Cox, K.G., and Gurney, J.J., 1975: Petrography and geological history of upper mantle xenoliths from the Matsoku Kimberlite pipe. *Phys.Chem.Earth.*, 9, 477-506.

Harte, B., Jackson, P.M. and R.M. Macintyre, 1981: Age of mineral equilibria in granulite facies nodules from kimberlites. *Nature*, 291, 147-148.

Hearn, B.C. and Boyd, F.R., 1975: Garnet peridotite xenoliths in a Montana, U.S.A., kimberlite. *Phys.Chem.Earth.*, 9, 247-256.

Henry, D.J. and Medaris, L.G.Jr., 1980: Application of pyroxene and olivine-spinel geothermometers to spinel peridotites in southwestem Oregon. *Am.J.Sci.*, 280-A, 211-231.

Hensen, B.J., 1973: Pyroxenes and Garnets as Geothermometers and Barometers.*Carnegie Inst.Wash.Yearbook*, 72, 527-535.

Hensen, B.J. and Essene, E.J., 1971: Stability of Pyrope-Quartz in the System $MgO-Al_2O_3-SiO_2$. *Contrib.Mineral.petrol.*, 30, 72-83.

Hensen, B.J., Schmid, R., and Wood, B.J., 1975: Activity composition relationships for pyrope-grossular garnet. *Contrib. Mineral.Petrol.*, 51, 161-166.

Hensen, B.J. and Green, D.H., 1973: Experimental study of the stability of cordients and garnet in pelitic compositions at high pressures and temperatures. III. Synthesis of experimental data and geological implications. *Contrib.Mineral.Petrol.*, 38, 151-166.

Herzberg, C.T., 1978: Pyroxene geothermometry and geobarometry: experimental and thermodynamic evaluation of some subsolidus phase relations involving pyroxenes in the system CaO-MgO-Al_2O_3-SiO_2. *Geochim. et Cosmochim. Acta.*, 42, 945-957.

Herzberg, C.T., 1978a: The bearing of phase equilibria in simple and complex systems on the origin and evolution of some well documented garnet Websterites. *Contrib.Mineral. Petrol.*, 66, 4, 375-382.

Hewins, R.H., 1975: Pyroxene geothermometry of some granulite facies rocks, *Contrib.Mineral.Petrol.*, 50, 205-209.

Holdaway, M.J., 1976: Mutual compatibility relations of the Fe^{2+}-Mg-Al silicates at 800°C and 3 kbar. *Am.J.Sci.*, 276, 285-308.

Holland, T.J.B., Navrotsky, A. and Newton, R.C., 1979: Thermodynamic parameters of $CaMgSi_2O_6$-$Mg_2Si_2O_6$ pyroxenes based on regular solution and co-operative disordering models. *Contrib.Mineral.Petrol.*, 69, 337-344.

Howells, S. and O'Hara, M.J., 1978: Low solubility of alumina in enstatite and uncertainties in estimated paleogeotherms. *Phil.Trans.Roy.Soc.Lond.*, A, 288, 471-486.

Howie, R.A. and Subramaniam, A.P., 1957: The paragenesis of garnet in charnockite, enderbite and related granulites. *Min.Mag.*, 31, 565-586.

Hsu, L.C., 1968: Selected phase relationships in the system Al-Mn-Fe-Si-O-H: A model for garnet equilibria. *J.Petrol.*, 9, 40-83.

Immega, I.P. and Klein, C. Jr., 1976: Mineralogy and petrology of some metamorphic Precambrian iron formations in southwestern Montana. *Amer.Mineral.*, 61, 1117-1144.

Irving, A.J., 1974: Geochemical and high pressure experimental studies of garnet pyroxenite and pyroxene granulite xenoliths from the Delegate basaltic breccia, Australia. *J. Petrol.*, 15, Pt 1, 1-40.

Ishii, T., 1975: The relations between temperature and compositions of pigeonite in some lavas and their application to geothermometry. *Min.Journ.*, 8, 1, 48-59.

Ito, K. and Kennedy, G.C., 1971: An experimental study of the basalt-garnet granulite-eclogite transition. *In* J.G.Heacock, ed., *The Structure and Physical Properties of the Earth's Crust*, pp.303-314. Am.Geophys.Union Geophys. Monogr. 14.

Jaffe, H.W., Robinson, P. and Tracy, R.J., 1978: Orthoferrosilite and other iron-rich pyroxenes in microperthite gneiss of the Mount Marcy area, Adirondack mountains. *Amer.Mineral.*, 63, 1116-1136.

James, P.R. and Black, L.P., 1981: A review of the structural evolution and geochemistry of the Archaean Napier Complex of Enderby Land, Australian Antarctic Territory (in press).

Jan, M. Qasim, and Howie, R.A., 1980: Ortho- and clinopyroxenes from the pyroxene granulites of Swat Kohistan, northern Pakistan. *Min.Mag.*, 43, 715-726.

Jan, M. Qasim and Howie, R.A., 1981: The mineralogy and geochemistry of the metamorphosed basic and ultrabasic rocks of the Jijal complex, Kohistan, N.W.Pakistan. *J.Petrol.*, 22, 1, 85-126.

Jenkins, D.M. and Newton, R.C., 1979: Experimental determination of the spinel peridotite to garnet peridotite inversion at 900°C and 1000°C in the system $CaO-MgO-Al_2O_3-SiO_2$, and at 900°C with natural garnet and olivine. *Contrib.Mineral.Petrol.*, 68, 407-419.

Jordan, T.H., 1975: The continental tectosphere. *Rev.Geophys.Space. Phys.*, 13, 1-12.

Jordan, T.H., 1978: Composition and development of the continental tectosphere. *Nature*, 275, 544-548.

Kamenev, E.N., 1972: Geological structure of Enderby Land *in* Adie R.J. (ed.), *Antarctic Geology and Geophysics*, pp. 579-583. Universitetforlaget, Oslo.

Kamenev, E.N., 1975: The geology of Enderby Land (in Russian) *Acad.Sci.USSR. Comm.Antarct.Res.Rep.*, 14.

Karsakov, L.P., 1973: Pyrope-bronzite-sillimanite schist of eastern Stanovik and the pressure-temperature conditions during its metamorphism. *Dokl. E.S.S.*, 210, 1, 187-190.

Kawasaki, T. and Matsui, Y., 1977: Partitioning of Fe^{2+} and Mg^{2+} between olivine and garnet. *Earth.Planet.Sci.Lett.*, 37, 159-166.

Kerrick, D.M. and Darken, L.S., 1975: Statistical thermodynamic models for ideal oxide and silicate solid solutions, with application to plagioclase. *Geochim.et Cosmochin. Acta.*, 39, 1431-1442.

Kitsul, V.I. and Kopylov, P.A., 1974: A find of garnetiferous ultramafic rocks on the Aldan Shield and their genesis. *Dokl. E.S.S.*, 209, 161-164.

Kolesnik, Yu.N., Nogteva, V.V., Arkhipenko, D.K., Orekhov, B.A. and Paukov, I.Ye., 1979: Thermodynamics of pyrope-grossular solid solutions and the specific heat of grossular at 13-300°K. *Geokhimiya*, 5, 713-721.

Kretz, R., 1963: Distribution of magnesium and iron between orthopyroxene and calcic pyroxene in natural mineral assemblages. *J.Geol.*, 71, 773-785.

Krogh, E.T., 1977: Evidence of precambrian continent-continent collision in western Norway. *Nature*, 267, 17-19.

Krylova, M.D. and Priyatkina, L.A., 1976: Hypersthene-sillimenite association in the Por'ya Bay granulite complex in the SW part of the Kola peninsula. *Dokl. E.S.S.*, 226, 148-151.

Lane, D.L. and Ganguly, J., 1980: Al_2O_3 solubility in orthopyroxene in the system $MgO-Al_2O_3-SiO_2$: A reevaluation, and mantle geotherm. *J.Geophys.Res.*, 85,B12, 6963-6972.

Lappin, M.A., 1974: Eclogites from the Sunndal-Grubse ultramafic mass, Almklovdalen, Norway and the T-P history of the Almklovdalen masses. *J.Petrol.*, 15, 3, 567-601.

Lappin, M.A., 1977: Crustal and in-situ origin of Norwegian Eclogites. *Nature*, 269, 730.

Lappin, M.A. and Smith, D.C., 1978: Mantle-equilibrated orthopyroxene eclogite pods from the Basal Gneisses in the Selje district, western Norway. *J.Petrol.*, 19, 3, 530-584.

Lindsley, D.H. and Dixon, S.S., 1976: Diopside-enstatite equilibria at 850°-1400°V, 5-35 kbar. *Am.J.Sci.*, 276, 1258-1301.

Lindsley, D.H. and Munoz, J.L., 1969: Subsolidus relations along the join hedenbergite-ferrosilite. *Am.J.Sci.*, 267A, 295-324.

Lovering, J.F. and White, A.J.R., 1969: Granulitic and eclogitic inclusions from basic pipes at Delegate, Australia. *Contrib.Mineral. Petrol.*, 21, 9-52.

Lutts, B.G. and Kopaneva, L.N., 1968: A Pyrope-Sapphirine rock from the Anabar massif and its conditions of metamorphism. *Dokl. E.S.S.*, 179, 161-163.

MacGregor, I.D., 1974: The system $MgO-Al_2O_3-SiO_2$: Solubility of Al_2O_3 in enstatite for spinel and garnet peridotite compositions. *Amer.Mineral.*, 59, 110-119.

MacGregor, I.D., 1979: Mafic and ultramafic xenoliths from the Kao kimberlite pipe. pp. 156-172 *in The Mantle Sample* (F.R. Boyd and H.O.A. Meyer, eds.). A.G.U., 1979.

Marakushev, A.A. and Kudryavtev, V.A., 1965: Hypersthene-sillimanite paragenesis and its petrological implication. *Dokl. E.S.S.*, 164, 145-148.

Matsui, Y, Syono, Y., Akimoto, S. and Kitayama, K., 1968: Unit cell dimensions of some synthetic orthopyroxene group solid solutions. *Geochem.J.*, 2, 51-70.

McCallum, M.E., Eggler, D.H., and Burns, L.K., 1975: Kimberlite diatremes in northern Colorado and southern Wyoming. *Phys.Chem.Earth.*, 9, 149-162.

McLelland, J.M. and Whitney, P.R., 1977: The Origin of Garnet in the Anorthosite-Charnockite suite of the Adirondacks. *Contrib.Mineral.Petrol.*, 60, 161-181.

McLelland, J.M. and Whitney, P.R., 1980: A generalised garnet forming reaction for Metaigneous rocks in the Adirondacks. *Contrib.Mineral.Petrol.*, 72, 2, 111-122.

Medaris, L.G.Jr., 1980: Petrogenesis of the Lien peridotite and associated eclogites - Almklovdalen, western Norway. *Lithos*,13, 339-353.

Mitchell, R.H., 1977: Ultramafic xenoliths from the Elwin Bay Kimberlite: the first Canadian paleogeotherm. *Can.J.Earth.Sci.*, 14, 1202-1210.

Mitchell, R.H., 1978: Garnet Lherzolites from Somerset Island, Canada and Aspects of the nature of perturbed Geotherms. *Contrib.Mineral.Petrol.*, 67, 341-347.

Mitchell, R.H., Carswell, D.A. and Clarke, D.B., 1980: Geological implications and validity of calculated equilibration conditions for ultramafic xenoliths from Pipe 200, Northern Lesotho. *Contrib.Mineral.Petrol.*, 72, 2, 205-218.

Moore, A.C., 1970: Descriptive terminology for the texture of rocks in granulite facies terraines. *Lithos*, 3, 123-127.

Mori, T., 1976: Pyroxene equilibria in ultramafic rocks. Unpubl.PhD Thesis. Aust.Nat.University.

Mori, T., 1978: Experimental study of Pyroxene Equilibria in the System CaO-MgO-FeO-SiO_2, *J.Petrol.*, 19, 1, 45-65.

Mori, T., and Green, D.H., 1975: Pyroxenes in the system $Mg_2Si_2O_6$-$CaMgSi_2O_6$ at high pressure.*Earth.Planet.Sci.Lett.*, 26, 277-286.

Mori, T. and Green, D.H., 1976: Subsolidus equilibria between pyroxenes in the CaO-MgO-SiO_2 system at high pressures and temperatures. *Amer.Mineral.*, 61, 616-625.

Mori, T. and Green, D.H., 1978: Laboratory duplication of phase equilibria observed in natural garnet lherzolites. *J.Geol.*, 86, 83-97.

Mysen, B.O. and Heier, K.S., 1972: Petrogenesis of eclogites in high grade metamorphic gneisses, exemplied by the Hariedland Eclogite, Western Norway. *Contrib.Mineral.Petrol.*, 36, 73-94.

Navrotsky, A., 1971: The Intracrystalline cation distribution and the thermodynamics of solid solution formation in the system $FeSiO_3$-$MgSiO_3$. *Amer.Mineral.*,56, 201-211.

Nehru, C.E. and Wyllie, P.J., 1974: Electron microprobe measurements of pyroxenes coexisting with H_2O undersaturated liquids on the join $CaMgSi_2O_6$-$Mg_2Si_2O_6$ -H_2O at 30 kbars with applications to geothermometry. *Contrib.Mineral.Petrol.*, 48, 221-228.

Newton, R.C., 1977: Thermochemistry of garnets and aluminous pyroxenes in the CMAS system. *in Thermodynamics in Geology* (D.G. Fraser, ed.) 29-55, 410pp. Dordrecht, Boston: D. Reidel Publishing Company, 1977.

Newton, R.C., Charlu, T.V., and Kleppa, O.J., 1977: Thermochemistry of high pressure garnets and clinopyroxenes in the system CaO-MgO-Al_2O_3-SiO_2, *Geochim. et Cosmochim.Acta.*, 41, 369-377.

Newton, R.C., Charlu, T.V., Anderson, P.A.M., and Kleppa, O.J., 1979: Thermochemistry of synthetic clinopyroxenes on the join $CaMgSi_2O_6$-$Mg_2Si_2O_6$. *Geochim. et Cosmochim.Acta.*, 43, 55-60.

Newton, R.C., Smith, I.V. and Windley, B.F., 1980: Carbonic metamorphism, granulites, and crustal growth. *Nature*, 288, 45-49.

Nixon, P.H. (ed.), 1973: Lesotho Kimberlites. Lesotho Nat.Develop. Corp. 1973, Transvaal Printers, Cape Town.

Nixon, P.H., 1973: The geology of Mothae, Solane, Thaba Putsoa and Blow 13, pp. 39-47. *In Lesotho Kimberlites* (P.H., Nixon, ed.), Lesotho Nat.Dev.Corp.

Nixon, P.H. and Boyd, F.R., 1973: Petrogenesis of the granular and shecored ultrabasic nodule suite in kimberlites. *In Lesotho Kimberlites* (P.H.Nixon, ed.), Cape and Transvaal printers, Cape Town.

Nixon, P.H. and Boyd, F.R., 1979: Garnet-bearing lherzolites and discrete nodule suites from the Malaita alnoite, Solomon Islands, S.W.Pacific, and their bearing on oceanic mantle composition and geotherm. pp.400-423 *in The Mantle Sample* (F.R.Boyd and H.O.A.Meyer, eds.) A.G.U., 1979.

Nixon, P.H., Reedman, A.J. and Burns, L.K., 1973: Sapphirine bearing granulites from Labwor, Uganda. *Min.Mag.*,39, 420-428.

Obata, M., 1976: The solubility of Al_2O_3 in orthopyroxenes in spinel and plagioclase peridotites and spinel pyroxenite. *Amer.Mineral.*, 61, 804-816.

Obata, M., 1980: The Ronda Peridotite: garnet-, spinel- and plagioclase-lherzolite facies and P-T trajectories of a high-temperature mantle intrusion. *J. Petrol.*, 21, 533-572.

O'Hara, M.J., 1977: Thermal history of excavation of Archaean gneisses from the base of the continental crust. *J.Geol.Soc. Lond.*, 134, 185-200.

O'Hara, M.J. and Mercy, E.L.P., 1966: Garnet-peridotite and eclogite from Bellinzona, Switzerland. *Earth.Planet.Sci.Lett.*, 1, 295-300.

O'Hara, M.J. and Howells, S., 1978: The enstatite-pyrope geobarometer, pp. 175-179. *in Progress in Experimental Petrology*, 4, N.E.R.C., 1978.

O'Hara, M.J. and Yarwood, G., 1978: High P-T point on an Archaean geotherm, implied magma gneisses by crustal anatexis and consequences for garnet-pyroxene thermometry and barometry. *Phil.Trans.Roy.Soc.Lond.*, A, 288, 441-456.

Oka, Y., 1977: A thermodynamic treatment of chemical reactions in orthopyroxene. *Geochem.J.*, 11, 101-106.

Oka, Y., 1978: Experimental study on the partitioning of Fe and Mg between garnet and olivine and its applications to kimberlites. *Jour.Fac.Sci.Hokkaido Univ.*, Serv. IV, 18(3), 351-376.

Oka, Y. and Matsumoto, T., 1974: Study on the compositional dependence of the apparent partition coefficient of iron and magnesium between coexisting garnet and clinopyroxene solid solution. *Contrib.Mineral.Petrol.*, 48, 115-121.

O'Neill, H. StS. and Wood, B.J., 1979: An experimental study of Fe-Mg partitioning between garnet and olivine and its calibration as a geothermometer. *Contrib.Mineral.Petrol.*, 70, 59-70.

Perkins, D. and Essene, E.J., 1977: A model for grossular activity in garnet solutions and applications to natural assemblages (abstr.) *EOS Trans.AGU*, 58, 523.

Perkins, D. and Newton, R.C., 1980: Compositions of Coexisting pyroxenes and garnets in the System $CaO-MgO-Al_2O_3-SiO_2$ at 900-1100°C and High Pressures. *Contrib.Mineral.Petrol.*, 75, 291-300.

Powell, R., 1978: The Thermodynamics of Pyroxene geotherms. *Phil.Trans.Roy.Soc.Lond.*, A, 288, 457-470.

Ravich, M.G. and Kamenev, E.N. 1975: *Crystalline of the Antarctic Basement platform*. John Wiley and Sons, New York.

Reid, A.M. and Dawson, J.B., 1972: Olivine-garnet reaction in peridotites from Tanzania. *Lithos*, 5, 115-124.

Rolfe, D.G., Nixon, P.H. and Boyd, F.R., 1973: The geology of the Kao kimberlite pipes, pp. 101-109. *In Lesotho Kimberlites* (P.H. Nixon, ed.), Lesotho Nat.Dev. Corp.

Ross, M. and Huebner, J.S., 1975: A pyroxene geothermometer based on composition-temperature relationships of naturally occurring orthopyroxene, pigeonite and augite. *Extended abstracts, international conference on geothermometry and geobarometry, Pennsylvania* State University.

Ross, M. and Huebner, J.S., 1979: Temperature-composition relationships between naturally occurring Augite, Pigeonite and Orthopyroxene at one bar Pressure. *Amer.Mineral.*, 74, 11-12, 1133-1155.

Sack, R.D., 1980: Some constraints on the thermodynamic mixing properties of Fe-Mg orthopyroxenes and olivines. *Caontrib.Mineral.Petrol.*, 71, 3, 257-270.

Savage, D., and Sills, J.D., 1980: High-pressure metamorphism in the Scourian of NW Scotland: evidence from garnet granulites. *Contrib.Mineral.Petrol.*, 74, 153-163.

Saxena, S.K., 1968: Distribution of iron and magnesium between coexisting garnet and clinopyroxene in rocks of varying metamorphic grade. *Amer.Mineral.*, 53, 2018-2024.

Saxena, S.K., 1969: Silicate solid solutions and geothermometry 4. Statistical study of chemical data on garnets and clinopyroxenes. *Contrib.Mineral.Petrol.*, 23, 140-156.

Saxena, S.K., 1976: Two-pyroxene Geothermometer: a model with an approximate solution. *Amer.Mineral.*, 61, 643-652.

Saxena, S.K., 1980: Pyroxene and garnet crystalline solutions *in Problems of Phyico-chemical Petrology*. D.S.Korzhinskii 80th anniversary volume. USSR acad Sci.Moscow.

Saxena, S.K. and Ghose, S., 1971: Mf^{2+}-Fe^{2+} order-disorder and the thermodynamics of the orthopyroxene solid solution. *Amer.Mineral.*, 56, 532-559.

Scharbert, H.G. and Kurat, G., 1974: Distribution of some elements between coexisting ferromagnesian minerals in Moldanubian Granulite facies rocks, Lower Austria. *Ischemako.Min.Petr.Mitt.*, 21, 110-134.

Schmid, R. and Wood, B.J., 1976:Phase relationships in granulite metapelites from the Ivrea-Verbana zone, northern Italy. *Contrib.Mineral.Petrol.*, 54, 255-279.

Schreyer, W. and Abraham, K., 1978: Symplectitic Cordierite-orthopyroxene-garnet assemblages as products of contact metamorphism of pre-existing basement granulites in the Vredefort Structure, South Africa, and their relations to pseudotachylite. *Contrib.Mineral.Petrol.*, 68, 53-62.

Sheraton, J.W., Offe, L.A., Tingey, R.J. and Ellis, D.J., 1980: Enderby Land, Antarctica - an unusual precambrian high-grade metamorphic terrain. *J.Geo.Soc.Aust.*, 27, 1-18.

Skinner, B.J. and Boyd, F.R., 1964: Aluminous enstatites. *Carnegie Inst.Wash.Yearbook*, 63, 163-165.

Smith, D.C., 1974: Pyroxene-olivine-quartz assemblages in rocks associated with the Nain anorthosite massif, Labrador. *J.Petrol.*, 15, 58-78.

Smith, D.C., 1980: A tectonic melange of foreign eclogites and ultramafites in west Norway; and reply by L.G. Medaris, Jr., *Nature*, 287, 366-368.

Sobolev, N.V., 1977: *Deep-seated inclusions in kimberlites and the problem of the composition of the upper mantle.* Amer.Geophys.Union., Washington, D.C.

Smith, D.C. and Levy, S., 1976: Petrology of the Green Knobs diatreme and implications for the upper mantle below the Colorado plateau. *Earth.Planet.Sci.Lett.*, 29, 107-125.

Stormer, J.C.Jnr. and Whitney, J.A., 1977: Two feldspar Geothermometry in granulite facies metamorphic rocks: Sapphirine Granulites from Brazil. *Contrib.Mineral.Petrol.*, 65, 123-133.

Takahashi, T. and Liu, L.G., 1970: Compression of ferromagnesian garnets and the effect of solid solutions on the Bulk Modulus, *J.Geophys.Res.*, 72, 29, 5757-5765.

Takeda, H., 1972: Crystallographic studies of coexisting aluminan orthopyroxene and augite of high-pressure origin. *J.Geophys.Res.*, 77, 5798-5811.

Tarney, J. and Windley, B.F., 1977: Chemistry, thermal gradients and evolution of the lower continental crust. *J.Geol.Soc.Lond.*, 134, 153-172.

Thompson, A.B., 1976: Mineral recations in pelitic rocks:
I. Prediction of P-T-X (Mg-Fe) phase relations
II. Calculation of some P-T-X (Fe-Mg) phase relations.
Am.J.Sci., 276, 425-454.

Thompson, J.B. Jr., 1967: Thermodynamic properties of simple solid solutions *in* P.H. Abelson, ed., *Research in Geochemistry*, 2, 340 (1967).